MODELLING MAGMATIC TRENDS IN TIME AND SPACE: ERUPTIVE AND MAGMATIC HISTORY OF TONGARIRO VOLCANIC COMPLEX, NEW ZEALAND

Volume I

A thesis

submitted in fulfilment

of the requirements for the Degree

of

Doctor of Philosophy in Geology

in the

University of Canterbury

by

B. J. Hobden

University of Canterbury

March 1997

Dedicated to the memory
of my brother, Allan

Ngauruhoe and Red Crater in serene mood as Ruapehu erupts in background, 25 September 1995.
Photo courtesy Thor Thordarson.

CONTENTS

ABSTRACT

Detailed mapping of volcanic stratigraphy in conjunction with 41 new K-Ar ages have been used to constrain a petrological model of Tongariro Volcanic Complex within a time-space framework. Over 400 samples form an extensive geochemical data base comprising whole-rock major and trace element data, together with whole-rock REE and isotopic analyses and mineral compositions for selected samples. These data have been used to investigate the complex interplay between magma batches on a variety of time scales and the time-space relationships of the subvolcanic plumbing system. This new integrated approach to the study of Tongariro has not been applied to many other composite volcanoes but is crucial in linking petrological models to realistic geological relationships.

Tongariro is a large (c.60 km^3), active, basaltic andesite to dacite composite cone complex situated near the southern end of the Taupo Volcanic Zone, New Zealand. A virtually continuous eruptive history of the Tongariro complex has been divided into 17 small (<2 km^3) to large (12 km^3) nested and overlapping volcano-stratigraphic or cone-forming units which represent the products (aa and block lava flows, welded scoria-spatter deposits, volcaniclastic tuff breccias) of many recurrent styles of eruptions from at least 30 discrete vents, active for varying periods of time (a few to tens of thousands of years) throughout Tongariro's known lifetime from c.275 ka to the present. Episodes of rapid cone growth have occurred at 210-200 ka (Tama 2 cone eruptive rate = 1 km^3/ka) and 130-80 ka (NE Oturere, SW Oturere and Tongariro Trig cones under construction), with development of the complex most recently dominated by the rapid growth (0.9 km^3/ka) of Ngauruhoe cone since 2.5 ka. There is no orderly time-space relationship between cone-building events; the locus of activity shifted non-systematically over the lifetime of the complex within a 13 km-long and 5 km-wide SW-NE aligned vent corridor.

Tongariro eruptive products vary in composition almost continuously from 53.0 to 64.2 wt% SiO_2 and 1.1 to 9.2 wt% MgO, forming a calc-alkaline, medium-K suite. Two-pyroxene andesites are volumetrically dominant, but hornblende is a significant phase confined to the older southern cones of Tama 1 and 2 and Pukekaikiore, and olivine is particularly prominent in the young (post-25 ka) eruptives, suggesting an overall time-space relationship with petrography and mineralogy. Tongariro rocks exhibit features typical of subduction-related magmas such as light-REE enriched patterns ($[Ce/Yb]_N$=1.8-3.9), relatively low high field strength abundances (e.g. Nb=2.7-6.7), and strongly spiked patterns on incompatible element spiderdiagrams. A wide range in $^{87}Sr/^{86}Sr$ (0.704442-0.706193) is accompanied by less variability in $^{143}Nd/^{144}Nd$ (0.512629-0.512862), Pb isotopic ratios ($^{206}Pb/^{204}Pb$=18.781-18.854, $^{207}Pb/^{204}Pb$=15.594-15.645, $^{208}Pb/^{204}Pb$=38.588-38.802), and $\delta^{18}O$ (+6.16-6.59).

Variation diagrams for the Tongariro cone-forming units reveal major diversity in the absolute elemental abundances for given SiO_2 contents, in the length, steepness and shape of chemical trends, and in the distribution of chemical groups within compositional space. However, certain volcano-stratigraphic units (e.g. the amphibole-bearing andesites

of the older southern cones) do share similar patterns of chemical ordering which suggest derivation from a common 'parental' magma reservoir and a similar early history. Nonetheless, considerable chemical variability in closely-related samples is common, and provides strong evidence for a higher level influence on magma compositions. Non-systematic relationships with age (compositional breaks, reversals and loops) along geochemical trends on variation diagrams and chemical stratigraphy plots cannot be modelled by fractional crystallization. These coincide with petrographic and mineralogical evidence for disequilibrium including plagioclase sieve textures, strong reverse zoning, co-existing high-temperature and low-temperature phases exhibiting reaction rims or corrosion, olivine phenocrysts with much higher Fo contents than expected from whole-rock Mg#, and bimodal or very widely ranging crystallization temperature estimates for some samples. These features suggest the involvement of multiple small batches of magma, rising from the various 'parental' reservoirs by differing ascent paths, within a complex subvolcanic plumbing system which has allowed varying degrees of interaction and magma mixing.

As indicated by the presence of quartzite xenoliths of the Torlesse metasedimentary basement, these magmas have also interacted with the crust, which represents an important means of introducing often wide compositional diversity of magmas on time scales as short as decades or centuries. A considerable variation in incompatible trace element ratios (e.g. Ba/Zr, Nb/Ta, La/Yb, Zr/Hf) and radiogenic isotopic compositions (e.g. Ngauruhoe $^{87}Sr/^{86}Sr$ ratios increase from 0.705470 in 1954 to 0.706165 in 1975) for closely-related samples, and the marked scatter of data evident on assimilation-fractional crystallization (AFC) process diagrams indicate that magmas have not evolved along a unique AFC trend but can more aptly be characterised as forming a 'family' of AFC trends or perhaps a series of 'one-off' AFC 'events' produced by contamination of numerous small and frequent Tongariro magma batches with varying amounts of compositionally heterogeneous Torlesse crust.

This investigation of chemically and isotopically diverse lavas related on time scales of 100 years (historic Ngauruhoe eruptives), 1000 years (Ngauruhoe, Red Crater and Te Mari Crater vents) and 10 000 years (0-10 ka young eruptives, 120-130 ka NE Oturere, 200-210 ka Tama 2) has demonstrated that the observed compositional variability is mainly developed at comparatively high crustal levels within a complex subvolcanic plumbing system by fractional crystallization and the mixing of numerous, small ($<<0.1$ km^3), short-lived (c.1 ka) magma batches coupled with variable amounts of crustal assimilation of a compositionally diverse Torlesse metasedimentary contaminant. These processes have been operating to similar effect throughout the lifetime of the Tongariro complex, although subtle differences in geochemical patterns suggest that the regularity or rate of magma batch production may have varied slightly. The young Ngauruhoe cone has been highlighted as a cameo study for which the well-constrained stratigraphy, enabled by the preservation of numerous young lava flows erupted over the last thousand years, provides a unique opportunity for detailed petrological modelling paying careful attention to age relationships. Five geochemically and isotopically distinct groups of magma reflect variable crustal contamination of many discrete magma batches within several independent shallow plumbing systems beneath Ngauruhoe.

LIST OF FIGURES

LIST OF TABLES

Chapter 1

Introduction

CHAPTER 1
INTRODUCTION

1.1 NATURE AND SCOPE OF STUDY

1.1.1 Significance of study

The multiple cones of the Tongariro Volcanic Complex evoke a complicated volcanological and magmatic evolution, yet the complex had not been mapped, dated or sampled in detail previously. This principally geochemical study incorporates stratigraphic and absolute age constraints in petrologic modelling, and addresses time-space relationships of the subvolcanic plumbing system, as well as the relationship between eruptive styles and magma compositions. As such, the study represents one of the few attempts to integrate time, volume and geochemical investigations of a long-lived composite volcano. Within the Taupo Volcanic Zone, the Tongariro complex is now the most comprehensively studied of the andesitic composite volcanoes, especially in the respect that extensive petrological data are tied into a relatively detailed chronology.

1.1.2 Background to approach taken for study

Many published studies of composite volcanoes are focused on the isotopic or trace element compositions of isolated samples from the lavas, with often little attention paid to the stratigraphy or eruptive history. This creates uncertainty in petrologic modelling (such as establishing parent-daughter relationships) as to whether the magmas considered are in fact capable of being genetically related in the manner tested by the model.

Some petrological studies, however, have placed a greater emphasis on attaining an integration with field data, often grouping the lavas and pyroclastics into eruptive series or stages (e.g. Hopson and Melson, 1990; Feeley et al., 1993; Feeley and Davidson, 1994), or concentrating on the variation of chemistry with stratigraphic position for well-constrained sections (e.g. Nixon, 1988b; Ferguson et al., 1992; Beddoe-Stephens et al., 1995), or highlighting the petrological trends during one particular historic eruptive episode (e.g. Gerbe et al., 1992; Clocchiatti et al., 1994).

A recent investigation of the eruptive chronology of the Mount Adams volcanic field in the Cascade Range (Hildreth and Lanphere, 1994) provides an excellent example of the potential for integration of time-volume-composition data. The study highlighted the importance of reconstructing the eruptive history as far back in time as possible to incorporate the older activity as well as the known historical record. Hildreth and Lanphere (1994) drew attention to issues such as the time-space relationship of subvolcanic plumbing systems, cyclic versus progressive evolution in magma compositions, and the importance of age relationships when assessing petrologic suites and lines of magmatic descent.

1.1.3 Nature and purpose of study

This thesis draws inspiration from the work of Hildreth and Lanphere (1994) and others (those cited above, plus Tatara-San Pedro Project Team, 1992), and seeks to understand detailed petrological data obtained for the Tongariro complex in the context of the volcano-stratigraphy developed during this study. Although essentially the entire complex has been mapped and sampled, the project has deliberately focused on several cameo studies (e.g. Ngauruhoe, NE Oturere), and thus these more well-constrained portions of the stratigraphy have provided a framework for understanding the complex as a whole. A significant contribution from this research has been establishing the relationship between the recent cone-building styles represented by the young eruptive products (on which most previous work had been focused) and the older volcanic stratigraphy - especially in terms of the eruptive pattern-frequency-volume and rates of magmatic differentiation.

This study has been conducted in association with Dr Bruce Houghton and Dr Ian Nairn from the Institute of Geological and Nuclear Sciences (GNS), Wairakei, who are involved in producing a detailed geological map and conducting physical volcanology studies on the Tongariro Volcanic Complex, and with Dr Marvin Lanphere of U.S. Geological Survey, Menlo Park, who has performed 41 K-Ar age determinations on Tongariro samples. Joint and independent field work for this thesis was carried out over a total period of about five months between 1991 and 1993.

To facilitate the study of temporal variations in magma chemistry, samples (over 400) of lava flows and pyroclastic units were collected stratigraphically from each cone-building sequence. The sample numbers referred to in descriptions and figure captions throughout this thesis are set out with their relevant information (location, rock type, field occurrence, etc.) in the tables of Appendix 1. K-Ar dating was used in conjunction with field data to identify a number of distinct volcano-stratigraphic units (Appendix 2), which then provided the framework for petrological modelling. Petrological data obtained for this study (Appendices 3-15) consist of petrographic analysis of thin sections, electron microprobe analysis of mineral compositions, whole-rock chemical analysis by XRF, rare earth and other trace element analysis by INAA, radiogenic isotope analysis (Sr, Nd, Pb) by TIMS, laser-fluorination oxygen isotope analysis, and accelerator mass spectrometry analysis of ^{10}Be. All the available information was used to develop a model for the eruptive and magmatic history of the Tongariro Volcanic Complex.

1.2 LOCATION, PHYSIOGRAPHY AND HISTORY OF STUDY AREA

1.2.1 Location and definition of study area

The Tongariro Volcanic Complex is situated in the centre of the North Island of New Zealand, near the southern end of the active Taupo Volcanic Zone (TVZ; Figs 1.1 and 1.2). The tectonic features of the TVZ are discussed in Section 1.4.2. This southern portion

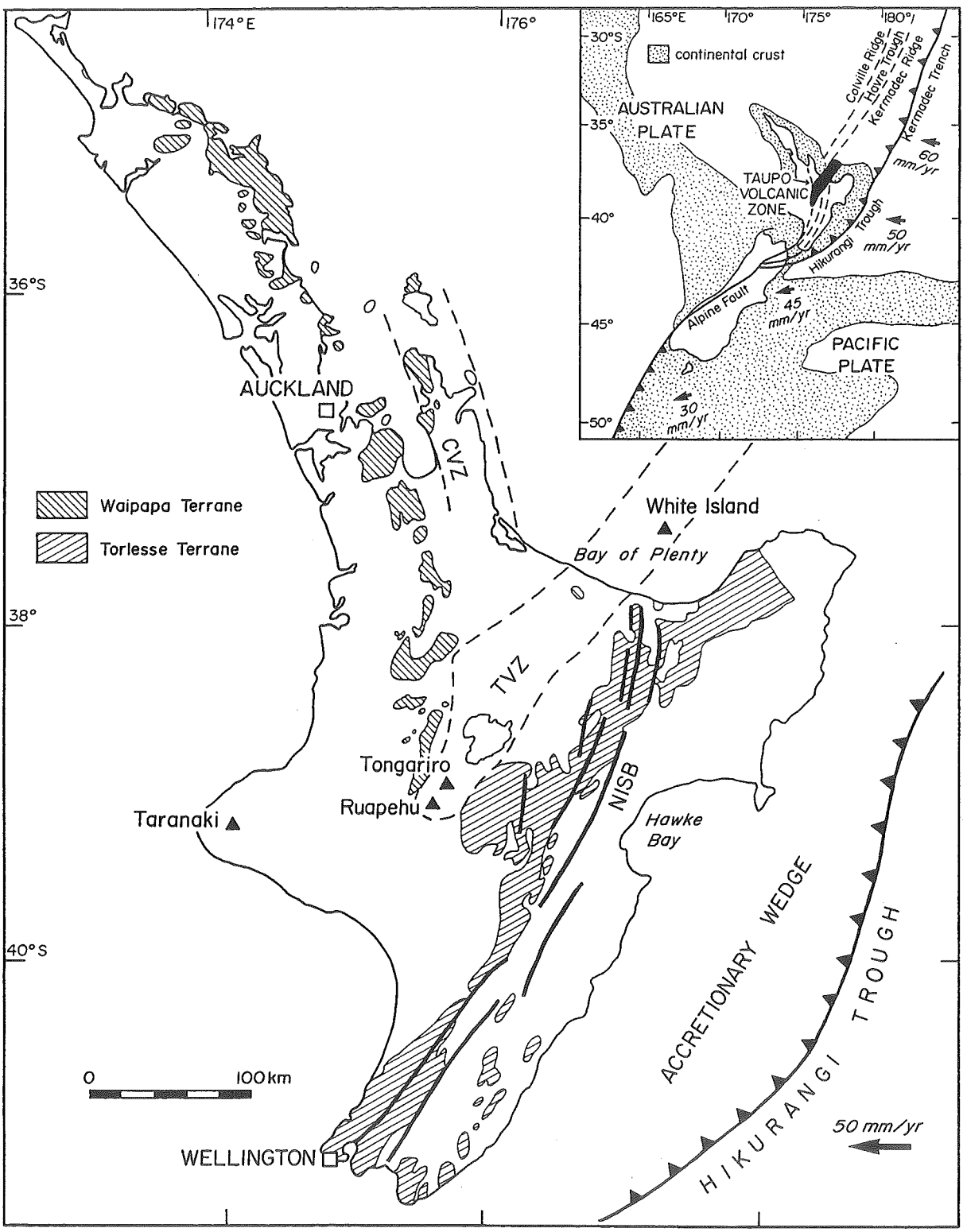

Figure 1.1 Map showing tectonic features of the North Island of New Zealand, setting of the Taupo Volcanic Zone (TVZ), and surface distribution of the Waipapa and Torlesse basement terranes. NISB = North Island Shear Belt. CVZ = Coromandel Volcanic Zone. Arrows indicate direction and rate of subduction of the Pacific Plate beneath the Australian Plate. Adapted from Graham et al. (1995) and Cole (1990).

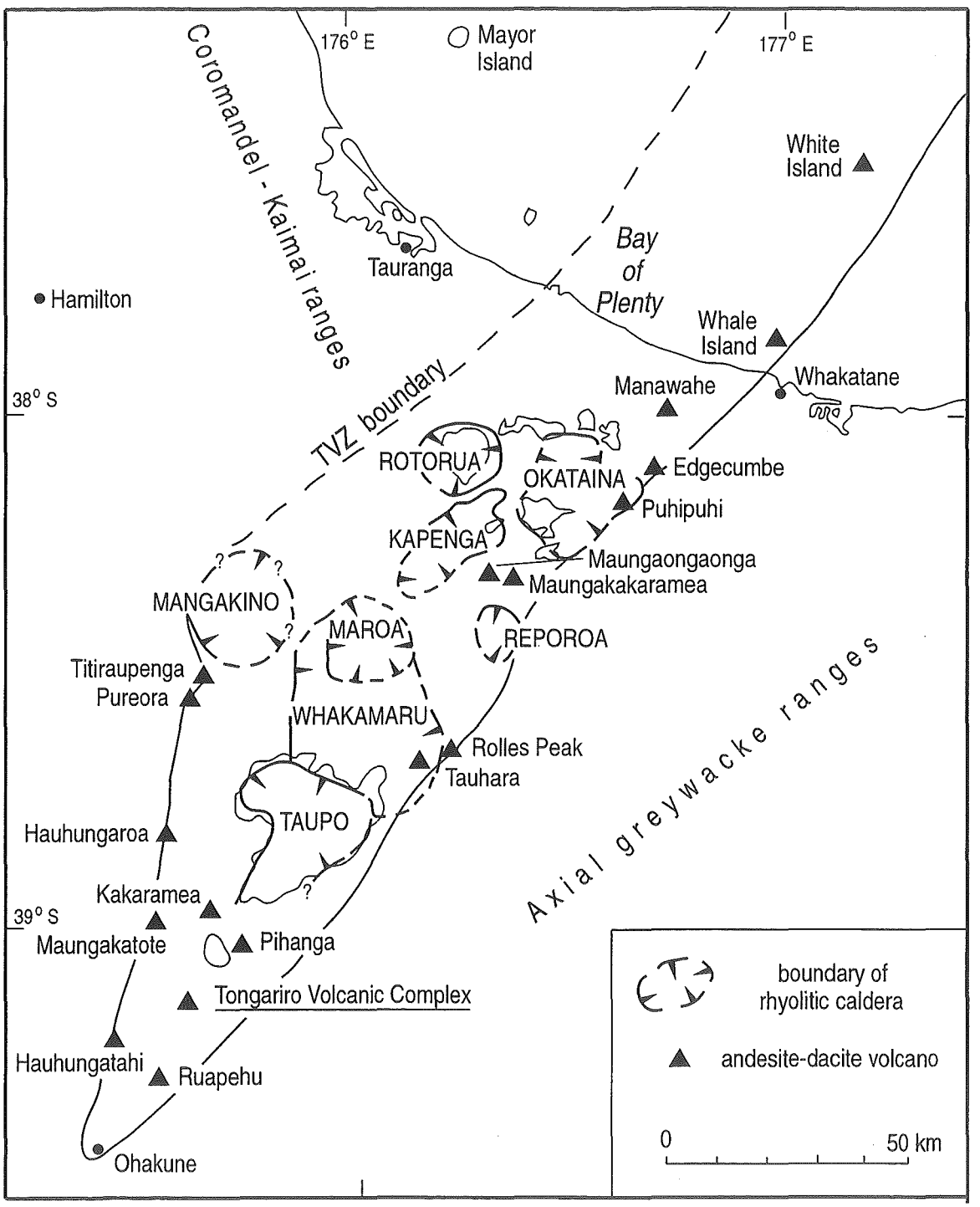

Figure 1.2 Map showing structural boundaries of rhyolitic calderas and locations of andesitic-dacitic composite cones and dome complexes. Adapted from Houghton et al. (1995) and Wilson et al. (1995)

of the zone is dominated by andesitic composite cones of various ages which have traditionally been classed together as the Tongariro Volcanic Centre (e.g. Grindley, 1960; Topping, 1974; Cole, 1978; Graham and Hackett, 1987; Graham et al., 1995). This is not an altogether satisfactory term because the use of "centre" for a collection of spatially distinct volcanic complexes each with its own magma feeding system is not consistent with its use for the rhyolitic centres to the north (Fig 1.2) where each centre is associated with just one magmatic system. Therefore the term Tongariro Volcanic Centre, as published, is not applicable to all of the andesite complexes south of Lake Taupo and may be re-defined in future work, but refinement of this nomenclature is not attempted here.

Two large andesitic volcanoes (Tongariro and Ruapehu), several smaller cones (Maungakatote, Kakaramea, Pihanga, Hauhungatahi, Pukeonake, Ohakune) and a distal ring plain occur at the southern end of TVZ (Fig 1.3). Over the last 250 ka, Ruapehu volcano (present volume 110 km^3) has erupted basalt to dacite lavas and pyroclastics from a variety of summit and flank vents during four major cone-building episodes (Graham and Hackett, 1987; Hackett and Houghton, 1989). The smaller cones have generally not been studied in detail: Maungakatote and Maungaku are two coalescing eroded andesite cones which may be <330 ka (Cole, 1978); Kakaramea-Tihia andesitic massif has been dated at 190-220 ka by Stipp (1968) but may be in part younger (Cole, 1978); Pihanga is a little dissected andesitic cone (Cole, 1978); Hauhungatahi is an eroded Miocene sequence of basaltic andesite lavas, ash and breccia overlying sediments, and was probably erupted from an eroded cone to the west ≥500 ka (Hackett, 1985); Pukeonake is a basaltic andesite scoria cone formed between 20 ka and 25 ka (Napp, 1983; Cole et al., 1986); and Ohakune Craters and associated basaltic andesite scoria cone - tuff ring are about 25 ka (Houghton and Hackett, 1984).

"Tongariro Volcano" encompasses a number of older (65-275 ka) cone-building episodes and younger (0-25 ka) active (or potentially active) cones and craters which have been defined as separate volcano-stratigraphic units in this study (Chapter 3). Because the term "volcano" is rather loosely defined and could also be used to refer to just one of the cones on Tongariro, the term "Tongariro Volcanic Complex" is preferred as a collective term to describe all the different cone-building sequences described in this study (although

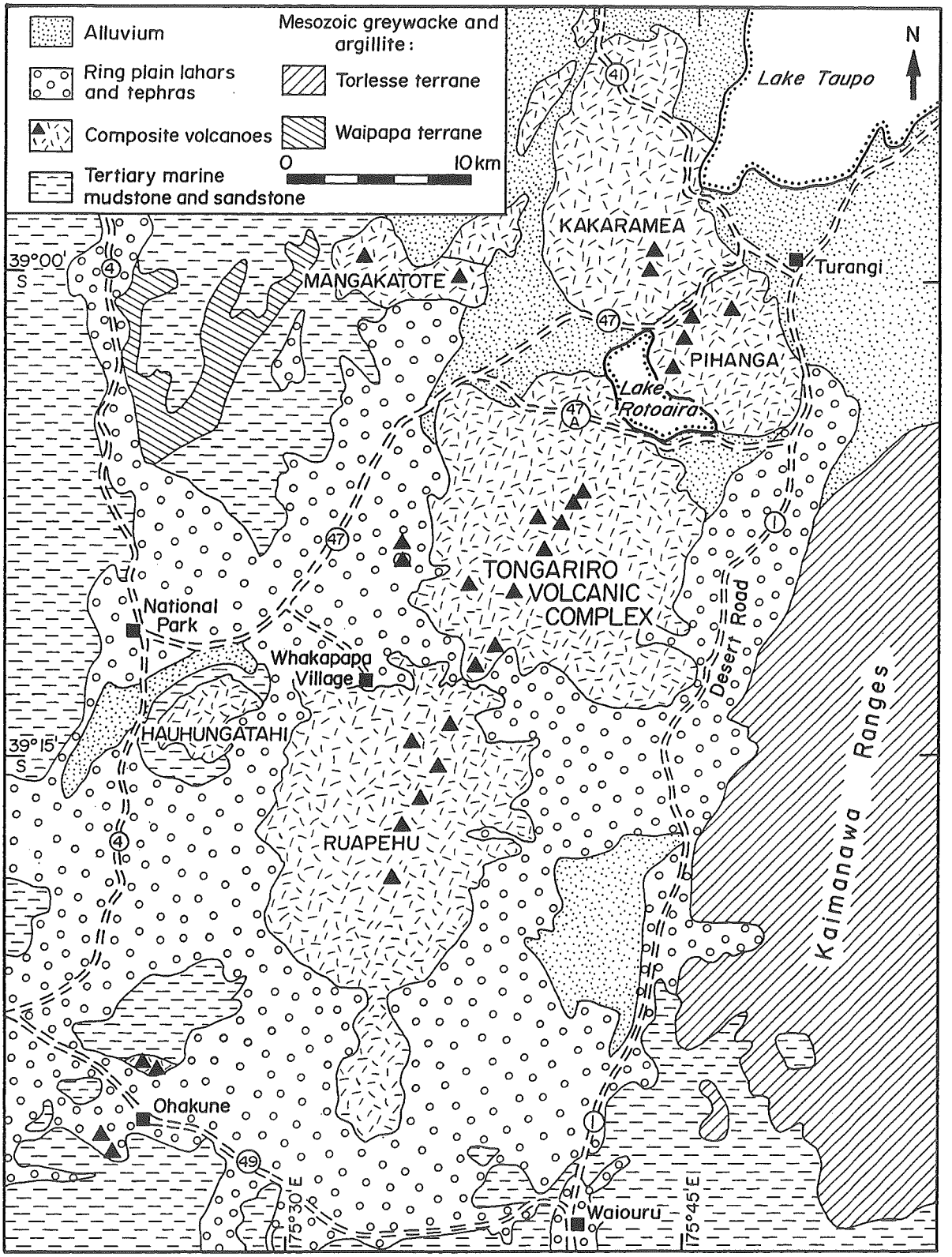

Figure 1.3 Map showing generalised geology of Tongariro Volcanic Centre and surrounding area, including distribution of alluvium, ring plain material, Tertiary sediments, and Mesozoic basement terranes. Main roads and settlements are also shown. Adapted from Beetham and Watters (1985), Hackett and Houghton (1989), and Cole (1990).

for brevity "the Tongariro complex", "Tongariro lavas", etc. are also used). The boundaries of the study area are therefore basically those of the proximal Tongariro Volcanic Complex (Fig 1.3), although one major valley system (Mangahouhounui) and the outer slopes of the volcanic edifice were not studied (Section 3.2.2).

1.2.2 Physiography

Tongariro Volcanic Complex covers approximately 200 km^2 and has a present (eroded) volume of approximately 60 km^3. Adding the c.15 km^3 (DRE) of Tongariro ring plain material to the volume calculated for the cones gives a total present volume of around 75 km^3. Taking a base level of 800 m above sea level, a significant proportion of the complex is over 600 m high (i.e. above 1400 m above sea level). There is no single summit to the volcanic edifice because the complex comprises a number of coalescing and overlapping cones, in various stages of erosion (Fig 1.4).

The landscape of the Tongariro complex is dominated by young post-glacial cones and craters which are roughly aligned in a SW-NE lineation (Figs 1.5 and 1.6). The symmetrical cone of Ngauruhoe forms the highest part of the complex (Figs 1.4 and 1.6), with a summit elevation of 2287 m above sea level. The smaller Red Crater scoria cone, North Crater spatter cone and Blue Lake crater are conspicuous in the central portion of the complex (Figs 1.6 and 1.7). The Te Mari Craters on the north slopes of the edifice (Figs 1.5 and 1.6) and the Tama Lakes craters to the south (Fig 1.5) complete the NE vent lineation. "Central Crater" and "South Crater" (Fig 1.5) were misnamed as craters by early visitors (Section 1.6.1); there is no evidence for an explosive origin and they are more likely to be cirque basins carved out by glaciers (cf. Topping, 1974). The Pukeonake scoria cone is a peripheral vent situated to the west of the complex (Fig 1.5).

The other topographic highs on the complex, e.g. Pukekaikiore, Mt Tongariro (Fig 1.7), Oturere Valley walls (Fig 1.7), Tama Lakes area (Fig 1.4), are ridges formed from the eroded remnants of older pre-glacial cones. These surviving cone-forming structures are generally of lower relief then the younger cones. The outer flanks of the complex are gently

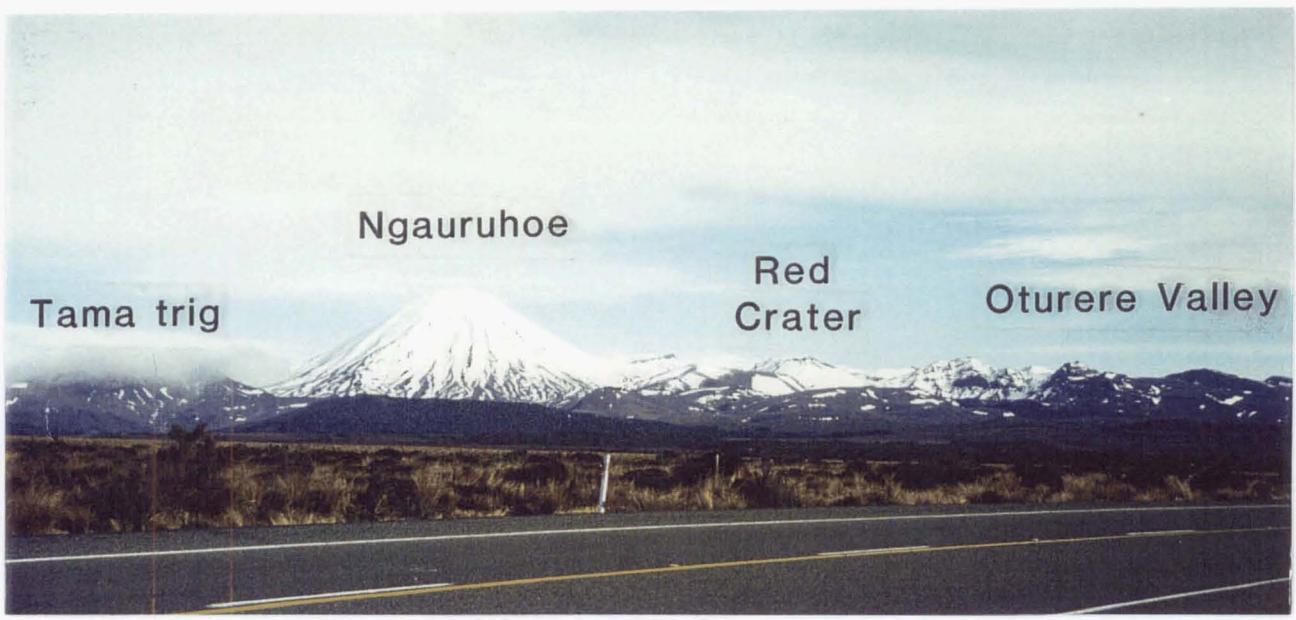

Figure 1.4 The young cone of Ngauruhoe dominates the skyline in this view of the Tongariro Volcanic Complex looking towards the northwest, from the Desert Road to the southeast.

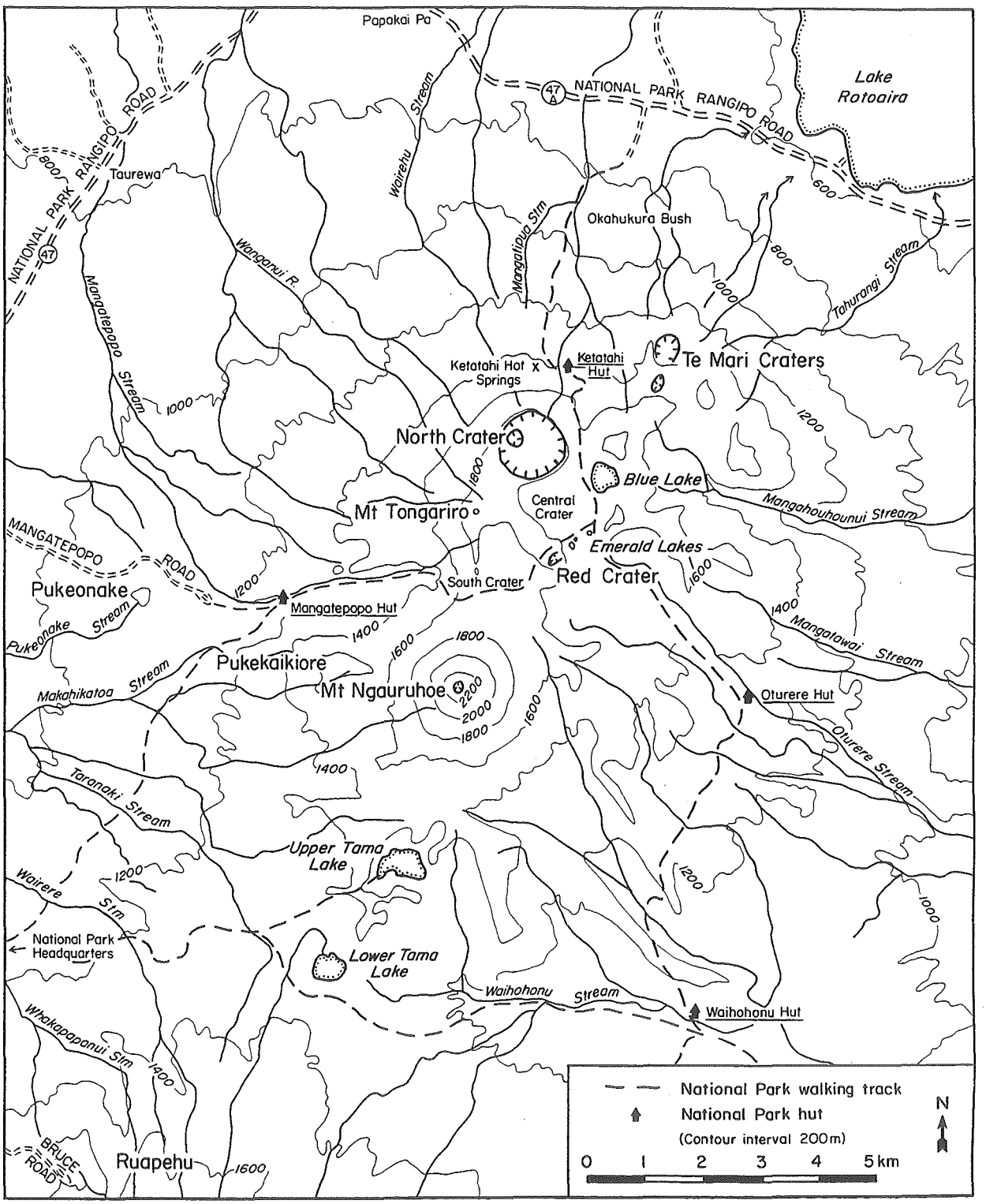

Figure 1.5 Location map for Tongariro Volcanic Complex showing topography, access roads, place names, National Park huts and walking tracks. Main stream courses only are shown.

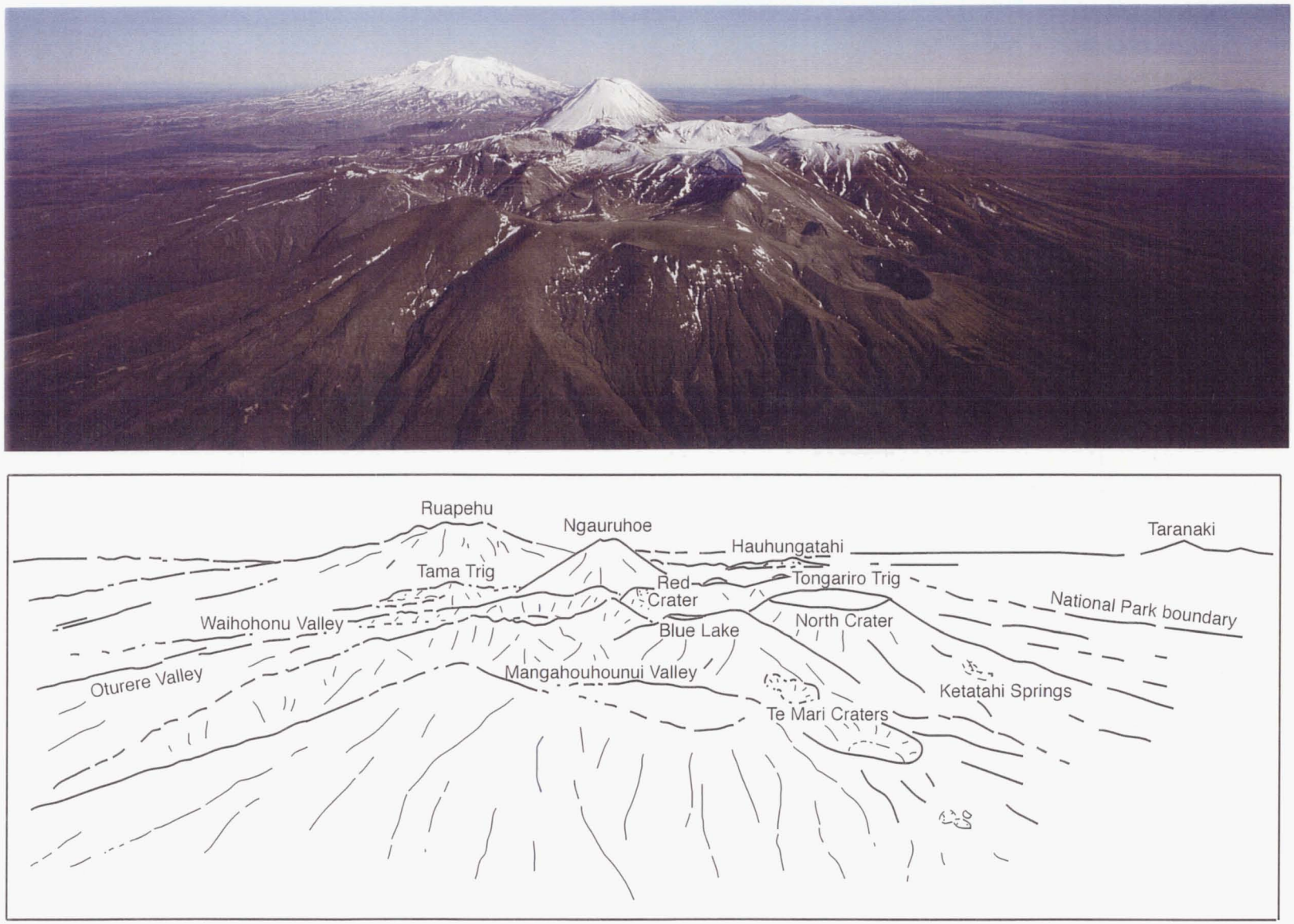

Figure 1.6 View of Tongariro Volcanic Complex looking towards the south. Ruapehu and Taranaki volcanoes in the background. Young cones & craters, older lava ridges, and valleys are labelled in the accompanying sketch. Photo courtesy of D.L. Homer, GNS Lower Hutt.

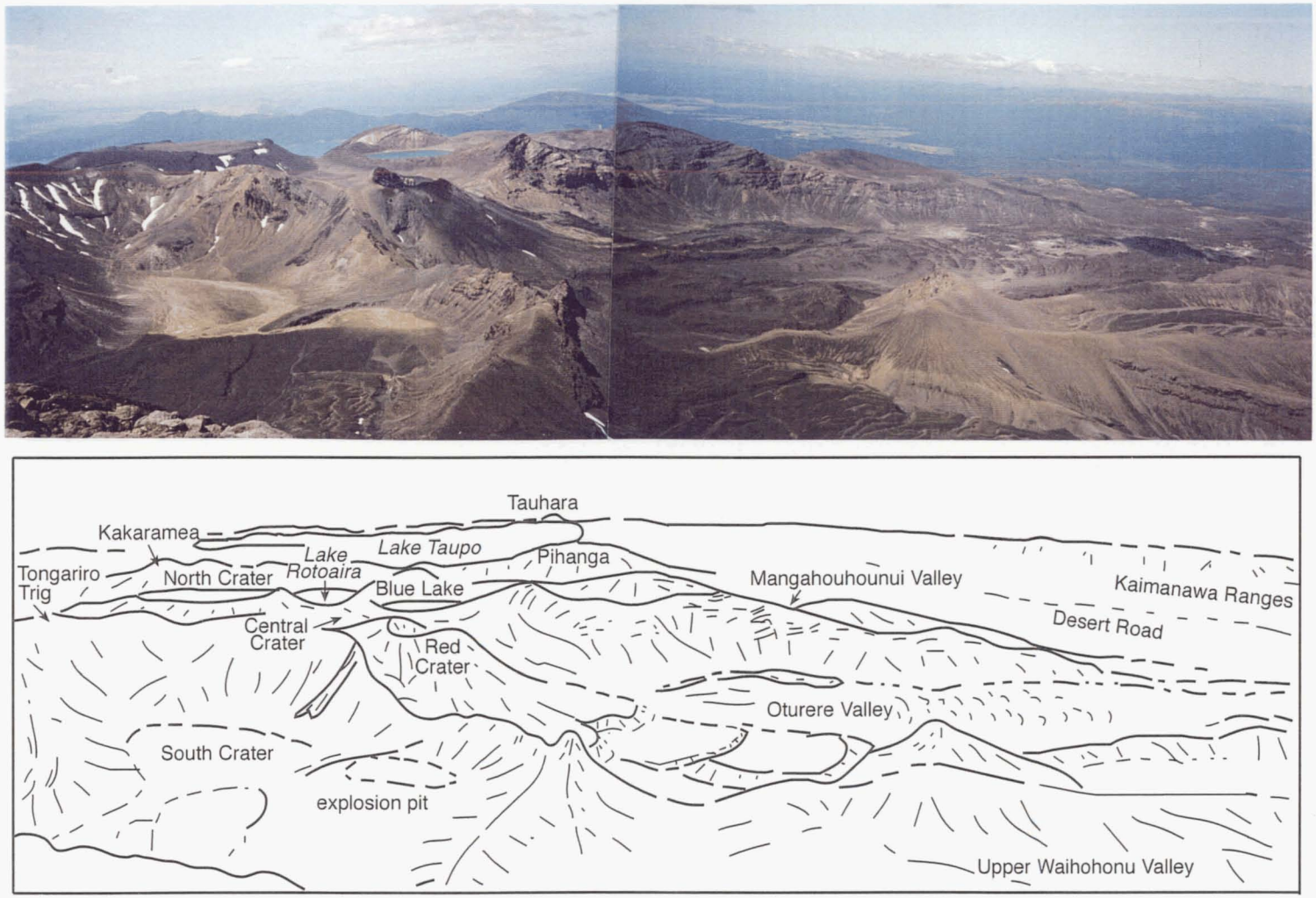

Figure 1.7 View of Tongariro Volcanic Complex looking towards the north. Kakaramea, Pihanga and Lake Rotoaira are in the background. Lake Taupo, Tauhara, and the Kaimanawa Ranges are in the far distance. Craters and valley systems are labelled in the accompanying sketch. Note Red Crater lava flows filling Oturere Valley. Photos courtesy of K.E. Cooper.

sloping, in contrast to the steep slopes of some of the young summit cones (e.g. the 30° slope of Ngauruhoe cone) (Fig 1.6).

Many streams drain radially down the slopes of the Tongariro complex (Fig 1.5), and several valleys have been further eroded by glaciation to form deep, flat-bottomed valleys (e.g. Waihohonu Valley, Oturere Valley, Mangatepopo Valley).The complex is basically divided into two catchments; streams on the western side drain into the Wanganui River which flows out to the west coast of the North Island, and streams on the eastern side drain into the Tongariro River which flows into southern Lake Taupo (and then out from the northern part of the lake as the Waikato River). Cold springs fed by rain water occur on the complex, including Soda Springs in Mangatepopo Valley, Ohinepango Springs and Waihohonu Springs.

Several small, roughly circular, cold lakes occupy explosion craters on the complex (Fig 1.5). Blue Lake (Fig 1.7) has a diameter of 400 m and is 16.5 m deep. The three Emerald Lakes have a maximum depth of 4.5 m, and owe their characteristic green colour to the entry of fumarolic sulphur into the lake and the ensuing formation of polysulphide ions (Christenson and Crump, 1994). Upper Tama Lake is 10.5 m deep, and Lower Tama Lake is 24 m deep (Michaelis, 1981). Blue Lake and the Emerald Lakes are noticeably acidic (pH = 3.1-5.2), whereas the Tama Lakes are neutral (Michaelis, 1981; Hochstein, 1985).

1.2.3 Climate

The high relief of the Tongariro complex and Ruapehu volcano forms a NE-SW trending barrier to the prevailing westerly winds which bring most of the rain. Consequently, rainfall on the northern and western sides is high (1800-3000 mm annually), whereas in the south and east conditions are slightly drier (annual rainfall down to 1100 mm) (Atkinson, 1981). It rains on average about 200 days of the year, and snows about 16 days of the year at Tongariro. At an altitude of 650 m the mean annual temperature is about 10°C, which drops to about 7°C at 1120 m (Atkinson, 1981). An average of 141 days of ground frost occurs at all times of the year at Tongariro (Atkinson, 1981),

contributing significantly to erosion by the processes of frost-heave and freeze-thaw. Wind erosion is also important, as winds blowing at 30-60 knots are commonly recorded, gusting up to 80 knots (Potton, 1987). Northwesterly winds gather speed as they are funnelled through Tama Saddle and have a significant drying effect on the land to the east of the volcanoes, helping to create the Rangipo Desert. No permanent snowfields or glaciers are present on the Tongariro complex, and the summit region is generally clear of snow during the height of summer (January to March) when field work is best carried out.

1.2.4 Past glaciations

The higher elevation of neighbouring Ruapehu volcano (2797 m) allows snow to exist all year round on the summit, which is also occupied by small, actively retreating alpine glaciers. Glaciers have existed in the past on the Tongariro complex, however, as evidenced by U-shaped valleys (Mangatepopo, Waihohonu, Oturere) and paired moraine ridges (Mangatepopo, Makahikatoa, and Waihohonu Valleys) (Figs 3.10, 3.15, 3.25).

Although various glacial features have been documented from Tongariro Volcanic Centre (Gregg, 1960; Mathews, 1967; Topping, 1974; Hackett, 1985), a definitive glaciation chronology has only been attempted for Mt Ruapehu (McArthur and Shepherd, 1990). However, because the Tongariro moraines are similar in their completeness, size, position, and degree of preservation to the Ruapehu moraines, McArthur and Shepherd (1990) noted that a correlation of the moraines was possible, which implied that ice fields of similar dimensions to those of Ruapehu (140 km^2) fed the Tongariro glaciers in late Otiran times.

Because glacial deposits on the Tongariro complex are often difficult to distinguish from volcaniclastic deposits or have been covered by subsequent volcanic activity, direct marine-terrestrial correlations (Pillans, 1994) have provided the best framework for a glaciation chronology in the central North Island. Using a combination of data from offshore deep sea cores (with established oxygen isotope chronology), and on-land loess sediments, river terraces, pollen analysis, tephra marker beds, magnetostratigraphy, and biostratigraphy, Pillans (1994) interpreted climatic changes over the last one million years

and established glaciation periods at approximately 10-70 ka (Otiran Glaciation), 135-200 ka (Waimean Glaciation), 250-265 ka (Waimaungan Glaciation), and 330-365 ka. Pillans et al. (1993) concluded that the interval 13-23 ka represents the period of greatest environmental change in the North Island and therefore can be regarded as the Last Glacial Maximum in this region (during which glaciation was of limited extent compared with the South Island). McGlone and Topping (1973, 1977, 1983) used pollen profiles from sediments in the Tongariro region to infer the Late Quaternary climate and vegetation history, and they determined that retreat of glaciers on the Tongariro complex began before 14 ka.

1.2.5 Vegetation

The nature of vegetation cover on Tongariro is of general interest, and has particular relevance in assessing the potential for charcoal preservation beneath lava flows - which can be used for ^{14}C dating of prehistoric flows (Section 3.4.2d). The first comprehensive botanical survey of the Tongariro area was carried out by Cockayne (1908), followed much later by an ecological survey and vegetation map presented by Atkinson (1981), and a popular guide by Gabites (1986). The lower slopes of Tongariro Volcanic Complex are dominated by tussockland-shrubland and some scrub on the western side, and by shrubland, kanuka-manuka scrub and mountain beech forest on the eastern side (Atkinson, 1981; Gabites, 1986). Podocarp forest of Hall's totara occurs on the north slopes below Ketatahi. Above about 1250 m (the normal tree line throughout much of the complex) the vegetation is restricted to sparse mosses, shrubs and tussock living amongst the rocky outcrops and scree (Atkinson, 1981).

Key factors influencing the distribution of vegetation on the Tongariro complex are altitude, poor soil drainage, the 1.8 ka Taupo ignimbrite (which overtopped Ngauruhoe and destroyed all vegetation on the complex), local andesitic eruptions (ash fall, lava flows, pyroclastic flows, lahars), erosion, and burning related to volcanic activity and fires lit by Maori and early European settlers. The two introduced plants which have caused the most concern about their rapid spread and ability to take over the natural vegetation are heather and the lodgepole pine. Introduced mammals, including the rat, stoat, rabbit, hare, possum,

pig, and deer, are also responsible for some of the damage to the natural vegetation. There are no large indigenous mammals on the complex, but there are many native species of birds and insects occupying the area.

McGlone and Topping (1973, 1977, 1983) found that the vegetation of the Tongariro region during the last 80 ka has ranged from dense podocarp-hardwood forest to sparse grassland-shrubland, reflecting changes in the equability of the climate. The present pattern of beech forest originated during the Last Glacial Maximum when forest was confined to small relict areas; the last 5000 years have seen significant expansion of beech forest (McGlone and Topping, 1977).

1.2.6 Geothermal features

Tongariro Volcanic Complex contains several small geothermal areas at Ketatahi Hot Springs, Te Mari Craters, Red Crater and Ngauruhoe. Most of these surface manifestations are believed to be fed by the same underlying vapour-dominated system (with an area of 15-20 km^2), formed from a combination of magmatic steam mixed with circulating meteoric water (Wilson, 1960; Moore and Brock, 1981; Hochstein, 1985). Equilibrium temperatures of 230-290°C have been inferred for the Tongariro geothermal system (Hochstein, 1985).

Ketatahi Springs (Fig 1.8), the major area of thermal activity on the Tongariro complex, are located on the northern slopes of North Crater (Fig 1.6), and the mineral-laden waters have long been respected for their medicinal powers by the local Maori people. Present at Ketatahi are fumaroles (some superheated up to 138°C), hot springs, mud pools and thermally altered ground with sulphur deposition covering an area of c.16 000 m^2 (Wilson, 1960; Moore and Brock, 1981). The hot springs discharge acid-sulphate waters (characterised by high concentrations of SO_4, B, Mg, NH_4, Ca; very low concentrations of Cl and F), and a maximum heat output has been estimated at 100-130 MW (Moore and Brock, 1981). Gregg (1960) found no evidence for major eruptions from Ketatahi, although a lahar was generated down the Mangatipua Stream in about 1895 (Fig 2.45).

Figure 1.8 Part of the Ketatahi Hot Springs on the north slopes of the Tongariro complex. View looking north toward North Crater.

The Red Crater activity, consisting of steaming ground (c.8000 m^2) with minor sulphur deposits, a few fumaroles (up to 95°C) and numerous steaming vents, contributes a total natural heat loss of c.20 MW (Hochstein, 1985). At Te Mari Craters, steaming ground (with minor sulphur deposits) covers an area of c.3000 m^2, which along with steam vents (up to 96°C) produces a natural heat loss of c.5 MW (Hochstein, 1985). Fumarole temperatures on Ngauruhoe had decreased to 78°C by April 1994, down from 90°C in 1993, after remaining stable at 94°C (boiling point for altitude) from 1986 to 1992 (Otway, 1994b).

1.2.7 Human history

The volcanoes of the Tongariro complex were *tapu* (sacred) to the Maori, who lived in settlements surrounding rather than on the mountains (Fig 1.9). To the local Maori of the Tuwharetoa tribe, the volcanoes are their *matua* (or parent of the land), the focus of their *mana* (influence, power), and recognised as their *tupuna* (or divine ancestors). The origin of many of the Maori place names on Tongariro, and some of the myths associated with the volcanoes are described in Section 1.3.1.

In order to maintain the *tapu* status of the mountains (providing protection especially from private *Pakeha* landowners), Te Heuheu Tukino IV (paramount chief of the Ngati Tuwharetoa; Fig 1.10) gifted the mountains of Tongariro, Ngauruhoe and Ruapehu to the people of New Zealand in 1887 in the form of a national park. The Tongariro National Park was the first in New Zealand and only the fourth in the world. The strength of the ties between the Te Heuheu line and Tongariro is demonstrated in the saying

> "Ko Tongariro te maunga; ko Taupo te moana; ko Ngati Tuwharetoa te iwi;
> ko Te Heuheu te tangata" (Tongariro is the mountain; Taupo the sea,
> Tuwharetoa the tribe; Te Heuheu the man).

Although they too were awestruck by the beauty and magnificence of the volcanoes, unlike the Maori the early *pakeha* did not hold them in such reverence. Accounts of some of the early European ascents of Tongariro and Ngauruhoe are detailed in Section 1.3.2. In

Figure 1.9 Motupoi Pa and Lake Rotoaira, looking across towards north slopes of the Tongariro complex. Print reproduced in Tongariro National Park 1:80 000 map (Infomap 272-04, Edition 4, Dept of Survey & Land Information, 1991) from Alexander Turnbull Library, Wellington.

Figure 1.10 Te Heuheu Tukino IV, chief of Ngati Tuwharetoa, photographed at Tokaanu in 1883. Print reproduced in Tongariro National Park 1:80 000 map (Infomap 272-04, Edition 4, Dept of Survey & Land Information, 1991) from National Museum, Wellington.

addition to general exploration, early (unsuccessful) attempts were made at sheep farming on the tussocklands on north Tongariro, but this endeavour was abandoned by 1900.

Not long after the establishment of the national park, tourism and recreation in the area quickly developed. The relative isolation of the central volcanic region was ended by the completion of the Desert Road (Figs 1.3 and 1.4) in 1894 and the main trunk railway line in 1908, and the building of accommodation facilities. Tramping, rock climbing and mountaineering are popular recreational activities in Tongariro National Park, and are catered for by a walking track system and huts on the mountain (Fig 1.5). The four park huts on the Tongariro complex (Mangatepopo, Ketatahi, Oturere, Waihohonu) each provide accommodation for 22-24 people, with additional camp sites available. The Department of Conservation (DOC) administers and maintains the park services from field centres in Whakapapa Village and nearby Turangi and Ohakune (Fig 1.3).

There are no ski fields on the Tongariro complex, so unlike Ruapehu where ski access roads extend to relatively high levels (c.1600 m above sea level), access roads to the start of walking tracks on Tongariro are more limited (Fig 1.5; Mangatepopo Road to 1120 m asl; Ketatahi access road to 760 m asl; Waihohonu track access from Desert Road at 960 m asl).

1.3 MAORI LEGENDS AND EARLY EUROPEAN ACCOUNTS

1.3.1 The Maori perspective: mountains of the gods

The Maori myths and legends explaining the central North Island volcanic activity were in many ways accurate foreshadowings of modern scientific interpretations. In particular, the Maori understood that a relationship existed between the alignment of volcanoes which we now term the Taupo Volcanic Zone. An early handbook for Tongariro National Park (Cowan, 1927) contains a detailed account of Maori history and legends of the region. Traditions of the local Maori are also described in Gregg (1960), Department

of Lands and Survey (1981), and Potton (1987). Two of the most enduring myths are related below from the above sources.

In earlier times, the Maori believed there to be a greater assemblage of mountains situated south of Lake Taupo than presently exists. Along with Mount Tongariro, Mount Taranaki stood to the south where the Tama Lakes now lie, and Mounts Tauhara and Edgecumbe (Putauaki) stood to the northeast in the area now occupied by Lake Rotoaira. All these mountains were gods and warriors, and all vied for the love of the beautiful Mount Pihanga to the north. In a fierce battle, Tongariro emerged victorious and became the proud husband of Pihanga. The defeated mountains departed in separate directions; Taranaki travelled fast and angrily westwards to his present location, Tauhara and Putauaki travelled to the north. In those days mountains were required to complete their journeys in one night, and so it came about that, whereas Putauaki travelled far to the north, the sad and lingering Tauhara only made it to the northeastern shore of Lake Taupo before the rising sun froze him in place.

During his exploration of the central North Island, the great *tohunga* (or priest) Ngatoro-i-rangi decided to climb Ngauruhoe and claim the surrounding land for his tribe, the Ngati Tuwharetoa. Upon reaching the summit in a snowstorm, Ngatoro-i-rangi called in desperation to his sisters in Hawaiki,

> "Ka riro au i te tonga! Haria mai he ahi moku!" (I am borne away by the cold south wind! Send fire to warm me!).

It was from words in this prayer - *"tonga"* (south wind) and *"riro"* (carried away) - that the name Tongariro was derived. Ngatoro-i-rangi's sisters responded by sending fire by way of an underground passage to White Island, Rotorua, Taupo and finally to Ngauruhoe, whereby Ngatoro-i-rangi was saved. Not so fortunate was his slave, *Auruhoe* (the volcano's namesake), who was thrown into the fiery crater to appease the volcano god Ruaimoko. This was the Maori explanation for the creation of the line of volcanoes through the North Island (the Taupo Volcanic Zone).

Other Maori place names on the Tongariro complex have their origins in local incidents or customs. For example, *Pukekaikiore* translates as the hill (puke) where rats (kiore) were eaten (kai) - in this case the "rats" were members of Ngati Hotu, defeated by Ngati Tuwharetoa. The *Te Mari Craters* were named after the chieftainess, Te Maari, who

died soon after a major eruption from the upper crater in 1868. Blue Lake was originally called *Te wai-whakaata-o-Te Rangihiroa* (Rangihiroa's mirror) in honour of Chief Te Rangihiroa who is said to have explored the Tongariro volcanoes in about 1750. The full name for the Tama Lakes is *Nga Puna a Tama* (the springs of Tama), named after Chief Tamatea who explored the area six centuries ago. *Ketatahi* means "one basket" - the Maori sometimes cooked a basket of food in the hot springs. Many of the other names refer to landscape features or vegetation (*manga*=stream, *puna*=spring, *roto*=lake, *wai*=water, *puke*=hill), e.g. *Makahikatoa* (stream of the manuka shrub); *Pukeonake* (evenly sloping hill); *Waihohonu* (deep river), *Rotopounamu* (greenstone lake) - the original name for Emerald Lakes.

1.3.2 Early European attitudes: would-be conquerors and scientists

The early European visitors to Tongariro showed little understanding or respect for the sacredness invested in the volcanoes by the Maori, and directed much of their energies towards outwitting the local Maori guardians of the *tapu* mountains. Gregg (1960) gave a good summary of all known previous observers, including a table listing early ascents of Ngauruhoe. The first pakeha to ascend Ngauruhoe was John Bidwill in 1839, who observed an ash eruption en route and was suitably impressed with the steaming crater to call it "the most terrible abyss I have ever looked into or imagined" (Hill, 1891; Cowan, 1927). When confronted with the angry Tuwharetoa chief upon his return, however, Bidwill only laughed and informed him that if the mountain was an *atua* (spirit) then he, Bidwill, must be a greater atua because he had got to the top of it.

Twelve years later in 1851 a second European, Henry Dyson, managed to evade the Maori and explore Ngauruhoe. The first specifically geological observations of the volcanoes were made by Hochstetter (1867), who prepared the first geological map of the area, despite not being able to actually climb onto the volcanoes! In defiance of Maori opposition, the first government survey of Tongariro and Ngauruhoe was carried out in 1882-1883, although it was later necessary to abandon the trig station set up on Ngauruhoe because the volcano was in a constant state of tremor (Cowan, 1927). These and many other subsequent visitors provided the first recorded descriptions of Ngauruhoe crater morphology, enabling the progressive changes in the number and dimensions of the summit

craters to be established. In addition, the early eruption narratives laid the foundation for later scientific work concerned with assessing the historical eruptive history. Some of these initial geological reports are described in Section 1.6.

1.4 REGIONAL TECTONIC AND GEOLOGIC SETTING

1.4.1 North Island plate boundary

The present convergence of the Pacific and Australian Plates in the New Zealand region has produced an active oceanic (Kermadec Arc - Havre Trough) and continental (Taupo Volcanic Zone - Hikurangi Trough) arc system characterised by a complex volcano-tectonic structure (Fig 1.1). Dramatic changes in volcanism occur at the sharp and relatively linear transition between oceanic crust, where (mostly submerged) mafic volcanoes prevail, and continental crust, where the Taupo Volcanic Zone (TVZ) is dominated by explosive rhyolitic volcanism (Gamble et al., 1993b, 1995). The plate tectonic setting is a convergent plate boundary involving a detached continental fragment rather than a true mainland continental margin such as South America.

The slightly oblique subduction beneath the North Island occurs at a rate of about 50 mm per year (Walcott, 1978). Westwards from the Hikurangi trough, the dip of the Benioff zone steepens considerably (as summarised by Cole, 1990) from 3-5° at depths of 0-25 km, increasing to 20-30° between 25 and 80 km, and changing to about 50° to a maximum depth of 250 km. A c.150 km wide accretionary prism is developed above the low-angle portion of the Benioff zone. Above the moderately dipping part there occurs a rapidly uplifting frontal ridge of Mesozoic meta-greywacke cut by the North Island Shear Belt (Fig 1.1). The volcanoes of TVZ occur about 80 km above the surface of the subducting slab (where the angle of subduction increases to c.50°), and the gap between the trench and TVZ covers a total distance of about 280 km.

1.4.2 Volcanic history and structure of Taupo Volcanic Zone

The Taupo Volcanic Zone, a NW-SE trending zone of late Pliocene to Quaternary volcanism and geothermal activity, is the surface expression of the westward subduction of the Pacific Plate beneath the North Island. The zone is approximately 300 km long and up to 60 km wide (Fig 1.2), the boundaries being defined by vent locations and caldera structural boundaries in a recent review by Wilson et al. (1995). TVZ is one of the most frequently active and productive systems in the world (Houghton et al., 1995), and is also characterised by anomalously high heat flow (4200±500 MW; Bibby et al., 1995), pervasive extensional tectonism (crust thinned to c.15 km), and high levels of crustal seismicity. Although a sub-volcanic basement has yet to be recognised, Wilson et al (1995) suggested that TVZ has erupted bulk volumes of 15-20 000 km^3 of volcanic material.

The onset of andesitic volcanism at c.2.0 Ma in TVZ was joined by (volumetrically dominant) rhyolitic caldera activity from c.1.6 Ma onwards (Houghton et al., 1995). Minor basaltic activity in TVZ is associated with tuff rings/scoria cones and fall deposits in the central TVZ, and as a subordinate component of the andesitic composite volcanoes (Wilson et al., 1995). Likewise, dacitic eruptions in TVZ are relatively rare and are mostly associated with dome complexes, andesite-dacite composite volcanoes, and fall/ignimbrite deposits from rhyolitic calderas (Wilson et al., 1995). Three stages in the evolution of TVZ have been identified by Wilson at al. (1995) (and refer to Fig 1.2):

1. *Old TVZ (2.0 to 0.34 Ma)*: Inception of the zone at c.2 Ma with andesitic activity at Hauhungaroa (2.0 Ma), Titiraupenga (1.85 Ma), Pureora (undated), Rolles Peak (0.71 Ma), Manawahe (0.43 Ma), Rotokawa (>0.34 Ma), Hauhungatahi (>0.34 Ma), and possibly Tongariro, Ruapehu and White Island. Caldera volcanoes active during this time were Kapenga and Mangakino.

2. *Young TVZ (0.34 Ma to 65 ka)*: Centres active during and after the Whakamaru-group eruptions (0.31-0.34 Ma) included the other caldera volcanoes Rotorua, Okataina, Kapenga, Reporoa, and Maroa. Composite cones active during this period were Maungakatote (<0.32 Ma), Tongariro (>0.34 Ma), Puhipuhi (0.23-0.28 Ma), Ruapehu (>0.22 Ma), Kakaramea (≥0.22 Ma), Tihia (undated), Tauhara (0.19 Ma),

Maungaongaonga (0.18 Ma), Maungakakaramea (undated), Pihanga (≥0.13 Ma), White Island (>65 ka), and Whale Island (>65 ka).

3. *Modern TVZ (<65 ka)*: The current active zone is represented by activity during and since the Rotoiti eruption (Okataina, c.0.065 Ma) and includes the rhyolitic centres of Okataina and Taupo (and to a lesser extent Rotorua, Kapenga, Maroa), and the composite volcanoes of White Island, Edgecumbe (1.8-5.5 ka), Tongariro, and Ruapehu.

A unifying and internally consistent overall model for the structure and evolution of TVZ has yet to be developed. Wilson et al. (1995) reviewed the three main models advocated by various authors (Fig 1.11), noting their disadvantages in explaining the features of TVZ. Major limitations arise from the lack of accurate age data, inadequate surface exposures, and the need for more detailed geological studies (Wilson et al., 1995). The models are summarised below.

1. *Migrating andesite arc model (Fig 1.11A).* TVZ is thought to represent part of the evolution of an arc which has been migrating SE across the North Island for the last c.20 Ma, accompanied by asymmetric crustal spreading. This model is particularly favoured by geophysical workers (e.g. Stern, 1986, 1987; Smith et al., 1989). But use of a more comprehensive age data base and consideration of all the geological evidence were factors cited by Wilson et al. (1995) which instead point to a distinct break between the NNW-SSE oriented Coromandel and Northland systems and the NE-SW oriented TVZ structure.

2. *Andesite-dacite arc plus rhyolite-basalt back-arc basin model (Fig 1.11B).* Cole (1979a, 1984, 1990) is the main proponent of this model which divides TVZ into an eastern arc marked by a line of andesite-dacite volcanoes, and a western marginal basin dominated by rhyolitic volcanism but with minor amounts of high-Al basalt. However, Wilson et al. (1995) point out that the andesite-dacite eruption products are not confined to the east and occur throughout TVZ, vents for basaltic and andesite/dacite activity overlap in time and space, and that there is evidence for interaction between rhyolite and andesite magmas in the proposed back-arc region.

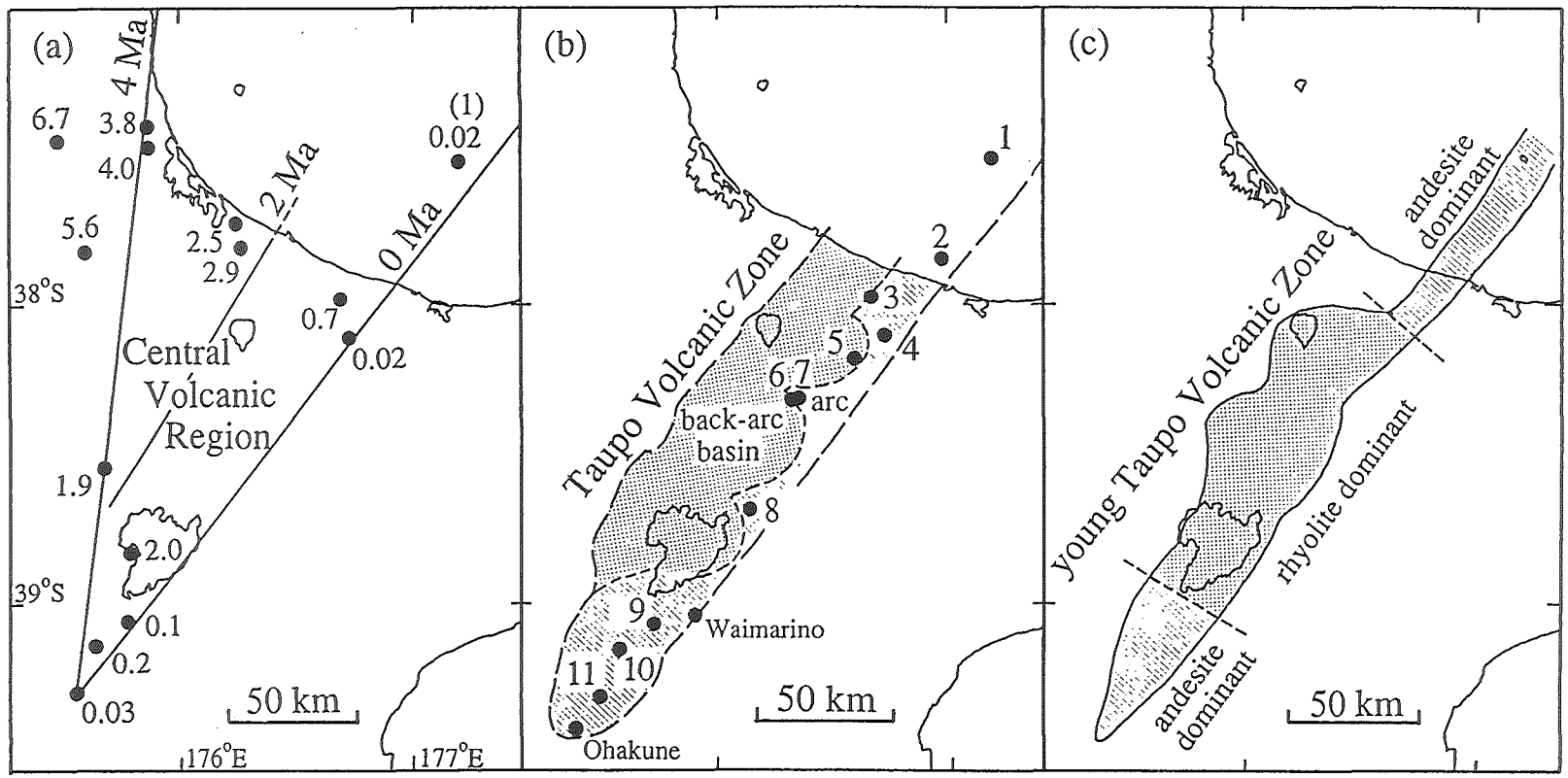

Figure 1.11 Maps showing the differing geometries of three models/summaries of the late Pliocene to Quaternary volcanism in the central North Island. From Wilson et al. (1995).

(a) The Central Volcanic Region (CVR) model of Stern (e.g. 1987). Points marked are K-Ar ages used by Stern to define the envelope of the CVR and derive time lines for the onset of andesitic volcanism.

(b) The TVZ model of Cole (e.g. 1990). Points marked are those centres used by Cole to define the 'arc'; 1 = White Island, 2 = Whale Island, 3 = Manawahe, 4 = Edgecumbe, 5 = Puhipuhi, 6 = Maungaongaonga, 7 = Maungakakaramea, 8 = Tauhara, 9 = Pihanga, 10 = Tongariro, 11 = Ruapehu.

(c) The segmented structure of young TVZ as noted by Healy (1962) and Wilson et al. (1984).

3. *Segmented TVZ model (Fig 1.11C).* Although not an explanatory model as such, Wilson et al. (1995) emphasize the pronounced segmentation of TVZ, first noted by Healy (1962) and subsequently remarked on by Wilson et al. (1984), Hackett and Houghton (1986), and Houghton et al. (1995). The NE and SW segments of TVZ comprise andesite-dacite composite volcanoes and no rhyolitic calderas; the central segment is dominated by a much higher geothermal heat flux and at least 8 rhyolitic centres (Fig 1.2) from which 34 caldera-forming eruptions have taken place (Wilson et al., 1995). The significance of this striking geographical division of TVZ into three segments has not been explained, but should be an essential component of any model for TVZ structure and evolution.

1.4.3 Pre-volcanic basement of Tongariro Volcanic Centre

The Tongariro Volcanic Complex is part of the concentration of andesitic material erupted in the southern segment of TVZ (Section 1.2.1). The general geology of the non-volcanic basement rocks has been mapped and described by Grindley (1960), Gregg (1960), and Beetham and Watters (1985). Because Tongariro magmas must ascend through these crustal rocks, attention has been focused on identifying the most likely contaminants of the magmas (e.g. Graham, 1987; Graham and Hackett, 1987).

Outcropping around the Tongariro Volcanic Centre are Mesozoic greywacke of both the Torlesse and Waipapa terranes, and Tertiary marine sediments (Fig 1.3). To the east of the ring plain and the Tongariro River, the Kaimanawa Ranges rise to above 1500 m and are composed of Torlesse sandstone and argillite, metamorphosed to very low grades (pumpellyite-actinolite) and containing abundant quartz veins (Beetham and Watters, 1985). The Waipapa sandstone and associated lithologies outcrop NW of Tongariro Volcanic Centre, and are less strongly metamorphosed (prehnite-pumpellyite) and quartz veined than their Torlesse counterpart (Beetham and Watters, 1985). To the south the Mesozoic basement is unconformably overlain by Early Pliocene marine sediments (Fleming and Steiner, 1951; Grindley, 1960), and to the NW Oligocene marine sediments overlie the Waipapa terrane (Gregg, 1960). There is no geophysical or geological evidence for an underlying ancient granite-gneiss terrane (Graham and Hackett, 1987).

1.4.4 Geophysical evidence beneath Tongariro Volcanic Centre

A tentative structural model has been developed for beneath Tongariro Volcanic Centre, based on a combination of two timed explosions (in Ruapehu Crater Lake and Lower Tama Lake), arrivals from eruption earthquakes at Ruapehu, and long-range crustal refraction studies (Latter, 1981). Sub-horizontal Tertiary marine sediments are inferred to underlie the volcanoes at about sea level, below which is a c.650 m thick layer of possible weathered greywacke, underlain (c.3 km beneath the volcanoes) by material considered to represent schistose greywacke (Latter, 1981). The base of the crust is thought to be at about 15 km beneath TVZ.

Using the location of zones of anomalously high S-wave attenuation to identify magma bodies, Latter (1981) found there to be at least three principal magma reservoirs beneath Ruapehu (2-9 km deep), and one beneath Ngauruhoe (3 km deep). The location of shallow (c.1 km) volcanic earthquakes and volcanic tremor has also been used at different times to infer possible magmatic intrusions beneath Ngauruhoe-Red Crater (Latter et al., 1990), Pukeonake (Latter et al., 1987), and North Crater (Latter at al., 1987).

1.4.5 Holocene faulting at Tongariro Volcanic Centre

NNE-trending normal faults (usually dipping towards the eruptive centres) cut across the Tongariro Volcanic Centre (Gregg, 1957b, 1960; Grindley, 1960; Mathews, 1967; Cole, 1990; Latter et al., 1990), in a trend paralleling that for TVZ overall. The vents of these volcanoes are also generally aligned NE-SW, and the faulting is believed to reflect magmatic intrusion into shallow crustal reservoirs (Cole, 1990). A relatively continuous fault or faults cross the Tongariro complex from Tama Lakes to North Crater. Mapping fault traces was not a part of this study, but work in progress by I.A. Nairn (pers. comm., 1995) involves identification of faults in detail and assessment of their relative ages and displacements.

1.5 VOLCANIC HAZARDS

This section provides an overview of the volcanic hazards present at Tongariro, based on the work of GNS scientists and others. Assessment and management of volcanic hazards in Tongariro National Park have centred on Ruapehu Crater Lake (Houghton et al., 1987; Latter, 1989; Montgomery and Keys, 1993), particularly the hazard posed by lahars (Otway et al., 1995), and the findings from these studies have been put to the test (and passed!) during the 1995-1996 eruption from Ruapehu. Without an active crater lake, volcanic hazards on the Tongariro Volcanic Complex are not quite the same as those on Ruapehu, but are similar in other respects.

1.5.1 Volcanic hazards present on Tongariro Volcanic Complex

An understanding of past eruptive styles and the history of volcanic activity is essential for identifying potential hazards and formulating management plans. Unlike Ruapehu, little is presently known of the lahar-producing eruptions which have contributed to the ring plain surrounding the Tongariro complex. Similarly, more studies are required before the hazard from major sector collapse or explosive dome disruption can be assessed.

However, eruptions in 1954-55 and 1974-75 have demonstrated the relatively localised and slight hazard posed by lava flows and pyroclastic avalanches respectively. Lacking ski fields like Ruapehu, the absence of settlements and installations in the probable flow paths on the volcanoes of the Tongariro complex means that these forms of volcanic activity only pose any threat if they extend well onto the ring plain. Ashfall from a substantial eruption is a more significant hazard which has the potential to affect much of the North Island, but would mostly be at the nuisance level only, unless a larger subplinian eruption occurred (documented in the tephrostratigraphy of the ring plain; Section 2.3.2e).

Latter (1989) presented a hazard map for Tongariro National Park in which he identified 3 km radius zones around Ngauruhoe, Red Crater and Te Mari Craters within which ballistic blocks, pyroclastic avalanches and base surges would pose a hazard in large eruptions. The map showed that pyroclastic avalanches from Ngauruhoe would most likely

be directed down Mangatepopo Valley and Waihohonu Valley, and those from Te Mari Craters to the N and NE. By selecting representative airfall deposits from studied subplinian eruptions, Latter (1989) was able to indicate zones (reaching up to 15 km from the source crater) which would receive over 50 cm of ash. The principle direction of tephra deposition is to the east. Latter (1989) also indicated that minor lahars or contamination of water courses were possible down the Mangatipua Stream from Ketatahi, and in several directions from Blue Lake crater.

1.5.2 Monitoring of volcanoes of the Tongariro complex

Surveillance of the Tongariro complex, principally Ngauruhoe, is carried out by scientists from the Institute of Geological and Nuclear Sciences at the Wairakei Research Centre. Background monitoring at present consists of periodic checks of various eruption parameters (Latter, 1986; Hurst, 1986), but there would be a significant upscaling in deployment of monitoring equipment and personnel in the event of renewed activity.

(a) **Seismic monitoring.** Volcanic seismicity is constantly recorded by a network of six permanent seismometers in the region (the Tongariro Volcano-Seismic Network): Maungaku (MGZ) NW of the complex; Ketatahi (KAV) on the north slopes of the complex; SW of Ngauruhoe (NGZ); the Chateau (CNZ) in Whakapapa Village; the Dome Shelter (DRZ) on Ruapehu; and Tukino (TUV) on the east slopes of Ruapehu. The seismic signals are telemetered to a central recording facility at Whakapapa Village, and the data are then transmitted to Wairakei and subjected to an automatic analysis system (EARSS) developed by New Zealand scientists. This way the background seismic pattern can be established and understood, and volcanic tremor and volcanic earthquakes can be identified.

Volcano-seismicity activity at Ngauruhoe has remained low since its last eruption in 1974-75, reflecting the continuing lack of volcanic activity at the cone (Sherburn, 1994, 1995). As the NGZ seismograph was only installed in 1976, it has not been possible to establish the relationship between volcanic earthquakes and eruptions, so progress in developing prediction models for Ngauruhoe has been limited (Hurst, 1986).

(b) **Deformation monitoring.** Geodetic measurements used to assess volcanic deformation at the Tongariro complex have been taken since 1978 (Otway, 1986), when three tilt-levelling patterns were established to monitor Ngauruhoe, Red Crater and Te Mari Crater. Tilt-levelling surveys are conducted every year or so, and to date have not indicated any significant tilt that might indicate magmatic intrusion (Otway, 1987, 1994b, 1995).

In 1983 a pattern to monitor horizontal deformation (ideally) annually was introduced, comprising six stations on the northern rim of Ngauruhoe crater which are fixed by electronic distance measurement (EDM) and theodolite angles from a base station near Tongariro trig (Otway, 1986). Surveys have not been conducted every year since 1983, but the half dozen or so surveys that have been carried out show no evidence for volcanic deformation (Otway, 1986, 1994a, 1995).

(c) **Fumarole and lake temperatures and chemistry.** Regular sampling of volcanic gases from fumaroles at the summit crater of Ngauruhoe allows their temperature and chemical composition to be monitored; a continuing decline in volcanic activity is indicated (Section 1.2.6). There are no hot crater lakes on the Tongariro complex, but temperatures and chemistry of Blue Lake, the Emerald Lakes and the Tama Lakes are checked periodically for any indications of thermal inflows or volcanic gas inputs (Christenson and Crump, 1994). The Ketatahi Hot Springs and Soda Springs are also monitored.

1.6 PREVIOUS WORK

An extensive literature dating back to last century exists for observations and later scientific studies of Tongariro Volcanic Complex. Modern detailed studies are somewhat more limited, particularly those taking the approach of this thesis. Near the beginning of most of the following chapters there is a section reviewing previous work on that specific aspect of Tongariro geology/petrology. This section therefore chiefly serves as an introduction to and overview of the literature, which is discussed in more detail in the

relevant chapters. In addition, a brief summary of work on other TVZ composite volcanoes and current models for andesite petrogenesis in TVZ are described.

1.6.1 Early workers

Since the time when Europeans first gained access to the volcanoes of the Tongariro complex in the mid nineteenth century (Section 1.3.2), there have been published accounts of the eruptions, crater morphology and general landscape features. These early, often lively and entertaining, reports were chronicled by Gregg (1960) and those of note are mentioned below.

Hochstetter (1867) provided some of the first geological observations of the central North Island volcanoes, and remarked upon the complicated volcanic system represented by the group of cones making up Tongariro. Thomas (1888, 1889) presented the first petrographic descriptions and partial chemical analyses of Tongariro rocks ("augite-andesites"), and gave the first comprehensive account of the geology of Tongariro and Ngauruhoe, including illustrations and a map of the summit area. Thomas (1889) named features such as North Crater, South Crater, Red Crater, and Blue Lake. More detailed topographic maps were published by the district surveyor, Cussen (1891), who also pointed out the NE-SW vent alignment. Some of these early observers were a little to eager to attribute the status of "crater" to any basin on the summit - hence South Crater (Thomas, 1889), Central Crater, West Crater (both Cussen, 1891), and Oturere Crater (Speight, 1908) - all of which are not considered to be of explosive origin (Section 1.2.2).

1.6.2 Eruption observations

Hill (1891, 1894) directed his attention to more volcanological observations, including an inspection of the products of the 1892 eruption of Upper Te Mari Crater -in which he no doubt inspired future generations of women geologists by conceding that even "the ladies could ascend the mountain...without much difficulty". Friedlaender (1898) provided a vivid account of a later eruption at Te Mari, and further emphasised the multiple cone nature of Tongariro.

Eruptions from the other active cone in historical times, Ngauruhoe, were the subject of many published descriptions (Sections 2.3.1a, 2.3.2b,d), e.g. Hector (1870), Johnston (1909), Cullen (1926), Grange (1928), Allen (1948, 1949), Battey (1949), Cloud (1951), Gregg (1956, 1957a), Nairn (1976), Nairn et al. (1976), Nairn and Self (1978). Summaries of the historic eruption record of Ngauruhoe are contained in Gregg (1960) and Cole and Nairn (1975) (Section 3.4.3). Marshall (1909) gave a very useful summary and comparison of past observations of Ngauruhoe crater morphology, as well as his own description and photographs, and accounts such as these (and e.g. Turner, 1911; Grange, 1928; White, 1929; Allen, 1948) have allowed a reconstruction of the development of the Ngauruhoe crater system over the last 150 years or so (e.g. Gregg, 1960; Section 3.4.8k).

1.6.3 Early mapping and geological surveys

The first systematic geological survey of the Tongariro National Park was carried out by Speight (1908), who discussed the geological history as well as the features of the present volcanic craters, but insisted on a catastrophic explosion as the means by which the summit of Tongariro was destroyed (as did others, e.g. Thomson, 1926; Grange and Hurst, 1929). There is no geological evidence for a large scale explosive removal of material from a single Tongariro cone; instead each cone-building sequence of the Tongariro Volcanic Complex was successively eroded (by glacial, fluvial and mass wasting processes), an option not considered by many early observers.

Grange and co-workers (1929, 1930, 1933) from the New Zealand Geological Survey (NZGS) conducted the first detailed geological and volcanological research of the National Park volcanoes, culminating in the publication of NZGS Bulletin No. 40 (Gregg, 1960). Grindley (1960) also mapped Tongariro as part of his 1:250 000 map of the Taupo region, although only going as far as differentiating the young cones and flows of Ngauruhoe, Te Mari Craters and Red Crater from Tongariro in general.

1.6.4 Modern studies

More recent work on Tongariro Volcanic Complex has involved assessment of the age and evolution of the complex (Sections 3.2.1, 3.3.1) and the tephrostratigraphy and tephrochronology of the ring plain material (Section 3.4.1). Various studies have also focused on particular aspects of the volcanic geology (see Chapter 2): welded spatter deposits of Blue Lake and North Crater (Healy, 1963; Mathews, 1967); Oturere Valley vent complexes (Mathews, 1967); vulcanian-style eruptions and pyroclastic avalanche deposits of Ngauruhoe (Nairn, 1976; Nairn and Self, 1978); Pukeonake scoria cone (Napp, 1983); Pukekaikiore and Mangatepopo Valley (Patterson and Graham; 1988); and the Tama Lakes area (Wahyudin, 1993).

Despite only being able to spend a week in the field, a visiting Canadian geologist (Mathews, 1967) provided some very useful new insights into the older structure and history of Tongariro. He recognised that the older Tongariro was composed of several separate cones, now eroded, and that there was no justification for invoking explosion or caldera subsidence to explain the present-day form (cf. previous workers). Mathews (1967) was also the first to describe vent breccias and steeply dipping lavas at Tongariro Trig and Oturere Valley (NE and SW walls).

The petrography (Section 4.2) and geochemistry (Section 6.2 and 7.2) of Tongariro lavas has principally been studied by Ewart and co-workers (1965, 1968, 1971, 1977), Clark (1960a,b), Cole (1978, 1979b, 1981, 1982), Cole et al. (1983), and Graham and co-workers (1985a, 1987, 1992, 1995). A discussion of the previous work on xenoliths found in Tongariro lavas is contained in Section 5.2. Publications on other aspects of Tongariro have already been noted: evidence for glaciation (Section 1.2.4); geothermal features (Section 1.2.6); pre-volcanic basement (Section 1.4.3); geophysical studies (Section 1.4.4); and faulting (Section 1.4.5).

In conclusion, the previous work on Tongariro Volcanic Complex had established a broad framework for study with regards the general geology, post-glacial volcanic history and petrology, but without significant age constraints and little was known in detail of the earlier evolution of the complex. Petrological studies had concentrated on the young eruptives, and few petrological samples were tied in to the volcanic stratigraphy. Some

areas of the complex, e.g. Oturere Valley and Waihohonu Valley, had only been visited infrequently (or not at all) by publishing geologists. Therefore the opportunity existed for the present study to develop a more detailed eruptive and magmatic history for the Tongariro complex, with petrological modelling incorporating time-space-volume relationships.

1.6.5 Other TVZ composite volcanoes

Within TVZ, andesite(-dacite) composite volcanoes are concentrated in the southern and northern regions (Section 1.4.2). However, within the central TVZ andesite also occurs as smaller volume cones or dome complexes (e.g. Titiraupenga, Pureora, Rolles Peak, Tauhara), buried edifices or discrete lava flows intersected in geothermal drillholes (e.g. Rotokawa), rare ignimbrites (e.g. in Mangakino area), and as end-member mixing compositions within silicic eruptives. These occurrences are summarised and presented in map form by Wilson et al. (1995), the petrogenesis of some of them is discussed by Graham et al. (1995).

The setting of the Tongariro complex (Fig 1.3) has already been described (Section 1.2.1). The other smaller cones that make up the Tongariro centre (Section 1.2.1) have not been mapped and sampled in the detail applied to Ruapehu and Tongariro, but have been included in general discussions which draw mostly on Ruapehu and Tongariro data (e.g. Graham et al., 1995).

The other large composite volcano situated south of Lake Taupo is, of course, Ruapehu volcano (Fig 1.3). This has been the subject of comprehensive study from both volcanological and petrological perspectives. Two PhD theses covered the geology (Hackett, 1985) and petrology (Hackett, 1985; Graham, 1985a) in some detail, although as no new age data were obtained it was difficult for these studies to reach firm conclusions regarding eruptive history and magmatic trends with time. However, from the detailed physical volcanology observations a division into four distinctive associations of lithofacies was possible (Hackett and Houghton, 1989; Section 2.4). From the petrological studies, a classification dividing Ruapehu lavas into six types was established (Graham and Hackett, 1987; Section 4.2), and the crustal contamination of Ruapehu lavas was highlighted -

including a detailed investigation of the xenoliths contained within the lavas (Section 5.2). It should be noted that some young eruptives from Tongariro Volcanic Complex (Ngauruhoe, Red Crater, Pukeonake, Pukekaikiore) were also included in these Ruapehu studies.

The andesite-dacite composite volcanoes occurring in and around the Bay of Plenty (Fig 1.2) have been studied in varying detail. The recent eruptive history of the largest and most active volcano, White Island, is well known (e.g. Houghton and Nairn, 1991; Graham and Cole, 1991), but the older portions of the complex are only just becoming more fully understood by work currently in progress. The nearby eroded volcanic remnant of Whale Island is also benefitting from recent study (Burt et al., 1996). On the mainland there is the Edgecumbe andesite-dacite dome complex (Duncan, 1970; Nairn and Wood, 1987), and the eroded cone of Manawahe (Broughton, 1988).

Although not part of TVZ, the basalt-andesite Taranaki Volcano to the west (Fig 1.1) is another young, large arc-related volcano in the North Island which warrants a mention in this discussion. The volcanic history and petrology has been described (Neall et al., 1986; Downey et al., 1994), comparisons made with basalts and andesites of TVZ (Price et al., 1992), and a recent crystal size distribution study has investigated magma residence times (Higgins, 1996).

1.6.6 Models for andesite petrogenesis in TVZ

Studies concerning andesite petrogenesis in TVZ are reviewed in more detail in Section 6.2 and 7.2. It is generally agreed that TVZ andesites were formed by similar processes to many other continental arc lavas around the world, i.e. differentiation of mantle-derived basaltic magmas. Clarification of the differentiation processes, specifically assimilation fractional crystallization (AFC), has been the focus of many studies (Cole, 1978; Cole et al., 1986; Graham and Hackett, 1987; Graham and Cole, 1991; Graham et al., 1995). Additional petrogenetic processes such as crystal accumulation and magma mixing have been invoked to explain some of the lava types identified by Graham and Hackett (1987), Patterson and Graham (1988), Graham and Worthington (1988), and Cole and Graham (1989).

One difficulty with this established approach of investigating TVZ petrogenesis is that often the geological (including chronological) context is ignored, thus impeding a fuller understanding of the magmatic evolution of individual volcanoes and TVZ as a whole (Wilson et al., 1995). Grouping TVZ eruptives by rock type (basalt, andesite, dacite, rhyolite) when assessing petrogenesis (e.g. Graham et al., 1995) gives rise to the problem of ages and locations being ignored in favour of broad overall petrogenetic models which may not be geologically feasible or realistic. As additional more detailed petrological studies are completed for individual volcanoes in TVZ (e.g. Taupo, Sutton et al., 1995), a more comprehensive and viable model for TVZ petrogenesis should emerge.

1.7 THESIS ORGANISATION

This study is chiefly concerned with integrating volcanological and geochronological information with petrological data, in order to develop petrogenetic models constrained in both time and space. To this end, the volcano-stratigraphic framework provides the basic structure for many chapters. The thesis is presented in two volumes; Volume 1 contains the eight chapters and references of the thesis, and Volume 2 contains the 15 appendices and the map.

Following on from Chapter 1: Introduction, the volcanological observations made during field mapping and sampling are described in Chapter 2: Products and styles of Tongariro volcanism, organised by type of volcanic product and eruptive style. The volcano-stratigraphic units are then defined and described in Chapter 3: Volcanic stratigraphy and eruptive history, with reference to the map (contained in back pocket of Volume 2) and new K-Ar age determinations. The chapter concludes with a discussion and summary of Tongariro's eruptive history.

The petrography of each volcano-stratigraphic unit and the overall mineralogy are then presented in Chapter 4: Petrography and mineralogy, which also contains sections dealing with crystallization conditions, evidence for magma mixing, and petrographic-stratigraphic trends. This is followed by Chapter 5: Xenoliths, an essentially petrographic

survey (but with limited chemical analyses) of the feldspathic and quartzose xenoliths present in many Tongariro lavas. Implications for crustal contamination processes are discussed.

The presentation, discussion and interpretation of chemical data is divided into two chapters. Chapter 6: Magma compositions of volcano-stratigraphic units: characterisation and relationships is concerned with the total data set of XRF analyses from the Tongariro complex, and discusses the chemical compositions and relationships between volcano-stratigraphic units. A model illustrating the magmatic history of the complex, linking in with the eruptive history established in Chapter 3, is presented. The subset of Tongariro samples for which more precise chemical and isotopic data are available is described in Chapter 7: Petrogenetic processes and time-space relationships: magma batches at Tongariro, which features an examination of magmatic stratigraphies on a variety of time scales for Ngauruhoe, other young eruptive units, NE Oturere, and Tama 2.

Chapter 8: Discussion and conclusions summarises the volcanological framework established from this study, and brings together and discusses the evidence for the various petrogenetic processes operating at a range of scales at Tongariro. The major findings of the study are highlighted, and the implications for our understanding of magma batch dynamics and the time-space relationships of composite volcano magmatic systems are considered.

Volume 2 contains Appendices 1-15 - a comprehensive data base and reference for general sample information, petrographic and mineralogical data, geochemical data, and full descriptions of analytical procedures. Each appendix is introduced and referred to in the appropriate chapters. The folded thesis map, Tongariro Volcanic Complex: Map of volcano-stratigraphic units, 1:25 000 is held in the back pocket of Volume 2.

Chapter 2

Products and Styles of Tongariro Volcanism

CHAPTER 2
PRODUCTS AND STYLES OF TONGARIRO VOLCANISM

2.1 INTRODUCTION

Eruptions of subduction-related cone volcanoes encompass virtually the complete spectrum of volcanic styles and any one composite volcano can exhibit a wide variety of primary volcanic products (e.g. Hackett and Houghton, 1989; Hildreth and Drake, 1992; Matthews et al., 1994). The Tongariro Volcanic Complex is no exception; eruptive styles range from quiet lava flow extrusion to mildly explosive strombolian fire-fountaining to powerful and violent vulcanian and plinian eruptions. These styles of activity represent volcanic hazards of varying degrees of severity (Section 1.5).

The volcanic products encountered during fieldwork (along with any relevant published descriptions) are summarised in this chapter. It is not intended as a detailed physical volcanology study, but rather serves to document the diversity of products present and volcanic processes operating at the Tongariro complex. This information is relevant to discussions of eruptive rates and patterns of cone growth (Chapter 3), and is also helpful in assessing the relative influence of such factors as conduit diameter, and magma composition, viscosity, yield strength, and gas content in determining eruptive style.

Although a broad spectrum of volcanic products can be erupted from a composite volcano, they often have contrasting distribution patterns on or around the volcano. In one of the most thorough facies models produced for a composite volcano, Hackett and Houghton (1989) highlighted the differential preservation of the products of Ruapehu volcano in the proximal and distal environments, neither of which preserve a complete

record of volcanism. Preserved primary products of explosive eruptions are generally confined to the distal ring plain, as accelerated erosion removes much of the pyroclastic material from the proximal cone. The cone itself is thus dominated by lava flows, and few products of effusive phases of activity reach the distal ring plain. This partitioning of eruptive products between proximal and distal localities is also a feature of the Tongariro complex, and therefore it is difficult to assess the contribution of effusive relative to explosive activity to the growth of the volcanic complex. Although lava flows are the most volumetrically important constituent of the cone, the significant deposits of volcaniclastic material preserved on the ring plain and the fact that historic eruptions have been overwhelmingly explosive in nature (over 60 tephra eruptions but only 3 lava flow-producing eruptions since 1839; Cole and Nairn, 1975) suggests that explosive eruptions have probably been of equal importance to effusive volcanism.

The eruptive products sampled from proximal Tongariro Volcanic Complex range almost continuously in composition from 53.0 to 64.2 wt% SiO_2 (hydrous data; anhydrous data are plotted in Fig 2.1) and are dominated by medium to light grey andesites, accompanied by minor dark grey basaltic andesites and light grey dacites (Fig 2.2). A broad correlation between magma composition and eruptive style is evident on the proximal cone; the basaltic andesites are predominantly erupted from scoria cones as strombolian falls or aa lava flows (e.g. Ngauruhoe, Red Crater, Pukeonake, Young SW Oturere), and at the other end of the spectrum, the dacites occur as either flow-banded, platey-jointed, thick lavas/coulees (e.g. SW Oturere) or pumiceous plinian ejecta (e.g. Tama Lakes). Many lavas are weakly to moderately vesicular and most are moderately to strongly porphyritic, whereas scoria is often aphyric (Section 4.3.1).

The products of Tongariro volcanism are described and illustrated in the next section, roughly in order of increasing explosivity, followed by a summary of the eruptive styles represented by these volcanic products. The chapter finishes with a comparison of the eruptive nature of the Tongariro complex with that documented for the neighbouring Ruapehu volcano.

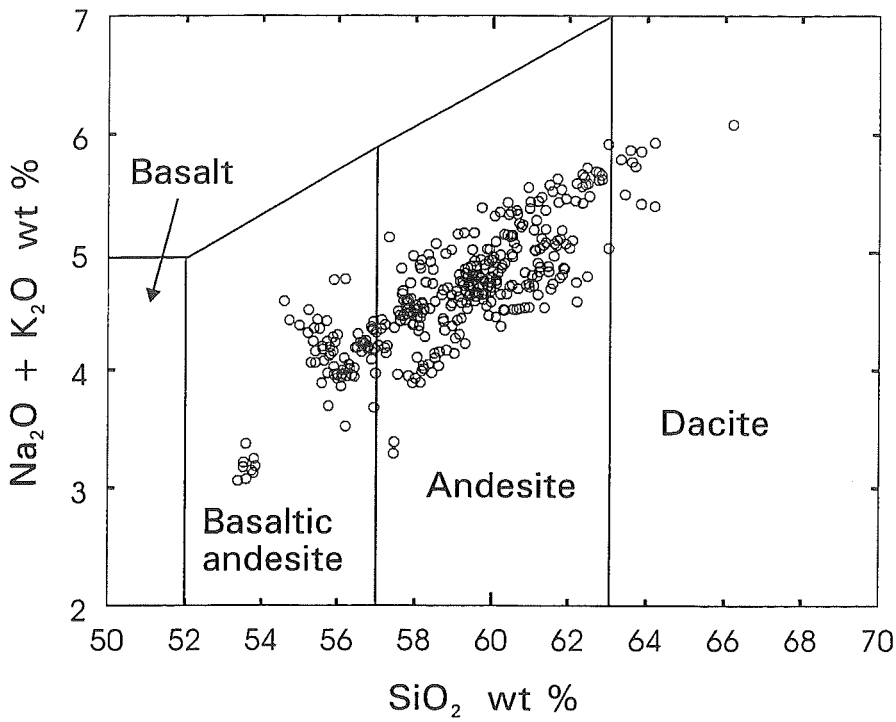

Figure 2.1 Tongariro analyses (n=370) plotted on a total alkali-silica (TAS) diagram (after Le Bas et al., 1986). Analyses recalculated anhydrous.

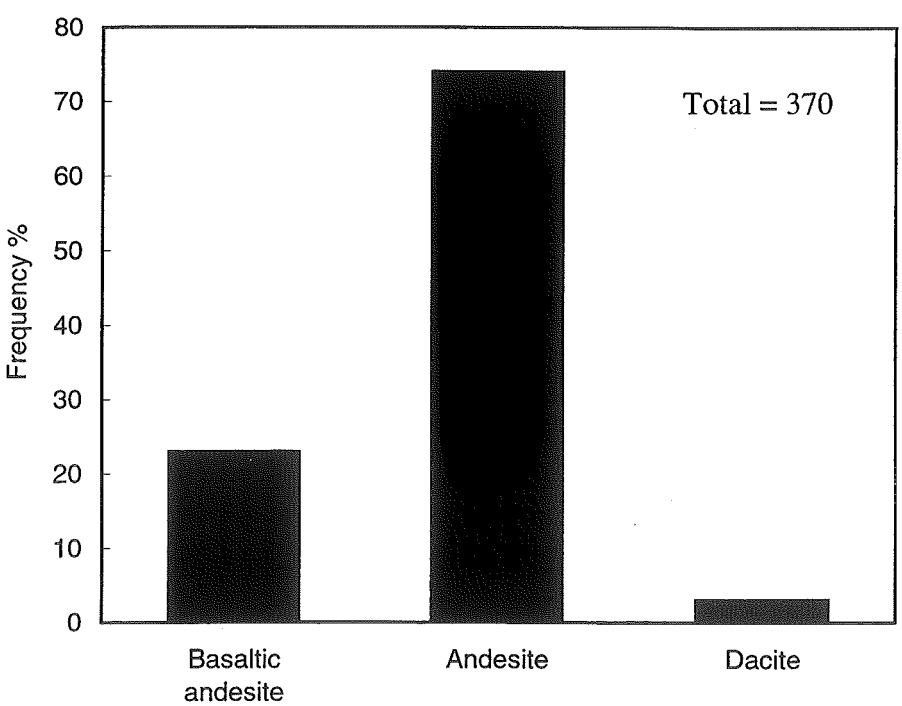

Figure 2.2 Relative proportions of basaltic andesite, andesite and dacite analysed from the Tongariro complex (based on TAS classification, Le Bas et al, 1986).

2.2 PRODUCTS OF TONGARIRO VOLCANISM

2.2.1 Lava flows, domes and dikes

Extrusion of numerous basaltic andesite to andesite block and rarely aa lava flows has been the principal means of cone construction for the Tongariro Volcanic Complex, and these are evident as young channel/valley-filling flows and older bluff- or cliff-forming outcrops everywhere around the complex. Lava domes are seldom seen, and exposures of dikes are likewise very rare. One solidified lava lake can be recognised in North Crater.

(a) **Lava flows.** On the Tongariro complex, young post-glacial flows with morphologic expression and good exposure can be classified as aa or block or transitional aa-block type whereas the older, less well-exposed flows are best described in terms of jointing type since the flow type cannot always be confidently determined.

Young pahoehoe flows

A minority of the young flows can be described as aa transitional to pahoehoe type, but the presence of some breccia in most of these flows precludes their classification as true pahoehoe flows. The thin, highly fluid post-1.8 ka basaltic andesite flows from Red Crater (e.g. Fig 2.3) are approaching pahoehoe morphology. Several of the thin basaltic andesite flows sampled on the upper slopes of Ngauruhoe are also transitional to pahoehoe flow type (e.g. TG500, TG507).

Young aa and block flows

Most Ngauruhoe flows (especially the basaltic andesites) are good examples of channel-confined aa (grading into block) lava flows comprising rubbly vesicular, scoriaceous flow tops and margins, and massive sheet interiors (Fig 2.4). The classic caterpillar-track motion of blocks collapsing off the slowly advancing flow front and being over-ridden and captured as a basal breccia layer was observed in the 1949 (Battey, 1949) and 1954 (Gregg, 1956) aa lava flows. Cross-sections through some pre-historic flows show significant development of a basal breccia and thin or absent upper breccia, suggesting

Figure 2.3 Thin (<1 m) Red Crater basaltic andesite aa lava flow, Central Crater (TG126).

Figure 2.4 Ngauruhoe basaltic andesite prehistoric aa lava flow, upper east Waihohonu Valley (TG181). Massive sheet lava (1-3 m thick) is surrounded by 0.5-1 m of scoriaceous rubbly breccia.

Figure 2.5 Ngauruhoe basaltic andesite prehistoric aa-block lava flow containing marginal levées and a central drained channel, Mangatepopo Valley (TG020).

that autobrecciation in its own right (rather than just entrainment of flow front breccia) was probably occurring at the base of these flows. The time taken for each of the historic lava flows (all from Ngauruhoe) to form was typically 1-2 days, with observed flows advancing at rates of up to c.300 metres per hour (Gregg, 1956). The entire 1954 eruption sequence of at least 10 lava flows was produced over a period of 4 months (Gregg, 1956).

The young flows display many features of classic aa to block flow morphology. Many flows have broad, expanded, steep lobate flow fronts which have spread out on the gentler slopes of the valley floor (e.g. Fig 3.27). These flow fronts are often thickened and bulbous, caused by cooling of the flow fronts and drainage of the relatively hot central parts of the flow (Stasiuk et al., 1993; Pinkerton and Wilson, 1994), leaving central depressions or channels and elevated marginal levées (Fig 2.5). These levées are thus a function of lava draining from the centre of the flow, and are not a constructional feature above the height of the flow surface. Some flows have multiple levées or a central ridge, such as observed during formation of Ngauruhoe flows in 1949 (Battey, 1949) and 1954 (Gregg, 1956), indicating flowage in multiple channels. Pressure ridges are developed in some Red Crater (Fig 2.6) and Ngauruhoe flows. These elongate ridges, which are perpendicular to flow direction in the central parts of the flow but sub-parallel at flow margins, probably form due to upward pressure from the molten lava flowing beneath the surface crust.

Youthful aa flow surfaces are a feature of the Ngauruhoe and Red Crater lava flows. A chaotic jumble of dm- to m-scale blocks (up to 4 m) with massive interiors and vesicular, rough exteriors characterises the surface of most flows (Figs 2.5 and 2.7). Some blocks are thermally stressed and shatter readily. Rounded accretionary lava balls up to 2 m in diameter were observed in several flows. A transition from aa to more block-type flow morphology is often observed from proximal to distal portions of the flow. The classic scoriaceous to clinkery aa flow surfaces (Fig 2.7) can change downflow to more blocky, undulating flow surfaces with relief of several metres and incorporating high aspect spires of lava (Fig 2.8). This transition reflects increased lava viscosity and yield strength downstream as a result of decreased gas content and temperature, and increased crystallinity (Lipman and Banks, 1987). Some of the older pre-historic Ngauruhoe flows have lost these youthful morphologies and have smoothed, more subdued relief and often vegetated flow

Figure 2.6 Part of the large Red Crater andesitic aa-block lava flow, Oturere Valley. Note pressure ridges.

Figure 2.7 Steep flow front of 30 June 1954 Ngauruhoe basaltic andesite aa lava flow, Mangatepopo Valley (TG023-025). Flow is 3-5 m thick (note person at right for scale).

Figure 2.8 Spinose flow surface of Ngauruhoe basaltic andesite prehistoric aa-block lava flow, Mangatepopo Valley (TG014).

surfaces. It is interesting to note, however, that even the 1954 lava flows have been colonised by small alpine mosses, herbs and shrubs. Many of the flows, of all ages, exhibit red high-temperature surface oxidation.

Lengths of young flows

Flow lengths of the young aa to block flows range from 0.5 to 7 km. Most of the narrow, channel-confined Ngauruhoe flows are at least 1.5 km long and have travelled down the steep slopes of the cone and beyond onto the valley floors (Figs 3.27 and 3.28), with several flows extending up to 5 km away into Makahikatoa and Waihohonu Valleys (Fig 3.30A). Several moderately-sized flows, 3-4 km long and 0.3-1.2 km wide (Fig 3.21), have been extruded from both the upper and lower Te Mari Craters.

The Red Crater flows tend to be shorter (0.5-1.5 km long; Fig 3.26), with the exception of the very long (7 km) and impressively thick (up to c.100 m) flow which fills the 1-1.5 km wide Oturere Valley (Figs 2.6 and 3.25). This flow is one of the pre-1.8 ka andesite flows which displays pressure ridges and a spinose surface, in contrast to the more fluid post-1.8 ka basaltic andesite flows from Red Crater. It is therefore interesting that the most far-travelled Red Crater flow is of the more viscous andesite; making it likely that a particularly high and constant effusion rate combined with restriction of flow width as it was channelled down the valley were the primary factors responsible for the enhanced flow length (cf. Walker, 1973; Pinkerton and Wilson, 1994). Conversely, lower and more variable effusion rates, marginal cooling and accidental breaching probably limit flow lengths elsewhere on the complex (cf. Pinkerton and Wilson, 1994). The shorter post-1.8 ka Red Crater basaltic andesite flows may have been spatter-fed and thereby partially air-cooled, limiting flow distance. Further field investigation of the largest Red Crater flow is required to determine whether a single flow progressed at this total thickness from initiation and subsequently lengthened down the valley, or whether it is a composite of several flows erupted within a short time period.

Magma composition does not appear to exert a particularly strong control on flow lengths. There is no obvious correlation between SiO_2 content and distance travelled for the younger lava flows of the Tongariro complex. In fact, there are several relatively silicic, far-travelled flows which strongly contradict the expected relationship. The obvious example is the largest Red Crater flow (discussed above), but also two of the most silicic Ngauruhoe

flows (TG205-206, 58.0-58.3 wt% SiO_2) flowed the furthest off the cone - almost 3 km into the Waihohonu Valley. The andesitic (59.9 wt% SiO_2) Te Mari Craters lavas also flowed some considerable distance (4 km) down the north flanks of the Tongariro complex. Conversely, many of the most basic lavas on the complex, such as some of the Red Crater post-1.8 ka basaltic andesites (53.0-53.7 wt% SiO_2), managed to travel only 500 m from their vent. The probable alternative factors to magma composition which control flow length were suggested above.

Aspect ratios of young flows

Most of the andesite (and basaltic andesite) flows have the high aspect ratios characteristic of composite volcano lavas. Flow thicknesses of young flows from Ngauruhoe and Red Crater are typically 3-5 m (Fig 2.7), but range up to about 10 m thick (excluding the unusually thick Red Crater flow discussed above). Much less common are the thin, widespread flows such as the one which flowed into Central Crater from Red Crater (1 m thick, 400 m wide; Fig 2.3). This basaltic andesite aa flow is one of the most primitive compositions from the Tongariro complex and thus illustrates the influence of chemical composition on lava viscosity when compared to the higher aspect ratio andesite flows. Factors other than viscosity can control flow width and thickness, however, as demonstrated by the Red Crater flow which flowed steeply down towards South Crater but stopped before reaching the crater floor (Fig 2.9), despite being of very similar composition to the flow in Central Crater. A lower effusion rate may have limited the extent of this flow.

Effects of topography on young flow morphology

Very steep surface slopes, like those encountered by the 1870 Ngauruhoe lavas as they descended over old lava bluffs, cause the flow to become incoherent and break up into loose blocks and scree at the steep flow front (Fig 3.28). The proximal portions of most Ngauruhoe flows are buried by scree on the steep slopes of the upper cone, giving them a somewhat rootless appearance. Lava flows of the 1954 eruption sequence were often observed in their initial stages overtopping the crater rim and flowing progressively further down the cone (Gregg, 1956), confirming that they did originate as flows from the crater rather than spatter remobilised further down the cone.

Figure 2.9 Steeply dipping, dark grey Red Crater basaltic andesite aa lava flow (TG127; centre right) which failed to reach the floor of South Crater.

Figure 2.10 Oxidised, autobrecciated base of andesite lava flow, SW Oturere Valley (TG178). Sheet lava overlies autobreccia of sub-angular clasts in fine matrix.

In addition to steepness of slopes, the pre-existing topography can affect flow morphology by acting as a barrier which forces a change in flow direction or divergence of multiple flow lobes around the obstacle. An excellent example of this phenomenon is the Ngauruhoe flow of 18 August 1954 which piled up to a thickness of about 15 m against the Pukekaikiore saddle, before being diverted around the southern end of the saddle, giving a decided kink near the end of the flow (Figs 2.47 and 3.27). Other 1954 Ngauruhoe flows contain small elongate windows into the underlying surface (Fig 3.27) caused by temporary branching out of flow lobes around higher relief of older lava flows.

Older lava flows

Older pre-glacial block lavas of the Tongariro complex have apparent thicknesses of 2-30 m, with an average thickness of about 9 m. Exposures of these older lava flows often provide good cross-sections though the thick (up to 2 m) autobrecciated margins and massive sheet interiors typical of andesitic flows (e.g. Fig 2.10). The autobreccia is typically best developed at the base of the flow, and comprises variably welded, angular to sub-rounded cm-dm clasts in a sparse to abundant oxidised interstitial matrix (Fig 2.10). Hackett and Houghton (1989) documented progressive changes in the character and proportion of autobreccia in Ruapehu lavas, with distance from vent. A similar transition is evident with Tongariro lavas; proximal exposures display only incipient brecciation (Fig 2.11) which increases in proportion to sheet lava and becomes less welded, more matrix-rich (Fig 2.10), and the clasts more rounded, in medial to distal localities. Exposures containing irregular zones of autobreccia carving up through the massive lava at steep angles from the brecciated base demonstrate the brittle-state process of autobrecciation whereby widening cracks propagate inwards into the moving flow and angular clasts are created as blocks crack and rotate; these clasts are ground into more rounded shapes and the proportion of finer-grained matrix increases with flow distance.

The non-brecciated interiors of these andesitic flows usually display one or more type of jointing pattern. Angular to rounded, sub-columnar to blocky joints on a metre-scale are most common (Figs 2.11-2.12). True columnar jointing is only really well-developed in the basal lavas of Pukekaikiore (Fig 2.13) and the older pre-existing lava in Red Crater. Many lavas exhibit intensive, cm-dm scale, sub-horizontal platey jointing (Fig 2.14), often in association with stretched vesicles and flow banding or foliation (Fig 2.15) which

Figure 2.11 Andesite lava flow containing angular blocky joints and incipient autobrecciation, Lower Te Mari Crater (TG346).

Figure 2.12 Andesite lava flow displaying sub-rounded blocky jointing, east of Te Mari Craters (TG347).

Figure 2.13 Sub-columnar jointing developed in andesite lava of Pukekaikiore (TG265).

Figure 2.14 Well-developed platey jointing on a cm-dm scale in andesite lava flow (TG178), upper east Waihohonu Valley.

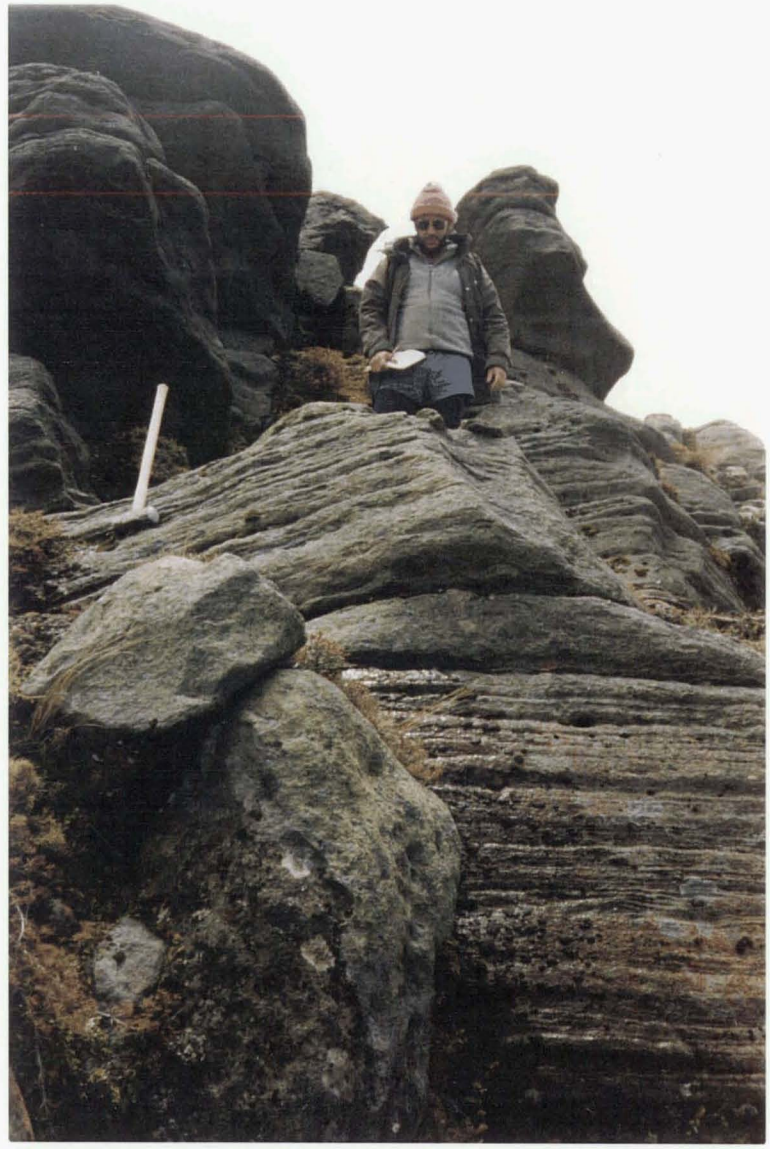

Figure 2.15 Flow-banded andesite lava flow (TG063), SW Oturere Valley.

reflect the sheared flow interior formed during laminar flow. Dacitic lavas are consistently platey-jointed and intensely flow-banded, often displaying flow folds, typical of these more viscous compositions. Field measurements of flow banding in over 50 lavas of the Tongariro complex have provided information on flow directions and steepness of the slopes down which they flowed (see also Section 3.2.2). Most of these older flows have dips of less than 30°; tectonically over-steepened dips of up to 80° often occur in old vent complexes. Platey jointing often occurs in conjunction with blocky jointing within one flow unit; the platey-jointed portion (often in the centre) reflecting the faster laminar flow of the hot flow interior

(b) **Domes.** The only convincing dome-like structure so far observed on the Tongariro complex is a small dome of silicic andesite in the Tama Lakes area (Fig 2.16). The approximate dome dimensions are an area of 250x250 m and a height of about 100 m. It may be that dome-building has been a more significant activity during development of the complex, but because domes are frequently related to and destroyed by explosive eruptions we do not often see them preserved on the cone (cf. Hackett and Houghton, 1989). Fragments of domes may be present in pyroclastic fall or sector collapse deposits on the ring plain.

Elsewhere on the complex, overthickened (up to 100 m thick) ponded lava flows approximate to a coulée/dome-like appearance with massive distorted columnar-slabby jointing fanning out and peeling off from the outcrop in an onion-skin type manner (e.g. Pukekaikiore, Fig 2.17; SW Oturere Valley, Fig 2.18). These andesitic flows are not silicic (and therefore viscous) enough, however, to be regarded as true domes or coulées.

(c) **Rheomorphic welded tuff.** Welded fall tuffs which are remobilised during post-depositional flowage are formed by the process of rheomorphism (Wolff and Wright, 1981; Cas and Wright, 1988). These rheomorphic tuffs and agglutinates are a response to rapid accumulation rate and associated intense welding of spatter deposited on a moderate slope.

Some of the welded tuffs and agglutinates present around North Crater, Blue Lake and Tongariro Trig are rheomorphic (see also Section 2.2.2a). They are characterised by

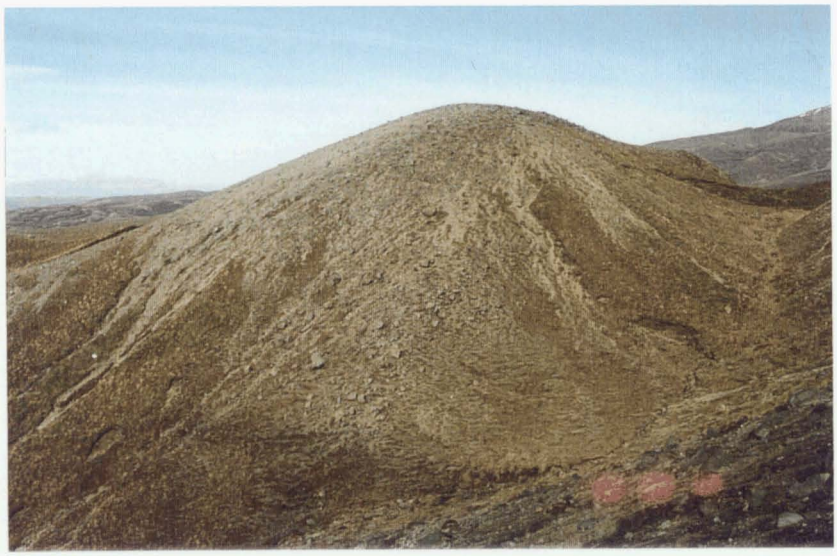

Figure 2.16 Silicic andesite dome, Tama Lakes (TG028). Photo courtesy of I.A. Nairn, GNS Wairakei.

Figure 2.17 Distorted columnar-slabby jointing in overthickened, ponded andesite lava, east side of Pukekaikiore (TG159). Photo courtesy of I.A. Nairn, GNS Wairakei.

Figure 2.18 (a) Up to 50 m thick, ponded-type, silicic andesite lava (TG228) contrasts with (b) thinner (4-10 m) overlying andesite flows (TG229-231), upper SW Oturere Valley.

a linear fabric caused by intense flattening and shearing out of lenticular clasts, and by an autobrecciated base and top (indicating they have indeed flowed). This fabric could sometimes be confused with flow banding in a lava flow, but there is usually subtle evidence for a pyroclastic origin: occasional lens-shaped flattened bombs may be distinguished; flattened blebs are too sharply terminated to be flow banding; the presence of rigid, unflattened lithic clasts; and the deposit is typically thinner (<0.5 m) than a lava flow.

(d) **Lava lake.** The 1 km-wide, flat-topped North Crater (Fig 1.6) represents a solidified lava lake associated with hawaiian-strombolian style fire-fountaining activity. Massive, columnar-jointed andesite of the lava lake is exposed to a depth of approximately 40 m within a 300 m-wide explosion pit (Fig 2.19), which mars the otherwise impressively flat surface of the North Crater cone. The relatively slow cooling in a ponded body of lava is accompanied by contraction leading to the development of vertical to sub-vertical joints perpendicular to the cooling surfaces - hence the moderately well developed columnar jointing present in the North Crater lava lake.

(e) **Dikes.** Despite quite detailed field coverage of the Tongariro complex, dikes are very seldom encountered. This lack of dikes is possibly partly a function of insufficient erosion of the older portion of the complex. The most obvious example of a dike is beautifully preserved within Red Crater (Fig 2.20); the lava has drained away to leave a 2-6 m-thick cavity or lava tube between the 1-2 m-thick quenched basaltic andesite walls of the dike.

Rare dikes have been observed in the SW Oturere Valley wall. A 1-2 m thick dark grey-black basaltic andesite dike intrudes welded tuffs (which exhibit heat effects at the dike margins) and appears to be related to the young SW Oturere ridge-capping black scoria deposit (I.A. Nairn, pers. comm., 1995). A more ambiguous candidate for an older dike occurs further down Oturere Valley in a part of the SW valley wall exhibiting orange-white hydrothermal alteration and steeply dipping lava flows (Fig 2.21). The possible dike is a 10-15 m thick vertical exposure of dm-scale columnar-jointed massive lava (Fig 2.21). Dike margins are not clearly delineated, but the occurrence of a dike-like intrusive body is in keeping with what appears to be an old vent area.

Figure 2.19 Massive, columnar-jointed andesite lava (TG196) of the North Crater lava lake, exposed in explosion pit.

Figure 2.20 Evacuated dike (TG342) exposed in south crater wall of basaltic andesite Red Crater scoria cone. Dike width is 3-8 m. Photo courtesy of I.A.Nairn, GNS Wairakei.

Figure 2.21 Dike-like vertical intrusive body (TG171) associated with hydrothermally-altered orange-white breccias and steeply dipping lava flows in old vent area in upper SW Oturere Valley.

2.2.2 Pyroclastic fall deposits

Material explosively ejected from a vent can accumulate as a pyroclastic fall deposit by fall from a high eruption column or by ballistic trajectory. The characteristics of the deposit vary depending on the kind of eruption, changes in eruptive style during the course of the eruptive phase, and distance from source. On Tongariro Volcanic Complex, pyroclastic fall deposits form minor to locally significant outcrops on the cone (welded spatter deposits, scoria cones, ballistic blocks), where their preservation chiefly depends on welding or burial by lava flows. Non-welded fall material is rare in the cone-forming sequences due to rapid erosion and re-working, but is of course an important constituent of the ring plain (medial-distal fall tephra deposits).

(a) **Welded spatter fall deposits.** Lava spatter cones built up around North Crater (Fig 1.6) and Blue Lake crater (Fig 1.6) during hawaiian-strombolian style fire-fountaining eruptions provide excellent outcrops (especially on crater rims) of near-vent or vent, variably welded, basaltic andesite to andesite spatter fall deposits. These welded "tuff breccias" or "agglomerates" were recognised by early workers (Healy, 1963; Mathews, 1967). Similar deposits are preserved in some of the older parts of the Tongariro complex such as around Tongariro Trig and upper NE Oturere Valley.

The hot, relatively fluid lava spatter has accumulated at varying rates around the vents to form layers (each layer generally <1-2 m thick) of welded tuff and agglutinate which mantle topography, and occasionally contain vertical cooling joints (Fig 2.22). Deposits often comprise a regular alternation of moderately-welded lapilli-bomb zones and sheet-like intensely welded agglutinate (Figs 2.23 and 2.24). Initial flattening of clasts occurs upon impact and is enhanced by post-depositional compaction and welding. Welding together of these hot spatter clasts is principally a function of accumulation rate (and therefore discharge rate); rapid accumulation increases the loading and compaction of underlying material, causing clasts to deform plastically and sinter together. The alternation in welding intensity exhibited by many spatter fall deposits can thus be correlated with rhythmic pulses of more or less intense fire-fountaining, and hence accumulation.

Figure 2.22 Andesitic welded tuffs and agglutinates on north slopes of North Crater. Note vertical cooling joints in foreground.

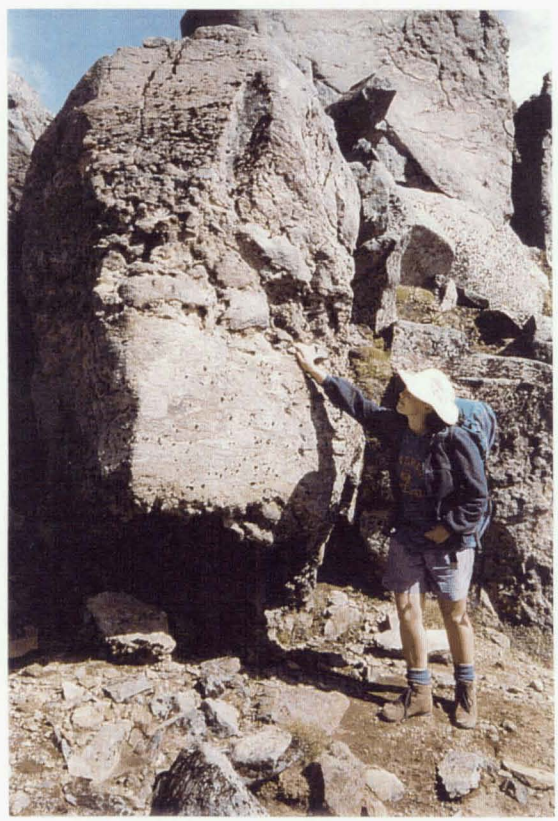

Figure 2.23 Variably welded, andesitic spatter fall deposit. Hand is placed on contact between lower zone of intensely-welded agglutinate and upper zone of moderately-welded tuff. Tongariro Trig (TG331).

Figure 2.24 Andesitic spatter fall deposits on southern rim of North Crater (TG195) with regular alternation of <1 m thick zones of moderately-welded lapilli-bombs and intensely-welded agglutinate.

Figure 2.25 Flattened and compacted lens-shaped bomb within intensely-welded andesitic agglutinate, North Crater (TG192).

Figure 2.26 Small (<5 cm) rigid lithic clasts within intensely-welded agglutinate, North Crater (TG195).

A pyroclastic origin is often not immediately obvious in the intensely-welded agglutinates, due to the extreme flattening of clasts into a linear fabric which resembles flow banding in a lava flow. Careful inspection usually reveals the occasional lens-shaped flattened bomb (Fig 2.25) or bombs plastically deformed over rigid lithic clasts (Fig 2.26). Further evidence for a pyroclastic derivation is provided when the welded agglutinate passes laterally into a non-welded fall deposit. An excellent example of this occurs on the western rim of Blue Lake crater where intensely-welded agglutinate grades laterally to moderately-welded scoria then to non-welded scoria fall over a distance of only 5-10 m. Very rapid lateral and vertical changes in welding are characteristic of the welded fall deposits on the Tongariro complex.

(b) **Scoria-tuff cones and medial-distal scoria fall deposits.** Basaltic andesite, coarse-grained scoria cones and sheets produced by strombolian-style eruptions occur with moderate frequency on the complex, generally interspersed with lava flow sequences. Several young scoria cones preserve primary cone morphology: the 1954 Ngauruhoe cone, Red Crater cone (Fig 3.24), and Pukeonake cone (Fig 3.13). The eruptions of Ngauruhoe in 1954 built up a sizeable spatter-scoria cone (basal diameter 200-300 m; height 50-60 m) in the summit crater. Exposures in the E-SE inner crater wall of the cone (Fig 2.27) reveal the following sequence (measured by I.A. Nairn and others): a c.20 m thick basal unit of poorly-bedded, black scoria bombs and blocks (with lithics) in an ash matrix; overlain by a c.8 m thick, yellow-light grey, densely-welded, blocky- to columnar-jointed scoria unit; overlain by c.25 m of well-bedded, red-black, scoria bomb-lapilli-ash beds (with lithics); and capped by c.10 m of red welded scoria from the 1974-75 eruption.

In Red Crater, dark red and black scoriaceous bombs and lapilli-ash are exposed in the crater walls and draping the crater rim and cone (Fig 2.28). The scoria overlies older light grey massive lavas. Exposures within the Pukeonake scoria cone reveal an alternation of dark grey to black, scoriaceous bomb and lapilli beds (bombs and blocks up to 1.5 m) with yellow-grey, well-sorted, bomb-bearing, lapilli-coarse ash beds (Topping, 1974; Napp, 1983; Hackett, 1985). Explosive activity at Pukeonake consisted of mild fire-fountaining eruptions with minor phreatomagmatic activity (Hackett, 1985).

Figure 2.27 Exposure through E-SE inner crater wall of Ngauruhoe 1954-55 scoria cone (see text for description of units). Total thickness is c.60 m. Uppermost c.10 m is red welded scoria from 1974-75 eruption.

Figure 2.28 Exposure through south wall of Red Crater scoria cone showing young red and black scoria and older light grey lava flow at right. Note evacuated dike in centre (cf. Figure 2.20).

Other young scoriaceous eruptive sequences on the Tongariro complex did not have the volume to build up a cone, or are preserved only as medial (to proximal) strombolian deposits, or may possibly represent proximal scoria from subplinian (rather than cone-building strombolian) eruptions (e.g. Hackett and Houghton, 1985). A small scoria mound and related lava flow occurs on the summit of Pukekaikiore (Fig 2.29). A tack- to moderately-welded scoria fall deposit in the Tama Lakes area consists of dm-sized cauliflower-breadcrusted bombs and minor wallrock lithics with relatively little fine matrix. The ridge along the upper SW Oturere Valley wall is topped by a relatively young scoria fall deposit which grades from black non- to tack-welded to moderately- to strongly-welded to bright red oxidised strongly-welded scoria from SE to NW, i.e. from distal to proximal localities. The c.15 m thick near-vent deposit is a coarsely-bedded, strongly-welded, highly oxidised slaggy bomb deposit (Fig 2.30). On the opposite side of Oturere Valley a different, laterally extensive, welded scoria fall deposit mantles the NE ridge with a relatively uniform thickness of 5-10 m (Fig 2.31). Rapid vertical transitions from moderately-welded scoria to intensely-welded agglutinate signify a pulsating eruption column and varying accumulation rates. The northern slopes of the complex are mantled by medial scoria fall deposits from North Crater and Blue Lake crater which vary from thin (<1 m), unconsolidated, non-welded lapilli to dm-m bomb deposits, to 2-6 m thick, massive to poorly-bedded, tack- to moderately-welded scoria units.

Scoria cones are also preserved within the older parts of the Tongariro complex, although their original forms are not always evident. An impressive scoria cone - tuff cone sequence over 40 m thick is present along the NE Oturere Valley wall (Fig 3.9). The sequence mantles autobrecciated lava flows and begins with a basal 4-6 m of cm-dm bedded, phreatomagmatic fine lapilli fall with angular blocks and intercalated fines-rich pyroclastic surge deposits (Fig 2.32A). This is overlain by 8-10 m of transitional strombolian-phreatomagmatic fall deposits with abundant fines and large angular and slabby blocks (Fig 2.32A). The scoria cone proper occupies the next 25+ m of the sequence and is well-bedded on a dm-scale, moderately-sorted, non- to moderately-welded up section, and comprises moderately- to highly-vesicular black basaltic andesite bombs, blocks and lapilli. Occasional lava flows are intercalated within the scoria sequence (Fig 2.32B). A spectacular angular unconformity between relatively flat-lying and steeply dipping scoria beds marks the transition from outer to inner wall environments, and rapid

Figure 2.29 Young andesitic scoria deposit (TG152-153) near summit of Pukekaikiore. Photo courtesy of I.A. Nairn, GNS Wairakei.

Figure 2.30 Oxidised, strongly-welded basaltic andesite scoria deposit, upper SW Oturere (TG165-166).

Figure 2.31 Variably-welded andesitic scoria fall deposit, NE Oturere Valley (TG262-263).

Figure 2.32 Portions of the NE Oturere Valley scoria cone. **A** - Hammer rests on contact between lava flow (TG119) and overlying phreatomagmatic lapilli-tuff and pyroclastic surge deposits, which grade up into transitional strombolian fall scoria deposits. **B** - Further up-sequence, black bomb and block beds of the scoria cone (TG242-244) contain intercalated dark grey-red autobrecciated lava flow (TG123) and thin light grey pyroclastic surge beds.

Figure 2.33 Scoriaceous tuff cone (TG340), Tongariro Trig. Lack of impact sag beneath large (c.80 cm) block implies lateral emplacement.

thinning from c.40 m to only a few metres thick over a short distance indicates proximity to vent. The main scoria cone sequence contains intercalated thin pyroclastic surge beds (Figs 2.32B and 2.43; Section 2.2.3f) and further up section there is a change to predominantly tuffaceous material. Large (<1 m) bombs in poorly-bedded ash grade up into more ash-rich bedded surge and co-surge fall deposits. This transition from dry strombolian to increasingly wet phreatomagmatic style suggests a multiple-vent eruption as it is uncommon for a vent environment to change from dry to wet during one eruption sequence.

Other older scoria-tuff cone deposits occur near Tongariro Trig and SW Oturere Valley. A thick (>30 m), dm-bedded, moderately-welded block and bomb-bearing tuff breccia sequence on the Tongariro Trig ridge comprises alternations of dark grey scoria in a pale grey ash matrix, with fines-rich, laminated, pale grey coarse ash-lapilli units (Fig 2.33). This deposit once again represents a tuff cone - scoria cone transition. A c.20 m thick scoria cone in upper SW Oturere Valley (TG240) lacks any tuff cone component and consists of dm-bedded, moderately- to strongly-welded, oxidised scoriaceous bombs and occasional angular lithic blocks.

(c) **Ballistic blocks.** Metre-sized ballistic blocks can be found near many of the young vents, including Ngauruhoe, Blue Lake, Te Mari Craters and North Crater. During the 1975 vulcanian eruption of Ngauruhoe, ballistic ejecta were thrown up to 2.8 km from the vent, with the largest blocks accumulating on Ngauruhoe summit in a deposit several metres thick (Nairn and Self, 1978). Ballistic blocks are mostly dense and massive, but may have slightly scoriaceous or breadcrusted surfaces (Fig 2.34), indicating expansion of a hot partially molten interior forming cracks on the cooled surface. Some blocks contain prismatic joints formed during cooling of the hot juvenile blocks, and jigsaw cracks formed due to impact shattering (Figs 2.35 and 2.36). Many of the Ngauruhoe blocks sit in still recognisable small impact depressions or pits, and ballistic blocks in general are often intensely shattered with fragments of the blocks found several metres away (Fig 2.36).

(d) **Medial-distal fall deposits.** Fine-grained, predominantly ash deposits are not commonly preserved on the cones as they tend to be thin, unconsolidated, and easily eroded or reworked. However, primary medial-distal fall from strombolian eruptions at Tongariro is sometimes preserved on top of relatively young but vegetated lava flows (e.g.

Figure 2.34 Breadcrusted-scoriaceous ballistic block, rim of Blue Lake crater.

Figure 2.35 Jigsaw cracks and prismatic cooling joints in ballistic block erupted during 1975 eruption of Ngauruhoe, Mangatepopo Valley.

Figure 2.36 Intensely shattered ballistic block displaying prismatic cooling joints, near Te Mari Craters. Photo courtesy of K.E. Cooper.

Figure 2.37 Pale cream Taupo pumice overlies red ash and black-brown andesitic lapilli-ash units in c.1 m thick tephra section preserved on top of Red Crater lava flow (T19/396 258), upper Oturere Valley.

Figure 2.38 Fall deposits exposed between upper Oturere and Waihohonu Valleys (T19/391 248).

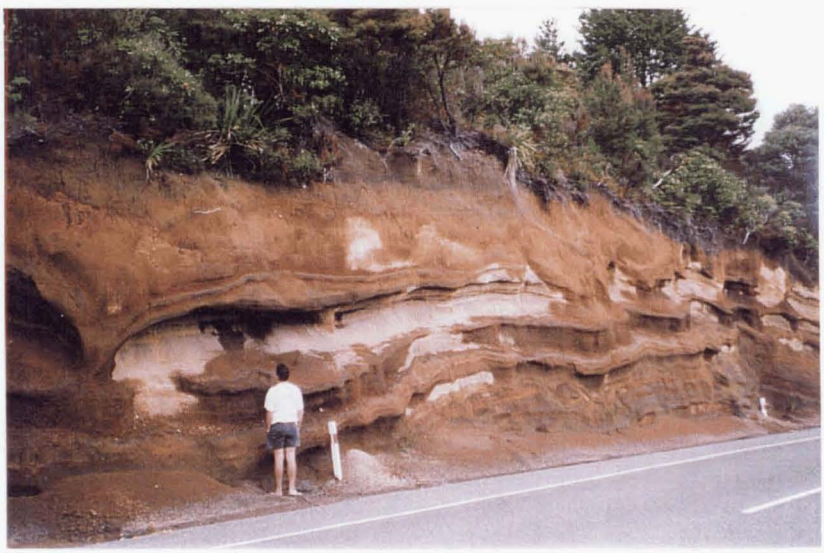

Figure 2.39 Thick sequence of mantle-bedded andesitic tephra on ring plain, exposed in road cutting on the Desert Road (approx T19/487 210), east of the Tongariro complex.

on Red Crater flows, Fig 2.37), or in small basins or valleys (e.g. between upper Oturere and Waihohonu Valleys, Fig 2.38). These deposits have not been examined in detail for the present study.

More significant deposits of primary distal fall from Tongariro subplinian-plinian eruptions are preserved on the surrounding ring plain in thick yellow-brown lapilli-ash sequences (Fig 2.39). The overall composition of the tephra is silicic andesite to dacite (Table 3.2; Donoghue, 1991). Two types of bed have been documented for the Holocene tephra deposits: dm-m thick massive or laminated ash with proximal lapilli beds; and dm-thick mantle and internally bedded lapilli beds (Hackett and Houghton, 1989). The prevailing westerly winds have influenced ash distribution around the cone so the thickest accumulations occur on the eastern side. The tephra sections contain distal material erupted from the Tongariro complex, but also from the neighbouring Ruapehu volcano and from the rhyolitic Taupo Volcanic Centre to the north. The tephra stratigraphy has been described by Topping (1973, 1974), Topping and Kohn (1973), Donoghue (1991), and Donoghue et al. (1995). Their work is summarised in Section 3.4.1 and Table 3.2.

2.2.3 Pyroclastic flows and surges

Explosive eruptions often produce dense mixtures of juvenile pyroclasts, lithics, magmatic volatiles, and external water which flow downslope under the influence of gravity. Termed pyroclastic or volcaniclastic density currents, these deposits can be divided into pyroclastic flows and pyroclastic surges - the high and low particle concentration end members, respectively (Sparks, 1976; Fisher and Schmincke, 1984; Cas and Wright, 1988; Carey, 1991). Such lateral emplacement of hot pyroclastic material has produced several small volume pyroclastic flow and surge deposits which are preserved on Tongariro Volcanic Complex.

Pyroclastic flow deposits are formed from hot, ground hugging flows which travel laterally as (sometimes partly fluidised) high particle concentration gas-solid dispersions. Pyroclastic flows may result from eruption column collapse or lava/dome collapse or lateral blast. The classification of pyroclastic flow deposits, based largely on vesicularity and chemistry of juvenile clasts, comprises three major subdivisions into block and ash flow,

scoria flow, and pumice flow (Wright et al., 1980; Cas and Wright, 1988; Smith and Roobol, 1982, 1990; Carey, 1991).

Pyroclastic surge deposits are formed from the lateral movement of pyroclasts as expanded, turbulent, low concentration gas-solid dispersions (Cas and Wright, 1988). A number of situations can generate a pyroclastic surge (phreatomagmatic and phreatic eruptions, pyroclastic flows, and pyroclastic falls), giving rise to at least three types of surge deposits: base, ground, and ash-cloud (Wright et al., 1980; Cas and Wright, 1988; Smith and Roobol, 1990; Carey, 1991).

(a) **1975 Ngauruhoe pyroclastic avalanche deposits.** The best example of a pyroclastic flow deposit on the Tongariro complex are the scoria flows or "pyroclastic avalanches" produced during the 1975 eruption of Ngauruhoe. Nairn and Self (1978) provide a detailed account of the 19 February 1975 pyroclastic eruption sequence and resulting deposits. Several pyroclastic avalanches were generated by partial collapse of the dense eruption columns and were funnelled into two main chutes down the northern flank of the cone - one of which is visible in Fig 2.40. The deposits comprise a sequence of overlapping, digitate tongues of dark grey basaltic andesite, with thin (1-1.5 m) lobate fronts (Figs 2.40 and 2.41). The surface of the deposit features conspicuous flow channels and marginal levées (Fig 2.42), indicating a high yield strength during the flow.

The deposit is coarse-grained and very poorly-sorted; fine ash and dense blocks and bombs are concentrated in the channels, whereas the levées and flow fronts are dominated by scoriaceous blocks up to 1 m in diameter (Fig 2.42). Bombs may have smooth, ropy surfaces or be vesiculated, breadcrusted or cauliflower-shaped. Dense, massive blocks lack any signs of plastic deformation, indicating that they were rigid when ejected. Some blocks have prismatic joints caused by stress release during cooling, showing that they were hot when ejected (temperatures of blocks in the deposit varied from >900°C to cold, Nairn and Self, 1978). Altered orange-white lithic blocks are also a component of the pyroclastic avalanche deposit.

Figure 2.40 19 February 1975 Ngauruhoe pyroclastic avalanche deposit (centre foreground), showing overlapping digitate flows with lobate fronts, Mangatepopo Valley.

Figure 2.41 Thin lobate flow front of 19 February 1975 Ngauruhoe pyroclastic avalanche.

Figure 2.42 Central flow channel and marginal levées developed in 19 February 1975 Ngauruhoe pyroclastic Zavalanche, Mangatepopo Valley.

(b) **1949 and 1954 Ngauruhoe pyroclastic avalanches.** Hot pyroclastic avalanches of a poorly sorted mixture of juvenile lava blocks and ash were also deposited during the 1949 and 1954 Ngauruhoe eruptions (Allen, 1949; Battey, 1949; Cloud, 1951; Gregg, 1956).

(c) **North Crater scoria flow.** A thin (<0.5 m) but relatively extensive scoria flow, believed to have erupted from North Crater, extends more than a kilometre downslope from the Tongariro trig ridge (I.A. Nairn, pers. comm., 1995) and is composed of fresh, black, vesicular andesitic lapilli and scoriaceous clasts.

(d) **Tama trig pumice flow (ignimbrite).** One small, wedge-shaped deposit of ignimbrite has been observed in a saddle northwest of Tama trig (T19/377 217; I.A. Nairn, pers. comm., 1994). Preservation of this moderately- to non-welded, oxidised, andesitic-dacitic blocky pumice flow deposit may have been enhanced by the existence of a topographic depression, as similar deposits have not been observed elsewhere on the complex. It is likely that much of the evidence for these small volume ignimbrite-producing eruptions has been removed from the cone.

(e) **Other older Tongariro pyroclastic flows.** Pyroclastic flow deposits in the older portions of the complex are generally less conspicuous than the post-glacial deposits where original overall geometry and morphology is preserved. However some massive, poorly-sorted, oxidised tuff breccias in old vent areas such as Tongariro Trig are likely to have a pyroclastic flow origin, although these deposits have not yet been studied in detail.

(f) **NE Oturere and Tongariro Trig pyroclastic surge deposits.** Within the scoria-tuff cone sequence in the upper NE Oturere Valley wall (Section 2.2.2b) are thin (<1 m), fines-rich, orange-brown to light grey, laminated lapilli tuffs deposited by phreatomagmatic pyroclastic surges (Fig 2.43). The surge beds exhibit planar- to wavy- to cross-bedding on a mm-cm scale. A lack of impact sags indicates that the lapilli and small blocks were carried along in the surge. A light blue-grey, draping co-surge ash fall deposit is often present (Fig 2.43).

Figure 2.43 Pale cream-grey laminated lapilli tuff deposited by a pyroclastic surge, with overlying pale blue-grey co-surge ash fall deposit, intercalated with scoria cone units, NE Oturere Valley (T19/414 263).

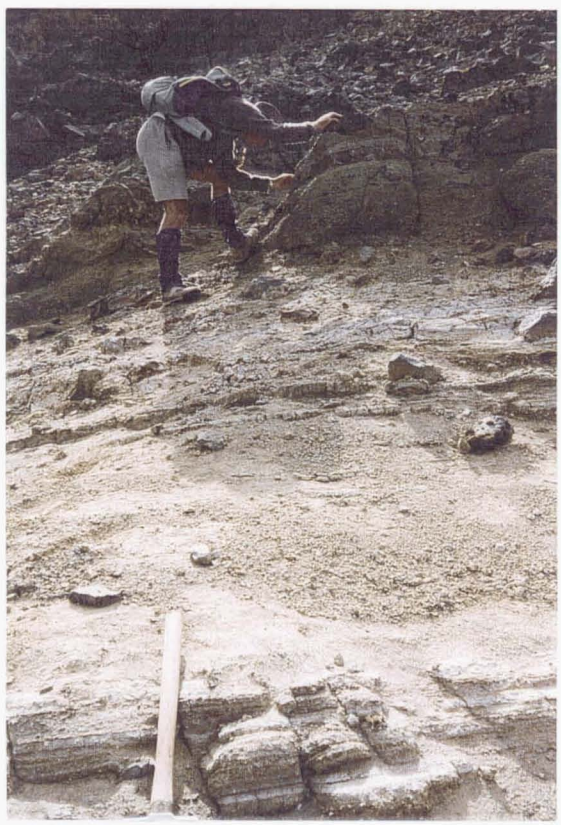

Figure 2.44 Orange-grey, subtly cross-bedded, lithic-rich lapilli tuffs which were probably deposited by a pyroclastic surge, upper NE Oturere Valley (T19/405 268).

Further up towards the head of NE Oturere Valley, in a near-vent sequence of tuffaceous breccias and welded agglutinates, deposits of orange-grey, cross-bedded, lithic-rich lapilli tuffs (Fig 2.44) probably also represent phreatomagmatic surge beds. A scoriaceous tuff cone sequence near Tongariro Trig contains fines-rich, bedded lapilli tuffs supporting large blocks which lack impact sags (Fig 2.33), indicating a pyroclastic surge origin is likely.

2.2.4 Epiclastic deposits

Epiclastic deposits are volcaniclastic sedimentary deposits formed by normal surface processes, e.g. gravitational collapse, weathering, wind reworking, debris flows, fluvial and slope processes (Cas and Wright, 1988). The depositional site for these epiclastic deposits is predominantly on the volcano flanks in fans or narrow valleys, or off the cone in volcaniclastic aprons or ring plains (Smith, 1991). During the lifetime of a composite volcano, periods of high eruptive activity generally contribute to the positive relief of the cone, whereas the longer repose periods between eruptions are dominated by normal surface processes operating at very high rates in comparison to other sedimentary environments (although the amount of available volcanic detritus is more limited compared to syn-/post-eruptive periods). Since the intervals of eruptive quiescence or repose usually exceed the duration represented by eruptive periods, epiclastic processes constitute a major phase of activity in the volcanic environment (Cas and Wright, 1988).

Epiclastic deposits encountered on Tongariro Volcanic Complex include pyroclastic material reworked or redeposited by processes such as debris avalanches, mudflows, and streamflows. The distinction between epiclastic and pyroclastic deposits is often ambiguous, but the presence or absence of features indicative of a gas phase and high temperatures of emplacement (e.g. gas-escape pipes, welding, red oxidation, prismatically-jointed clasts, carbonised vegetation) often serve to identify the origin of the deposit. Much work is required on the epiclastic deposits of the Tongariro complex, although some of the ring plain deposits have been described within the context of the more detailed studies of the Ruapehu volcano deposits (Hackett and Houghton, 1989; Donoghue, 1991; Palmer et al., 1993; Hodgson, 1993 ;Donoghue et al., 1995).

(a) **Debris avalanche deposits.** An incoherent rock mass dislodged by a rockfall or slide associated with sector collapse (e.g. 18 May 1980 Mt St Helens eruption) flows at great speed off the volcano to form a massive, extremely poorly sorted deposit in valleys and out onto the ring plain. Unlike the distinctive hummocky debris avalanche deposits that characterise parts of the ring plains of the two other major andesitic composite volcanoes, Taranaki and Ruapehu, the Tongariro complex lacks evidence for any such similar deposits. However, recognition of one volcanic debris avalanche deposit exposed on the northern flank during excavations for the Tongariro Power Scheme ("Te Whaiau formation"; Palmer et al., 1991), provides the basis for a forthcoming investigation of these deposits on the Tongariro complex (V.E. Neall, pers. comm., 1995).

There does not appear to have been any very recent sector collapse or cone destruction event at the Tongariro complex because there is no geomorphic expression for the hummocky terrain expected to be associated with such an event. It is possible that a high output of tephra could have buried the evidence for any debris avalanche deposits. However, it is more likely that the lava flow-dominated structure of Tongariro's multiple cone complex is more stable than, for example, the steep Taranaki cone which consists of high proportions of unconsolidated volcaniclastics (cf. Palmer et al., 1991).

(b) **Lahar and hyperconcentrated stream deposits.** Mass flow of volcaniclastic debris, with water acting as an interstitial medium, transports large volumes of material off cone volcanoes and onto the ring plain by a continuum of flow processes from lahars to hyperconcentrated flows to more dilute stream flows. Lahars are typically massive, matrix- to clast-supported muddy to sandy gravels, whereas dilute stream flow deposits contain structures such as channels and cross-bedding, and comprise sands or gravels with intercalated sand lenses (Smith and Lowe, 1991).

An historic lahar, named the Mangatipua Formation by Topping (1974), flowed down the north flanks of the cone from Ketatahi Springs in about 1895. The deposit comprises angular to sub-rounded, cm-dm sized clasts in a yellow sandy matrix (Fig 2.45). In gully exposures in the Tama Lakes area (e.g. Fig 3.23), ash-rich pyroclastic units are intercalated with poorly sorted, massive to weakly bedded, heterolithologic muddy sandy gravels containing large angular to sub-rounded clasts and boulders up to 1.5 m in diameter.

Figure 2.45 Historic lahar deposit of c.1895 exposed in Mangatipua stream, near Ketatahi Springs. Deposit is poorly-sorted and comprises angular to sub-angular clasts in a yellow-orange sandy matrix.

Figure 2.46 Basaltic andesite lava (TG115) overlies orange-brown laharic breccia, NE Oturere Valley. Lahar deposit is massive and poorly-sorted, and contains sub-angular to rounded clasts up to 2 m in diameter.

These are thought to represent lahar and hyperconcentrated flow deposits. Older deposits of poorly to moderately sorted, massive to poorly bedded, matrix-rich to matrix-poor breccias and conglomerates have been observed in SW and NE Oturere Valley walls (Fig 2.46) and are also interpreted to be formed by lahars and hyperconcentrated (?to more dilute) stream flows.

The extensive lahar and hyperconcentrated flow deposits on the ring plain surrounding Ruapehu have been described by Donoghue (1991), Palmer et al. (1993), and Hodgson (1993). Similar detailed work has not yet been completed for the ring plain of the Tongariro complex, although Topping (1974) noted sections of laharic breccias and conglomerates exposed on the ring plain and also reported outcrops of lahar deposits in the north of the complex - thought to be derived from Blue Lake and North Crater.

2.3 STYLES OF TONGARIRO VOLCANISM

2.3.1 Effusive volcanism

On Tongariro Volcanic Complex, magma has been erupted as coherent lava flows mostly from central vents, although quiet fire fountaining and overspilling from a lava lake ponded in a crater has also contributed to the effusive products - including rheomorphic spatter and the solidified lava lake itself.

(a) **Lava flow extrusion.** The presence of degassed magma is a prerequisite for quiet extrusion of lava flows. The style of lava flow eruption on the Tongariro complex then seems to be controlled in part by the viscosity and yield strength of the magma. The transition between aa and block flow types represents the increasing importance of brittle over plastic behaviour, and is largely governed by viscosity.

Basaltic andesite flows are more often of aa type, and their mafic composition produces long flow distances and occasionally a thin, widespread nature. The andesitic lava flows (and often the distal ends of aa flows) tend to be block flows, with high aspect ratios

and often spinose flow surfaces indicating the higher viscosity and yield strength typical of andesitic lavas. Some silicic andesites and dacites on the complex form very thick, ponded-type flows with development of extreme flow banding, further illustrating the influence of viscosity and consequently magma composition on style of flow.

However, flow behaviour is not solely determined by magma composition; factors other than magma viscosity and yield strength also affect the style of lava extrusion. Effusion rate, topographic channelling, the thermal efficiency of the flow process, and steepness of the underlying slope all play a role in producing the diversity of lava flow characteristics present on the Tongariro complex.

The dominance of lava flows in old and young successions on the cone shows that they have been consistently produced throughout the growth of the complex, and therefore the conditions for effusive volcanic activity have routinely existed. The only historic lava flows have been observed from Ngauruhoe in 1949 and 1954 (Figs 2.47 and 2.48; Battey, 1949; Gregg, 1956), and these accounts describe typical aa flow movement and associated (preceding and contemporaneous) explosive strombolian activity, and the formation of hot pyroclastic avalanches (characteristically associated with andesitic lavas; Cas and Wright, 1988). Each lava flow formed relatively quickly, reaching its maximum length in 1-2 days. The observations of collapsing brecciated flow fronts and molten flow interiors can be ascribed to the caterpillar-track type motion of aa lava flows. Autobrecciation is also an important process occurring in lava flows of the Tongariro complex, and is an effective means of breaking down massive lava into more easily eroded clasts and matrix, thus contributing reworked material to the ring plain.

(b) Lava lake formation. Lava lakes typically form from weak explosive eruption of basaltic magma and are common on Hawaiian shield volcanoes. The Tongariro complex contains one well-preserved solidified lava lake in North Crater which is composed of andesitic lava. The andesitic magma must have had a very low initial gas content and have been relatively hot for it to behave in such a fluidal manner. This high-

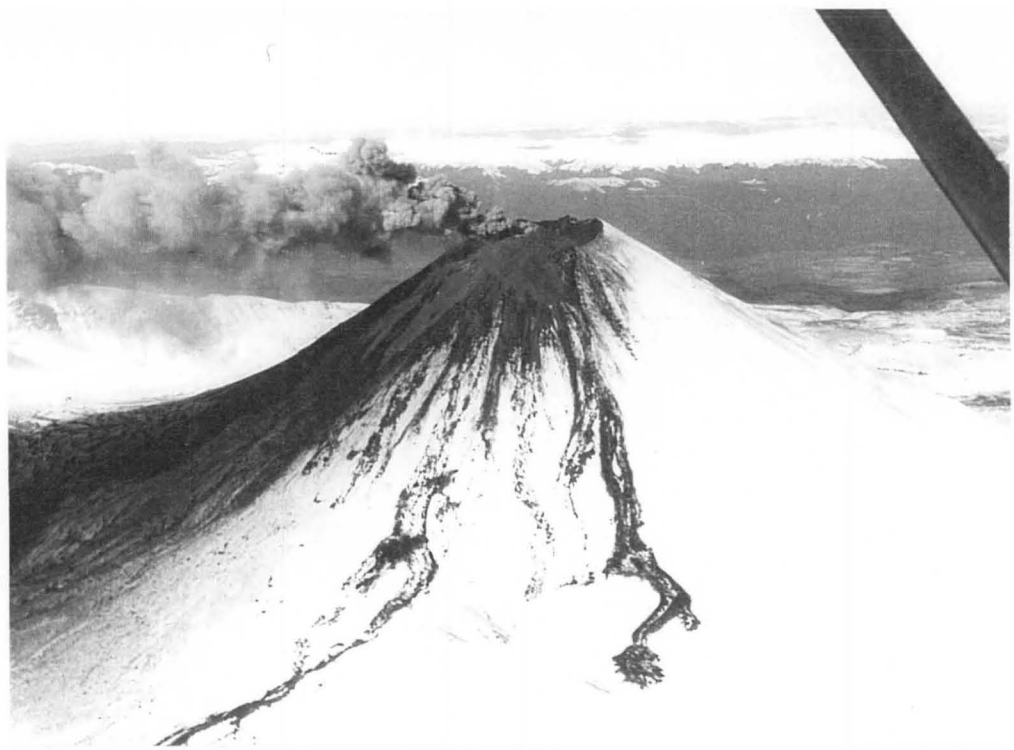

Figure 2.47 1954 eruption of Ngauruhoe showing dark lava flows of June, July and August standing out on the snow-covered western flanks of the cone. The northern slopes on the left have been blackened by falling ash. Photo taken by J. Healy on 3 September 1954 (print courtesy of GNS Wairakei).

Figure 2.48 Incandescent lava fountaining on the night of 16 September 1954 during the 1954-55 strombolian eruption of Ngauruhoe. A lava flows moves down the western flank of the cone. Photo taken from Pukekaikiore saddle by E.F. Lloyd (print courtesy of GNS Wairakei).

temperature character is confirmed by Fe-Ti geothermometry; calculations for one sample of the lava lake yield a maximum temperature of 1116°C, well above most temperature estimates for other lavas on the complex (Section 4.6.2).

In addition, the North Crater vent was probably much wider and more open than most other vents on the complex. This wide basin-shaped vent, together with a relatively low magma discharge rate, would have enabled decoupling of the magmatic volatiles from the magma, allowing gases to escape and the lava to accumulate in a pond within the crater. Disruption of the lava lake surface by the emerging gases caused periodic fire fountaining and deposition of spatter deposits around the crater rim (Section 2.3.2a).

2.3.2 Explosive volcanism

Most andesitic eruptions are explosive (Walker, 1982), as demonstrated on Tongariro Volcanic Complex where over 95% of the eruptions witnessed in historic times were entirely explosive in nature. The range of eruptive styles at Tongariro can be pieced together from the preceding description of the pyroclastic deposits, supplemented by several published visual observations of actual eruptions.

Pyroclastics are fragmented in two ways: (1) rapid exsolution of magmatic volatiles (induced by decompression and/or crystallization); and (2) the interaction between hot magma and water whereby the external water flashes to steam (i.e. phreatomagmatic eruption). The styles of Tongariro explosive volcanism are discussed in order of approximately increasing degree of explosivity: hawaiian, strombolian, phreatic-phreatomagmatic, vulcanian, and plinian. There are, of course, gradations between these categories of activity, and the style of explosive activity may also change during the course of a single eruption.

(a) **Hawaiian volcanism.** Mildly explosive eruptions of basic magma via a low pulsating eruption column or "fire" fountain are termed hawaiian style eruptions. Evidence for such eruptions can be observed in the welded lava spatter deposits of North Crater, Blue Lake, Tongariro Trig and upper Oturere Valley (Section 2.2.2a). These formed when jets of fountaining lava fell back around the vent area, creating localised deposits draping the

crater rims and building up spatter ramparts around the vents. At least one of the craters of these spatter cones contained a large ponded lake of lava (Sections 2.2.1d and 2.3.1b). Some of the welded spatter deposits were remobilised and flowed to create rheomorphic welded tuffs (Section 2.2.1c).

Hawaiian style volcanism on the Tongariro complex has involved andesitic magma as opposed to the more characteristic basaltic composition. Factors such as high magmatic temperatures and low magmatic volatile contents, however, have helped determine the eruptive style (see Section 2.3.1b).

(b) **Strombolian volcanism.** Increasing explosivity signals the progression from hawaiian to strombolian style eruption. Strombolian activity involves discrete explosions each generated when one or more large gas bubbles burst through the magma surface and eject the fragmented magma of the bubble skin as pyroclasts. Because of the relatively low column height, most of the ejecta (predominantly scoriaceous to fusiform bombs and lapilli) falls back near the vent to form a scoria cone. Strombolian eruptions may generate significant lava flows, such as occurred from Ngauruhoe and Red Crater. Strombolian volcanism on the Tongariro complex has built up scoria cones of basaltic andesite composition at Ngauruhoe, Red Crater, Pukeonake, Oturere Valley, and Tongariro Trig (Section 2.2.2b).

Strombolian eruptions of Ngauruhoe during 1948-49 and 1954-55 have been witnessed and well-documented (Allen, 1948; Battey, 1949; Gregg, 1956). Prolonged fire fountaining between June and September of 1954 (Fig 2.48) built up a sizeable scoria cone within the main crater of Ngauruhoe, a section through which is described in Section 2.2.2b. Ash explosions occurred spasmodically throughout the eruptive period, with dark eruption columns (over 1 km high) observed which deposited ash and lapilli on the cone (Fig 2.47) and carried ash as far away as Taupo, 65 km to the northeast (Gregg, 1956). Some particularly sharp explosions were accompanied by visible shock waves immediately preceding ash emission (Gregg, 1956). Vigorous lava fountaining episodes culminated in the extrusion of at least 10 lava flows down the western flank (Figs 2.47 and 2.48; Section 2.2.1a).

Strombolian volcanism also played a role in prehistoric times on the Tongariro complex. Scoria cones such as those in NE Oturere Valley were formed within otherwise monotonous sequences of lava flows, often creating angular unconformities where lava flows have banked up against a wedge of scoria.

(c) **Phreatic - phreatomagmatic volcanism.** Phreatic eruptions are steam explosions caused by the interaction of external water with magmatic heat and/or volatiles. The water may be encountered in the form of ground water, a crater lake, hydrothermal fluids, or water-saturated sediment. These explosions may create craters within the country rock, for example the Emerald Lakes and associated NE trending line of pit craters (Fig 3.24) were created in this manner. Lithic fragments thought to have been ejected from Emerald Lakes were identified by Topping (1974) in tephra deposits in Oturere Valley and on the Red Crater flow in Central Crater, and the phreatic explosions were interpreted to be post-Taupo pumice, i.e. <1.8 ka.

Phreatomagmatic eruptions occur with significant direct input of magma and involve the fragmentation of new magma as well as country rock. Fine-grained, poorly-sorted deposits of phreatomagmatic volcanism are present in some of the older parts of the Tongariro complex, particularly NE Oturere Valley and Tongariro Trig, where they occur in scoria cone sequences. The changing proportion of phreatomagmatic surge and fall deposits (Sections 2.2.2b and 2.2.3f) to scoria represents a changing balance between wet and dry phases of the eruption - or the involvement of more than one vent (Section 2.2.2b).

The Te Mari Craters, on the north slopes of complex, were often observed steaming vigorously or in eruption during last century (Gregg, 1960; Cole and Nairn, 1975) and these were probably mostly phreatic to phreatomagmatic eruptions. As well as large quantities of steam, the ejection of mud, boulders, ash and pumice or molten lava during some of the eruptions has also been described (Hill, 1894; Friedlaender, 1898). No substantial deposits of these ejecta have been preserved, however.

(d) **Vulcanian volcanism.** Vulcanian style eruptions are common from andesitic composite volcanoes, and involve short-lived violent (probably phreatomagmatic) explosions which produce small eruption columns and often generate small-volume

Figure 2.49 Collapse of eruption column to produce a pyroclastic avalanche deposit, 90 seconds after commencement of Ngauruhoe eruption at 1810 hours, 19 February 1975. Photo taken from Mangatepopo Valley looking east (Pukekaikiore in foreground) by G.T. Hancox (used with permission).

pyroclastic flows. The often cited 1974-75 eruption of Ngauruhoe (Self, 1975; Nairn, 1976; Nairn et al., 1976; Nairn and Self, 1978; Self et al., 1979) provided a classic example of a vulcanian eruption sequence.

The eruption of 19 February 1975 was observed closely and began with voluminous gas-streaming, followed by violent cannon-like explosions which ejected ballistic blocks up to 2.8 km from the vent (Section 2.2.2c), and were accompanied by atmospheric shock waves and condensation clouds (Nairn, 1976; Nairn and Self, 1978). Dense eruption columns up to 10 km high underwent partial collapse to form pyroclastic avalanches (of both fresh magmatic and older lithic blocks) down the flanks of the cone (Section 2.2.3a; Fig 2.49; Nairn and Self, 1978). Vulcanian pyroclastic fall deposits are characteristically thin and unlikely to be preserved. Near to Ngauruhoe the fall deposit comprised 3-4 cm of scoria-ash, and thinned to 1 mm of ash at 21 km along the dispersal axis (Nairn and Self, 1978). Maximum initial ejecta velocities of around 400 m s^{-1} (Nairn, 1976) were linked to high explosion gas pressures caused by magmatic intrusions rapidly heating meteoric water confined beneath a solidified lava cap (Nairn and Self, 1978; Self et al., 1979).

(e) **Sub-plinian - plinian volcanism.** The largest eruptions are comparatively steady, high-energy events in which a powerful gas jet and high convective eruption column (usually <20 km) disperse widely voluminous amounts of relatively silicic scoria, pumice and ash. Extensive sub-plinian to plinian pyroclastic fall deposits are preserved on the ring plain of the Tongariro complex (Section 2.2.2d). These have been studied within the context of tephrochronology and stratigraphy by Topping (1973, 1974), Donoghue (1991) and Donoghue et al. (1995).

Topping (1973, 1974) mapped tephra distributions for post-glacial eruptions and produced isopach maps and identified probable source vents; his work has recently been revised by Donoghue et al. (1995) (see Section 3.4.1). The deposits of individual eruptions are preserved in thicknesses of up to 1 m or more near vent, and have estimated volumes of 0.2-2.8 km^3 and dispersal areas of over 10^3-10^4 km^2 (Topping, 1973; Hackett and Houghton, 1989). Many of these eruptions are best described as sub-plinian.

2.4 DISCUSSION AND SUMMARY

The general field survey of Tongariro Volcanic Complex contained in this chapter shows that this volcano comprises a wide variety of erupted products, which often occur together in vertical successions (e.g. NE Oturere Valley wall) characterised by rapid lithological changes and complex alternations of lava flows with pyroclastic and epiclastic deposits. A lateral change in eruptive products (related to preservation) is also evident; lava flows and localised pyroclastic deposits dominate the proximal cone whereas widespread pyroclastic fall deposits and reworked volcaniclastic material dominate the distal part of the complex. The styles of volcanism exhibited by Tongariro Volcanic Complex can be summarised as:

1. repeated effusion of numerous aa and block lava flows from many summit and flank vents on the complex, with some lavas extending up to 7 km down valleys towards the ring plain,
2. occasional formation of lava lakes ponded in craters, during frequent hawaiian to strombolian fire fountaining eruptions, forming significant but localised welded spatter deposits and scoria cones,
3. small phreatic to phreatomagmatic eruptions creating explosion craters or tuff cones and pyroclastic surge deposits, often associated with scoria cone growth,
4. vulcanian style eruptions with associated pyroclastic flows or avalanches, the frequency of which is difficult to determine due to low preservation potential,
5. relatively infrequent subplinian to plinian eruptions which deposit extensive tephra on the ring plain.

The styles, and therefore the products, of Tongariro volcanism are determined by a complex interplay of controlling factors. Magma composition plays an influential role whereby the basaltic andesites tend to be erupted as aa lava flows or scoria, andesites as block flows or welded spatter, and silicic andesites to dacites as overthickened flows/coulées or scoriaceous-pumiceous fall. So on a first order level it is apparent that the more mafic magmas erupt less violently. This theme is explored in further detail in later chapters on the geochemistry of the eruptive products (Chapters 6 and 7). Gardner et al.

(1995) found that the range in eruptive intensity of Mt St Helens results more from differences in the composition of erupting magma, rather than conduit diameter. Other workers have emphasised conditions in the vent (e.g. vent radius, gas content, magma viscosity) which were believed to exert the major influence over style of activity (e.g. Walker, 1982; Wilson et al., 1980).

Some of these other controls on Tongariro volcanism can be related to magma composition and include temperature, viscosity, yield strength, and volatile content of the magma. Effusion rate, or magma discharge rate, also has obvious implications for e.g. extent of magma degassing, volume of deposit, degree of welding. Physical aspects of the vent (size, presence of blockage, presence of water, etc.) and surrounding topography (slope, presence of barrier, channelling, etc.) also contribute to the diversity of eruptive styles, and differences within one type of eruptive product, e.g. flow direction, length, aspect ratio and surface morphology of lava flows.

The detailed facies model developed for Ruapehu volcano (Hackett and Houghton, 1989) can be applied to the Tongariro complex and allows useful comparisons to be made. Hackett and Houghton (1989) identified a four-fold division of the Ruapehu deposits into associations of lithofacies:

1. Central and flank vent association
2. Proximal (cone-forming) association
3. Distal (ring plain) association
4. Satellite vent association

The two composite volcanoes share many features in common. Like Ruapehu, the Tongariro complex is made up of a number of cones, each associated with a vent which may be either a central vent as exemplified by some of the post-glacial cones (e.g. Ngauruhoe crater, Red Crater, North Crater), or a flank vent. The presence of welded fall deposits and vent breccias in the older parts of the complex indicate the vent areas (central and/or flank) for the pre-glacial cones. The spacing of the central vents at Tongariro is broadly similar to that at Ruapehu.

Concurring with Ruapehu's cone-forming association, massive and autobrecciated lavas also dominate the cones of the Tongariro complex. Tongariro's ring plain, which coalesces with that of Ruapehu, is also where the distal primary fall deposits are concentrated. Stream and slope processes on the cone make an important contribution to epiclastic deposition on the ring plain. The Pukeonake scoria cone, situated only a few kilometres west of the Tongariro complex edifice, is recognised as belonging to the satellite vent association.

There are differences in detail, however, regarding the relative abundance of facies on Tongariro and Ruapehu. The vent association on the Tongariro complex is less well exposed than on Ruapehu volcano because Ruapehu is higher and more deeply eroded. The general absence of dikes in the proximal cone-forming association on Tongariro may similarly be related to the degree of erosion; on Ruapehu the dikes only occur in the oldest, most deeply eroded sections. A history for the ring plain, and particularly debris avalanche deposits, is less well established for Tongariro than it is for Ruapehu. Ring plain studies of the most recent (<25 ka, especially those c.10 ka) tephras erupted from Ruapehu volcano and the Tongariro complex have revealed differences in composition; high pumice contents typify the former, and darker scoria characterise the latter (Donoghue, 1991; A.S. Palmer, pers. comm., 1995).

In comparison to other composite volcanoes in general, Tongariro Volcanic Complex exhibits the variability in cone morphology, eruptive style and products which is a characteristic trait of many of these composite cone complexes. Stratigraphic complexity and the preferential distribution of the different primary volcanic products in near-vent locations or on the ring plain is also a common feature encountered on other composite volcanoes. The influence of sedimentary processes on composite volcanoes has come to be recognised more recently, and the importance of epiclastic reworking as a significant activity on the Tongariro complex has been acknowledged. The large number of excellently preserved historic and youthful prehistoric lava flows erupted from the complex - especially from Ngauruhoe (over 70 recognisable flows and pyroclastic units) -is perhaps a feature which distinguishes it from many other composite volcanoes and provides an exciting opportunity for well-constrained geochemical analysis.

Chapter 3

Volcanic Stratigraphy and Eruptive History

CHAPTER 3
VOLCANIC STRATIGRAPHY AND ERUPTIVE HISTORY

3.1 INTRODUCTION

A major aim of this project was to establish a detailed volcano-stratigraphy and geochronology for the Tongariro Volcanic Complex, thereby enabling an integration of time-volume data with geochemical data. This aim has been achieved by a combination of detailed field mapping, sampling, and K-Ar determinations. Field mapping was carried out in collaboration with the Institute of Geological and Nuclear Sciences, and K-Ar age determinations by U.S. Geological Survey, Menlo Park (Section 1.1.3). The purpose of this chapter is therefore to explain the methodology employed and to describe the 17 volcano-stratigraphic units identified on the complex.

This part of the project represents the first detailed division of Tongariro geology in terms of units constrained by absolute age limits. Estimation of the present and original volumes of each unit has then been used with the new age data to provide constraints on the rates of cone growth and to investigate the relationships between different magma batches and magma reservoirs (in terms of their size, state, lifespan, and degree of independence). In this way a more detailed model of Tongariro magmatism can be built up. This approach marks a significant departure from previous broad generalisations of Tongariro stratigraphy, and as a consequence permits greater insight into the Tongariro complex.

3.2 FIELD MAPPING AND SAMPLING PROCEDURE

3.2.1 Previous Work

Prior to the current detailed mapping of Tongariro Volcanic Complex, only generalised geological maps were available. The first geological mapping of the Tongariro National Park was carried out in the 1930's by Grange and co-workers, but the maps were not published until 1960 (Gregg, 1960). The Tongariro complex was treated as one large massif with only the young flows from Ngauruhoe and Red Crater outlined. Similarly, in Grindley's (1960) 1:250 000 map of the Taupo region, only the obvious young lavas from Ngauruhoe, Red Crater, Te Mari Crater, North Crater and Pukekaikiore were differentiated from Tongariro in general.

Mathews (1967) produced a slightly more elaborate geological map which included a distinction between young (Holocene) and older lavas and pyroclastics, inferred positions of old vents, faults, moraine, alluvium, and lahar deposits. Topping (1974) further developed Mathews' (1967) map by adding age limits from tephrochronology. Cole (1978) presented a refined version of Topping's (1974) map, and it is these two geological maps which have been referred to by subsequent workers on the Tongariro complex.

3.2.2 Present mapping

During the course of field mapping, coverage of about 80% of the volcanic edifice was achieved; the northwest and northeast slopes, and Mangahouhounui Valley to the east were not visited. The diminishing outcrop on the outer flanks of the complex made visitation of these areas an unproductive use of the time available during field seasons. Significant outcrop does occur in the walls of Mangahouhounui Valley where over 300 m of welded pyroclastic fall deposits and lava flows are exposed (I.A. Nairn, pers. comm., 1995). Future work in this area would benefit a fuller understanding of Tongariro's eruptive history.

Outcropping volcanic rocks were mapped at a scale of 1:12 500 for presentation at 1:25 000 on the thesis map (contained in map pocket, Volume 2). The base map was an enlargement of the 1:50 000 NZMS 260 Sheet T19 and uppermost part of Sheet T20 (the latter for coverage of Lower Tama Lakes). Aerial photographs obtained from NZ Aerial Mapping Ltd (Hustings), at a scale of approximately 1:25 000, were also used to aid mapping and sample location. Series SN8440, runs E19-24, F19-24 and G19-24 (all taken on 30 January 1985) gave comprehensive coverage of most of the Tongariro complex, with most mapping possible with just E22, F20, F22 and G21. An additional older (25 October 1980) set of photographs, Series SN5752 runs A4-5, was necessary for use in the Lower Tama Lake area.

The thesis map is not a complete geological map in that faults (Section 1.4.5), alluvium, 1.8 ka Taupo eruption deposits (Section 3.4.2c), and moraine and other glacial deposits (Section 1.2.4) are not shown. The approach has been to depict the present outcrop expression of older cone-building sequences and young eruptive units (collectively termed volcano-stratigraphic units) in dark colour shadings, and the inferred extent of each unit (i.e. including the area covered by scree or vegetation) in corresponding lighter colour shading. Old vent areas are depicted by cross hatching and eight were identified based on a combination of features including: the presence of intense hydrothermal alteration (often of vent breccias), projected convergence of radiating dip patterns, steep and opposing dips, thick scoria deposits, and more rarely, dikes or domes. Measurements of flow banding and dip directions of lava flows are plotted on the map. More recent vents are easily recognised as geomorphologically-defined craters, cones and/or proximal scoria deposits, and 25 vents of young eruptives have been shown on the map by star symbols. Note that vent localities are also summarised on Figure 3.4.

3.2.3 Volcano-stratigraphy

On the basis of 41 new K-Ar age determinations (Section 3.3.2) in conjunction with field data (e.g. identification of older vent areas, patterns of lava flow directions), six pre-glacial (275-65 ka) cone-forming sequences were defined in the course of mapping (see Fig 3.2 and Section 3.5): Tama 1(t1), Northeastern Oturere (no), Tama 2 (t2), Pukekaikiore

(pk), Southwestern Oturere (so), and Tongariro Trig (tt). Eleven young intra- and post-glacial (<c.25 ka) eruptive units are also recognised (see Fig 3.2 and Section 3.5.8): Young NE Oturere (yno), Pukeonake (pn), Blue Lake (bl), North Crater (nc), Young Pukekaikiore (ypk), Young SW Oturere (yso), Te Mari Craters (tm), Tama Lakes (tl), Red Crater (rc), South Crater explosion pit (scp), and Ngauruhoe (ng). This division into volcano-stratigraphic units, particularly of the older part of the complex, is a significant refinement of the previous broad division into an older group (>20 ka) of strongly eroded lavas, and a younger group (<20 ka) of lavas which display primary volcanic morphology (Topping, 1974; Cole and Nairn, 1975; Cole, 1978). This study therefore represents the first detailed eruptive chronology of the pre-glacial portions of the Tongariro complex (Section 3.6.1). Two- to three-letter abbreviations (identified in Table 3.3) for each volcano-stratigraphic unit are incorporated as labels on the map in conjunction with the colour coding of the units.

3.2.4 Sampling

A total of 410 samples of Tongariro lavas and pyroclastics were collected over the course of this study. Sampling was conducted within a stratigraphic context, further constrained by K-Ar dating, to ensure meaningful petrological modelling could be carried out (see Section 1.1 for discussion of the benefits of this approach). Many samples were collected from thick (>100 m), near-vertical, lava-volcaniclastic sequences exposed along the walls of deep glaciated valleys. The use of field photographs of these vertical sections proved an effective method of accurate sample location. Although some lava flows could be traced for 1 to 2 km along valley walls, total correlation of sampled sections on a flow-by-flow basis was not possible due to most flows being laterally discontinuous. Appendix 1 contains tabulated information on sample location, field occurrence, volcano-stratigraphic unit, rock type, and analytical treatment. Appendix 2 contains the best interpretation possible, given available field information and K-Ar dating, of the sampling stratigraphy of each volcano-stratigraphic unit.

The Mangahouhounui Valley represents the only major omission in the comprehensive sampling of the complex, although there is also the potential for further

sampling of Te Mari Craters lavas and Tama Lakes ejecta. Otherwise, very detailed sampling of all cone-building sequences has yielded almost 400 petrological samples which are considered representative of the exposed portions of the complex. Mapping and sampling of eruptive products on the ring plain was beyond the scope of this project. Two samples (TG035 and TG036) collected from the Lower Tama Lakes area are Ruapehu-derived lavas, and have therefore been omitted from all appendices apart from Appendix 1 and Appendix 15 (the latter contains age, mineralogical and chemical data pertaining to these two samples). Ruapehu lavas are compared with those from the Tongariro complex in discussions throughout the thesis, particularly in Sections 6.7.

3.3 K-AR AGE DETERMINATIONS

Although the post-glacial history of Tongariro Volcanic Complex was reasonably well-established (Section 3.4.1), age data for the earlier phases of activity were very limited and the acquisition of 41 new K-Ar age determinations has greatly improved our understanding of the sequence of older cone-building episodes. It is also important in providing an absolute time framework for the stratigraphy, enabling determination of the life span and size of magma batches at the Tongariro complex and the degree of linkage between them.

3.3.1 Previous work

Earlier workers to touch upon the age of early Tongariro lavas include Gregg (1960), Stipp (1968), and Topping (1974). Stipp (1968) dated three lavas from the complex (Tama Lakes, Mangatepopo Valley, northern Tongariro), which when recalculated (Hobden et al., 1996) give ages of 266±3 ka, 107±10 ka, and 85±3 ka respectively.

Gregg (1960) and Topping (1974) discussed the other minimal geochronological evidence available. The first pyroxene-andesite pebbles to be deposited into the Wanganui

Basin from the southern end of the Taupo Volcanic Zone appeared during the Nukumaruan Stage (c.1.5-1.1 Ma) of the early Pleistocene (Fleming, 1953), but these were probably derived from the older andesitic cones of Titiraupenga and Pureora (northwest of Lake Taupo), rather than signalling the initiation of volcanism at Tongariro or Ruapehu. Andesitic lava exposed at Beggs Pool in the Tongariro River east of the Tongariro complex has reversed polarity and was therefore interpreted by Topping (1974) to have been erupted in the Matuyama Reverse Chron (i.e. >0.73 Ma). Topping (1974) also noted Whakamaru Ignimbrite (c.0.34 Ma) overlying andesitic material. The relationship between these andesite lavas to the east of the complex (described in drill logs of the Tongariro Power Development project) and those sampled and dated for this project is unknown. The Tongariro complex is unlikely to be much older than a few hundred thousand years, however, as the lifetime of an andesitic composite volcano rarely spans more than 0.5 Ma (cf. Cas and Wright, 1988; Hildreth and Lanphere, 1994).

3.3.2 New data

The results of the 41 new K-Ar age determinations are summarised in Table 3.1, and these data and their implications are also presented and discussed in brief by Hobden et al. (1996). The relevant techniques employed are outlined in Appendix 8.1. The K-Ar age measurements were carried out on whole-rock samples by M.A. Lanphere at USGS, Menlo Park. Hildreth and Lanphere (1994) discuss the suitability of K-Ar age calibration for Quaternary composite volcanoes and demonstrate this through their successful and comprehensive dating programme for the Mt Adams volcanic field. Together with the data from Stipp (1968), the new Tongariro data generally form an internally consistent data set in agreement with most stratigraphic evidence, and appear to adequately encompass the ages of all identified volcano-stratigraphic units (although the base of the moderately eroded older portions of the volcanic complex is not exposed). Within the NE Oturere sequences, however, several ages do not fit into the established stratigraphy, probably indicating excess argon in these samples (Section 3.5.3a).

Table 3.1 K-Ar age data for samples from Tongariro Volcanic Complex, arranged by volcano-stratigraphic unit.

Sample	Volcano-stratigraphic unit	Map label	Grid reference (T19 or T20)	K_2O (wt%)	$^{40}Ar^*$ (10^{-13} mol/g)	%Ar (rad)	Age (ka)	s.d. (ka)
New data								
TG330	Tongariro Trig	tt	379 261	1.58	1.470	3.5	64	11
TG147	Tongariro Trig	tt	370 256	1.44	1.645	9.4	79	9
TG144	Tongariro Trig	tt	370 263	1.81	2.388	10.5	91	7
TG138	Tongariro Trig	tt	351 261	2.04	3.249	12.6	110	6
TG235	SW Oturere	so	388 256	1.93	1.888	2.5	68	11
TG077	SW Oturere	so	400 247	1.35	1.501	2.3	77	14
TG228	SW Oturere	so	390 255	2.05	2.409	3.1	81	17
TG051	SW Oturere	so	414 236	1.33	1.672	6.8	87	10
TG182	SW Oturere	so	391 242	2.25	2.935	13.8	91	9
TG298	SW Oturere	so	397 208	1.23	1.614	1.2	91	31
TG178	SW Oturere	so	394 243	2.02	2.754	14.2	95	10
TG084	SW Oturere	so	417 225	1.42	1.995	7.4	97	10
TG171	SW Oturere	so	399 250	1.75	2.582	9.8	103	12
TG080	SW Oturere	so	401 247	1.45	2.289	7.6	109	13
TG086	SW Oturere	so	422 227	1.95	3.213	15.1	114	9
TG151	Pukekaikiore	pk	353 245	1.32	2.289	2.0	121	23
TG265	Pukekaikiore	pk	347 251	1.31	2.973	5.3	158	14
TG155	Pukekaikiore	pk	354 240	1.42	3.899	19.5	190	9
TG292	Tama 2	t2	391 213	1.35	3.961	12.4	203	11
TG383	Tama 2	t2	368 220	1.50	4.412	22.2	204	13
TG373	Tama 2	t2	367 229	1.29	3.781	17.0	204	15
TG382	Tama 2	t2	367 225	1.35	3.996	22.3	206	14
TG300	Tama 2	t2	399 222	1.06	3.167	16.8	207	18
TG389	Tama 2	t2	375 216	1.42	4.252	25.3	208	14
TG294	Tama 2	t2	384 213	1.32	3.972	19.3	209	16
TG103	NE Oturere	no	416 255			1.8	89	21
TG047	NE Oturere	no	424 240	1.21	1.798	3.2	103	18
TG227	NE Oturere	no	400 265	1.22	1.820	4.3	104	13
TG258	NE Oturere	no	412 268	1.43	2.172	4.8	105	12
TG247	NE Oturere	no	413 264	1.52	2.664	6.9	122	10
TG109	NE Oturere	no	415 259	1.15	2.024	7.1	123	16
TG114	NE Oturere	no	412 261	1.80	3.283	3.3	123*	10
TG123	NE Oturere	no	414 264	1.36	2.497	7.3	128	12
TG249	NE Oturere	no	413 265	1.30	3.410	8.5	164*	12
TG098	NE Oturere	no	420 249	1.24	3.106	14.3	173	10
TG400	NE Oturere	no	405 267	1.14	3.310	3.5	202	23
TG111	NE Oturere	no	413 256	1.29	4.266	13.9	229	11
TG048	NE Oturere	no	422 246	1.33	4.750	15.8	247	10
TG028	Tama 1	t1	359 205	1.50	4.675	19.5	216	14
Tn89	Tama 1	t1	354 199	1.14	4.385	16.1	266	12
TG136	Tama 1	t1	355 197	1.08	4.237	6.2	273	22
*Stipp (1968)***								
3257	Tongariro Trig		353 259				107	10
3258	?northern Tongariro		391 373				85	3
3254	Tama 1		354 205				266	3

* indicates the average of 2 measurements

** recalculated using decay constants of Steiger & Jager (1977)

The age data in Table 3.1 have been arranged according to volcano-stratigraphic unit. The K-Ar age determinations and sample localities are shown within the context of schematic boundaries of these cone-forming sequences in Figures 3.1 and 3.2 respectively. Each cone-forming sequence, or eruptive unit, is described in detail in Section 3.5. There is no systematic time-space relationship of the pre-glacial cones (Fig 3.2), and there was some overlap between successive cones so that often two cones were erupting over the same time period (Fig 3.3). The overlapping of error bars for all dated samples throughout the history of the complex (Fig 3.3) demonstrates eruptive continuity except for possibly a small break between 150 and 140 ka, and the longer ?quiescence between c.65 and 25 ka (see below).

The inferred older vent areas are roughly aligned SW-NE, very similar to the modern vent configuration, suggesting no great change in the magmatic plumbing system during the last glaciation interval (Fig 3.4). Taken together, the positions of the old and young vents thus define a 13 km-long and 5 km-wide vent corridor which contains around 30 recognised eruptive sites (Fig 3.4).

Because the Tongariro complex is not sufficiently deeply eroded to reveal its base, it is not possible to assess the time gap between the oldest dated lava and the true date of initiation of cone growth. The significant portions of the complex with no surface exposure may represent an earlier period in Tongariro's history beyond the oldest dated lava presently known from this study. Growth of the visible portion of the complex, however, had commenced by the time interval 250-275 ka. Remnants of this early activity are exposed in the southern (Tama 1) and possibly northeastern (NE Oturere) sectors of the complex. A major eruptive episode in the southern part of the complex built up a cone relatively rapidly between 210 and 200 ka (Tama 2). The NE Oturere cone continued to grow until about 90 ka, and the Pukekaikiore cone was also built during this time interval (between 190 and 120 ka). The two youngest pre-glacial cone-building episodes took place between 115 and 65 ka at SW Oturere and Tongariro Trig.

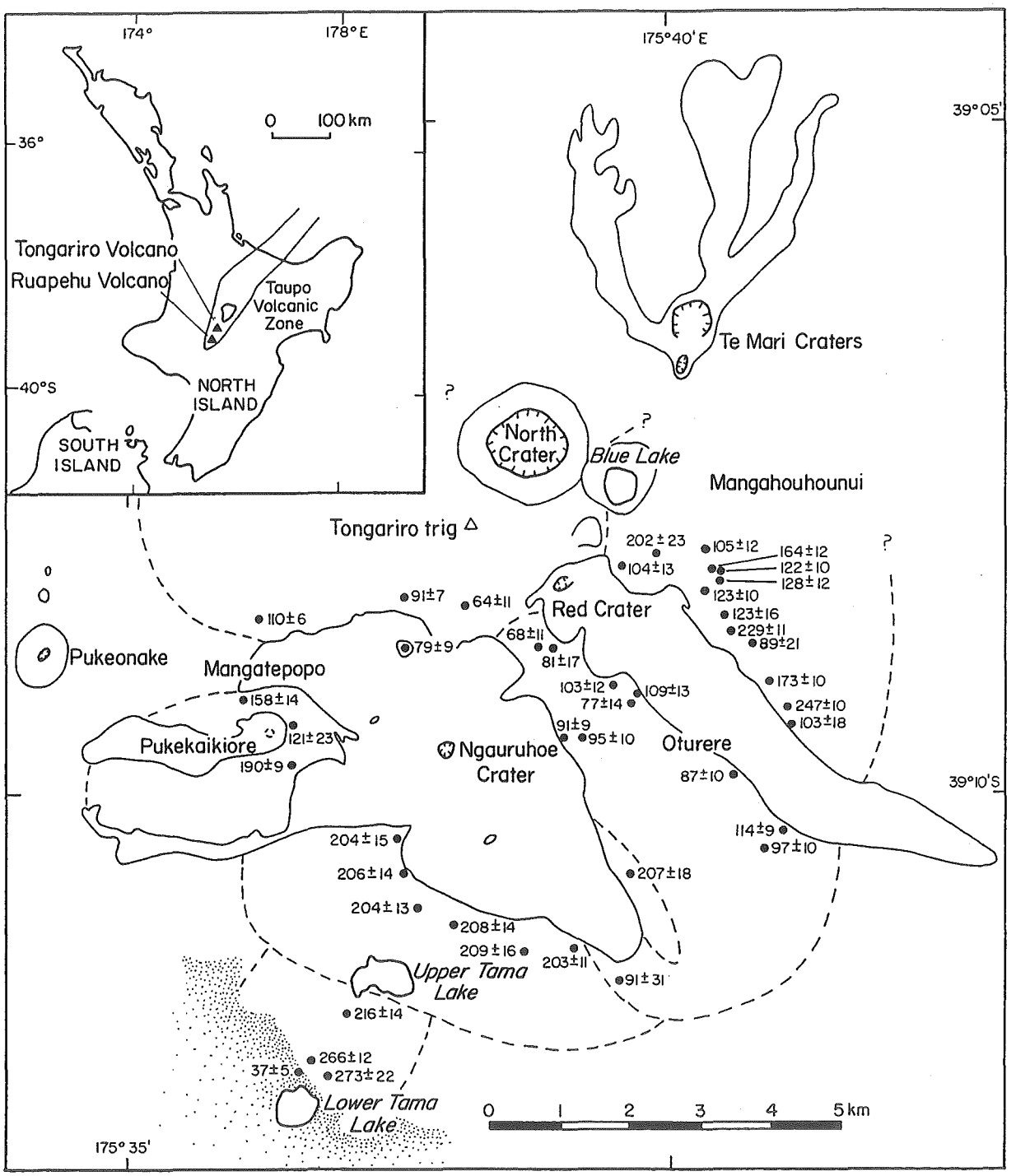

Figure 3.1 Location of samples with K-Ar age determinations (ka) on the Tongariro Volcanic Complex. In the stippled area around Lower Tama Lake, Tongariro lavas are overlain by younger flows from the adjacent Ruapehu composite volcano to the south.

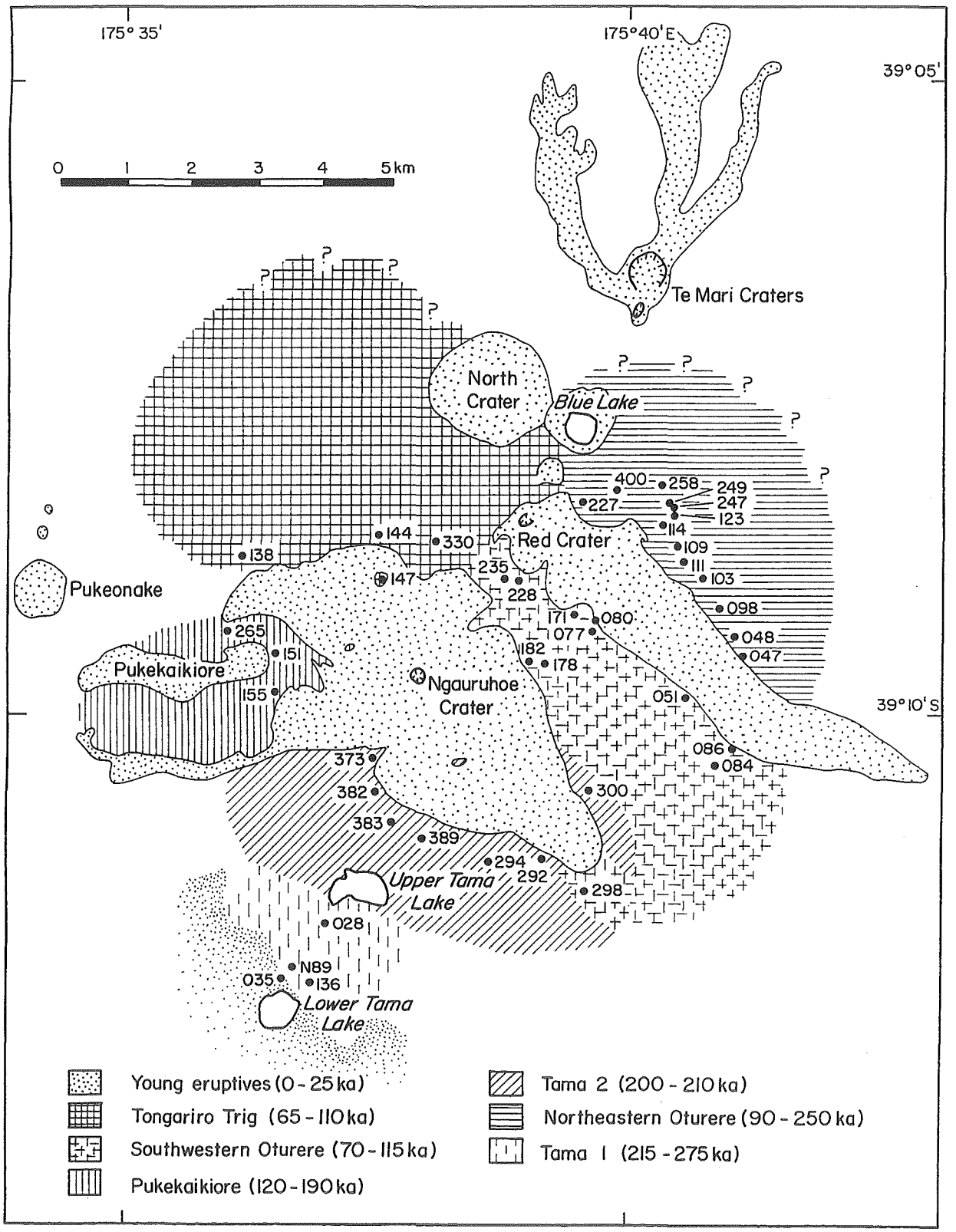

Figure 3.2 Schematic sketch map showing exposed cone-forming sequences of Tongariro Volcanic Complex, and the numbers of those samples selected for K-Ar dating. Stippled area around Lower Tama Lake represents Ruapehu lavas.

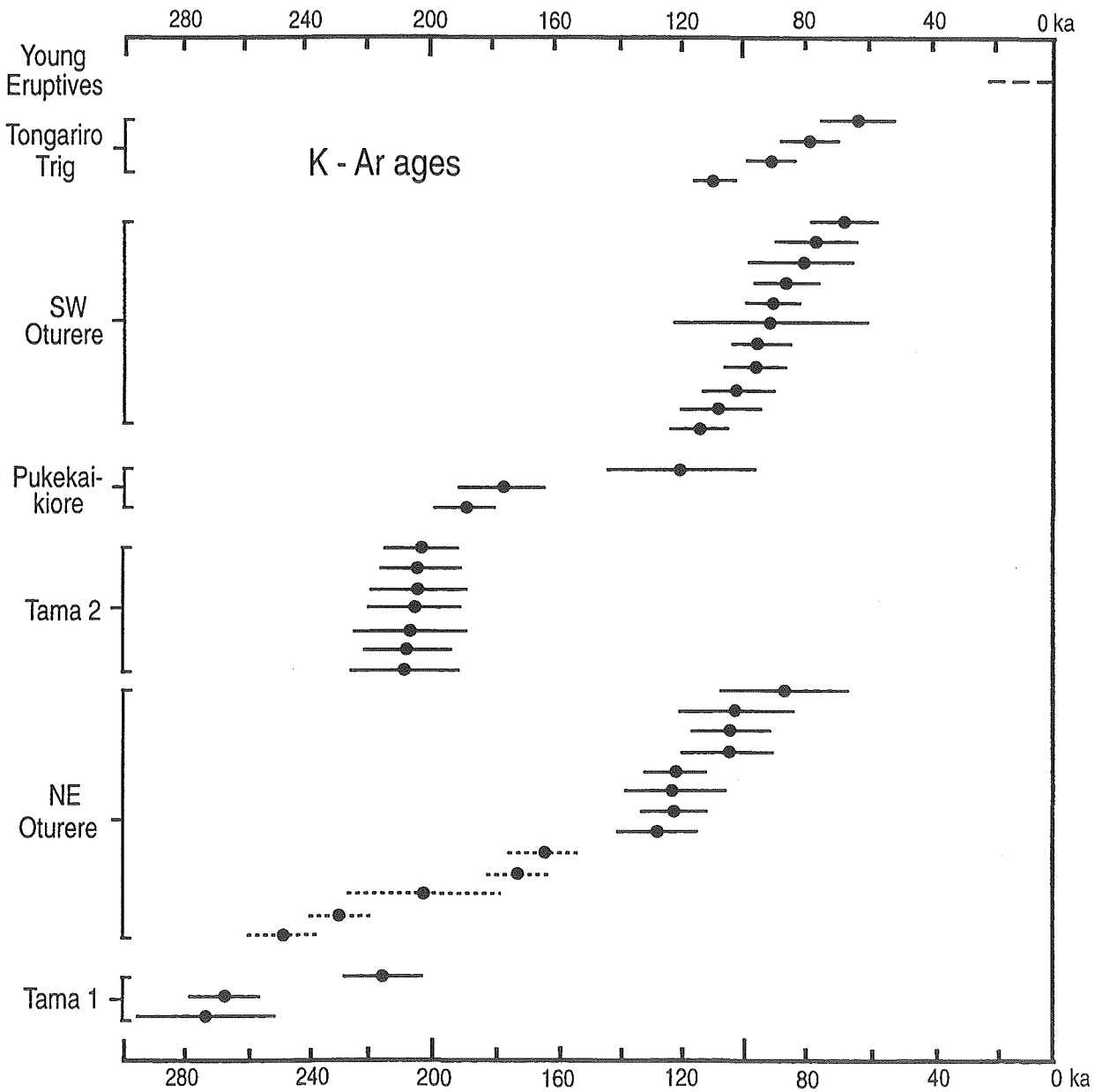

Figure 3.3 K-Ar age determinations for Tongariro Volcanic Complex, arranged by volcano-stratigraphic unit. Error bars (1 sd) are shown for each sample (see Table 3.1). Dotted error bars indicate several NE Oturere age determinations which may be affected by excess argon (Section 3.5.3a). Dashed line represents age range of young eruptive units (determined principally from tephrochronology; Section 3.4)

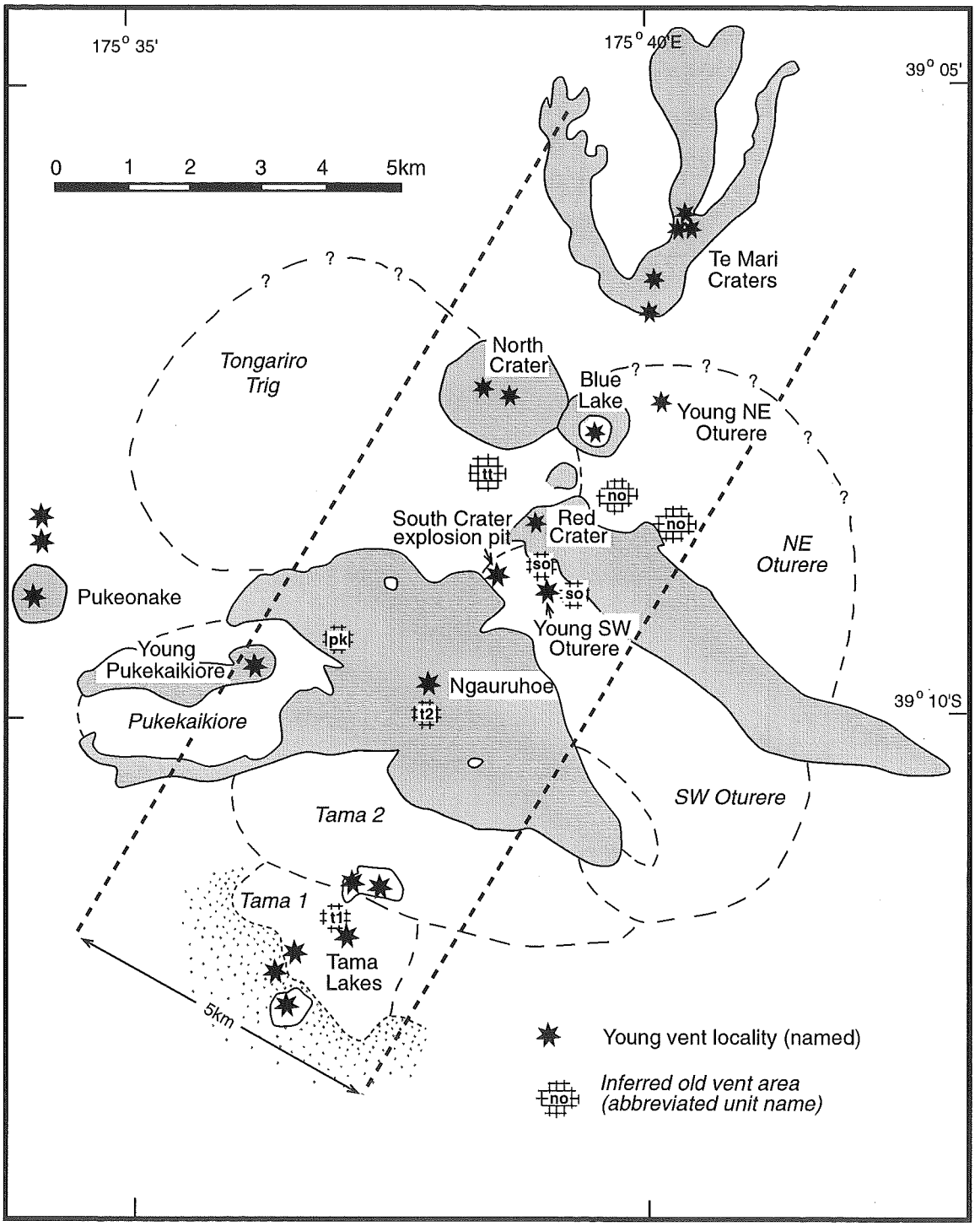

Figure 3.4 Schematic sketch map of Tongariro Volcanic Complex showing inferred vent areas of pre-glacial cone-forming sequences and vent localities of young eruptives. Note SW-NE alignment of both the old and young vents enclosed in a 13 km-long and 5 km-wide vent corridor (dashed lines). See Table 3.1 for unit abbreviations. Stippled area around Lower Tama Lake represents Ruapehu lavas.

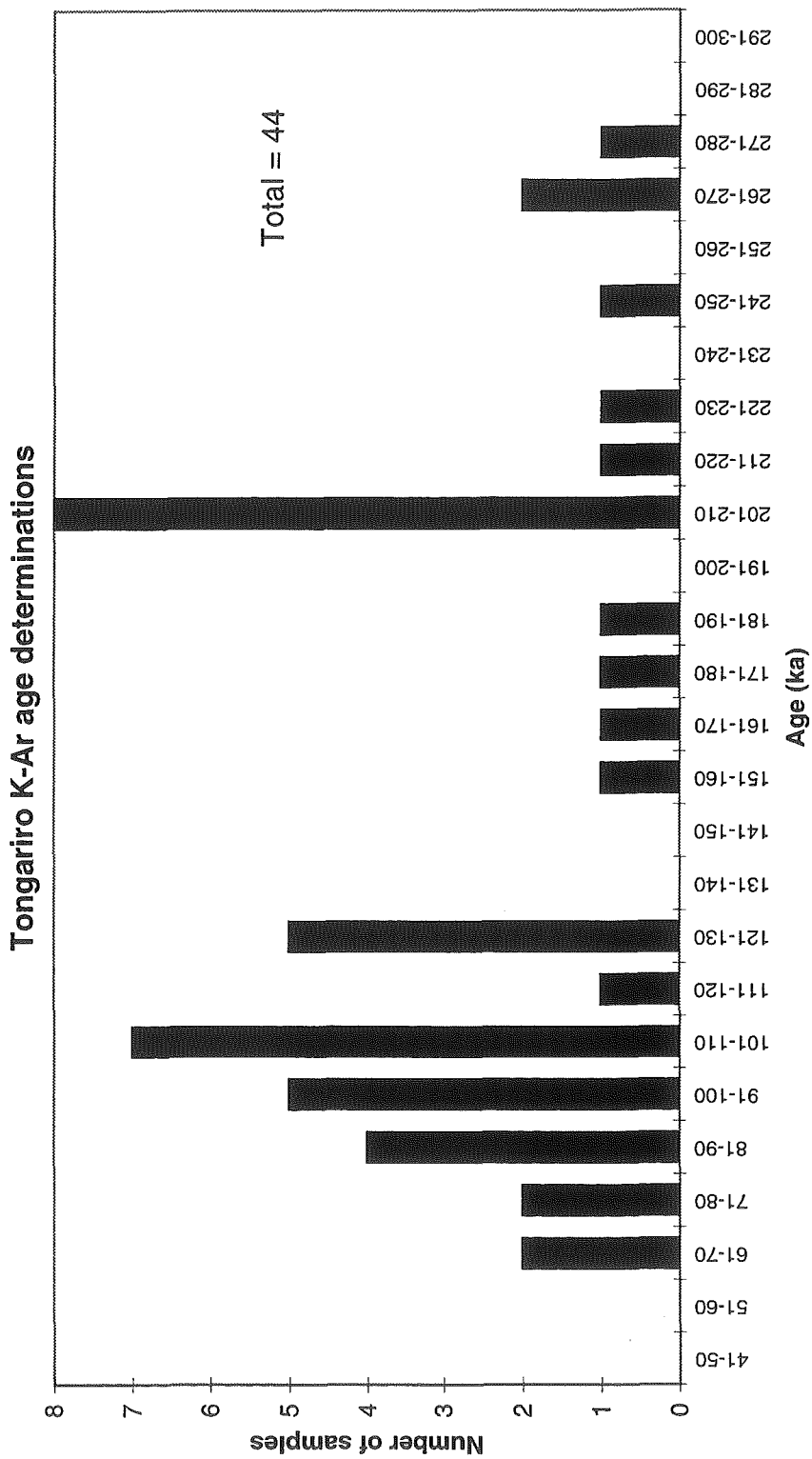

Figure 3.5 Histogram of distribution of K-Ar age determinations (41 from this study, 3 recalculated from Stipp, 1968) from Tongariro Volcanic Complex.

The modern summit cones and craters represent a much younger portion of the complex. The available age data imply a period of relative quiescence from about 65 ka to around 25 ka when the comparatively complex system of vents of the "young eruptives" (Section 3.4) was established. This "time gap" is unlikely to be a function of the limitations of the dating method; if this were the case then more failed samples would be expected (i.e. those too young to be accurately dated by the K-Ar method) since most of the (exposed) stratigraphic range of the complex was sampled. Nevertheless, the absence of data from northwestern Tongariro and Mangahouhounui Valley, and the possibility that some younger material may have been overlooked for dating purposes, indicates that the preservation of 65-25 ka eruptive products cannot be discounted. Conversely, rocks of this age range may have existed but were subsequently eroded during the Otiran Glaciation (c.70-10 ka; Pillans, 1994), which coincides with the "time gap" (see Section 1.2.4 for further information on glaciations of the Tongariro complex). Either way, it is quite likely that there was no real lull in eruptive activity, although this is difficult to confirm.

Figure 3.5 illustrates the distribution of K-Ar age determinations in the form of a histogram which shows the concentration of dated samples in rapid cone-building episodes during 210-200 ka and 130-80 ka. Thus the rate of cone growth has varied throughout the eruptive history of the Tongariro complex. Similarly, the durations of cone-building episodes varies from several relatively long-lived cones (active for >50 ka) to the short-lived Tama 2 cone (formed in less than 10 ka) (Fig 3.3).

3.4 ESTABLISHING THE RECENT ERUPTIVE HISTORY

The young eruptive units of Tongariro Volcanic Complex, that is those less than about 25 ka, have been defined using a different approach to that used for the older cone-building sequences. Because the young eruptives form easily recognisable landscape-forming entities their boundaries are generally self-evident in the field, whereas the eroded pre-glacial cones required absolute age determinations (K-Ar) and use of flow direction indicators to define their spatial (and temporal) limits.

Determining the ages of the young eruptives, however, is more straightforward. The evidence for the age of each young eruptive unit is discussed in Section 3.5.8. The ages of most of the proximal lava and volcaniclastic units are constrained (with varying confidence) by tephra chronology relationships on the ring plain. A review follows of the established work and ongoing investigations of the tephrostratigraphy and chronology of the Tongariro complex and Ruapehu volcano ring plains (Section 3.4.1). It is hoped that in the very near future these separate studies of the proximal cones (this study) and ring plain tephras (other workers) will be integrated into a unifying model for the geochronology and eruptive history of the Tongariro Volcanic Complex. The potential of other dating methods which could be applied to the proximal lava flows is also discussed (Section 3.4.2), and the historic eruptive record is summarised (Section 3.4.3).

3.4.1 Review of post-glacial tephrostratigraphy studies

The post-glacial history of the Tongariro complex was first determined in earnest by Topping (1973, 1974) and his work has provided the basis for more recent (and ongoing) investigations and revisions by workers of Massey University (Donoghue, 1991; Cronin et al., 1994, 1996; Donoghue et al., 1995) which to date have concentrated on the Ruapehu segment of the ring plain. Donoghue et al. (1995) provides a good summary of the early investigations of andesitic fall tephras prior to the work of Topping.

Topping (1973, 1974) established the andesitic tephrochronology using ^{14}C age determinations and interbedded rhyolitic marker fall tephras. This work was summarised by Hackett and Houghton (1989; Sections 2.2.2d and 2.3.2e). In tracing these andesitic fall tephras south into the Ruapehu ring plain, Donoghue et al. (1995) identified new tephra formations and revised some of Topping's (1973, 1974) tephrostratigraphy. A summary of the stratigraphy, chronology and composition of andesitic fall tephras (from 22.5 ka to present) preserved on the Tongariro-Ruapehu ring plain is presented in Table 3.2. Some of these tephras have been convincingly linked back to their sources on the proximal cones by construction of isopach maps. Eruptions from Ngauruhoe, Red Crater, Tama Lakes, Te

Table 3.2 Summary of stratigraphy, chronology and composition of andesitic tephras preserved on the Tongariro-Ruapehu ring plain, after Topping (1973, 1974), Donoghue (1991) and Donoghue et al. (1995). RC = Red Crater. TMC = Te Mari Craters. Solid lines depict the major ferromagnesian minerals; dashed lines represent those present in minor or trace amounts.

Subgroup	Formation	Age (ka)	Member	Volume (km^3)	Probable source	Ferromagnesian minerals oliv cpx opx hbl	SiO_2 wt% glass (gl) or whole-rock (wr)
Tongariro Subgroup	Ngauruhoe Formation & Tufa Trig Formation	0 - 1.8	Tf18 - Tf1	1.3	Ngauruhoe (and RC, TMC) Ruapehu Crater Lake	———	63.6 - 64.5 (gl)
	Mangatawai Tephra	1.8 - 2.5			Principally Ngauruhoe		
	Papakai Formation	2.5 - 9.7	black ash-2 and -1 orange lapilli-2 and -1	1.5	Principally Tama Lakes & northern Tongariro craters, subordinate contribution from Ruapehu		
	Mangamate Formation	9.7 - 9.78	Poutu Lapilli	0.91	Blue Lake	———	
			Wharepu Tephra	0.27	Tama Lakes		
			Ohinepango Tephra		Tama Lakes		
			Waihohonu Lapilli	0.49	Tama Lakes	———	53.7 (wr)
			unnamed tephra				
			Oturere Lapilli	0.48	Tama Lakes	———	
			Te Rato Lapilli	0.10	North Crater	---———	57.2 - 63.5 (wr)
	unnamed tephra	c.9.78 - 10					
	Pahoka Tephra	c.9.8 - 10		0.28	North Crater	---———	59.5 - 63.1 (wr)
Tukino Subgroup	Okupata Tephra	c.10 - 13		0.20	Ruapehu	---——---	
	Rotoaira Lapilli	13.8		0.20	Lower Te Mari Crater	---———	59.0 (gl)
	Bullot Formation	10 - 22.5	Ngamatea lapilli-2 & -1 Pourahu Member Shawcroft Lapilli L18 - L1	0.19	Ruapehu	---——---	54.2 - 72.6 (gl + wr)

Mari Craters, North Crater, Blue Lake, and Ruapehu volcano are recorded in the ring plain fall tephra deposits (Table 3.2). Current work is underway to document the tephrostratigraphy beyond 22.5 ka (e.g. Cronin et al., 1994, 1996).

3.4.2 Dating methods applicable to prehistoric (Holocene) lavas

As mentioned above, the young craters, cones, and lava flows of the proximal part of the complex are principally dated by correlation with associated ring plain tephras (or by observation if they are produced by historic eruptions). Use of the existing tephrochronology provides an effective means of closely estimating the age of most proximal young eruptives, and would be further enhanced by refinement of the tephrostratigraphy.

Dating on a more precise level, however, especially of the numerous prehistoric lava flows of the Tongariro complex, is problematic - but important for constraining petrological models. In leaving the relative certainty of historic eruption accounts to explore the older history of a cone, the eruptive record becomes less complete due both to burial of older lavas by more recent flows and to deeper weathering and erosion. Unless the lava flows are overlapping or superimposed so that their relative ages are readily apparent, it is often difficult to estimate the order in which they were extruded. The relative degree of weathering and/or vegetation of flows is not always a reliable indicator. Useful young ash marker beds are not often present, and when they are they usually only provide a broad guide for distinguishing relatively older and younger flows. Radiocarbon dating and paleomagnetic dating are more reliable techniques for dating Holocene events, but these methods have not been applied to lava flows of the Tongariro complex, and indeed, may not even be suitable.

Most of the prehistoric flows have been erupted from Ngauruhoe and Red Crater. The various approaches used (and those with potential) to reconstruct the prehistoric eruptive history of Ngauruhoe (Section 3.5.8k) and Red Crater (Section 3.5.8i) are described below. The best approximation of the stratigraphic ordering of these flows is

presented in Appendix 2, and has implications for subsequent geochemical modelling (Sections 6.6.8i and k, and Section 7.5).

(a) **Superimposition of flows.** The overlapping relationships between successive lava flows are certainly the most obvious and convenient indicators of relative (although not absolute) age. In Mangatepopo Valley, and to a lesser extent in Waihohonu Valley, some of the Ngauruhoe prehistoric flows may be chronologically ordered in this manner (Fig 3.30A). Battey (1949) was the only previous worker to produce a detailed map of the flows in Mangatepopo Valley, numbered in probable order of extrusion (flows I to XI). His work has been slightly modified in this study; flow II is interpreted to be much younger, and flow XI much older than Battey's (1949) original order (Appendix 2.1). Some of the flows from Red Crater, the five in Oturere Valley, can readily be ordered from inspection of their overlapping relationships evident on an aerial photograph (Fig 3.26; Appendix 2.3), and this was done by Topping (1974).

On both Ngauruhoe and Red Crater, the older flows tend to be those at lowest elevations (many on the valley floors) and greatest distances from source. This is partly a function of burial of shorter older flows higher up on the cones by younger flows, and the fact that there are generally fewer long flows than short ones. Complete burial by younger lavas may have substantially lowered the number of recognised older flows, although this is difficult to evaluate. However, due to the steep upper slopes of especially the Ngauruhoe cone (where not even the proximal ends of historic flows remain) and the prominent geomorphologic expression of the recognised prehistoric flows, it is likely that the present distribution of older lava flows preserved on and around the cones of Ngauruhoe and Red Crater does not differ significantly from the original distribution.

There is a limit to the usefulness of superimposition of lava flows for indicating relative age, however, because many of the prehistoric lavas have flowed down different sectors of the cone (particularly at Ngauruhoe) and there is no way to gauge the relative age of the geographically separate groups of flows. Even within one sector the flows may be positioned side by side so that no overlapping occurs.

(b) **Relative weathering and vegetation of flows.** To some extent the degree of weathering, erosion and vegetation of a lava flow may be taken as a guide to its age relative to other flows (Section 2.2.1a). There are problems inherent to this approach, however, and caution must be exercised when decisions of relative age rest solely on degree of weathering or vegetation. Topping (1974) attempted to order some of the Red Crater flows using degree of weathering judged from chemical analyses of scoria lying on the surface of the flows. The validity of this approach is questionable. Rubin et al. (1987) noted that extrapolation of historical weathering rates to Hawaiian lava flows >1 ka yielded much older dates than those ultimately derived by ^{14}C measurements. The extent of vegetation of a flow surface obviously bears some relationship to the time available for colonisation by plants, but is complicated by the existence of varying microclimates around the volcanic cone (particularly contrasts in rainfall; e.g. Holcomb et al., 1986) - which also affect the degree of chemical weathering.

(c) **Tephra marker beds.** The best young ash marker bed present on the Tongariro complex is the rhyolitic pumice fall and ignimbrite deposit from the 1.8 ka Taupo eruption. Typically small ponds of the Taupo material are preserved sporadically around the proximal part of the complex, beneath or on top of lava flows or within andesitic tephra successions. Occurrences noted during fieldwork for this study include: Waihohonu Valley (T19/377 224; T19/407 201); Tama Lakes (T20/354 196); Mangatepopo Valley (T19/343 249, T19/346 255 and T19/371 257); South Crater (T19/384 254); and Oturere Valley (T19/423 236, T19/417 237, T19/410 258, T19/398 255).

Figure 2.37 shows the typical appearance of Taupo pumice overlying andesitic tephra (Mangatawai Tephra) on a Red Crater lava flow, and Figure 3.6 shows one of the occurrences of thicker (<2 m) valley-ponded Taupo ignimbrite on the large Red Crater flow in Oturere Valley. Topping (1974) measured three tephra sections on Red Crater lava flows (numbers 477, 479, and 481) containing Taupo pumice and Mangatawai Tephra indicating that they were extruded prior to c.2.5 ka. Although the thick Mangamate Tephra (c.9.8 ka) was noted by Topping (1974) elsewhere on eastern Tongariro complex, he did not observe it overlying the Red Crater lavas and therefore concluded that they were younger than 9.8 ka. No Taupo pumice occurs on the Red Crater flows in Central Crater, South Crater

Figure 3.6 Exposure of valley-ponded Taupo ignimbrite on Red Crater lava flow, Oturere Valley (T19/417 237, west of Oturere Hut). The deposit is c.1.5 m thick and comprises yellow to creamy white, massive, matrix-rich ignimbrite containing pumice blocks up to 25 cm. Note person for scale.

and upper NE Oturere Valley and these were considered by Topping (1974) to be <1.8 ka. On his schematic geological map, Topping (1974) mapped the oldest Red Crater flow (filling Oturere Valley) as 3.4-9.7 ka, the next one (to two) oldest as 1.8-3.4 ka, the next 3 oldest (upper Oturere Valley) as 1.8-2.5 ka, and the youngest as 0.5-1.8 ka.

Tephra from the 1.8 ka Taupo eruption has not been observed so frequently on or under the prehistoric Ngauruhoe lava flows. Taupo ignimbrite-derived pumice occurs on one of the oldest flows (TG016) in Mangatepopo Valley, and beneath one of the flows (TG285) in Waihohonu Valley. More thorough searching in the field would possibly reveal more instances of Taupo pumice preserved amongst the lavas, although it appears that the majority of the geomorphologically distinct Ngauruhoe lavas evident today were extruded after 1.8 ka, in the latter part of the cone's lifetime. Topping (1974) notes that the older flows in western Mangatepopo Valley and Makahikatoa Valley overlie Mangatawai Tephra and therefore are >1.8 ka. On Topping's (1974) schematic map he depicts all other Ngauruhoe flows in Mangatepopo Valley as post-1.8 ka which appears reasonable given available field evidence, but his contention that all Makahikatoa and Waihohonu flows are >1.8 ka is not backed up by any evidence and may be pure conjecture, especially since one of the Waihohonu Valley flows can be shown to be post-1.8 ka (see above).

Topping (1974) also used tephra marker beds to date approximately other young lava flows and deposits elsewhere on the Tongariro complex. The large lava flow north of Lower Te Mari Crater is overlain by part of the Papakai Tephra and thus its age was estimated by Topping (1974) to be 6-9.7 ka (Section 3.5.8g). The smaller lava flow NE of Lower Te Mari Crater was thought to be associated with the 13.8 ka Rotoaira Lapilli eruption (Topping, 1974). Topping (1974) described the 14.7 ka rhyolitic Rerewhakaaitu Ash in a tephra section exposed on top of the olivine andesite lava flow erupted from the summit of Pukekaikiore (Section 3.5.8e), and accordingly assigned an age of c.14.7 ka to the Pukekaikiore flow. It does seem rather unlikely that this ash derived from the Okataina Centre could be traced so far south, but until Topping's (1974) tephrostratigraphy is reassessed it is probably best to keep to his interpretation. At Pukeonake scoria cone (Section 3.5.8b), c.22.6 ka Taupo-derived Oruanui Tephra overlies the scoria, providing a minimum age for the final eruptions of the cone (Topping, 1974) which is generally accepted.

(d) Radiocarbon dating. The best method for determining the ages of prehistoric lava flows - which are too young to be directly dated by isotopic analysis - is the technique of radiocarbon dating (Lockwood and Lipman, 1980). Use of the ^{14}C method for dating material beneath lava flows has increased markedly in the last two decades, as demonstrated by the comprehensive data base of radiocarbon dates that now exists for Hawaiian lava flows (Rubin et al., 1987). An example of how ^{14}C dating can greatly enhance understanding of a volcano's eruptive history is provided by the study of Lockwood and Lipman (1987), in which they reconstructed a detailed prehistoric eruptive chronology and made estimations of eruptive rates for Mauna Loa Volcano, based principally on over 140 ^{14}C dates.

Lockwood and Lipman (1980) produced guidelines for the recovery of datable charcoal beneath young Hawaiian pahoehoe and aa basaltic flows. Obviously the first criterion is that living woody material must be present. Although charcoal nearly always forms when forests are buried by lava flows, it usually burns to ash before the overlying flow cools (Lockwood and Lipman, 1980). The favourable circumstances which determine preservation of the charcoal are restricted oxygen circulation or temperatures which remain below about 500°C. Taking these factors into consideration, Lockwood and Lipman (1980) found that carbonised wood (particularly plant rootlets) was commonly preserved beneath all parts of pahoehoe flows (where oxygen availability is restricted), but only beneath the margins of aa flows (where temperatures are lower).

Is there the potential to apply ^{14}C dating to prehistoric lava flows from Ngauruhoe? Surviving natural forest is confined to small scattered localities around the complex; much of the forest cover was removed by Maori and early European fires, and later tussock fires (Topping, 1974; Section 1.2.5). The present day environment around the Ngauruhoe cone is not particularly suited to charcoal formation; vegetation is all but absent on the scree-covered flanks of the cone, and consists mostly of small subalpine mosses and herbs lower down in the valleys (Section 1.2.5). However, some small woody shrubs are present, and these have the potential to be carbonised. McGlone and Topping (1973, 1977, 1983) described the Late Quaternary vegetation history of the Tongariro region; they recognised changing patterns of forest, scrub and grassland distributions. It appears that the past (and

probably the present) nature of vegetation on the Tongariro complex was conducive to at least some charcoal formation beneath over-riding lava flows.

Because the flows are of the brecciated aa and block type, circulating oxygen would inhibit preservation of the charcoal, although the slightly lower temperatures of emplacement of basaltic andesite and andesite lavas (compared to Hawaiian basalts) may enhance charcoal preservation. Because no areas of carbonised organic matter were observed incidentally during sampling of the Ngauruhoe lavas, it is likely that they are only preserved in special local environments which may be difficult to find. However, the great advantage of obtaining absolute ages for prehistoric flows by ^{14}C dating would justify a detailed investigation of the occurrence of datable charcoal beneath any of these lavas.

(e) **Other methods.** Paleomagnetic dating is often a very useful means for dating volcanic rocks. Topping (1974) used the occurrence of reversals of polarity to approximately date several distal lavas of the Tongariro complex, but these were all older than 100 ka. Prehistoric lavas may be dated by using an established reference curve for the secular variation (SV) of the geomagnetic field, a technique which has the potential to exceed the precision of ^{14}C dating (e.g. Holcomb et al., 1986). However, independent age control (usually by radiocarbon dating) is required to constrain the SV curve, and this has precluded the establishment of a reliable, well-constrained SV curve for the Tongariro complex.

The dendrochronology method of dating is seldom applicable to volcanic deposits, but Topping (1974) used tree-ring dating to date the large lava flow which flowed NE from Upper Te Mari Crater. The flow was already known to be younger than the 1.8 ka Taupo pumice. A Hall's totara which grew at the eastern margin of the flow since around the time of lava extrusion was used to provide an approximate age of the Upper Te Mari Crater lava flow of c.450 years (an extrusion date of close to 1528 A.D.) (Topping, 1974).

3.4.3 Historic eruption record

The latest activity on Tongariro Volcanic Complex has occurred in historic times, with records dating back to 1839 and up to as recently as 1975, when the last eruption (from Ngauruhoe) took place. Section 1.6.2 refers to some of the earliest accounts from European travellers and scientists. The region around the Tongariro complex was relatively isolated and inaccessible to the Europeans prior to the completion of the railway and improvement of accommodation facilities in the early 1900s. For this reason, some uncertainty exists about details of some of the earliest reported eruptions, particularly those of last century. Nevertheless, the historic eruption record is overall very good and a valuable means by which to constrain the time dimension in petrological models of the immediate past and present magma reservoir dynamics beneath the Tongariro complex.

Most historic eruptions have been from Ngauruhoe, but Red Crater and Upper Te Mari Crater have also been active since observations were recorded. Ash and steam eruptions were reported from Red Crater in 1855, 1859, ?1885-1887 and ?1890 (summarised in Gregg, 1960; Cole and Nairn, 1975). During the 1926 eruption of Ngauruhoe, Red Crater was also reported in eruption (Cullen, 1926), but this is probably erroneous since newspaper reports from other perspectives around the mountain described the steam plume from Ngauruhoe drifting across Red Crater, which most likely gave it the appearance of also being in eruption from a viewpoint in Turangi (D.M. Johnston, pers. comm., 1994). Upper Te Mari Crater produced eruptions (of mostly steam, Section 2.3.2c) in 1869, 1886, 1888, 1892-1893 and 1896 (summarised by Gregg, 1960; Cole and Nairn, 1975).

Ngauruhoe has been intermittently active since the first steam eruption was recorded in 1839; over 60 eruptive episodes of strombolian-vulcanian (Sections 2.2.2b, 2.2.3a, 2.3.2b & d) and effusive styles (Sections 2.2.1a, 2.3.1a) have occurred in the last 150 years or so (Cole and Nairn, 1975). Many eruptions were confined to steam or ash emissions, but lava flows were extruded in 1870 (Gregg, 1960), 1949 (Allen, 1949; Battey, 1949) and 1954 (Gregg, 1956), and pyroclastic avalanches in 1974-1975 (Nairn et al., 1976; Nairn and Self, 1978). A scoria cone was built up in the inner crater during the 1954-1955 eruption, and the crater morphology has undergone many changes since observations began (Gregg,

1960). Since the 1975 eruption, activity at Ngauruhoe has reached an all time low with only weak fumarolic activity (Otway, 1994b). The 20 years which have elapsed since the last Ngauruhoe eruption represent the longest period in the last 150 years without an eruption.

3.5 VOLCANO-STRATIGRAPHIC UNITS

3.5.1 Introduction

As discussed in Section 1.1.2, magmatic models are most viable when set in the context of the eruptive history of the volcano. For the Tongariro Volcanic Complex, the integration of geochronology with petrology has been made possible by a new K-Ar dating programme, in association with detailed field investigations. And rather than just dividing the eruptive products into broad stages in the development of the complex, the available data have enabled a more comprehensive volcano-stratigraphy to be developed (Section 3.2.3).

These units are summarised in Table 3.3, depicted in schematic map form in Figure 3.2, and described in full in Sections 3.5.2 - 3.5.8. The volcano-stratigraphic map (back pocket, Volume 2) shows in more detail the data for lava flow direction which were used, in conjunction with inferred vent areas and K-Ar ages, to define the boundaries of the older units (Sections 3.2.2 and 3.2.3). For each volcano-stratigraphic unit, the location and areal extent of outcrop, together with the unit age and duration of cone-building are described. Volume estimates for the present and original cone edifices are also presented (Table 3.3). The estimated present volumes do not sum to the total present volume of 60 km^3 for the cone complex (Section 1.2.2) because the calculations for individual units do not account for those portions of the stratigraphy not exposed at the surface.

The volume and age data were used to calculate the approximate long-term magma eruption rate over the lifetime of each major cone (Table 3.3); information which has implications for the dynamics of the sub-volcanic plumbing system (including perhaps

Table 3.3 Summary of volcano-stratigraphic units of Tongariro Volcanic Complex. Ages of the 11 young eruptive units (Ngauruhoe to Young NE Oturere) inferred from tephrostratigraphy and tephrochronology; ages of the 6 older cone-building sequences (TongariroTrig to Tama 1) derived from K-Ar age data. Note that estimates of original volumes for the young eruptive units are believed to be close approximations to reality, whereas errors are attached to the estimates for the older cone-forming units because the original dimensions of the older cones are less certain. Eruptive rates are average magma production rates for the major cones; see Table 3.4 for inferred instantaneous magma production rates for some of the younger, single large explosive events.

Volcano-stratigraphic unit	Map label	Approximate age (ka)	Estimated present volume (km^3)	Estimated original volume (km^3)	Approximate eruptive rate (km^3/ka)	Approx. number of exposed lava flows/ pyroclastic units	Location of known vent(s) or inferred vent area(s)	Composition (rock type and wt% SiO_2)	Proximal (and distal where known) eruptive products
Ngauruhoe	ng	0 - 2.5	2.2	2.2	0.88	80	summit crater of cone (T19/375 242)	basaltic andesite - andesite 54.2 - 58.6 wt% SiO_2	Aa to block lava flows, scoria cone within summit crater, (1954-55), pyroclastic avalanches (1974-75), ballistic blocks, tephra of Ngauruhoe Formation and Mangatawai Tephra
South Crater explosion pit	scp	1.8 - c.2	<<0.01	<<0.01		<<5	southern end of South Crater, between Ngauruhoe and Red Crater (T19/386 256)	andesite 57.8 wt% SiO_2	Scoria bomb and block deposit
Red Crater	rc	0 - c.3	0.3	0.3	0.1	15	summit crater of cone (T19/392 264), and Emerald Lakes (T19/395 266, T19/398 267) - 250m and 500m NE of Red Crater	basaltic andesite - andesite 53.0 - 61.1 wt% SiO_2	Transitional pahoehoe to aa and aa to block lava flows, scoria cone, dikes, tephra of Ngauruhoe Formation (and Mangatawai Tephra?)
Tama Lakes	tl	c.10	0.1	0.1		10	upper lake (T19/362 211, T19/366 210), lower lake (T20/352 193), and craters between the lakes (T19/361 203, T19/353 201, T20/350 199)	basaltic andesite - dacite 56.1 - 64.2 wt% SiO_2	Pumice-lapilli-ash fall deposits, scoria bombs, welded scoria fall deposits, tephra of Papakai Formation and Mangamate Formation
Te Mari Craters	tm	0 - 14+	0.2	0.2		15	upper (T19/410 293) and lower (T19/412 299) craters, and explosion pits (T19/414 305, T19/415 306, T19/416 305) - 500m NE of Lower Te Mari Crater	andesite 57.5 - 60.2 wt% SiO_2	Lava flows, ballistic blocks, vent tuff breccia in upper crater, tephra of Ngauruhoe Formation, ?Papakai Formation and Rotoaira Lapilli
Young SW Oturere	yso	c.10 - 14	<<0.01	<<0.01		<5	about 1km south of Red Crater in SW Oturere Valley (T19/394 253)	basaltic andesite - andesite 55.0 - 57.4 wt% SiO_2	Welded scoria fall deposit
Young Pukekaikiore	ypk	c.15	<0.1	<0.1		<5	scoria mound on summit of Pukekaikiore (T19/352 245)	andesite 56.9 - 57.4 wt% SiO_2	Scoria mound, lava flows
North Crater	nc	10 - c.15	0.5	0.5		25	centre of flat-topped crater (T19/388 283), and explosion pit in west part of crater (T19/385 284)	basaltic andesite - andesite 56.3 - 60.1 wt% SiO_2	Welded tuffs and agglutinates (spatter fall; some rheomorphic), lava spatter cone, solidified lava lake, scoria fall and flow deposits, ballistic blocks, tephra of Mangamate Formation (Te Rato Lapilli) and Pahoka Tephra

(continued over)

Table 3.3 (continued) Summary of volcano-stratigraphic units of Tongariro Volcanic Complex. Ages of the 11 young eruptive units (Ngauruhoe to Young NE Oturere) inferred from tephrostratigraphy and tephrochronology; ages of the 6 older cone-building sequences (TongariroTrig to Tama 1) derived from K-Ar age data. Note that estimates of original volumes for the young eruptive units are believed to be close approximations to reality, whereas errors are attached to the estimates for the older cone-forming units because the original dimensions of the older cones are less certain. Eruptive rates are average magma production rates for the major cones; see Table 3.4 for inferred instantaneous magma production rates for some of the younger, single large explosive events.

Volcano-stratigraphic unit	Map label	Approximate age (ka)	Estimated present volume (km^3)	Estimated original volume (km^3)	Approximate eruptive rate (km^3/ka)	Approx. number of exposed lava flows/ pyroclastic units	Location of known vent(s) or inferred vent area(s)	Composition (rock type and wt% SiO_2)	Proximal (and distal where known) eruptive products
Blue Lake	bl	10 - c.20	0.1	0.1		15	lake-filled crater (T19/400 277)	andesite 56.8 - 59.9 wt% SiO_2	Welded tuffs and agglutinates (spatter fall; some rheomorphic), lava spatter cone, scoria fall deposits, ballistic blocks, tephra from Mangamate Formation (Poutu Lapilli)
Pukeonake	pn	c.23	0.3	0.5		10	centre of scoria cone (T19/320 258), and two smaller cone remnants (T19/321 266, T19/322 269) - 750m and 1km north of Pukeonake	basaltic andesite 56.5 - 57.0 wt% SiO_2	Scoria cone, lava flows
Young NE Oturere	yno	c.20+	<<0.01	<<0.01		<5	north of Oturere Valley, about 1km NE of Blue Lake (T19/411 280)	andesite 57.6 - 58.1 wt% SiO_2	Welded scoria fall deposit
Tongariro Trig	tt	65 - 110	10 ± 4	12 ± 5	0.27 ± 0.11	45	area eastwards along ridge from Tongariro trig (centred on T19/385 271)	andesite - dacite 57.0 - 62.3 wt% SiO_2	Welded tuffs and agglutinates (spatter fall; some rheomorphic), lava flows, scoriaceous tuff breccias, lapilli tuff, vent breccias
SW Oturere	so	70 - 115	3 ± 1	5 ± 2	0.11 ± 0.05	65	at least 2 areas in SW wall of Oturere Valley: c.0.5km south of Red Crater (T19/398 251) and c.1.5km SE of Red Crater (T19/391 257)	andesite - dacite 57.2 - 65.5 wt% SiO_2	Lava flows (some ponded and overthickened), welded agglutinates, scoria cone, tuff breccias
Pukekaikiore	pk	120 - 190	2 ± 0.5	6 ± 2	0.09 ± 0.02	15	probably c.1km NE of present-day summit of Pukekaikiore (T19/362 249)	basaltic andesite - andesite 59.8 - 61.8 wt% SiO_2	Lava flows (some ponded and overthickened)
Tama 2	t2	200 - 210	6 ± 1	10 ± 2	1.00 ± 0.20	55	c.0.5km south of Ngauruhoe crater (area centred on T19/375 235)	basaltic andesite - andesite 56.4 - 63.0 wt% SiO_2	Lava flows, pumice flow deposit, tuff breccias
NE Oturere	no	90 - 250	5 ± 1	11 ± 2	0.37 ± 0.07 (applies to main period 100-130ka)	75	at least 2 areas in NE wall, Oturere Valley: c.1km east of Red Crater (T19/403 266) & c.2km east of Red Crater (T19/411 261)	basaltic andesite - andesite 55.4 - 62.2 wt% SiO_2	Lava flows, welded agglutinates, tuffaceous scoria cone, pyroclastic surge deposits, tuff breccias, scoria fall deposits
Tama 1	t1	215 - 275	1 ± 0.5	2 ± 1	0.03 ± 0.02	10	probably centred on lava dome 1km SW of Upper Tama Lake (T19/358 204)	andesite 59.5 - 62.6 wt% SiO_2	Lava flows and domes

variable crust thickness, local stress regimes) and the constraints operating on petrological processes. The relationship between magma composition and eruptive rate is explored in Chapter 6. Because the volume estimates essentially ignore the volume of pyroclastics and reworked material lost to the ring plain (and beyond), the calculated rate is perhaps more accurately described as the *rate of cone growth* rather than *eruptive rate*. It is difficult to incorporate a rate of explosive activity to obtain a true eruptive rate with time. Note that it was not appropriate to calculate an average magma production rate for most of the young eruptives. These units instead provide a window into the instantaneous eruptive rates of discrete events (Table 3.4; Section 3.5.8), as opposed to the average rates calculated for the larger cones - which combine high discharge explosive events with slower background magma production (lava flows, cone construction, and intervals of non-eruption). The number of (exposed) lava flows within each unit (Table 3.3) also gives an impression of the frequency of eruption. The volume-time relationships for the Tongariro complex as a whole are discussed in Section 3.6.2.

The eruptive products and styles of volcanism displayed by each cone (as represented by each volcano-stratigraphic unit) are also described. Because of the tendency for products of the most explosive phases of activity to be preserved only on the ring plain (Section 2.1), it is generally difficult to assess the role of (particularly) subplinian-plinian style eruptions for the older cones (for which ring plain tephrostratigraphy has not been established). The nature of the available outcrops and the extent of sampling of each unit are noted. The sampling sequences for stratigraphic sections (Appendix 2) are referred to. The composition of the eruptive products from each unit, in terms of rock type and SiO_2 range, is summarised in Table 3.3 and Figure 3.7, and remarked upon for each unit in the following sections.

Figure 3.7 Samples from Tongariro Volcanic Complex according to rock type (TAS classification) and volcano-stratigraphic unit.

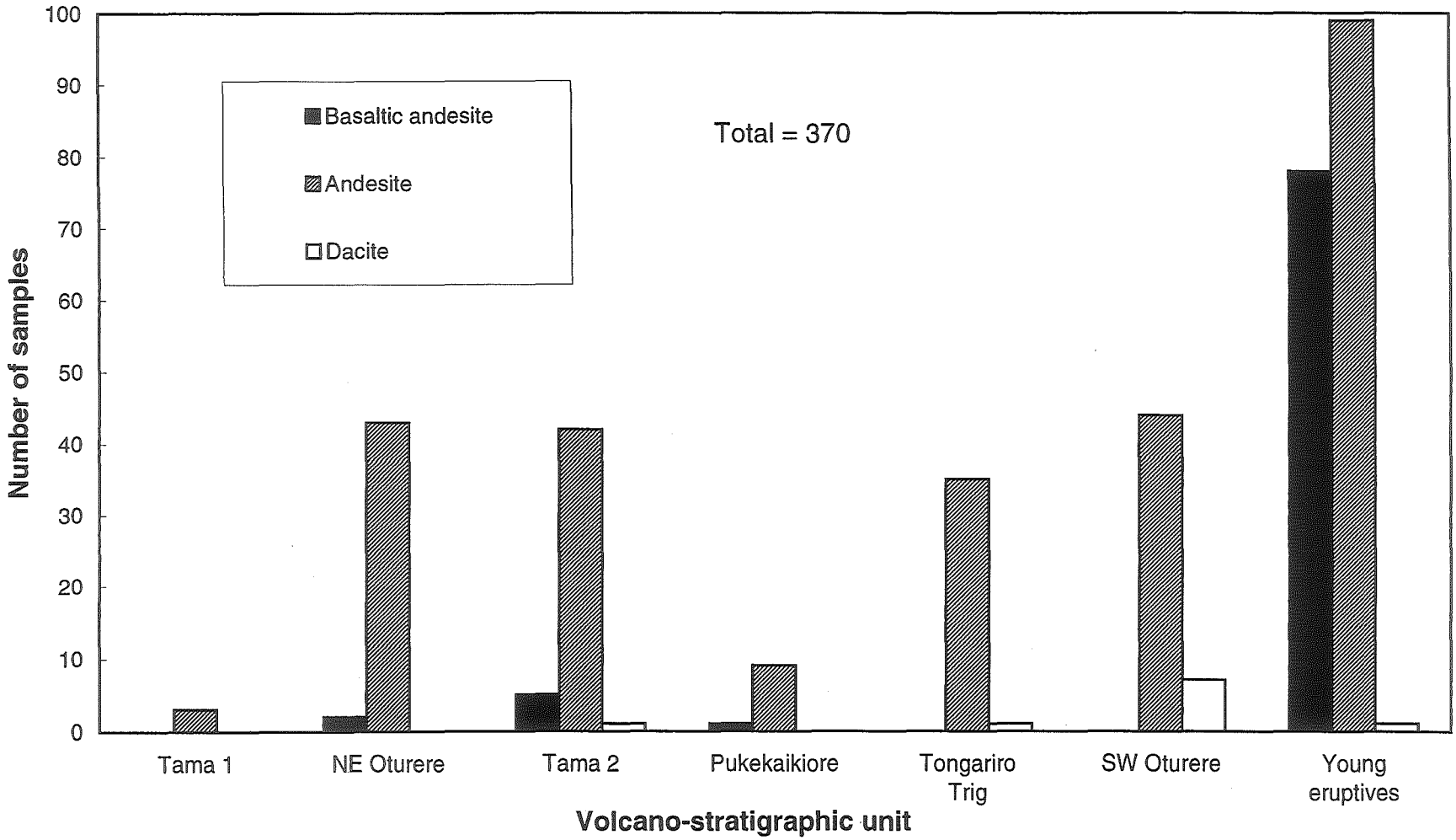

3.5.2 Tama 1 [*t1*] (215-275 ka)

(a) Stratigraphy. The low ridges preserved between the explosion craters of the Tama Lakes area in the southwest (Figs 3.2, 3.8 and 3.11) are the oldest exposed rocks on the Tongariro complex, yielding ages between 273±22 ka and 216±14 ka (Table 3.1). Construction of the Tama 1 cone therefore lasted for at least 60 ka. Note that the young Ruapehu lavas exposed in the walls of the Lower Tama Lake crater were erroneously assumed by Wahyudin (1993) to be the oldest lavas outcropping in the Tama Lakes area. The present small area (3 km^2) and volume (c.1 km^3) of the cone remnants, together with the dominance of scree over in situ outcrops, meant that sampling of this unit was more limited than for the other units and a detailed internal stratigraphy could not be established (see Appendix 2.17). Tama 1 eruptives are silicic andesites ranging from 59.5 to 62.6 wt% SiO_2.

(b) Lithofacies. Lava flows and domes, only about 10 of which are preserved, represent the proximal eruptive products of the Tama 1 cone (Table 3.3). Little evidence of the original morphology of the lava flows is preserved, and they are typically quite weathered. The youngest dated sample (TG028; 216±14 ka) is from a small (c.250 m diameter, c.100 m high) silicic andesite dome (Section 2.2.1b, Fig 2.16) situated between Upper and Lower Tama Lakes, which displays conspicuous cm-scale flow banding.

(c) Discussion. The dome probably represents the youngest product erupted and marks the vent area for the Tama 1 cone in general (Fig 3.4). Along with quiet effusion of lava flows and domes, explosive dome destruction also probably occurred, which may explain the origin of the oldest (c.273 ka) samples (TG046, TG136) which are hornblende andesite fragments found only as scree. The original extent of this early cone is difficult to estimate because of concealment beneath younger lavas from Ruapehu in the south (37±5 ka, Appendix 15) and from Tama 2 in the north, removal of material during the c.10 ka Tama Lakes explosive episode, and general erosion of the cone. An estimated original volume of c.2 km^3 gives an approximate eruptive rate of 0.03 km^3/ka, the lowest of the cone-building units (Table 3.3).

Figure 3.8 View of south side of Tama 1 cone remnants, looking towards the north with Ngauruhoe in the background. North side of Lower Tama Lake and two other c.10 ka explosion craters are visible in middle distance. Photo courtesy of I.A. Nairn, GNS Wairakei.

3.5.3 Northeastern Oturere [*no*] (90-250 ka)

(a) Stratigraphy.

Introduction: geography and spatial extent

Possibly whilst the Tama 1 cone was still active in the southern part of the complex, the Northeastern Oturere cone(s) began to form in the north - now represented by the thick sequence of at least 75 andesitic lava flows and intercalated pyroclastic units preserved in the NE wall of the valley (Figs 1.7, 3.2, 3.9, 3.10). The present remnants of the cone cover 26 km^2 and have an approximate volume of 5 km^3 (Table 3.3). Most of the outcrop is concentrated in the steep, 200-300 m high walls of the NE side of the Oturere valley, providing an opportunity for detailed stratigraphic sampling (Appendix 2.16).

Internal stratigraphy

The sequence has been subdivided into 8 discrete packets (subunits 'a' to 'h') within each of which consistent stratigraphic relationships can be determined. Each packet is bounded by unconformities to adjacent packages, and angular unconformities also occur within some packages - notably subunit 'd' (Appendix 2.16).

Age relationships

The majority of dated lavas fall into a rapid cone-building period which took place between 130 and 100 ka (Fig 3.5). Because they do not all fit well with the inferred stratigraphic relationships, several of the older K-Ar ages are viewed with caution and may in fact represent erroneous age determinations due to excess argon. Further K-Ar dating of adjacent samples is being carried out to test the validity of these older ages. The oldest dated lavas occur at localities along the length of the valley wall (Fig 3.1); at the lower end (TG048, 247±10 ka), towards the middle (TG111, 229±11 ka), and in the upper part (TG400, 202±23 ka). An upper scoria sequence described below (TG120-TG248) and an underlying stack of lavas (TG114-119), illustrated in Fig 3.9, comprise c.200 m of continuous stratigraphy which was erupted at essentially the same time (three K-Ar dates all within error; 128±12 ka, 123±10 ka, 122±10 ka).

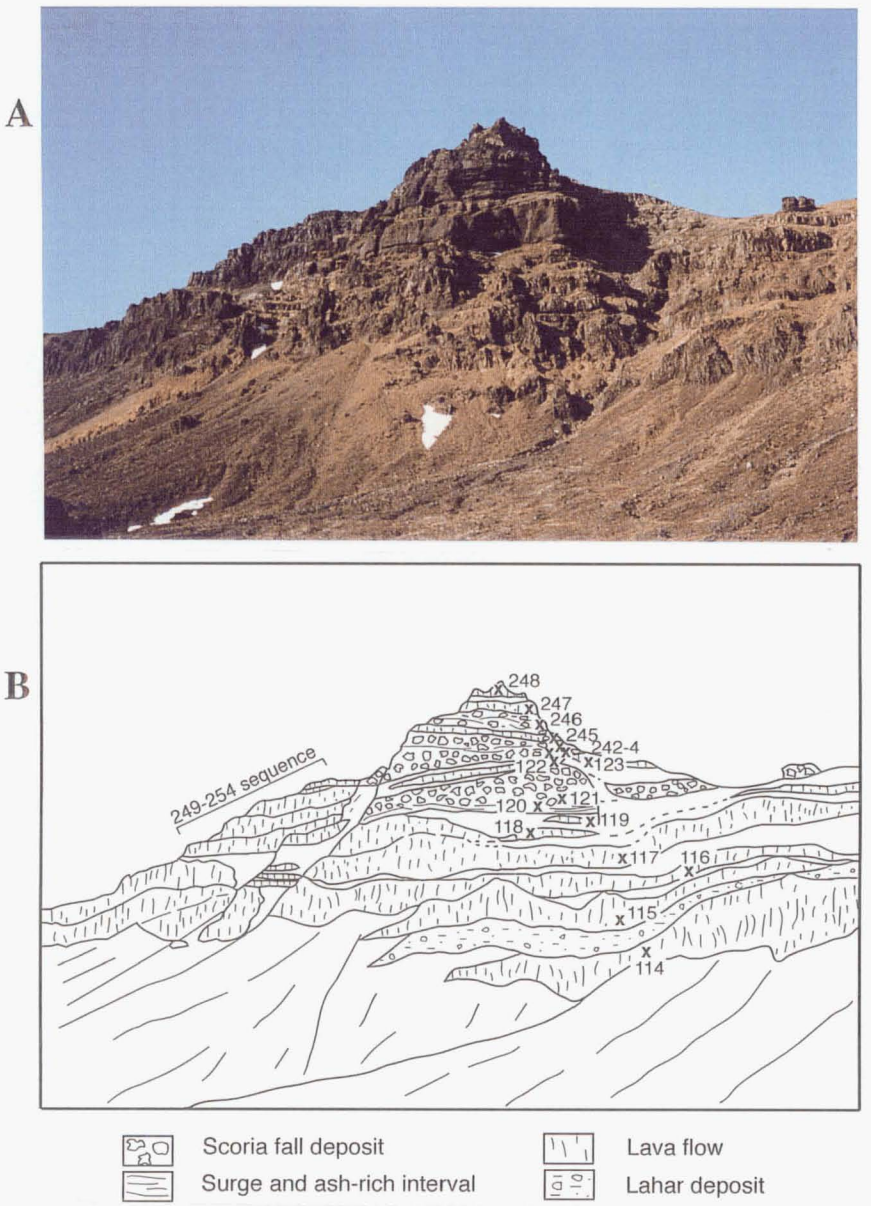

Figure 3.9 View of part of subunit 'd' of NE Oturere stratigraphy, showing a c.200m thick vertical sequence of lavas and volcaniclastic deposits. Numbered sample locations are marked with a cross (all have TG prefix).

Figure 3.10 View of upper NE Oturere Valley wall, looking east towards the Kaimanawa ranges. note the angular unconformities separating packages of lava and scoria.

Chemistry

The vast majority of NE Oturere eruptive products are andesitic - only a few basaltic andesite lava flows have been identified (Fig 3.7) - and they span a compositional range of 55.4-62.2 wt% SiO_2 (Table 3.3). The thick lava-scoria section of subunit 'd' provides an opportunity for detailed magmatic stratigraphy (Sections 4.8, 6.6.3c and 7.5.4).

(b) Lithofacies.

Sheet/autobrecciated lavas

The numerous autobrecciated lava flows range in thickness from 2 to 30 m (similar to the overall range for older Tongariro lavas, Section 2.2.1a), but are typically 3-8 m thick and display blocky to platey jointing. The lava flows are not laterally continuous along the entire length of the valley wall but form lenses of sheet lava enclosed in envelopes of autobreccia, and rarely pyroclastic material.

Scoria cones

A scoria cone sequence occurs in a c.250 m thick section of lava flows (Figs 3.9 and 3.10) labelled subunit 'd' of the NE Oturere stratigraphy described in Appendix 2.16. Angular unconformities between the packages of lava flows and scoria deposits allow further subdivision of subunit 'd' (Fig 3.10; Appendix 2.16), although they do not necessarily indicate a large time break if they are merely a function of lavas banking up against the depositional slope of a wedge of scoria. Mathews (1967) also drew attention to this internal structure evident in the NE Oturere valley wall. The 40 m+ thick scoria cone (Figs 2.32 and 3.9, Section 2.2.2b) with intercalated phreatomagmatic surge beds and ash-rich intervals (Fig 2.43, Section 2.2.3f) occurs sandwiched between lava flows (TG119 at the base; TG247 at the top). Lava flows are also contained within the scoria sequence (TG122, TG123, TG245).

Laharic tuff breccias

Near the base of the subunit 'd' section a c.3 m thick, orange-brown, poorly-sorted tuff breccia occurs between two lava flows (TG114 and TG115; Figs 2.46 and 3.9). The breccia, considered to be of laharic origin (Section 2.2.4b), consists of subangular to rounded <2 m-diameter boulders of massive non-vesicular andesite set in a fine to coarse ash matrix.

Proximal fall deposits

In the head of the valley, intensely-welded agglutinates and near-vent tuff breccias (partly visible in foreground of Fig 3.10) have been sampled as subunits 'a' (104±13 ka) and 'b' (202±23 ka) of the NE Oturere stratigraphy (Appendix 2.16). The spatter-fed agglutinate deposits of subunit 'a' display extreme flattening of clasts and are interpreted to be very proximal. The tuff breccias have been hydrothermally-altered to white-orange colours, and comprise a chaotic unsorted deposit of metre-sized dark magmatic blocks/bombs, lithic clasts, and ash matrix.

Phreatomagmatic surge deposits

Bedded lithic-rich lapilli tuff units (Fig 2.44) within subunit 'b' are thought to represent phreatomagmatic surge beds (Section 2.2.3f).

(c) **Discussion.**

Original cone geometry

The lava flows generally have low to moderate dips (8-27°), and the dip direction swings round from towards the NW and N in the head of the valley to towards the NE and E further down the valley (see map, back pocket, Volume 2). These lava flows are believed to have flowed from a (now mostly eroded) central vent to the west of the valley wall (Fig 3.4), in the area now occupied by the Oturere Valley. Part of this central vent and flank vents, however, are preserved in the NE wall in the form of scoria fall deposits, welded agglutinates and hydrothermally-altered vent breccias.

Eruptive style

In summary, the andesitic eruptive products of the NE Oturere cone represent a wide range of eruptive styles possibly operating over a considerable period of time, which have created a complex stratigraphy of alternating lavas and pyroclastics. Quiet effusion of lava flows has been the dominant style of activity. However, significant volumes of welded spatter and scoria fall deposits also signify that Hawaiian- to Strombolian-style volcanism (Sections 2.3.2a & b) has played a role in the growth of the NE Oturere cone. In addition, occasional magma-water interaction has triggered episodes of phreatomagmatic activity, producing surge and co-surge fall deposits (Section 2.3.2c).

Erupted volume and eruptive rate

The combination of deep glacial erosion of the Oturere Valley and general erosion of the edifice is assumed to have removed a substantial proportion of the NE Oturere cone, which probably had an original volume of around 11 km^3 (Table 3.3). For the main cone-building period of 100-130 ka, a moderate eruptive rate of approximately 0.37 km^3/ka has been calculated (Table 3.3). Recognition of at least 75 separately distinguishable lava flow and pyroclastic units (Table 3.3, Appendix 2.16) attests to the high frequency of eruption during certain periods of cone growth.

3.5.4 Tama 2 [*t2*] (200-210 ka)

(a) Stratigraphy. Concurrent with the early NE Oturere activity, and after cessation of Tama 1 cone-building, a major cone (Tama 2) formed over much of the southern part of the Tongariro complex between 209±16 ka and 203±11 ka (Table 3.1). At least 55 lavas across the breadth of the 17 km^2 remaining outcrop of the Tama 2 cone (Fig 3.1) cluster tightly within this c.10 ka period (Fig 3.5). No continuous thick stratigraphic sections are preserved, but most of the lavas could be sampled within the context of small groups of stacked flow units (subunits 'a' to 'l'; Appendix 2.15).The Tama 2 cone mostly erupted hornblende-bearing andesite lavas with minor basaltic andesite flows, covering a compositional range of 56.0-63.0 wt% SiO_2 (Fig 3.7, Table 3.3).

(b) Lithofacies. The lavas are exposed along ridges north of upper Tama Lake (subunits 'd'-'g', 'j'), and to the west on Tama trig (subunit 'l') and the SW wall of Waihohonu valley (subunit 'a') (Fig 3.11), as well as a smaller eroded remnant on the NE Waihohonu Valley wall (subunit 'h'). The flows are typically 2-6 m thick (range 2-20 m), and blocky- to columnar-jointed. Two outcrops of hydrothermally-altered lavas and poorly-sorted tuff breccias (subunits 'b' and 'c', e.g. Fig 3.12) are exposed as windows into the upper slopes of the Ngauruhoe cone.

(c) Discussion. The lava flows dip away to the S-SW to form a preserved flank from the mostly eroded large cone. The now-concealed central vent is located beneath the Ngauruhoe cone to the south of the present crater (Fig 3.4).The hydrothermally-altered lavas and breccias probably represent eroded flank vents of the Tama 2 cone (one of which,

Figure 3.11 View from Ngauruhoe summit of the south part of the Tongariro complex. Waihohonu Valley is in the foreground; the valley wall, Tama trig ridge (centre left), and ridges north of Upper Tama Lake comprise the outcrops of the Tama 2 cone. Tama 1 lavas are preserved in the ridges between the Upper and Lower Tama Lakes. Ruapehu volcano is in the background.

Figure 3.12 Window of Tama 2 hydrothermally-altered lavas and tuff breccias (TG371-373) exposed in the SW flank of Ngauruhoe, near the inferred location of the now-concealed central vent for the Tama 2 cone.

subunit 'b', was also mapped as an old vent by Mathews, 1967). Apart from the dominant mode of eruptive style, lava flow effusion, evidence for at least one small volume ignimbrite-producing eruption is preserved near Tama trig (subunit 'i'; Section 2.2.3d) Significant erosion of the Tama 2 cone (and its partial concealment beneath the Ngauruhoe cone) has reduced its dimensions from a probable original volume of c.10 km^3 to a present estimated volume of c.6 km^3 (Table 3.3). With at least 55 recognised lava flows and an eruptive rate of around 1.0 km^3/ka (Table 3.3), the Tama 2 cone represents the most rapid eruptive episode in the history of cone-building on the Tongariro complex.

3.5.5 Pukekaikiore [*pk*] (120-190 ka)

(a) Stratigraphy. Soon after activity had ceased at the Tama 2 cone, and whilst the NE Oturere cone was still active, another major cone (Pukekaikiore) grew in the west part of the complex (Figs 3.2 and 3.28). The c.70 ka lifespan of Pukekaikiore is bracketed by the ages 190±9 ka and 121±23 ka (Table 3.1), but more age determinations are required to clarify the history and internal stratigraphic relationships of this cone. The eroded edifice of the Pukekaikiore cone is a crescent-shaped hill situated west of Ngauruhoe (Fig 3.13; subunit 'a', Appendix 2.14), in addition to some scattered outcrops in Makahikatoa Valley to the south (subunit 'b'). The present area (6 km^2) and volume (c.2 km^3) of the Pukekaikiore cone rank it as the second smallest (after Tama 1) of the pre-glacial cones preserved on the Tongariro complex. Relatively limited sampling opportunities are afforded by the c.15 (predominantly andesitic; Fig 3.7) lava flows identified on the present cone, which range from 55.6 to 61.8 wt% SiO_2 (Table 3.3).

(b) Lithofacies. Exposures on Pukekaikiore are dominated by the thick (<100+ m) lavas outcropping around the margins which are either approaching a coulée-type with massive distorted jointing (Fig 2.17, Section 2.2.1b), or are more regularly columnar-jointed lavas (Fig 2.13, Section 2.2.1a).

(c) Discussion. The Pukekaikiore lavas dip away from the inferred vent area situated to the east of the cone (Fig 3.4) and are now buried by Ngauruhoe lavas. Topping (1974) tentatively suggested that Pukekaikiore represented a multiple flow cumulodome.

Figure 3.13 The eroded remnants of the Pukekaikiore cone, as viewed from the summit of Ngauruhoe looking west. Dark Ngauruhoe 1954 lava flows encroach on Pukekaikiore hill in the foreground. The small scoria cone of Pukeonake is visible in the background, to the left of Mangatepopo Road.

Figure 3.14 Part of the SW Oturere cone; over 100 m of alternate autobrecciated lava flows and bedded pyroclastic units exposed in the upper valley wall. Black tack-welded scoria deposit (TG176) at top of sequence represents the Young SW Oturere volcano-stratigraphic unit.

Patterson (1986) recognised Pukekaikiore as the remnant of an old cone separate from the Tongariro trig area, although he suggested that the vent was on the top of Pukekaikiore hill, near the young Pukekaikiore vent. He also rather dubiously inferred the complexly-jointed overthickened eastern lavas to represent many thin, rapidly cooled flow units (Patterson, 1986). Assuming that considerable erosion has occurred (to form Mangatepopo Valley) and that part of the Pukekaikiore cone is concealed beneath Ngauruhoe, the original volume of the Pukekaikiore cone is estimated at about 6 km^3, which manifests as a low eruptive rate of approximately 0.09 km^3/ka (Table 3.3).

3.5.6 Southwestern Oturere [*so*] (70-115 ka)

(a) Stratigraphy.

Introduction: geography and spatial extent

After the Pukekaikiore cone became inactive, and near the tail end of cone-forming eruptions at the NE Oturere cone, eruptive activity shifted to the middle-SE sector of the complex (Fig 3.2).The main outcrops of the eroded cone occur along the length of the SW wall of the Oturere Valley (subunits 'b'-'f', Appendix 2.13; Figs 2.18, 3.14, 3.25), in addition to exposures in the upper NE (subunits 'g' & 'i') and lower SW (subunit 'h') Waihohonu Valley and the South Crater - Oturere Valley saddle (subunits 'a'-'b'). The SW Oturere lavas travelled down a probably already glacially-eroded valley which had left a remnant of Tama 2 cone lavas now preserved in the NE Waihohonu Valley wall (Fig 3.2). The present area covered by the SW Oturere cone is about 26 km^2 and the present volume is estimated at 3 km^3 (Table 3.3).

Internal stratigraphy

At least 65 lava flows and pyroclastic units are recognised, and these have been subdivided into 9 discrete packets (subunits 'a' to 'i'; Appendix 2.13), some of which are divided internally by angular unconformities (e.g. subunit 'b').

Age relationships

The SW Oturere cone began to form at around 114±9 ka and grew for c.45 ka until about 68±11 ka (Table 3.1). A number of stratigraphic sequences have been identified along the length of the valley wall (subunits 'b' to 'f', Appendix 2.13). The older flows occur near

the lower end of the valley (subunit 'f'; 114±9 ka, 97±10 ka, 87±10 ka). Slightly younger overall packages of lavas are exposed in the mid-valley sections (subunits 'c' & 'd'; 109±13 ka, 103±12 ka, 77±14 ka), and the upper valley contains some of the youngest lavas (subunit 'b'; 81±17 ka, 68±11 ka). There is a pronounced unconformity (and probably quite large age difference) between the lower lavas of subunit 'b' (TG228-235) and the overlying agglutinate and scoria deposits (TG236-240). It is unclear whether or not there is also an unconformity between the lower overthickened (coulée-type) lavas at the base of subunit 'b' and the lavas of the vent area (subunit 'c') further to the south along the valley wall. Lavas exposed near the present western limits of the cone (subunits 'g'-'i') are of intermediate ages (95±10 ka to 91±9 ka).

Chemistry

The predominant rock type is andesite, although a small proportion of dacite lava does occur (Fig 3.7). SW Oturere eruptives are among the most silicic on the complex, ranging from 57.2 to 65.5 wt% SiO_2 (Table 3.3).

(b) Lithofacies.

Sheet/autobrecciated lavas

Lava flow thicknesses vary from 2 to 50 m, and contrasting overthickened flows (coulées) and thin flows often occur in the same sequence (Fig 2.18). Autobrecciated flow margins are common (Fig 2.10). Many flows display blocky jointing, and many have well-developed platey jointing (Fig 2.14) and flow banding (Fig 2.15) (Section 2.2.1a).

Scoria cone

A small (c.20m thick) scoria cone deposit (TG240) tops a sequence of lava flows and welded agglutinates (subunit 'b') in the upper part of the valley. The deposit consists of dm-bedded, oxidised and welded scoria bombs, with dense angular lithics up to 1m diameter.

Proximal fall and vent breccia deposits

A pyramidal outcrop of welded agglutinates and lava (TG236-239) occurs near the head of the valley (part of subunit 'b'). Also in the head of the valley, on the saddle between South Crater and Oturere Valley, hydrothermally-altered breccias are exposed which comprise both andesite clasts and dense angular lithic blocks (<0.5m). Rare dikes exposed

in the walls of SW Oturere Valley are associated with areas of intense hydrothermal alteration and steeply-dipping units (Fig 2.21) believed to indicate the location of an old vent area

Epiclastic deposits

Epiclastic deposits of lahars and hyperconcentrated streams are also a feature of the SW Oturere stratigraphy (Section 2.2.4b). For example, site TG160 comprises a c.2m thick, dm-bedded, well-sorted, matrix-poor fluvial conglomerate, and a 3-4m thick poorly bedded, matrix-rich lahar/debris avalanche deposit..

(c) Discussion.

Original cone geometry

Lava flow directions and flow banding measurements indicate opposing and often steep (<86°) dips (see map, back pocket, Volume 2) in areas also characterised by hydrothermally-altered breccias and dike-like intrusive bodies (Fig 2.21). At least two of these areas, in the mid-upper valley (subunit 'c') and near the South Crater-Oturere saddle (subunit 'b'), are assumed to be close to vents (Fig 3.4). Mathews (1967) recognised the same two vent areas as cores of earlier cones.

Eruptive style

Lava flow effusion was joined in many places by Hawaiian-Strombolian spatter-scoria fall activity (Sections 2.3.2a & b), evident as intercalated units (e.g. Fig 3.14) or discrete scoria cones (e.g. TG240, back from the upper valley wall).

Erupted volume and eruptive rate

Considerable erosion of the SW Oturere cone removed material from the Oturere and Waihohonu Valley areas, and part of the cone is probably buried beneath the east flanks of the Ngauruhoe cone. Taking into consideration an original volume of approximately 5 km^3, a relatively low eruptive rate of c.0.11 km^3/ka is implied (Table 3.3).

3.5.7 Tongariro Trig [*tt*] (65-110 ka)

(a) Stratigraphy. The last of the older pre-glacial cones (Tongariro Trig) formed in the north of the complex (Fig 3.2) not long after activity had commenced from the SW Oturere vents, and the two cones were erupting contemporaneously. Tongariro Trig cone-building occurred over c.45 ka (the same duration as the SW Oturere cone) and is dated between 110±6 ka and 64±11 ka (Table 3.1); however supplementary dating would be of benefit to allow further unravelling of the stratigraphy. The Tongariro Trig cone is relatively large, covering a present area of 23 km^2 and with an estimated present volume of 10 km^3 (Table 3.3). About 45 separate lava flows and pyroclastic units can be distinguished as 6 packages (subunits 'a' to 'f', Appendix 2.12). These flows and agglutinates are predominantly andesites (Fig 3.7) with SiO_2 content in the range 57.0-62.3 wt% (Table 3.3).

(b) Lithofacies. The oldest eruptive products of the Tongariro Trig cone (dated at 110±6 ka and 91±7 ka) are exposed as long, thin (2-10 m) to moderately thick (15-30 m), westwardly-dipping andesitic lava flows in the north wall of the Mangatepopo Valley (Fig 3.15; subunit 'f', Appendix 2.12). Patterson (1986) distinguished one thick lava outcrop in the lower valley (TG138; 110±6 ka) as a vent area (the "Mangatepopo labradorite andesite") separate from Tongariro Trig, but this is not supported by other evidence. A window of 79±9 ka Tongariro Trig lavas is revealed on the NNW slopes of Ngauruhoe (subunit 'e'; seen in the left of Fig 3.28). Younger lava flows are joined by welded agglutinate units (64±11 ka; Fig 2.23, Section 2.2.2a) in the head of Mangatepopo Valley and along the Tongariro trig - South Crater ridge (subunits 'b' & 'd'). Scoria-tuff cone deposits (Fig 2.33; Section 2.2.2b) and hydrothermally-altered (to varying degrees) lapilli-tuff breccias (subunit 'a'; Figs 3.16-3.18; Sections 2.2.2a, 2.2.3e-f) also crop out in this area.

Figure 3.15 View from Ngauruhoe summit looking NW at lavas and agglutinates of the Tongariro Trig cone exposed in the north wall of Mangatepopo Valley. Tongariro Trig - South Crater ridge at right. Historic and pre-historic lavas from Ngauruhoe fill Mangatepopo Valley in the foreground.

Figure 3.16 Eroded spines of hydrothermally-altered vent breccias exposed in the NE wall of South Crater. View towards the north.

Figure 3.17 Hydrothermally-altered proximal lapilli-tuff breccias (TG334-335) outcropping on the Tongariro Trig ridge. Photo courtesy of I.A. Nairn, GNS Wairakei.

Figure 3.18 Closer view of outcrop in Figure 3.17. Photo courtesy of I.A. Nairn, GNS Wairakei.

(c) **Discussion.** In addition to lava effusion and Hawaiian-style fire-fountaining (Section 2.3.2a), more explosive styles of volcanism were displayed by the Tongariro Trig cone. Strombolian-style scoria eruptions (Section 2.3.2b) and phreatomagmatic surge and fall eruptions (Section 2.3.2c) occurred from vents (Fig 3.4) near the Tongariro Trig - South Crater ridge. This general area (in the left of Fig 1.7) also contains the hydrothermally-altered breccias which represent vent breccias, pyroclastic flows and surges, and fall deposits. Mathews (1967) also identified old vent areas in the vicinity of Tongariro Trig. Glacial erosion of the cone (forming Mangatepopo Valley, South Crater, Central Crater) and concealment beneath post-glacial cones (North Crater, Blue Lake, Red Crater) has reduced Tongariro Trig cone volume from a probable original volume of around 12 km^3 (Table 3.3). This translates into a moderate eruptive rate of approximately 0.27 km^3/ka (Table 3.3).

3.5.8 Young eruptives (0-c.25 ka)

Late-stage volcanic activity on the Tongariro complex is represented by a relatively complex system of intra- to post-glacial vents established from c.25 ka onwards. Further K-Ar dating is required to assess whether or not the "time gap" between the conclusion of cone-building at Tongariro Trig (c.65 ka) and commencement of the young eruptives phase (c.25 ka) is real (Section 3.3.2).

Descriptions of each volcano-stratigraphic unit of the young eruptives follow a more condensed format to that used above for the older cones, although because primary morphology features are preserved and ring plain tephrostratigraphy is often known, more information about eruptive histories (including observed eruptions) and styles can be obtained (especially for Ngauruhoe). In addition, less uncertainty surrounds estimates of original volumes (most are under 1 km^3). In general, the present volume is taken to be essentially the same as the original volume for most of the young eruptives. The proportions of basaltic andesite, andesite and dacite for each young eruptive are shown in Figure 3.19. In addition to the summary information contained in Table 3.3, a generalised guide to instantaneous eruption rates is presented in Table 3.4. Known eruption volumes and durations were used to calculate rates for historic Ngauruhoe eruptions, and tephra dispersal

Figure 3.19 Samples from the young eruptives of Tongariro Volcanic Complex according to rock type (TAS classification).

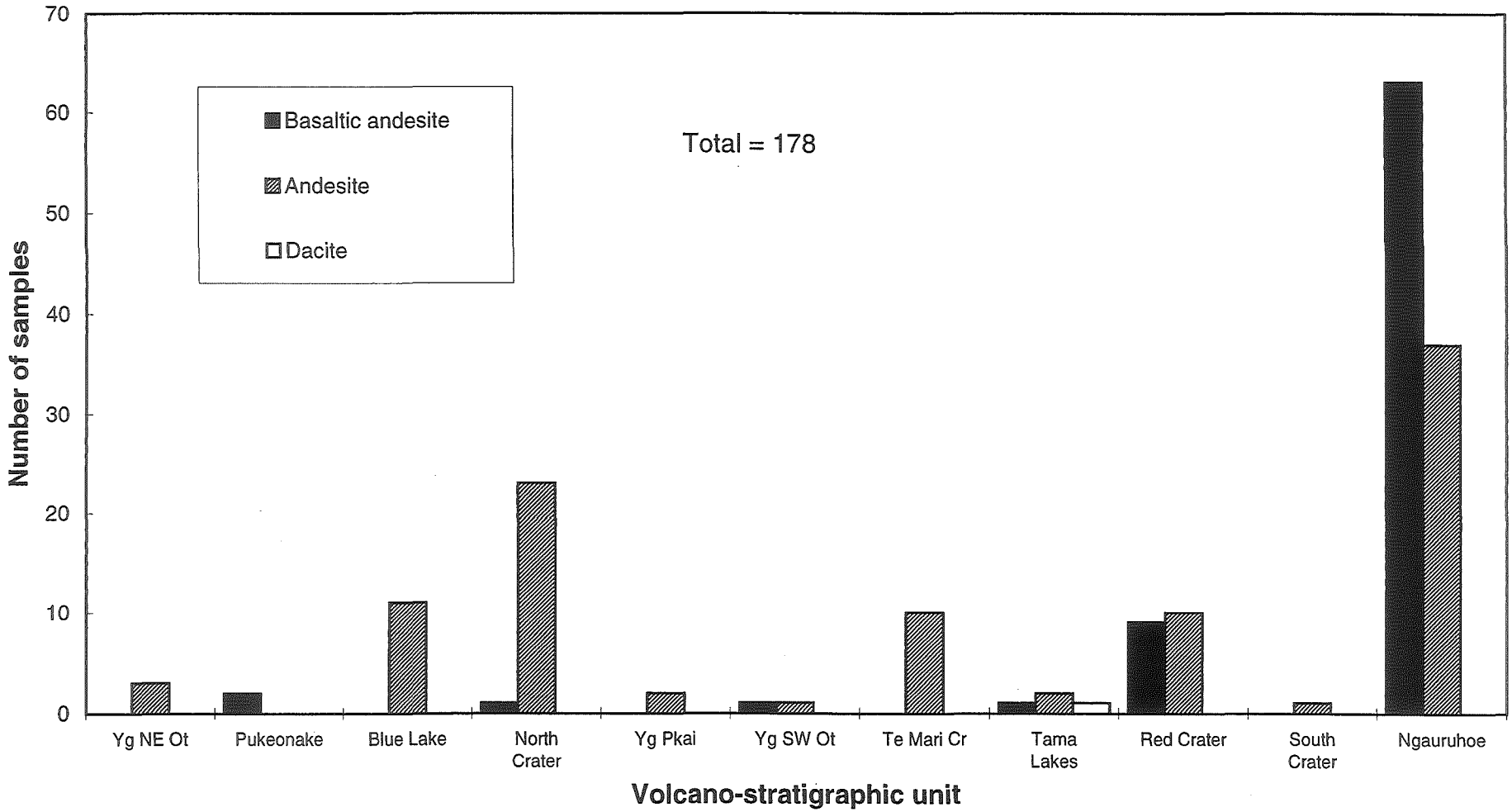

Table 3.4 Inferred instantaneous magma production rates during some historic and prehistoric eruptions from the Tongariro Volcanic Complex. Historic eruptive rates have been calculated with reasonable precision from available data; prehistoric eruptive rates are inferred from dispersal characteristics of the tephra and are approximate only.

Volcano-stratigraphic unit	Approximate age (ka)	Lava flows and/or tephra representing discrete eruptive events (if applicable)	Approximate instantaneous eruptive rate (m^3/s)
Ngauruhoe	0 - 2.5	19/2/1975 pyroclastic avalanche & fall deposit	70
		4/6/1954 - 26/9/1954 lava flows	1
		30/6/1954 lava flow	4
		10/2/1949 - 12/2/1949 lava flow & pyroclastic avalanche	4
South Crater explosion pit	1.8 - c.2		1 - 10
Red Crater	0 - c.3		1 - 10
Tama Lakes	c.10	c.9.7-9.8 ka Wharepu Tephra, Mangamate Formation	10^4
		c.9.7-9.8 ka Ohinepango Tephra, Mangamate Formation	10^3
		c.9.7-9.8 ka Waihohonu Lapilli, Mangamate Formation	10^4
		c.9.7-9.8 ka Oturere Lapilli, Mangamate Formation	10^4
Te Mari Craters	0 - 14+	c.13.8 ka Rotoaira Lapilli	10^3
Young SW Oturere	c.10 - 14		1 - 10
Young Pukekaikiore	c.15		1 - 10
North Crater	10 - c.15	c.9.7-9.8 ka Te Rato Lapilli, Mangamate Formation	10^3
		c.9.8-10 ka Pahoka Tephra	10^3
Blue Lake	10 - c.20	c.9.7-9.8 ka Poutu Lapilli, Mangamate Formation	10^4
Pukeonake	c.23		1 - 10
Young NE Oturere	c.20+		1 - 10

characteristics were used to infer approximate magnitudes of eruption rates for prehistoric events.

Recent work by Ian Nairn (GNS Wairakei) and Tetsuo Kobayashi (University of Kagoshima, Japan) has involved mapping proximal-medial fall deposits in the northern part of the complex and linking them in with the established ring plain chronology. Personal communications from Ian Nairn concerning some of their findings relevant to this study are acknowledged throughout the text.

(a) **Young NE Oturere [*yno*] (c.20+ ka).** Possibly the oldest of the young eruptive units, the Young NE Oturere welded scoria fall deposit caps a c.500 m long segment of the upper NE Oturere Valley ridge (Fig 2.31, and see map in back pocket of Volume 2). Although not dated by an absolute dating method, the unit is believed to be c.20 ka (possibly much older) because it is overlain by c.14 ka Rotoaira Lapilli and must also be pre-glacial (i.e. pre-Oturere Valley) as no scoria is preserved south of the ridge (I.A. Nairn, pers. comm., 1995). The three samples taken from the Young NE Oturere unit are andesites with a narrow SiO_2 range of 57.6 to 58.1 wt% (Fig 3.19; Table 3.3).

This 5-10 m thick, low-volume (<<0.01 km^3) unit is described in Section 2.2.2b. The scoria thinly mantles the slopes to the north of the ridge to a postulated (now-concealed/eroded) vent in the head of the Mangahouhounui Valley, east of Blue Lake (Fig 3.4). It is not clear whether or not the unit represents the eroded remnants of strombolian-style scoria eruptions or the proximal deposit of a more widespread subplinian eruption (Section 2.2.2b).

(b) **Pukeonake [*pn*] (c.23 ka).** Not strictly part of the Tongariro Volcanic Complex, the Pukeonake scoria cone and associated vents represent satellite eruptions from a N-S fissure peripheral to the main complex, about 5 km WNW of Ngauruhoe crater (Fig 3.2). The c.140 m high Pukeonake cone (Fig 3.13) is mostly tussock-covered, but an erosional gully (enhanced by quarrying) provides access to the interior of the cone, where c.30 m of bedded pyroclastics (Section 2.2.2b) are overlain by the c.22.6 ka rhyolitic Oruanui Tephra from the Taupo caldera (Section 3.4.2c). The absence of a conspicuous paleosol or erosional break indicates that the Pukeonake cone formed not long before the Oruanui Tephra (Hackett, 1985). Up to five valley-confined, 5-10 m thick lava flows are

exposed W and NW of the cone (e.g. at Mahuia Rapids, TG280) and are probably of a similar age to the cone. North of the main Pukeonake cone are the eroded remnants of two other cones, now consisting only of lava, with no pyroclastics preserved (Hackett, 1985).

Taken together, the scoria cones and lava flows cover about 55 km^2 (Topping, 1974) and have a volume of c.0.3 km^3, which may have originally been up to c.0.5 km^3 (Table 3.3). The products of these strombolian eruptions (Section 2.3.2b) are basaltic andesites with 56.5-57.0 wt% SiO_2 (Fig 3.19; Table 3.3). Only limited study and sampling (Appendix 2.10) of the Pukeonake volcano-stratigraphic unit was undertaken as it has already been investigated by Topping (1974), Napp (1983), and Hackett (1985).

(c) **Blue Lake *[bl]* (10-c.20 ka).** The age of the c.0.1 km^3 Blue Lake cone (Figs 1.6 and 1.7), situated in the northern part of the Tongariro complex summit area (Fig 3.2), is constrained by the c.9.7 ka subplinian eruption of the Poutu Lapilli (part of the Mangamate Formation, Table 3.2), with other eruptive products which may be as old as 15-20 ka (I.A. Nairn, pers. comm., 1995). Eruptions from Blue Lake could therefore have lasted for up to 10 ka. The Poutu Lapilli is almost 1 m thick at its type section, and has a tri-lobed distribution centred on Blue Lake (Topping, 1973; Donoghue et al., 1995). The eruptive products sampled from the Blue Lake unit are all andesites (Fig 3.19), ranging in composition from 56.8 to 59.9 wt% SiO_2 (Table 3.3).

The lake-filled crater (Section 1.2.2) is surrounded by a rim (up to c.100 m high) built up of thin (2-3 m thick), draping, welded agglutinates (Fig 3.20) deposited during hawaiian-style fire-fountaining eruptions (Sections 2.2.2a, 2.3.2a). Platey-jointed 3-5 m thick lava flows can be recognised intercalated between the intensely welded agglutinate units and rheomorphic flows (Section 2.2.1c), creating short stratigraphic sequences of up to 15 units in places around the rim (e.g. Fig 3.20, subunit 'a', Appendix 2.9). Scoria bomb beds (subunit 'b'; Section 2.2.2b) display rapid lateral transitions from proximal, oxidised, moderately- to intensely-welded agglomerate, to medial/distal, non-oxidised, non-welded scoria fall material. Up to metre-sized, breadcrusted-scoriaceous ballistic blocks are scattered around the crater rim and the northern slopes of the Blue Lake cone (Fig 2.34, Section 2.2.2c).

Figure 3.20 Northern inner and outer wall of Blue Lake crater; agglutinate-lava sequence of subunit 'a' (Appendix 2.9) at right, welded scoria fall deposits of subunit 'b' (Appendix 2.9) in centre and to left. View looking towards the east.

(d) **North Crater [*nc*] (10-c.15 ka).** The c.0.5 km^3 flat-topped North Crater spatter cone in the NW part of the summit area (Figs 1.6, 1.7, 3.2) was built up at about the same time as the one at Blue Lake, although it is probably not quite as old (I.A. Nairn, pers. comm., 1995). Activity lasted for about 5 ka, culminating with subplinian eruptions around 9.8-10 ka (Table 3.2) which produced the SE-dispersed Pahoka Tephra and the NE-dispersed Te Rato Lapilli (of the Mangamate Formation) (Topping, 1973, 1974; Donoghue et al., 1995). All the sampled North Crater products are andesites except for one basaltic andesite pyroclast (TG308), and the SiO_2 content is in the range 56.3-60.1 wt% (Fig 3.19, Table 3.3).

The 1 km-wide, level surface of North Crater is a solidified lava lake (Sections 2.2.1d and 2.3.1b); a section through which has been sampled (subunit 'a', Appendix 2.8) in a c.40 m-deep explosion pit (Fig 2.19). Remnants of the encircling crater rim are composed of 1-10 m thick welded agglutinates, and rheomorphic tuffs (subunits 'b' and 'c'; Figs 2.22, 2.24-2.26; Sections 2.2.1c and 2.2.2a), formed during hawaiian-strombolian style fire-fountaining eruptions (Section 2.3.2a). A relatively extensive 2-4 m thick scoria flow (TG316-317) exposed on the SW slopes is believed to have been erupted from North Crater (Section 2.2.3c), and other scoria fall deposits (<6 m thick) are preserved north and south of North Crater (subunits 'd' and 'e'). Some of the lava flows on the NW slopes below North Crater were probably erupted from the young cone, whereas others were derived from older, pre-existing vents (I.A. Nairn, pers. comm., 1995). Approximately 25 exposed lavas and pyroclastic units attest to the relative frequency of eruptions.

(e) **Young Pukekaikiore [*ypk*] (c.15 ka).** A young scoria deposit from a vent on the summit of Pukekaikiore (Fig 3.2) was also the source of two relatively thin, overlapping aa-block lava flows which extended up to 2.5 km to the west (Fig 2.29; Section 2.2.2b). Topping (1974) identified c.14.7 ka Rerewhakaaitu Ash interbedded with Young Pukekaikiore lapilli and ash, and this provides an approximate age for the unit (Section 3.4.2c). The sampled scoria and lava flow (Appendix 2.6) are a distinctive olivine-andesite with 56.9-57.4 wt% SiO_2 (Fig 3.19, Table 3.3). The Young Pukekaikiore unit covers 1.5 km^2, but was not a substantial cone-building unit - with a volume of only <0.1 km^3 (Table 3.3).

(f) **Young SW Oturere [*yso*] (10-14 ka).** A young, variably welded scoria fall deposit (<15 m thick) mantles c.1 km of the ridge on the SW side of Oturere Valley and covers about 0.5 km^2 (Figs 2.30 and 3.14, Section 2.2.2b). The unit is probably of post-glacial age as the scoria is interbedded with post-glacial tephras in places, although because the inferred vent out at the south margin of the valley (Fig 3.4) has been removed, it may be of "intra-glacial" age (I.A. Nairn, pers. comm., 1995). A thin dike intruding welded tuffs beneath the ridgeline is probably associated with the Young SW Oturere strombolian-style eruption (Section 2.2.1e). The low volume (<<0.01 km^3) scoria deposit is basaltic andesite to andesite, with SiO_2 from 55.0 to 57.4 wt% (Fig 3.19, Table 3.3).

(g) **Te Mari Craters [*tm*] (0-14+ ka).**

Stratigraphy

At least 15 lava flows and pyroclastic units can be recognised from the northernmost vents identified on the Tongariro complex, Te Mari Craters (Figs 1.6 and 3.2), where activity probably began about 13.8 ka with the subplinian eruption of the NE- and SE-dispersed Rotoaira Lapilli from the Lower Te Mari Crater (Table 3.2; Topping, 1973). The eastern lava flow on the north slopes (not sampled) and probably some of the flows exposed in the lower crater walls (subunit 'b', Appendix 2.5) were also erupted at this time (Topping, 1973, 1974; Section 3.4.2c). The large levéed flow directly north of Lower Te Mari Crater (TG027, subunit 'a') is overlain by Papakai Formation, leading Topping (1974) to suggest an age of c.6-9.7 ka (Section 3.4.2c).

The youngest lava flows have come from the Upper Te Mari Crater, most of them directed in multiple, overlapping lobes down the NW slopes and one into the lower crater (Fig 3.21). These flows are younger than the Taupo pumice (i.e. <1.8 ka) and have been tree-ring dated by Topping (1974) at c.0.45 ka (c.1500AD) (Section 3.4.2e). Eruptions from Te Mari Craters during the last 1.8 ka have contributed to the Ngauruhoe Formation tephra, and possibly between 2.5 and 9.7 ka to the Papakai Formation tephra (Table 3.2, Topping, 1973). Historic phreatic and phreatomagmatic eruptions were observed from Lower Te Mari Crater by the Maori and early Europeans (in 1839 & 1867; Gregg, 1960), and from Upper Te Mari Crater between 1868 and 1897 (Sections 1.6.2, 2.3.2c, 3.4.3). With a duration of activity spanning at least 14 ka, the Te Mari Craters represent the most long-lived of the young eruptives. The sampled flows are all andesitic (Fig 3.19) with SiO_2 ranging from 57.5 to 60.2 wt% (Table 3.3).

Figure 3.21 View of Te Mari Craters, looking towards the SE. Lava flows from the Upper Te Mari Crater have flowed NW down the lower slopes and also into the Lower Te Mari Crater. Note the lavas exposed within the lower crater wall, and the small ephemeral lake in the crater floor. Photo courtesy of D.L. Homer, GNS Lower Hutt.

Figure 3.22 Hydrothermally-altered blocky tuff breccias exposed in the eastern inner wall of Upper Te Mari Crater. See text for full description.

Lithofacies and Discussion

The 3-4 km long lava flows (Section 2.2.1a) on the northern slopes (subunit 'a'), and those exposed within the lower crater (subunit 'b') and to the east (subunit 'c') are typically 2-8 m thick and blocky (Figs 2.11 and 2.12) to platey-jointed. Some flows display levée development. Excellent exposure of c.40 m of the inner walls of the upper crater (Fig 3.22) reveals the following sequence: an upper, red-black, bedded tuff breccia; a lower, red-grey, massive mega-block tuff breccia (lithics <2-3 m); and a central, hydrothermally-altered, orange-white vertical vent structure infilled with blocky tuff breccia. The large (400 m wide, 80 m deep) lower crater used to be called Sulphur Lagoon last century when it was partly occupied by a shallow yellow lake, but now only an ephemeral small pool of water exists (Fig 3.21) - although minor sulphur deposits accompany steaming ground and fumaroles (Section 1.2.6). Several small explosion pits on the outer slopes of the lower crater (Fig 3.4) mark the northernmost vents of the Tongariro complex. Ballistic blocks found scattered in the vicinity of Te Mari Craters (Fig 2.36) are further evidence of explosive eruptions (Section 2.2.2c).

The crater-topped cones and lava flows of the Te Mari unit cover 6 km^2, and represent a relatively small volume of c.0.2 km^3 (Table 3.3). A wide range of eruptive styles have been recorded from Te Mari Craters, ranging from effusion of lava flows (some large), to phreatic and phreatomagmatic explosions, to subplinian lapilli fall events.

(h) Tama Lakes [*tl*] (10 ka).

Stratigraphy

The Tama Lakes unit is represented by six 20-50 m deep explosion craters (three of which are filled by the Lower and Upper Tama Lakes) and c.0.1 km^2 of pyroclastic material preserved in the surrounding (proximal) area (Fig 3.4, and see map, back pocket of Volume 2). These are the southernmost vents of the Tongariro complex, and occur superimposed on the oldest exposed lavas, those of the Tama 1 cone (Figs 3.8 and 3.11).

Eruptions of the Tama Lakes craters occurred during a period of intense volcanic activity on the complex at around 10 ka, represented by the Pahoka Tephra, Mangamate

Figure 3.23 Volcaniclastic sequence of lithic-rich tuff beds preserved from c.10 ka Tama Lakes eruptions, in gully near Lower Tama Lake. See text for full description. Photo courtesy of I.A. Nairn, GNS Wairakei.

Formation tephras, and early Papakai Formation tephras (Table 3.2). The Tama Lakes have been identified as the source for four members of the 9.7-9.8 ka Mangamate Formation (Oturere Lapilli, Waihohonu Lapilli, Ohinepango Tephra, Wharepu Tephra) with E-SE dispersal axes, and some of the lower (c.9.7 ka) Papakai Formation tephras (Table 3.3; Topping, 1973; Donoghue et al., 1995). Relatively limited sampling of the Tama Lakes ejecta (Appendix 2.4) reveals them to span the widest compositional range of any of the units of the Tongariro complex; basaltic andesite to dacite, 56.1-64.2 wt% SiO_2 (Fig 3.19, Table 3.3).

Lithofacies and Discussion

Basaltic andesite bombs (e.g. TG137) occur within volcaniclastic sequences exposed in stream gullies around the Tama Lakes (Fig 3.23). These thick sections comprise alternations of dm-bedded, well-sorted, lapilli-ash phreatomagmatic fall units, with massive to poorly-bedded, poorly-sorted, heterolithologic muddy sandy gravel laharic and fluvial deposits which contain <1 m rounded boulders (Section 2.2.4b). A c.1 m thick, coarse, andesitic welded fall unit (TG029-034) is exposed for c.20 m along the ridge between Upper and Lower Tama Lakes and it is not apparent whether the deposit represents strombolian or proximal subplinian style eruptions (Section 2.2.2b). The dacitic banded pumice ejecta (Tn141a) collected by I.A. Nairn was also erupted during the c.10 ka subplinian eruptions, but probably from a different (but nearby) vent to that/those from which the other Tama Lakes ejecta were erupted. The styles of volcanism represented by the Tama Lakes ejecta thus range from strombolian to phreatomagmatic to subplinian. Wahyudin (1993) also described several sections through the young Tama Lakes tephras.

(i) Red Crater [*rc*] (0-c.3 ka).

Stratigraphy

Well after eruptions had ceased at Tama Lakes, and concurrent with activity at Te Mari Craters, the Red Crater scoria cone began to form through a series of strombolian eruptions coupled with the formation of at least 10 moderate to large lava flows, which have produced a total volume of about 0.3 km^3 (Table 3.3). Red Crater is situated near the centre of the Tongariro complex at the head of the Oturere Valley and surrounded by ridges of the much older lavas of the NE Oturere, SW Oturere and Tongariro Trig cones (Figs 1.7 and 3.2) The lower age limit for the Red Crater volcano-stratigraphic unit is uncertain

(Section 3.4.2c), but Topping (1974) noted that some of the older flows underlie the 1.8-2.5 ka Mangatawai Tephra (Fig 2.37), providing at least a minimum age for the unit. Historic ash and steam eruptions were observed from Red Crater in the latter half of last century from 1855 to probably 1890 (Section 3.4.3), and since then sulphurous steaming ground and fumaroles have remained active (Section 1.2.6). Red Crater eruptions have contributed material to the 0-1.8 ka Ngauruhoe Formation tephras (Table 3.2), and there is also probably a component of Red Crater distal fall in the 1.8-2.5 ka Mangatawai Tephra (Topping, 1974). An average magma production rate of 0.1 km^3/ka has been calculated for Red Crater cone (Table 3.3).

Lithofacies and Discussion

The Red Crater cone is composed of dark red and black, variably welded basaltic andesite scoria (TG128-129, Appendix 2.3) which drapes older light grey columnar-jointed lava (Fig 2.28, Section 2.2.2b), probably of the Tongariro Trig cone (TG344). Several basaltic andesite dikes are exposed within the c.60-80 m deep crater, one of which is preserved as a hollow lava tube (Fig 2.20, Section 2.2.1e). Phreatic eruptions during the last 1.8 ka (Topping, 1974) have created a line of explosion pits NE of Red Crater, three filled by the Emerald Lakes (Figs 3.4 and 3.24, Section 1.2.2), which mirror the overall NE vent lineation of the Tongariro complex.

There is a two-fold division of the 10 sampled Red Crater lava flows (Fig 3.26, Section 2.2.1a; Appendix 2.3; Topping, 1974) into:

1. At least 5 post-1.8 ka (Taupo pumice), thin pahoehoe transitional to aa, basaltic andesite flows in South Crater (TG127, Fig 2.9), Central Crater (TG126, Fig 2.3), and Oturere Valley (TG112, TG130-131).
2. At least 5 pre-1.8 ka (Taupo pumice), aa to block, andesite flows in Oturere Valley (TG053, TG087-090, TG113, TG132-135) which contain transverse pressure ridges and spinose surfaces. The largest pre-1.8 ka flow is unusually long (7 km) and thick (<100 m) (Figs 2.6 and 3.25, Section 2.2.1a). Taupo pumice (Fig 2.37) and ignimbrite (Fig 3.6) overlie these older Red Crater flows.

The largest Red Crater flow fills the floor of the Oturere Valley and has an estimated minimum volume (c.0.3 km^3) which is several orders of magnitude greater than any other

Figure 3.24 Red Crater scoria cone and the NE-aligned phreatic explosion craters filled by the Emerald Lakes. View looking towards the SW, Ngauruhoe in background at left.

Figure 3.25 View looking NW up the Oturere Valley towards the Red Crater scoria cone. Note the pressure ridges on the long andesite flow filling the valley floor. The Oturere hut is visible in the foreground at right near the north margin of the flow. Ngauruhoe is prominent in the background at left. Photo courtesy of D.L. Homer, GNS Lower Hutt.

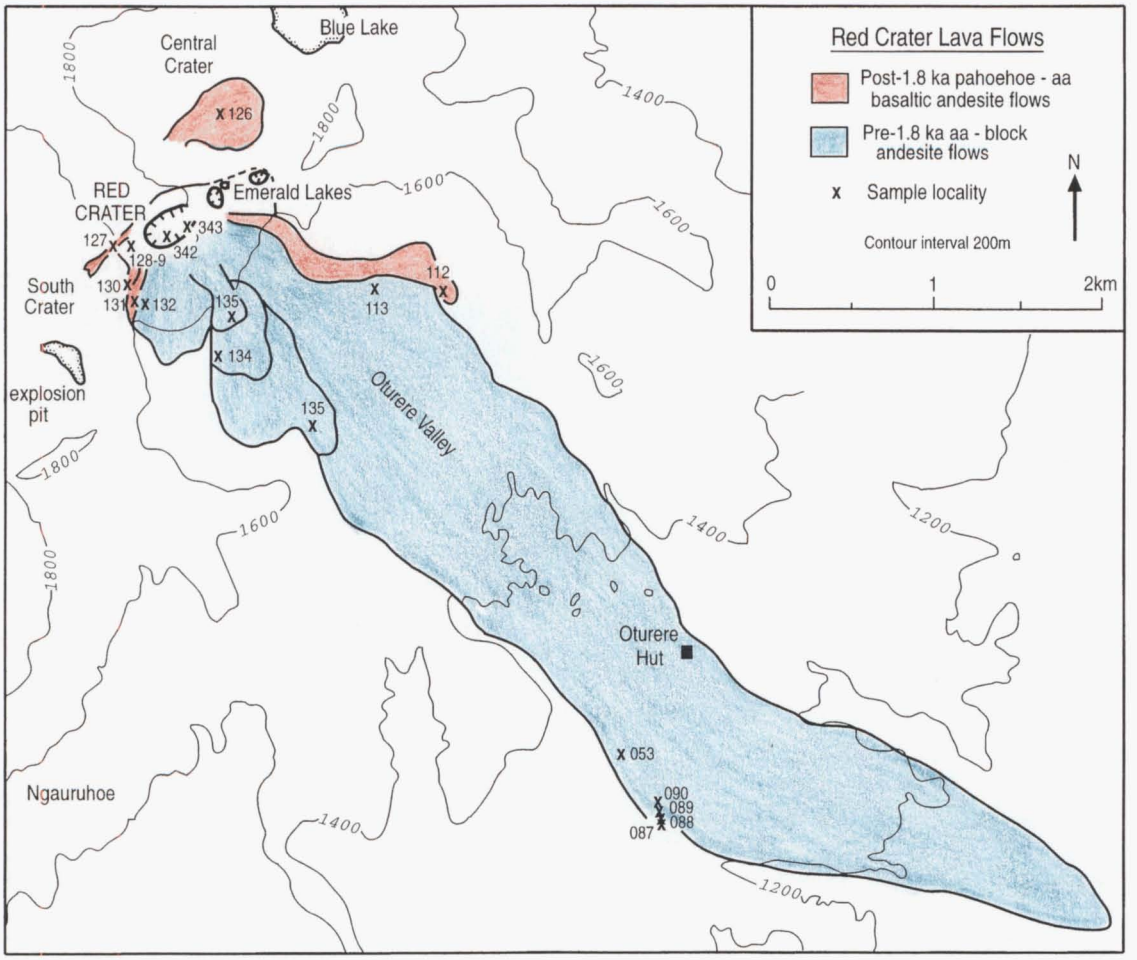

Figure 3.26 Map of Red Crater lava flows and sample localities, showing distribution of the two different lava types. See volcano-stratigraphic map in back pocket of Volume 2 for more detail.

of the Red Crater flows (c.0.003 - 0.0003 km^3). Since this is the oldest preserved flow from Red Crater, it could represent an initial near-emptying of the magma reservoir after which time no significant replenishment occurred and only relatively small remnants of magma were erupted to produce the subsequent (and much smaller volume) andesite flows. Injection of more basic magma after 1.8 ka is implied by the younger basaltic andesite flows which have SiO_2 contents of 53.0-53.7 wt%, quite distinct from the andesite flows which range from 59.1 to 61.1 wt% (Fig 3.19, Table 3.3). There was obviously a significant change in magmatic chemistry and eruptive style sometime around 1.8 ka to produce these two very different groups of lavas.

(j) **South Crater explosion pit [*scp*] (c.1.8-2 ka).** The South Crater unit is a small exposure (<<0.01 km^3) in the explosion pit at the southern end of the South Crater basin, at the base of the Ngauruhoe cone (see map in back pocket, Volume 2). Almost exactly half-way on a direct line between the Ngauruhoe and Red Crater vents, the young South Crater eruption could represent a leak from the magmatic reservoir or dike feeding the other two cones. The one sample (TG276, Appendix 2.2) collected from the fresh andesitic scoria deposit contains 57.8 wt% SiO_2 (Fig 3.19, Table 3.3).

A c.7 m thick sequence preserved in a small gully contains a basal c.4 m of hydrothermally-altered, orange-white, poorly-sorted tuff breccia with blocks <1 m which probably represent wallrock erupted from the explosion pit. Above this is a 2.3 m thick unit comprising fresh, black, juvenile andesitic scoriaceous lapilli and blocks (<20 cm), which equates with the magmatic phase of the eruption. This unit contains intercalated Mangatawai Tephra (1.8-2.5 ka) and is overlain by c.0.5 m of 1.8 ka Taupo ignimbrite; these tephras thus constrain the age of the South Crater explosion pit eruption to between c.1.8-2 ka.

(k) **Ngauruhoe [*ng*] (0-2.5 ka).**

Stratigraphy

Introduction: geography and spatial extent: The youthful symmetrical cone of Ngauruhoe forms a prominent feature near the centre of the Tongariro complex (Figs 1.4, 1.5), rising to an elevation of 2287 m above sea level and covering 15 km^2. The cone itself is about 900 m high, and has steep sides sloping at c.30° (Fig 3.27). Ngauruhoe, established

Figure 3.27 View of Ngauruhoe cone and summit crater, looking towards the east. Note dark 1954 lavas in foreground diverging around eastern margin of Pukekaikiore. Lavas have flowed into South Crater (muddy pond in explosion pit visible at upper left), Mangatepopo Valley (out of view to left), Makahikatoa Valley (centre right foreground), and Waihohonu Valley (middle distance at right). Ridges of Tama 2 remnant lavas are visible at right. Photo courtesy of D.L. Homer, GNS Lower Hutt.

Figure 3.28 Historic (dark grey, upper cone) and prehistoric lavas (medium grey to brown, lower cone and valley floor) from Ngauruhoe which have flowed into Mangatepopo Valley. Multiple-lobed 1975 pyroclastic avalanche deposit visible in centre, to the right of which is the 1949 lava flow, and some of the 1954 flows are visible on far right flank of cone (Pukekaikiore in background at right). Tongariro Trig lava bluff at left is surrounded by two 1870 lava flows, and part of the main Tongariro Trig outcrop is visible at far left.

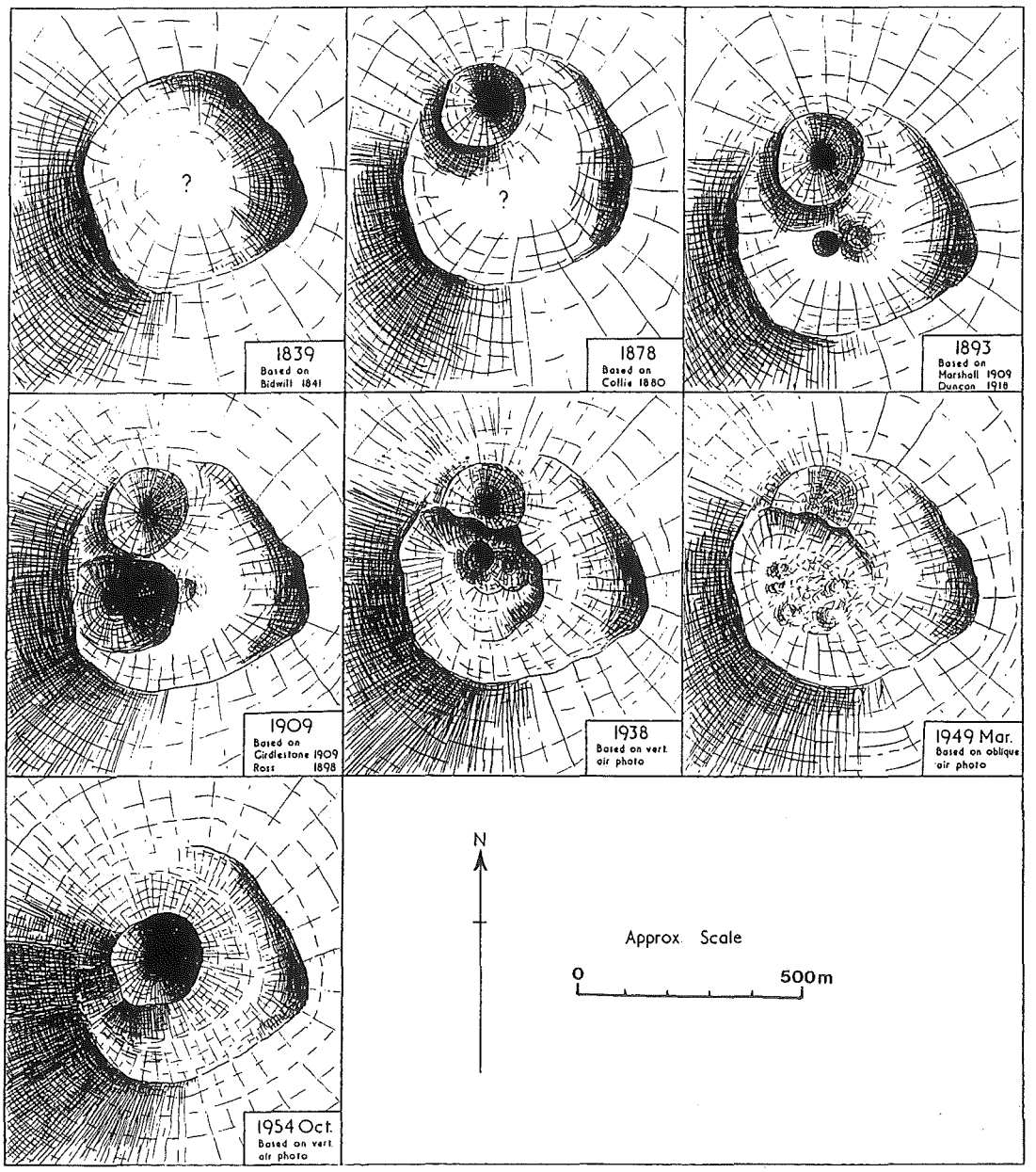

Figure 3.29 Sketch maps showing historical changes in Ngauruhoe crater morphology from 1839 to 1954, from Gregg (1960).

in an area where several of the older cones intersected, has buried the vents for the Tama 2 and Pukekaikiore cones (Fig 3.4), and produced lavas which have flowed into and partially filled several glacially-eroded valleys (Mangatepopo, Figs 3.28 and 3.15; Makahikatoa, Fig 3.27; Waihohonu, Fig 3.27). Lavas were preferentially directed into these glacial valleys because the long extinct, eroding edifices of the Tama 2, Pukekaikiore, SW Oturere and Tongariro Trig cones were still high enough to deny Ngauruhoe lavas access to other areas.

The summit of Ngauruhoe consists of a 400 m wide crater which has undergone frequent changes during the last 150 years of observation. These changes are summarised by Gregg (1960) (Fig 3.29), who also presented an impressive series of early photographs of the crater taken between 1886 and 1956. Up until the 1850's the crater comprised one large deep vent with almost vertical walls. Sometime during the 1850's a NW subcrater formed and this remained for 100 years until buried by the eruptions of 1954. A south subcrater appeared in the 1890's which became the locus for the main activity, and around which a scoria cone was built in 1954-55 which in the process completely buried the remains of the NW subcrater. The outer crater rim is highest on the SE side, and the present active crater is about 60 m deep with a sequence of the 1954-55 and 1974-75 scoriaceous material preserved in the E-SE inner wall (Fig 2.27, Section 2.2.2b).

Age relationships: The central vent eruptions began around 2.5 ka, when Ngauruhoe-derived fall material can first be identified from isopach maps for the <0.8 m thick 1.8-2.5 ka Mangatawai Tephra (Table 3.2; Gregg, 1960; Topping, 1973; Donoghue et al., 1995). The majority of the cone-building evidently took place in these first c.700 years (Topping, 1974); Ngauruhoe tephras make a lesser contribution to the 0-1.8 ka deposits (Ngauruhoe Formation), which are dominated by Ruapehu-derived products (Tufa Trig Formation) (Table 3.2; Topping, 1973; Donoghue et al., 1995). Ngauruhoe has been nearly continuously active in historic times (Section 1.6.2; Gregg, 1960), with major eruptions in 1870, 1949, 1954-55, and 1974-75 (Section 3.4.3). Disappointingly (especially for younger geologists), Ngauruhoe is currently experiencing its longest recorded period of quiescence since observations began in 1839, with only weak (and declining) fumarolic activity occurring at present (Section 1.2.6).

Internal stratigraphy and Chemistry: Comprehensive sampling of lava flows (and pyroclastic avalanches and scoria) from all sectors of the volcano has enabled the construction of a detailed volcano-stratigraphy (Appendix 2.1). Superimposition relationships or tephra chronology were sometimes lacking or inadequate for establishing relative ages of some of the prehistoric flows (Section 3.4.2), but overall the Ngauruhoe sequence is relatively well-constrained. On the basis of field relationships and inferred flow chronology, the lava flows have been divided into 5 groups (Fig 3.30A) which also have a chemical distinction (Fig 3.30B). Figure 3.31 summarises the progression of eruptions with respect to the different lava groups, and introduces their basic chemical parameters (discussed in detail in Chapters 6 and 7). The majority (64%) of Ngauruhoe lavas are basaltic andesites, 36% are andesites (Fig 3.19). SiO_2 contents range from 54.2 to 58.6 wt% (Table 3.3, Fig 3.30B).

Lithofacies

Most Ngauruhoe lavas are channel-confined, aa (to block) flows with marginal levées and lobate flow fronts expanded onto the valley floors (Figs 2.4, 2.5, 2.7, 2.8; Section 2.2.1a).

Prehistoric lavas (Groups 1A-3A): The oldest of the exposed Ngauruhoe lavas are >1.8 ka because they overlie Taupo pumice (Section 3.4.2c). These lavas were directed in several directions down the flanks of the cone (Figs 3.30A and 3.31a); Group 1A lavas flowed east and south into the Waihohonu Valley and NW into Mangatepopo Valley, and one Group 3B lava (TG529) flowed the furthest of all Ngauruhoe lavas (5 km) west into Makahikatoa Valley. Based on available evidence, all other sampled Ngauruhoe flows are considered to be <1.8 ka (Section 3.4.2c). The next sequence of lavas, Group 1B, were channelled down the N-NW side of the cone into Mangatepopo Valley and towards South Crater (Figs 3.30A and 3.31b). In contrast, the following lava-producing eruptions (Group 2) sent several relatively long (<3 km) flows down the south flanks into Waihohonu Valley (Figs 3.30A and 3.31c). Group 3A lavas flowed in a more SW direction into the upper west Waihohonu Valley (Figs 3.30A and 3.31d).

Group 3B lavas and pyroclastics: Lava flow direction changed once more when the youngest prehistoric flows (Group 3B and a few from Group 1B), together with historic

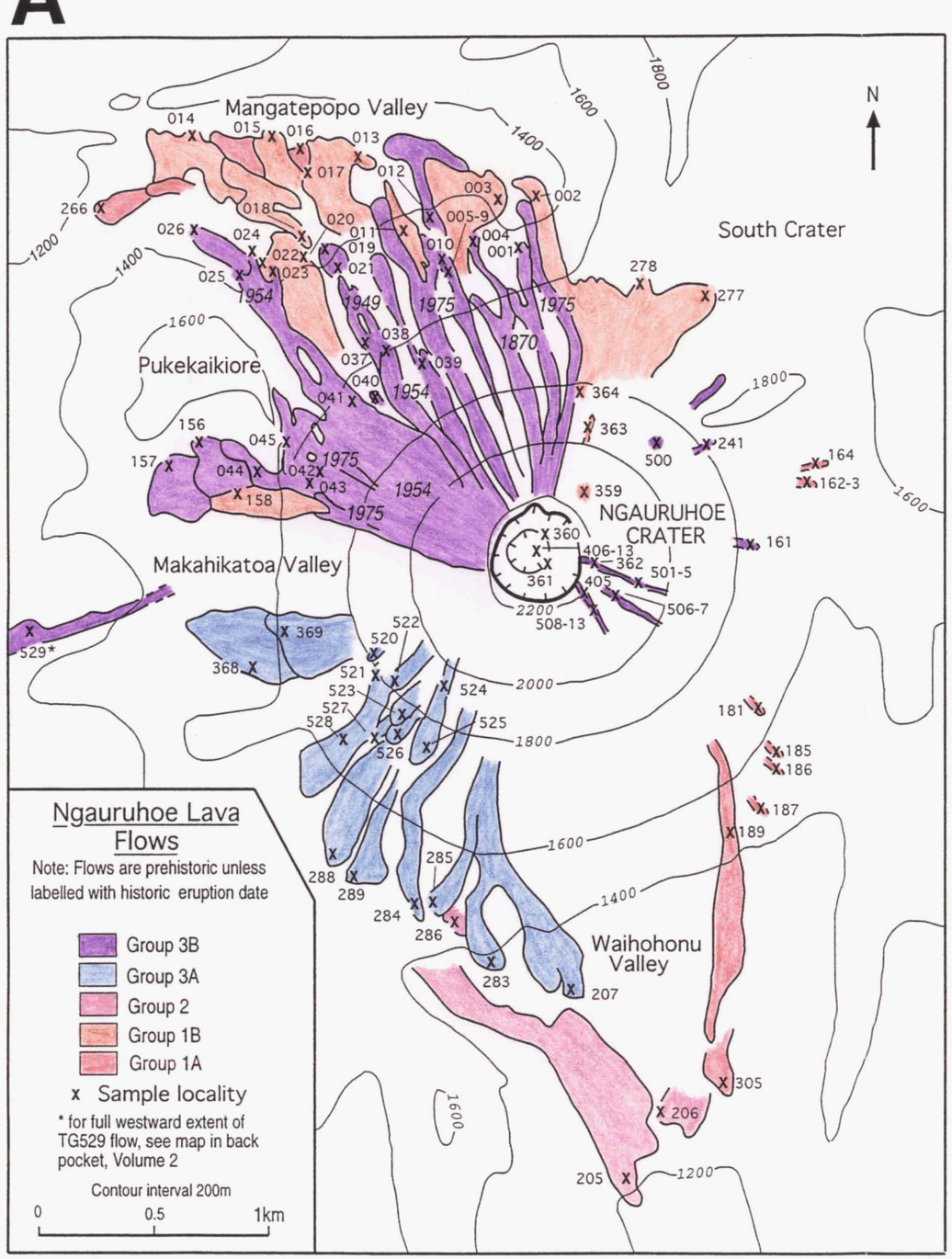

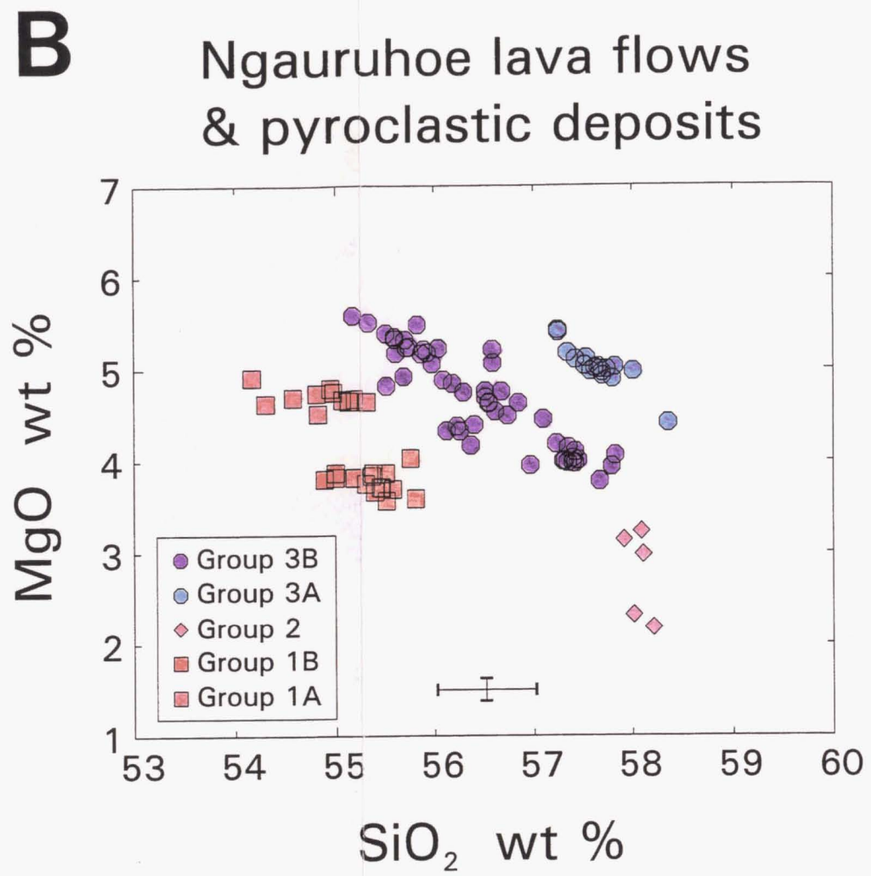

Figure 3.30 **A.** Map of Ngauruhoe lava flows and sample localities, showing distribution of the 5 lava groups. See volcano-stratigraphic map in back pocket of Volume 2 for more detail.
B. Ngauruhoe samples plotted on a graph of SiO_2 versus MgO showing chemical distinction between the 5 lava groups. All data recalculated anhydrous. Error bars represent total error (2 sd from mean; Section A8.3.3).

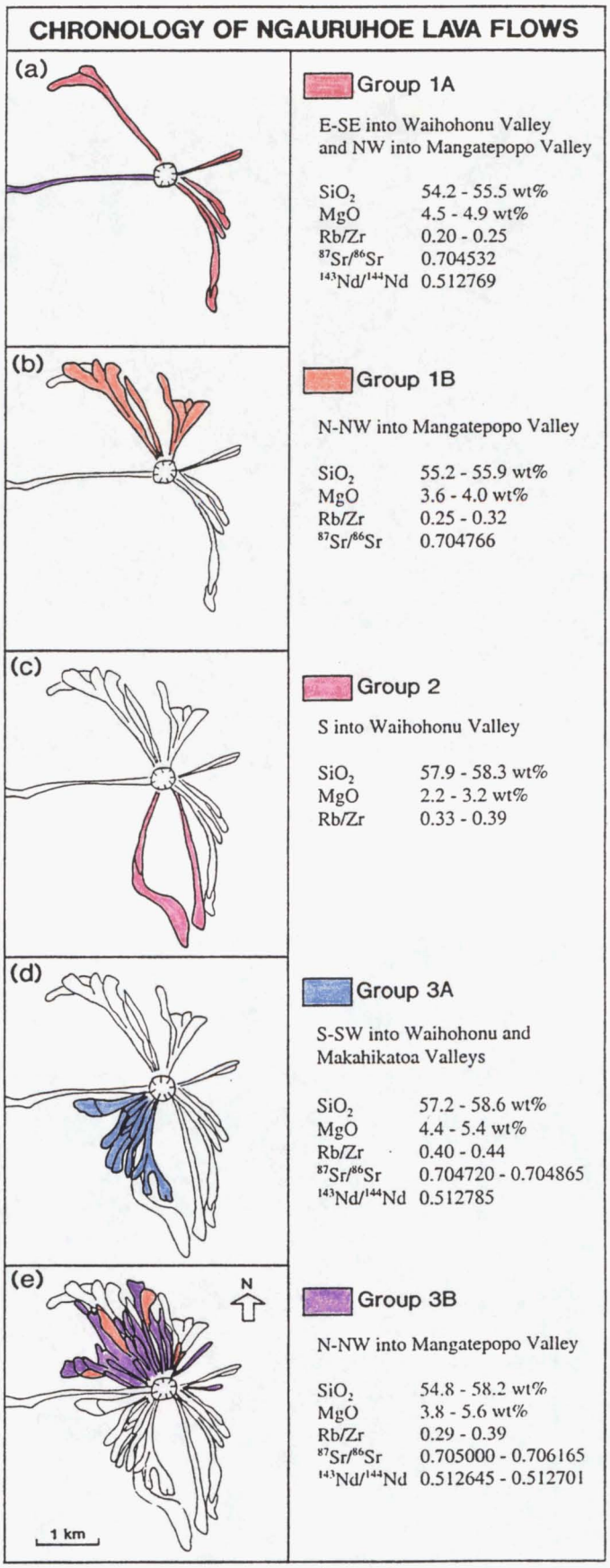

Figure 3.31 Chronology of Ngauruhoe lava flows preserved on the cone, with respect to the 5 identified lava groups. See text for discussion. Geochemical features of lava groups are described in Chapters 6-7. Note that several flows from Groups 1B and 3B were erupted during different time intervals from the majority of flows of their respective group.

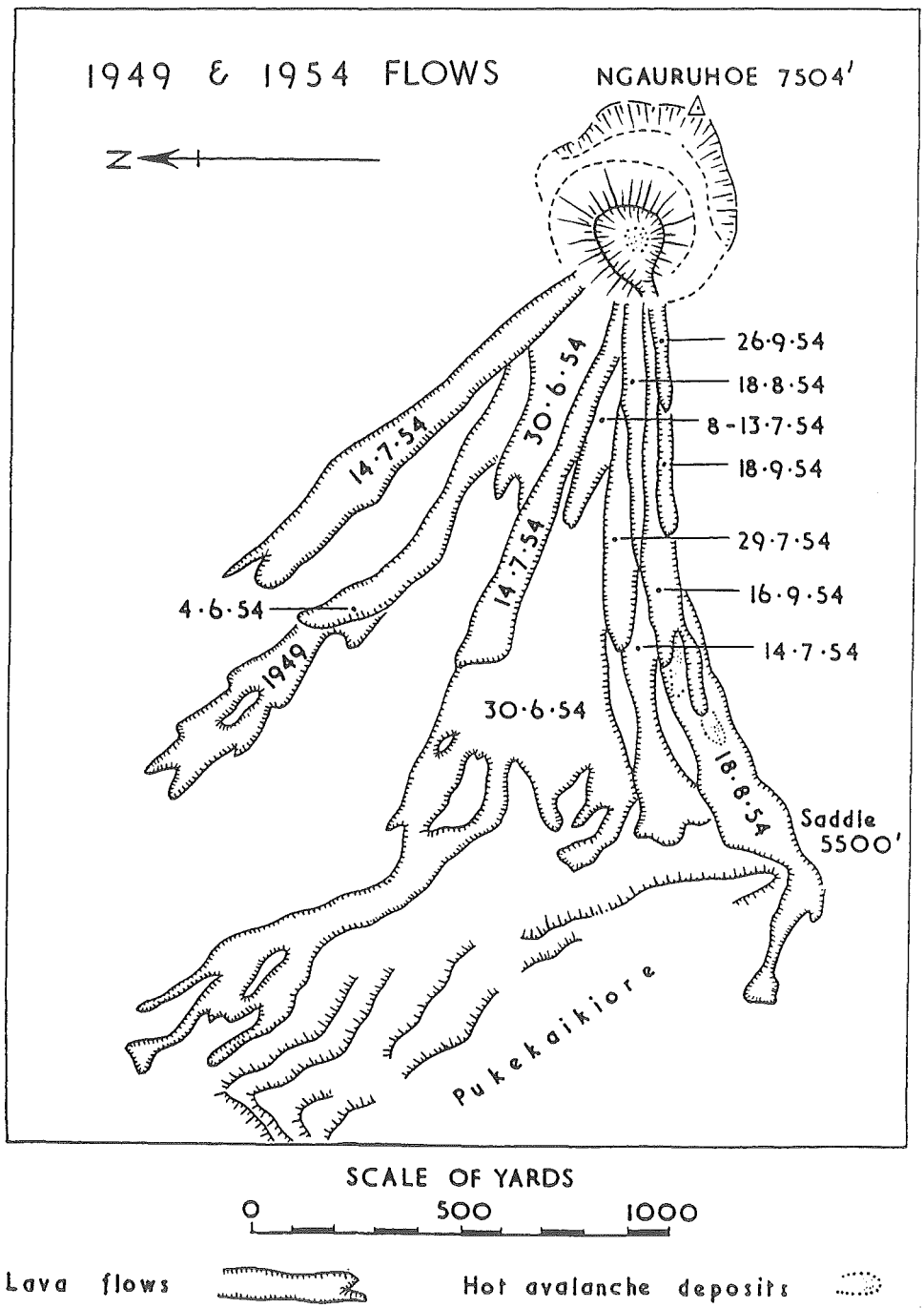

Figure 3.32 Map showing distribution of 1954 lava flows from Ngauruhoe (after Gregg, 1956).

flows (Group 3B), followed the paths taken by the earlier Group 1B lavas down the N-NW sector of the cone (Figs 3.30A and 3.31e). Only three historic eruptions have produced lava flows (Section 3.4.3). Because of lack of direct observation, there has been some confusion over the 1870 flows (discussed by Gregg, 1960), but it is now generally accepted that these are the two dark lavas (TG001, TG004) which have flowed down the north side and terminated either side of the old Tongariro Trig bluff (Fig 3.30A). The 1949 eruption was closely observed (Allen, 1949; Battey, 1949) and produced one lava flow and two pyroclastic avalanches to the NW (TG019, P9997). Likewise, the 1954-55 eruption was well-documented (Gregg, 1956; Steiner, 1958) and generated at least 10 lava flows down the NW-NNW flanks (Fig 3.32) over a 4 month period. The 1954-55 scoria cone is described in Section 2.2.2b. No further lava flows have been produced from Ngauruhoe, but new magmatic material was erupted in 1974-75 (Nairn et al., 1976; Nairn and Self, 1978) and preserved in the form of pyroclastic avalanche deposits on the NW slopes (Figs 2.40-2.42; Section 2.2.3a,b) and large ballistic blocks (Fig 2.35; Section 2.2.2c).

Discussion

Distribution of lavas: Flow direction appears to be controlled by crater morphology; groups of flows of similar age are channelled through low points of the crater rim (as demonstrated by historic eruptions), which have been variably located during Ngauruhoe's eruptive history. Occasionally, short-lived abberations in wind direction have allowed spatter to overtop the higher parts of the crater rim to form small detached flows down the less favoured side of the cone (e.g. the E-SE flows). Overall, there is not an even radial distribution of lava flows preserved on Ngauruhoe; instead they are concentrated in the N-NW and SW sectors - which probably represent the two most accessible exit points from the summit crater in recent times.

Eruptive style: Activity at Ngauruhoe has been characterised by effusive (Fig 2.47, Section 2.3.1a), strombolian (Fig 2.48, Section 2.3.2b), vulcanian (Fig 2.49, Section 2.3.2d) and possibly subplinian styles of activity, which have produced a correspondingly wide range of eruptive products.

Erupted volume and eruptive rate: Ngauruhoe has an estimated volume of 2.2 km^3, the largest volume of the young eruptive units (Table 3.3). The frequency of eruption from

Ngauruhoe is demonstrated in both the large number of recognisable lava flows and pyroclastic units (c.80) and in the relatively high eruptive rate of c.0.88 km^3/ka - second only to that of the Tama 2 cone (Table 3.3). Approximate instantaneous eruptive rates calculated for the lava flow-producing eruptions vary from 1-4 m^3/s, whilst the 1975 pyroclastic avalanche eruption occurred at a rate of c.70 m^3/s (Table 3.4). Eruptive style obviously exerts a strong control over the rate of magma production for a particular eruption. When converted to km^3/ka, the historic eruptive rates are much greater (c.20-2200 km^3/ka) than the average eruptive rate calculated over Ngauruhoe's life span (0.88 km^3/ka; Table 3.3). Obviously this average rate does not represent a constant growth rate; it incorporates periods of high discharge as well as periods of low magma production or quiescence. The instantaneous eruptive rates represent the operation of relatively high-level processes in and above the shallow magma reservoir, whereas the average long-term rate of cone growth calculated for Ngauruhoe (and estimated for the older cones) is controlled by deeper processes.

3.6 DISCUSSION AND SUMMARY

The eruptive history of the Tongariro Volcanic Complex has been determined by a combination of new detailed field mapping and K-Ar age determinations, with referral to the published tephrostratigraphic record. Careful delineation of all map units and attention to field relationships allowed reconstruction of original cone geometries and estimation of original cone volumes. The good age control obtained for the study enabled interpretations of eruptive frequency, eruptive rate, and the interrelationships between magmatic plumbing systems. The Tongariro complex comprises six relatively large, nested and overlapping pre-glacial cone-forming units (with variably directed sectorial lava aprons from each), upon which eleven mostly post-glacial eruptive units or cones are superimposed. These units have been described in detail within a new volcano-stratigraphic framework developed for this study. The growth of the Tongariro complex in terms of the successive cone-forming units is illustrated schematically in Figure 3.33.

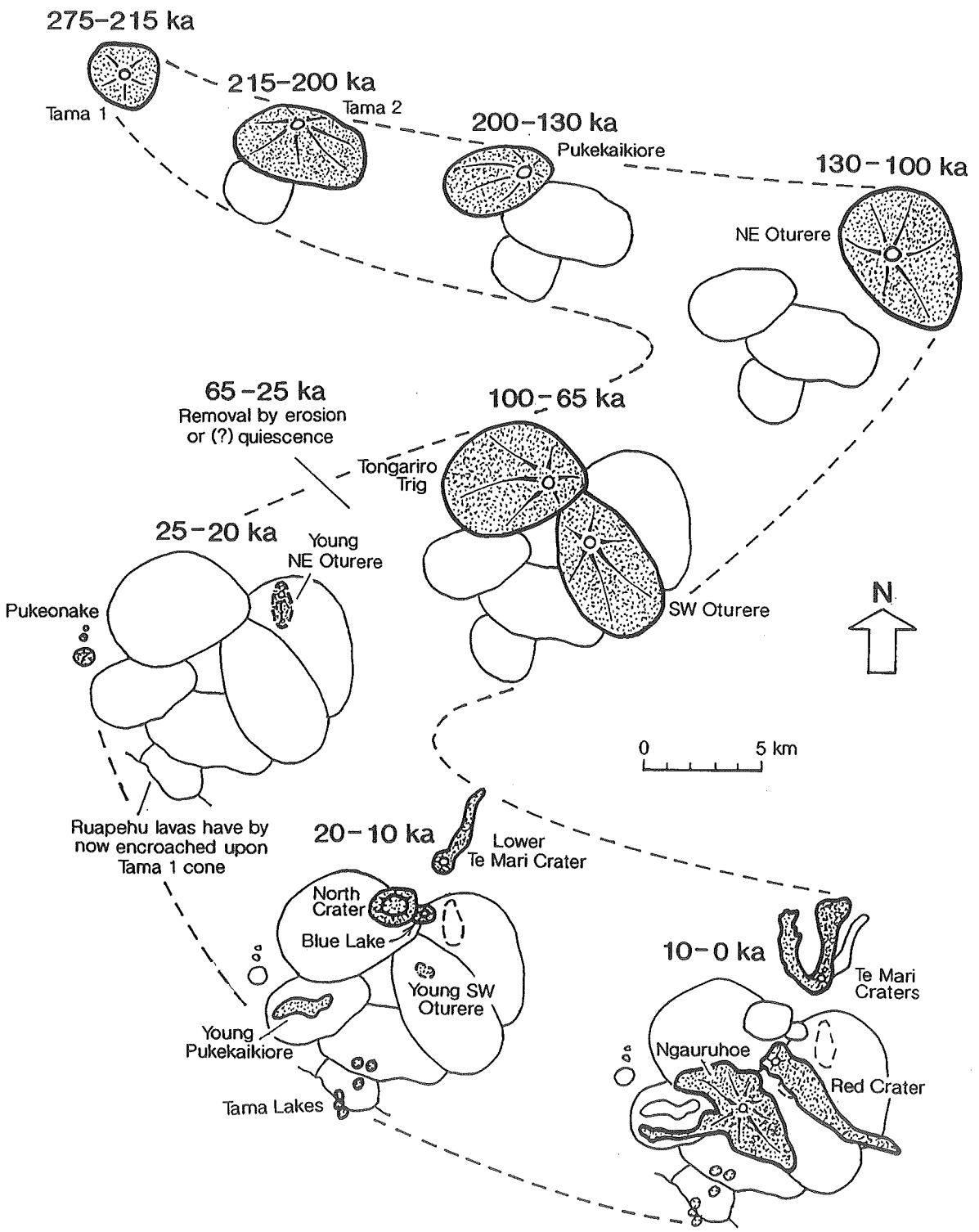

Figure 3.33 Schematic representation of the growth of the Tongariro Volcanic Complex, showing main periods of cone-building.

3.6.1 Summary of eruptive chronology

The earliest known history of the complex is recorded in the hornblende-bearing silicic andesite lava flow and dome remnants exposed in the Tama Lakes area (Tama 1 cone; c.275-215 ka; Fig 3.33A). Although partial concealment beneath younger flows together with explosive and erosive removal of parts of the cone make the original extent of Tama 1 difficult to estimate, it appears to have been comparatively small in volume (c.2 km^3) with a low eruptive rate of 0.03 km^3/ka. Activity remained focused in the south of the complex with the rapid growth (1.00 km^3/ka) of the large (c.10 km^3) Tama 2 cone between c.210 and 200 ka (Fig 3.33B). At least 55 hornblende-phyric andesite lava flows have been mapped dipping southwards away from hydrothermally-altered vent breccias exposed on the flanks of Ngauruhoe. The final phase of this concentration of hornblende-andesite production in the southern portion of the complex is represented by the Pukekaikiore cone situated just west of the Tama centres (Fig 3.33C). This cone, of moderate proportions (c.6 km^3 original volume) and low eruptive rate (0.09 km^3/ka), was active between c.190 and 120 ka, producing thick, columnar-jointed silicic andesite flows from a vent now concealed beneath Ngauruhoe.

The first obvious indication of the SW-NE vent corridor which dominates the overall Tongariro vent configuration is provided by the NE Oturere cone, which represents a shift in vent location from the south to the northeast by at least 130 ka when an intense period of activity commenced (Fig 3.33D). It is debatable whether or not growth of the NE Oturere cone was initiated earlier than this, but between 130 and 100 ka the bulk of the c.11 km^3 cone was formed (0.37 km^3/ka) by eruption of more than 70 andesitic block lava flows and intercalated scoria-tuff deposits, now exposed as thick stratigraphic sequences (bounded by angular unconformities) in the glacial valley wall. Erosion of the glacial valley is believed to have removed most of the central vent for the NE Oturere cone, although some remnants of proximal fall deposits and hydrothermally-altered vent breccias are preserved in the upper valley wall.

As activity waned in the northeast, the central portion of the complex between the southern hornblende-bearing cones and NE Oturere was filled with material erupted synchronously from two cones, SW Oturere and Tongariro Trig, between 115 and 65 ka

(Fig 3.33E). Thick stacks of andesitic-dacitic autobrecciated lavas, pyroclastic and epiclastic deposits are exposed along the walls of the SW Oturere and north Mangatepopo valleys and South-Central Crater. The Tongariro Trig cone appears to have originally been larger (12 km^3) and more productive (0.27 km^3/ka) than the SW Oturere cone (5 km^3, 0.11 km^3/ka), although the SW Oturere cone preserves evidence of a greater number of flows and pyroclastic units (c.65) compared to the Tongariro Trig cone (c.45). Old vent areas can be recognised for both cones, in the form of extensively hydrothermally-altered lavas and lapilli-tuff breccias, dike-like intrusive bodies, proximal scoria and spatter deposits, and lava flows with steep and opposing dips.

Following a possible lull in eruptive activity between c.65 and 25 ka, the complex system of vents comprising the"young eruptives", small-volume cones and pyroclastic deposits, was established on the eroded remnants of the six older cone-forming units. Recognisable original cone and flow morphology has been preserved for most of these units, and they dominate the summit landscape and skyline. These young eruptives were typically more mafic than those erupted previously, with generally higher proportions of olivine-bearing basaltic andesites.

The basaltic andesite Pukeonake scoria cone, lava flows, and associated vents formed c.23 ka and represent the only known eruptions *peripheral* to the main Tongariro complex (Fig 3.33F). At this time, back on the main edifice, a cluster of small cones was starting to form on the north flanks. The Young NE Oturere scoria fall deposit, Blue Lake spatter cone, North Crater spatter cone and lava lake, and Te Mari Crater cone were constructed over the period c.25-10 ka (Fig 3.33F-G). Discrete eruptions also occurred further to the south (Young SW Oturere scoria deposit, Tama Lakes explosions) and west (Young Pukekaikiore scoria deposit and lava flows) during the same time interval (Fig 3.33G). Many of these eruptions occurred around 10 ka, signifying that this was a period of intensive volcanic activity and peak productivity of magma for the Tongariro complex.

The most recent activity has taken place within the last 3 ka from new vents near the centre of the complex at Red Crater and Ngauruhoe, and has continued in the north from Upper Te Mari Crater (Fig 3.33H). Eruptions from the Red Crater vent have built up a small scoria cone and sent small to large lava flows in many directions, with ash and

steam eruptions occurring last century. By far the most productive of all the post-glacial vents has been that of Ngauruhoe, which has issued numerous lava flows (c.80 exposed) and built a 2.2 km^3 cone within its 2.5 ka lifetime at an average rate of 0.88 km^3/ka. Ngauruhoe has been frequently active in historic times and last erupted in 1975. The Upper Te Mari Crater has also erupted historically, but has not produced a lava flow since c.1500AD.

3.6.2 Time-space-volume relationships

(a) **Sequence of vent locations.** The preceding survey of Tongariro eruptive history reveals a rather non-systematic time-space relationship between cones. Although the early part of Tongariro history saw a concentration of activity in the southern part of the complex, the locus of subsequent activity did not progress in an ordered manner northeastwards up the vent corridor. Instead, eruptions switched from the northeast (NE Oturere) back south (SW Oturere and Tongariro Trig), and finally northern (Young NE Oturere, Blue Lake, North Crater, Te Mari Craters), southern (Tama Lakes) and central (Young Pukekaikiore, Young SW Oturere, Red Crater, Ngauruhoe) vent locations were all exploited by magmas erupted during the final "young eruptives" stage. This pattern indicates that a certain degree of flexibility in magma ascent and storage was allowed by the tectonic regime affecting the region, and that quite an intricate complex of magma plumbing systems existed beneath the volcanic edifice. Despite the seemingly random nature in which magmas find their way to the surface over time, all of the 30 or so recognised vents are confined to a 13 km-long and 5 km-wide SW-NE aligned vent corridor which parallels the alignment of the Taupo Volcanic Zone.

(b) **Persistent activity.** Although the time of inception of the Tongariro Volcanic Complex is not known for certain, from the earliest signs of activity at around 275 ka to the present day the magmatic system has remained almost constantly activated. This is demonstrated by the overlapping in time of successive cone-building events such that usually at least two cones were under (varying stages of) construction over the same time period. Thus melt generation and magma supply have been ongoing processes for most of Tongariro's lifetime. Only one possible major period of repose has been identified, between

c.65 and 25 ka, but the lack of lavas dated from this period could equally be attributable to their removal by glacial erosion or to sampling bias.

(c) **Rates and durations of cone-building.** Growth of the Tongariro complex may have been virtually continuous, but this growth did not occur at a steady rate. The periods during which a noticeable upsurge in magma production occurred were c.210-200 ka (growth of Tama 2 cone) and c.130-80 ka (main growth phases of NE Oturere, SW Oturere and Tongariro Trig cones). The very high cone-building eruptive rate of Tama 2 ($1km^3/ka$) is an order of magnitude larger than the rates of some of the other cones. Around 50% of the lavas and pyroclastics making up the Tongariro complex was erupted during the130-80 ka period of accelerated activity. The durations of cone-building at any one vent also varied, ranging from the short-lived (<10 ka) Tama 2 cone to comparatively long-lived cones which were active for >50 ka before the locus of activity shifted elsewhere.

3.6.3 Styles of eruption

The wide variety of eruptive product types at Tongariro reflect an equally wide range of eruption styles. There is no obvious progression or pattern to the occurrence of different eruptive styles through time. The preserved products of Tongariro are dominantly effusive, although this may be a slightly biased view since evidence of explosive eruptions is often removed. Ample evidence for Hawaiian-Strombolian style spatter-scoria eruptions and phreatomagmatic activity exists throughout most of Tongariro's history, but is perhaps concentrated more in the latter half of its lifetime. Many of these lava flows and pyroclastics are exposed in thick continuous sequences in valley walls which allow determination of detailed stratigraphies involving division into internally consistent subunits. The extent and nature of the distal tephras representing subplinian-plinian style eruptions are not fully known and are the subject of ongoing research by other workers. Until the ring plain and proximal cone histories are linked together into a unified model of Tongariro's development, it will be difficult to have much more than a general impression that this most explosive style of eruption was indeed a feature of many of the cone-forming events on Tongariro.

3.6.4 Relationship between early and later cone-building styles

This study provides the opportunity for a comparison between the early cones and the better-preserved young cones. One obvious drawback to a simple comparison is that the eruptive history is a lot more detailed for the young eruptives than it is for the pre-glacial cones. Poorer cone preservation and age control for the older units mean that in defining each of these cone-forming units there is no alternative but to (often unknowingly) bracket several "young eruptive"-type units together because they cannot be clearly recognised as individual entities. Thus calculations of erupted volume and duration of cone-building are not strictly analogous. Notwithstanding this problem, it is still possible to make some useful observations. Comparable eruptive rates have been calculated for both old and young cones; for example, the high magma output of Ngauruhoe (0.9 km^3/ka) almost matches that of Tama 2 (1.0 km^3/ka). The location of older vents shifts non-systematically with time as is the case for the young vents, and together with the fact that vents of all ages share the same vent corridor alignment it appears that similar magmatic plumbing system dynamics have endured for most of Tongariro's development. Despite the lower levels of preservation for the pre-glacial cones, the same variety of eruptive products and hence eruption styles can be found represented by the earlier history of the complex as are demonstrated by the most recent cones.

3.6.5 Implications for composite volcanoes

It is difficult to assess with any degree of certainty how typical Tongariro's eruptive behaviour and history is compared to other composite volcanoes. This is because very few similar time-volume-composition studies have been conducted. In general, the lifespan, size, and eruptive products of the Tongariro complex all have aspects in common with other andesite volcanoes (e.g. Hackett and Houghton, 1989; Ferguson et al., 1992; Feeley et al., 1993). A more useful comparison is with the detailed investigation of Mount Adams by Hildreth and Lanphere (1994). Their implications for understanding the workings of composite volcanoes are duplicated in the findings for this study of the Tongariro complex.

An important result of the Mount Adams study was that the construction of an arc volcano often encompasses several growth spurts when magma production rates were particularly high, interspersed with much longer periods of sporadic, low-level background activity (Hildreth and Lanphere, 1994). The investigation of Tongariro also reveals a pattern of long-term behaviour whereby certain periods of peak productivity were responsible for adding significant volumes to the cone complex. Thus volumetric eruption rates are generally more meaningful when calculated within the context of the time scales of a detailed volcano-stratigraphy. Otherwise, if only an average rate for the lifetime of the volcano had been estimated, the unique rhythms in varying peak and background magma production rates now evident for Tongariro's history would not have been revealed.

Chapter 4

Petrography and Mineralogy

CHAPTER 4
PETROGRAPHY AND MINERALOGY

4.1 INTRODUCTION

Considering the extent of sampling on the Tongariro Volcanic Complex (approximately 80% of exposed lavas; Section 3.2.2) and the resultant large number of thin sections (395 from a total of 410 lava samples), the general petrography of Tongariro lavas is now well known and is described in this chapter. Following on from the volcano-stratigraphic framework established in Chapter 3, a principle aim of this chapter is to apply the variability in petrography, mineralogy, and crystallization conditions to the volcano-stratigraphic units. This is possible to varying degrees, depending on the amount of mineral chemistry data that are available for the different units. Identification of differences within and between units in terms of textures, phenocryst assemblages, modal abundances, disequilibrium features, mineral compositions, equilibration temperatures, fO_2, etc. contributes to our understanding of Tongariro's magmatic trends within the construct of time-space relationships. These observations are reported in the following sections, and represent a necessary forerunner to discussions of whole-rock chemical compositions (Chapters 6 and 7).

After some general observations on the overall mineralogical and textural characteristics of Tongariro eruptives (Sections 4.1-4.3), the first main part of this chapter is devoted to description and discussion of an investigation into the petrographic traits of the volcano-stratigraphic units (Section 4.4). Results of a microprobe and textural study of the main phases contained in Tongariro lavas are then presented and discussed in Section 4.5. Mineral compositional data are then utilised to assess the crystallization conditions of

magmas from a variety of units (Section 4.6). A special section draws together and discusses the strands of evidence for the magma mixing processes which have been ubiquitous throughout Tongariro's magmatic history (Section 4.7). And finally ,a case study of NE Oturere examines stratigraphic variations in petrography and mineralogy, and what these changes mean for magmatic conditions and processes involved (Section 4.8). A table summarising the petrographic variations within and between volcano-stratigraphic units (Table 4.6) is included at the end of the chapter along with the final summary (Section 4.9). However some of the major implications of the data presented in this chapter are briefly summarised below:

1. Although the typical mineral assemblage dominated by plagioclase along with orthopyroxene and clinopyroxene prevails on the Tongariro complex, hornblende is a significant phase confined to the older southern cones of Tama 1 and 2, and Pukekaikiore, and olivine is particularly prominent in the young eruptives, suggesting an overall time-space relationship with petrography and mineralogy.

2. Apart from any obvious differences in the presence or absence of hornblende or olivine, the mineralogical variability between volcano-stratigraphic units is generally more subtle (given the constraints of the available data) with the main distinction being the degree of disequilibrium displayed (see next point).

3. Evidence for disequilibrium between phenocryst phases and groundmass and the involvement of magma mixing processes is especially prevalent in lavas from Tama 2, NE Oturere, SW Oturere, Pukeonake, Red Crater, and Ngauruhoe, and includes: plagioclase containing zones of intense concentrations of glass inclusions (sieve texture) coinciding with major compositional breaks/reversals and inner resorption surfaces; strongly reverse and/or patchy zoned crystals; co-existing high-temperature and low-temperature phases showing evidence of disequilibrium such as resorption (corroded/embayed crystal edges) and reaction rims; olivine phenocrysts with much higher Fo contents than expected from whole-rock Mg#; and bimodal or very widely ranging crystallization temperature estimates for some samples.

4. Where possible, mineral compositions were used to infer crystallization conditions and these calculations revealed some subtle differences between and within some units (e.g. Ngauruhoe lava groups appear to have crystallized at slightly different temperatures), although more mineral analyses are required to assess this variation more fully. Overall crystallization conditions encompass equilibration temperatures of 850-1100°C, oxygen fugacities on or up to 1 log unit above the NNO buffer curve, relatively low total pressures of <7 kb (possibly only 1-3 kb), and water contents of up to 2-5 wt% H_2O.

5. On the basis of variations in phenocryst mineralogy and abundances, grainsize, vesicularity, and other textures, at least three episodes of magma recharge and mixing have been identified in the NE Oturere subunit 'd' stratigraphic sequence. These subtle cyclical changes in magma petrography and chemistry suggest that multiple batches of magma and differing ascent histories have played an important role over a relatively short period of time (<10 ka?).

Sixty-two samples were chosen for detailed petrographic analysis (Appendix 3) and these correspond to the samples for which precise trace element and isotopic data have been obtained. The remaining 333 thin sectioned samples received more limited study; brief descriptions of these samples are presented in Appendix 4. A representative selection of 35 samples was point-counted to give modal % phenocryst proportions (Appendix 5). Mineral compositions were determined by electron microprobe analysis for a subset of 24 samples (Appendix 9), and were subsequently used to assess crystallization conditions. Unlike the comprehensive petrographic study, the mineral chemistry data presented here represent a preliminary investigation only.

The following mineral abbreviations are used when listing mineral assemblages: plag = plagioclase, oliv = olivine, cpx = clinopyroxene (or aug = augite), opx = orthopyroxene, hbl = hornblende, ox = Fe-Ti oxides (magnetite and ilmenite), ap = apatite, qtz = quartz. Grain size measurements are given for the maximum crystal dimension, as observed in thin section. Precise mineral compositions (mol% An, mol% En, etc.) are only given for analysed samples and therefore may not be truly representative of (or may be

missing for) those volcano-stratigraphic units for which limited (or no) microprobe data are available.

Petrography and mineralogy throughout Tongariro are generally rather homogeneous, although there are some broad differences between lavas of some of the different volcano-stratigraphic units (Section 4.4). Typically, the Tongariro rocks are two-pyroxene-plagioclase andesitic lavas which commonly contain Fe-Ti oxides, and often olivine or hornblende. The phenocryst mineralogy of Tongariro lava is thus similar to that of typical calc-alkaline andesites and basaltic andesites (calcic plag + augite + opx + Timag ± oliv ± hbl; Ewart, 1982). The occurrence of olivine and hornblende allows the Tongariro lavas to be divided into three broad petrographic groupings (Fig 4.1):

1. Plag + oliv + cpx + opx ± ox (rare ap, qtz)
2. Plag + cpx + opx ± ox (rare ap, qtz)
3. Plag + cpx + opx + hbl + ox (rare oliv, ap, qtz)

Minor aphyric lavas are also present on the complex. Figure 4.1 shows the relative proportions of the petrographic groups for all thin-sectioned Tongariro lavas. The dominant group is the two-pyroxene assemblage which accounts for 60% of the samples. Olivine-bearing lavas constitute a significant minority (30%), with the hornblende-bearing lavas being less common (less than 10% of samples). Hornblende and olivine, however, are not mutually exclusive; some hornblende-bearing lavas contain rare (typically <<0.5 modal %) olivine phenocrysts or microphenocrysts (usually surrounded by reaction rims), but these lavas are still classed within grouping 3 for petrographic purposes.

There is no clear relationship between petrographic group and chemically-determined rock type (Fig 4.2). Features of note are that olivine is a significant phase in andesite as well as basaltic andesite, and that hornblende is restricted to andesitic lavas.

The typical crystallization sequence for a Tongariro andesite (determined principally from textural relationships in thin section) is plagioclase, followed by Fe-Ti oxides, then orthopyroxene and clinopyroxene. Olivine, when present, crystallizes early along with or just after plagioclase. Clinopyroxene also tends to be an earlier crystallizing phase in the

Figure 4.1 Petrographic groupings for all thin-sectioned Tongariro samples.

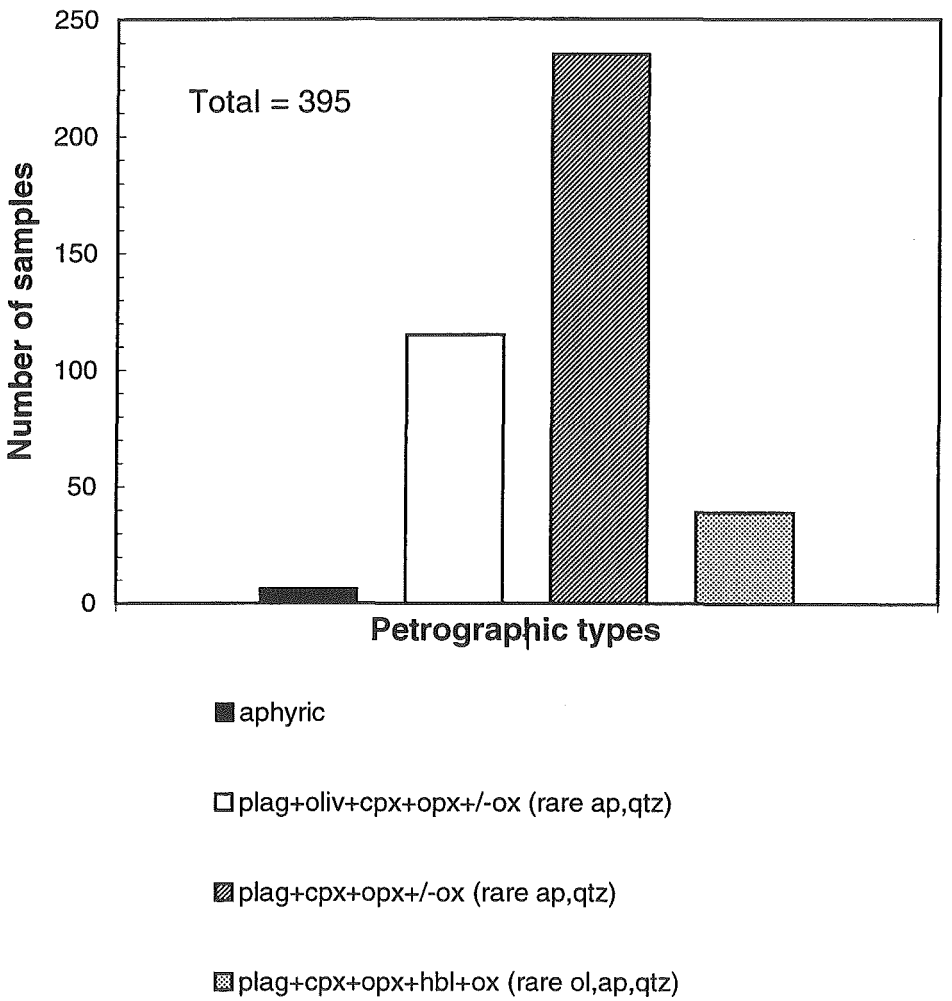

Figure 4.2 Petrographic groupings of Tongariro lavas according to rock type (TAS classification).

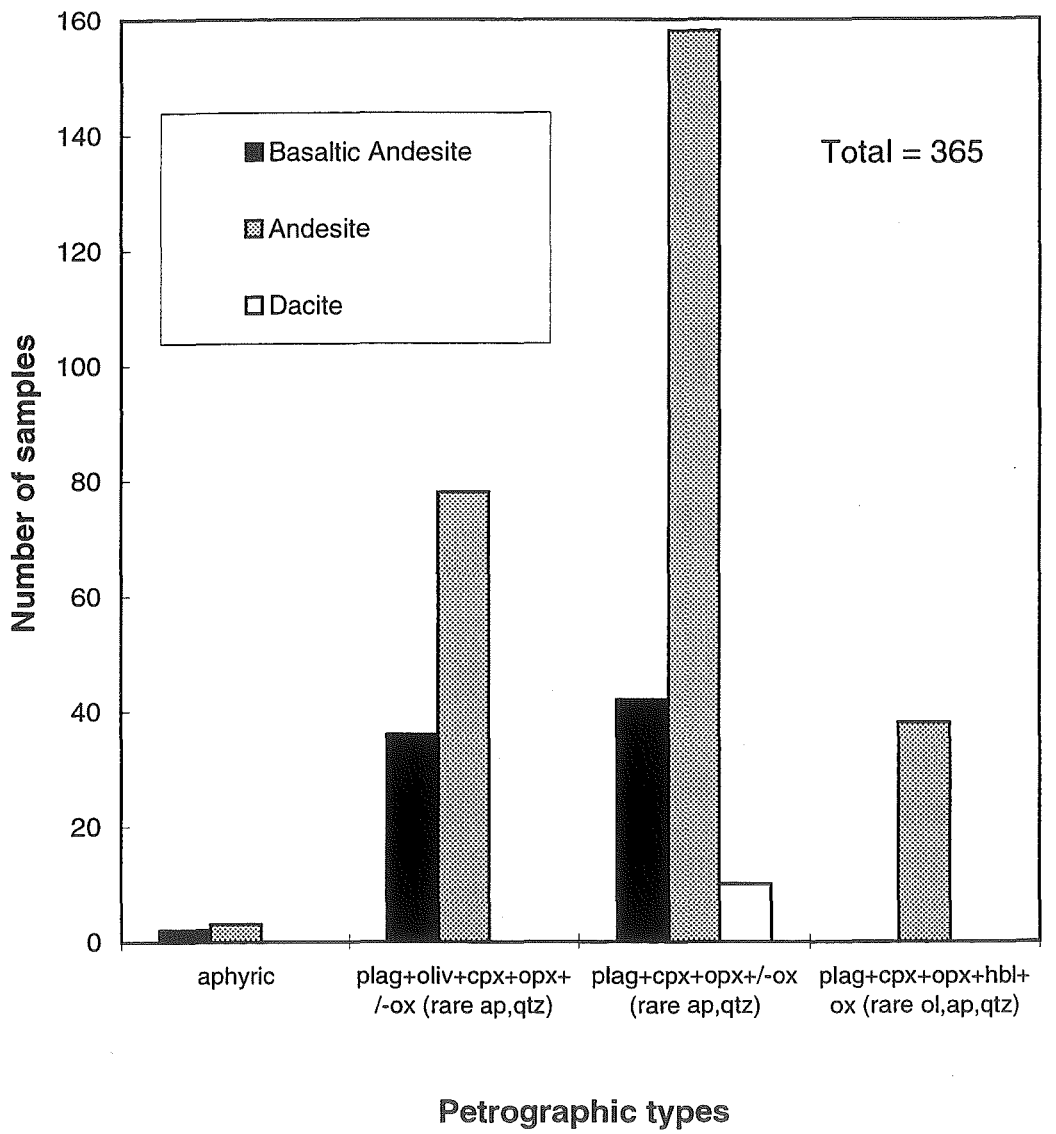

olivine-phyric lavas. Hornblende-bearing lavas appear to have crystallized mostly in the order: plagioclase, Fe-Ti oxides, hornblende + orthopyroxene ± clinopyroxene, apatite.

Although Tongariro lavas have been grouped petrographically in order to assess broad trends and patterns, these groups do not form the basis of a classification. Because of the fine grain size and glassy nature of many volcanic rocks, chemical classifications are generally more important and more useful than petrographical ones. Since a chemical analysis is available for 365 out of 395 thin sectioned Tongariro samples it is logical to adopt the standard TAS chemical classification system (Section 2.1).

With respect to petrography, the overall dominance of plagioclase phenocrysts (generally 60-90% of the total phenocryst assemblage) and lack of feldspathoids, alkali feldspar or quartz puts all Tongariro lavas in the basalt/andesite field of the QAPF classification diagram of Le Maitre (1989). Minor dacite lavas, as classified on the TAS diagram, lack quartz phenocrysts and therefore do not plot as dacites on the QAPF diagram. There is no definitive way to distinguish between basalt and andesite (including basaltic andesite) petrographically, hence the chemical TAS classification has been employed. The traditional division by An% (An>50 = basalt; An<50 = andesite) has been shown to be invalid (Gill, 1981), as most andesites contain plagioclase more calcic than An_{50} (e.g. Tongariro plagioclase compositions range from An_{45} to An_{90}; Section 4.5.2) so An% is not a determinative characteristic of andesite. The presence of orthopyroxene and lack of abundant olivine are often indicative of andesite. Virtually all Tongariro lavas contain orthopyroxene phenocrysts which are typically predominant over clinopyroxene. Olivine is usually only a minor phase (generally less than 10% of the total phenocryst assemblage) in Tongariro lavas.

4.2 PREVIOUS WORK

This study expands greatly on earlier work on Tongariro petrography. It involves more extensive and more representative sampling, covering a greater area of the volcanic

complex and a lengthier period of eruptive history. It is also significant in that the stratigraphic context of sampling provides the potential to tie in petrographic trends with temporal geochemical changes and thus derive a more complete picture of the petrogenesis.

Battey (1949) and Steiner (1958) provided the first significant contributions to Tongariro petrography in their descriptions of glassy two-pyroxene (± olivine) andesites erupted from Ngauruhoe in 1949 and 1954 respectively. Clark (1960a) gave a useful summary of early published petrographical work, and then, based on a relatively comprehensive study of about 300 thin sections from Tongariro Volcanic Centre, he described and classified the lavas on the basis of phenocryst content. Clark (1960a) proposed five petrographic types:

1. Labradorite andesite (plag>>pyx)
2. Labradorite-pyroxene andesite (plag≥pyx)
3. Pyroxene andesite (pyx>>plag)
4. Olivine andesite
5. Hornblende andesite

This initial classification scheme was followed, with slight modification to incorporate chemically-determined lava types, by Ewart (1965), Cole (1978), Cole et. al. (1983, 1986), Hackett (1985), Graham (1985a), and Patterson (1986). Representative modal analyses were presented by all these authors. These primarily petrographic classifications were limited by the factors mentioned in Section 4.1.

Because Graham and Hackett (1987) found this scheme difficult to apply and relate to petrogenetic models, they subdivided the lavas of Ruapehu and related vents into six types - still based largely on petrography, but refined using chemical and isotopic compositions - as follows:

Type 1: *Plagioclase-pyroxene phyric lavas.* Basalt to dacite. Plag>pyx>oliv. Volumetrically dominant type occurring throughout Ruapehu, plus Ngauruhoe 1954 and Red Crater. Derived from low-Al_2O_3 basalt by AFC.

Type 2: *Plagioclase-phyric lavas.* Two Wahianoa Formation (Ruapehu) andesites. Abundant plagioclase glomerocrysts. AFC plus crystal accumulation.

Type 3: *Pyroxene-(olivine)-phyric lavas.* Ruapehu andesite to dacite. Abundant pyroxene-rich glomerocrysts. AFC plus crystal accumulation.

Type 4: *Pyroxene-phyric lavas.* Rare Ruapehu andesites with unusual chemistry. Contain hornblende. Origin remains equivocal.

Type 5: *Olivine-pyroxene-phyric lavas.* Parasitic vents (Hauhungatahi, Ohakune, Pukekaikiore, Waimarino). Basalt to basaltic andesite. No plagioclase phenocrysts. Derived from primitive tholeiitic basalt (Waimarino?) by fractional crystallization with variable crustal assimilation.

Type 6: *Hybrid lavas.* One Mangawhero Formation (Ruapehu) lava and Pukeonake. Disequilibrium textures indicate origin by magma mixing of tholeiitic (Type 5) basalt with Type 1 andesite-dacite in a 1:1 ratio.

An additional three lava types have been described from Tongariro and elsewhere in the TVZ:

Type 7: Plagioclase-pyroxene-phyric andesites from the Pukekaikiore-Upper Tama Lake area of Tongariro. Type 7 lavas differ chemically from Type 1 lavas, and are interpreted to represent fractional crystallization of a basaltic parent without crustal assimilation (Patterson and Graham, 1988).

Type 8: The essentially aphyric (2% plag + cpx ± opx ±hbl) Type 8 andesites occur only at Rolles Peak, Tauhara (Graham and Worthington, 1988).

Type 9: Type 9 andesites are the 1977 ejecta from White Island and are geochemically similar to Type 6 lavas (Cole and Graham, 1989).

Graham et. al. (1995) reviewed these 9 lava types and concluded that the scheme allowed adequate classification of most TVZ andesites and basaltic andesites described to date.

This lava classification will not be adopted in this study because it represents a different approach from that being undertaken for the Tongariro complex. Geochronological and stratigraphic relationships are used initially to group Tongariro lavas into volcano-stratigraphic units (Chapter 3), and for each unit the petrography, mineralogy and geochemistry is described (Chapters 4, 6, and 7). In this way, any petrological trends or groupings can be assessed within the more meaningful context of time-space relationships, rather than rock types representing a wide range of ages and locations within TVZ (cf. Graham et. al., 1995). However, these time-space groupings identified in lavas of the Tongariro Volcanic Complex are compared to Graham and Hackett's (1987) Ruapehu

lava types in a later section on whole-rock chemical compositions and relationships (Section 6.7).

Donoghue (1991) provided information on the mineralogy of andesitic tephras erupted from Tongariro Volcanic Complex (see Table 3.2). This will be referred to where appropriate, but a comprehensive comparison between mineral compositions of the tephras and their associated proximal deposits or lavas is beyond the scope of this study. Electron microprobe analyses of Tongariro phenocryst phases are contained in the following studies (location of Tongariro samples indicated in brackets): Cole (1978; partial analyses of Ngauruhoe 1954 and Tama Lakes), Hackett (1985; Pukeonake), Graham (1985a; Red Crater), Patterson (1986; Pukekaikiore), Graham and Hackett (1987; Ngauruhoe 1954), Patterson and Graham (1988; Ngauruhoe, Red Crater and Pukekaikiore), Donoghue (1991; Tongariro tephras), Donoghue et. al. (1991; Mangamate Tephra, Tongariro), and Wahyudin (1993; Tama Lakes). The new mineralogical data presented in this chapter complement the existing analyses but also extend the data base further back into Tongariro's history to include analyses of some of the older lavas (SW Oturere, Tama 2, NE Oturere, Tama 1). However, a more comprehensive and representative study of Tongariro mineral chemistry is required.

4.3 GENERAL TEXTURES AND MODAL ANALYSES

4.3.1 Hand specimen

In hand specimen, Tongariro lavas range from dark grey to black basaltic andesites to medium/light grey andesites and dacites, and display several textural and structural features recognisable in the field. Phenocrysts are conspicuous, especially plagioclase, although the groundmass tends to be microcrystalline or glassy. Many lavas are weakly to moderately vesicular, and in some samples (especially scoria) vesicles make up more than 10% of total rock volume. The moderate to high crystal contents and vesicularity of Tongariro magmas contribute to their increased viscosity, and eruption as mainly block lava

flows (Section 2.2). Vesicles are typically 0.1-20 mm in diameter (some coalesced) and spherical, ellipsoidal or irregular in shape.

Often vesicles have been stretched out (up to 40 mm long) and aligned sub-parallel to the flow direction. Tabular plagioclase phenocrysts may also be flow-aligned, and these flow effects have imparted a relatively flat-lying, mm-cm scale banding (rarely folded) or cm-dm scale platyness to some lavas. Compositional banding occurs infrequently and is discussed in Section 4.7.1. Another structure widely recognised in Tongariro lavas is the occurrence of mm-cm sized xenoliths (see Chapter 5).

Generally, Tongariro lavas appear relatively fresh and unaltered in both hand specimen and in thin section. The historic and young pre-historic lavas are especially pristine. All phenocryst phases are typically unaltered, except for hornblende crystals which are commonly rimmed (often pseudomorphed) by oxide minerals. Some lavas display pink to red high-temperature oxidation effects, often at autobrecciated flow margins. A minority of lava outcrops had orange/brown/grey altered surfaces, but these could usually be avoided during sampling. Areas of hydrothermal alteration (e.g. Tongariro trig, South Crater, upper NE Oturere Valley, upper SW Oturere Valley) were also disregarded during petrological sampling. Localised yellow-green (probably deuteric) alteration of some North Crater and Blue Lake samples could not be totally avoided. Overall, alteration (noted in "Comments" in Appendix 1) was relatively minor.

4.3.2 Textures in thin section

Tongariro lavas are fine-grained, and holocrystalline to hypocrystalline. Glass, where present, is usually a minor constituent of the groundmass occurring as small, indeterminate, pale to medium brown (often devitrified) patches interstitial to groundmass crystals (intersertal texture in some samples). Care must be taken in distinguishing densely packed, overlapping, tiny groundmass crystals (which confer a brown amorphous character to the groundmass) from glass. However, unequivocal glass often occurs as unaltered brown patches (up to 1 mm across) trapped in the interstices of glomerocrysts (e.g. TG027, TG134, TG156). This suggests that these glomerocrysts are xenocrystic, since glomerocryst interstices are unlikely places for the only glass present (which is often the case) to form

upon eruption. Instead, the glass probably formed when residual melt in a wallrock fragment (ripped from the sides of the magma reservoir or from the conduit walls) rapidly solidified upon incorporation into the more evolved host magma. Lava bombs (eg. TG212, TG242, TG327) tend to be among the more glass-rich samples, and a few exhibit vitrophyric textures of phenocrysts set in an almost entirely glassy matrix (Fig 4.3). Rarely, glass-rich silicic andesites or dacites (eg. TG055) display perlitic cracking.

The most noticeable textural feature of Tongariro lavas is their moderately to strongly porphyritic nature (Fig 4.4), with phenocryst contents typically 20-40%. Aphyric lavas are rare (less than 2% of samples), indicating that Tongariro magmas almost invariably partially crystallized on the way to the surface. Phenocryst maximum diameters are typically 1-2 mm, but most crystal populations encompass 0.1-0.4 mm microphenocrysts ranging up to relatively large (<5 mm) phenocrysts. This gradational variation in grain size imparts a seriate texture common to many Tongariro lavas. A distinctly bimodal grain size distribution is observed in a minority of Tongariro samples (eg. TG126 contains crystals approximately 0.3 mm or 2.0 mm).

The majority of large crystals (particularly plagioclase and pyroxene) occur as glomerocrysts (glomeroporphyritic texture) rather than as discrete phenocrysts (Fig 4.4). This indicates preference for heterogeneous nucleation. Some glomerocrysts may be cognate xenoliths from the same magma body, but these are difficult to distinguish from clusters of phenocrysts (see above).

Groundmasses range from microcrystalline to cryptocrystalline, and many are glass-bearing or glass-rich giving rise to intersertal or more rarely vitrophyric textures (see above). Sub-parallel alignment of small plagioclase laths (due to laminar flow) commonly imparts a sub-trachytic texture to the groundmass of many Tongariro lavas. These aligned laths often swirl around the larger phenocrysts, which themselves may also be roughly aligned. Groundmass microlites are dominated by euhedral to subhedral acicular lathlike or tabular plagioclase, accompanied by subhedral stubby prismatic to anhedral pyroxene (mostly orthopyroxene) and euhedral equant or anhedral granular Fe-Ti oxides (mostly magnetite), all generally less than 0.05-0.1 mm. Concentration of tiny magnetite crystals

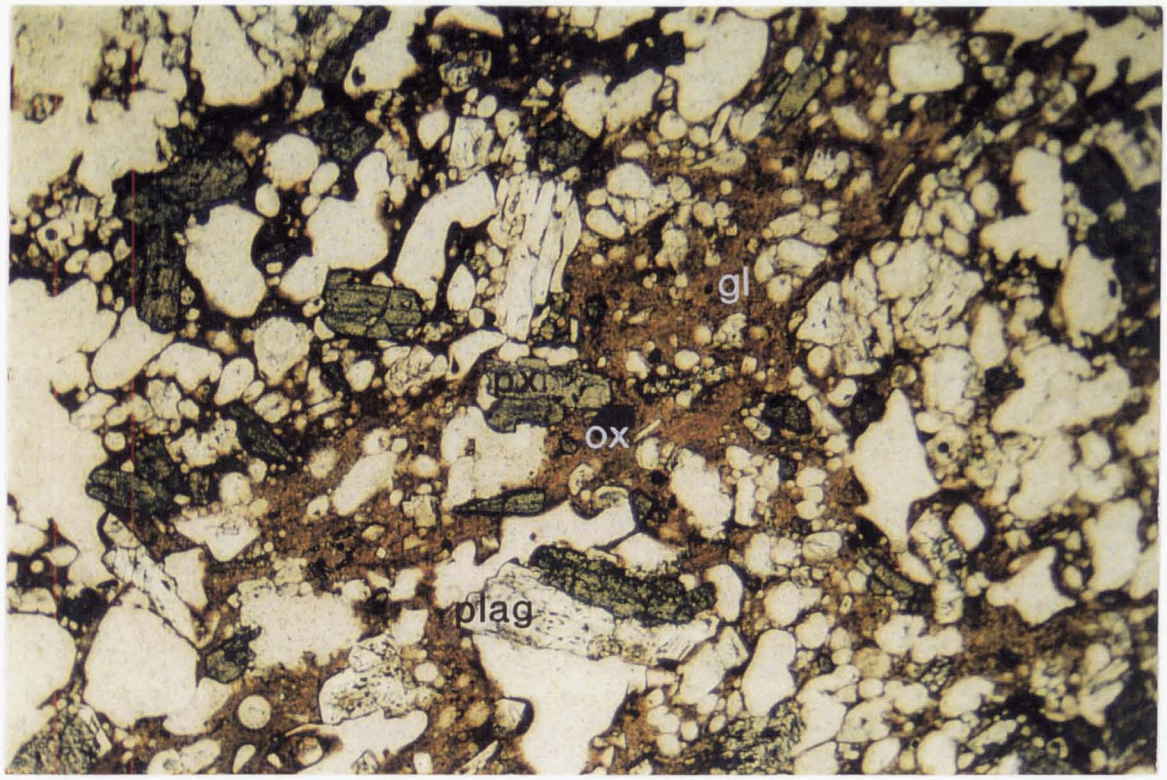

Figure 4.3 Vesicular, vitrophyric andesite lava bomb (TG327, Tongariro Trig). Phenocrysts of plagioclase (plag), pyroxene (px), & Fe-Ti oxides (ox) set in brown glass (gl). View length 7.9 mm (ppl).

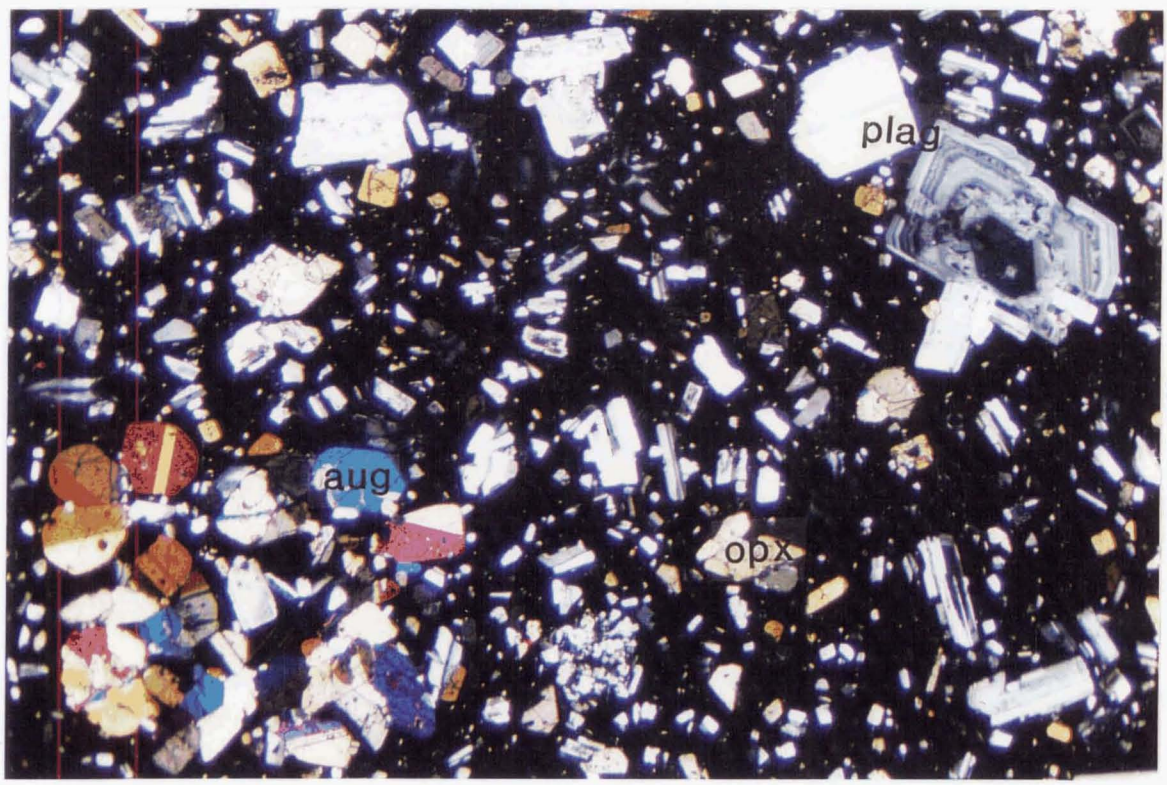

Figure 4.4 Strongly porphyritic-glomeroporphyritic, seriate andesite, (TG510, Ngauruhoe Group 3B). Zoned and sieved plagioclase (plag), orthopyroxene (opx), and augite (aug) glomerocryst. View length measures 7.9 mm (cpl).

into sub-parallel layers imparts a fine-scaled (mm) banding to the groundmass of a few samples (eg. TG022).

4.3.3 Modal mineralogy

Point-counting of 35 representative thin sections revealed total phenocryst contents ranging from 12.3 to 41.5 modal %. Figure 4.5 presents these results in the form of a histogram, with samples arranged in order of increasing SiO_2 content from basaltic andesites through to dacites. Total phenocryst contents show only a weak positive correlation with increasing SiO_2. General observation of the entire Tongariro thin section collection suggests that andesites and dacites are typically more porphyritic than the basaltic andesite lavas.

The proportion of plagioclase to mafic phenocrysts increases with increasing SiO_2 from a ratio of about 1:1 in the basaltic andesites to about 3:1 in the dacites (Fig 4.5). Plagioclase is obviously the single most abundant phase in nearly all the lavas (average 19 modal %). Clinopyroxene is generally present in higher proportions in the basaltic andesites (average 6 modal %) than the andesites (average 4 modal %), whereas orthopyroxene content is more constant throughout the compositional range (average 4 modal %). Olivine is a minor constituent of the phenocryst assemblage (generally <2 modal %) and is more abundant in the low-SiO_2 lavas, although it is noteworthy for its persistence into more silicic magmas (dropping out at around 61.5 wt% SiO_2) - usually surrounded by pyroxene reaction rims. Hornblende is restricted to the more silicic andesites, and is normally resorbed and rimmed or pseudomorphed by oxide minerals so that usually <5 modal % hornblende is observed in thin section. Exceptions are samples TG136 and Tn144 which contain up to 18 modal % of relatively unaltered hornblende. Fe-Ti oxides occur in almost 90% of Tongariro lavas. Typically, 0.5-2 modal % magnetite ± ilmenite is present throughout the compositional range, although higher Fe-Ti oxide contents generally occur in the more silicic andesites and dacites.

Figure 4.6 demonstrates the relationship between modal % of phenocrysts and whole-rock MgO. In a similar trend as that with increasing SiO_2, plagioclase contents increase steadily and markedly with decreasing MgO. Modal clinopyroxene and olivine

Figure 4.5 Modal abundance of phenocrysts for 35 point-counted Tongariro samples ranked in order of increasing SiO2 content. Modal data is contained in Appendix 5, SiO2 contents in Appendix 10.

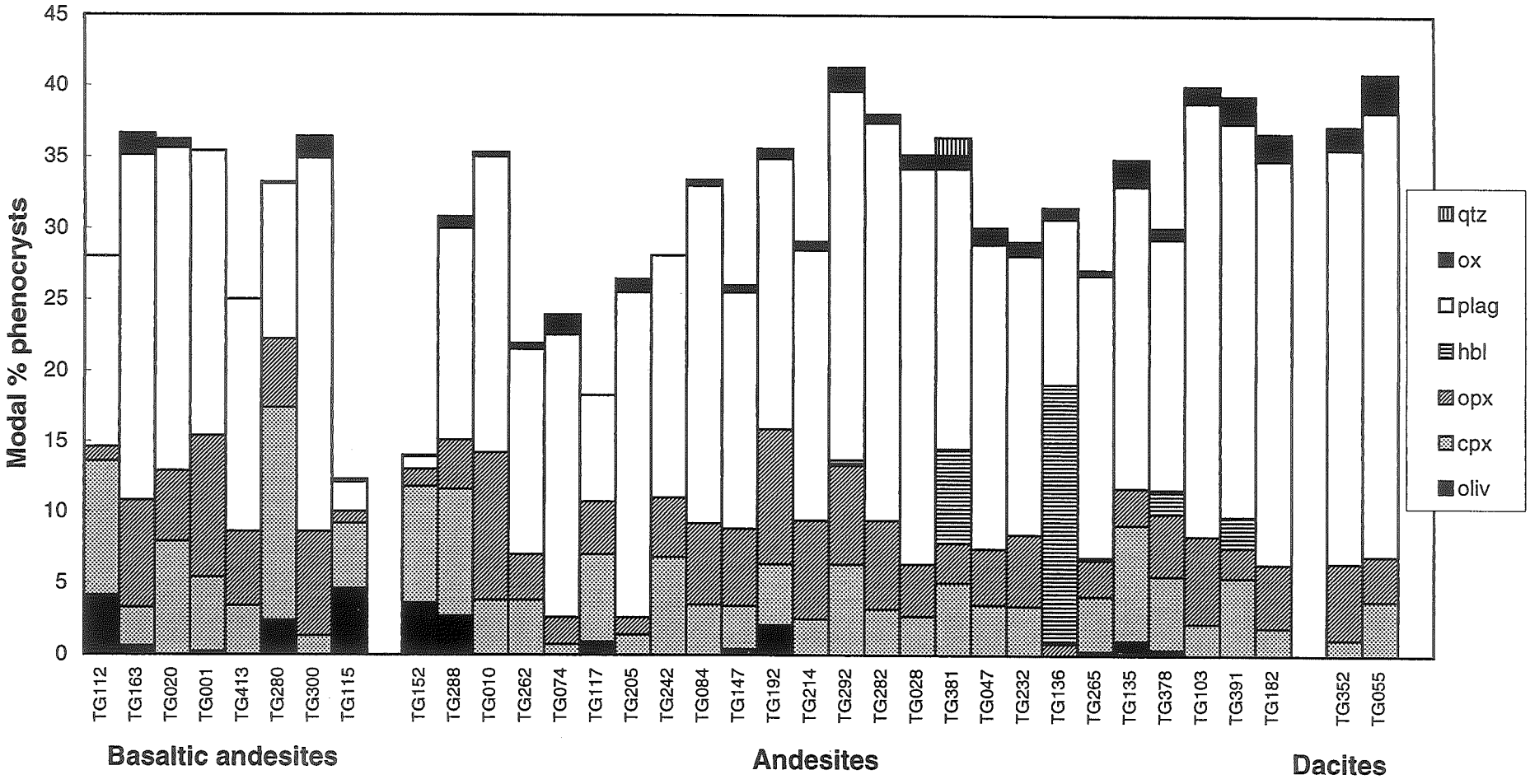

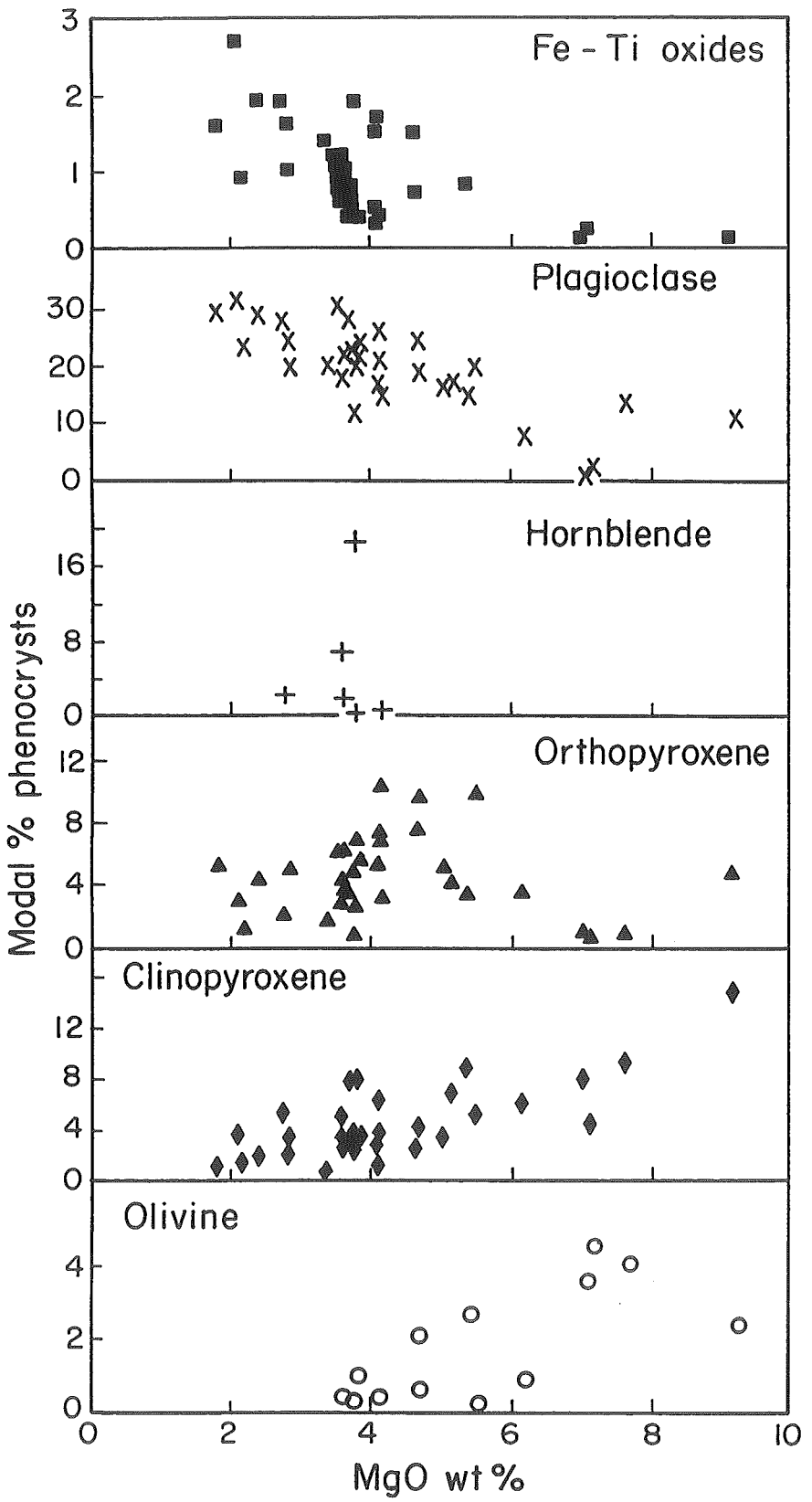

Figure 4.6 Modal abundance of phenocrysts in Tongariro lavas plotted versus whole-rock MgO. Modal data are contained in Appendix 5; MgO contents in Appendix 10.

show a strong positive correlation with MgO, falling in abundance as MgO decreases. Olivine disappears from the phenocryst assemblage at around 3.5 wt% MgO. Orthopyroxene abundance initially increases with decreasing MgO, but then levels out or decreases slightly between 4.0 and 3.5 wt% MgO. The paucity of hornblende samples precludes the identification of any trend, but it does not seem to appear as a phenocryst until whole-rock MgO falls below about 4 wt%. Modal Fe-Ti oxide increases slightly with decreasing MgO.

Looking for overall trends and patterns in modal mineralogy and whole-rock chemical composition is useful to some extent, but is limited by the problem of trying to compare all volcano-stratigraphic units together. Point-counting of many more thin sections is required to allow an adequate assessment of individual units. However, the general petrographic characteristics of each volcano-stratigraphic unit are examined in the following section.

4.4 PETROGRAPHY OF VOLCANO-STRATIGRAPHIC UNITS

4.4.1 Introduction

Figure 4.7 shows the relative proportions of the petrographic groupings identified in Section 4.1 for each Tongariro volcano-stratigraphic unit. This summary diagram provides a framework for discussion of the petrography of individual units (the geology of each unit is described in Section 3.5). Despite some variation in sampling intensity between units, a few general observations can be made. Lavas of the young cones are frequently olivine-bearing, whereas the older cones are dominated by two-pyroxene-plagioclase lavas and erupted proportionately fewer olivine-phyric lavas. This petrographic trend is also reflected in whole-rock chemistry; lavas were overwhelmingly andesitic in composition during the early part of Tongariro's history, whereas the young cones have erupted almost as much basaltic andesite as andesite lava (Section 3.5.1). The most recent lavas appear to represent the most primitive compositions erupted from the Tongariro complex.

Figure 4.7 Tongariro samples according to petrographic group and volcano-stratigraphic unit.

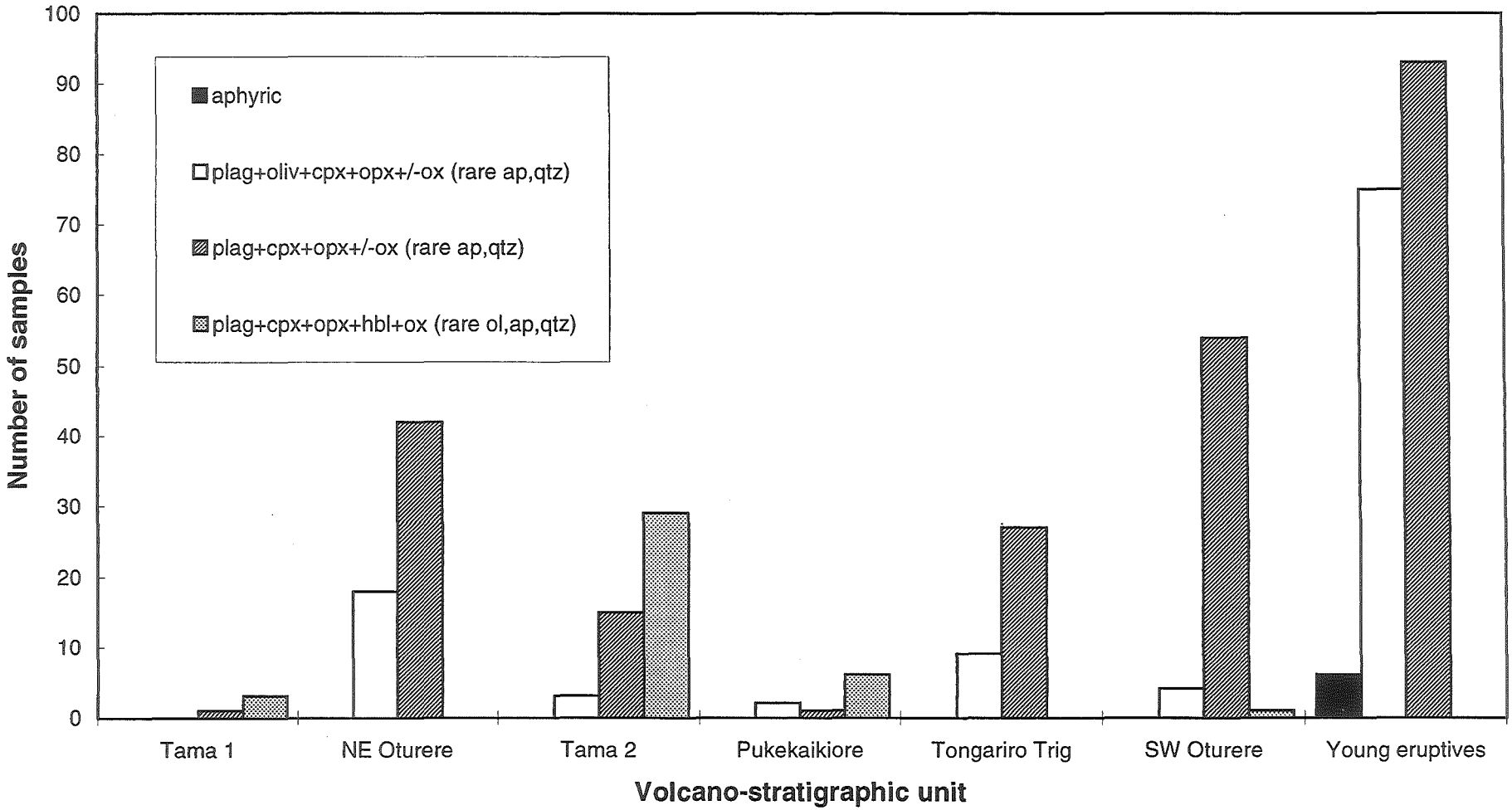

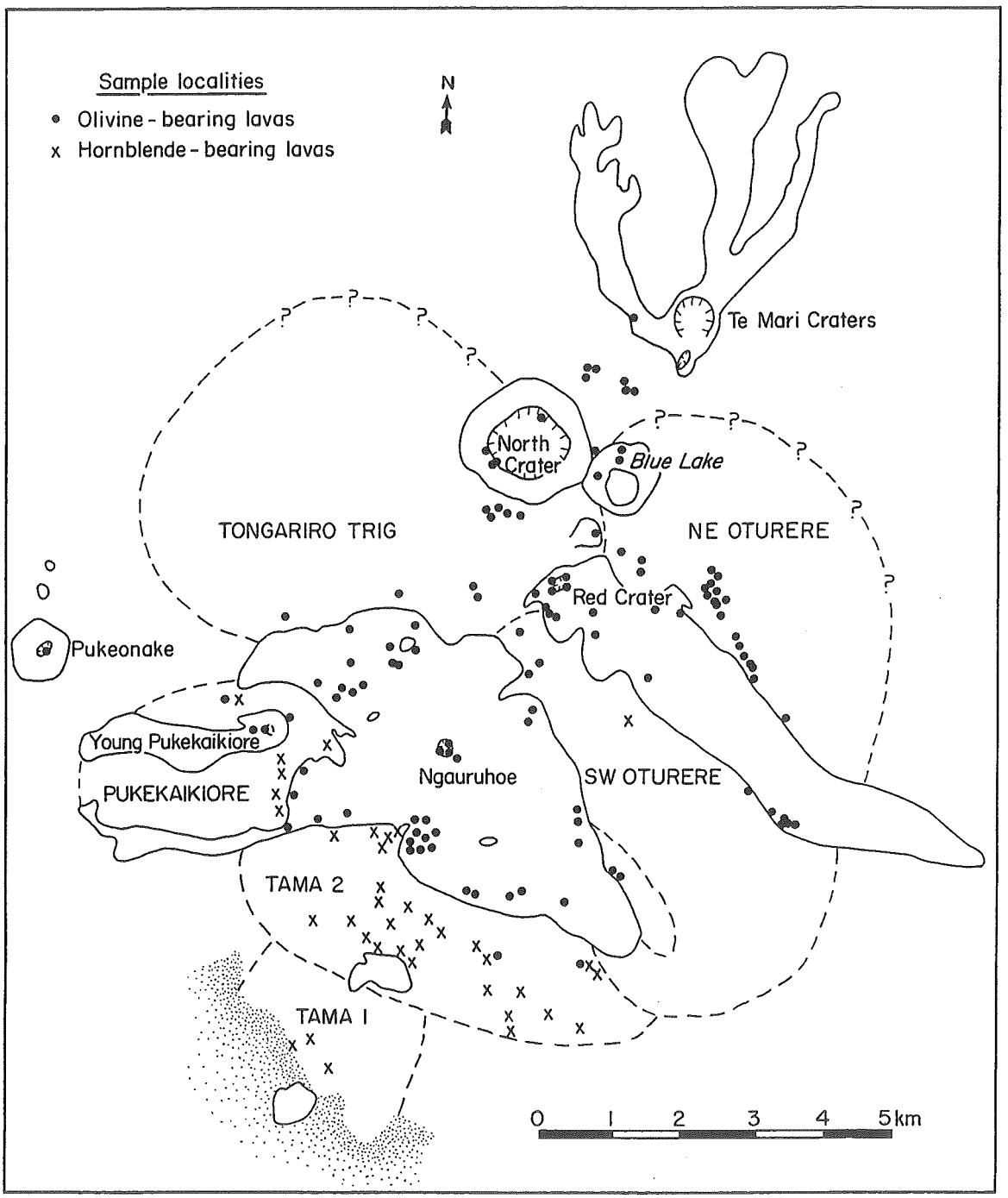

Figure 4.8 Spatial distribution of hornblende-bearing (x) and olivine-bearing (•) Tongariro lavas (sample localities plotted) with respect to volcano-stratigraphic units. Note that sample localities for lavas which lack olivine or hornblende are not shown. See Chapter 3 for further explanation of volcano-stratigraphic units.

The location of olivine-bearing and hornblende-bearing lavas sampled on Tongariro is depicted in Figure 4.8. Olivine-bearing lavas are concentrated in the younger cones (especially Ngauruhoe and Red Crater) and the older cones in the northeast (NE Oturere, Tongariro Trig), with only minor occurrences in Tama 2, Pukekaikiore, and SW Oturere. Hornblende-bearing lavas are almost entirely restricted to the older southern cones, principally Tama 1, Tama 2, and Pukekaikiore. This suggests more hydrous conditions in the magma system feeding these cones, possibly in combination with more rapid magma ascent prior to eruption which ensured preservation of the pressure-sensitive hornblende phenocrysts (see Section 4.5.4).

Petrographic features typical of each volcano-stratigraphic unit are described below (and summarised in Table 4.6 in Section 4.9). Further details of the zoning schemes, inclusions, resorption and reaction textures of each phenocryst phase are given in Section 4.5. For the purposes of this study, sieve texture (mainly in plagioclase) is described relative to the estimated proportion of crystals which are sieved: weak (<20%), moderate (20-70%), or strong (>70%).

4.4.2 Tama 1

The limited sampling (4 samples, partly a function of limited exposure; Section 3.5.2) of the Tama 1 volcano-stratigraphic unit means that it is difficult to assess whether or not these samples are representative of the petrography of the Tama 1 lavas. All the samples lack olivine and most contain hornblende phenocrysts (Fig 4.7).

The oldest samples (TG046, TG136; 273±22 ka) are the most hornblende-rich of any lavas sampled on the entire Tongariro Volcanic Complex. These lavas are holocrystalline, strongly porphyritic- glomeroporphyritic, seriate andesites (Fig 4.9). The microcrystalline groundmass is composed of plagioclase, pyroxene and Fe-Ti oxide crystals of a distinctly coarser grain size than other Tongariro lavas (Fig 4.9B). This is largely due to the stubby prismatic to tabular crystal habit of the plagioclase which contrasts with the acicular laths common to the groundmasses of most Tongariro lavas.

Phenocrysts and microphenocrysts range in size from about 0.2 to 3.5 mm and constitute about 30% of the mode. Euhedral-subhedral, pale to dark green hornblende phenocrysts constitute up to 18 modal %, and are surrounded by rims of oxides ± plag+px of varying thicknesses (0.03-0.2 mm; Fig 4.9B). The green colour of Tama 1 hornblendes differs from other Tongariro hornblendes (which are red-brown), and the compositional range is narrower for Tama 1 (ferri-tschermakitic hornblendes or tschermakites) compared with other Tongariro hornblendes (which also encompass magnesio-hornblende, edenitic hornblende and magnesio-hastingsite; see Section 4.5.4). Some of the Tama 1 hornblende microphenocrysts have been completely pseudomorphed by the fine-grained plagioclase and pyroxene, but have retained euhedral crystal shapes as defined by oxide rims. Euhedral-subhedral plagioclase (An_{57-89}) makes up <12 modal % and displays patchy, oscillatory and strong normal zoning, and a weak sieve texture. Sparse (<1 modal %) subhedral orthopyroxene (En_{62-67}) and Fe-Ti oxides complete the phenocryst assemblage.

Tn89 (266±12 ka) is petrographically similar to the lavas described above, but phenocrysts are smaller (generally <1.5 mm), hornblende is less abundant (<5 modal %), and pyroxene (including clinopyroxene) is more abundant (c.10 modal %). The youngest lava sampled from Tama 1 (TG028; 216±14 ka) differs somewhat from the other lavas, lacking hornblende and containing a much finer-grained groundmass. TG028 is a holocrystalline, strongly porphyritic (35 modal %) two-pyroxene andesite.

Of the analysed andesites of "old" Tama Lakes sampled by Wahyudin (1993), there are three which correlate with the old Tama 1 lavas mapped for this study. Samples D11 (T19/354205) and D74 (T19/361207) are strongly porphyritic andesites containing phenocrysts of plagioclase (24 modal %, An_{52-82}), orthopyroxene (5-6 modal %, En_{62-73}), augite (3-5 modal %, $Ca_{41}Mg_{44}Fe_{15}$ - $Ca_{42}Mg_{41}Fe_{17}$), and Fe-Ti oxides (1-3 modal %, magnetite). These samples (D11, D74) appear to be comparable to sample TG028. Another sample (D2-T20/354196) contains 11 modal % pale to dark brown hornblende which has a slightly more alkali-rich composition (ferroan pargasitic hornblende and edenitic hornblende) than the hornblende analysed from TG136.

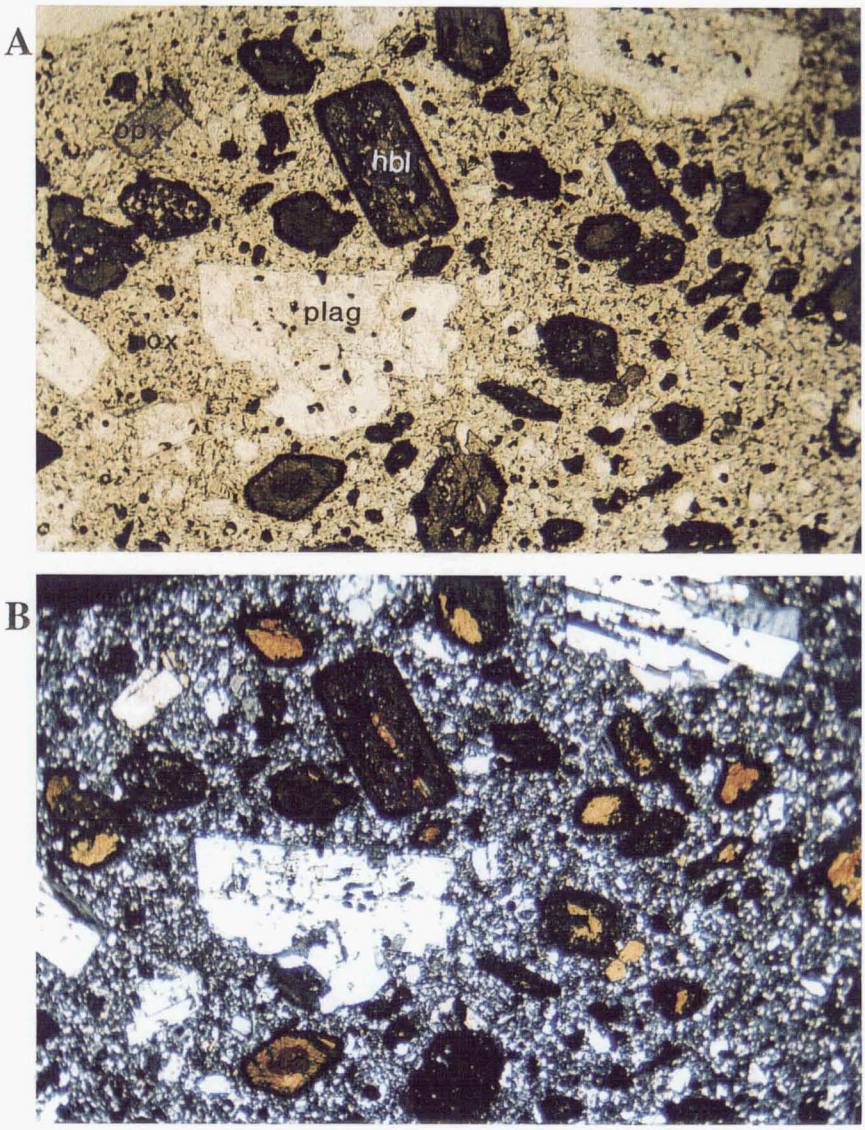

Figure 4.9 Tama 1 andesite (TG136). Green hornblende (hbl), plagioclase (plag), orthopyroxene (opx) and Fe-Ti oxide (ox) phenocrysts in a coarse-grained groundmass. View length 7.9 mm (A-ppl; B-cpl).

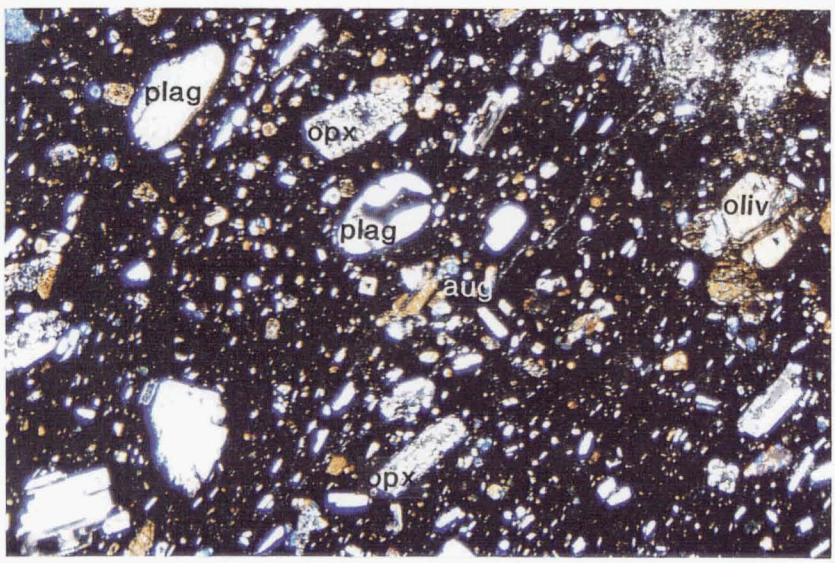

Figure 4.10 NE Oturere andesite (TG108). Coarsely sieved/fractured orthopyroxene (opx), resorbed plagioclase with sieved rims (plag), resorbed olivine (oliv), & augite (aug). View length 7.9 mm (cpl).

4.4.3 Northeastern Oturere

Comprehensive sampling of the NE Oturere lava-scoria sequence permits a representative survey of the petrography of this cone (possibly active from c.250 to 90 ka). A preliminary investigation of petrographic variation with stratigraphic position is described in Section 4.8. Olivine-bearing andesites account for 30% of the lavas sampled, but the majority (70%) are two-pyroxene andesites (Fig 4.7). The relative abundance of phenocryst phases can be summarised: plag>>cpx≥opx±oliv±ox. The lavas are hypocrystalline to holocrystalline, moderately to strongly porphyritic-glomeroporphyritic, seriate andesites (only two lavas are basaltic andesites).

Phenocrysts constitute 12-40% of the mode, and are typically 0.1-3 mm. Euhedral-subhedral plagioclase (An_{46-82}), which usually exhibits patchy, oscillatory, and strong normal or reverse zoning and is weakly to strongly sieved, is nearly always the dominant phase (6-30 modal %) apart from rare exceptions (e.g. TG105, TG118-119) when cpx≥plag. Clinopyroxene phenocrysts (2-7 modal %) are mostly subhedral and are augite ($Ca_{41}Mg_{52}Fe_7$ - $Ca_{41}Mg_{38}Fe_{21}$), and some exhibit strong normal or reverse zoning. Subhedral-anhedral orthopyroxene (En_{55-86}; normal and reverse zoning) constitutes 1-6 modal % and appears to be a less stable phase; phenocrysts are often embayed, coarsely sieved or fractured, or rimmed by clinopyroxene (Fig 4.10). Olivine (Fo_{72-87}; 0.5-4 modal %), when present, is subhedral to anhedral and is also commonly resorbed, fractured or suffering rim alteration. Euhedral to anhedral Fe-Ti oxide microphenocrysts (mostly magnetite) are present in over 75% of NE Oturere lavas but make up a very minor part of the phenocryst assemblage (generally <1 modal %). Subhedral to anhedral xenocrystic quartz occurs in two samples (TG108 and TG245) and has a corroded appearance. The wide compositional range, reverse zoning, resorption and sieve textures common to many phenocrysts (particularly plagioclase and orthopyroxene) suggest disequilibrium and the involvement of magma mixing processes.

4.4.4 Tama 2

The Tama 2 cone represents the greatest concentration of hornblende-bearing lavas on the Tongariro complex (27 flows; Fig 4.8), especially in the area immediately north of

Upper Tama Lake. These flows were also erupted over the relatively short time period of about 10 000 years (cone formed between 210 and 200 ka). The majority (62%) of Tama 2 lavas contain hornblende; only 6% are olivine-bearing, and the remainder are two-pyroxene andesites (Fig 4.7). Relative phenocryst abundances are typically plag>>cpx≥opx>hbl>ox±oliv±ap. Tama 2 flows are hypocrystalline (rarely holocrystalline), moderately to strongly porphyritic-glomeroporphyritic, seriate basaltic andesite or andesite lavas (Fig 4.11).

Phenocryst contents range from 26 to 42 modal %, and grain size ranges from 0.2 to 3 mm. Euhedral-subhedral plagioclase (An_{48-82}) constitutes typically 16-28 modal % and displays oscillatory and patchy zoning, and moderate to strong sieve texture. Clinopyroxene (1-5% of mode) is euhedral-subhedral and augite in composition ($Ca_{42}Mg_{42}Fe_{17}$ - $Ca_{40}Mg_{40}Fe_{21}$). Orthopyroxene (En_{63-69}) makes up 2-7 modal % and is euhedral to subhedral. Red-brown hornblende (0.5-7 modal %) cover a range of compositions from magnesio- to tschermakitic-hornblende, to edenitic hornblende, to magnesio-hastingite. Most Tama 2 hornblende phenocrysts are subhedral-anhedral, resorbed and surrounded by (Fig 4.11A) or more commonly pseudomorphed (Fig 4.11B) by oxide minerals. More rarely, the reaction rim is composed of plagioclase and pyroxene (±Fe-Ti oxides). Subhedral-anhedral Fe-Ti oxide microphenocrysts constitute less than 2% of the mode. Distinctive, but minor (0.1 modal %), red-brown pleochroic, prismatic apatite appears in some lavas. Rare olivine and quartz crystals are embayed and rimmed by reaction products. TG293 is compositionally banded and has fractured plagioclase (Fig 4.12). These features (along with sieve textures and heterogeneous glass compositions) are interpreted as evidence for magma mixing (Section 4.7).

4.4.5 Pukekaikiore

The somewhat restricted sampling of Pukekaikiore (9 samples) has still revealed a range of petrographic types in this relatively long-lived unit (120-190 ka); hornblende-bearing (Fig 4.8), olivine-bearing, and two-pyroxene lavas (Fig 4.7). The characteristic relative phenocryst abundances are: plag>>cpx≥opx>hbl>ox±oliv. One lava contains rare embayed quartz crystals.

A

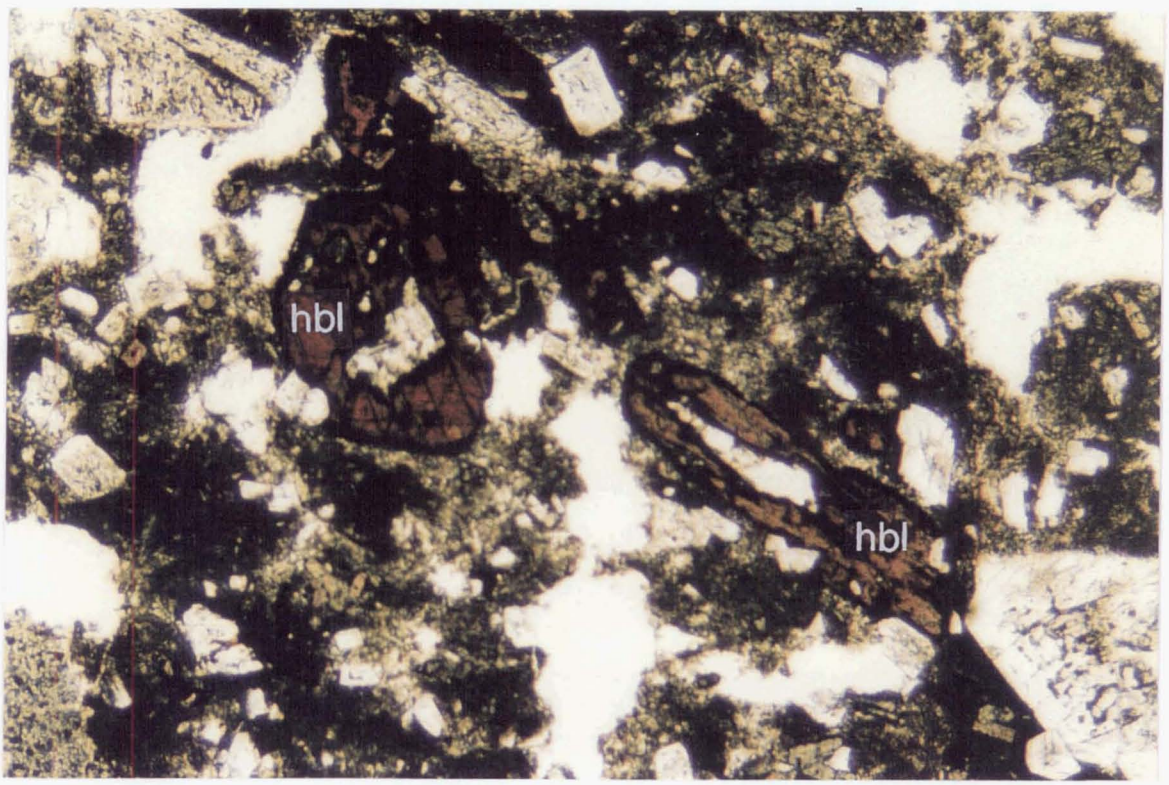

B

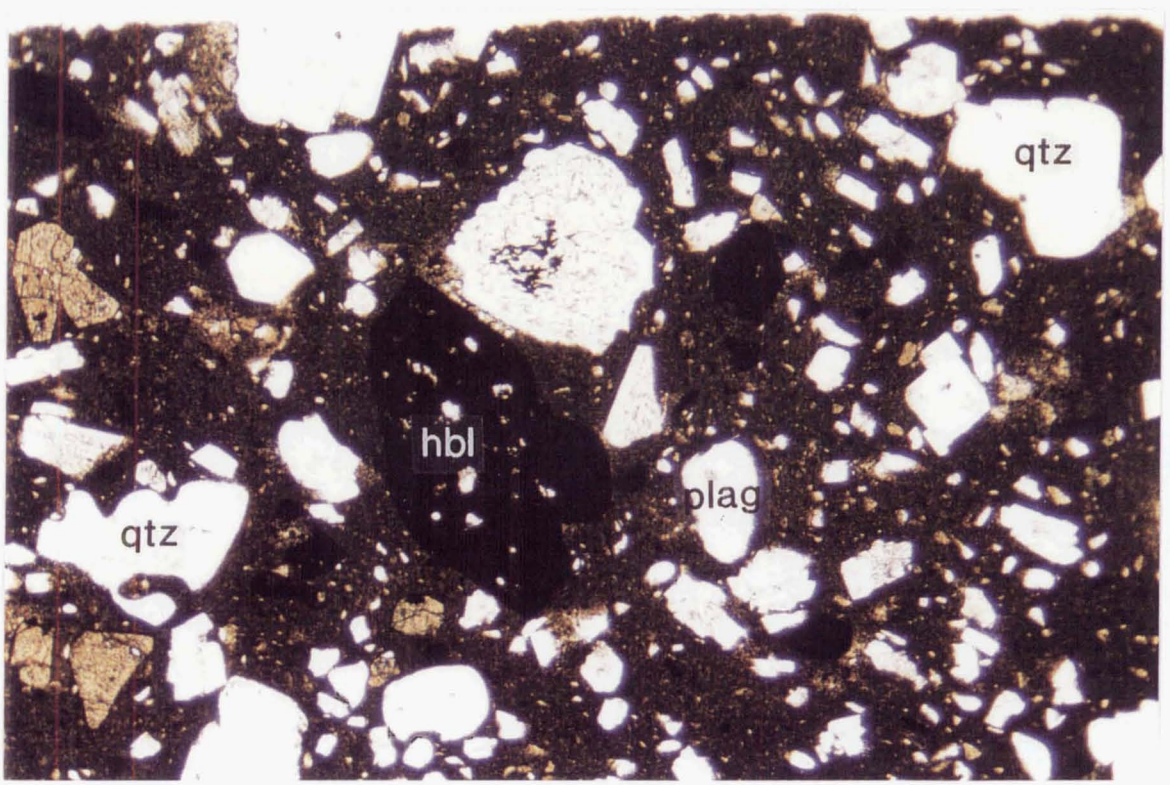

Figure 4.11 Tama 2 hornblende andesites. **A-** Red-brown hornblende phenocrysts partially resorbed and rimmed by oxides (TG376; view length 6.3 mm; ppl). **B-** Hornblende phenocrysts pseudomorphed by oxides. Note also the rounded, resorbed plagioclase and quartz (TG381; view length 7.9 mm; ppl).

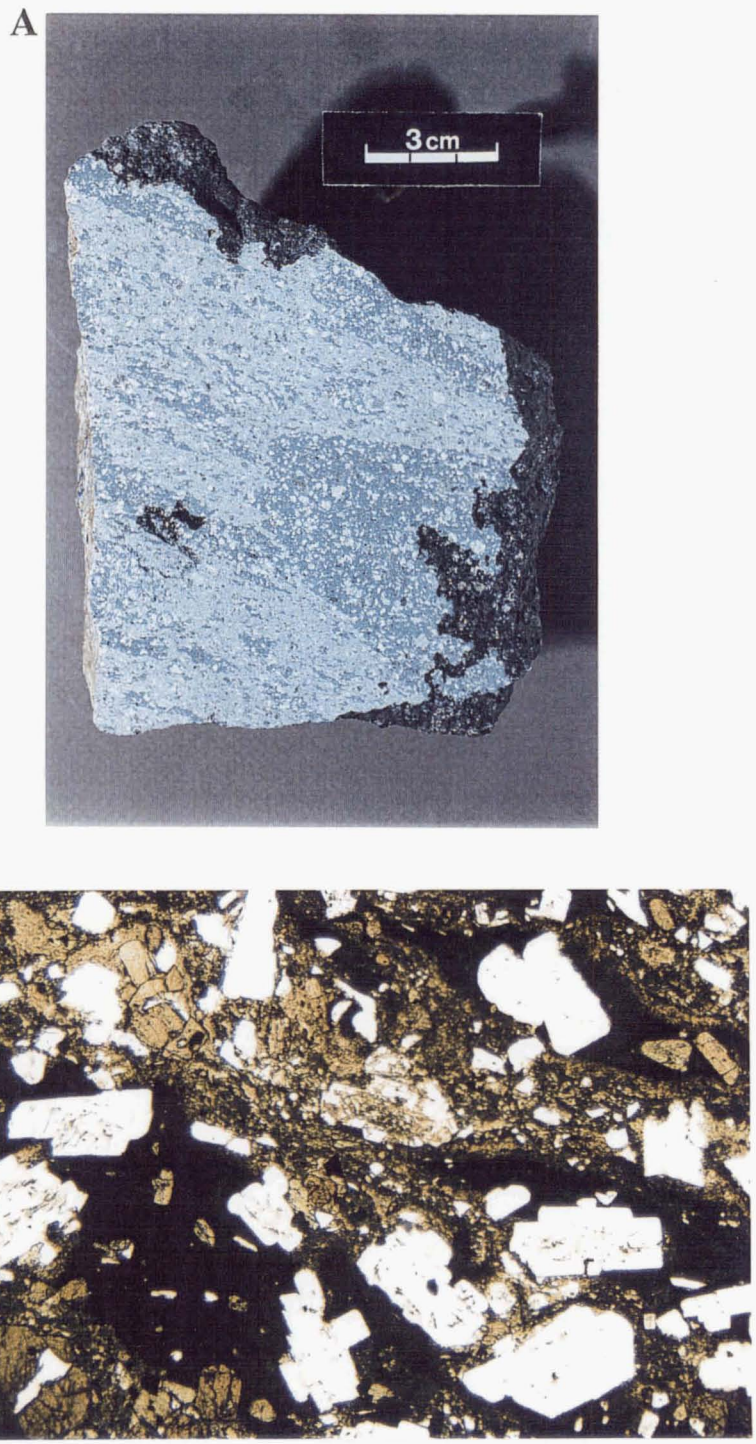

Figure 4.12 Banded andesite lava (TG293), Tama 2. Irregular bands and patches (1-30 mm thick) of microcrystalline and glassy andesite. **A-** hand specimen; **B-** photomicrograph, view length 7.9 mm (ppl).

Pukekaikiore lavas are hypocrystalline or holocrystalline, moderately to strongly porphyritic-glomeroporphyritic, seriate (grain size 0.1-3.5 mm) andesites. They are similar to Tama 2 lavas (Section 4.4.4), but the hornblende in Pukekaikiore lavas is much more severely resorbed and nearly always pseudomorphed by oxide minerals or occasionally fine-grained plag+px+ox (original pleochroic hornblende is extremely rare). Relatively fine-grained (typically <0.5 mm), clinopyroxene-rich glomerocrystic aggregates are common. Limited microprobe analysis by Patterson (1986) of one Pukekaikiore lava sample gave the following mineral compositions: plagioclase An_{57-71}, orthopyroxene En_{54-58}, augite $Ca_{42}Mg_{47}Fe_{11}$ - $Ca_{42}Mg_{37}Fe_{21}$, olivine Fo_{88}..

4.4.6 Southwestern Oturere

The lava sequences of SW Oturere cone (70-105 ka) have been sampled in detail, and the petrography is consistently plag>>opx≥cpx>ox for most (92%; Fig 4.7) of the samples. Four samples contain olivine and one is hornblende-bearing (Fig 4.7). SW Oturere lavas are holocrystalline to hypocrystalline, moderately to strongly porphyritic-glomeroporphyritic, seriate basaltic andesites to dacites.

Phenocrysts constitute 24-41 modal % and range in size from 0.1-3 mm. Euhedral-subhedral plagioclase (An_{46-88}) makes up 17-31% of the mode and is commonly oscillatory and/or patchy-zoned (normal and reverse), and weakly to moderately sieved. Similar to TG293 from Tama 2 (Section 4.4.4), plagioclase in TG182 is fractured and the cracks are filled with silicic glass (Fig 4.13) implying a magma mixing origin (see Section 4.7). Orthopyroxene (En_{56-80}) is subhedral to anhedral and constitutes 2-6% of the mode. Clinopyroxene (1-8 modal %) is typically subhedral-anhedral, and augite in composition ($Ca_{43}Mg_{47}Fe_{10}$ - $Ca_{39}Mg_{41}Fe_{20}$). Subhedral-anhedral Fe-Ti oxides (<3 modal %) are mostly magnetite but several ilmenite-rich lavas were encountered (e.g. TG080, TG240). Olivine (Fo_{70-84}), where present, is resorbed and rimmed by pyroxenes, and makes up less than 1 modal %. TG080 contains hornblende (<0.5 modal %) which is pale to dark brown, resorbed, and rimmed by oxide minerals.

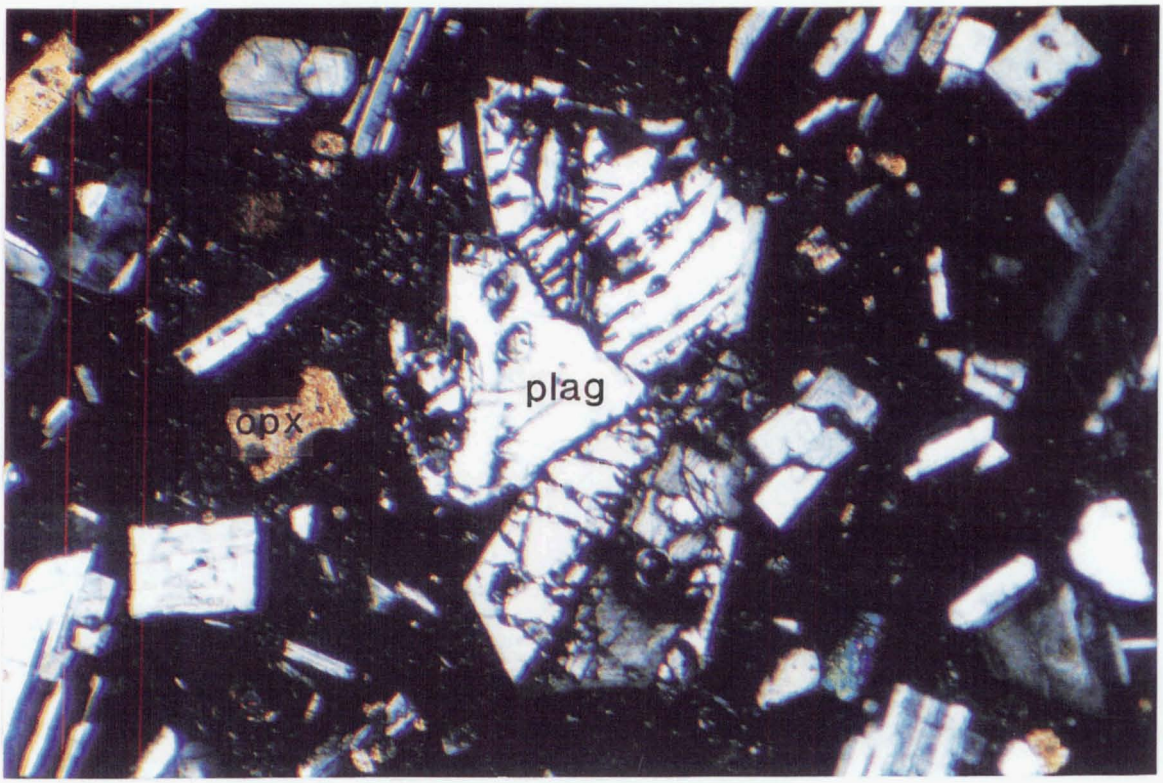

Figure 4.13 Fractured plagioclase (plag), with cracks filled with silicic glass. SW Oturere andesite lava flow (TG182). View length measures 3.2 mm (cpl).

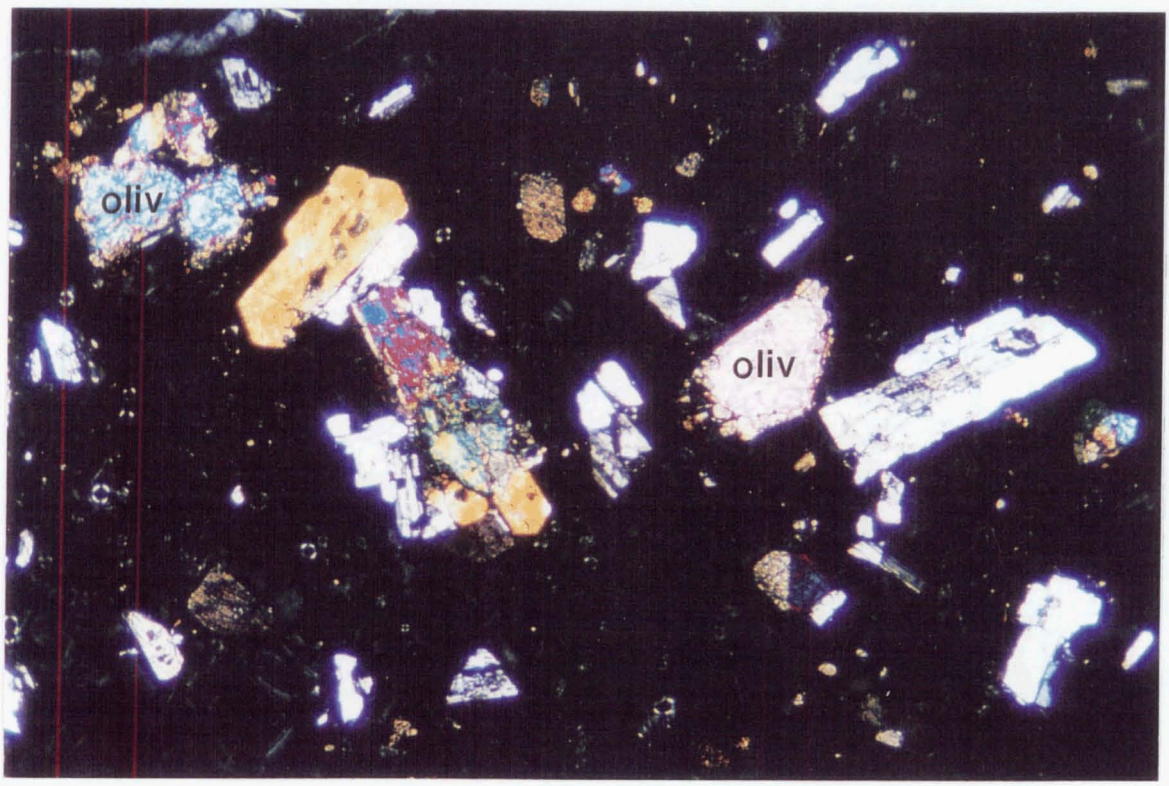

Figure 4.14 Resorbed olivine (oliv) surrounded by reaction rim of pyroxene and plagioclase, Tongariro Trig andesite lava bomb (TG317). View length measures 6.3 mm (cpl).

4.4.7 Tongariro Trig

The lava flows, scoria and agglutinates erupted from Tongariro Trig cone (65-110 ka) are predominantly (75%) two-pyroxene andesites (and one dacite), but a significant minority (25%) contain olivine (Fig 4.7). The relative phenocryst abundances can be summarised: plag>>opx≥cpx>ox±oliv. Lavas are holocrystalline to hypocrystalline, typically moderately porphyritic-glomerporphyritic (16-28 modal % phenocrysts), and seriate (grain size range: 0.1-3 mm). The flattening of pyroclastic clasts in the welded agglutinates imparts a banded texture to many of these samples.

Euhedral-subhedral plagioclase constitutes 10-20% of the mode and typically displays oscillatory (and often patchy) zoning, and weak to moderate sieve textures. Euhedral-subhedral orthopyroxene (2-5 modal %) and clinopyroxene (2-4 modal %) are occasionally resorbed or sieved. Subhedral olivine (generally <1 modal %) is also frequently resorbed and rimmed by reaction products (Fig 4.14). Fe-Ti oxide microphenocrysts are a minor but consistent part of the mineral assemblage.

4.4.8 Young eruptives

The lava flows, scoria and agglutinate erupted from the young (mostly post-glacial) cones on the Tongariro Volcanic Complex have excellent exposure and have been comprehensively sampled (over 170 samples). As noted in Section 4.4.1, the more primitive magma compositions of the young cones (relative to the older cones) are reflected in the high proportion(43%; Fig 4.7) of olivine-bearing magmas. This common occurrence of olivine-bearing lavas, and lack of hornblende-bearing lavas, in the young cones is also illustrated in Figure 4.8.

The relative proportions of the petrographic groups for each of the young cones are presented in Figure 4.15. Almost all of the exposed flows and deposits of the young cones have been sampled; Te Mari Craters and Tama Lakes are the only units requiring further sampling (Section 3.2.4). Therefore the petrographic variation illustrated in Figure 4.15 is considered to be representative of the young cones. The key observation which can be made

Figure 4.15 Samples from the young eruptives of Tongariro Volcanic Complex according to petrographic group.

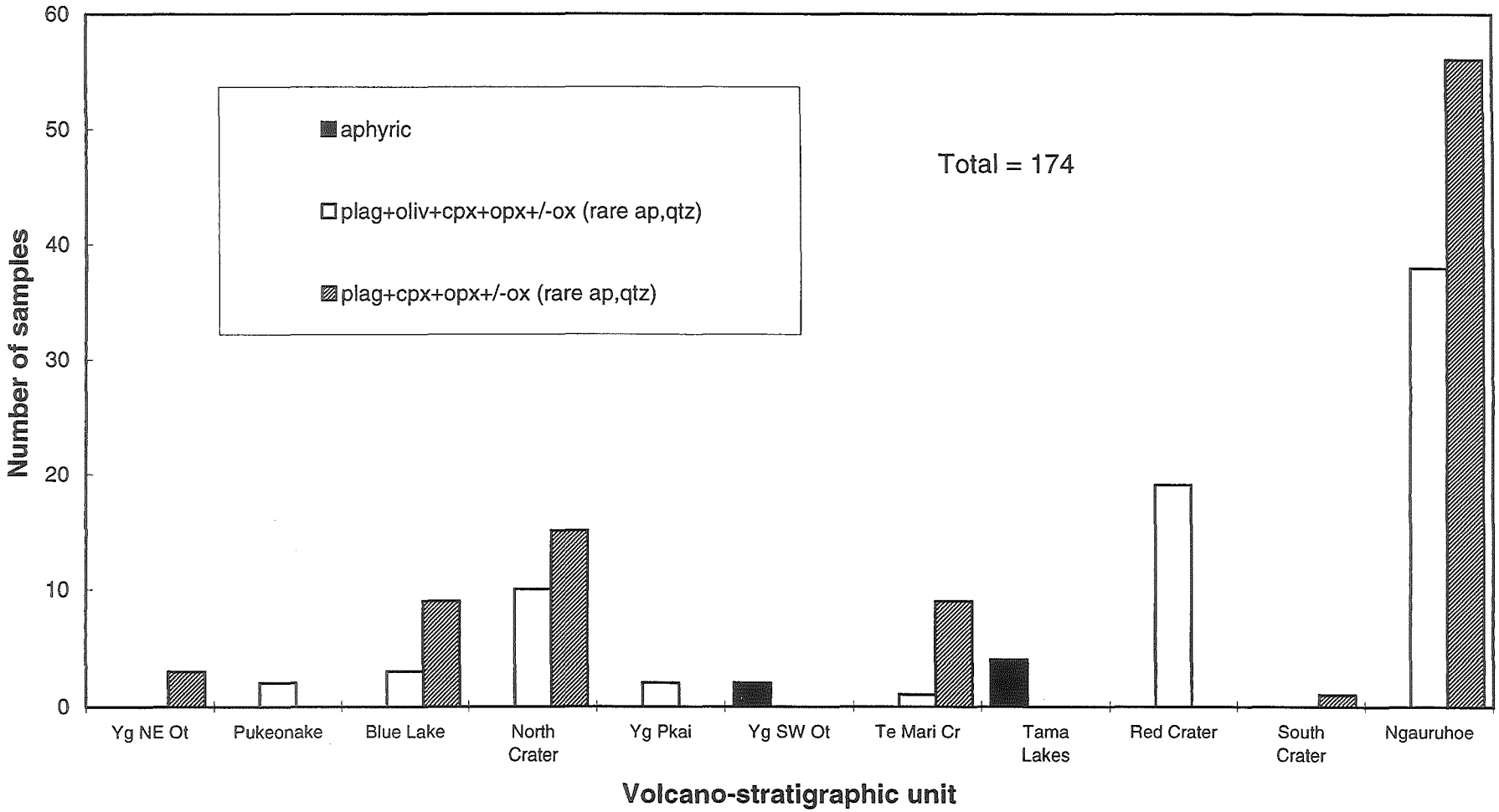

is that most of the young cones (apart from Young NE Oturere, Young SW Oturere, South Crater) have erupted olivine-bearing lavas. Although the few lavas sampled from Tama Lakes lack olivine, they are probably not representative of the cone because they are aphyric, sampling is incomplete, plus Wahyudin (1993) has described olivine-phyric lava bombs from Tama Lakes ejecta (see Section 4.4.8f). The petrography of each of the cones will be described in turn below.

(a) Young NE Oturere. The three samples of lava bombs and blocks from the Young NE Oturere scoria deposit are glass-rich, hypocrystalline, moderately porphyritic two-pyroxene andesites. Phenocrysts constitute up to 22 modal % and grain size ranges from 0.1 to 1.5 mm. Euhedral-subhedral plagioclase (c.15 modal %) displays oscillatory zoning and weak to moderate sieve texture. Subhedral orthopyroxene (c.4 modal %), clinopyroxene (c.3 modal %) and Fe-Ti oxides (<1 modal %) complete the phenocryst assemblage.

(b) Pukeonake. Samples of the scoria (TG279) and lava flow (TG280) from Pukeonake cone have similar petrography. They are hypocrystalline, moderately to strongly porphyritic-glomeroporphyritic, seriate basaltic andesites. Phenocryst contents range from 20 to 33 modal %, and grain size ranges from 0.2 to 4 mm. Euhedral-subhedral plagioclase (An_{50-74}; 8-11 modal %) displays oscillatory, patchy, and some strong reverse zoning, and moderate sieve textures (Fig 4.16B). Euhedral-subhedral augite ($Ca_{42}Mg_{51}Fe_8$ - $Ca_{34}Mg_{45}Fe_{21}$) often displays reverse zoning, and makes up 6-15% of the mode. Subhedral orthopyroxenes (En_{65-86}; 4-5 modal %) are: (i) large, strongly reversely-zoned grains with clear resorbed cores and sieved rims; and (ii) smaller, normally-zoned, sieved grains which are the same composition as the rims of the larger grains (Fig 4.16A). Subhedral-anhedral olivine (Fo_{86-95}; 2 modal %) contains chrome spinel inclusions, and is surrounded by a reaction rim of orthopyroxene (Fig 4.16). Rare (<<1 modal %) Fe-Ti oxide microphenocrysts and inclusions are also present.

The rimming of resorbed grains with more Mg- or Ca-rich overgrowths, sieve textures, and strong reverse zoning all suggest magma mixing between a high temperature magma composition ($An_{>70}$, Fo_{90}, En_{80-85}, Fe-poor augite, Cr-spinel) and a low temperature magma composition ($An_{<70}$, En_{65-70}, Fe-rich augite, Fe-Ti oxides) (Section 4.7). These

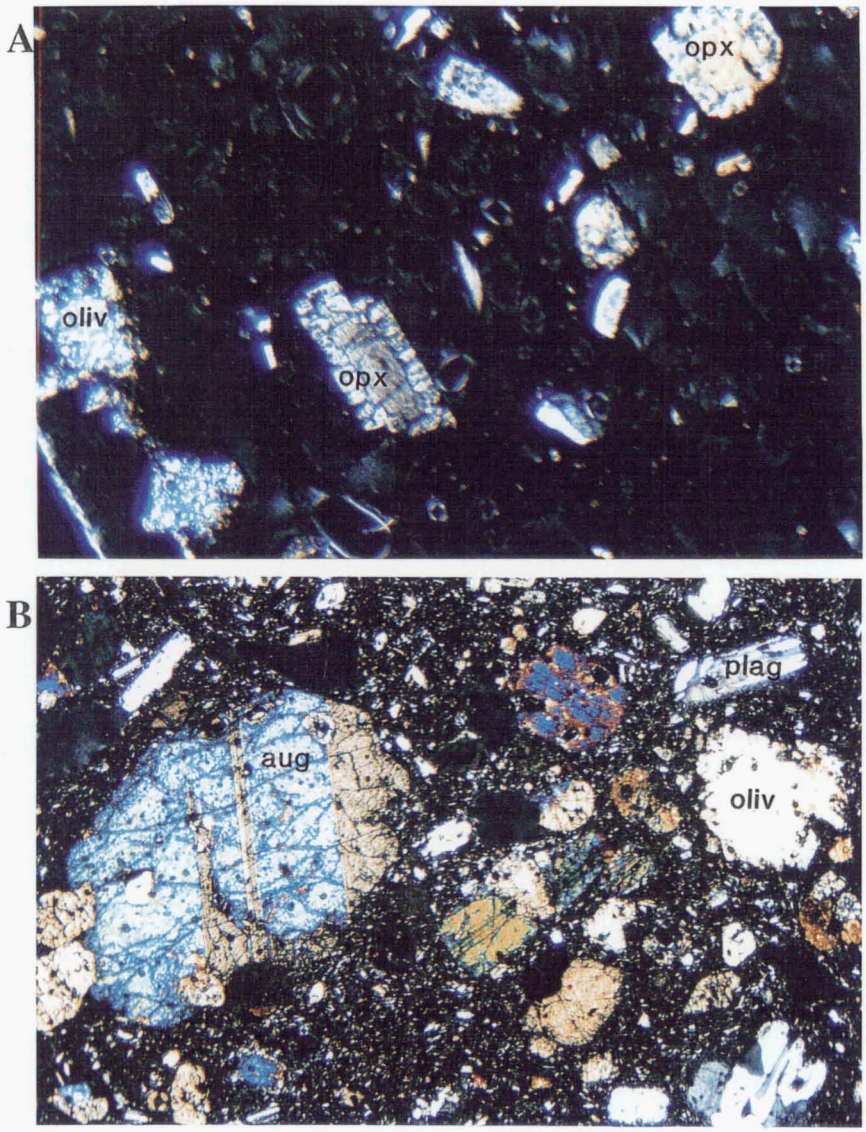

Figure 4.16 Pukeonake basaltic andesite. **A**-TG279; **B**-TG280. Orthopyroxene (opx) with resorbed cores and sieved rims, resorbed olivine (oliv) & plagioclase, and augite. View lengths 5 mm (A) & 7.9 mm (B) (cpl).

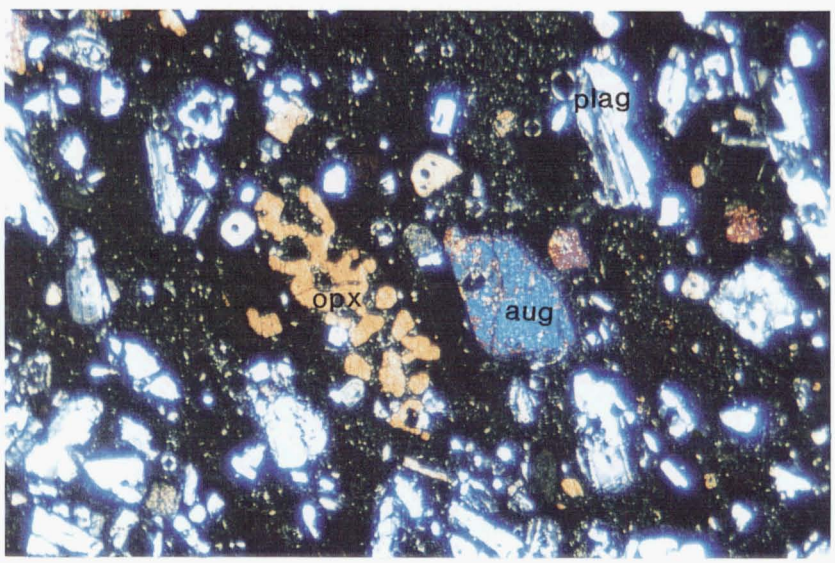

Figure 4.17 Rare corroded and embayed orthopyroxene (opx) occurs along with plagioclase (plag) and augite (aug) phenocrysts in Blue Lake andesitic scoria (TG214). View length measures 5 mm (cpl).

disequilibrium features have also been described by Graham and Hackett (1987) who assigned Pukeonake to their Type 6 hybrid lavas category (Section 4.2). Rare peridotite xenoliths observed by Graham and Hackett (1987) and Hackett (1985) were interpreted as either upper mantle xenoliths or cumulates from primitive basaltic magma.

(c) **Blue Lake.** The welded agglutinates and lava flows exposed in the NE inner crater wall are hypocrystalline, moderately porphyritic-glomeroporphyritic (<30 modal % phenocrysts), seriate (grain size 0.1-2 mm) andesites with weakly sieved plag>>opx>cpx>ox. Rarely, orthopyroxene phenocrysts are extensively corroded and embayed (Fig 4.17). Some of the agglutinates display a banded texture of flattened, stretched out clasts. Glass-rich scoria bombs and blocks sampled around the outer crater wall also contain olivine, and the plagioclase is moderately sieved.

(d) **North Crater.** The phenocryst assemblage of andesite samples from the solidified lava lake is plag>opx≥cpx>ox. Some of the welded agglutinates sampled on the crater rim and NE slopes also contain olivine. In general, North Crater lavas are richer in pyroxene than lavas of the older cones, which tend to have much higher plagioclase: pyroxene ratios. All the lavas are hypocrystalline (many are glass-rich), moderately to strongly porphyritic-glomeroporphyritic (16-36 modal % phenocrysts), and seriate (grain size 0.1-2 mm). Some agglutinates have banded or trachytic groundmass textures.

Euhedral-subhedral plagioclase (An_{58-80}; 15-19 modal %) displays moderate to strong normal, reverse & patchy zoning, and coarse sieve textures comprising pale brown vermicular glass inclusions (Fig 4.18). Euhedral-subhedral orthopyroxene (En_{58-75}; 6-10 modal %) and augite ($Ca_{43}Mg_{49}Fe_9$ - $Ca_{41}Mg_{38}Fe_{22}3$; 3-4 modal %) both show some normal and reverse zoning. Anhedral resorbed olivine (Fo_{69-82}; <3 modal %) is normally-zoned and rimmed by pyroxene. Subhedral-anhedral magnetite and ilmenite microphenocrysts make up <1 modal %.

(e) **Young Pukekaikiore.** The c.15 ka andesite lava (TG152) and scoria (TG153) erupted from a vent on the summit of Pukekaikiore is unique amongst Tongariro lavas for the absence of large plagioclase phenocrysts. The andesites are holocrystalline to hypocrystalline, weakly to moderately porphyritic (cpx>oliv>opx; 10-20 modal % phenocrysts), and seriate (grain size 0.2-2 mm).

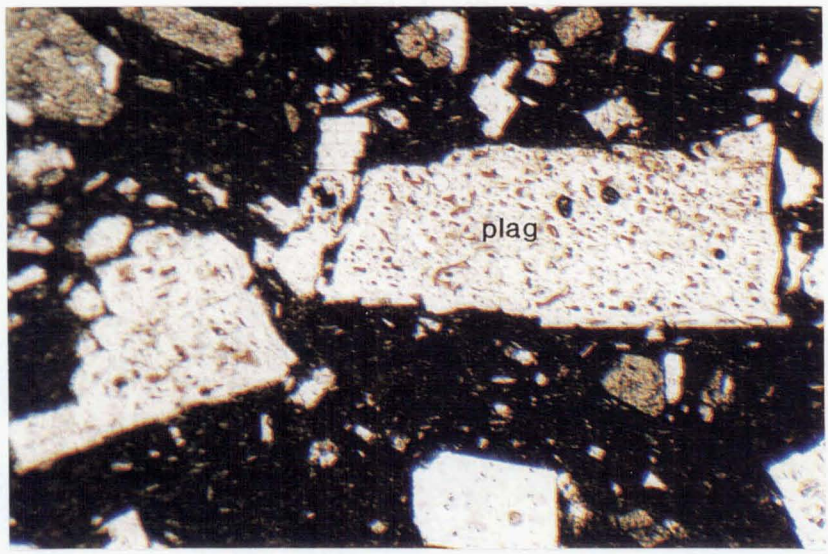

Figure 4.18 Sieve texture in plagioclase (plag), North Crater andesite (TG196). View length 3.2 mm (ppl).

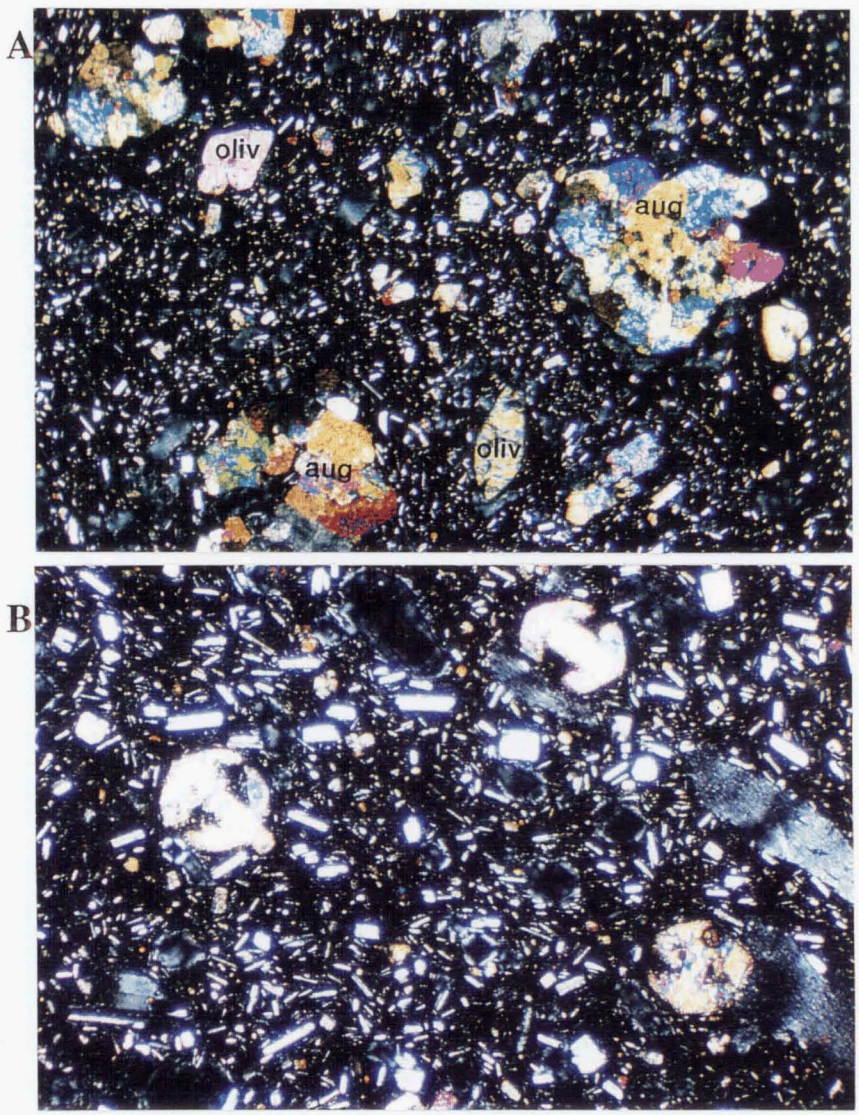

Figure 4.19 Young Pukekaikiore andesite (TG152). **A-** augite (aug) glomerocrysts and olivine (oliv) phenocrysts, view length 7.9 mm (cpl); **B-** quenched skeletal olivine phenocrysts, view length 2.6 mm (cpl).

The mineral compositions quoted below were determined by Patterson (1986) and Patterson and Graham (1988) but do not constitute representative analyses. Small (<0.1 mm) euhedral plagioclase (An_{73-75}) microphenocrysts are rare (<1 modal %), but plagioclase laths are a common constituent of the groundmass. The dominant phenocryst phase is subhedral augite ($Ca_{40}Mg_{52}Fe_7$; 8-15 modal %) which occurs most commonly in glomeroporphyritic aggregates (Fig 4.19A). Subhedral orthopyroxene (En_{78-83}) constitutes generally <2 modal %. Subhedral and quenched skeletal olivine (Fo_{80-82}; Fig4.19B) constitutes typically 2-4 modal %. Subhedral Fe-Ti oxide microphenocrysts are a minor occurrence (<<1 modal %). The Pukekaikiore olivine-pyroxene-andesite has been modelled as originating from a tholeiitic basalt parental magma by fractional crystallization and variable crustal contamination (Graham and Hackett, 1987; Patterson and Graham, 1988; Graham et. al., 1995).

(f) **Young SW Oturere.** Three lava bombs sampled from the Young SW Oturere scoria fall are hypocrystalline, glass-rich and aphyric, containing <2 modal % phenocrysts (cpx±opx±plag±oliv). The plagioclase, where present, is strongly sieved.

(g) **Te Mari Craters.** Sampling of lava flows erupted from Te Mari Craters is incomplete. The c.6-9.7 ka flow (TG027) from the lower crater is a hypocrystalline, strongly porphyritic- glomeroporphyritic, seriate andesite with plag>>opx≥cpx>ox. The plagioclase in TG027 is moderately sieved and displays distinctive patchy and oscillatory zoning (Fig 4.20). Lavas exposed in the walls of Lower Te Mari Crater and to the east of the lower crater are petrographically similar to TG027, but many are also glass-rich.

The c.1500 AD flows (TG281-282) from the upper crater are hypocrystalline (glass-rich), moderately to strongly porphyritic-glomeroporphyritic (38 modal% phenocrysts), seriate andesites with moderately sieved plag>>opx=cpx>ox>oliv. The photomicrograph of a feldspathic xenolith in TG282 (Figure 5.8) also shows part of the host andesite lava.

(h) **Tama Lakes.** Limited sampling of bombs in the c.10 ka tephra erupted from the various Tama Lakes craters has shown them to be glass-rich, essentially aphyric basaltic andesites to andesites. They typically contain less than 4 modal % phenocrysts of subhedral moderately sieved plagioclase (<2 mm), subhedral clinopyroxene <1 mm), and in one basaltic andesite bomb (TG137), hornblende microphenocrysts (<0.2 mm).

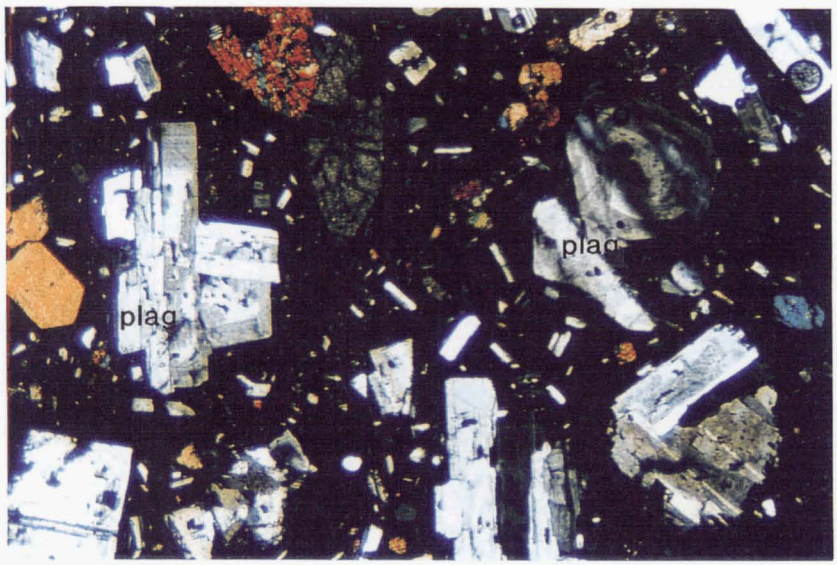

Figure 4.20 Oscillatory- and patchy-zoned plagioclase (plag) phenocrysts, Te Mari Craters andesite (TG027). View length measures 5 mm (cpl).

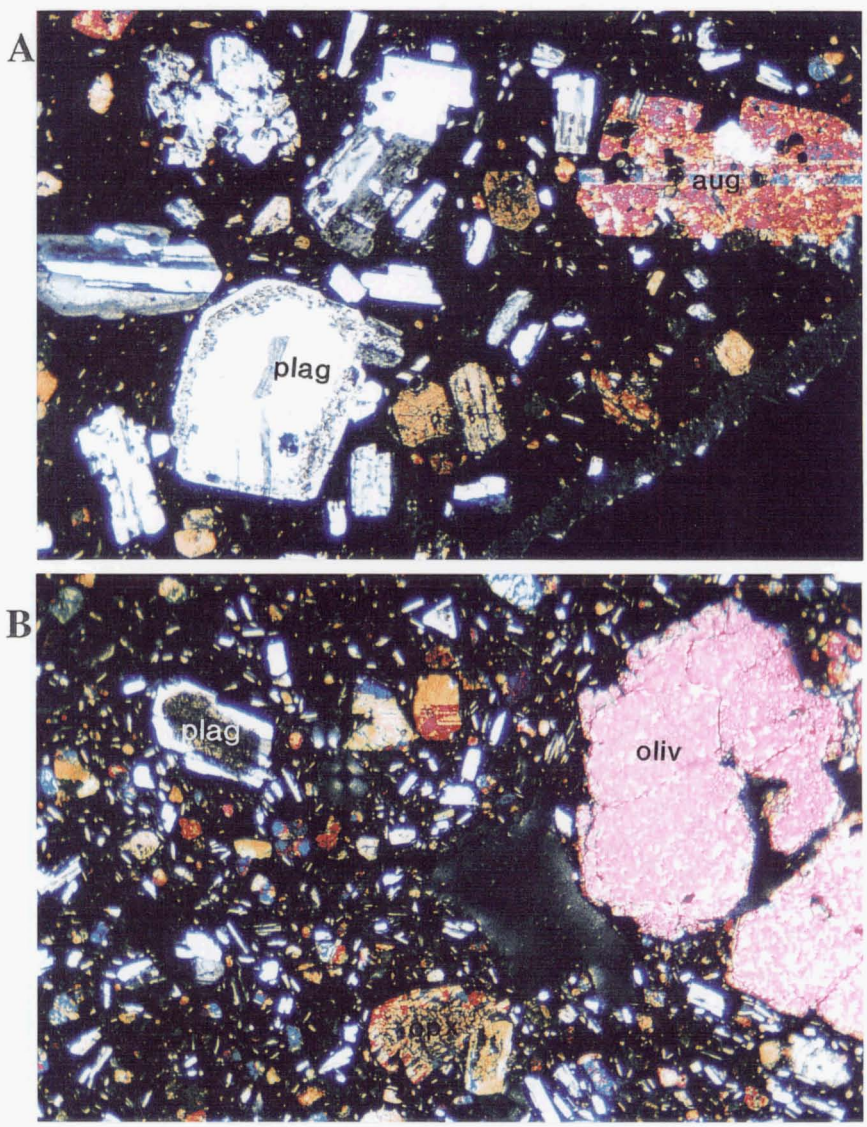

Figure 4.21 Sieved plagioclase (plag), augite (aug), orthopyroxene (opx) with augite rims, and olivine (oliv), Red Crater lavas. **A**-TG134 andesite; **B**-TG126 basaltic andesite. View lengths measure 6.3 mm (cpl).

Groundmasses range from glassy to cryptocrystalline to microcrystalline, and may display a trachytic texture of aligned plagioclase laths. Banded pumice ejecta (Tn141a) has also been sampled, although unfortunately no thin section is available for this sample. Most of these Tama Lakes samples contain up to 4 modal % hornblende- and plagioclase-phyric dacite inclusions, thought to be cognate volcanic xenoliths of the older Tama 1 lavas erupted in the same area (Fig 5.4; Section 5.4).

Wahyudin (1993) presented mineral analyses from two moderately porphyritic basaltic andesite bombs (samples D3-T20/356197 and D61-T20/357198) which were found in the young (c.10 ka) Tama Lakes tephra (probably the same exposure from which TG137 was collected). The phenocryst assemblage is: 12-14 modal % plagioclase (An_{57-81}); 1-2 modal % augite ($Ca_{45}Mg_{48}Fe_7$ - $Ca_{37}Mg_{45}Fe_{18}$); <1 modal % orthopyroxene (En_{61}); 2-4 modal % olivine (Fo_{64-84}); and 1-6 modal % Fe-Ti oxides (magnetite and ilmenite) (Wahyudin, 1993).

(i) **Red Crater.** The olivine-bearing lava flows erupted from Red Crater are all hypocrystalline, moderately to strongly porphyritic (27-35 modal % phenocrysts) with seriate (grain size 0.2-3 mm) or bimodal (0.3, 1-2 mm) crystal populations. Unlike other Tongariro lavas, those from Red Crater do not exhibit pronounced glomeroporphyritic textures. The flows can be subdivided into the pre-1.8 ka andesites and post-1.8 ka basaltic andesites (Section 3.5.8i).

The older andesites (Fig 4.21A) have relative phenocryst proportions of plag>>cpx>opx>oliv>ox. Euhedral-subhedral plagioclase (An_{45-73};15-21 modal %) displays oscillatory, patchy, normal and reverse zoning, and moderate sieve textures (Fig 4.21A). Subhedral-anhedral augite ($Ca_{43}Mg_{49}Fe_7$ - $Ca_{43}Mg_{40}Fe_{18}$; 7-8 modal %) is often reversely zoned. Subhedral-anhedral orthopyroxene (En_{58-76};2-3 modal %) are rimmed by clinopyroxene. Euhedral-anhedral olivine (Fo_{82-84}; 1-2 modal %) is occasionally rimmed by pyroxene or plagioclase. Magnetite and ilmenite microphenocrysts make up less than 2 modal %.

The younger basaltic andesites (Fig 4.21B) lack significant Fe-Ti oxides and are more olivine-rich (plag>cpx>oliv>opx) than the older lavas. Euhedral-anhedral plagioclase (An_{51-81}; 13-15 modal %) exhibits strong reverse zoning, along with patchy and oscillatory

zoning, and is resorbed and strongly sieved. Euhedral-subhedral augite ($Ca_{43}Mg_{49}Fe_8$ - $Ca_{45}Mg_{38}Fe_{17}$; 9-10 modal %) and olivine (Fo_{74-89}; 4-7 modal %) are dominant over orthopyroxene (En_{60-68}; 1-2 modal %) which is rimmed by clinopyroxene (Fig 4.21B).

The mineral compositions given here agree with those obtained by Graham (1985a), who classified Red Crater lavas as Type 1 (Graham and Hackett, 1987).

(j) **South Crater.** The scoria thought to have erupted from the South Crater explosion pit is a hypocrystalline, strongly porphyritic-glomeroporphyritic andesite with a phenocryst assemblage of plag>>opx>cpx>>ox.

(k) **Ngauruhoe.** A high proportion (40%) of Ngauruhoe lavas are olivine-bearing, and the remainder are two-pyroxene basaltic andesites or andesites (Fig 4.15). The relative phenocryst abundances can be summarised: plag>>opx≥cpx±oliv±ox. The individual lava groups (see Section 3.5.8k) exhibit petrographic groupings broadly related to their whole-rock MgO content (Fig 3.30B). Lavas with MgO>4 wt% (Groups 1A, 3A, and the high-MgO part of 3B) are usually olivine-bearing; lavas with MgO<4 wt% (Groups 1B, 2, and the low-MgO part of 3B) have little or no olivine (Fig 4.22).

Textures of Ngauruhoe lavas are similar for all groups: hypocrystalline (many glass-rich), moderately to strongly porphyritic-glomeroporphyritic (25-37 modal % phenocrysts), seriate (grain size: 0.1-5 mm), and occasionally sub-trachytic groundmasses. Photomicrographs of representative Ngauruhoe lavas illustrate their common petrographic features (Figs 4.4. 4.23-25). The mineralogy typical of each Ngauruhoe lava group is summarised in Table 4.1 and reveals only subtle differences between the groups. Similarly, on a time scale an order of magnitude smaller than that covering the whole of Ngauruhoe's lifetime, the historic lavas of Group 3B do not display any particularly marked differences, except for the presence or absence of minor olivine, and very slight differences in phenocryst modal abundances. Note, however, that some caution must be applied to this view since the level of detail applied to the study of Ngauruhoe mineralogy has the scope to be greatly enhanced.

Figure 4.22 Petrography of Ngauruhoe lava groups.

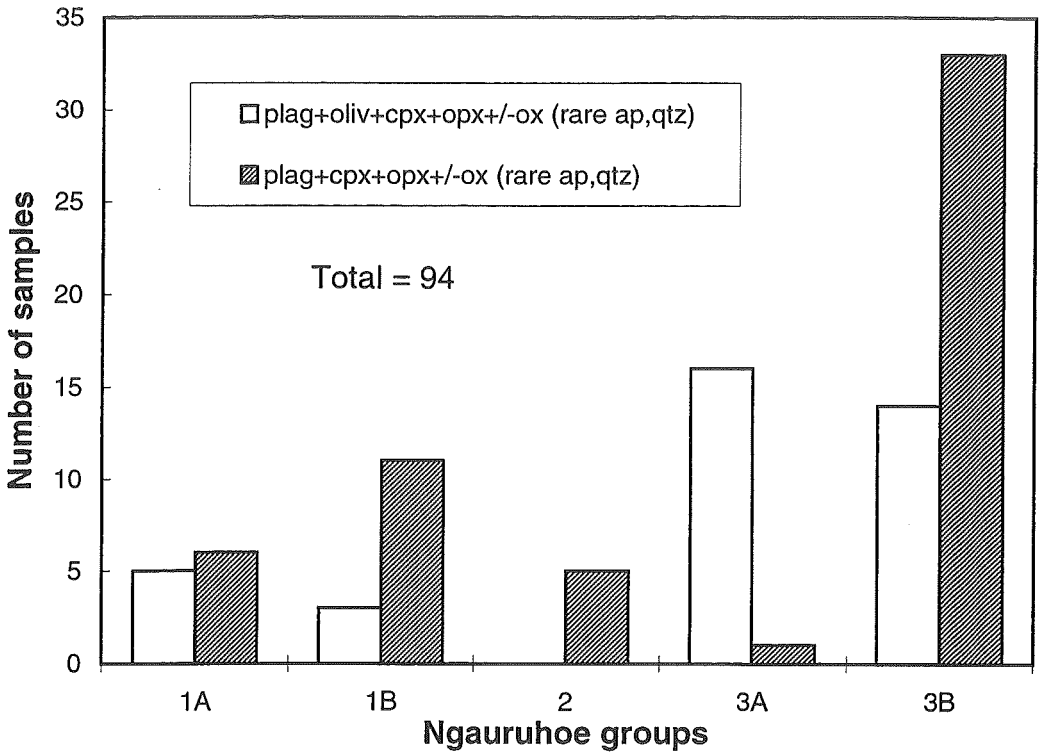

Table 4.1 Characteristic mineralogy of Ngauruhoe lava groups. N = normal zoning; R = reverse zoning; n.a. = not analysed.

	Group 1A	**Group 1B**	**Group 2**	**Group 3A**	**Group 3B**
PLAG	24 modal % An_{57-90} N+R mod sieved	23 modal % An_{58-88} N+R mod sieved	20 modal % n.a. mod sieved	15 modal % An_{54-74} wk sieved	20 modal % An_{60-82} N+R str sieved
OPX	8 modal % En_{63-71}	5 modal % En_{63-67}	4 modal % n.a.	4 modal % En_{61-76} R	10 modal % En_{62-70}
CPX	3 modal %, N $Ca_{41}Mg_{47}Fe_{12}$ - $Ca_{37}Mg_{44}Fe_{19}$	8 modal %, N $Ca_{40}Mg_{43}Fe_{17}$ - $Ca_{39}Mg_{41}Fe_{20}$	3 modal % n.a.	9 modal %, R $Ca_{39}Mg_{47}Fe_{14}$ - $Ca_{39}Mg_{39}Fe_{22}$	5 modal %, N+R $Ca_{39}Mg_{50}Fe_{11}$ - $Ca_{35}Mg_{41}Fe_{24}$
OLIV	<1 modal % Fo_{67} opx rims			3 modal % Fo_{80-91} N opx/cpx rims	<1 modal % Fo_{80}
OX	1 modal %	<1 modal %	<1 modal %	<1 modal %	

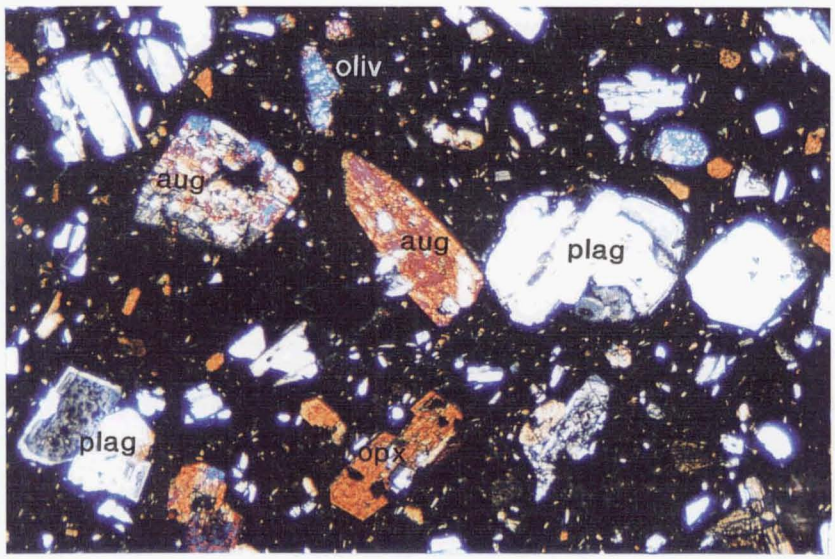

Figure 4.23 Ngauruhoe Group 3A andesite (TG288). Phenocrysts of olivine (oliv), augite (aug), sieved and oscillatory-zoned plagioclase (plag), and orthopyroxene (opx). View length measures 6.3 mm (cpl).

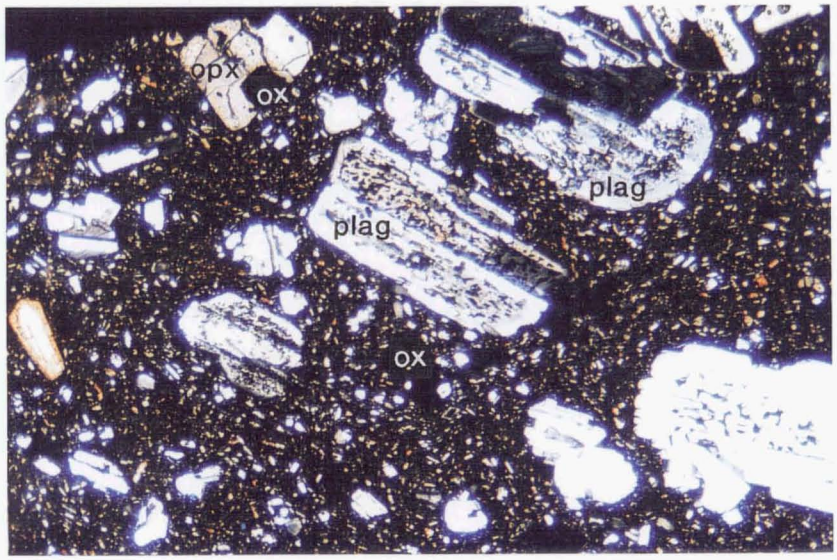

Figure 4.24 Ngauruhoe Group 2 andesite (TG508). Sieved and zoned plagioclase (plag), orthopyroxene (opx) and Fe-Ti oxides (ox) in a microcrystalline groundmass. View length measures 6.3 mm (cpl).

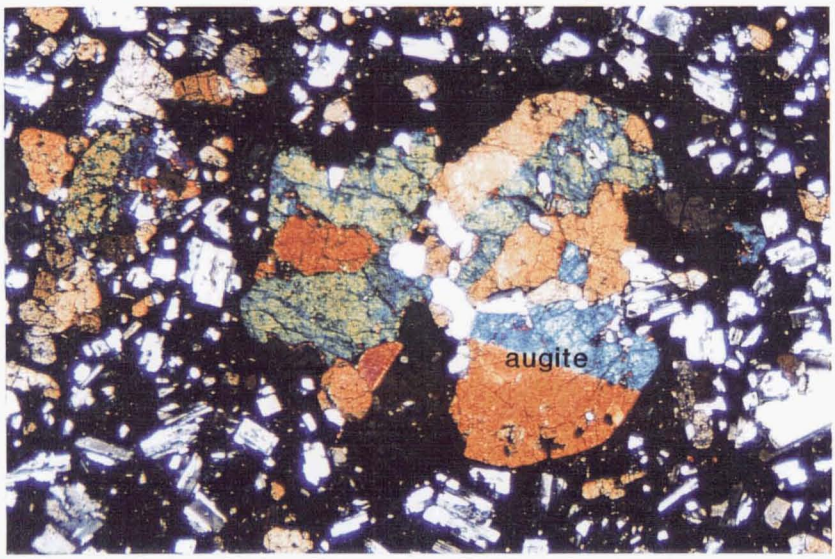

Figure 4.25 Ngauruhoe Group 1A basaltic andesite (TG164), view length measures 6.3 mm (cpl).

4.5 MINERAL COMPOSITIONS

Tongariro mineral chemistry was investigated with several aims in mind. Precise analyses could be used to determine the range of compositions present and the degree of chemical disequilibrium in any one sample or unit, which might confirm the suspicion already formed that magma mixing has played an important role in Tongariro petrogenesis. The other essential role of the mineral analyses was to provide data for use in establishing crystallization conditions such as temperature and oxygen fugacity (see Section 4.6). Chemical analyses of mineral phases were obtained using the University of Otago electron microprobe (see Appendix 8.2 for analytical procedures). Mineral data for 24 selected Tongariro samples are presented in Appendix 9. Iron recalculations and cation site occupancies were calculated using the PetMin computer programme (see Appendix 9 for details).

4.5.1 Olivine

Olivine is present as a minor (<2 modal %) phenocryst phase in almost a third (Fig 4.1) of the sampled Tongariro lavas, particularly in the basaltic andesites but also in the more silicic andesites (Fig 4.2). Three olivine morphologies can be recognised:

1. Relatively large (1-3 mm) and abundant (3-7 modal %) euhedral to subhedral phenocrysts (and xenocrysts?) (Figs 4.19A, 4.21B) occur in a minority of the more basic lavas (e.g. TG115, TG126, TG152).
2. Small (0.2-0.4 mm), rare (<<1 modal %) skeletal crystals with double-arrowhead shapes occur in TG152 (Fig 4.19B). (NB. Donoghue et al. (1991) document the occurrence of distinctive skeletal olivine morphologies in four members of the Tongariro-derived Mangamate Tephra which were thought to represent supercooling related to magma mixing).
3. Small (0.1-0.8 mm) subhedral to anhedral resorbed microphenocrysts, often rimmed with granular opx±cpx±plag±ox (Figs 4.14, 4.16, 4.23), and rarely fractured and altered to iddingsite (Fig 4.10), are the most common type of olivine encountered in thin section - usually comprising <1-2% of the mode.

Olivine compositions range from Fo_{96} to Fo_{67}, a slightly wider range than that determined for Ruapehu olivines (Fo_{74-94}) by Graham and Hackett (1987) (Fig 4.34). Individual crystals are relatively homogeneous with only weak normal zoning (core - rim variation of 1-4 mol% Fo, rarely up to 13 mol% Fo).

Pukeonake lavas contain the most Fo-rich olivines (Fo_{86-96}), and Ngauruhoe Group 1A the most Fo-poor olivines (Fo_{67}) (Fig 4.35). Otherwise, there are overlapping compositional ranges for olivines of the different units. However, as the analysed samples are not representative of all Tongariro lavas, further generalisations about the units should not be made. Orthopyroxene rims on olivines (plotted in Fig 4.35) are either markedly more Fe-rich than the olivines (Ngauruhoe Group 3A, Pukeonake) or slightly more Mg-rich (Ngauruhoe Group 1A, NE Oturere).

Overall, maximum Fo contents of Tongariro olivines show a positive correlation with whole-rock $100Mg/(Mg+Fe^{2+})$ ratio (Mg#) (Fig 4.26). Distribution coefficients (K_D) calculated for the partitioning of Fe and Mg between olivine phenocrysts and liquids (host rocks) range from 0.13 to 0.73 (Table 4.2). The equilibrium range of K_D values determined for basalts (K_D=0.26-0.36; Roeder and Emslie, 1973) and andesites (K_D=0.25-0.33; Ussler and Glazner, 1989) is plotted on Figure 4.26. Most Tongariro lavas - including andesites with up to 61 wt% SiO_2 - have high-Fo olivine cores in equilibrium with whole-rock Mg#. However, one NE Oturere lava (TG098) and especially one Ngauruhoe lava (TG163) have olivine cores with Fo contents much lower than indicated from their host rock Mg# (e.g. TG163 has Fo_{67} olivine compared to an expected equilibrium value of Fo_{80}). In contrast, lavas from Pukeonake, Ngauruhoe Group 3A and to a lesser extent, post-1.8 ka Red Crater, all contain more forsteritic olivine than expected from the Mg# of their host rocks. Together with observations of other disequilibrium features in these three lava groups (Sections 4.4, 4.7), these results suggest the involvement of magma mixing processes. Three of the high-Fo olivine-bearing lavas (TG279, TG280, TG289) also contain chrome spinel inclusions in the olivine phenocrysts.

Of the minor elements (Fig 4.27), MnO (0.00-0.44 wt%) shows a strong negative correlation with increasing Fo content; CaO (0.03-0.27 wt%) does not display any obvious correlation with Fo; NiO (0.00-0.66 wt%) increases in a steepening trend with increasing Fo; Cr_2O_3 (0.00-0.38 wt%) was detected in a minority of crystals, and like NiO it is

Table 4.2 Summary of calculations pertaining to olivine - liquid equilibria.

Unit	Group	Sample	N°. olivine analyses	Olivine Fo range	Host Rock 100 Mg/(Mg + Fe^{2+})	K_D range
Ngauruhoe	3B	TG001	2	80.7 - 80.4	58.6	0.34
	1A	TG163	2	67.3 - 66.9	54.5	0.58 - 0.59
	3A	TG288	10	91.0 - 80.2	61.0	0.15 - 0.39
	3A	TG289	10	91.3 - 77.6	57.1	0.13 - 0.38
Red Crater	post-1.8ka	TG112	8	88.5 - 76.9	65.0	0.24 - 0.56
	post-1.8ka	TG126	9	88.9 - 74.0	64.5	0.23 - 0.64
	pre-1.8ka	TG134	5	83.1 - 82.0	59.3	0.30 - 0.32
	pre-1.8ka	TG135	5	84.2 - 81.8	57.0	0.25 - 0.30
North Crater		TG192	8	81.9 - 69.3	60.0	0.33 - 0.67
Pukeonake		TG279	14	95.5 - 86.0	73.7	0.16 - 0.45
		TG280	12	94.4 - 87.0	74.1	0.17 - 0.43
SW Oturere		TG051	2	77.6 - 76.4	54.2	0.34 - 0.37
		TG240	9	84.1 - 69.8	62.8	0.32 - 0.73
NE Oturere		TG098	4	78.0 - 71.9	57.5	0.38 - 0.53
		TG115	12	87.3 - 84.8	68.2	0.31 - 0.38

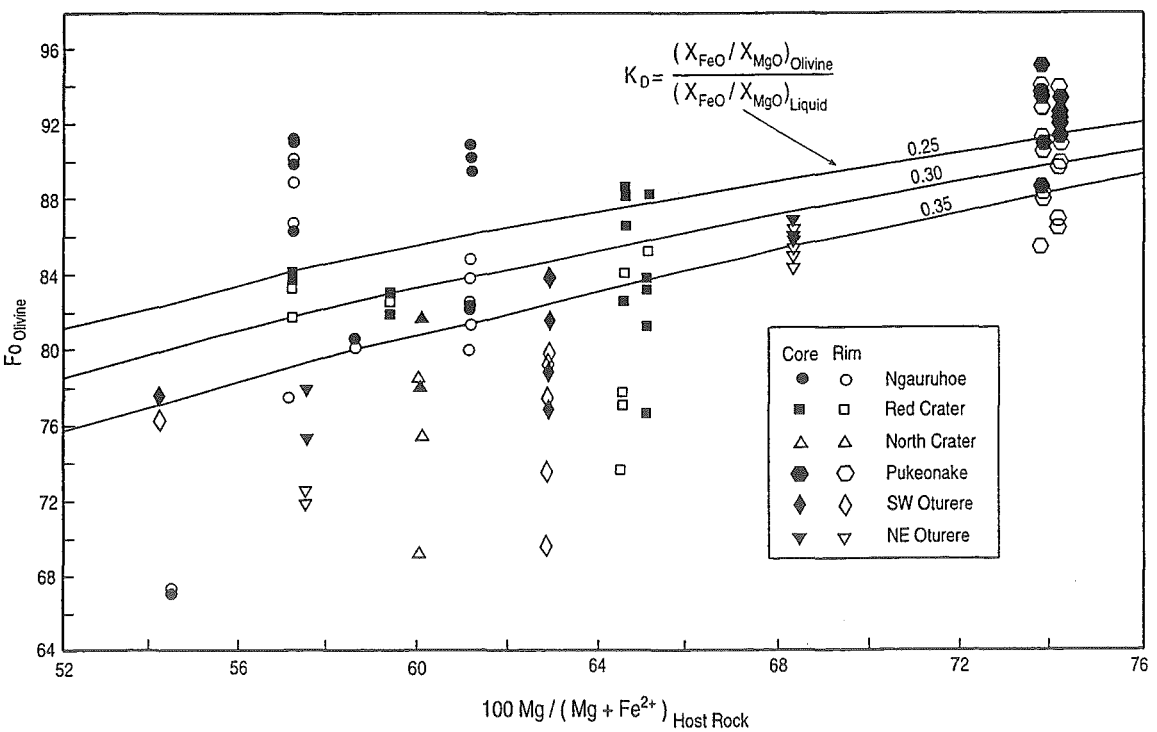

Figure 4.26 Forsterite (Fo) contents of Tongariro olivines plotted versus 100Mg/(Mg+Fe^{2+}) of the host rock, assuming Fe_2O_3/FeO=0.3. Closed and open symbols represent core and rim compositions respectively. Curves denote equilibrium range of K_D values for basalt-andesite obtained by Roeder & Emslie (1970) and Ussler & Glazner (1989).

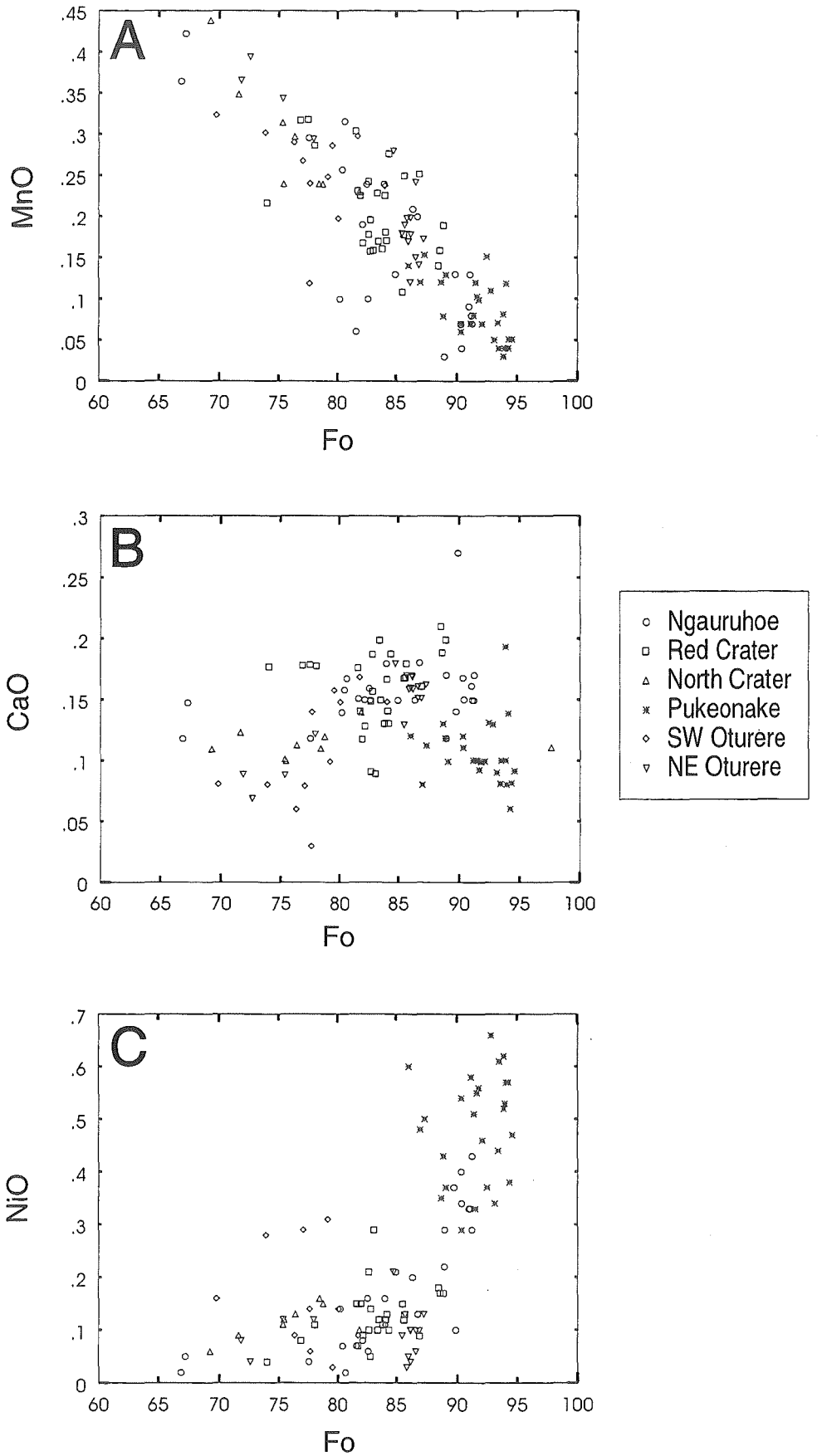

Figure 4.27 Minor element abundances (wt%) plotted versus Fo (mol%) contents for Tongariro olivines.

restricted to the more Mg-rich olivines. Since most olivines contain constant CaO contents of 0.10-0.20 wt%, low pressure crystallization is implied (Stormer, 1973), although olivines with CaO <0.1 wt% (and especially those also with >Fo_{90}) may have a xenocrystic high pressure origin (e.g. Pukeonake olivines).

4.5.2 Plagioclase

Plagioclase phenocrysts are ubiquitous and abundant (average 19 modal %) in Tongariro lavas, with the exception of the Young Pukekaikiore olivine-pyroxene andesite (Section 4.4.8e). Plagioclase ranges in size from 0.1 to 3.0 mm and is generally euhedral to subhedral, but displays a wide variety of zoning patterns, resorption features and sieve textures (see below). Apart from the frequent glass inclusions (sieve texture), plagioclase crystals may also occasionally contain inclusions of pyroxene and/or Fe-Ti oxides. Plagioclase is also a major groundmass phase in all lavas.

Plagioclase compositions range from An_{90} to An_{45} (i.e. dominantly labradorite to bytownite), which is similar to the range of An_{89-40} obtained for Ruapehu plagioclases (Graham and Hackett, 1987). Compositional ranges for phenocryst cores within each volcano-stratigraphic unit and often within single samples are almost as wide as the overall range; typically spanning 20-35% in An content (Fig 4.28). There is no systematic relationship between An% and whole-rock SiO_2 content. For example, Red Crater basaltic andesites (c.53 wt% SiO_2) contain An_{51-81} plagioclase; a SW Oturere andesite (TG240, 58.1 wt% SiO_2) contains An_{55-88} plagioclase; and a Tama 1 andesite (TG136, 60.7 wt% SiO_2) contains An_{57-89} plagioclase.

Or contents are less than 4 mol% for all Tongariro plagioclases, with most samples containing 0.2-1.5 mol% Or and the higher Or contents correlating with the more K_2O-rich lavas. However, much of the K_2O is concentrated in groundmass glass because normative plagioclase calculations predict much higher Or contents of up to 20 mol% (TG055, see Appendix 11).

Most Tongariro plagioclase phenocrysts exhibit complex oscillatory zoning (e.g. Figs 4.4, 4.20, 4.23, 4.24, 4.33), detailed microprobe analysis of which is beyond the scope of the current investigation. Often over 50 zones can be counted in one crystal at x500

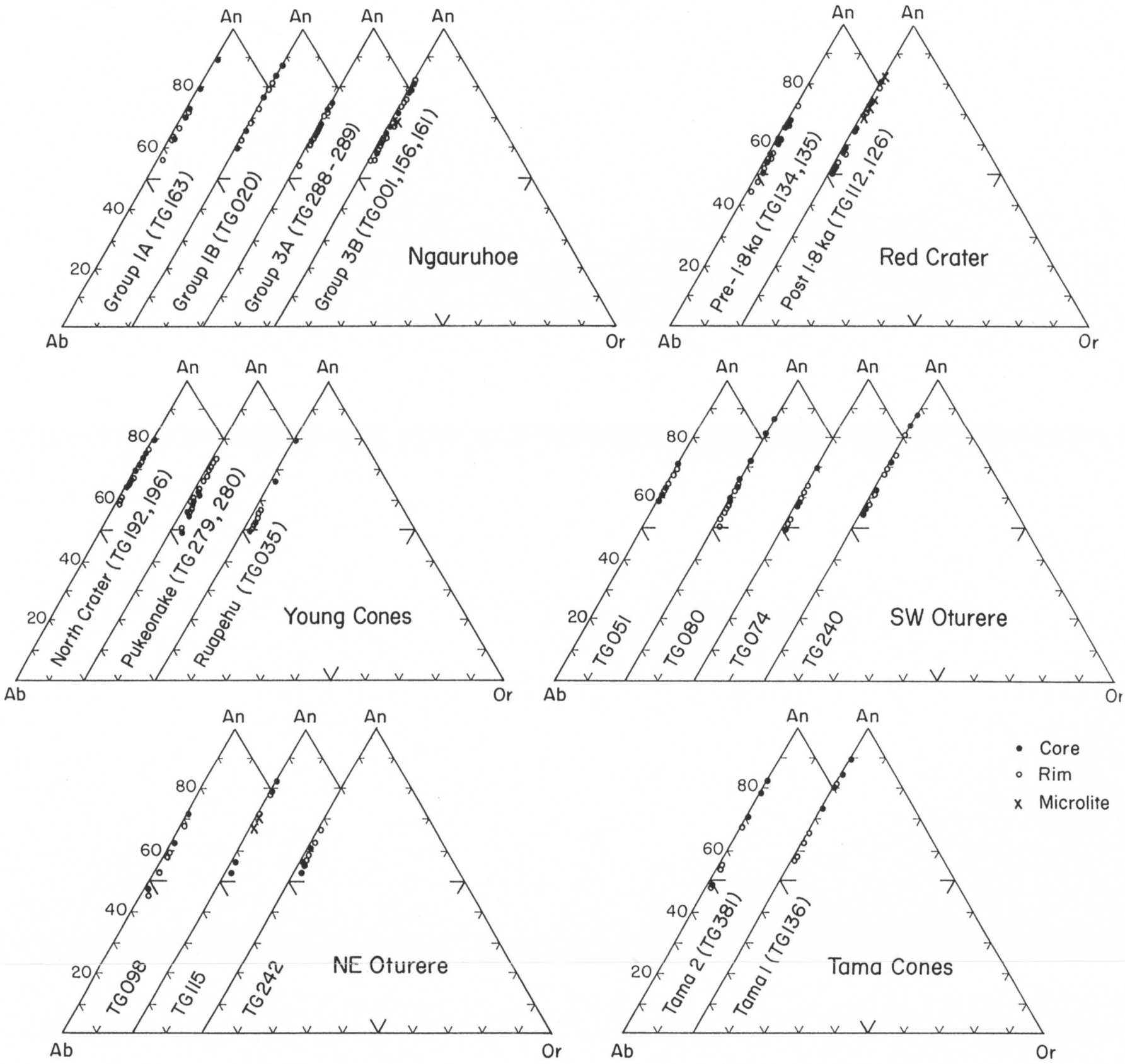

Figure 4.28 Electron microprobe analyses of plagioclase from Tongariro by volcano-stratigraphic unit (some units not represented). Note that one sample (TG035) is from a Ruapehu flow in the Tama Lakes area (see Sections 6.5 and 7.6). Those units with limited mineral data are plotted for convenience in sets of overlapping graphs. Each point represents an analysis. Mineral data are tabulated in Appendix 9.

magnification. The exact mechanisms responsible for oscillatory zoning remain a matter of debate. Abrupt major compositional changes in oscillatory zoning profiles were attributed by Nixon and Pearce (1987) to magma mixing. Pearce (1993) favoured a model involving the cycling of plagioclase phenocrysts around a turbulently convecting magma reservoir, where the balance between growth and dissolution determines their survival. Pearce (1993) found that most zoning profiles result from simple convection and do not require a major change in composition of the magma reservoir, such as that produced by magma mixing between basalt and rhyolite compositions.

Analyses of cores and rims reveal few homogeneous crystals and overall normal zoning for many Tongariro plagioclases (i.e. fractional crystallization), with typically 4-20 (and up to 30) mol% An variation within one crystal. However, other crystals are reversely-zoned with often distinctly more An-rich rims (core-rim variation 3-26 mol% An). The few crystals for which analyses of intermediate zones are also available typically display normal zoning from core to intermediate crystal region, and reverse zoning from intermediate to rim (e.g. TG098, crystal 3: An_{51}-An_{47}-An_{58}). These thin calcic rims can be readily observed in thin section.

Although the overall range in plagioclase compositions is similar for all the volcano-stratigraphic units, there are also some notable contrasts even within volcano-stratigraphic units (Fig 4.28). Of the Ngauruhoe lavas, Group 1A and 1B have the most An-rich compositions (An_{57-90}) and particularly strong normal zoning (e.g. An_{90}[core], An_{63}[rim]). Plagioclases of Group 3A lavas have a more narrow compositional range (An_{54-74}) and exhibit reverse (e.g. An_{64}[core], An_{74}[rim]) as well as normal zoning. Group 3B An% ranges from 60 to 82 mol% and the plagioclase phenocrysts generally display moderate normal and reverse zoning.

The normally-zoned (An_{74}[core] - An_{45}[rim]) plagioclase phenocrysts of the pre-1.8 ka Red Crater andesites contrast with the more An-rich (up to An_{81}) and strongly reversely-zoned (An_{54}[core] - An_{79}[rim]) post-1.8 ka basaltic andesites (Fig 4.28). The plagioclase compositions in these younger lavas define an almost bimodal distribution with sodic cores rimmed by calcic overgrowths, calcic microlites, and calcic cores surrounded by sodic rims. These features suggest injection of more basic magma into the post-1.8 ka Red Crater magma reservoir.

Pukeonake lavas also contain plagioclase phenocrysts which exhibit pronounced reverse zoning (An_{50}[core] - An_{74}[rim], Fig 4.31), which along with other mineralogical evidence also points to magma mixing. Plagioclases in TG115 NE Oturere and TG381 Tama 2 lavas also span a wide compositional range and display strong zoning and calcic microlites (Fig 4.28). See Section 4.7 for further discussion of magma mixing.

The majority of Tongariro lavas contain plagioclase phenocrysts displaying sieve textures - intense concentrations of minute glass inclusions, often arranged zonally within the crystal. Clear, inclusion-free crystals are the exception rather than the rule. The intensity of sieving with respect to the crystal population of each sample has been ranked as weak (<20% sieved), moderate (20-70% sieved), or strong (>70% sieved) in the petrographic descriptions contained in Appendices 3 and 4. Figure 4.29 shows that most lava samples contain moderately to strongly sieved plagioclase crystal populations.

A variety of sieve patterns are displayed by Tongariro plagioclases:

1. Rounded, intensely sieved resorbed cores are surrounded by clear, euhedral mantles and rims (Figs 4.21B, 4.30) in a minority of samples.
2. More commonly, rounded unsieved cores (often only the resorbed remnants) are mantled by an intermediate zone or multiple zones of glass inclusions, surrounded by a thin (<0.025 mm), clear, euhedral (or rounded) rim (Fig 4.31). These sieve zones often display patchy zoning - irregularly-shaped areas of uniform extinction coinciding with the glass inclusions (Figs 4.20, 4.32), suggesting that the patchy zoning originates through resorption (Vance, 1965). The sieved zones vary in thickness (0.025 - 0.1 mm) and may extend from the core to inner rim, rendering the crystal almost completely sieved (Figs 4.11, 4.18). Multiple sieve zones are often separated by clear, oscillatory-zoned regions (Fig 4.33).
3. In other crystals, only a relatively thin sieved inner rim exists in an otherwise clear crystal, which may be euhedral (Fig 4.21A) or rounded and embayed (Fig 4.10).

The intensity of sieving *within* a crystal varies from only a few randomly scattered (Fig 4.3) or crystallographically aligned (Fig 4.4) coarse glass inclusions, to dense

Figure 4.29 Relative intensity of sieve texture in plagioclase for all Tongariro lavas (excluding aphyric lavas). The proportion of the plagioclase crystal population which displays sieve textures is used to arbitarily classify sieving intensity as weak (<20%), moderate (20-70%), or strong (>70%).

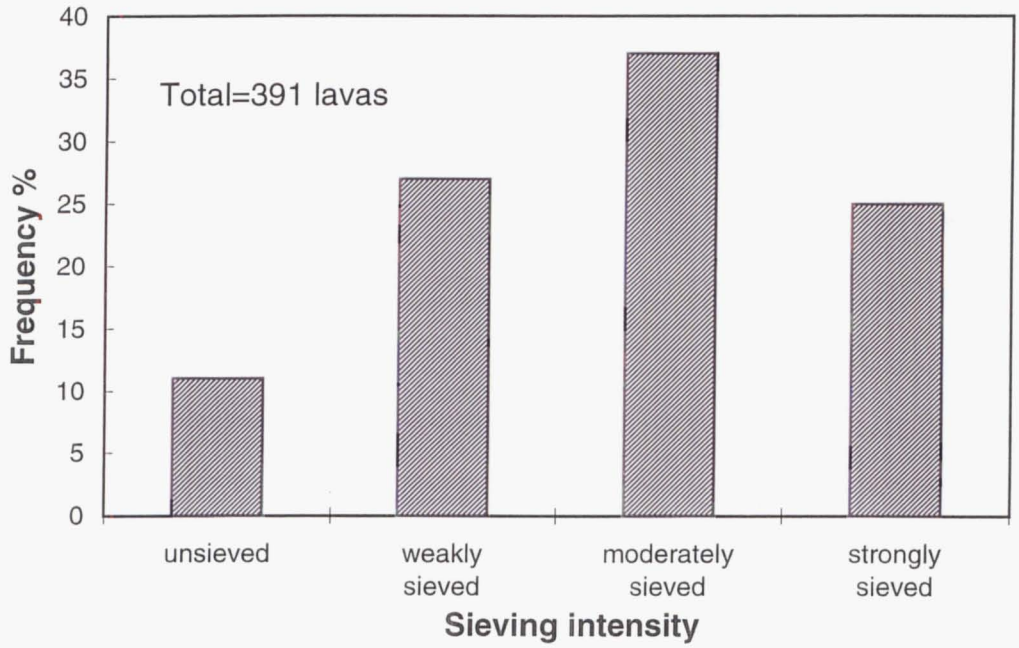

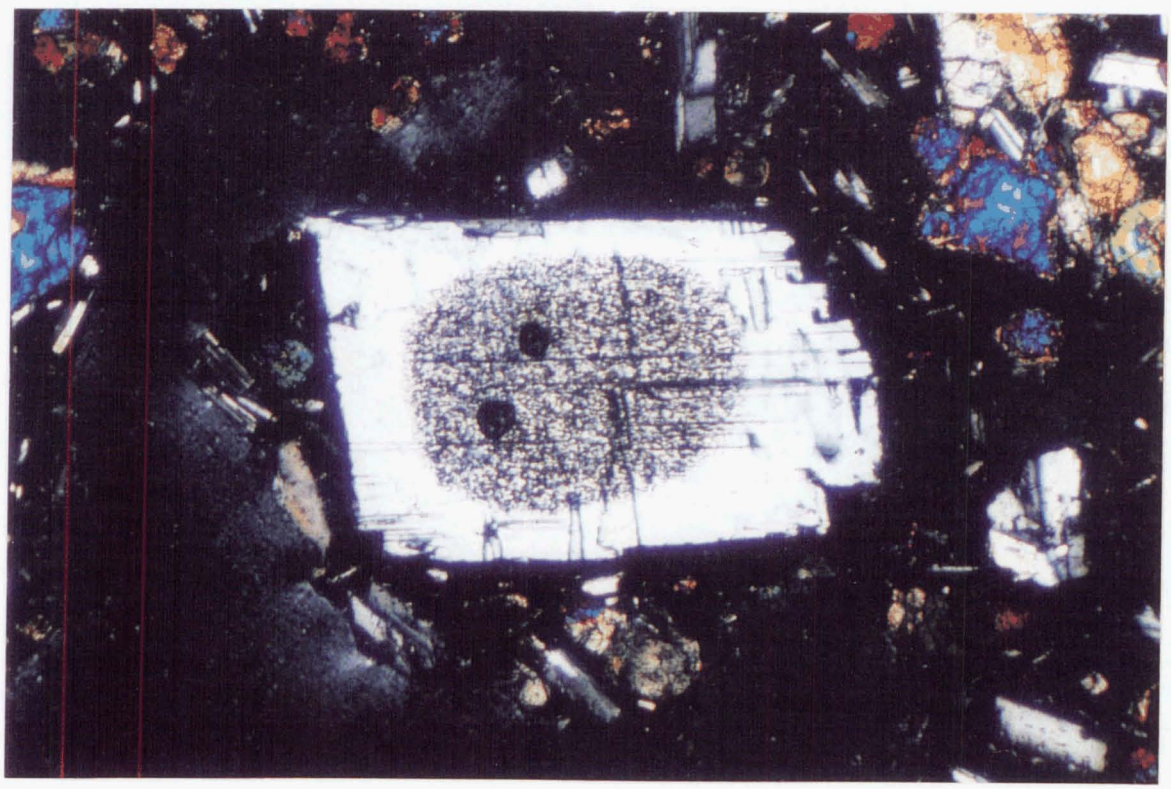

Figure 4.30 Plagioclase phenocryst with rounded, sieved core and euhedral, clear rim. Red Crater basaltic andesite (TG126). View length measures 2 mm (cpl).

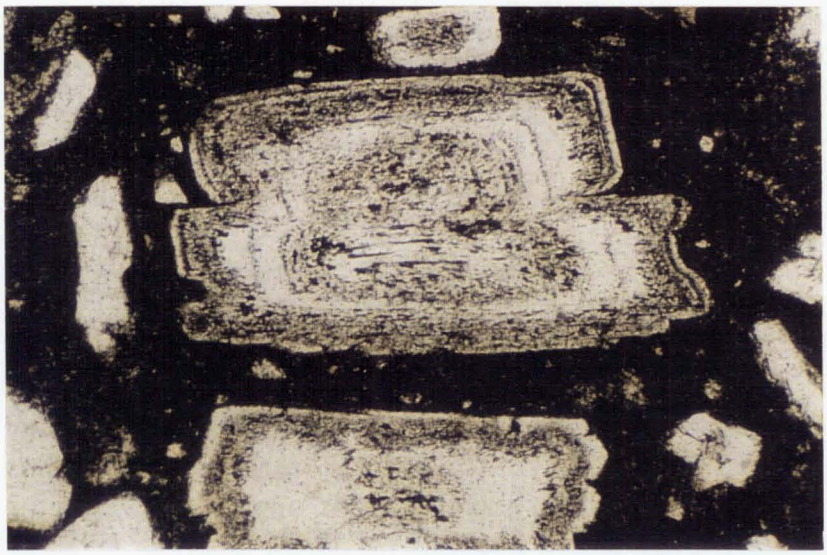

Figure 4.31 Plagioclase with multiple sieved zones, Tama 2 bas. andesite (TG299). View length 2 mm (ppl).

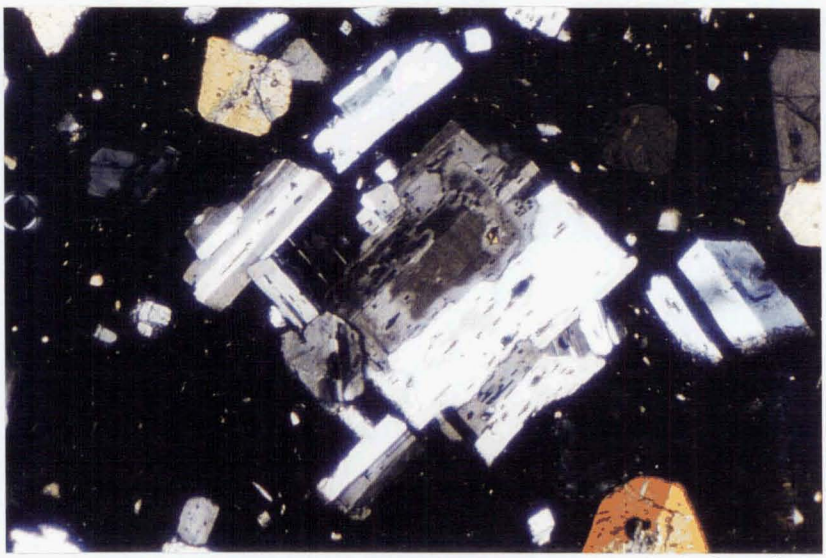

Figure 4.32 Blocky glass inclusions and patchy zoning in Ngauruhoe plagioclase phenocrysts (TG529). View length measures 2 mm (cpl).

Figure 4.33 Strongly oscillatory zoned plagioclase with multiple sieved zones, Tama 2 basaltic andesite (TG299). View length 3.2 mm (cpl).

concentrations of fine glass inclusions (Figs 4.21B, 4.30). The shape of inclusions ranges from blocky-rectangular (often parallel to twinning or zoning; Fig 4.32), to rounded-blebby (Fig 4.18), to vermicular interconnected networks (Fig 4.24). The colour of the glass varies from pale to dark brown, and is occasionally devitrified.

These sieve textures indicate major resorption episodes during crystal growth. Further evidence for resorption is found in the optically-distinct, irregular, internal resorption surfaces which often coincide with major compositional discontinuities and truncate zoning. There is the potential for a much more detailed study on Tongariro plagioclase textures which is unfortunately beyond the scope of this present study. However, these general petrographic observations can lead to at least a preliminary interpretation of the origin of the sieve textures.

Similar sieve textures and zoning patterns have been interpreted by many workers to result from magma mixing (e.g. Dungan and Rhodes, 1978; Lofgren and Norris, 1981; Tsuchiyama, 1985; Nixon and Pearce, 1987; Stamatelopoulou-Seymour et al., 1990; Stimac and Pearce, 1992). Experimental investigations by Tsuchiyama (1985) have shown that crystals more sodic than the plagioclase in equilibrium with the surrounding melt dissolve to give rounded shapes (at T>liquidus; or retain euhedral outlines at T≤liquidus) and sieved, more calcic rims. Those crystals more calcic than the plagioclase in equilibrium with the melt continue to grow with more sodic, euhedral overgrowths.

In many Tongariro plagioclase crystals there is a definite compositional difference between sodic cores and sieved mantles/rims (e.g. TG126, analyses 0148-9: An_{54}[core], An_{79}[rim]) which equates with Tsuchiyama's (1985) reaction textures produced by magma mixing. Most of the strongly reversely-zoned crystals described earlier in this section also display sieve textures, indicating a strong disequilibrium with their host lava. Other sieved crystals exhibit less pronounced compositional breaks which may indicate magma mixing between closely related (andesitic) compositions rather than the classic basalt - dacite/rhyolite magma mixing.

Because of the other supporting evidence for magma mixing (e.g. disequilibrium mineral assemblages, see Section 4.7), these sieve textures may reasonably be interpreted as originating in such a way. However, often there is no significant difference in

composition between the sieved and unsieved crystal portions, or between coexisting sieved and unsieved plagioclase. In these cases, and in the absence of other criteria indicative of magma mixing, rapid decompression (Pearce et al., 1987; Nelson and Montana, 1992) may be responsible for producing (particularly the coarse) sieve textures. In all likelihood, Tongariro plagioclase sieve textures are often the result of combined magma mixing and rapid decompression, although it is difficult to assess the relative contributions of these two processes.

4.5.3 Pyroxene

Pyroxene is the dominant mafic phase in Tongariro lavas (Fig 4.5), and both orthopyroxene (enstatite; 1-10 modal %) and clinopyroxene (augite; 1-15 modal %) phenocrysts occur in most lavas. Augite generally decreases in abundance from basaltic andesites to andesites, whereas orthopyroxene remains relatively constant and is usually the dominant pyroxene in andesites (Figs 4.5, 4.6). Pyroxene is also an important groundmass constituent.

Pyroxene phenocrysts range in size from 0.1 to 5.0 mm and are typically euhedral to subhedral, although some crystals may be anhedral and resorbed. A minority of samples contain pyroxenes which are fractured or display coarse sieve textures (Figs 4.10, 4.16). A significant minority of orthopyroxene crystals are surrounded by overgrowths or reaction rims of augite; orthopyroxene rims on augite are rare. Continuously-rimmed orthopyroxene crystals (e.g. in Red Crater lavas, Fig 4.21B) are also often resorbed (rounded) and/or sieved, whereas discontinuously-rimmed orthopyroxene crystals (augite on surfaces parallel c-axis; e.g. TG283) do not exhibit such disequilibrium features. Many pyroxene phenocrysts contain inclusions of Fe-Ti oxides and less commonly plagioclase, and some orthopyroxenes contain augite inclusions.

The compositional fields for analysed Tongariro pyroxenes are similar to the fields of published Ruapehu pyroxenes (Fig 4.34), apart from a few more Fe-rich orthopyroxene and pigeonite analyses from Ruapehu. Tongariro augites have a relatively restricted range in composition ($Ca_{35-46}Mg_{35-52}Fe_{7-24}$); orthopyroxenes exhibit more variable and more Fe-

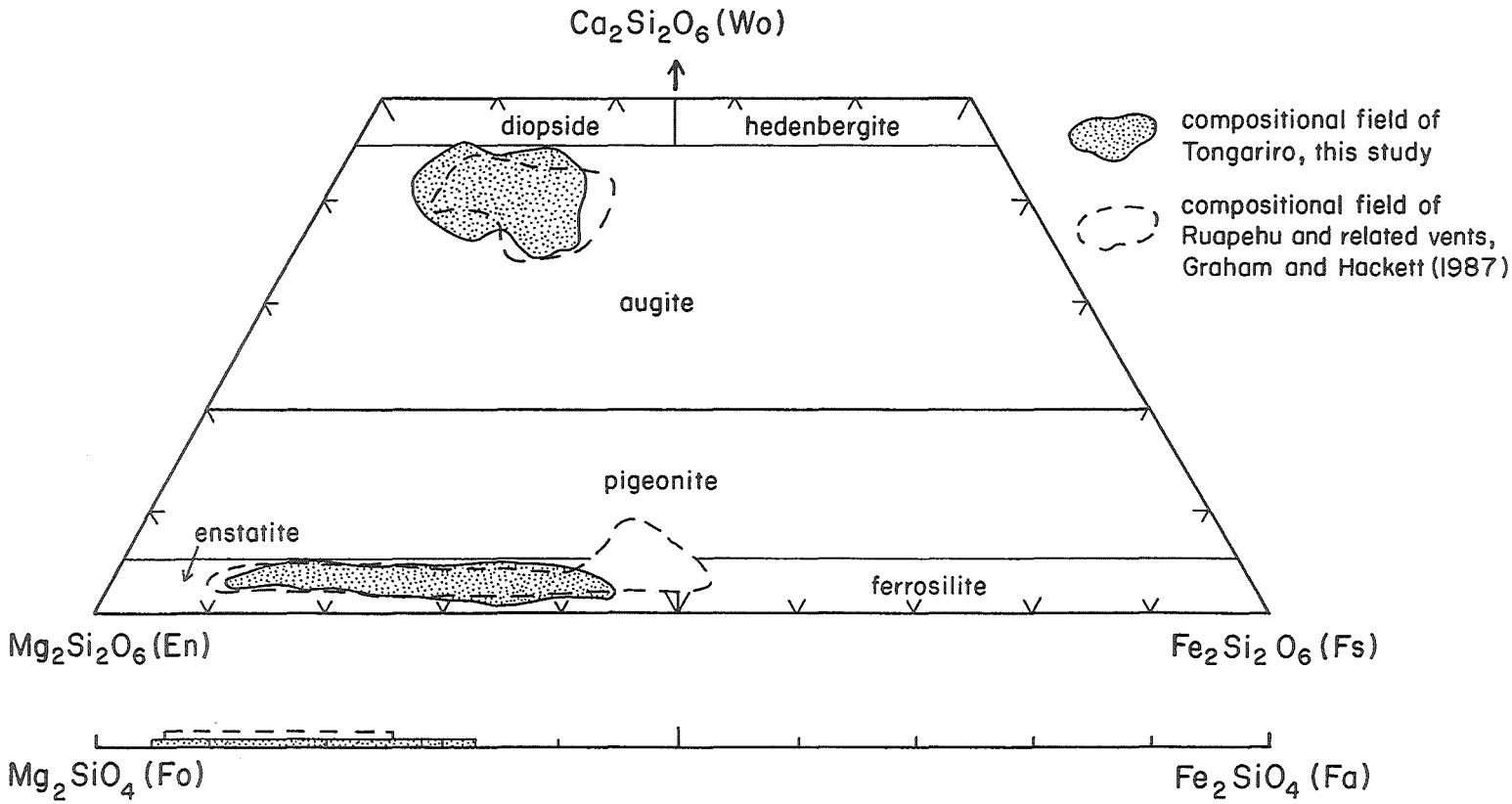

Figure 4.34 Compositional fields of pyroxenes and olivine from Tongariro (all electron microprobe analyses). The fields of Ruapehu and related vents (dashed lines; Graham and Hackett, 1987) are shown for comparison. Pyroxene classification after Morimoto (1989).

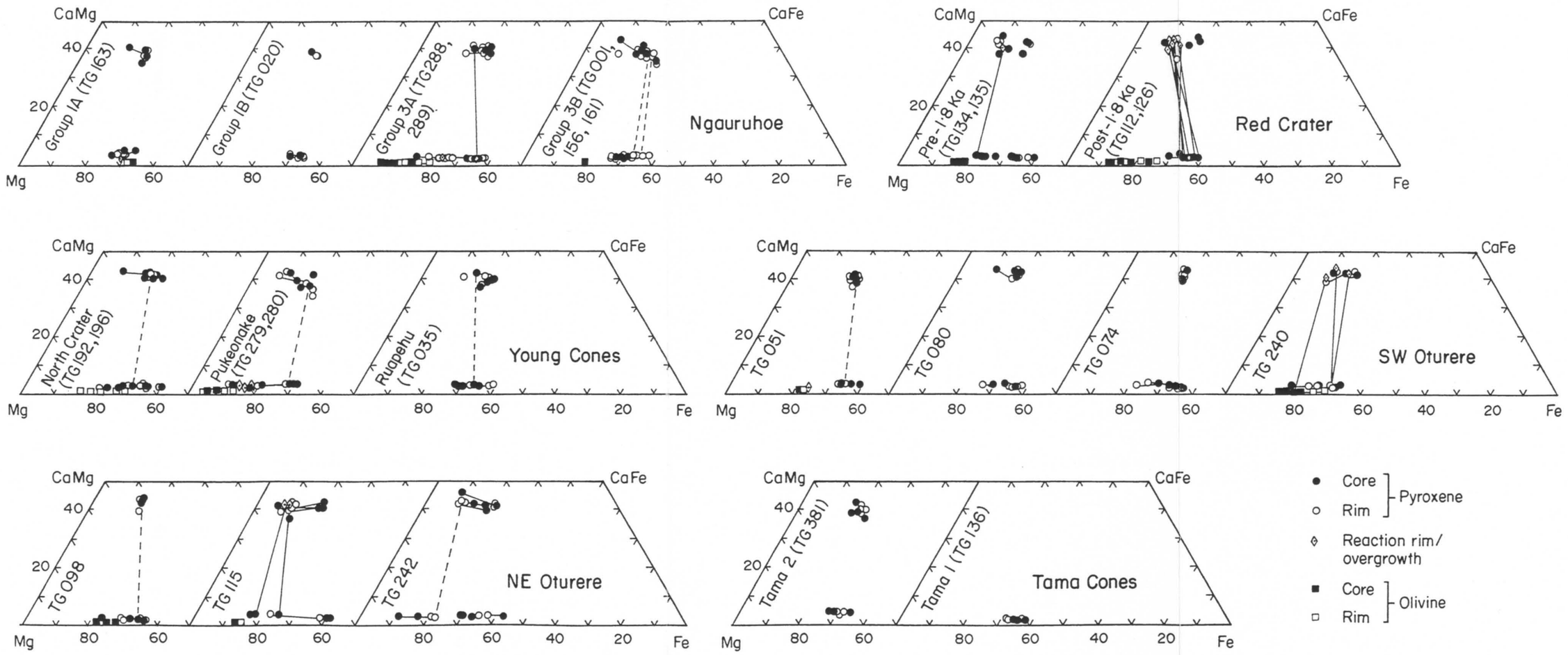

Figure 4.35 Electron microprobe analyses of pyroxenes (quadrilateral) and olivines from Tongariro by volcano-stratigraphic unit (some units not represented). Note that one sample (TG035) is from a Ruapehu flow in the Tama Lakes area (see Sections 6.5 and 7.6). Those units with limited mineral data are plotted for convenience in sets of overlapping graphs. Each point represents an analysis. Solid tie-lines join core-rim analyses made within a single crystal, and include reaction rims. Dashed tie-lines join adjacent pyroxenes in a single sample. Mineral data are tabulated in Appendix 9.

rich compositions ($Ca_{1-5}Mg_{55-86}Fe_{11-42}$) than coexisting augites (Fig 4.34). Analyses of glomerocrysts comprising adjacent clinopyroxene and orthopyroxene crystals produce tie-line configurations which suggest that, for these samples, equilibrium is closely approached (Fig 4.35). Tongariro pyroxene compositions are similar to those quoted by Ewart (1982) for calc-alkaline basaltic andesites and andesites.

$100Mg/(Mg+Fe^{2+})$ ratios (Mg#) for augite range from 64 to 88, and for orthopyroxene from 57 to 94, showing no systematic variation with whole-rock SiO_2 content. For example, the maximum Mg# for orthopyroxenes in Red Crater basaltic andesite TG112 (53.4 wt% SiO_2) is 67; for NE Oturere basaltic andesite TG115 (56.4 wt% SiO_2) it is 83; for Ngauruhoe andesite TG161 (58.2 wt% SiO_2) it is 66; and for NE Oturere andesite TG098 (61 wt% SiO_2) it is 76. However, the Mg# of both pyroxenes varies more systematically with whole-rock FeO*/MgO; showing an overall slight decrease with increasing FeO*/MgO (Fig 4.36). The clinopyroxene Mg# values are generally greater than and of a more restricted range than in orthopyroxene. Increasing maximum Mg# for pyroxenes also broadly correlates with increasing whole-rock Mg#.

In comparing the different volcano-stratigraphic units (Fig 4.35), augite compositional ranges are similar overall, with some displaying slightly wider ranges (e.g. NE Oturere), whereas orthopyroxene compositions are more variable with respect to Fe/Mg ratios. Ngauruhoe Group 3A lavas have much more Mg-rich orthopyroxene phenocrysts than the other Ngauruhoe groups. There is also a significant difference between Red Crater orthopyroxenes in pre-1.8 ka andesites (En_{58-76}) and post-1.8 ka basaltic andesites (En_{60-68}). Orthopyroxene phenocrysts in NE Oturere lava TG242 span a particularly wide compositional range (En_{56-88}). Tama 1 orthopyroxenes are noticeably lower in the Wo component (<2 mol%) compared to most other Tongariro units (which generally contain >2.5 mol% Wo).

Tongariro pyroxenes typically appear homogeneous under the microscope, but even limited microprobe analysis reveals many to be weakly to moderately zoned (Fig 4.35). Augite phenocrysts may be relatively homogeneous in composition, exhibiting core-rim

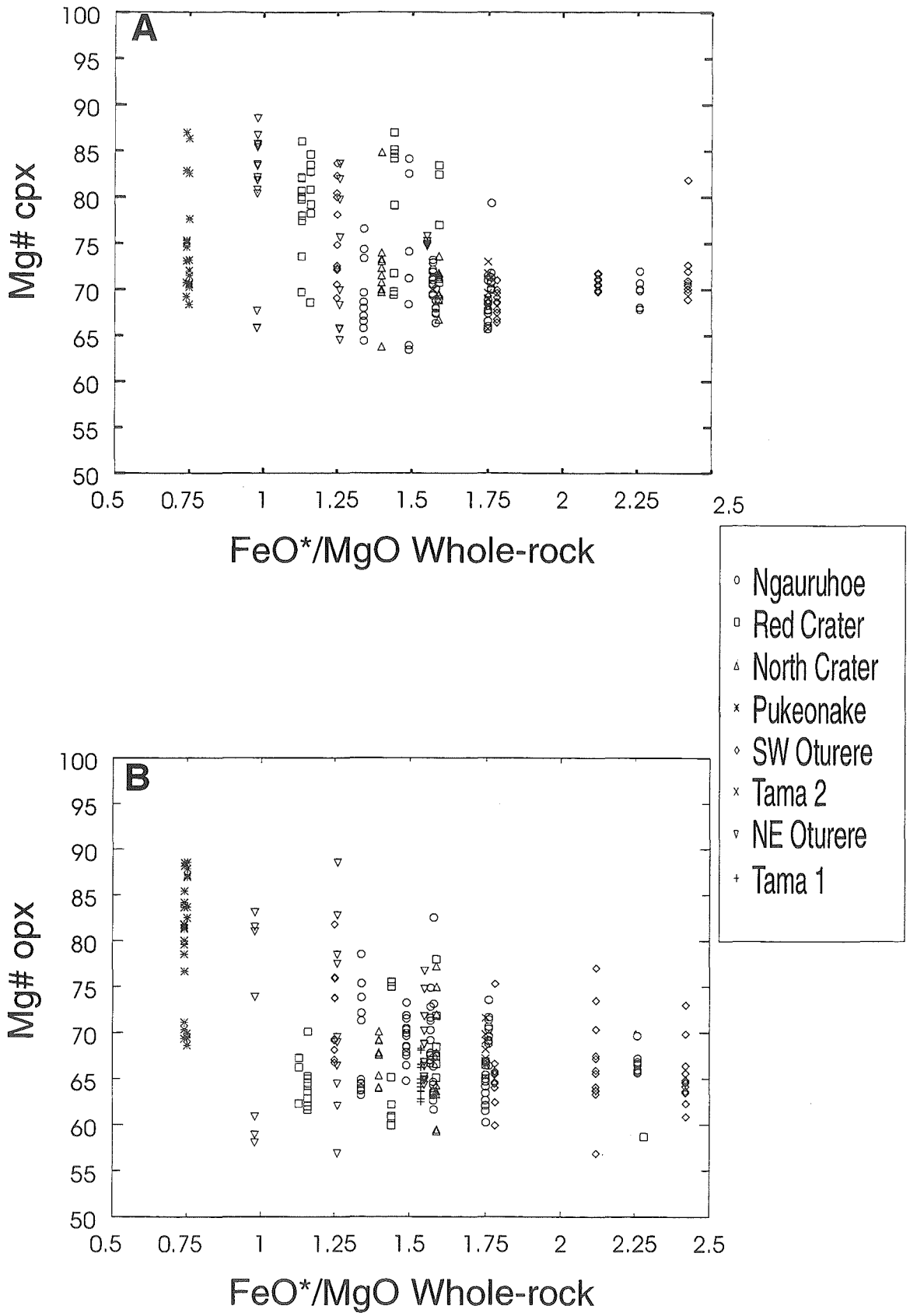

Figure 4.36 Mg# [100Mg/(Mg+Fe^{2+})] of Tongariro clinopyroxenes (A) and orthopyroxenes (B) plotted versus FeO*/MgO of the host rock (assuming Fe_2O_3/FeO=0.3).

variations of less than 3 mol% of end-member components, but some display moderate normal zoning from Mg- and Ca-rich cores to Fe-rich rims (e.g. TG242, crystal 2: $Ca_{46}Mg_{46}Fe_9$[core], $Ca_{41}Mg_{39}Fe_{20}$[rim]). Moderate reverse zoning from Fe-rich cores to Mg-rich rims is also displayed by some augites, especially those from Red Crater, Pukeonake, SW Oturere (TG240), and NE Oturere (TG115, TG242) lavas (e.g. TG115, crystal 4: $Ca_{41}Mg_{39}Fe_{20}$[core], $Ca_{42}Mg_{50}Fe_8$[rim]).

Orthopyroxene phenocrysts are typically weakly zoned (normal or reverse both equally as common) with up to 5 mol% En variation within one crystal. Normal zoning is rarely stronger (e.g. TG242, crystal 1:En_{86}[core], En_{76}[rim]), but moderate to strong reverse zoning (>10 mol% En variation) occurs in a significant minority of orthopyroxene phenocrysts from Ngauruhoe Group 3A, Pukeonake, and NE Oturere (TG115) lavas (e.g. TG279, crystal 9: En_{66}[core], En_{86}[rim]). Although weak reverse zoning may be produced by decompression (Kontak et al., 1984) or a late-stage increase in fO_2 (Luhr and Carmichael, 1980), such pronounced reverse zoning as described above is more likely related to magma mixing processes (cf. Sakuyama, 1978, 1981; Nixon, 1988a; Feeley and Davidson, 1994).

Solid tie-lines joining orthopyroxene cores with augite reaction rims/overgrowths (Fig 4.35) show that many of these rims have Fe/Mg ratios too high to be in equilibrium with their cores (e.g. post-1.8 ka Red Crater pyroxenes). Along with petrographic evidence of resorption at the core-rim boundary, these Mg-rich augite rims imply crystallization from more basic magma (cf. Sakuyama, 1979).

There is a concurrence of other disequilibrium features in some samples. Lavas with strongly reversely-zoned pyroxene and disequilibrium augite rims on orthopyroxene often also contain disequilibrium forsteritic olivine (Section 4.5.1) and sieved, reversely-zoned plagioclase (Section 4.5.2). These lavas (which include those from Red Crater, Pukeonake, and NE Oturere) appear to be the result of magma mixing processes.

Non-quadrilateral components (mainly Al_2O_3, TiO_2, Na_2O) occur in relatively low concentrations in both augite and orthopyroxene (<6.4 wt% Al_2O_3; <1.6 wt% TiO_2; <0.5 wt% Na_2O). MnO content increases with increasing FeO*, with a maximum of 1.1 wt% MnO for a TG074 orthopyroxene. Cr_2O_3 is present in significant amounts

(<0.9 wt%) in the more Mg-rich augites in lavas from Red Crater, Pukeonake and NE Oturere. NiO contents are low and variable, but reach 0.16 wt% NiO in some Mg-rich orthopyroxenes, although there is not such a consistent relationship between Mg# and NiO content as there is for Mg# and Cr_2O_3 content.

4.5.4 Amphibole

Prior to this study, amphibole had only been reported from one or two lavas near Tama Lakes (Ewart, 1971; Cole et al., 1986; Wahyudin, 1993). Detailed sampling has now revealed that amphibole phenocrysts occur in about 10% of the sampled Tongariro lavas (40 lava flows; Fig 4.1), specifically in the relatively silicic andesites from the older southern cones, particularly Tama 1, Tama 2, and Pukekaikiore (Fig 4.8). Amphibole is generally restricted to less than 5 modal % (rarely up to 18 modal %), and ranges in size from 0.4 to 3.0 mm. It may be euhedral elongate prismatic, but is typically subhedral-anhedral and resorbed and rimmed or pseudomorphed by oxides ± plag ± pyx (Figs 4.9 & 4.11). Amphibole phenocrysts from Tama 1 lavas and from one Tama 2 ignimbrite (Tn144) have a distinctive pale to dark green pleochroism (Fig 4.9) whereas all other Tongariro amphiboles are red-brown (Fig 4.11). Some amphiboles contain inclusions of Fe-Ti oxides or plagioclase.

The extent of the reaction rims surrounding or pseudomorphing the amphibole phenocrysts varies within and between samples, and warrants further discussion because of their significance regarding amphibole preservation. The presence of amphibole phenocrysts in a lava has implications for magmatic conditions, particularly pressure and water content. Experimental work indicates that pressures greater than 2 kb and water contents of >4 wt% are required for hornblende crystallization in andesitic melts (e.g. Rutherford and Devine, 1988). Because amphibole undergoes a pressure-dependent breakdown reaction during magma ascent prior to eruption, its preservation depends on the magma ascent rate - which may or may not be slow enough for some remnant amphibole crystals to survive complete breakdown. Therefore many magmas could have experienced amphibole crystallization at a deeper level, but a slow magma ascent (and/or prolonged storage in a shallow magma reservoir) may have destroyed the evidence and lava petrography may then provide no clues as to the former presence of these hydrous,

relatively high pressure crystallization conditions. Trace element chemistry, however, may provide evidence for amphibole fractionation (e.g. Romick et al., 1992).

The rims on Tongariro amphiboles are of two types. The majority of rims (those from Tama 2, along with Pukekaikiore and SW Oturere) are composed almost entirely of Fe-Ti oxides and can be as thin as 5-30 μm (e.g. TG387), but are usually much thicker (Fig 4.11A) or completely replace the amphibole (Fig 4.11B). This type of amphibole reaction product was termed 'black' type by Garcia and Jacobson (1979) and is generally interpreted to form by oxidation and dehydrogenation during or after extrusion. Some Tongariro amphiboles also contain black rims which cut through crystals. The black amphibole pseudomorphs vary greatly from large (<2 mm) and euhedral to small (0.4 mm) and rounded, indicating the reaction may proceed to varying degrees, ultimately destroying the crystal.

The second type of reaction rim observed on Tongariro amphiboles, particularly those from Tama 1 lavas, comprises a fine- (5-20μm) to medium-grained (<500μm) aggregate of anhedral plag+opx+cpx+ox, termed 'gabbroic' type by Garcia and Jacobson (1979). These reaction rims form as a result of reduced water content of the coexisting melt produced magma ascent, although an origin by mixing with new hotter or low-H_2O magma cannot be totally discounted for Tongariro - which has so much evidence for magma mixing. Amphibole glomerocrysts are rimmed only on the outside crystal edges in contact with the melt.

In an experimental study on amphibole in Mt St Helens dacite, Rutherford and Hill (1993) calibrated ('gabbroic') amphibole reaction rim width with decompression time which allowed estimates of magma ascent rates. Although measurement of rim widths on Tongariro amphiboles is not as precise as in the experimental study, they all appear thicker than 30μm which would indicate that these magmas probably spent several weeks ascending from an approximately 5-7 km deep magma reservoir to the surface (Rutherford and Hill, 1993, Fig 6). Despite the uncertainties in extrapolating the experimental results to Tongariro amphiboles, the connection between amphibole rim width (or presence at all) and decompression time suggests that those Tongariro lavas which contain amphibole may principally reflect relatively fast magma ascent compared to amphibole-free lavas, and not necessarily higher pressure, more hydrous crystallization conditions. Lavas which lack

amphibole may still at some time have experienced the conditions necessary for its crystallization, but slower magma ascent could have removed the evidence. Certain aspects of these lavas' whole-rock chemistry, however, provide further clues for the role of amphibole crystallization (Chapters 6 and 7).

The only occurrence of unrimmed amphibole on the Tongariro complex is from a small andesitic ignimbrite from Tama 2 (Tn144). Pristine, green, euhedral-subhedral hornblende phenocrysts are abundant and form sharp, "clean" contacts with the surrounding glass. A much more rapid magma ascent than other amphibole-bearing Tongariro magmas is implied, and this correlates with the explosive style of eruption.

Amphibole compositions for only two Tongariro samples, TG136 and TG381, were determined by electron microprobe (Table A9.5, Appendix 9). Difficulties were encountered in finding fresh remnant cores large enough to be analysed. All analysed Tongariro amphiboles have $(Ca+Na)_{M4}>1.34$ and $(Na)_{M4}<0.67$, and can therefore be classified as calcic amphiboles after Leake (1978). Most of the calcic amphiboles also have $(Na+K)_A<0.50$ and extend from magnesio-hornblende through tschermakitic hornblende to tschermakite. Three amphibole analyses from TG381 have $(Na+K)_A>0.50$; two are edenitic hornblendes and the other classifies as magnesio-hastingsite. Overall, the Tongariro amphibole compositions are typical of orogenic andesites (Gill, 1981; Ewart, 1982).

Tama 1 amphibole (TG136) has a relatively narrow compositional range (ferri-tschermakitic hornblende to ferri-tschermakite; Si=6.15-6.35 atoms per formula unit [a.p.f.u.]), relatively high ferric iron content (Fe^{3+}=1.11-1.56 a.p.f.u.), consistent Al^{tot} concentrations (1.72-2.06 a.p.f.u.), and relatively low Ti concentrations (Ti=0.11-0.16 a.p.f.u.). In contrast, Tama 2 amphibole (TG381), has a wider compositional range which also encompasses magnesio-hornblende, edenitic hornblende and magnesio-hastingsite (Si=6.19-6.79 a.p.f.u.), lower Fe^{3+} (0.23-0.96 a.p.f.u.), more variable Al^{tot} concentrations (1.34-2.11 a.p.f.u.), and slightly higher Ti (0.16-0.22 a.p.f.u.).

Tongariro amphiboles exhibit no apparent trend on a plot of Al^{IV} vs. $(Na+K)_A$ (Fig 4.37) which might suggest increasing temperature. A positive correlation between Al^{IV} and (Na+K) cations in the A site of amphibole phenocrysts has been demonstrated

Figure 4.37 Al (IV) vs. (Na+K) A site occupancy for Tongariro hornblendes.

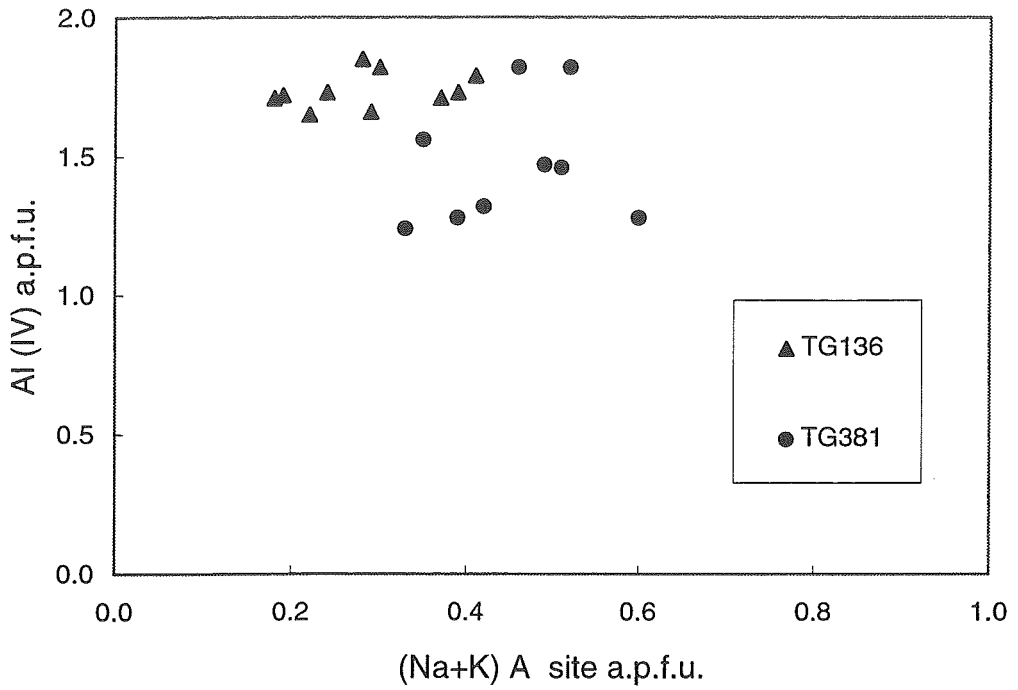

Figure 4.38 Al(tot) versus Mg# for Tongariro hornblendes

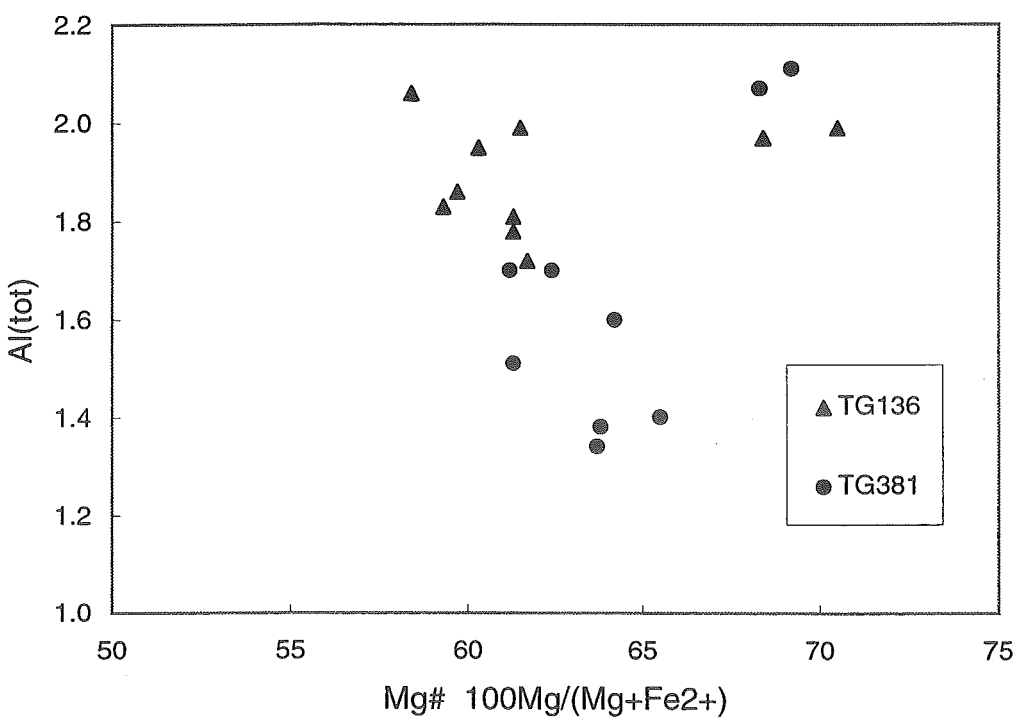

experimentally to coincide with increasing crystallization temperatures (Jakes and White, 1972; Helz, 1973). The limited number of analyses available for Tongariro amphiboles probably prevents any useful interpretation from such a plot.

Figure 4.38 illustrates the overall higher and more limited Al^{tot} range of most TG136 hornblendes compared to the more variable Al^{tot} of TG381 hornblendes. Although only a limited number of analyses are available, the two samples show only limited overlap on the plot of Al^{tot} versus $100Mg/(Mg+Fe^{2+})$ ratio (Mg#). The four high-Mg# analyses may indicate influx of a more basic magma involved in magma mixing. On the other hand, the few outlier analyses of high or low Mg# may indicate failure to analyse a representative population of hornblende for each sample, which may in fact range continuously between the extreme Mg# compositions. More detailed investigation of Tongariro hornblendes is required to further assess this relationship.

Mg# of Tongariro hornblendes range from 58 to 71 (TG136) and 61-69 (TG381), and are thus only slightly lower overall than the Mg# of their coexisting pyroxenes (62-67, TG136; 65-73, TG381). Of the hornblendes which have both a core and rim analysis (mostly from TG136), many show weak to moderate reverse zoning from Fe-rich cores to Mg-rich rims (e.g. TG136, crystal 2: Mg#=60 [core], Mg#=71 [rim]). Reverse zoning in hornblendes may be the result of magma mixing (Sakuyama, 1979) or an increase in fO_2 (Mason, 1978). Other crystals appear to be more homogeneous (e.g. TG381, crystal 4: Mg#=64 [core], Mg#=64 [rim]).

Because amphibole is not a common phenocryst in lavas from the Tongariro complex and the Tongariro Volcanic Centre in general, it is appropriate to compare the amphibole compositions found in this study with those of previous workers. Ewart (1971) identified a tschermakitic hornblende from Tama Lakes andesite. Hackett (1985) presented limited microprobe data on the rare brown or green amphibole phenocrysts found in two silicic andesites and one dacite at Ruapehu; these classified as ferroan pargasitic hornblendes. In a survey of the whole of Tongariro Volcanic Centre, Cole et al. (1986) noted hornblende occurrences in only Tama Lakes and Maungakatote lavas. The only other full amphibole analyses available for Tongariro lavas come from a recent MSc thesis (Wahyudin, 1993), which describes mostly ferroan pargasitic hornblende and edenitic hornblende in two samples from the Tama Lakes area.

Recent work on the young andesitic tephras from the eastern sector of the Tongariro-Ruapehu ring plain reveals that some contain hornblende. The c.9.8 ka Te Rato Lapilli (Mangamate Tephra), inferred to have erupted from North Crater on Tongariro (Topping, 1973) is rich in pargasitic hornblende (Donoghue et al., 1991). Donoghue (1991) analysed amphiboles from other tephras derived from Tongariro (Poutu Lapilli, Oturere Lapilli) and Ruapehu (Bullot Formation), which she classified (after Leake, 1978) as ferroan pargasite, pargasite, pargasitic hornblende, ferroan pargasitic hornblende, pargasitic hornblende, edenite, tschermakitic hornblende, and magnesio-hornblende. Cronin et al. (1994) examined tephras up to c.80 ka and assigned the hornblende-bearing tephras to a Tongariro source, based on their rarity in Ruapehu lavas.

In general, amphibole compositions determined in this study are similar to those found by other workers on Tongariro and neighbouring cones. The occurrence of hornblende in young tephras but its absence in the associated lavas on the cone (e.g. Te Rato Lapilli and North Crater lava/agglutinate) suggests a connection between this hydrous mineral and episodes of explosive volcanism. If magmas containing amphibole preferentially erupt as fall deposits rather than lava flows, the units are more likely to be preserved on the ring plain than on the cone itself. Until the tephra stratigraphy and tephra chronology is better known, it is not possible to assess whether the occurrence of hornblende in Tongariro lava flows (as documented in this study) is a true reflection of the abundance of hornblende in Tongariro magmas. Even then, breakdown reactions leading to the disappearance of amphibole from the phenocryst assemblage ensure that an element of uncertainty will remain.

4.5.5 Oxides

The majority (almost 90%) of Tongariro lavas contain Fe-Ti oxide minerals, principally magnetite but also ilmenite, as a minor phase (typically 0.5-1 modal %). Fe-Ti oxides occur throughout the compositional range, but tend to be more abundant (<3 modal %) in the silicic andesites and dacites (Figs 4.5 and 4.6). Chrome spinel is restricted to sparse inclusions in olivine phenocrysts of several basaltic andesite to andesite lavas (e.g. TG240, TG279-280, TG289).

(a) **Magnetite and ilmenite.** Fe-Ti oxides occur as euhedral to anhedral microphenocrysts (generally <0.5-1.0 mm; Figs 4.3, 4.9, 4.24), and more commonly in pyroxene glomerocrysts (Figs 4.13, 4.24) or as inclusions in pyroxene (and occasionally plagioclase and amphibole) phenocrysts. Most Fe-Ti oxides appear homogeneous and unexsolved when viewed with the petrological microscope. However, Ti scans with the electron microprobe revealed that some magnetite grains in a minority of Tongariro samples contain fine ilmenite lamellae, formed during subsolidus oxidation (Negendank, 1972). Magnetite is also an important constituent of the groundmass of most Tongariro lavas. Fe-Ti oxides also commonly surround hornblende phenocrysts in reaction rims, or replace them entirely as pseudomorphs (Section 4.5.4).

Figure 4.39 shows the compositional range of Tongariro Fe-Ti oxides with respect to the solid solution series magnetite-ulvöspinel and hematite-ilmenite. Ulvöspinel (Usp) contents of magnetite range from 1 to 61 mol%, but most analyses yield 25-40 mol% Usp, which is within the typical range for calc-alkaline volcanics (Gill, 1981; Frost and Lindsley, 1991). Ulvöspinel does not show any systematic relationship with whole-rock SiO_2 or TiO_2. Tongariro ilmenites contain 7-25 mol% hematite in solid solution and exhibit less compositional variability than the magnetites. Fe-Ti oxide compositions are occasionally variable within samples (e.g. TG240: Usp_{25-61}, Hem_{11-19}), but are more commonly homogeneous.

Differences between volcano-stratigraphic units are generally slight, although the hornblende-bearing lavas of Tama 1 and Tama 2 contain magnetites with noticeably lower Usp contents (1-27 mol%) than other Tongariro magnetites. The highest Usp contents were recorded in analyses from a variety of volcano-stratigraphic units, often in olivine-bearing lavas: SW Oturere (TG240, Usp_{61}); North Crater (TG196, Usp_{55}); Ngauruhoe (TG156, Usp_{55}; TG288, Usp_{45}); and Pukeonake (TG279, Usp_{45}). These differences between units appear to correlate primarily with differing mafic phenocryst assemblages. Carmichael (1967) noted this relationship between TiO_2 content of Fe-Ti oxides and composition of the co-existing ferromagnesian silicate phenocrysts; TiO_2 decreases in the order oliv-opx-hbl+biot.

The magnetite phenocrysts for which both core and rim analyses were obtained often have slightly more Ti-rich (and occasionally more Mg-rich & Fe-poor) cores than

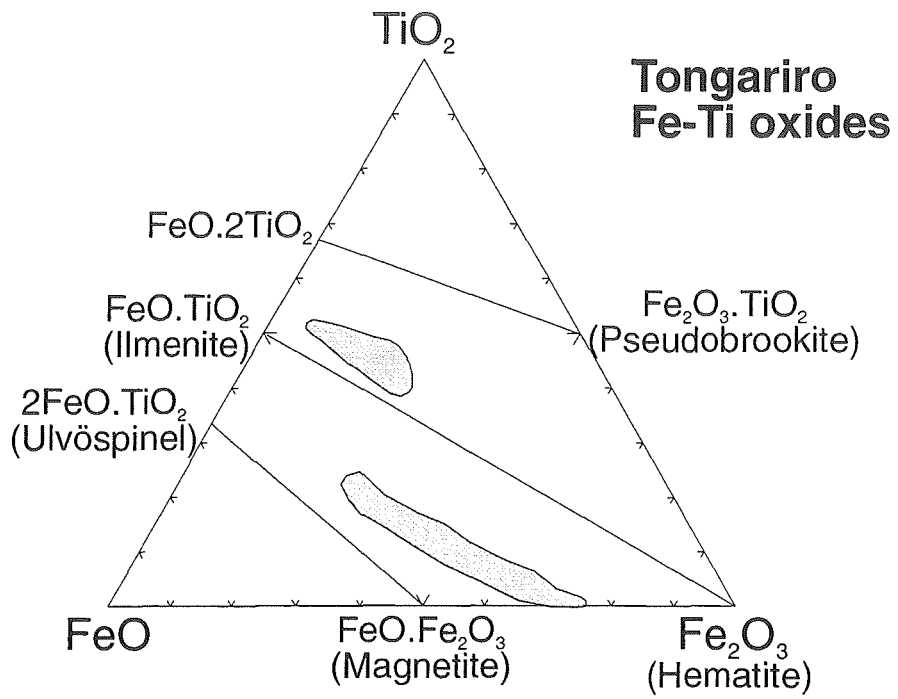

Figure 4.39 Compositional fields of Tongariro Fe-Ti oxide solid solution series magnetite-ulvöspinel and hematite-ilmenite, plotted in the system FeO-Fe_2O_3-TiO_2. Mineral data are tabulated in Appendix 9.

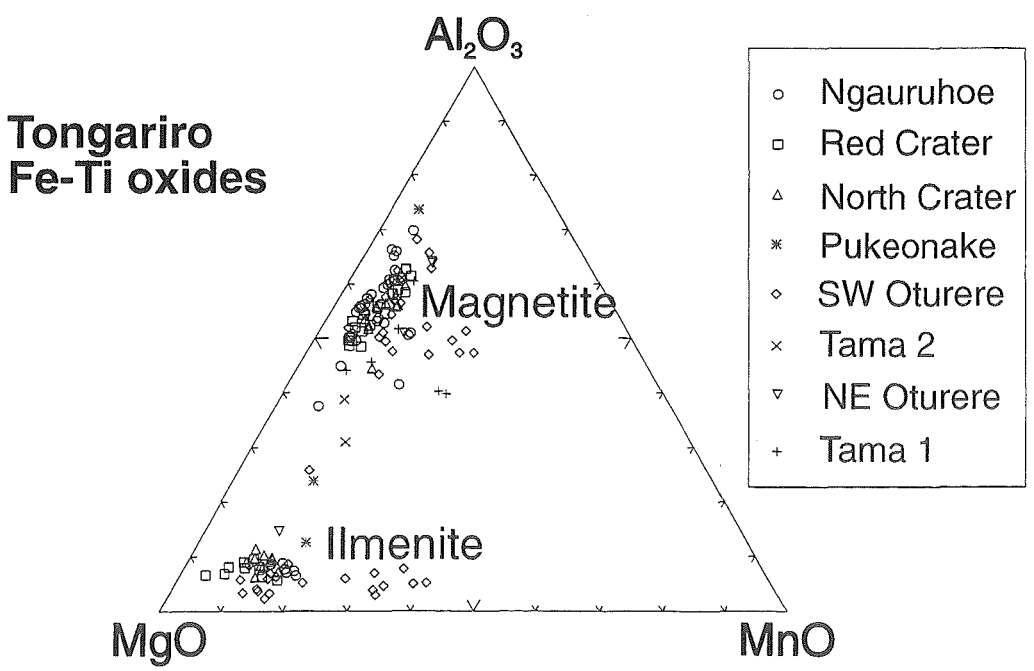

Figure 4.40 Minor element abundances (wt%) for Tongariro Fe-Ti oxides, plotted in the system MgO-MnO-Al_2O_3.

rims (e.g. TG126, crystal 3: 11.94[core] - 11.71[rim] wt% TiO_2), but are also homogeneous or with cores poorer in Ti than rims (e.g. TG020, crystal 4: 9.20[core] - 10.42[rim] wt% TiO_2). TiO_2 contents range from 0.3 to 20.9 wt% but most magnetites contain 10-15 wt% TiO_2. Al_2O_3 and MgO contents are quite variable, 0.6-7.5 wt% and 0.5-5.5 wt% respectively, and reach somewhat higher abundances than those typical of calc-alkaline volcanics (1-3 wt%; Frost and Lindsley, 1991). The minor elements also vary: 0.15-1.4 wt% MnO, 0.0-1.0 wt% Cr_2O_3, 0.0-0.16 wt% NiO, 0.0-0.3 wt% CaO, and together with Al_2O_3 and MgO, indicate partial substitution for Fe^{3+} and Fe^{2+} within the magnetite structure.

R_2O_3 contents (Fe_2O_3 + Al_2O_3 + Cr_2O_3) of Tongariro ilmenites range from 7 to 25 mol%, a range encompassing slightly more Fe_2O_3-poor compositions than typical for ilmenites in orogenic andesites (15-25 mol% R_2O_3; Gill, 1981). TiO_2 contents are 37.5-48.0 wt% and MgO reaches as high as 6.6 wt%, but is typically less than 3 wt%. MnO, Al_2O_3, and Cr_2O_3 all occur in abundances less than 1 wt%.

Relationships between three of the minor elements (MgO, MnO, Al_2O_3) are shown in Figure 4.40 for all analysed Tongariro Fe-Ti oxides. The magnetites are richer in Al_2O_3 but poorer in MgO compared to the ilmenites. Several analyses plot as intermediate compositions between the main fields for magnetite and ilmenite. These analyses correspond to oxides with exsolution lamellae or oxides included in hornblende phenocrysts. The majority of analyses cluster in a narrow region on the MnO-poor side of the triangular plot (Fig 4.40). Fe-Ti oxides become progressively depleted in Al_2O_3 and MgO, and enriched in MnO, with increasing whole-rock SiO_2 (Carmichael, 1967; Bacon and Hirschmann, 1988). Because most Tongariro oxides have similar (relatively high) Mg/Mn values they are likely to have crystallized within a similar and relatively narrow temperature range. Several Red Crater oxide pairs have higher Mg/Mn values than other Tongariro oxides, indicating higher-temperature crystallization. The only samples to show appreciable enrichment in MnO are from the higher-SiO_2 lavas of TG080 (SW Oturere) and TG136 (Tama 1), which apparently crystallized Fe-Ti oxides at lower temperatures than other Tongariro magmas.

(b) Chrome spinel. Chrome spinel occurs as small (<0.2 mm), rare, dark red-brown to opaque, euhedral to subhedral inclusions within olivine phenocrysts (Fo_{86-92}

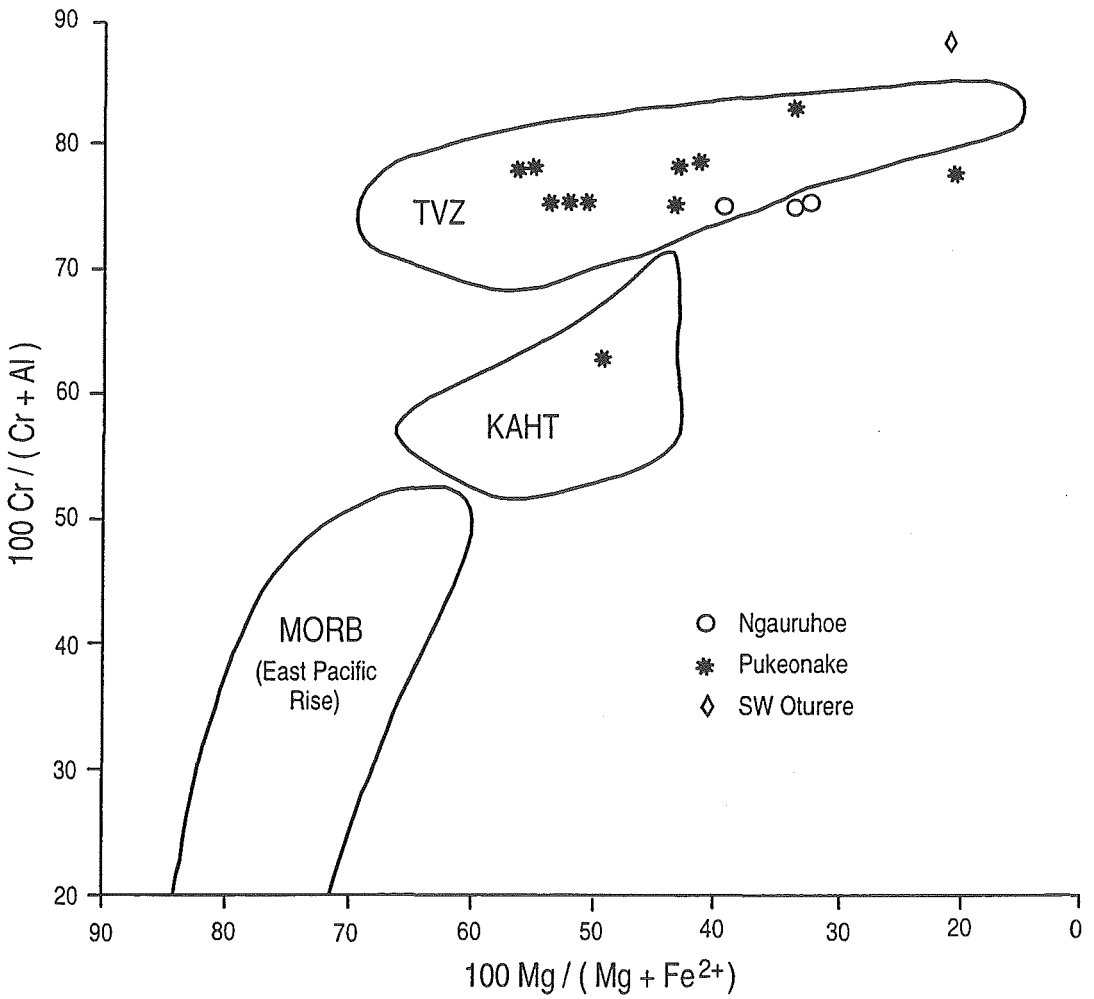

Figure 4.41 Electron microprobe analyses of chrome spinels from the Tongariro Complex. Compositional fields of the Taupo Volcanic Zone (TVZ), Kermadec Arc and Havre Trough (KAHT) (both from Gamble et al., 1993b), and East Pacific Rise MORB (Natland, 1989) are shown for comparison. Mineral data are tabulated in Appendix 9.

cores) of some of the more Mg-rich basaltic andesites (TG279-280; 8.9-9.2 wt% MgO) and andesites (TG240, TG289; 4.4-5.5 wt% MgO). Less commonly, a chrome spinel grain may occur included in an olivine or pyroxene glomerocryst.

Microprobe analyses of 15 chrome spinels from 3 samples (Table A9.8, Appendix 9) show them to be rich in chrome (42.6-56.2 wt% Cr_2O_3), characterised by 100Cr/(Cr+Al) from 62.8 to 88.3 and by 100Mg/(Mg+Fe^{2+}) from 20.5 to 55.7 (Fig 4.41). Thus the compositional range of Tongariro chrome spinels is similar to those from TVZ basalts (Gamble et al., 1993b) and arc-related lavas in general (Dick and Bullen, 1984), and significantly wider than mid-ocean ridge basalt spinel compositions (Dick and Bullen, 1984).

4.5.6 Apatite

Euhedral-subhedral prismatic apatite occurs as a minor (<0.1 modal %) phase in some Tongariro andesites. Of particular note is the red-brown pleochroic variety found in many of the hornblende-bearing Tama 2 andesites. These microphenocrysts (up to 1.0 mm, but generally <0.2 mm) probably owe their red colour to exsolution of iron oxides; some grains contain thin opaque-filled cracks and these grains tend to be redder than those where the opaques are less prominent or absent. No microprobe analyses of Tongariro apatites were obtained.

4.5.7 Quartz

Rare xenocrystic quartz has been observed in lavas from several Tongariro volcano-stratigraphic units: NE Oturere (TG108, TG245), Tama 2 (TG381), Pukekaikiore (TG154), and Ngauruhoe (TG411). Typically only 1-3 quartz grains are present per thin section, but TG381 contains about 1 modal % quartz. The quartz is always subhedral to anhedral, resorbed and corroded (Fig 4.11B) and is not in equilibrium with the host lava, which often also contains olivine (e.g. TG108, TG154, TG411). The quartz grains in TG381 have associated fringing tridymite and some spherulite development, and are associated with a colourless glass more silicic than the dominant brown andesitic glass. Together with other

mineralogical evidence for disequilibrium in these lavas, the quartz crystals are interpreted as relict phenocrysts from a lower-temperature, more silicic magma involved in a magma mixing event (see Section 4.7).

4.5.8 Glass

Three Tongariro glass analyses were made during microprobe analysis of Tongariro minerals. Only limited glass compositions were obtained because of the difficulty in finding an area of fresh glass large enough for analysis (see Section 4.3.2).

The glass analyses from a pre-1.8 ka Red Crater lava flow (TG134) and the North Crater lava lake (TG196) are presented with their whole-rock compositions in Table 4.3. The glass occurs interstitially within glomerocrysts (plag-opx, analysis 0329G; cpx-opx, analysis 0484G) and as an inclusion within a plagioclase phenocryst (analysis 0484G). Glass is more SiO_2-poor (65.9 wt% SiO_2) in the olivine-bearing Red Crater andesite than in the North Crater andesite (72.2-76.6 wt% SiO_2). An increase in SiO_2, Al_2O_3 (and Na_2O, K_2O) and a decrease in FeO*, MnO, MgO, and CaO from whole-rock to glass compositions is consistent with differentiation by fractional crystallization. However, more glass analyses more representative of Tongariro groundmass compositions would be required to further assess differentiation processes and to make comparisons between volcano-stratigraphic units.

Table 4.3 Tongariro glass and whole-rock compositions. GC = glomerocryst. incln = inclusion. n.a. = not analysed. Whole-rock FeO_t calculated assuming $Fe_2O_3/FeO = 0.3$.

	TG134: Red Crater andesite		**TG196: North Crater andesite**		
Modal % phenocrysts	15% plag 7% cpx 1% ox	2% opx 2% oliv 73% gmass	15% plag 1% ox	6% opx 75% gmass	3% cpx
	whole-rock	glass	whole-rock	glass	glass
Analysis		0329G		0474G	0484G
Location		plag-opx GC		plag incln	cpx-opx GC
SiO_2	59.47	65.86	59.20	72.18	76.55
TiO_2	0.70	0.21	0.78	0.63	0.85
Al_2O_3	16.02	19.97	17.11	15.05	11.68
FeO_t	6.48	1.33	6.50	2.23	3.86
MnO	0.12	0.00	0.12	0.04	0.02
MgO	4.49	0.04	4.08	0.69	0.29
CaO	7.23	4.88	6.93	3.26	1.32
Na_2O	3.10	6.18	3.25	3.39	2.86
K_2O	1.52	1.44	1.45	2.33	4.12
P_2O_5	0.14	n.a.	0.15	n.a.	n.a.
LOI	-0.39	n.a.	-0.42	n.a.	n.a.
TOTAL	99.60	99.91	99.88	99.80	101.55

4.6 CRYSTALLIZATION CONDITIONS

4.6.1 Pyroxene thermometry

All but one (TG136) of the 24 Tongariro samples for which mineral data have been obtained have coexisting clinopyroxene and orthopyroxene phenocrysts suitable for use in the graphical two-pyroxene thermometer of Davidson and Lindsley (1989). The molar proportions of pyroxene end-members were projected onto the quadrilateral using the calculations of Lindsley and Anderson (1983), available in a subroutine in the PetMin computer programme (see Appendix 9 for details). Since pyroxenes in which Wo+En+Fs<90% (i.e. nonquadrilateral components or "others" >10%) were omitted from the geothermometry calculations, the two-pyroxene temperature estimates are probably accurate to ±50°C (Lindsley, 1983). A pressure of 2 kb was assumed in the calculations (see Section 4.6.3).

Because each pyroxene of a pair yields an independent estimate of temperature, a check for consistency and equilibrium conditions can be made. Temperature estimates for most Tongariro clinopyroxenes are in good agreement with their orthopyroxene counterparts. Rarely, samples show a temperature disparity between pyroxene pairs (e.g. TG289: cpx=700-900°C; opx=1000-1100) which can often be related to petrographic evidence for disequilibrium and magma mixing processes.

Projected compositions of all Tongariro pyroxenes with "others" <10% are plotted on the temperature-contoured pyroxene quadrilateral (Fig 4.42A; after Lindsley, 1983) and indicate that Tongariro pyroxenes formed over a large temperature range of approximately 600 to 1200°C, although most data points are concentrated between the 900°C and 1100°C temperature contours. There is only a moderate difference between temperature estimates for basaltic andesites (typically 950-1200°C) and andesites (typically 850-1100°C), with a weak overall trend of decreasing temperature with increasing whole-rock SiO_2 content.

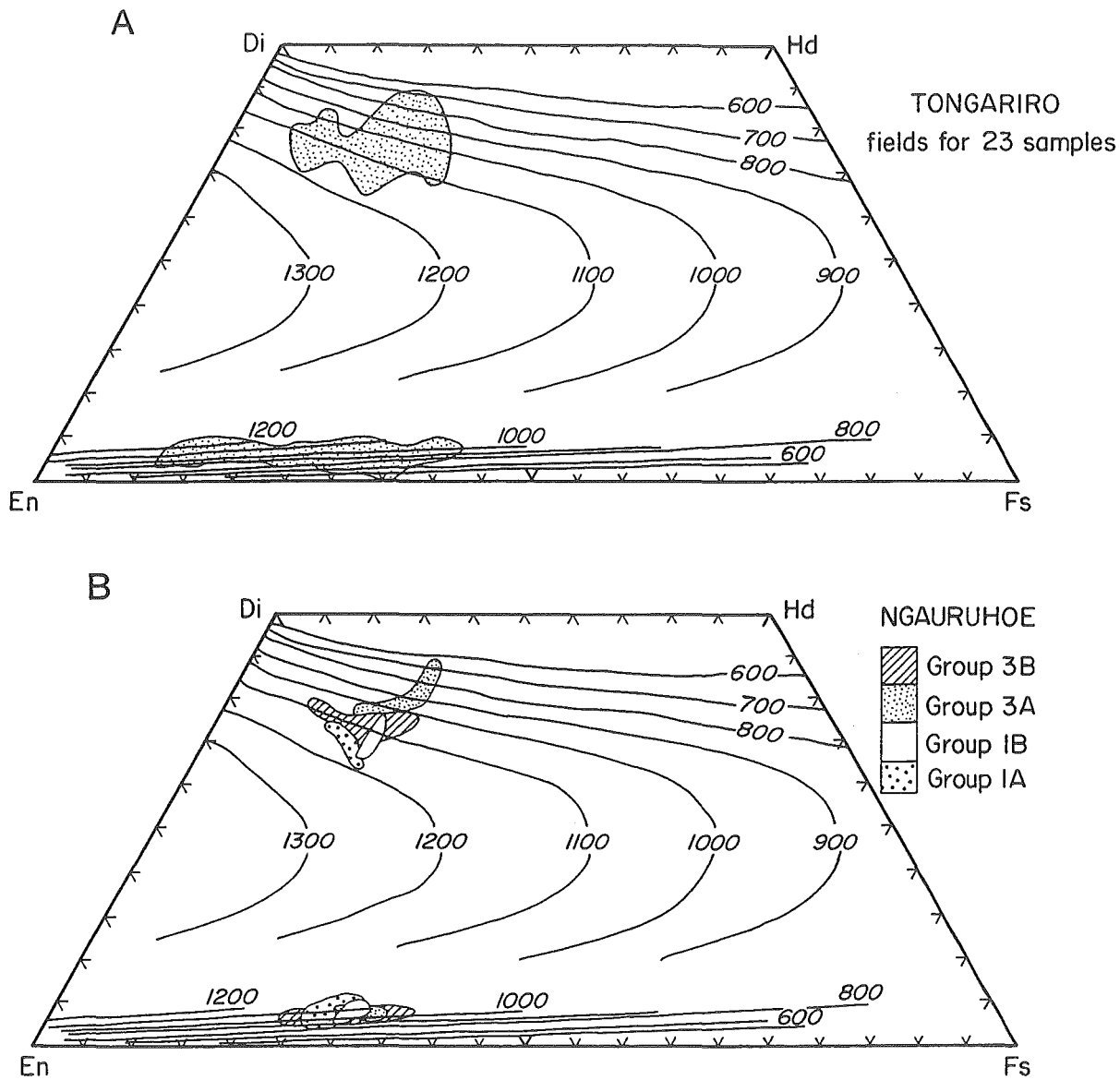

Figure 4.42 Compositions for coexisting pyroxene pairs projected according to the calculation scheme of Lindsley (1983) and plotted on the pyroxene quadrilateral. Temperature contours (°C, Lindsley, 1983) indicate range of equilibration temperatures for (**A**) all analysed Tongariro pyroxenes, and (**B**) pyroxenes from Ngauruhoe lava groups.

Table 4.4 Temperature estimates using Davidson & Lindsley's (1989) graphical two-pyroxene thermometer for selected Tongariro lavas. Pressure set at 2 kb for calculation. Errors quoted by Lindsley (1983) are +/-50°C.

Unit	Group	Sample	Range T (°C) for sample	Range T (°C) for group/unit
Ngauruhoe	3B	TG001	1000 - 1100	1000 - 1100
		TG156	1000 - 1100	
		TG161	1000 - 1100	
	3A	TG288	950 - 1100	700 - 1100
		TG289	700 - 1100	
	1B	TG020	1000 - 1200	1000 - 1200
	1A	TG163	1000 - 1150	1000 - 1150
Red Crater	Post-1.8 ka	TG112	800 - 1050	800 - 1050
		TG126	900 - 1000	
	Pre-1.8 ka	TG134	900 - 1100	900 - 1150
		TG135	900 - 1150	
North Crater		TG192	950 - 1050	800 - 1050
		TG196	800 - 1000	
Pukeonake		TG279	1000 - 1200	1000 - 1200
		TG280	1100 - 1200	
SW Oturere		TG051	950 - 1050	800 - 1100
		TG074	800 - 1100	
		TG080	900 - 1100	
		TG240	900 - 1100	
Tama 2		TG381	600 - 1100	600 - 1100
NE Oturere		TG098	800 - 1100	800 - 1200
		TG115	850 - 1200	
		TG242	950 - 1100	

These Tongariro temperature estimates span a wider range and encompass lower temperatures than the temperatures derived using the method of Lindsley (1983) from mostly Ruapehu coexisting pyroxenes of between 1200°C (basalt) and 1050°C (dacite) by Graham and Hackett (1987) and Graham et al. (1995). The only other previous geothermometry calculations for Tongariro lavas come from Wahyudin (1993) who used Lindsley's (1983) two-pyroxene thermometer to estimate equilibration temperatures of 720-1050°C for a volcanic bomb (D61) from a young Tama Lakes tephra deposit (equivalent to sample TG137), and 600-950°C for old Tama lavas (D57 and D66) equivalent to and in reasonable agreement with the TG381 Tama 2 lava (600-1100°C).

Estimated temperature ranges for the 23 Tongariro samples are presented according to volcano-stratigraphic unit in Table 4.4. Temperature ranges of most units overlap, although Pukeonake is notable for its high temperature overall (1000-1200°C), whereas Ngauruhoe and Tama 2 lavas appear to represent particularly broad temperature ranges of 500°C (700-1200°C and 600-1100°C respectively).

Subtle differences in pyroxene compositions and equilibration temperatures between the Ngauruhoe lava groups are revealed in Figure 4.42B (note that no mineral data are available for Group 2). Two-pyroxene thermometry suggests that magmas of the older Groups 1A and 1B equilibrated at higher temperatures overall (1000-1200°C) than the younger Groups 3A and 3B. Group 3A pyroxene analyses span the greatest temperature range (700-1100°C) and encompass the lowest calculated temperatures. Group 3B pyroxenes appear to have equilibrated over the narrowest temperature range (1000-1100°C), even though they represent the widest range of Fe/Mg ratios of all the Ngauruhoe lava groups. Temperature ranges for clinopyroxene and orthopyroxene do differ somewhat, suggesting disequilibrium conditions in some of these Ngauruhoe lavas.

Variation within other volcano-stratigraphic units is more difficult to assess with the limited data available. There does not appear to be a significant difference between pre-1.8 ka and post-1.8 ka Red Crater lavas (Table 4.4). The four samples from SW Oturere also have similar temperature ranges (Table 4.4), and it is interesting to note that the younger and much higher MgO scoria sample (TG240) contains pyroxenes which indicate crystallization over the same temperature range as much lower MgO lavas (e.g. TG080). NE Oturere samples have relative temperatures consistent with their degree of

fractionation; pyroxenes in the basaltic andesite TG115 indicate crystallization temperatures of up to 1200°C, compared to the silicic andesiteTG098 which crystallized at temperatures as low as 800°C (Table 4.4).

4.6.2 Fe-Ti oxide thermometry and oxygen fugacity

Coexisting ilmenite and magnetite in some Tongariro lavas provide a means to estimate temperature (T°C) and oxygen fugacity (fO_2) using the geothermometer of Anderson and Lindsley (1988), which unlike earlier models takes into account the effects of Mg and Mn. Because ilmenite is typically scarce or absent in Tongariro lavas, it was not possible to obtain Fe-Ti oxide temperature estimates representative of all volcano-stratigraphic units. In addition, a thorough search for ilmenite during microprobe analysis yielded only one or two ilmenite grains per polished section for some samples (e.g. TG135, TG279) which does not provide a true indication of the full range of crystallization temperatures for those samples. Fe-Ti oxide thermometry calculations were processed using the PetMin computer programme (see Appendix 9 for details). Calculated T-fO_2 values are probably within the errors of around ±50°C and ±1 log unit fO_2 originally quoted by Buddington and Lindsley (1964). A pressure of 2 kb was assumed for calculation purposes.

Ideally, oxide pairs used in geothermometry calculations should display petrographic evidence for equilibration such as contact directly with each other or via continuous glass. Most Tongariro oxides, however, occur as inclusions within silicate phenocrysts or as microphenocrysts within crystalline groundmasses. Therefore only oxide pairs which satisfy the Mg/Mn equilibrium partitioning criterion of Bacon and Hirschmann (1988) were used to calculate temperatures (Fig 4.43). At high Mg/Mn values some of the analyses (e.g. TG289) deviate slightly above the error envelope of the best-fit equilibrium line (Fig 4.43), but this is consistent with a small temperature and/or compositional dependence on partitioning confirmed in experimental studies mentioned by Bacon and Hirschmann (1988).

Results of the Fe-Ti oxide estimates of temperature and oxygen fugacity are presented in Table 4.5 and Figure 4.44. Volcano-stratigraphic units represented are Ngauruhoe (Group 3A, TG289), Red Crater (pre-1.8 ka, TG134-135), North Crater

Figure 4.43 Mg/Mn (atomic) for 35 ilmenite-magnetite pairs in selected Tongariro lavas. Best fit equilibrium line (heavy solid line) is surrounded by error envelope of +/-2sd, as determined by Bacon & Hirschmann (1988).

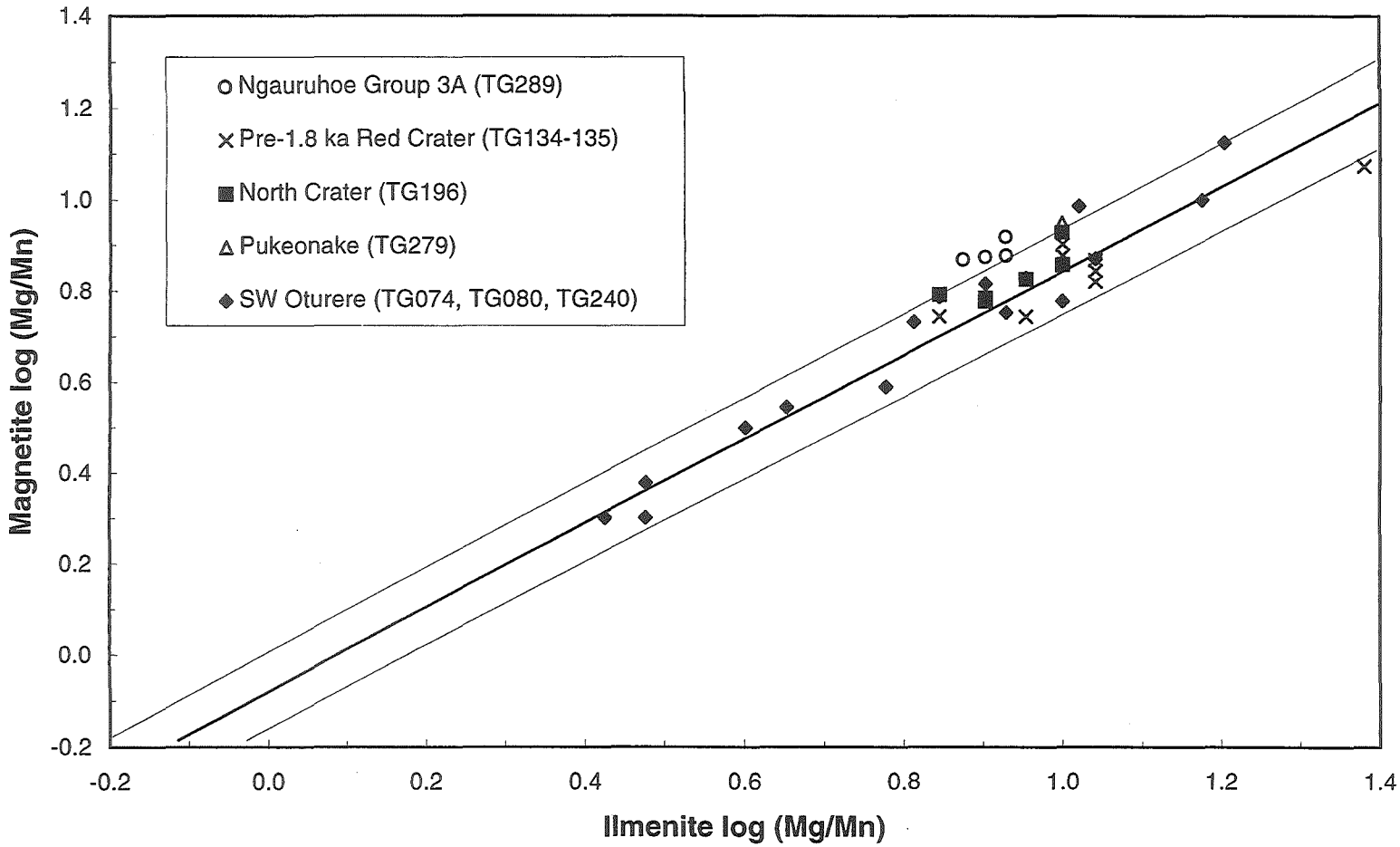

Table 4.5 Temperature (T) and oxygen fugacity (fO_2) calculations (using Anderson and Lindsley's [1988] geothermometer for coexisting Fe-Ti oxides) for selected Tongariro lavas. Pressure set at 2 kb for calculation. Errors quoted by Buddington & Lindsley (1964) are ±50°C and ±1 log unit fO_2. sd = standard deviation.

Unit	Sample	Ilmenite Analysis	Magnetite Analysis	T (°C) (Anderson & Lindsley, 1988)	$-\log_{10} fO_2$	Range T (°C) for sample	Mean (±2sd) T(°C) for sample
Ngauruhoe	**TG289**	1467N	1418N	820	12.9	820-862	846 ± 32
Group 3A	58.62 wt% SiO_2	1468N	1444N	862	12.0		
		1466M	1464C	844	12.5		
		1465M	1471M	856	12.1		
Red Crater	**TG134**	0294N	0286N	951	10.2	861-951	904 ± 53
Pre-1.8 ka	59.47 wt% SiO_2	0285N	0288C	911	10.7		
		0292R	0290R	907	10.8		
		0296C	0291C	881	11.1		
		0299C	0295C	861	11.6		
		0297C	0298C	920	10.5		
		0293C	0300N	899	10.9		
	TG135	0369C	0355C	885	11.1	885	
	60.94 wt% SiO_2						
North Crater	**TG196**	0504C	0487C	937	10.9	861-1116	945 ± 168
	59.20 wt% SiO_2	0494C	0488C	964	10.5		
		0498R	0490C	876	12.3		
		0497C	0501R	1116	8.5		
		0491C	0503C	916	11.3		
		0500R	0505C	861	12.5		
Pukeonake	**TG279**	1296C	1298C	1055	9.3	1055	
	56.99 wt% SiO_2						
SW Oturere	**TG074**	0777C	0775C	842	12.9	741-842	802 ± 87
	57.57 wt% SiO_2	0780C	0776C	822	13.6		
		0778C	0779C	741	15.5		
	TG080	1110C	1076C	860	12.2	846-918	879 ± 48
	59.78 wt% SiO_2	1114C	1077C	899	11.0		
		1106C	1079C	870	11.8		
		1109C	1089C	846	12.4		
		1111C	1112C	879	11.9		
		1115C	1116C	918	10.6		
	TG240	1184C	1151C	906	11.0	791-1175	910 ± 233
	57.81 wt% SiO_2	1191C	1180C	839	12.1		
		1188C	1181C	1175	8.0		
		1182C	1187C	934	10.6		
		1189C	1190C	852	11.8		
		1193C	1192C	791	13.4		
		1183C	1194C	873	11.3		

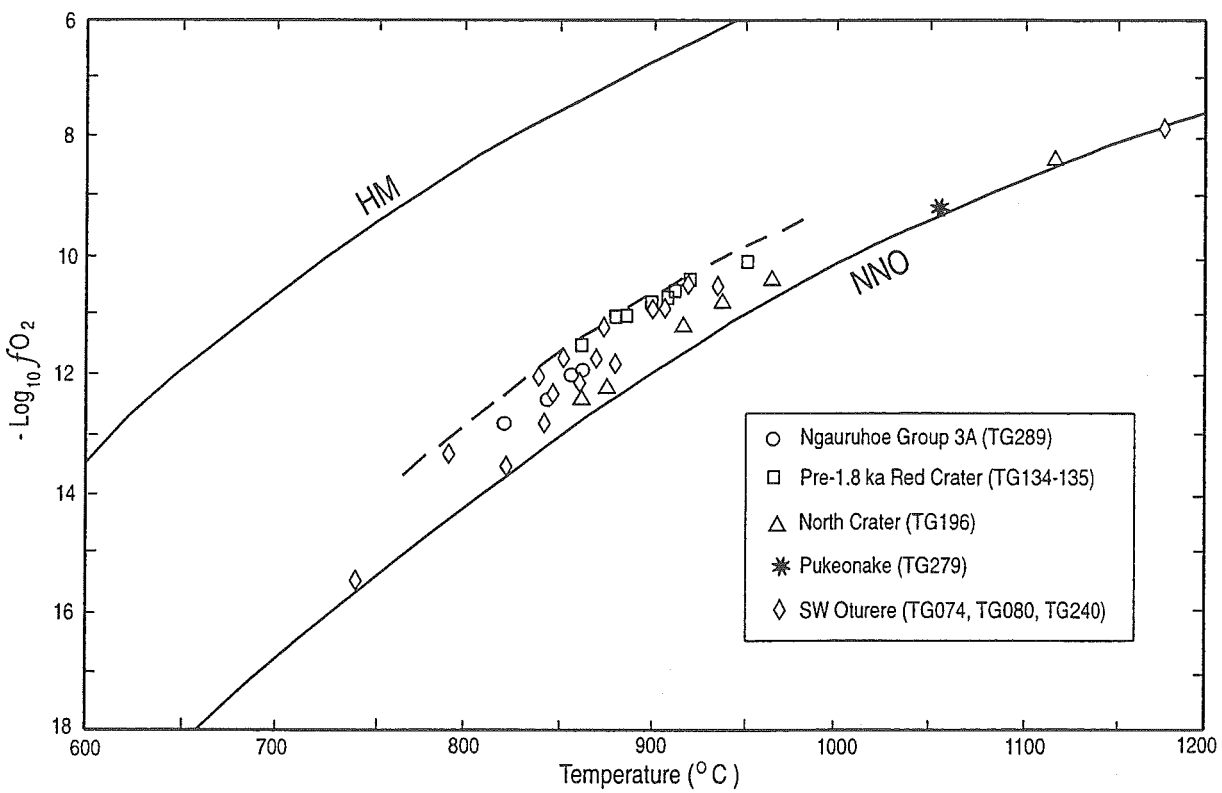

Figure 4.44 Plot of temperature and oxygen fugacity using coexisting Fe-Ti oxides (after Anderson and Lindsley, 1988) for selected Tongariro lavas. Errors quoted by Buddington and Lindsley (1964) are ±50°C and ±1 log unit fO_2. Dashed curve is the T-fO_2 trend defined by TG134-135 and TG240. Nickel-nickel oxide (NNO) buffer curve from Huebner and Sato (1970) and hematite-magnetite (HM) buffer curve from Carmichael et al. (1974).

(TG196), Pukeonake (TG279), and SW Oturere (TG074, TG080, TG240). All samples are 2-pyroxene (± olivine) andesite lavas (apart from the Pukeonake basaltic andesite) spanning a narrow SiO_2 range of 57.6 to 60.9 wt%. There is no systematic relationship between temperature estimates and the limited range of whole-rock SiO_2 contents. The overall temperature range calculated for these Tongariro lavas is 741 to 1175°C, but most of the oxide pairs yield temperatures between 840 and 950°C (Table 4.5; Fig 4.44).

Some of the samples yield a relatively restricted range of estimated temperatures (±30-50°C; e.g. TG080, TG134, TG289), whereas others cover a very wide temperature interval of up to 384°C (TG240, 791-1175°C) (Table 4.5). The very high temperature estimate from TG240 probably indicates magma mixing involving injection of more basic magma into the SW Oturere magma reservoir. This may also be the case for TG196, although the 255°C spread of estimated temperatures (861-1116°C) may instead indicate thermal stratification of the North Crater lava lake. The one Fe-Ti oxide temperature estimate from Pukeonake (TG279) is 1055°C and is likely to represent the high-temperature end-member of magma mixing (Section 4.4.8b).

In the T-fO_2 plot (Fig 4.44), Tongariro analyses lie on or up to 1 log unit above the Ni-NiO (NNO) buffer curve of Huebner and Sato (1970), coinciding with the typical fO_2 range of orogenic andesites in general (Gill, 1981; Frost and Lindsley, 1991). Data points for TG074, TG196 and TG279 lie on the NNO buffer curve, whereas TG134-135 and TG240 oxides form an array of points parallel to and offset about 1 log unit above the NNO buffer curve (dashed curve, Fig 4.44). TG289 oxides plot 0.5-1 log unit above the NNO buffer curve, and TG080 oxides define a trend with a steeper slope than the NNO buffer curve; these samples share a T-fO_2 trend similar to that for orthopyroxene-bearing silicic rocks (Carmichael, 1967). Coexisting oxides from hornblende-phyric Tongariro lavas have not been analysed, so no comparison can be made with Carmichael's (1967) T-fO_2 trend for amphibole-bearing rocks which is displaced to higher fO_2 values.

4.6.3 Total pressure

Quantitative estimation of total pressure during crystallization of Tongariro magmas is hampered by the lack of an appropriate geobarometer to apply to Tongariro mineral

assemblages. However, some trial thermodynamic calculations were carried out along the lines of Barton and Wyers (1991), although the results are subject to uncertainties stemming from the inherent assumptions of the thermodynamic approach (Frost and Lindsley, 1992). Using activity-composition relations between olivine, clinopyroxene and plagioclase, and standard-state thermochemical data (see Barton and Wyers, 1991, for details), total pressures in the range of 1-2 kb were calculated for TG289 (Ngauruhoe) and TG134 (Red Crater). Applying the α_{SiO2} of TG289 and TG134 to the petrogenetic grid of DePaolo (1979) yields pressure estimates of 4 kb and 2 kb respectively. Errors of ±1-2 kb for these two methods (Barton and Wyers, 1991) add further uncertainty to the results. More rigorous use of thermodynamic methods is really beyond the scope of this study.

The more general observation that pressures are likely to be low (<7 kb, and probably only a few kb) can be made from various mineralogical evidence. Tongariro pyroxene phenocrysts generally have low abundances of nonquadrilateral components (Section 4.5.3) which therefore preclude crystallization pressures >10 kb (cf. Green, 1972). The low Al^{VI} contents of amphiboles in TG136 (Al^{VI}=0.06-0.25 a.p.f.u.) and TG381 (Al^{VI}=0.05-0.30 a.p.f.u.) indicate crystallization within the crust (Helz, 1973; Allen et al., 1975; Allen and Boettcher, 1978, 1983; Rutherford et al., 1985). The relatively high and constant CaO contents of most Tongariro olivine phenocrysts implies low pressure crystallization, although Pukeonake olivines with CaO<0.1 wt% and >Fo_{90} may have a higher pressure origin (Stormer, 1973; Section 4.5.1).

Further support for low crystallization pressures in Tongariro magmas comes from limited seismic studies in the vicinity of Tongariro. Using patterns of anomalously high S-wave attenuation, Latter (1981) identified potential magma reservoirs beneath Ngauruhoe at about 2-3 km depth, and beneath Ruapehu at 2-9 km depth (Section 1.4.4). Based on similar methods, Latter and Ahmed (1992) postulated the existence of a magma reservoir beneath NW Tongariro at a depth of 4-9 km. These depths equate with pressures of about 1 to 3 kb. However, these seismically-identified magma reservoirs may only be very temporary shallow reservoirs rather than where the bulk of phenocryst crystallization occurred.

4.6.4 Water content

Similar problems to those of pressure estimation are encountered in estimating water contents for Tongariro magmas. Most lavas contain anhydrous mineral assemblages, and the ubiquity of plagioclase phenocrysts (indicating it is the liquidus phase) implies less than 2-5 wt% water is required in the melt (high water contents suppress plagioclase stability; Eggler, 1972; Eggler and Burnham, 1973; Gill, 1981). Most Tongariro magmas are probably hydrous to some extent, however, because of the relatively high anorthite contents of plagioclase (P_{H2O}>1 kb are required for plagioclase >An_{50} to crystallize at T<1100°C for andesitic magma; Gill, 1981). Hornblende-bearing lavas must have magma water contents of >4-5 wt% (e.g. Merzbacher and Eggler, 1984; Rutherford and Devine, 1988).

4.6.5 Discussion and summary of crystallization conditions

Estimates of magmatic intensive parameters are often difficult to obtain, but are vital in providing constraints on modelling the dynamics and evolution of magmatic plumbing systems. Estimated temperatures and pressures of crystallization can constrain geochemical models. Pressure and volatile contents also have obvious implications for depths of magma reservoirs, evolutionary paths of magmas, and understanding explosive volcanism. Quantification of the pre-eruptive conditions of Tongariro magmas provides an important contribution towards modelling the petrological and volcanological evolution of the complex. However, the limitations imposed by Tongariro mineral assemblages on choice of geothermometry, etc. methods, together with the non-representative subset of Tongariro samples analysed for mineral compositions, preclude a thorough and accurate quantification of Tongariro magmatic conditions.

Evidence of disequilibrium (related to magma mixing) in many Tongariro lavas requires caution when applying mineral thermometers to these lavas. Attempts have been made to assess equilibrium conditions (e.g. Mg/Mn partitioning in Fe-Ti oxide pairs) so that the results of geothermometry calculations can provide a useful guide to pre-eruptive temperatures of some Tongariro magmas. However, the limitations imposed by the available mineral data and presence of mineral assemblages appropriate for

geothermometry mean that the calculated temperatures are not representative of Tongariro lavas as a whole and therefore must remain as a guide only, pending further microprobe analysis of a broader range of Tongariro lavas.

As is often the case (Lindsley and Frost, 1992), temperatures calculated using two-pyroxene thermometry are generally spread over a higher and wider temperature range than those estimated from Fe-Ti oxide thermometry (e.g. TG134: 2-pyx T=900-1100°C; Fe-Ti ox T=861-951°C), beyond the ±50°C error on these two thermometers. It is possible that the lower temperatures given by the Fe-Ti oxide thermometer may be the result of cooling sufficiently slow enough for some unmixing to have occurred. Oxides are very prone to resetting so that the temperature and oxygen fugacity that they record may not reflect the conditions of the original magma reservoir (Lindsley and Frost, 1992).

In summary, the majority of Tongariro lavas assessed by geothermometry calculations appear to have crystallized at temperatures of 850-1100°C, oxygen fugacities on or up to 1 log unit above the NNO buffer curve, relatively low pressures of less than 7 kb (possibly only 1-3 kb), and water contents of up to 2-5 wt%. These crystallization conditions are typical of andesitic magmas in general (e.g. Gill, 1981; Frost and Lindsley, 1991; Johnson et al., 1994).

Pukeonake magmas equilibrated at higher temperatures (1000-1200°C) and possibly higher pressures than most other Tongariro magmas. Some magmas (e.g. TG240, TG381) yield very wide temperature ranges (300-500°C) or exhibit bimodal temperature estimates, which together with other evidence suggests magma mixing was a significant process in the evolution of these lavas. The hornblende-bearing lavas of Tongariro (particularly Tama 1 and Tama 2) represent higher magmatic water contents of at least 4-5 wt% H_2O. The low pressure estimates suggest that Tongariro magma reservoirs are typically located at relatively shallow crustal levels (<3 km depth), although some magmas may have experienced a polybaric evolution with magma stalled at mid-crustal levels (c.7 km).

4.7 PETROGRAPHIC AND MINERALOGICAL EVIDENCE FOR MAGMA MINGLING AND MIXING

Throughout this chapter, reference has been made to features of petrography and mineralogy suggestive of magma mixing. These features are now brought together and summarised. There are five lines of evidence in Tongariro lavas that, when considered together, demonstrate the importance of magma mixing processes in Tongariro petrogenesis. In addition, magma mixing is suggested by glomerocrysts with relatively abundant glass (which seem out of place in glass-poor host rocks); the nearly crystallized magma of more primitive (cognate) wallrock has mixed with the host rock magma (Section 4.3.2).

4.7.1 Compositional banding

Observable in the field and under the microscope, dark and light banding of TG293 from Tama 2 (Section 4.4.4, Fig 4.12) corresponds to mingling of two compositionally similar (Section 6.6.4) magmas just prior to eruption. Such compositional banding, however, is rare in Tongariro lavas. Some of the pumice collected from the Tama Lakes ejecta (Tn141a) has distinctive dark and light bands which may represent mixing of a small volume of basalt injected into a large volume of dacite (e.g. Kouchi and Sunagawa, 1985), or pre-eruptive mixing of layers in a compositionally-zoned magma reservoir (e.g. Giannetti and Luhr, 1983).

4.7.2 Sieve textures

Most Tongariro lavas (Fig 4.29) contain plagioclase phenocrysts which are riddled with minute glass inclusions - which along with inner resorption zones and rounded/mantled crystal shapes indicate major resorption events have occurred (Section 4.5.2, Figs 4.30-4.33). Although some of these sieve textures probably represent resorption due to just rapid decompression (Pearce et al., 1987; Nelson and Montana, 1992), other sieved crystals display pronounced compositional breaks and reversals between sieved and

unsieved zones and therefore are more likely to represent reaction textures created by magma mixing (Tsuchiyama, 1985). Less extreme compositional differences within many sieved crystals point to mixing of relatively similar magma compositions.

Sieve textures indicative of magma mixing are particularly prevalent in Pukeonake and Red Crater lavas (Sections 4.4.8b and 4.4.8i). Several lavas (TG182, TG293) also contain fractured plagioclase whose cracks are filled with glass more silicic than whole-rock compositions (Sections 4.4.4 and 4.4.6). Pyroxene phenocrysts are also occasionally sieved (e.g. in NE Oturere lavas, Section 4.4.3).

4.7.3 Reverse and patchy zoning

Strong reverse and/or patchy zoning occurs in many Tongariro phenocrysts, especially in sieved plagioclase crystals. Calcic overgrowth rims and calcic microlites are interpreted as responses to injections of more basic magma into the system, with core-rim variation of up to 25 mol % An (e.g. in lavas from Ngauruhoe Groups 3A & 3B, Pukeonake, Red Crater, NE Oturere, Tama 2; Sections 4.4 and 4.5.2). In some samples the phenocryst rims themselves span a wide compositional range (<20 mol % An; e.g. TG020, TG288) indicating that they cannot all have been in equilibrium with the host liquid prior to eruption. Patchy zoning is often closely associated with resorption surfaces and glass inclusions (Section 4.5.2). Once again a magma mixing origin best explains these features.

Moderate to strong reverse zoning also occurs in augite and orthopyroxene phenocrysts in a significant minority of samples from several units (Ngauruhoe Group 3A, Red Crater, Pukeonake, SW Oturere, NE Oturere). With core-rim variations of up to 20 mol % En (Section 4.5.3), these instances of reverse zoning are most likely to be related to magma mixing processes (e.g. Nixon, 1988a). Many hornblende phenocrysts also display moderate reverse zoning (Section 4.5.4) which could result from magma mixing (Sakuyama, 1979), although increased fO_2 may be the cause (Mason, 1978).

4.7.4 Disequilibrium mineral assemblages

Coexisting high-temperature and low-temperature phases in disequilibrium in the same lava provide further evidence of magma mixing. Resorbed xenocrystic quartz derived from a ?dacitic magma occurs in several basaltic andesite and andesite samples (Section 4.5.7) such as TG381 which also contains heterogeneous glass comprising patches of pale silicic and brown basic glass. The corroded crystal shapes and lack of protective clinopyroxene coronas suggest little impediment to dissolution; quartz residence times in basaltic melt may be as short as 12 hours (Donaldson, 1985) implying very short time intervals between magma mixing and eruption of these lavas. Disequilibrium is usually relatively subtle in Tongariro mineral assemblages, and more extreme assemblages such as albite + quartz + biotite + hornblende coexisting with An-rich plag + Mg-rich olivine+pyroxene are absent.

Disequilibrium between phenocrysts and their groundmass is also revealed by mineral chemistry. Lavas from Ngauruhoe, Red Crater and Pukeonake all contain more forsteritic olivine than expected from the whole-rock Mg# (Section 4.5.1). Resorbed orthopyroxenes are surrounded by euhedral Mg-rich augite rims in lavas from Red Crater, Ngauruhoe and NE Oturere (Section 4.5.3). These Mg-rich compositions are associated with the influx of high-temperature magma during a mixing event.

4.7.5 Disparate crystallization temperature estimates

Geothermometry calculations for some Tongariro lavas produced bimodal or very widely ranging crystallization temperature estimates (Section 4.6). Coexisting Fe-Ti oxides in SW Oturere sample TG240 mostly equilibrated at 865±46°C (Table 4.5), but one ilmenite-magnetite pair equilibrated at 1175°C and was therefore probably derived from a high-temperature magma influx. Ngauruhoe Group 3A and Tama 2 pyroxene analyses span temperature ranges of 700-1100°C and 600-1100°C respectively, suggesting mixing of low-temperature and high-temperature magmas.

4.7.6 Summary

Apart from determining the extent of magma mixing processes contributing to Tongariro petrogenesis, demonstration of equilibrium (or disequilibrium) is required for certain petrological calculations and modelling (e.g. geothermometry). It is apparent from the petrography and limited mineral chemistry that magma mixing does play a significant role in the Tongariro magmatic system, and therefore must be incorporated into models of magma reservoir dynamics and petrogenesis.

The nature of magma end-members prior to mixing often can be inferred from the resorbed cores of disequilibrium phenocrysts, whilst a record of the interaction between the different magmas is often exhibited by the phenocryst rims. Sieve textures, strong reverse and patchy zoning, and disequilibrium mineral assemblages occur together in some of the lavas from Ngauruhoe, Red Crater, Pukeonake, SW Oturere, Tama 2, and NE Oturere. Compositional banding and disequilibrium temperature estimates for some samples provide further evidence for magma mixing.

Similar petrographic characteristics have been used to demonstrate episodic replenishment and magma mixing in other calc-alkaline magma reservoirs (Sakuyama, 1978; Nixon and Pearce, 1987; Nixon, 1988a). However, unlike many of these studies of mixing between basalt and dacite magmas, Tongariro lavas often appear to result from mixing of less disparate (basaltic andesite - andesite) compositions.

4.8 PETROGRAPHIC TRENDS CORRELATED WITH STRATIGRAPHY: EXAMPLE FROM NE OTURERE

Detailed sampling of the thick stack of andesitic lavas and pyroclastics comprising subunit 'd' of the NE Oturere stratigraphic sequence (Appendix 2.16) provides an opportunity to investigate changes in mineralogy and geochemistry with time. This theme is also explored further in Sections 6.6.3c and 7.5.4. The four K-Ar age determinations available for subunit 'd' are all within error (ranging from 105±12 ka to 128±12 ka),

suggesting that this sequence was erupted over probably less than 10 ka. Subunit 'd' consists of over 200m of continuous stratigraphy (Fig 3.9; Section 3.5.3) which can essentially be divided into 3 packages: a lower sequence of lava flows, a middle sequence of scoria deposits with interbedded tuffs and lava flows, and an upper sequence of lava flows. These packages are separated by angular unconformities (Fig 3.10) which also signify certain petrographic differences. These relationships are summarised in Fig 4.45.

4.8.1 Lower sequence

The lowermost lava flow (TG114), separated from overlying lavas by a lahar deposit, has only weakly sieved plagioclase, less olivine, lower MgO, and higher SiO_2 contents than the lavas above (Fig 4.45). TG114 does, in fact, belong to a different chemical group than the rest of the eruptives in subunit 'd' (Section 6.6.3c). The five autobrecciated lava flows (TG115-119) erupted after deposition of the lahar all contain abundant olivine and clinopyroxene phenocrysts, and have much higher MgO and lower SiO_2 contents compared with TG114 (Fig 4.45). In particular, the first of these lavas (TG115) is a basaltic andesite with strongly sieved and resorbed plagioclase, clinopyroxene, and orthopyroxene indicative of a major magma mixing event. There is a sharp reversal in chemical trends from TG114 to TG115, after which TG116 to TG119 maintain relatively constant chemical compositions (Fig 4.45). As a whole, this lower package of lavas is also distinguished from the rest of subunit 'd' by a lack of vesicles, a lack of glomerocrysts (except TG114), and the relatively coarse grainsize of the groundmass crystals (Fig 4.45).

4.8.2 Middle sequence

A change in eruptive style is signalled by the thick scoria sequence which dominates the middle part of the stratigraphy of subunit 'd'. In contrast to the lower lavas, olivine is absent, plagioclase is much more abundant than pyroxene, and orthopyroxene is present in similar proportions to clinopyroxene (Fig 4.45). Phenocrysts often occur as glomerocrysts, unlike the lower section. The eruptives of this middle section are often strongly vesicular, with crypto- to microcrystalline groundmasses, some of which are glass-rich. There is a subtle change in chemical composition towards slightly higher SiO_2 and lower MgO

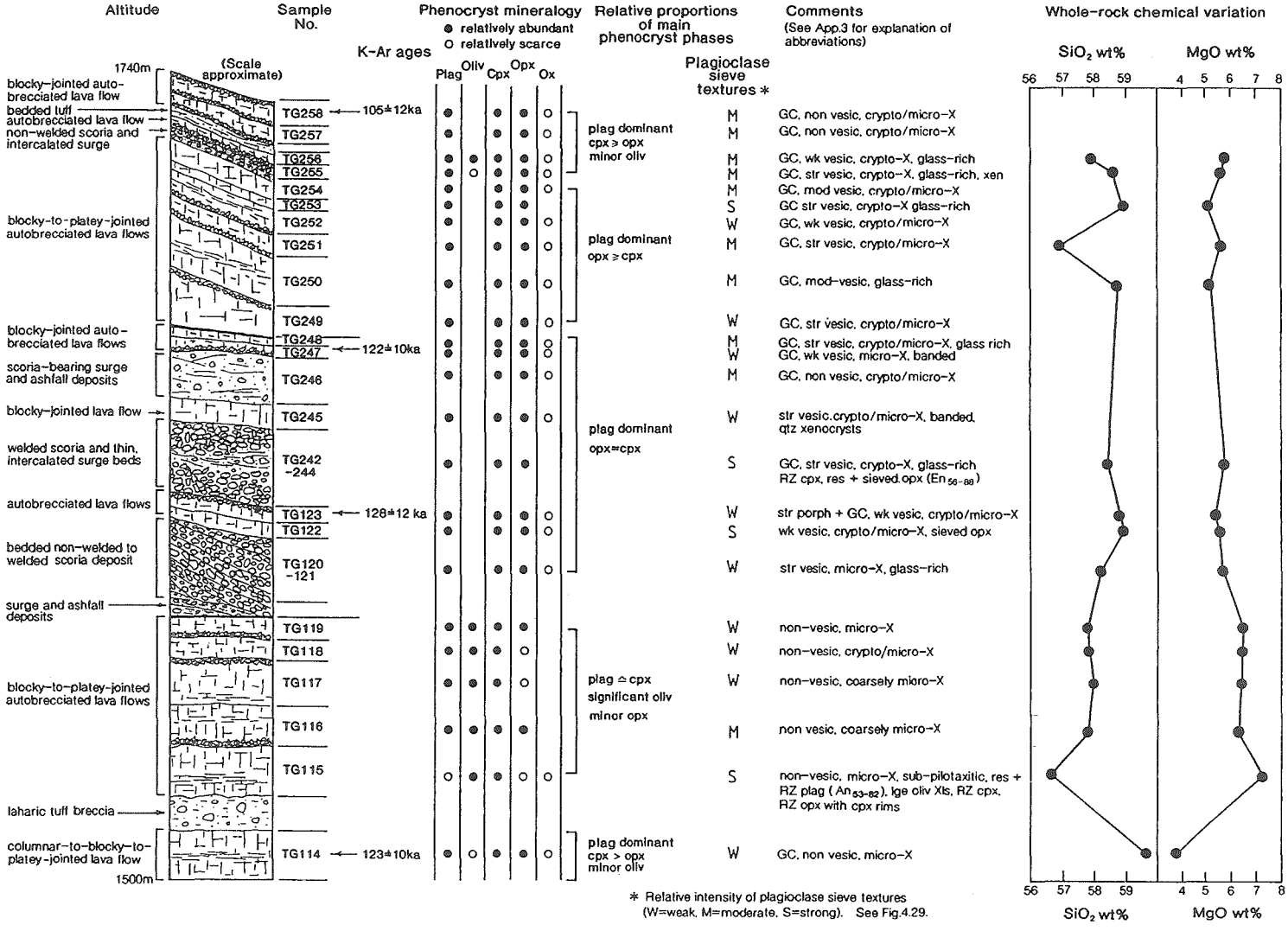

Figure 4.45 Stratigraphic column for NE Oturere subunit 'd' lava-pyroclastic section showing relationship of stratigraphy to phenocryst mineralogy, proportions, textures, and whole-rock MgO and SiO_2 contents. See text for discussion.

contents (Fig 4.45) which is suggestive of fractional crystallization, although lack of data in the upper part of the sequence prevents a clear picture of chemical variability. Magma mixing must have occurred during production of this middle sequence, as indicated by strongly sieved plagioclase and orthopyroxene, pronounced reverse zoning and wide compositional ranges of some phases, presence of disequilibrium quartz crystals, and compositional banding (Fig 4.45).

4.8.3 Upper sequence

The upper sequence of steeply-dipping autobrecciated lava flows (with two intercalated thin scoria and tuff units) have phase assemblages also dominated by plagioclase, but the orthopyroxene:clinopyroxene ratio decreases and olivine enters the crystallizing assemblage upsection (Fig 4.45). Glomeroporphyritic texture is prevalent, degree of vesicularity is highly variable, and groundmasses tend to be cryptocrystalline and often glass-rich (Fig 4.45). The relative intensity of sieve textures in plagioclase phenocryst populations is variable, but most are moderately sieved. Basaltic andesite lava TG251 imparts a pronounced break in the chemical trends (especially SiO_2), and was found to possess a quite distinctive chemical signature which sets it apart from the two main chemical groups of the NE Oturere eruptives (Section 6.6.3c).

4.8.4 Discussion

Although this stratigraphic section does not provide a complete characterisation of petrological changes with time, the sampling is adequate to at least highlight some major, and some more subtle, contrasts in mineralogy and whole-rock chemical composition. The variability cannot simply be explained by fractional crystallization processes alone. Variations in phenocryst mineralogy and abundances, grainsize, vesicularity, and other textures suggest that multiple batches of magma and differing ascent histories have played a part during the life of the NE Oturere magmatic system. Magma mixing has already been established as an important process occurring at NE Oturere (Sections 4.4.3, 4.7). More detailed characterisation of petrography and especially mineral compositions would allow firmer limitations to be placed on the timing and magnitude of the chemical cycles within

this NE Oturere sequence. Crustal xenoliths occur in only one unit (TG255 scoria), but the role of crustal assimilation can be more readily examined using precise trace element and isotopic means (Chapter 7).

In summary, dense olivine andesite and basaltic andesite lavas (TG114-119) characterised by one major compositional reversal were succeeded by plagioclase-dominant, olivine-free, alternating andesitic scoria and lava flow units (TG120-123, TG242-248) with ample petrographic evidence for at least one magma mixing event. These eruptives were in turn followed by a series of chemically variable, vesicular, glassy, olivine-bearing andesite to basaltic andesite lava flows (TG249-258) also characterised by an injection of basic magma. Although the available whole-rock chemical data indicate a relatively narrow compositional range for subunit 'd' (56.4-59.7 wt% SiO_2, 3.7-7.1 wt% MgO), subtle cyclical changes in magma petrography and chemistry occur up through the section, indicating periodic magma recharge and mixing over a relatively short period of time (<10 ka?).

4.9 SUMMARY

Throughout the growth of the Tongariro Volcanic Complex, eruptive products have been dominated by very porphyritic two-pyroxene andesites (and very minor dacites). Hornblende-pyroxene andesites were also erupted from the older southern cones (Tama 1, Tama 2, Pukekaikiore), whereas the young eruptives contain olivine-bearing basaltic andesites and andesites. Other petrographic and mineralogical differences between the volcano-stratigraphic units are relatively subtle, but are summarised as best as possible in Table 4.6.

Olivine (Fo_{67-92}; <2 modal %) typically occurs as resorbed microphenocrysts in almost a third of Tongariro lavas. Plagioclase phenocrysts (An_{45-90}; average 19 modal %) display complex zoning patterns, sieve textures, and resorption features, and single samples often contain wide core compositional ranges of 20-35 mol% An. Orthopyroxene ($Ca_{1-5}Mg_{55-86}Fe_{11-42}$; 1-10 modal %) is usually dominant over augite ($Ca_{35-46}Mg_{35-52}Fe_{7-24}$; 1-15

Table 4.6 Summary of petrographic and mineralogic characteristics and derived information for volcano-stratigraphic units of Tongariro Volcanic Complex. All information is discussed in the appropriate section(s) of Chapter 4 and/or is contained within Appendices 3-5. Tsch=tschermakite, ed=edenitic, hast=hastingsite, m.m.=magma mixing, other abbreviations as for Appendices 3 and 9. Phase proportions are modal % from point-counting or visual estimation. Mineral composition data (and hence estimates of crystallization conditions) were not available for all units. See Section 4.4.8j for information on South Crater.

	Relative phenocryst abundances and range in total phenocryst contents	PLAG	OPX	CPX	OLIV	HBL	OX	Other	Crystallization conditions	Degree of variation within unit	Notable features
Tama 1	hbl>plag>>opx≥ox 30-35 modal % phenocrysts	12-24% An_{52-89}, N oscil+patch Z wk sieved	1-6% En_{62-73}	0-5% augite $Ca_{41}Mg_{44}Fe_{15}$ (from Wahyudin,1993)		<18% pale-dark green ferri-tsch hbl or tsch ox±plag±px rim/psm altn	<3%		>4-5 wt% H_2O (presence of hbl)	hbl restricted to older flows	most hbl-rich Tong eruptives, v.str porph
NE Oturere	plag>>cpx≥opx±oliv±ox 12-40 modal % phenocrysts	6-30% An_{46-82}, N+R oscil+patch Z wk-str sieved	1-6% En_{55-86}, N+R sieved + embayed cpx rims	2-7% augite, N+R $Ca_{41}Mg_{38-52}Fe_{7-21}$	0-4% Fo_{72-87} often res, fr, rim altn		<1%	<1% (rarely <5%) fsp xen rare qtz xenocrysts	800-1200°C (pyx)	subunits similar or variable PC propns (Section 4.8)	strong petrographic evidence for magma mixing
Tama 2	plag>>cpx≥opx>hbl>ox±oliv±ap 26-42 modal % phenocrysts	16-28% An_{48-82}, N oscil+patch Z mod-str sieved	2-7% En_{63-69}	1-5% augite $Ca_{40-42}Mg_{40-42}Fe_{17-21}$	rare embayed crystals reaction rims	<7% red-brown Mg-hast or Mg-/tsch-/ed-hbl ox±plag±px rim/psm altn	<2%	<<1% red-brown apatite <1% (rarely <5%) fsp xen rare qtz xenocrysts	600-1100°C (pyx) >4-5 wt% H_2O (presence of hbl)	subunits similar, variable oliv	str hbl presence str evidence for m.m. str porph
Pukekaikiore	plag>>cpx≥opx>hbl>ox±oliv 27 modal % phenocrysts	20% An_{57-71} oscil+patch+sector Z mod-str sieved	3% En_{54-58} (from Patterson, 1986)	4% augite $Ca_{42}Mg_{37-47}Fe_{11-21}$ (from Patterson, 1986)	<2% Fo_{88} (from Patterson, 1986)	<1% severely res + psm	<1%	<2% fsp xen rare qtz xenocrysts	>4-5 wt% H_2O (presence of hbl)	hbl restricted to older flows	cpx>opx evidence for m.m.
SW Oturere	plag>>opx≥cpx>ox±oliv 24-41 modal % phenocrysts	17-31% An_{46-88}, N+R oscil+patch Z wk-mod sieved	2-6% En_{56-80}, N+R	1-8% augite $Ca_{39-43}Mg_{41-47}Fe_{10-20}$	<1% Fo_{70-84} res, pyx rim		<3%	<3% fsp xen	800-1100°C (pyx) 740-1175°C (ox) 8-15.5 $-\log_{10}fO_2$	subunits generally similar with slight PC propn variations	str evidence for m.m.
Tongariro Trig	plag>>opx≥cpx>ox±oliv 16-28 modal % phenocrysts	10-20% oscil+patch Z wk-mod sieved	2-5%	2-4%	<1% often res, reaction rims		<1%	<<<1% red-brown apatite <4% fsp xen		subunits similar, subtle variation in oliv+cpx propns	
Yg NE Oturere	plag>>opx>cpx>>ox <22 modal % phenocrysts	15% oscil Z, wk-mod sieved	4%	3%			<1%	<1% fsp xen		similar	
Pukeonake	plag≥cpx>opx>oliv>>ox 20-33 modal % phenocrysts	8-11% An_{50-74}, R oscil+patch Z mod sieved	4-5% En_{65-86}, R resorbed + sieved 2 crystal populations	6-15% augite, R $Ca_{34-42}Mg_{45-51}Fe_{8-21}$	2% Fo_{86-95} crsp inclusions opx rims		<<1%	Cr-spinel inclns in oliv	1000-1200°C (pyx) 1055°C (ox) 9.3 $-\log_{10}fO_2$	similar	high Fo (<95) oliv v.str evidence for m.m.
Blue Lake	plag>>opx>cpx>ox±oliv <30 modal % phenocrysts	19% wk-mod sieved	4-7% rarely corroded	3%	occur in glassy scoria		<1%	<1% fsp xen rare qtz xen		PC propns differ betw. scoria + lava	
North Crater	plag>opx≥cpx>ox±oliv 16-36 modal % phenocrysts	15-19% An_{58-80}, N+R patch Z mod-str sieved	6-10% En_{58-75}, N+R	3-4% augite, N+R $Ca_{41-42}Mg_{38-49}Fe_{9-22}$	<3% Fo_{69-82}, N pyx rims		<1%	<1% fsp xen rare qtz xen	800-1050°C (pyx) 860-1120°C (ox) 8.5-12.5 $-\log_{10}fO_2$	presence of oliv and Xlzn temps vary	rel. pyx+oliv-rich wide range Xlzn temps
Yg Pukekaikiore	cpx>oliv>opx 10-20 modal % phenocrysts		<2% En_{78-83} (from Patterson, 1986)	8-15% augite $Ca_{46}Mg_{52}Fe_7$ (from Patterson, 1986)	2-4% Fo_{80-82} some skeletal Xls		<<1%	<4% qtz xen		similar	lack plag PC oliv+augite-rich
Yg SW Oturere	aphyric (cpx±opx±plag±oliv) <2 modal % phenocrysts	(str sieved)						1% fsp xen		similar	
Te Mari Craters	plag>>opx≥cpx>ox±oliv 38 modal % phenocrysts	28%, oscil+patch Z mod sieved	6%	3%	rare		<1%	≤1% fsp xen		similar	
Tama Lakes	aphyric (plag+cpx) <4 modal % phenocrysts	12-14% An_{57-81} (from Wahyudin, 1993)	<1% En61 (from Wahyudin, 1993)	1-2% augite $Ca_{37-45}Mg_{45-48}Fe_{7-18}$ (from Wahyudin, 1993)	2-4% Fo_{64-84} (from Wahyudin, 1993)		1-6%	<2% hbl-plag lithics <4% qtz-fsp xen		contrast between BA-A bombs and banded pumice	hbl dacite lithics in BA-A bombs
Red Crater	plag>cpx>opx≥oliv±ox 27-37 modal % phenocrysts	13-21% An_{45-81}, N+R oscil+patch Z mod-str sieved	1-3% En_{58-76} cpx rims	7-10% augite, N+R $Ca_{43-45}Mg_{38-49}Fe_{7-18}$	1-7% Fo_{74-89} rare plag/pyx rims		<2%		900-1150°C (pyx) 861-951°C (ox) 10-11.5 $-\log_{10}fO_2$	post-1.8 ka subunit has more oliv + m.m. evidence	rel. oliv-rich str evidence for m.m.
Ngauruhoe	plag>>opx≥cpx±oliv±ox 23-37 modal % phenocrysts	15-24% An_{54-90}, N+R oscil+patch Z wk-str sieved	4-10% En_{61-76}, R	3-9% augite, N+R $Ca_{35-41}Mg_{39-50}Fe_{11-24}$	0-3% Fo_{67-91} pyx rims		<1%	rare crsp inclns in oliv 0-6% fsp and/or qtz xen rare qtz xenocrysts	700-1200°C (pyx) 820-862°C (ox) 12-13 $-\log_{10}fO_2$	subtle differences in oliv propns, cpx:opx and Xlzn temps	most contain oliv str evidence for m.m. qtz xen common

modal %), and both may be moderately to strongly zoned. Green or red-brown hornblende (mostly magnesio-hornblende to tschermakite; generally <5 modal %) is typically resorbed and rimmed or pseudomorphed by oxides ± plag ± pyx. Minor phases are dominated by magnetite, and also include ilmenite, chrome spinel, apatite, and quartz.

Crystallization conditions (deduced from mineralogy) for the majority of Tongariro lavas are: equilibration temperatures of 850-1100°C; oxygen fugacities on or up to 1 log unit above the NNO buffer curve; relatively low total pressures of <7 kb (possibly only 1-3 kb); and water contents of up to 2-5 wt% H_2O.

An important finding from this investigation of Tongariro petrography and mineralogy is the involvement of magma mixing (often between magmas of very similar composition) in the petrogenesis of many lavas, particularly those from Ngauruhoe, Red Crater, Pukeonake, SW Oturere, Tama 2 and NE Oturere. These lavas display a combination of features indicative of a magma mixing origin, including sieved plagioclase phenocrysts with major compositional breaks and reversals at resorption surfaces, strong reverse and patchy zoning, bimodal or very widely ranging crystallization temperature estimates, disequilibrium mineral assemblages, and compositional banding. At least three episodes of magma recharge and mixing have been identified in the NE Oturere subunit 'd' stratigraphic sequence, on the basis of variations in petrography and chemical composition over a period of approximately 10 ka.

Chapter 5

Xenoliths

CHAPTER 5
XENOLITHS

5.1 INTRODUCTION

Xenoliths are inclusions in magmatic rocks which may be either *cognate* or *accidental* (McBirney, 1989). Cognate xenoliths are those genetically related to their host magma, such as volcanic fragments from lava flows that predate but are from the same igneous complex as the host, or plutonic equivalents of the volcanic host (magma chamber cumulates). Accidental xenoliths bear no direct relationship to their host magma and may be wall rocks of older igneous, metamorphic, or sedimentary lithologies. Severe alteration often obscures the origin of accidental xenoliths.

Accidental xenoliths may be derived from all levels down to the source region of the magma. Mafic and ultramafic mantle and deep crustal xenoliths have not been sampled from the Tongariro Volcanic Complex, except for the satellite cone of Pukeonake. Hackett (1985) and Graham and Hackett (1987) describe peridotite xenoliths from Pukeonake basaltic andesite lava and scoria (see also Section 4.4.8b). Ultramafic xenoliths are rarely associated with volcanoes at convergent plate boundaries. Instead, assimilation of felsic materials at upper crustal levels is considered one of the main petrogenetic processes (Maury and Didier, 1991). However, occurrences of metasedimentary upper crustal xenoliths are not as well documented as those of mafic and ultramafic xenoliths. Perhaps this can be related to the overall worldwide predominance of mafic and ultramafic xenoliths, which Sachs and Stange (1993) attribute to the more efficient assimilation of felsic xenoliths by *ablation* (where xenolith melt is continuously removed by the viscous flow of the host magma, allowing new xenolith melt to be produced) compared with the

less effective *dissolution*-controlled assimilation experienced by mafic and ultramafic xenoliths.

Metasedimentary xenoliths are often extensively altered and melted, and as a consequence have received attention in studies of thermal metamorphism and melting processes (e.g. Sigurdsson, 1968; Maury et al., 1978; Graham et al., 1988). However identification of the original lithologies of metasedimentary xenoliths is not always based simply on textures and mineralogy, and instead is often inferred from knowledge of basement lithologies expected to underlie the volcano. This can lead to circular arguments as xenoliths are "matched up" to the preferred basement rocks. This approach may inhibit the inherent value of xenoliths in providing information on the sub-volcanic basement.

Tongariro lavas contain abundant xenoliths of two main types: cognate feldspathic xenoliths occur in lavas of all volcanic-stratigraphic units except Tama 1 (which has been inadequately sampled); accidental quartzose xenoliths are mainly confined to the young cones, especially Ngauruhoe historic lavas. Cognate volcanic xenoliths, inclusions of andesitic or dacitic lava, have been identified in a few samples. Xenoliths were not specifically sampled and most examples described below (and in Appendices 6 & 7) were incidental to lava collection. There is a sampling bias towards xenoliths from the Ngauruhoe 1975 pyroclastic avalanche deposit because of the abundance and accessibility of especially quartzose xenoliths in this unit. About half the thin sections examined contained at least one mm-sized feldspathic xenolith; these usually comprised up to 1% of the mode, but some lavas were relatively xenolith-rich and contained up to 6% of feldspathic xenoliths.

Because of the limited sampling this is not a truly representative study of Tongariro xenoliths. A more comprehensive study has been carried out on Ruapehu and Ngauruhoe xenoliths (Hackett, 1985; Graham, 1985a, 1987; Graham and Hackett, 1987; Graham et al., 1988, 1990) and it is interesting to compare those findings with this precursory survey of Tongariro xenoliths. Even though this investigation is of a preliminary nature, the following conclusions have been reached which are at odds with those of previous studies:

1. The feldspathic xenoliths common to most Tongariro lavas are interpreted as cognate to Tongariro magmas, and not related to gneissic basement as maintained by Graham (1987).

2. Petrographic features of the quartzite xenoliths, common especially in Ngauruhoe lavas, provide evidence for an origin as quartz veins rather than as quartzose segregations of gneissic sandstone as proposed by Graham (1985a, 1987).

5.2 PREVIOUS WORK

Early accounts of Tongariro geology contain mention of foreign inclusions in the lavas (Speight, 1908; Grange and Williamson, 1930). Battey (1949) noted the inclusion-rich nature of the Ngauruhoe 1949 lava and attributed a quartz-wollastonite xenolith to thermally metamorphosed Tertiary sandy limestone. Cloud (1951) reported abundant coarse-grained andesitic inclusions in the Ngauruhoe 1949 lava.

Tongariro xenoliths were first given serious attention by Steiner (1958) who described quartzose, feldspathic and vitrified xenoliths from Ngauruhoe 1954 lava. He. concluded that the xenoliths originated from an acid gneiss which underlies the greywacke basement beneath the volcano. Steiner (1958) advanced the hypothesis that fragments of quartzo-feldspathic gneiss engulfed by the Ngauruhoe magma had suffered thermal expansion and separated into quartz-rich and feldspar-rich relict bands. No xenoliths of Tertiary sediments, greywacke or rhyolite were recorded.

Clark (1960a) described cognate crystal aggregates, andesitic wall rock metamorphosed to basic hornfels, rhyolite fragments, and thermally altered quartzose xenoliths, but did not speculate on the origin of the latter. Subsequent publications dealing with Tongariro petrogenesis include only brief mention of xenoliths (Ewart and Stipp, 1968; Cole, 1978; Blattner and Reid, 1982; Cole et al., 1986) until the substantial contribution made by Graham and co-workers.

Based on the work of two PhD theses (Graham, 1985a; Hackett, 1985) the wide variety of xenoliths found in "Tongariro Volcanic Centre" (principally Ruapehu) were divided into seven main types (Graham, 1985a, 1987; Graham and Hackett, 1987; Graham et al., 1988, 1990):

1. *Igneous xenoliths* (Type IX) including near-surface volcanic inclusions (some hydrothermally altered), glomerocrysts, and cumulate nodules of dunite, harzburgite, pyroxenite, gabbro, and norite.
2. *Upper crustal xenoliths* (Type UCX) which have suffered only minor mineralogical and chemical modification including porcellanite derived from Tertiary calcareous siltstones near Ohakune, rare inclusions of metagreywacke similar to Torlesse suite lithologies, and two calc-silicate xenoliths thought to represent limestone within the Torlesse.
3. *Vitrified metagreywacke xenoliths* (Type VX) occurring only in Ngauruhoe 1954 and Pukeonake lavas, and represent Torlesse rocks which have undergone pyrometamorphism (Graham et al., 1988).
4. *Quartz-rich xenoliths* (Type QX) including rare garnet-bearing schists (QXa) and abundant metaquartzites (QXb). QXa are principally confined to one stratigraphic unit (Iwikau Member pyroclastics, Ruapehu), and are internally segregated into contrasting mineral assemblages: (1) qtz + calcic plag + cpx ± titanite ± ilm; and (2) sodic plag + garnet ± opx ± biotite ± rhyolitic glass (Graham, 1985a, 1987). The widespread QXb often comprise almost 100% quartz, but some contain minor anorthite + diopside ± wollastonite ± spinel (Graham, 1985a, 1987). Because the metaquartzites (QXb) contain minerals found in assemblage (1) of the schists (QXa), Graham (1985a, 1987) interpreted the metaquartzites to be quartzose segregations of the schist and suggested a common genesis for Types QXa and QXb as relict bands of quartzofeldspathic gneissic Torlesse basement (after Steiner, 1958).
5. *Feldspar-rich xenoliths* (Type FRX) including rare biotite schists (FRXa) and abundant pyroxene hornfels (FRXb). The metamorphic textures, relict foliations, and high pressure-temperature mineral assemblages of FRXb did not support an origin as cognate plagioclase cumulates. Instead, an origin linking FRX to gneissic basement was favoured. The pyroxene hornfelses (FRXb) were considered restites after extraction of melt from biotite schist (FRXa) (Graham, 1987).

6. *Spinel-rich xenoliths* (Type SRX) are uncommon but widespread and are thought to represent metamorphosed disaggregated micaceous layers of gneiss.
7. *Meta-igneous granulite xenoliths* (Type MIX) are relatively abundant and it has been proposed that they are fragments of altered oceanic crust and thus provide rare samples of the lower crustal basement beneath TVZ (Graham et al., 1990).

In summary, Graham and co-workers relate most of the metasedimentary xenoliths (Types VX, QX, FRX and SRX) to Torlesse terrane greywacke, regionally metamorphosed to gneiss near the base of the crust and/or contact metamorphosed during igneous activity. They use this evidence to infer that assimilation of rhyolitic melt - derived from partial melting of greywacke-gneiss - is involved in andesite petrogenesis in Tongariro Volcanic Centre (Graham and Hackett, 1987) and Taupo Volcanic Zone (Graham et al., 1992). Despite the wide variety of xenolith types described from Ruapehu and related vents, Graham (1985a) considered only a minority to be important crustal contaminants of the andesitic magma. Further details and a critique of these models will be given in Sections 5.5 and 5.6 where pertinent to interpretation of Tongariro xenoliths.

In addition, Donoghue (1991) used the presence of schist xenoliths within Mangamate Tephra and Pahoka Tephra as diagnostic of a Tongariro source. These xenoliths were thought to be equivalent to the low-grade metagreywacke xenoliths of Hackett (1985).

5.3 GLOMEROCRYSTS AND XENOCRYSTS

Apart from the cognate volcanic and feldspathic xenoliths, and accidental quartzose xenoliths (Sections 5.4 - 5.6), Tongariro lavas also contain glomerocrysts and rare xenocrysts.

Millimetre-sized clots or glomerocrysts of crystals the same size and mineralogy as the phenocrysts are common in Tongariro lavas (see Section 4.3.2) and in most andesites (Gill, 1981). These are mostly interpreted as phenocryst aggregates, but some could

represent cognate crystal cumulates detached from the sides, roof or floor of magma reservoirs. A clear distinction between glomeroporphyritic clusters and cognate xenoliths cannot easily be made, although the occurrence of glass exclusively within some glomerocrysts suggests a xenocrystic origin (Section 4.3.2). Because they are genetically related to the magma in which they occur and have not substantially altered its composition, glomerocrysts will not be considered further. However, note that cognate gabbroic xenoliths (20-30 cm in diameter) have been described from Ruapehu lavas (Graham, 1985a; Hackett, 1985). Gabbroic inclusions of this size were not observed in Tongariro lavas.

Xenocrysts are often difficult to distinguish from phenocrysts or phenocrysts undergoing reaction. Xenoliths which have undergone intergranular melting will be disaggregated into separate xenocrysts and dispersed in the magma. The only obvious occurrence of xenocrysts in Tongariro lavas are rare quartz crystals found in association with magma mixing (see Section 4.5.7 and Fig 4.11B).

5.4 VOLCANIC XENOLITHS

Pale grey hornblende-dacite volcanic xenoliths (<2 cm diameter; Fig 5.1) occur in andesite bombs (TG029-34, TG137) erupted from Tama Lakes, and were probably derived from the older Tama 1 cone lavas. A lava clast (TG513) from a welded fall deposit on Ngauruhoe contains mm-sized pale grey andesite xenoliths which contrast with the denser, darker grey groundmass of the host lava (Fig 5.2). The andesite xenoliths have sharp but irregular contacts with their hosts, and unmodified igneous textures with plagioclase and orthopyroxene phenocrysts in a crystalline groundmass.

Three less obvious examples of volcanic xenoliths, TG267A, TG530 and TG532, come from the Ngauruhoe 1975 pyroclastic avalanche deposit. TG267A is a 20x15 cm glassy, strongly vesicular, fine-grained feldspathic xenolith interpreted as a pumiceous inclusion. It has a relict volcanic texture with sparse phenocrysts of plagioclase and pyroxene, along with devitrified volcanic fragments (Fig 5.3). Most of the non-glassy

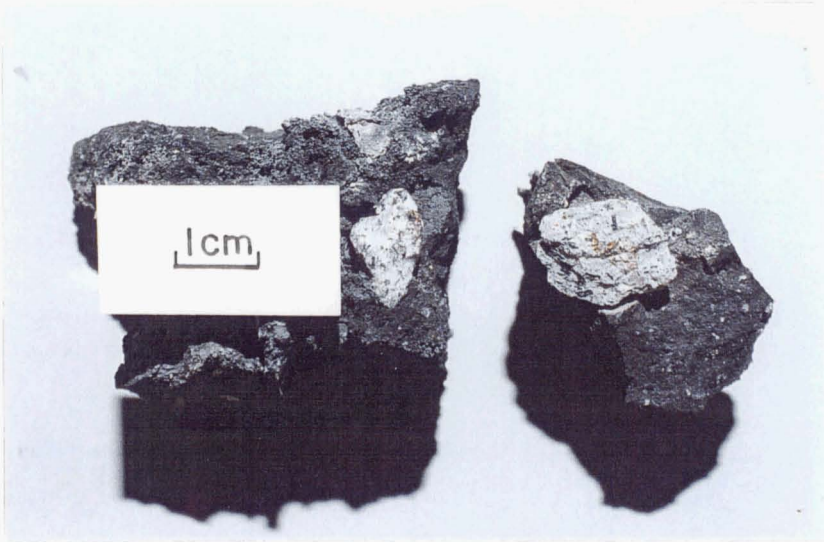

Figure 5.1 Hornblende-dacite cognate xenoliths in andesite bomb (TG030), Tama Lakes.

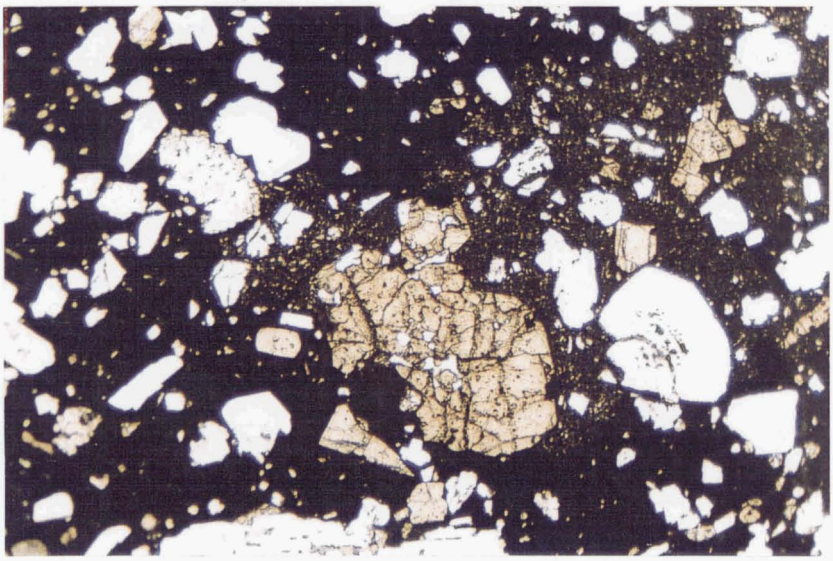

Figure 5.2 Inclusion of porphyritic andesite (with microcrystalline groundmass) contrasts with glassy groundmass of host andesite (TG513), Ngauruhoe welded fall deposit. View length measures 7.9 mm (cpl).

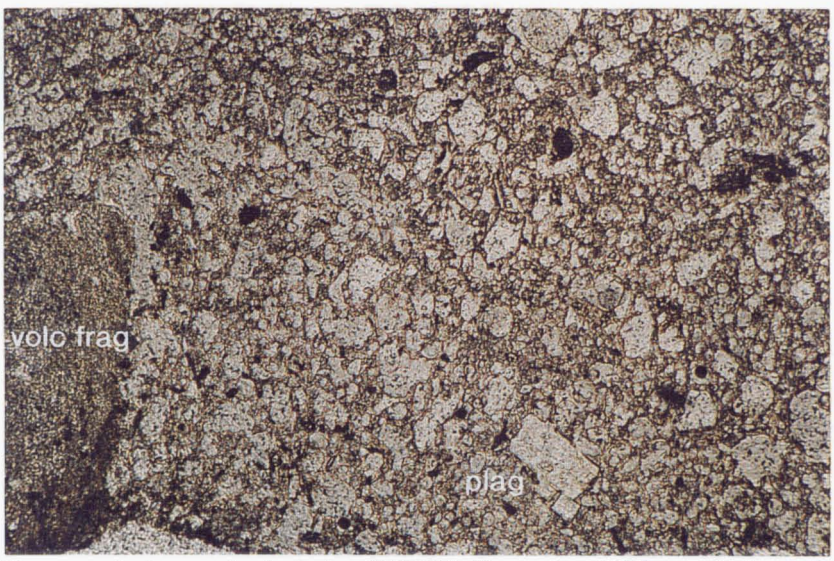

Figure 5.3 Glassy, vesicular pumice inclusion (TG267), Ngauruhoe 1975 pyroclastic avalanche deposit. Note relict plagioclase phenocrysts (plag) and devitrified volcanic fragment (volc frag). View length 3.2 mm (ppl).

portion of the rock is composed of poikilomosaic sanidine - a secondary feldspar which grew during either sanidinite facies contact metamorphism, or devitrification of some of the glass. Fine-grained to glassy silicic-intermediate igneous rocks are easily recrystallized to quartz/feldspar aggregates, with phenocrysts pseudomorphed by secondary minerals (Spry, 1969). The presence of two glass compositions in thin section, together with weak banding observed in hand specimen, suggests that magma mingling may have occurred within the pumice. A distinctive band of andesite within the pumice xenolith probably represents injection of the host magma into the xenolith. The xenolith also contains several quartzite xenoliths with clinopyroxene-glass reaction coronas.

A chemical analysis from part of the xenolith sample (TG267B; Appendix 7) has high SiO_2 (63.9 wt%) and high CaO (21.6 wt%) which suggests a wollastonite quartzite mineralogy similar to TG269. The relationship between the feldspathic thin section (sample TG267A) and the calc-silicate chemical analysis (TG267B) is somewhat obscure. A possible explanation for the discrepancy could be that TG267A is from the margin of the quartzite xenolith and represents mingling of xenolith and host melt in a vesicular boundary zone (cf. TG531, Section 5.6.3). This would then account for the contrasting glass compositions and the presence of quartzite fragments within TG267A.

TG530 (30x20 cm) is a cordierite-bearing, micro- to cryptocrystalline rock (Fig 5.4) with relict igneous textures such as subhedral feldspar phenocrysts pseudomorphed by cordierite. Petrographic determination of the groundmass was difficult due to its fine-grained to amorphous nature, but XRD analysis revealed anorthite, tridymite, sillimanite and cordierite. These minerals are consistent with an origin as high-grade, thermally metamorphosed clay and carbonate rocks. TG530 was probably once a hydrothermally altered volcanic fragment, with cordierite and calc-silicates having replaced the clay-carbonate mixture during contact metamorphism.

TG532 (5x3 cm) is a finely banded, devitrified feldspathic xenolith (Fig 5.5) which represents a fragment of a flow-banded volcanic rock. Two distinct feldspathic layers (<1 cm wide) of fine-grained anhedral plagioclase and Fe-Ti oxides (devitrification products) are surrounded by vesicular glassy andesite. Aligned subhedral tabular plagioclase crystals define planes of flow-banding.

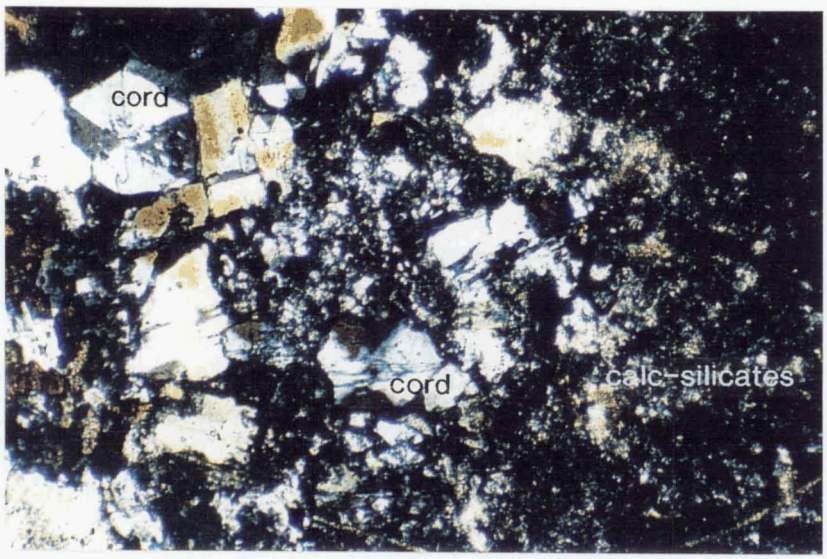

Figure 5.4 Sector-twinned cordierite (cord) and calc-silicates replacing hydrothermally altered volcanic fragment (TG530), Ngauruhoe 1975 pyroclastic avalanche deposit. View length measures 2.6 mm (cpl).

Figure 5.5 Flow-banded, devitrified volcanic xenolith (TG532), Ngauruhoe 1975 pyroclastic avalanche deposit. **A**-hand specimen; **B**-photomicrograph, view length measures 6.3 mm (cpl).

Volcanic-derived cognate xenoliths may exist in other pyroclastic deposits on Tongariro, but have not been observed in samples collected for this study. If the xenoliths are very similar in colour, texture and composition to the host lava they may be easily overlooked. Graham (1985a) describes volcanic xenoliths incorporated in Ruapehu lava flows which have mineralogy and whole-rock chemistry indicative of a common origin with their host magma. Thus assimilation of volcanic xenoliths is not expected to have a significant influence on andesite petrogenesis.

5.5 FELDSPATHIC XENOLITHS

5.5.1 Petrography

A selection of representative feldspathic xenoliths is described in Appendix 6. Cognate feldspathic xenoliths are ubiquitous in Tongariro lavas, although their grey colour makes them less noticeable in the grey-black andesitic host rock than the white quartzose xenoliths (Fig 5.6). The feldspathic xenoliths are generally very small (<1 mm, rarely <10 cm) and therefore unsuitable for whole-rock chemical analysis. Xenolith shapes range from subrounded to subangular, and equant to elongate to irregular.

The xenoliths are composed typically of 90-100% plagioclase and 0-10% orthopyroxene ± Fe-Ti oxides ± glass in a subhedral-equigranular, fine-grained (0.01-0.2 mm) texture (Fig 5.7). Rarely, xenoliths contain coarser-grained (<1 mm) irregular bands (e.g. TG081, TG282A; Fig 5.8).

Plagioclase crystals are euhedral-subhedral, stubby tabular to square, and sometimes twinned and/or zoned. Some crystals contain fine glass inclusions (possibly due to decompression melting) and Fe-Ti oxide inclusions. Anhedral-subhedral orthopyroxene and rarely clinopyroxene occur interstitial to the plagioclase. Fe-Ti oxide crystals are subhedral with square cross-sections, or are anhedral granules. Ovoid patches of densely crowded

Figure 5.6 Small inconspicuous cognate feldspathic xenoliths (indicated by arrows) within Ngauruhoe 1949 basaltic andesite (TG019). Note the more obvious white quartzite xenolith.

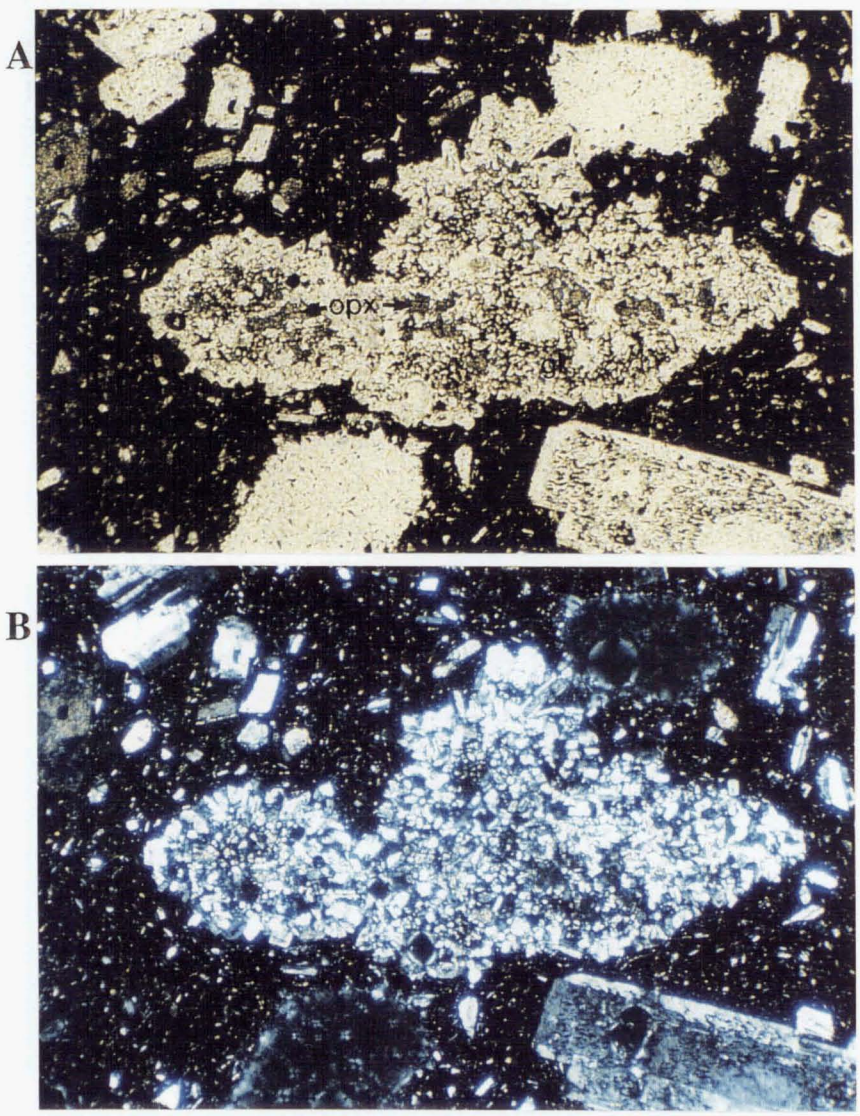

Figure 5.7 Fine-grained cognate feldspathic xenolith with plagioclase and orthopyroxene (opx) set in brown glass (gl). Ngauruhoe 1870 basaltic andesite (TG001). View length measures 2.6 mm (**A**-ppl; **B**-cpl).

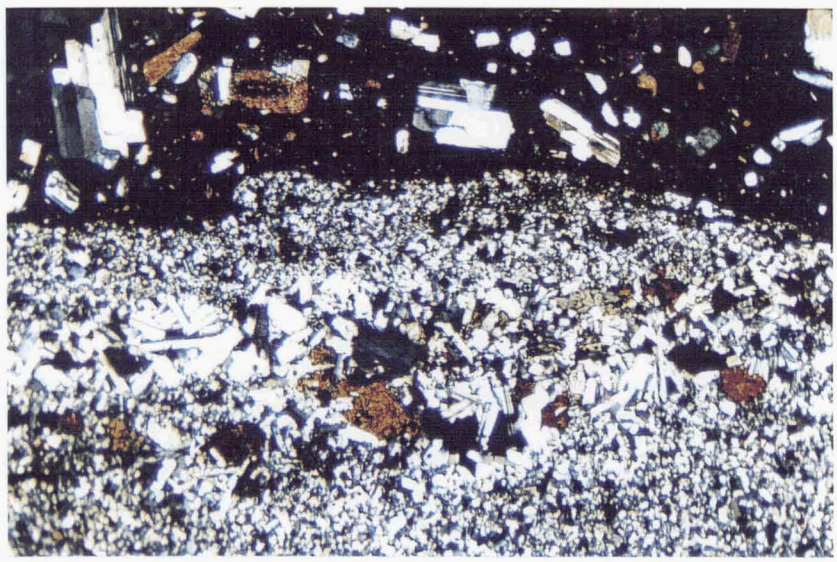

Figure 5.8 Relatively coarse band within fine-grained feldspathic xenolith (TG282A), c.1500AD lava flow, Upper Te Mari Crater. View length measures 7.9 mm (cpl).

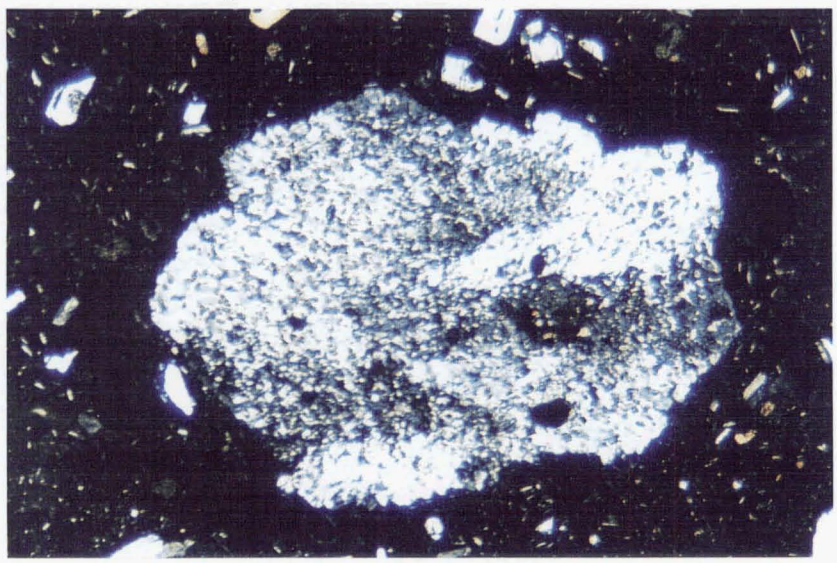

Figure 5.9 Recrystallized feldspathic xenolith, Ngauruhoe basaltic andesite (TG002). View length 5 mm(cpl).

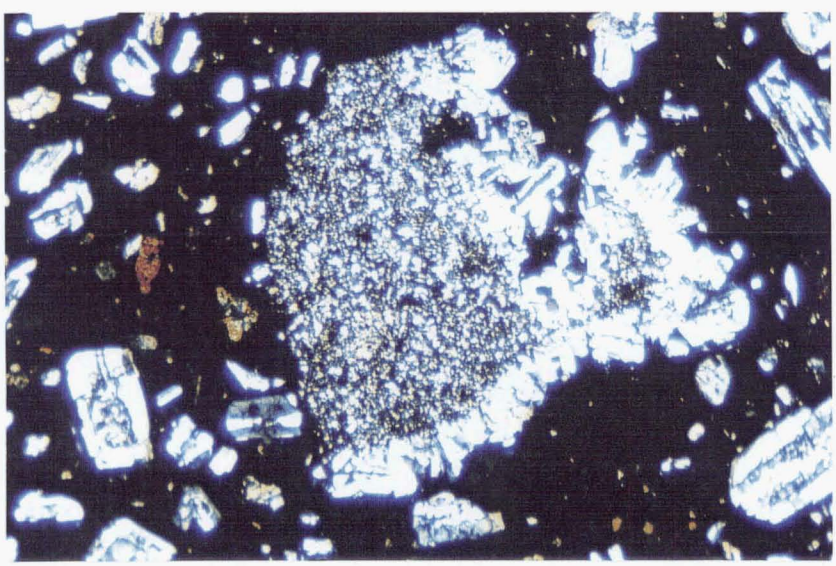

Figure 5.10 Nucleation of phenocrysts on feldspathic xenolith, Tama 2 andesitic lava flow (TG287). View length measures 6.3 mm (cpl).

granular/vermicular Fe-Ti oxides occur in the centre of some xenoliths and may represent the breakdown product of an Fe-rich mineral such as orthopyroxene. One xenolith (TG081) contains several large (<3 mm) poikiloblastic sanidines, which have probably grown during thermal metamorphism of the entrained xenolith. Medium to dark brown glass (sometimes partly devitrified) often occurs interstitially and completely surrounds some crystals (Fig 5.7). TG010 contains larger (0.1-0.3 mm wide) patches and streaks of glass.

Some feldspathic xenoliths (e.g. TG008) have a more recrystallized appearance than those described above. There is a gradation between xenoliths of euhedral-subhedral plagioclase set in glass (typical of primary igneous crystallization), and those of anhedral plagioclase with irregular serrated grain boundaries which lack interstitial glass. These recrystallized feldspathic xenoliths can be termed pyroxene hornfels as they have experienced thermal metamorphism in the hot near-magmatic environment.

Rare xenoliths show evidence of extensive recrystallization. TG002 contains a 4.0x2.5 mm feldspathic xenolith composed of fine-grained anhedral plagioclase (and sparse orthopyroxene and Fe-Ti oxides) which is optically continuous in large patches or sectors (Fig 5.9). It is not clear whether this xenolith represents recrystallization of one large crystal or several intergrown crystals. TG022 contains a 3x2 mm coarse feldspathic xenolith which is partly recrystallized to finer, anhedral grains.

5.5.2 Xenolith-host lava contact

Feldspathic xenoliths show no reaction with the enclosing magma and appear to be in chemical equilibrium with the host composition. Xenolith margins are typically irregular and often have subhedral-euhedral plagioclase crystals protruding into the host groundmass (Fig 5.7).

TG287 contains a fine-grained (0.02-0.1 mm) feldspathic xenolith (4.0x3.5 mm) which is partly surrounded by a fringing rim of coarser-grained (<0.5 mm) tabular plagioclase crystals of similar appearance to the host phenocrysts (Fig. 5.10). The long

dimensions of the fringing crystals are perpendicular to the xenolith margin. This coarse rim represents phenocrysts which have nucleated and grown on the relatively cold xenolith.

5.5.3 Origin of feldspathic xenoliths

The feldspathic xenoliths described above are interpreted as cognate coarse-grained equivalents of the host groundmass, thermally metamorphosed to varying degrees. They are thought to represent hypabyssal crystallization from the melt at the margins of relatively narrow magma conduits. Flowage differentiation, when phenocrysts are concentrated towards the centre of liquid flowing in a conduit, renders the conduit margins devoid of phenocrysts. Multiple magma conduits are likely, and hence most conduit margins may be adjacent to relatively warm igneous rock rather than cold wallrock (which would give rise to chilled margins). This moderately slow, in situ crystallization (with no fractionation) would be expected to produce xenoliths of the same composition as aphyric lavas or groundmass. Unfortunately no chemical analyses are available for the feldspathic xenoliths. However the xenolith mineral assemblage of plag + opx + Fe-Ti oxides is identical to that of most Tongariro groundmasses. Thus the presence of these feldspathic xenoliths has little effect on magma compositions, unlike the more dramatic effect of contamination by quartzose xenoliths (Section 5.6). The rare banding and variation in grain size exhibited by a few feldspathic xenoliths could be expected at the margins of magma conduits.

Graham (1987) describes abundant and widespread pyroxene hornfels xenoliths in Ruapehu lavas. These have essentially the same mineralogy as the feldspathic xenoliths described here, but layering of orthopyroxene + Fe-Ti oxides with plagioclase is common (unlike the Tongariro xenoliths) and interpreted as relict metamorphic foliation (Graham, 1987). The occurrence of almandine garnet and cordierite in just one sample was used as evidence of high pressure-temperature conditions. Graham (1987) cited metamorphic textures, high pressure-temperature mineral assemblages, and elevated $^{87}Sr/^{86}Sr$ compositions as supportive of an origin linking the pyroxene hornfels xenoliths to gneissic Torlesse basement, rather than fine-grained plagioclase cumulates.

I believe that Graham (1987) presents insufficient evidence for a deep-seated metasedimentary origin. Graham (1987) could have misinterpreted the banding (as observed in Tongariro xenoliths) as metamorphic layering. Almandine garnet and cordierite can form during contact metamorphism so it is not necessary to invoke a high pressure gneissic origin. The xenolith $^{87}Sr/^{86}Sr$ compositions of 0.70570, 0.70702 and 0.70800 quoted by Graham (1987) are not notably higher than the Tongariro isotopic range (0.704442-0.706193; Section 7.4.1). Petrographic observations of this study lead to the interpretation of the feldspathic xenoliths as representing cognate, hypabyssal crystallization of melt at the margins of narrow magma conduits.

5.6 QUARTZITE XENOLITHS

5.6.1 Petrography

A variety of quartzose xenoliths, mostly from historic Ngauruhoe lavas, are described in Appendix 6. They range from small (2-5 mm) subangular to subrounded inclusions within andesite, to larger (2-8 cm) intact xenoliths (Figs 5.11, 5.12) - often easily separated from the host lava - which were individually thin sectioned. Much larger, boulder-sized, xenoliths (<1 m diameter) were described from the Ngauruhoe 1954 lava flows by Steiner (1958). The medium- to coarse-grained white quartzite xenoliths are the most conspicuous type, providing a marked contrast with their dark grey to black andesite host (Fig 5.11).

(a) Quartz. Xenoliths are typically composed of 60-100% quartz. A whole-rock chemical analysis of quartzite xenolith TG273B (Appendix 7) is dominated by almost 90 wt% SiO_2, illustrating the very simple chemical composition of these xenoliths. Grain sizes range from 0.1 to 4.0 mm (average c.0.5-1.0 mm). The texture is typically a granoblastic mosaic; equidimensional quartz with straight grain boundaries meeting at triple-point junctions (Fig 5.13). This coarse-grained mosaic texture is characteristic of high temperature annealing (static recrystallization) during contact metamorphism. Less

Figure 5.11 Quartzite xenoliths in Ngauruhoe 1975 pyroclastic avalanche deposit and Ngauruhoe 1954 lava.

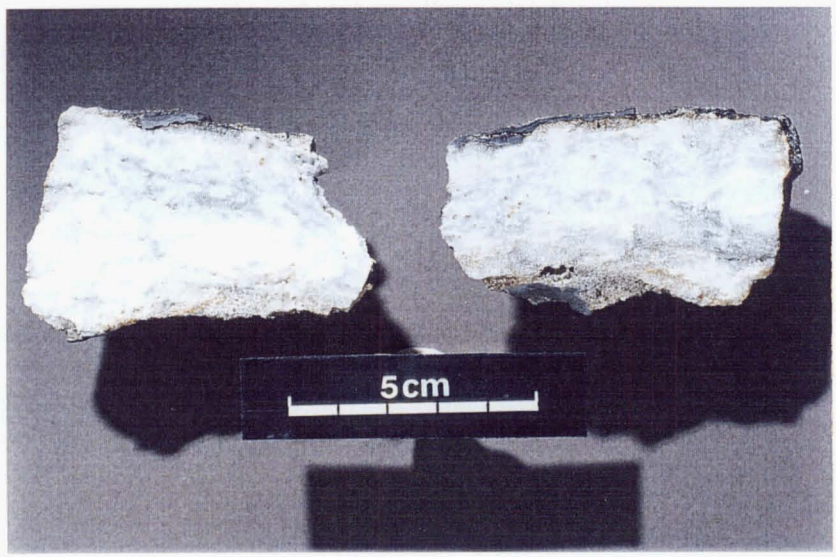

Figure 5.12 Quartzite xenolith from Ngauruhoe 1975 pyroclastic avalanche deposit (TG269). Note pale green-grey bands and patches of calc-silicate minerals.

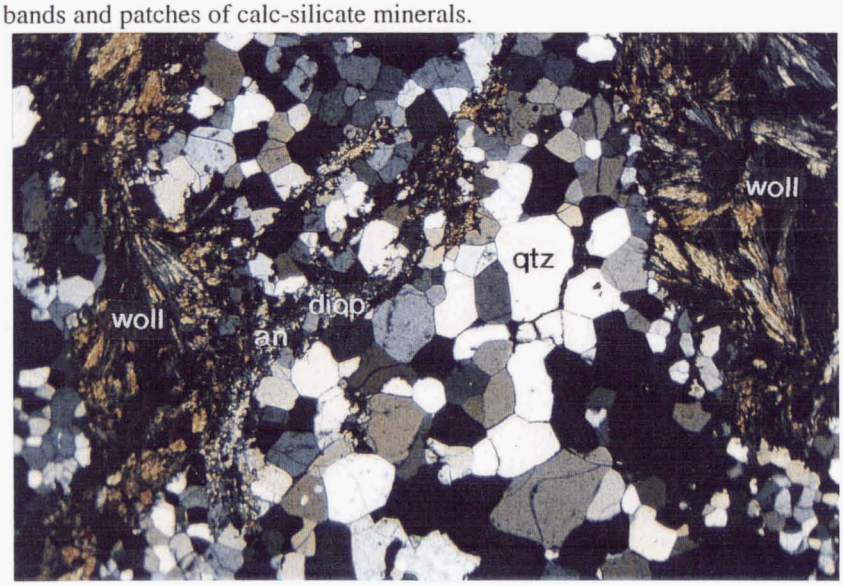

Figure 5.13 Quartzite xenolith (TG269) composed of granoblastic quartz mosaics (qtz) and irregular bands and patches of fibrous wollastonite (woll), anorthite (an), and diopside (diop). View length 7.9 mm (cpl).

common are slightly elongate quartz grains with serrated grain boundaries, indicating an incomplete grain boundary migration. Some grains display weak undulose extinction. Quartz grains in TG271 contain small negative crystals and low refractive index fluid inclusions; these probably grew in the presence of hydrothermal fluid (H_2O, CO_2?).

(b) Calc-silicates. In addition to ubiquitous quartz, many of the xenoliths contain 5-40% calc-silicates: wollastonite, anorthite, and minor diopside. These comprise a stable assemblage typical of thermally metamorphosed calcareous minerals. The calc-silicates are concentrated together in irregular patches or bands (0.5-10 mm thick) between quartz mosaics (Fig 5.13), and as thin irregular bands or trails (generally 0.05-0.2 mm thick) within the quartz. These thin bands often cross-cut the dominant banding, and are overgrown by larger quartz grains in places (Figs 5.13 - 5.15). Wollastonite crystals are euhedral-subhedral tabular (0.2-3.5mm long) and fibrous (0.2-2.5 mm long), with the characteristic position of the OAP across the cleavages. Anorthite crystals are small (<0.2 mm), anhedral, high relief, and sometimes twinned. Colourless to pale green clinopyroxene, probably diopside, occurs as small anhedral grains (generally <0.6 mm, but rarely <2 mm). The very high Ca content of quartzite xenolith TG269 (23.9 wt% CaO; Appendix 7) is consistent with its wollastonite-rich nature.

(c) Sanidine. One of the quartzite xenoliths examined, TG021A, contains about 30% sanidine with lesser (10%) calc-silicates. The anhedral, low relief sanidine crystals are generally <0.5 mm, but some are much larger (<3 mm) poikiloblasts (Fig 5.16). Sanidine is a characteristic phase of the sanidinite facies of contact metamorphism, indicating very high temperatures (>c.800°C) at very low pressures (<c.2 kbar).

The development of mesoperthite texture in some sanidine grains (Fig 5.16) appears unusual for a rock in such a high temperature volcanic environment. Although exsolution in feldspars of intermediate composition almost always takes place in the volcanic situation, it yields typically a cryptoperthite texture which is invisible under the microscope (Brown and Parsons, 1993). Mesoperthites require a period of slower cooling to develop. Hence this quartzite must have been temporarily removed from the hot environment after initial heating in the sanidinite facies, in order for the newly grown sanidine to microscopically exsolve. A possible scenario is as follows: wall rock of the magma conduit is thermally metamorphosed and sanidine grows; magma flow temporarily wanes or is diverted into

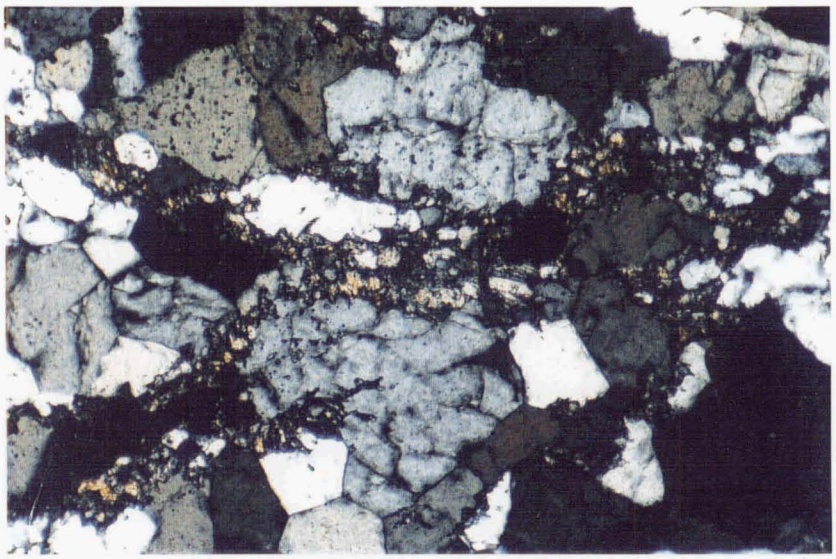

Figure 5.14 Detail of quartzite xenolith (TG271) showing thin, irregular bands of calc-silicates which are overgrown by larger quartz grains in places. View length measures 2 mm (cpl).

Figure 5.15 Thin irregular cross-cutting calc-silicate bands in quartzite (TG271). View length 7.9 mm (ppl).

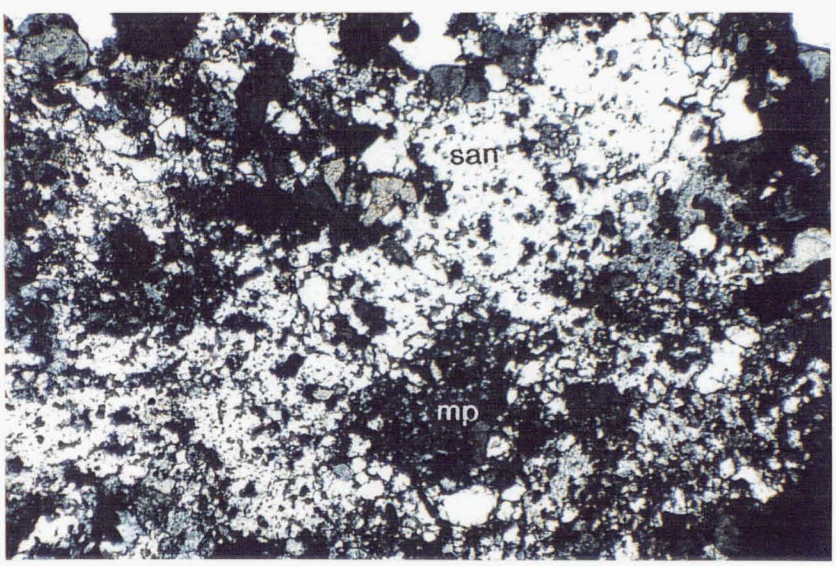

Figure 5.16 Large poikiloblastic sanidine grain (san) and smaller mesoperthite sanidine grain (mp) within quartzite xenolith (TG021A). View length measures 3.2 mm (cpl).

another conduit, allowing wall rock to cool and mesoperthite texture to develop; magma flow is re-established and wall rock fragments are incorporated as xenoliths prior to eruption. The development of the mesoperthite texture would have to take place very near to the surface (i.e. very low pressure), otherwise at deeper levels the feldspars would completely exsolve and be separate (and in any case, intermediate alkali-feldspar does not exist at high pressures).

5.6.2 Partial melting of xenoliths

Colourless glass commonly occurs along quartz grain boundaries (Fig 5.17), especially in triangular gaps between crystals, and in places the grains are "floating" in patches of glass. This provides evidence of partial melting within the xenolith, which is also supported by the "sugary" or granular texture of many quartzite xenoliths in hand specimen - suggesting loss of an intrinsic part of their structure. This felsic partial melt could infiltrate the host magma and, by virtue of its contrasting composition, could contaminate and alter the host magma composition. Intergranular melting is a powerful mechanism for disaggregating xenoliths, ultimately into separate xenocrysts, which are dispersed throughout the enclosing magma and are more rapidly assimilated than a larger intact xenolith. This important petrogenetic process of crustal assimilation is discussed in Section 8.5. Note that although pure quartz has a high melting temperature (1170°C at P_{H2O}=1 kbar), only small amounts of feldspar are necessary to depress the melting point to allow quartz to melt at temperatures of around 700-800°C at P_{H2O}=1 kbar (Tuttle and Bowen, 1958).

Contact metamorphism under the high temperature conditions of the sanidinite facies can readily melt xenoliths entrained in basic magma (a process also known as pyrometamorphism). Many of the Tongariro quartzite xenoliths which only have thin rims of melt at grain boundaries must have been heated and partially melted very near to the surface, and then erupted soon after to prevent further melting and actual disintegration of the xenoliths. Extensive melting produces highly vitrified xenoliths known as buchites. TG534 is one such example (Figs 5.18-5.20): colourless, vesicular glass containing small euhedral orthopyroxene and opaque minerals surrounds discontinuous bands and

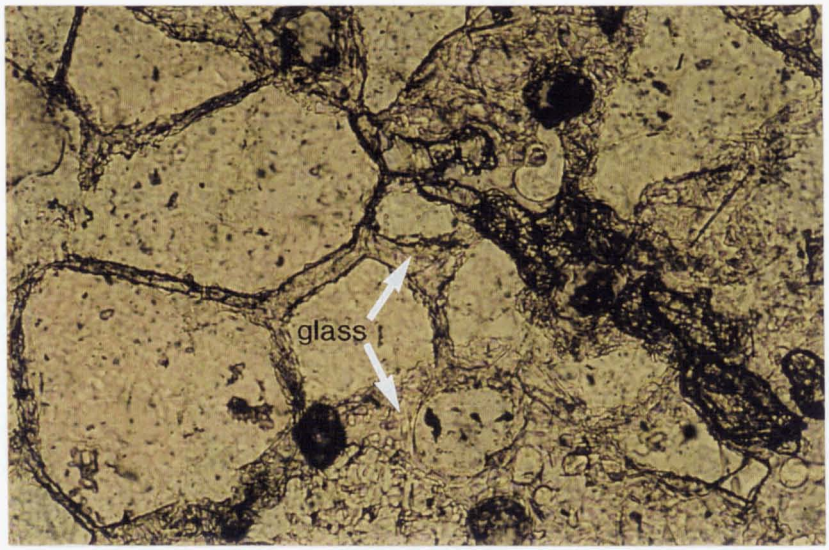

Figure 5.17 Glass along grain boundaries of quartz, TG021A quartzite xenolith. Note small grains "floating" in patch of glass at bottom of photo. View length measures 0.7 mm (ppl).

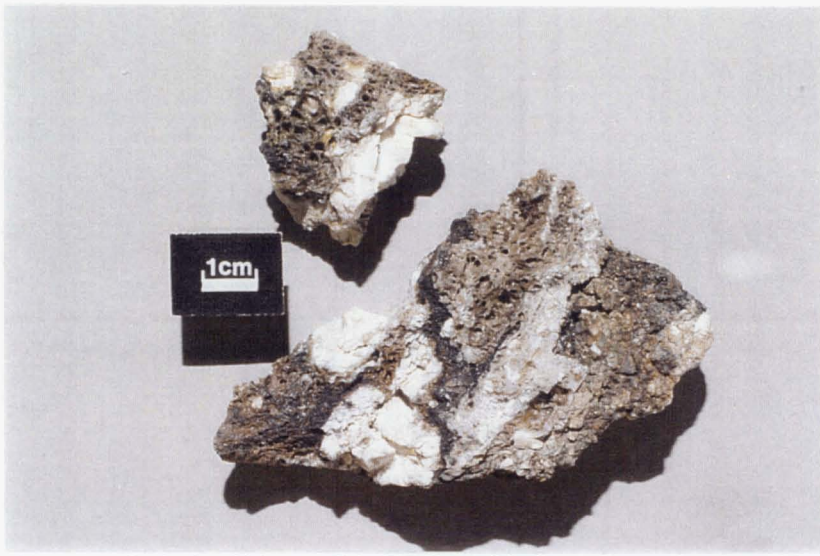

Figure 5.18 Glassy, vesicular buchitic xenolith (TG534) with discontinuous bands and fragments of quartzite and feldspar-opaque material. Ngauruhoe 1975 pyroclastic avalanche deposit.

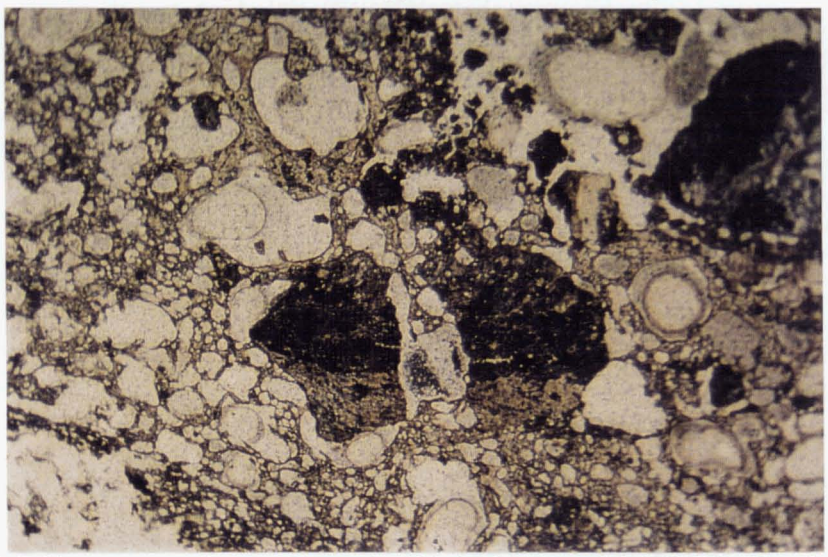

Figure 5.19 Feldspar-opaque fragment (centre) within buchitic xenolith (TG534). View length 7.9 mm (ppl).

A

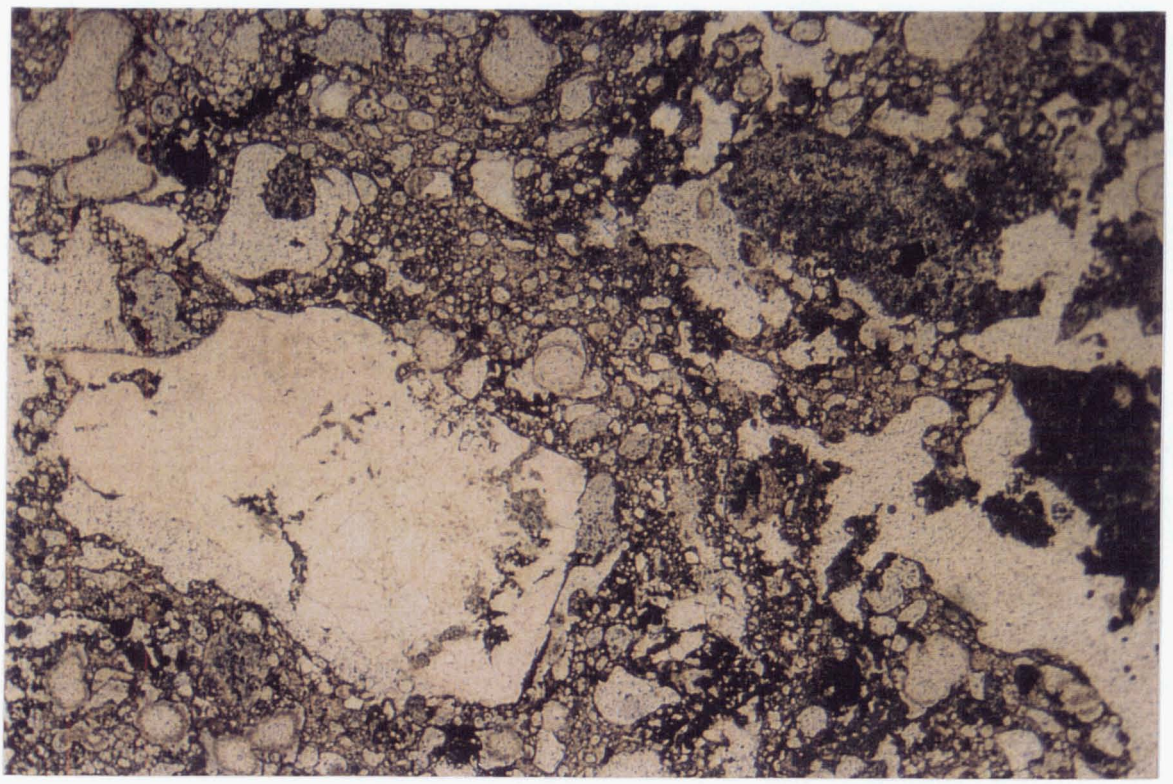

B

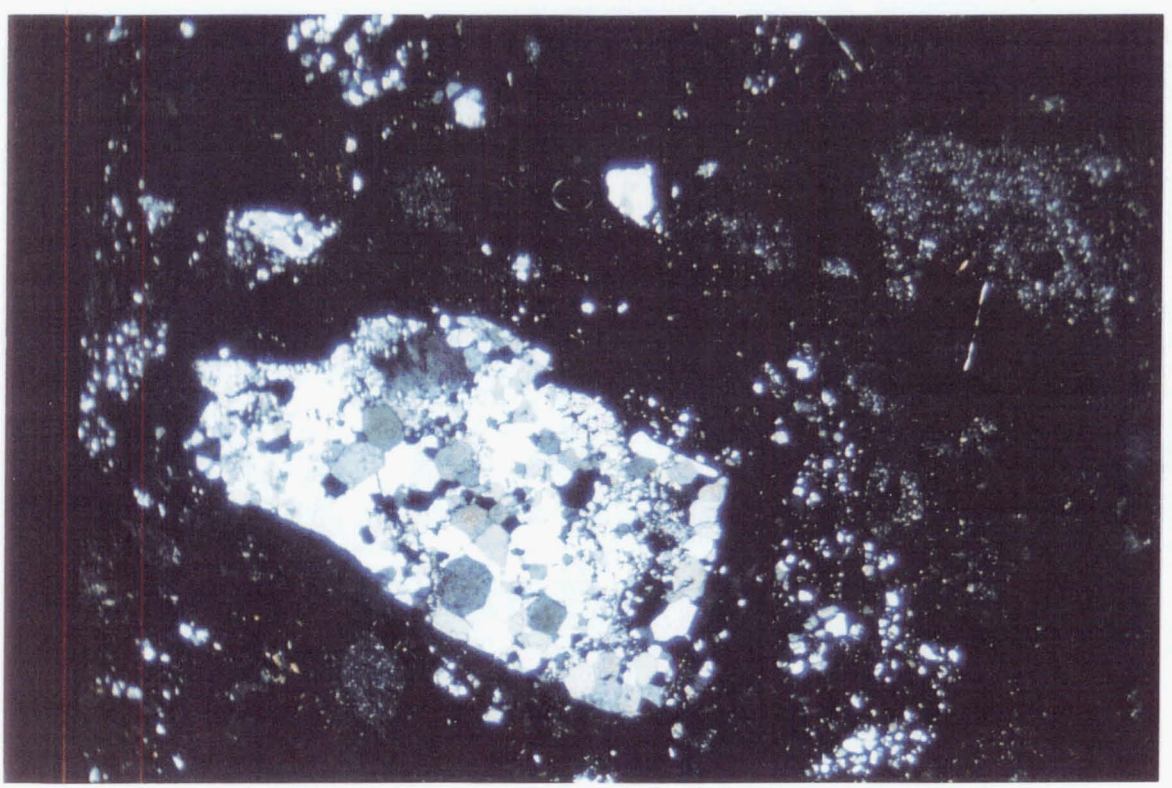

Figure 5.20 Quartzite and feldspar-opaque fragments within glassy, vesicular buchitic xenolith (TG534). View length measures 7.9 mm (**A**-ppl; **B**-cpl).

subangular fragments of refractory quartzite (± calc-silicates) and banded feldspar-opaque material.

Building on the observations of Steiner (1958), Graham et al. (1988) investigated the mineralogy and chemistry of buchitic metagreywacke xenoliths from Ngauruhoe 1954 lavas. These xenoliths comprise up to 80% glass and up to 50% vesicles, and contain quartz-rich and quartz-poor layers which are contorted and/or discontinuous over a few centimetres. Fragmented veins of quartz, wollastonite and calcic plagioclase were reported in some xenoliths. Euhedral cordierite, orthopyroxene and spinel crystals in the glass were interpreted as breakdown products of phengite and chlorite which are both common constituents of Torlesse greywacke and argillite (Graham et al, 1988). Cordierite has not been identified in TG534, but otherwise the xenolith appears similar to the buchitic xenoliths described by Graham et al (1988) and probably has the same fused Torlesse greywacke origin.

5.6.3 Xenolith-host lava contact

Most quartzite xenoliths show no reaction with the enclosing magma and have smooth, sharp contacts with the host lava. Quartz grains are often broken across the xenolith-host boundary. This general lack of reaction suggests only a short residence time for the xenoliths in the magma prior to eruption. Xenoliths were probably also entrained in the magma at earlier stages but have reacted extensively and assimilated with the host magma, thus destroying any evidence of their existence.

One of the quartzite xenoliths, however, does show evidence of reaction with the host magma. TG153 contains a xenolith surrounded by a discontinuous, irregular zone of colourless, vesicular glass up to 2 mm wide, which is in turn rimmed by a zone (<1 mm wide) of 0.2-0.6 mm, subhedral, prismatic clinopyroxene crystals (Fig 5.21). This reaction relationship between quartz and andesitic magma illustrates the simplest case of assimilation of a phase with which the liquid is undersaturated (McBirney, 1979). The TG153 rim equates to Sato's (1975) inner Zone I of clinopyroxene-glass coronas around quartz xenoliths, which result from alkali enrichment in corona glass (increasing the

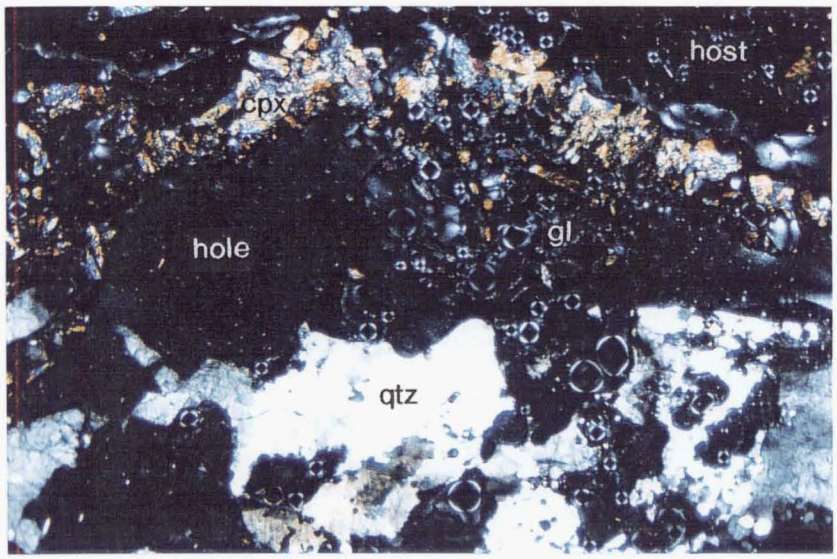

Figure 5.21 Quartzite xenolith (qtz) in young Pukekaikiore andesite (TG153; host) with a reaction rim of vesicular glass (gl) and clinopyroxene (cpx). View length measures 7.9 mm (cpl).

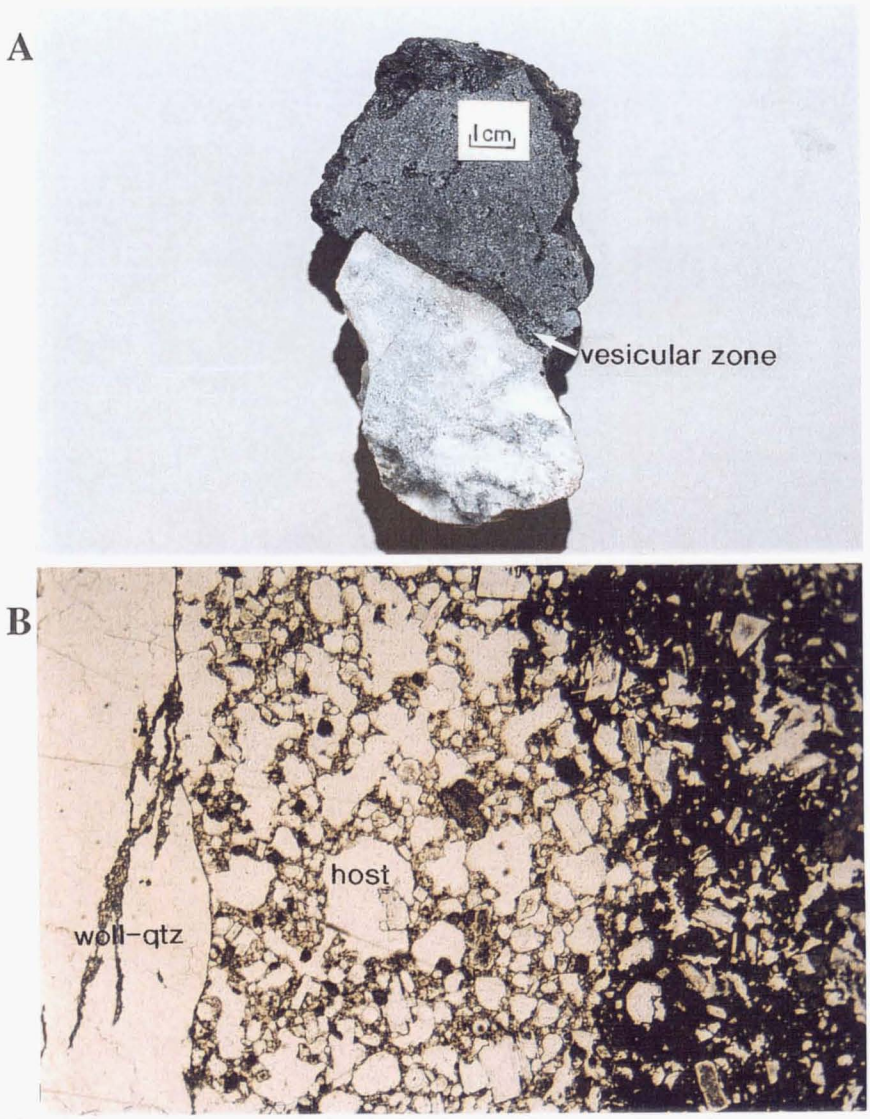

Figure 5.22 Glassy, vesicular zone of andesite (host) adjacent wollastonite-quartz (woll-qtz), Ngauruhoe 1975 pyroclastic avalanche deposit (TG531). **A**-hand specimen; **B**-photomicrograph, view length 7.9 mm (ppl).

effective CaO concentration) causing clinopyroxene to crystallize in orthopyroxene andesite. Graham (1987) also described such clinopyroxene-glass coronas around quartz-rich xenoliths from Ruapehu. He attributed them to extraction of partial melts from the xenolith which interact diffusively with the host magma. TG153 is a sample from the young Pukekaikiore olivine andesite scoria, noteworthy for its complete lack of plagioclase phenocrysts and relatively high MgO content (7 wt%). Development of clinopyroxene-glass reaction rims may be dependent on magma temperature and thus rims only occur in the more basic magmas, and are absent from the more evolved Tongariro andesites which also contain quartzite xenoliths.

A wollastonite-quartzite xenolith (TG531) found in the Ngauruhoe 1975 pyroclastic avalanche deposit has a sharp boundary across the quartz grains, but is surrounded by zones of progressively less silicic, vesicular glassy lava (Fig 5.22). A distinct 3-5 mm wide zone of pale brown, highly vesicular, glassy porphyritic andesite immediately contacts the xenolith. This zone is bordered by an irregular 8-15 mm wide zone of medium brown glassy andesite, which is in turn surrounded by dark brown andesite of the unaffected part of the host lava. This texture is likely to represent mingling of silicic partial melt of the xenolith with liquid of the host andesite, which quenched and vesiculated because of the decrease in pressure associated with rapid ascent. It is possible that CO_2 released during the reaction of calcite and quartz (producing wollastonite) is one of the vapour phases exsolved on quenching.

5.6.4 Origins of quartzite xenoliths

Firstly, these xenoliths are quartzites, as opposed to orthoquartzites - which would have dusty margins separating overgrowth cement from the original sandstone grains. A well-recrystallized quartz-dominated rock can originate in several ways: as a sandstone, as chert, or as quartz-vein material. Each of these possibilities is considered below, and it is argued that a quartz vein origin best satisfies the available petrographic evidence.

(a) Sandstone. The irregularity of the calc-silicate layering, or in places patches rather than layering, precludes a calcareous quartz sandstone origin. Although contact metamorphism brings about a coarsening in grain size, primary sedimentary structures such

as bedding are frequently preserved. The large patches of quartz and irregular, cross-cutting calc-silicate patches and bands represent the original structure of the rock, and contrast with the regular, continuous beds expected of a bedded limey sandstone. The calc-silicate layering is also too closely spaced (0.05-0.2 mm wide layers) for a sandstone.

Graham (1985a) documented rare Torlesse metagreywacke xenoliths (assemblage quartz+albite+chlorite+muscovite+epidote), with relict graded bedding, from Ruapehu and Tongariro (Type UCX). No such xenoliths were observed in the small collection made for this study, but it is useful to note the unlikelihood of the quartzite xenoliths described above being derived from Torlesse sandstone itself. Apart from the issue of bedding structures, even if the significant feldspar-mica component of the sandstone had been melted or reacted, some evidence of glass patches or reaction products would be expected. Instead, the Tongariro quartzites are composed of very pure "clean" quartz quite unlike the Torlesse.

Barley (1987) described abundant metasedimentary xenoliths within dacites of the mid-Cretaceous Mt Somers Volcanics, Canterbury, New Zealand, which were erupted onto an eroded surface of Torlesse sediments. The xenolith assemblage consists of quartz + alkali feldspar + plagioclase + orthopyroxene ± biotite ± garnet ± hercynite ± sillimanite and was interpreted as metamorphosed Torlesse sediments (Barley, 1987). This is a useful example of a more certain identification of Torlesse xenoliths.

(b) **Chert.** There is also the possibility that the Tongariro quartzites could represent a recrystallized, layered, quartz-rich chert with some Ca-rich impurities. However the irregularity of the calc-silicate layers is difficult to reconcile with origin as a chert.

(c) **Quartz veins.** Origin as a calcite/dolomite-quartz vein is a more probable explanation of the Tongariro quartzite xenoliths. The xenoliths show growth structures reminiscent of a crack-seal process of vein growth, defined by Ramsey (1980) as a process of repeated closely-spaced brittle cracking, accompanied by repeated sealing of the cracks by precipitation. Each burst of cracking does not always follow the previous cracks, giving rise to irregular, cross-cutting textures. The thin calc-silicate bands in the Tongariro quartzites represent minor calcite/dolomite precipitated along with the quartz, and record a succession of opening events in irregular configurations typical of a crack-seal style of vein growth. Grain coarsening and recrystallization during contact metamorphism has

caused quartz grains to overgrow the calc-silicate layers. This grain coarsening also indicates an initially fine grain size inconsistent with a coarse-grained high grade metamorphic rock such as a gneiss (cf. Graham, 1985a, 1987; Section 5.2).

These features are very similar to those observed in quartz-dolomite veins in the Ordovician Greenland Group slates of the West Coast of the South Island (see Shelley, 1975). The irregular banding is overgrown and enclosed by the coarse, recrystallized quartz; the Greenland Group quartz vein provides a suitable model for the textures observed in Tongariro quartzites.

Relating these quartz veins to basement lithologies beneath the Tongariro complex is difficult, partly because of the uncertainty of what is actually down there (xenoliths provide one of the major lines of evidence!), and partly because quartz veins can occur in many lithologies. The Tongariro quartzite xenoliths lack any evidence of the host rock to the vein. Such evidence could be debris trails of the host rock which were trapped when a crack opened then sealed in by further growth. The likely candidates are for quartz veins within the Tertiary sequence, or within the Torlesse greywacke basement rocks (Section 1.4.3). Because the isotopic composition of the three xenoliths analysed (Appendix 7, Fig 7.23) is very similar to measured Torlesse isotopic compositions, it is perfectly conceivable that they originated from quartz veins within the Torlesse basement. Beetham and Watters (1985) noted that quartz veins were common in the Torlesse sandstone encountered during tunnelling for the Tongariro Power Development project in the western Kaimanawa Range, adjacent to the Tongariro Volcanic Complex.

An important observation in Graham's (1985a) descriptions of the metagreywacke xenoliths is the occurrence of quartz-calcite veins. This provides further support for a Torlesse quartz vein origin to explain the Tongariro quartzite xenoliths. Prominent cross-cutting quartz veins in schistose metagreywacke xenoliths found in Tongariro tephras were described by Donoghue (1991). Graham (1985a) and Graham et al. (1988) also noted cross-cutting veins of quartz, wollastonite and plagioclase within the Ngauruhoe buchitic xenoliths. A chemical analysis of one vein (VUW 17472, Graham, 1985a) is very similar to the TG269 analysis. Two wholly calc-silicate xenoliths dominated by wollastonite (+ anorthite ± quartz) were considered, however, to represent limestone within the Torlesse (Graham, 1985a).

Although Graham (1985a) described quartz-calcite and quartz-wollastonite veins within Torlesse metagreywacke, he did not ascribe a vein origin to his quartz-rich xenoliths (Type QX; Section 5.2). These metaquartzites have the same mineralogy as those described from Tongariro in this study and could reasonably be expected to share a similar quartz vein origin, although lack of description of calc-silicate/quartz textural relationships makes this more difficult to assess. In the light of petrographic descriptions and interpretations of the present study, there seems to be no compelling reason to attribute the Tongariro quartzite xenoliths to gneissic Torlesse sandstone itself - as favoured by Graham (1985a, 1987) to explain his Type QX xenoliths.

5.7 DISCUSSION AND SUMMARY

5.7.1 Crustal contamination

Although xenoliths provide the most obvious evidence for contamination of magma, there is no simple relationship between xenolith abundance and the amount of contamination that has taken place. This is because xenoliths not in equilibrium with their host magma will melt, dissolve, or react. As a result, thorough assimilation of xenoliths - leading to their absence in lava samples - may be mistaken for a lack of contamination. Furthermore, incorporation of xenoliths just prior to eruption precludes significant reaction with the magma; in this case the presence of xenoliths does not necessarily indicate extensive contamination. Experiments by Tsuchiyama (1986) showed that digestion of xenoliths by partial melting was mainly dependent on host magma temperature, not xenolith size. The time required for complete xenolith digestion varied from about 1000 years at a few °C superheating, to a few days at 100°C superheating (Tsuchiyama, 1986). Based on these digestion rates Tsuchiyama (1986) concluded that survival of many xenoliths was contingent upon their incorporation into a magma just prior to eruption.

5.7.2 Why do we not see recognisable greywacke basement preserved more often as xenoliths in Tongariro lavas?

The scarcity of greywacke xenoliths can be explained by the high susceptibility of this rock to rapidly melt/react, disaggregate and be consumed by the enclosing magma. In a study of the melting of pelitic xenoliths in Wehr Volcano, Germany, Grapes (1986) found that plagioclase had been preferentially consumed with respect to quartz, which remained as the most abundant relict phase. Because it is highly likely that Torlesse greywacke does underlie the Tongariro complex, it is probable that fragments of greywacke have been incorporated and digested by the magma, and this is supported by isotopic data and assimilation-fractional crystallization trends (Section 7.4). So Torlesse probably has contaminated Tongariro magmas, but because of its fusible nature we do not see much petrographic evidence (i.e. xenoliths) for this process. The rare metagreywacke xenoliths described by Graham (1985a) must represent greywacke basement incorporated just prior to eruption.

5.7.3 Why do quartz-rich xenoliths predominate in Tongariro lavas?

Xenoliths composed mainly of a single mineral and very rich in a component such as silica (e.g. quartz veins) are very difficult to assimilate not just because of their refractory nature, but also because incorporating such high concentrations of a single component requires dissemination through large volumes of magma (McBirney, 1979). So although quartz veins, chert, etc. are likely to be minor constituents of the basement rocks, these will be over-represented in the xenolith population because of their high survival rate, unlike the majority of the basement constituents (feldspar, micas, etc.) which have disappeared through melting or reaction. In a study of quartzose xenoliths in Auckland basalts, Searle (1962) came to a similar conclusion that minor quartz veins or cherty beds within the basement greywacke had preferentially survived even though they represented only a small proportion of the sedimentary material originally engulfed by the magma. This issue of xenolith abundance and preservation is not always taken into account. For example, Graham (1987) dismissed an origin as chert within Torlesse basement because the relative abundance of quartzite xenoliths was "inconsistent with their rarity in the source terrane" -

even though he admitted a chert origin was difficult to deny on chemical or petrographic grounds.

It is interesting to consider relationships between the abundance of quartz veins in the Torlesse and the abundance of quartzite xenoliths in Tongariro magmas. From the preceding discussion, it has been suggested that quartz veins (now represented by quartzite xenoliths) could be the only component of the Torlesse which (more or less) survives incorporation into Tongariro magmas (but minor partial melting has been documented; Section 5.6.2). Based on this assumption, and using an estimate of the absolute abundance of quartz veins in the Torlesse, it is possible to use the abundance of quartzite xenoliths in Tongariro lavas (up to c.2 modal %) to make a rudimentary calculation of the total amount of Torlesse assimilated.

If quartz veining were very minor or virtually absent in some parts of the Torlesse, comprising say 1% of the total volume, then using the upper limit of xenolith abundance of 2% this would imply 100x2=200% by volume Torlesse assimilated in a given volume of Tongariro magma! This is clearly untenable since Tongariro magmas do not have the composition of melted Torlesse rocks. It is more reasonable to assume that these Tongariro magmas have assimilated parts of the Torlesse which contain a higher proportion of quartz veins. The amount of veining in Torlesse rocks is variable (both areally and with depth), and may range from c.10% in low grade (pumpellyite-phrenite) rocks to locally c.30% (especially in schistose Torlesse). No quantitative estimates were reported from the Tongariro Power Development work through the Torlesse basement, but Beetham and Watters (1985) noted that 1-100 mm wide quartz veins were widespread. Therefore, it is more likely that the quartzite xenolith-rich Tongariro magmas (mostly from Ngauruhoe) encountered Torlesse containing perhaps 10-20% quartz veins, implying 10x2=20% or 5x2=10% Torlesse assimilation respectively. These are more feasible estimates of maximum amounts of crustal contamination and are in broad agreement with chemical and isotopic modelling of assimilation fractional crystallization (AFC) processes (Section 7.4).

5.7.4 Conclusions

The main findings of the Tongariro xenolith study can be summarised as follows:

1. Cognate feldspathic xenoliths are common in all volcano-stratigraphic units, and are interpreted as coarse-grained equivalents of the host groundmass which crystallized hypabyssally at conduit margins - in contrast to the origin put forward by Graham (1987) linking feldspar-rich xenoliths to gneissic basement.

2. Quartzite xenoliths are particularly common in Ngauruhoe lavas. The thin, irregular, closely-spaced layering of calc-silicates between the quartz grains points towards an origin as quartz veins - as opposed to the gneissic sandstone origin proposed by Graham (1985a, 1987).

3. It is probable that the quartz veins were derived from the Torlesse metasedimentary basement, and represent perhaps the only component to commonly survive assimilation. Variable quartzite xenolith abundances in Tongariro lavas of up to c.2 modal % therefore imply variable crustal contamination (<c.10-20%) by Torlesse basement containing relatively more or less abundant quartz veins.

It is quite possible that Graham and co-workers have collected and described different xenolith types from those of this preliminary study of Tongariro xenoliths. No true schists analogous to their Type QXa have been found (although perhaps this is not surprising considering their rarity on Ruapehu). A more detailed study is required to resolve this problem. Future xenolith studies in Tongariro, and Taupo Volcanic Zone in general, will be crucial in determining the crustal structure beneath TVZ. At present, it appears that Tongariro feldspathic xenoliths cannot easily be interpreted in terms of Graham's (1987) model for a deep-seated metasedimentary origin, and instead are suggestive of a cognate origin. I must also draw the interim conclusion that the small selection of Tongariro quartzites examined in this study cannot be reconciled with Graham's (1985a, 1987) gneissic Torlesse interpretation, and are better explained as thermally metamorphosed calcite/dolomite-quartz veins which may, however, have originated within the Torlesse basement.

Chapter 6

Magma Compositions of Volcano-Stratigraphic Units: Characterisation and Relationships

CHAPTER 6
MAGMA COMPOSITIONS OF VOLCANO-STRATIGRAPHIC UNITS: CHARACTERISATION AND RELATIONSHIPS

6.1 INTRODUCTION

A comprehensive geochemical data base has been obtained for the Tongariro Volcanic Complex. This encompasses all volcano-stratigraphic units and thus provides the opportunity to interpret compositional data within a time-space-volume framework (Section 1.1). Major and trace element compositions of 370 Tongariro samples are given in Appendix 10. All but seven of these samples have thin section petrographic descriptions (Appendices 3 and 4). CIPW norms are presented in Appendix 11. XRF analytical procedures and data quality assessments are contained in Appendix 8, Sections 8.3.1-3. A more extensive and more precise trace element and isotopic data base (Appendix 13) is used to further investigate Tongariro magmatic trends in time and space (Chapter 7). Throughout the discussion, major and trace element concentrations are reported as analysed (i.e. on a hydrous basis), whereas all data have been recalculated volatile-free for plotting purposes.

In the following sections, Tongariro lavas and pyroclastics are classified on the basis of their chemical composition, and overall chemical trends for the complex are presented. This establishes a broad framework within which time-space-volume-composition relationships may be examined. The chemistry of each volcano-stratigraphic unit is then examined in turn, and related to eruptive style, volume and rate (determined in Chapters 2 and 3), in addition to petrographic characteristics and mineral compositions (determined in Chapter 4). The relationships between the units are examined, and petrological trends

over the lifetime of the complex are identified and discussed. The Tongariro data are also considered with respect to trends shown by Ruapehu volcano.

This approach, investigating Tongariro magmatic trends within the time-space framework of the established volcano-stratigraphy, has revealed some important findings which can be briefly summarised as follows:

1. variation diagrams for the Tongariro cone-forming units reveal differences in the absolute elemental abundances for given SiO_2 contents, in the length, steepness and shape of chemical trends, and in the distribution of chemical groups within compositional space;
2. certain volcano-stratigraphic units do share, however, similar patterns of chemical ordering which suggest derivation from a common deep magma reservoir, e.g. the amphibole-bearing andesites of southern cones (Tama 1, Tama 2, Pukekaikiore);
3. other compositionally distinct units nevertheless often exhibit analogous trend patterns which may signify a common high level differentiation history involving (to varying degrees) magma mixing, fractional crystallization and crustal contamination;
4. a relatively complex history is envisaged for the plumbing system of the Tongariro Volcanic Complex, in which different configurations and combinations of both deep and shallow magma reservoirs, some operating independently and others interconnected, have existed at different time periods throughout Tongariro's development.

6.2 PREVIOUS WORK

As for the earlier work on Tongariro petrography (Section 4.2), this study represents a significant expansion of the existing geochemical data base and also differs from previous work in that petrological samples were collected and grouped within a specific volcano-stratigraphic context. Whole-rock chemical analyses of Tongariro rocks (principally the

young eruptives) have been published by several authors, but very few lavas from the older parts of Tongariro (and none from SW and NE Oturere) had been analysed. A recent review (Graham et al., 1995) provides a useful survey of the petrology of Tongariro Volcanic Centre andesites and of TVZ lavas in general.

The first (partial) chemical analyses were made over a hundred years ago on samples from Ngauruhoe, Red Crater and North Crater (Thomas, 1889). Much later, the 1954 eruption of Ngauruhoe provided an impetus for new analytical work and presentation of unpublished analyses of other historic (1928, 1949) and prehistoric Ngauruhoe lavas, a Red Crater lava, and the young Pukekaikiore flow (Steiner, 1958). These same analyses were also brought together by Clark (1960a). Both authors used variation diagrams to show that a relationship existed between Tongariro andesites and other TVZ lavas. The focus was on overall trends rather than individual volcanoes, and Clark (1960a) maintained that any petrogenetic model developed for Tongariro andesites should also be applicable to all TVZ eruptives. These authors favoured variable crustal contamination of parental basalt magma, in conjunction with limited fractional crystallization, as the main process (accompanied by minor crystal accumulation) responsible for producing Tongariro andesites.

Ewart (1965) and Ewart and Stipp (1968) reviewed the work of Steiner (1958) and Clark (1960a), and included additional analyses of hornblende andesites from Tama Lakes. Ewart and co-workers (1968, 1977) presented trace element and radiogenic isotope compositions (Section 7.2) which supported an origin for the andesites from a basic parent magma assimilating Mesozoic sediments. Although Topping's (1974) PhD study of Tongariro Volcanic Centre principally concentrated on tephrostratigraphy and chronology, lava flows from Red Crater (10), Lower Te Mari Crater (2), Pukekaikiore (1) and Pukeonake (4) were also analysed for major element compositions. The eruption of Ngauruhoe in 1974-75 provided further opportunity for analysis of historical eruptives; major element data were presented by Nairn et al. (1976) and Nairn and Wood (1987).

Further analyses were presented by Cole (1978) for Te Mari Craters, Tongariro, Pukekaikiore and Pukeonake, and by Cole (1979b) for 12 samples of 1954 Ngauruhoe lavas. Cole (1978) represents the first published study devoted solely to Tongariro Volcanic Centre lavas, in which they are classified as calc-alkaline andesites and low-Si andesites.

Tectonic assimilation of accretionary wedge sediments with basalt of the downgoing slab was proposed in conjunction with fractional crystallization for derivation of the andesites (Cole, 1978). Cole (1979a, 1981, 1982) and Cole et al. (1983) discussed the origin of andesites within the general context of TVZ petrogenesis, noting that all lavas show evidence of crustal contamination.

More recent work on Tongariro Volcanic Centre petrology has focused on a detailed study of Ruapehu volcano (Hackett, 1985; Graham, 1985a; Graham and Hackett, 1987), for which a relatively large geochemical data base (including isotopic compositions; Section 7.2) was obtained (144 XRF analyses; Hackett, 1985). Analyses from Ngauruhoe 1954, Red Crater, Pukekaikiore and Pukeonake were included in the studies, although the Tongariro complex itself was not investigated. Graham and Hackett (1987) discuss Ruapehu petrogenesis within the context of six lava types, which are summarised in Section 4.2. Assimilation fractional crystallization (AFC) was recognised as the dominant process producing the majority of Ruapehu lavas, with some also showing evidence of crystal accumulation or magma mixing (Graham and Hackett, 1987). An ideal parental basalt could not be found on Ruapehu, so a basalt found to the NE at Waimarino (Fig 1.11) and a less primitive Ruapehu basalt were used to model subsequent fractional crystallization and contamination by Torlesse terrane greywacke (see Section 7.2).

New analyses of andesite lavas exposed in the Mangatepopo Valley wall, on Pukekaikiore, and in the Tama Lakes area (Patterson, 1986; Patterson and Graham, 1988; Wahyudin, 1993) were noteworthy for representing the sparse petrological investigations of portions of the older part of the Tongariro complex. Because no detailed volcano-stratigraphic framework was available, however, the geochemical trends could not be satisfactorily tied in to a Tongariro eruptive history. Instead, lavas were grouped into the lava types of Graham and Hackett (1987), and a new lava type (Type 7; Patterson and Graham, 1988) was identified. The TVZ lava types now number nine (Section 4.2), and have recently been reviewed by Graham et al. (1995). For reasons outlined in Section 4.2, this lava classification scheme is not followed for this study, although comparisons are made (Section 6.7; Chapter 7).

6.3 CHEMICAL CLASSIFICATION

The composition of Tongariro eruptive products was introduced in Section 2.1 where a TAS diagram was presented (Fig 2.1) which showed basaltic andesites, andesites and minor dacites ranging from 53.0 to 64.2 wt% SiO_2. Dacites had not previously been reported from the Tongariro complex (the four dacites identified by Wahyudin, 1993, as old Tama Lakes lavas are actually young overlying Ruapehu lavas). The three broad petrographic groupings identified in Section 4.1 do not correspond to any particular rock type, although olivine is (predictably) absent in dacites, and hornblende occurs only in the andesite lavas (Fig 4.2).

These data define a calc-alkaline, medium-K trend (Figs 6.1 and 6.2) in keeping with the pattern established for other TVZ andesites (Graham et al., 1995). All Tongariro rocks plot in the calc-alkaline field on an AFM diagram, apart from the Red Crater basaltic andesites which occur on the calc-alkaline - tholeiitic dividing line (Fig 6.2). There is no coherent trend evident on the AFM diagram, but most samples display only limited iron enrichment.

All Tongariro eruptives are hypersthene- and quartz-normative, with corundum appearing in the norms of several slightly altered samples (Appendix 11). There is significant correspondence between modal and normative mineralogy; an, ab, or, di, hy, mt, il and ap in the norm correspond to the observed phenocryst phases plagioclase, clinopyroxene, orthopyroxene, Fe-Ti oxides, and apatite (Section 4.1). However, the existence of up to 23% Q in the norm is generally not matched by modal quartz abundances (<1% in only a few lavas; Section 4.5.7), and the lack of normative ol contrasts with the typically <2 modal % found in almost a third of Tongariro samples (Section 4.5.1). The occurrence of <5% hornblende in the mode of some samples (Section 4.5.4) cannot, of course, be reflected in normative compositions.

Even when the total Tongariro data set of whole-rock analyses is crowded onto one diagram (Fig 6.1), several different trends are evident within the broad envelope represented by Tongariro analyses. These trends and groupings can be examined more

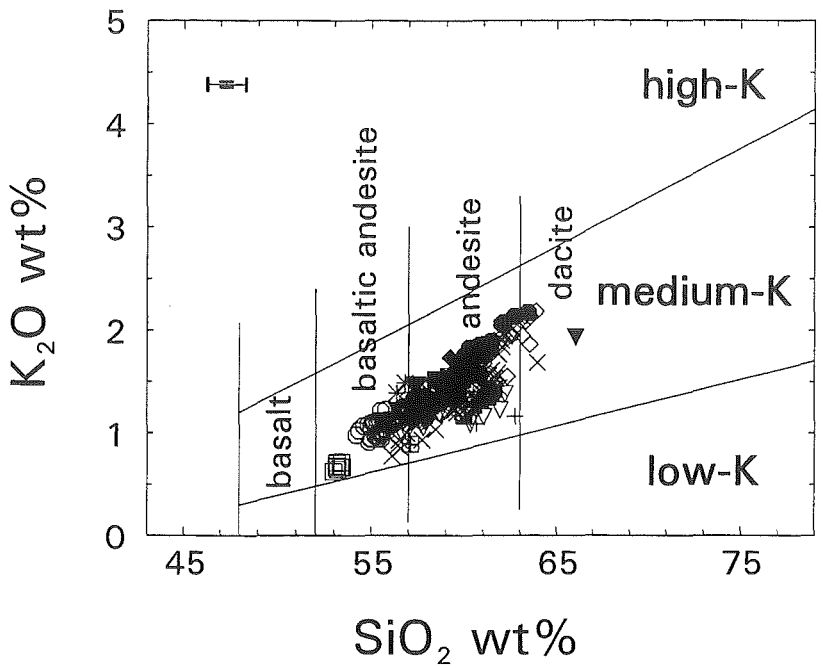

Figure 6.1 K_2O-SiO_2 classification diagram of all Tongariro samples (plotted according to volcano-stratigraphic unit) showing that they are medium-K type. After Le Maitre et. al. (1989). Key for unit symbols shown below. All data recalculated anhydrous. Error bars represent total error (2 sd from mean; Section A8.3.3).

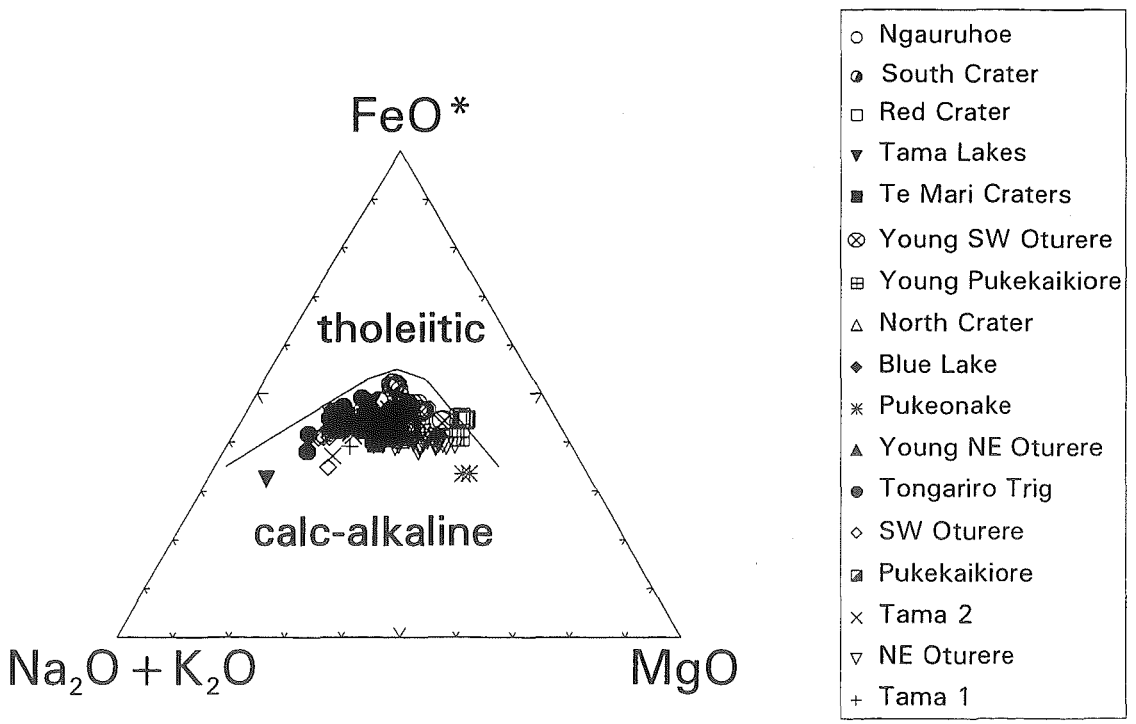

Figure 6.2 Alkali - FeO* - MgO (AFM) classification diagram of all Tongariro samples (plotted according to volcano-stratigraphic unit) showing their calc-alkaline character. After Irvine and Barager (1971). All data recalculated anhydrous.

readily by first looking at individual volcano-stratigraphic units (Section 6.6). However, it is apparent from Figure 6.1 that the most primitive compositions are those most recently erupted, from Red Crater (whose basaltic andesites sit slightly apart from the main body of Tongariro data) and Ngauruhoe. The most evolved compositions were produced during the middle part of Tongariro's eruptive history (Tongariro Trig, SW Oturere, Tama 2) -apart from the dacite of the young Tama Lakes ejecta (which is separated by a small - almost 2 wt% - SiO_2 gap from the other dacites). Because of the comprehensive data base, these small breaks at either end of the Tongariro compositional range are probably real rather than an artifact of incomplete sampling.

Despite these distinctions, magma compositions of the different units generally overlap, so that an overall systematic petrological evolution with time cannot be invoked for Tongariro eruptives. Andesitic and basaltic andesitic magma has been consistently erupted throughout the lifetime of the Tongariro complex, although basaltic andesite compositions have been more prevalent during the latter stages of Tongariro's development (Fig 3.7).

$100Mg/(Mg+Fe^{2+})$ [Mg#] ranges from 36.6 (Tongariro Trig) to 70.8 (Pukeonake), but without Pukeonake the highest Mg# is 65 (NE Oturere). Although possessing high Mg#, MgO, Cr, Ni, and olivine Fo contents (Fo_{86-95}), the Pukeonake eruptives also contain relatively high concentrations of incompatible elements and exhibit clear petrographic evidence for magma mixing (Section 4.7), and therefore cannot be considered as primary magmas. In fact, no Tongariro eruptives have the primitive characteristics representative of direct mantle melts. A plot of $100Mg/(Mg+Fe^{2+})$ versus SiO_2 (Fig 6.3) shows more clearly the grouping of data points into distinct trends or clusters, often coinciding with separate volcano-stratigraphic units. The highest $100Mg/(Mg+Fe^{2+})$ values (>60) belong to Pukeonake eruptives, Red Crater post-1.8 ka basaltic andesites, Young Pukekaikiore scoria, and part of a NE Oturere trend (Fig 6.3). A lower trend of Tongariro Trig eruptives, along with a few samples from Ngauruhoe, Tama Lakes and Tama 2 comprise the lowest (<40) $100Mg/(Mg+Fe^{2+})$ values.

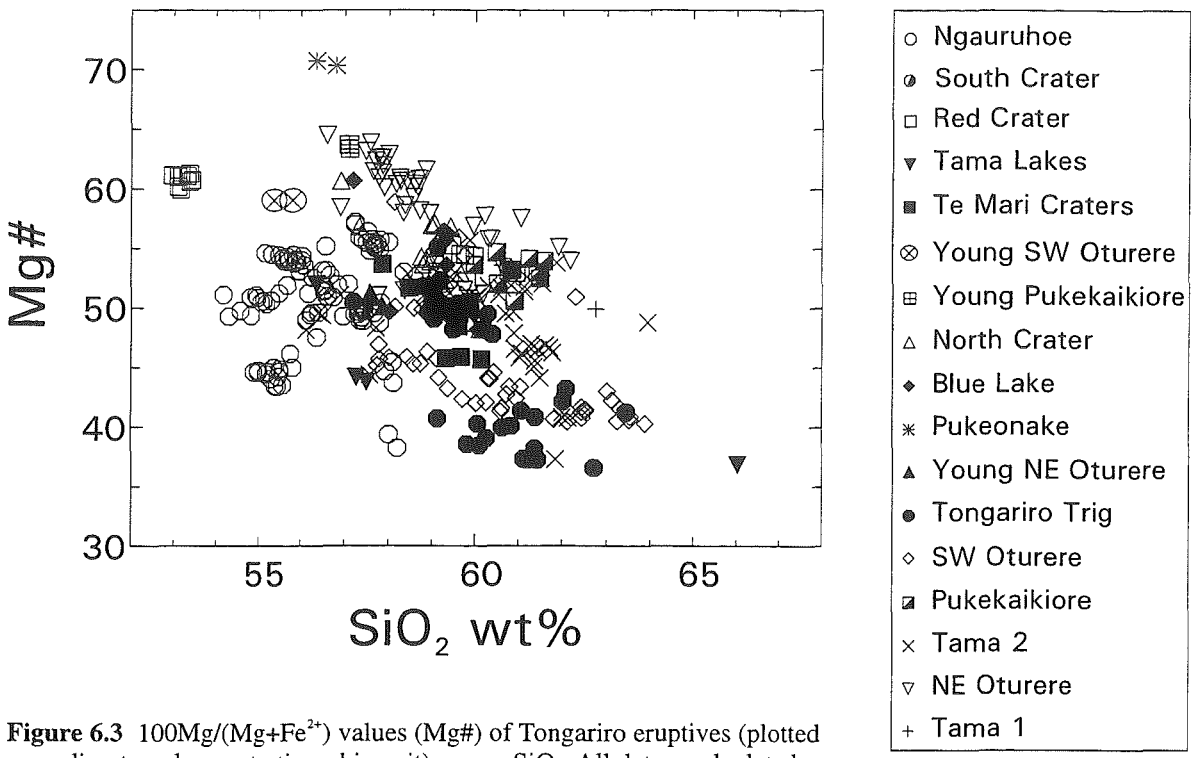

Figure 6.3 100Mg/(Mg+Fe^{2+}) values (Mg#) of Tongariro eruptives (plotted according to volcano-stratigraphic unit) versus SiO_2. All data recalculated anhydrous.

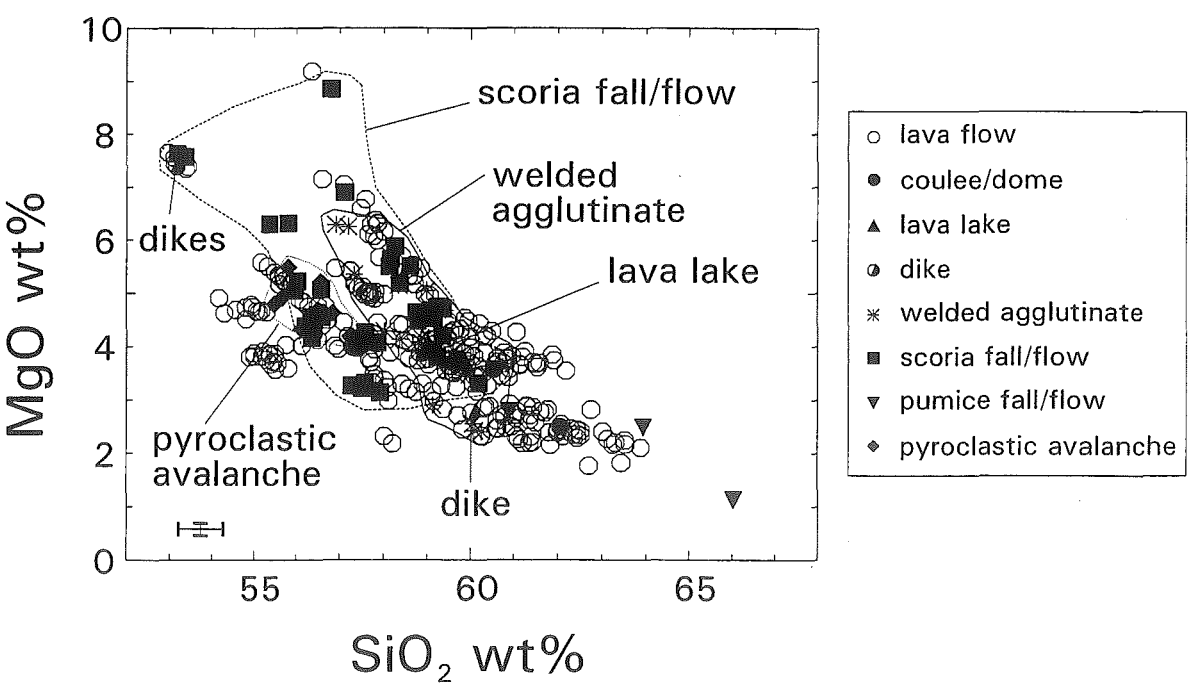

Figure 6.4 MgO-SiO_2 diagram of all Tongariro samples plotted according to type of eruptive product (not volcano-stratigraphic unit as for other figures), showing partial control of magma compositionon eruptive style. All data recalculated anhydrous. Error bars represent total error (2 sd from mean; Section A8.3.3).

6.4 RELATIONSHIP BETWEEN CHEMICAL COMPOSITION AND ERUPTIVE STYLE

When the total set of Tongariro analyses is plotted according to type of eruptive product on a diagram of MgO versus SiO_2 (Fig 6.4), it is apparent that magma chemistry has, to a certain extent, an influence on eruptive style. It has already been noted in Sections 2.1 and 2.4 that the more mafic the magma, the less likely it will have been erupted violently. When considering the chemical compositions and trends of each volcano-stratigraphic unit (Section 6.6), relationships between eruptive style and magma composition are described in more detail. General relationships, with reference to Figure 6.4, are outlined below.

Tongariro magmas covering almost the entire compositional range are erupted as lava flows (Fig 6.4), and this is the dominant eruptive product preserved in the Tongariro complex. It is not practicable to further subdivide samples into pahoehoe, aa and block flow type because lava flows often exhibit characteristics transitional between these end members, and for the older flows it is not usually possible to determine flow type with any degree of certainty. However, for the younger flows it is apparent that generally only the basaltic andesites were erupted as aa flows (or the rare pahoehoe flows). The relatively rare overthickened flows (coulées) and domes are of evolved lower MgO (<4 wt%), higher SiO_2 (>60 wt%) composition compared to the overall Tongariro field (Fig 6.4) - as would be expected for such viscous effusive land forms.

The chemical composition of the solidified products of the North Crater lava lake do not differ markedly from the majority of Tongariro products, and plot in a small coherent group near the middle of the Tongariro field on the MgO-SiO_2 plot (Fig 6.4). Factors such as a wide flaring vent geometry have probably been more influential than magma composition in promoting this hawaiian-strombolian fire-fountaining style of eruption (Section 2.3.1b). Similarly, the chemistry of magmas emplaced as dikes (rarely observed on the Tongariro complex) may not play a particularly important role in determining the style of eruption (or intrusion) since both mafic (Red Crater) and more

silicic (SW Oturere) dikes have been sampled (Fig 6.4). This conclusion must be tempered with the acknowledged poor exposure of dikes on the complex (Section 2.2.1e).

Of the explosive styles of volcanism, the hawaiian-strombolian style, andesitic welded agglutinates and rheomorphic tuffs form a moderate to high MgO (2.4-6.2 wt%) and low to moderate SiO_2 (56.3-60.1 wt%) field on Figure 6.4. This field is overlapped by that for the strombolian style, basaltic andesite to andesite, scoria fall deposits, which also extends to more MgO-rich (<8.9 wt%) and SiO_2-poor (>53.0 wt%) compositions (Fig 6.4). The vulcanian pyroclastic avalanche deposits were erupted exclusively from Ngauruhoe and plot in a relatively small field (overlapping with the field for scoria fall deposits) in the moderate MgO and low SiO_2 part of the overall Tongariro field. There is evidently some compositional control on these eruptive styles that requires involvement of the least evolved magmas. In contrast, pumiceous pyroclastic (fall and flow) deposits from Tama Lakes and the Tama 2 cone represent some of the most evolved compositions (Fig 6.4), especially the dacitic plinian ejecta from Tama Lakes (64.2 wt% SiO_2). Of course, one chemical parameter not analysed for this study is volatile content, therefore the influence particularly of water contents on eruptive styles cannot be directly accounted for.

6.5 OVERALL CHEMICAL TRENDS ON VARIATION DIAGRAMS

Before examining each volcano-stratigraphic unit in turn (Section 6.6), it is useful to note the overall range in major and trace element compositions for the Tongariro complex as a whole, and demonstrate the different patterns and families of trends which indicate a more complex magmatic history. These diagrams of a comprehensive sample population (370) thus show that caution is required when interpretations are sought from smaller data sets of samples for which separate trends may not be well defined, and whose stratigraphic context may be poorly understood or unknown. Unknowingly trying to relate samples from different volcano-stratigraphic/geochemical groups may lead to geologically-unrealistic chemical models.

SiO_2 shows the greatest variability between samples and is used as the differentiation index in the variation diagrams which follow. Different symbols have been used for each unit allowing preliminary comparisons between them to be made. Overall, Tongariro eruptives contain major and trace element abundances in the characteristic range for calc-alkaline andesites, as summarised by Gill (1981). However, a minority of Tongariro samples are somewhat higher in MgO and Cr than documented for typical andesites (Gill, 1981).

The relationships between units is discussed in more detail in Section 6.6, where, on selected diagrams, the compositional fields for each unit are progressively superimposed to develop an overall picture of the magmatic history of the complex (summarised in Section 6.6.9). The important chemical characteristics and trends of each unit (which are related to volcanological and mineralogical features) are also discussed in more detail in Section 6.6.

6.5.1 Major elements

For the Tongariro complex as a whole contents of CaO, TiO_2, Fe_2O_3*, MnO, and MgO decrease, and Na_2O and K_2O increase with increasing SiO_2 (Fig 6.5); trends to be expected from fractional crystallization involving the observed phenocryst phases (plagioclase, orthopyroxene, clinopyroxene, Fe-Ti oxides, some olivine, some hornblende). It is not possible to simply relate samples of this entire Tongariro suite by fractional crystallization models, however, because the low SiO_2 samples (mostly from Red Crater and Ngauruhoe) which would typically be chosen to represent "parents" are in fact much younger than most of the higher SiO_2 samples which would traditionally be selected as "daughter" compositions. In addition, the predominantly straight rather than curved trends, and the considerable scatter in many elements (e.g. Al_2O_3, TiO_2, MgO, Na_2O, K_2O) suggest that processes other than closed system fractional crystallization are operating in complex subvolcanic plumbing systems, effectively blurring simple liquid lines of descent.

(a) **Aluminium.** The scatter evident on the plot of Al_2O_3 versus SiO_2 (Fig 6.5A) reflects the variable abundance of (mainly) plagioclase phenocrysts (especially low in

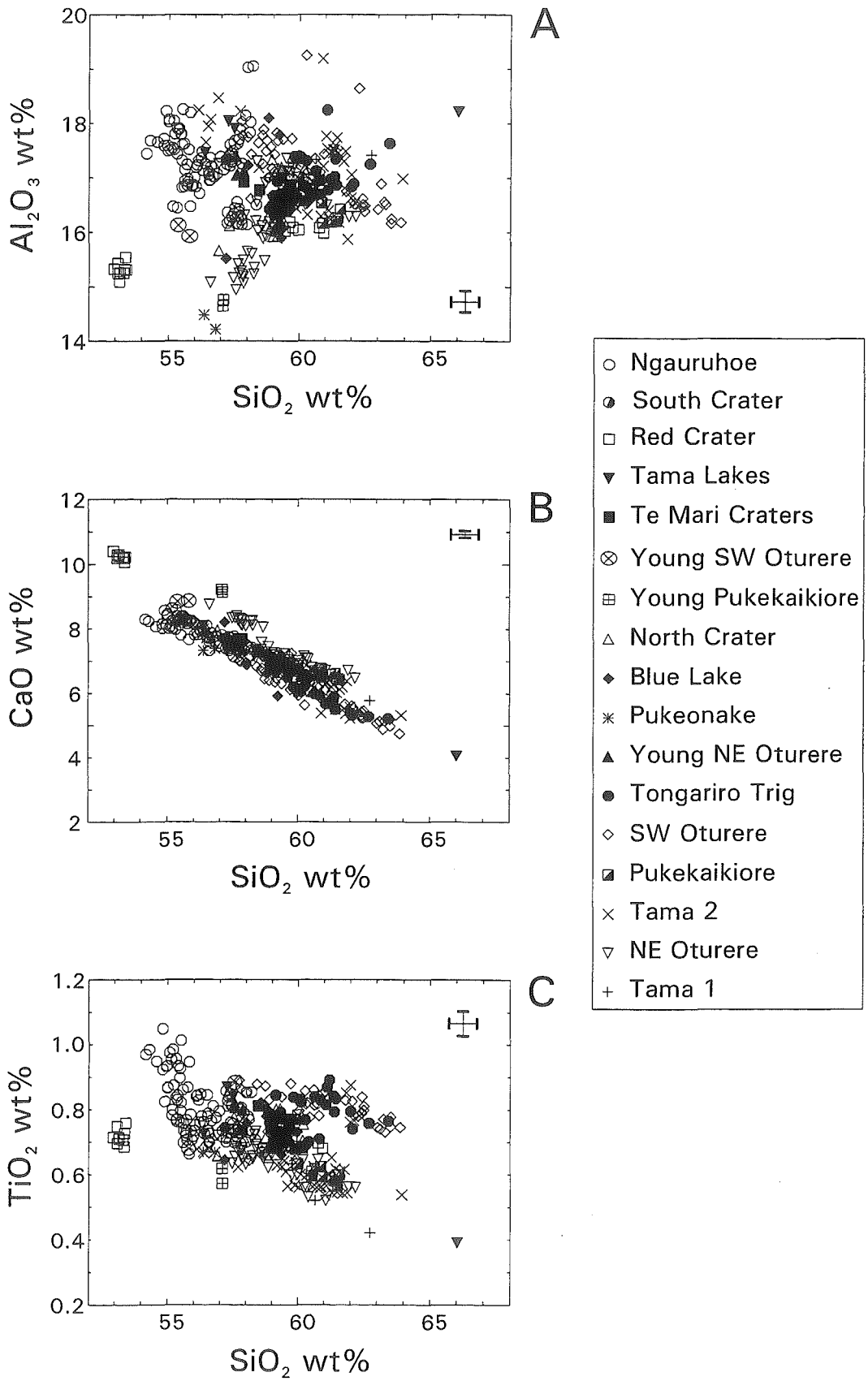

Figure 6.5 Major element concentrations in Tongariro eruptives (plotted according to volcano-stratigraphic unit) versus SiO_2. All data recalculated anhydrous. Error bars represent total error (2 sd from mean; Section A8.3.3).

samples from Pukeonake, Young Pukekaikiore, post-1.8 ka Red Crater, and part of NE Oturere; Section 4.4); but the majority of samples form a very broad family of weakly decreasing trends with increasing SiO_2. Tongariro Al_2O_3 concentrations are relatively high, ranging from 14.3 to 19.1 wt%; the few particularly high Al_2O_3 samples (TG174, 205, 508, Tn144d) may represent some plagioclase (and hornblende for Tn144d) accumulation, which is supported by petrographic observations. The scattered trend is also consistent with the samples not being derived from a single parent.

(b) Calcium. CaO (3.9-10.5 wt%) forms a relatively coherent negative trend when plotted against SiO_2 (Fig 6.5B), although certain volcano-stratigraphic units define separate sub-parallel trends, and the slightly higher-CaO trends of post-1.8 ka Red Crater, Young Pukekaikiore and NE Oturere are reflected in a higher relative proportion of clinopyroxene in the phenocryst assemblage (Section 4.4). The lowest CaO sample (Tn141a, Tama Lakes pumice) is also the highest SiO_2 sample, and indicates the continuation of the sub-linear trend into the data-poor dacitic end of the Tongariro compositional range (Fig 6.5B). The negative correlation between CaO and SiO_2 is consistent with fractionation of plagioclase and clinopyroxene. CaO/Al_2O_3 decreases with increasing SiO_2 (not shown), providing further evidence for significant clinopyroxene fractionation in association with plagioclase fractionation.

(c) Titanium. A rather complex pattern emerges on the TiO_2 versus SiO_2 variation diagram (Fig 6.5C), for which variable Ti-magnetite and ilmenite abundances are probably at least partly responsible. This diagram also suggests clearly that different volcano-stratigraphic units of similar age represent different magma batches (even when close in age). The post-1.8 ka Red Crater samples sit in a comparatively low TiO_2 position relative to their SiO_2 content, whereas the Ngauruhoe lavas have much higher TiO_2 concentrations (maximum 1.1 wt%) which define a sharply decreasing TiO_2 trend with increasing SiO_2 (Fig 6.5C). This decreasing trend is generally followed by most other Tongariro samples, except some from Tongariro Trig, SW Oturere and Tama 2 which remain at relatively constant TiO_2 values until around 62 wt% SiO_2 where they begin to decrease in a trend roughly paralleling the main trend (Fig 6.5C). This broad envelope of decreasing trends is rather poorly represented at the high SiO_2 end by three scattered

samples (Fig 6.5C); Tn89 (Tama 1), Tn144e (Tama 2), and the lowest (0.4 wt%) TiO_2 sample Tn141a (Tama Lakes).

(d) Iron. Like CaO, Fe_2O_3* (total iron expressed as Fe_2O_3) forms a relatively tight cluster of decreasing (slightly concave upward) sub-linear trends with increasing SiO_2 (Fig 6.5D), consistent with removal of pyroxene and Fe-Ti oxide phases (sometimes along with olivine or hornblende) by fractional crystallization. Fe_2O_3* contents vary from 3.7 wt% (Tn141a, Tama Lakes) to 9.8 wt% (TG342, Red Crater dike).

(e) Manganese. MnO data are the least precise of all the major elements and analytical data are rounded to 0.01 wt%, but despite this limitation it is clear that an overall trend of decreasing MnO with increasing SiO_2 exists (Fig 6.5E), reflecting fractionation of the same mineral phases responsible for the Fe_2O_3* trend. The Tama Lakes pumice, Tn141a, has noticeably higher MnO than expected if it were to follow the overall negative correlation.

(f) Magnesium. MgO is one of the better major element discriminators between volcano-stratigraphic units, and the MgO-SiO_2 plot was therefore chosen as a basis for comparison between units in Section 6.6. An overall negative correlation and slightly concave downward curvilinear trend is evident on the MgO-SiO_2 variation diagram (Fig 6.5F), but data plot in several distinct trends and clusters and note that at any one value of SiO_2 there is a correspondingly wide range in MgO concentrations (particularly for the least silicic lavas).

MgO contents range from the anomalously high Pukeonake lavas and scoria (TG279-280) at 9.2 wt%, to a low of 1.1 wt% for the Tama Lakes pumice (Tn141a). The Ngauruhoe lavas plot in several different discrete groups and trends; the post-1.8 ka Red Crater lavas form their own separate group; NE Oturere lavas define a steeply decreasing trend; Tongariro Trig, SW Oturere and Tama 2 lavas lie on more shallow overlapping trends. To some extent the overall negative correlation between MgO and SiO_2 reflects fractionation of olivine and pyroxene. However, some of the low SiO_2 samples also have low MgO contents and the different groups cannot be logically related by fractional crystallization, suggesting that they represent different magma batches. There is not a

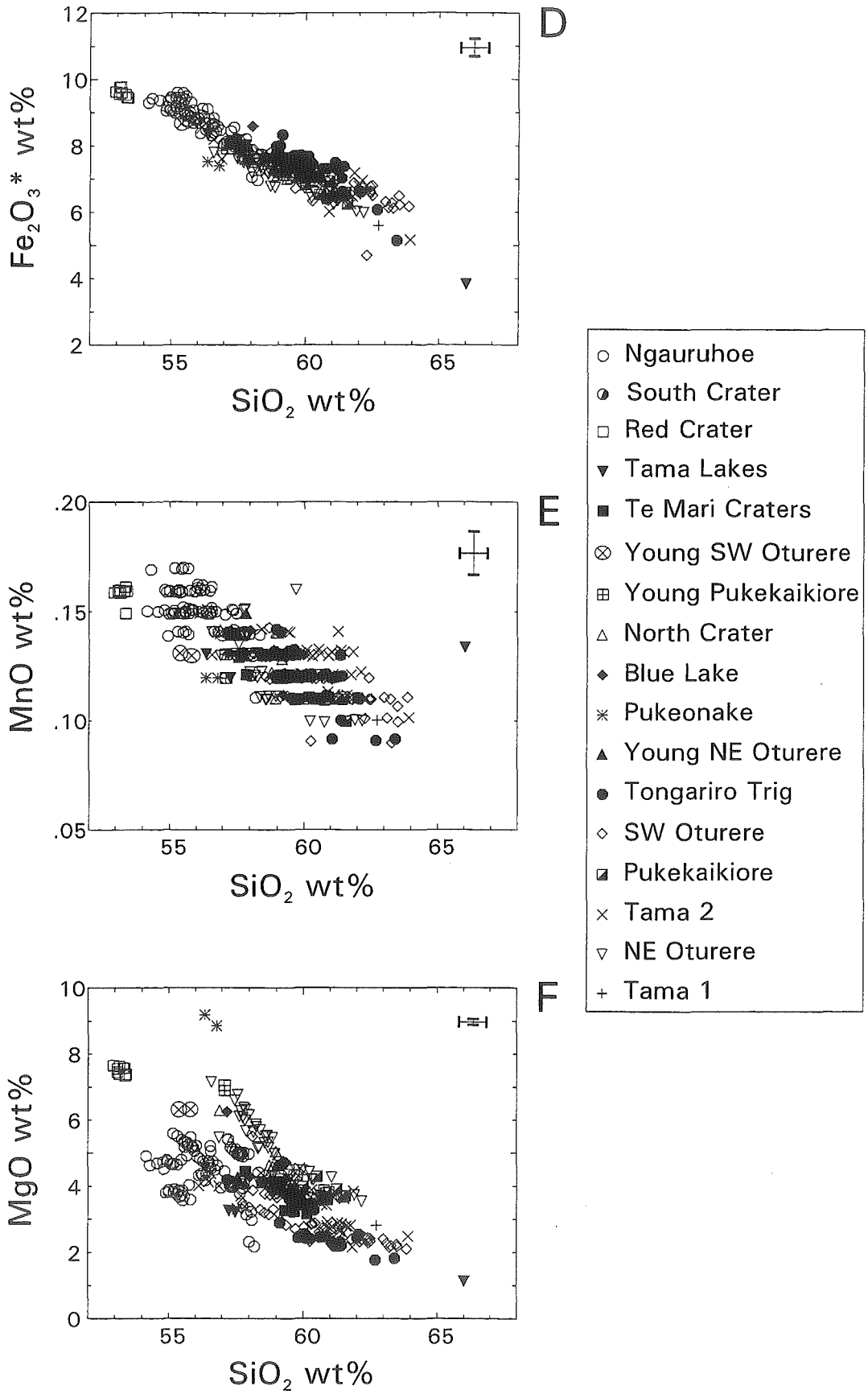

Figure 6.5 (continued) Major element concentrations in Tongariro eruptives (plotted according to volcano-stratigraphic unit) versus SiO_2. All data recalculated anhydrous. Error bars represent total error (2 sd from mean; Section A8.3.3).

particularly strong overall correlation between MgO and Fe_2O_3*, and iron does not appear to be as effective as MgO in distinguishing different magma batches.

(g) **Sodium.** The variation diagram for Na_2O versus SiO_2 (Fig 6.5G) shows an overall positive correlation, but a moderate amount of scatter does occur. Na_2O is generally incompatible with the fractionating mineral assemblage. Concentrations of Na_2O vary from 2.4 wt% (Red Crater and Young Pukekaikiore samples) to 4.0 wt% (Tama Lakes pumice). To a certain degree the dispersal on the Na_2O-SiO_2 plot corresponds with different volcano-stratigraphic units. In particular, some of the Ngauruhoe lavas have notably high Na_2O contents relative to their low SiO_2, and the SW Oturere lavas define a trend of high and relatively constant Na_2O (above the Tongariro positive main trend) across a SiO_2 range of 57.2 to 63.5 wt%.

(h) **Potassium.** K_2O shows a stronger positive correlation with SiO_2 (Fig 6.5H) than does Na_2O, indicating that it behaves even more incompatibly. Several different subparallel trends are apparent - particularly in the hornblende-bearing lavas from Pukekaikiore, Tama 2 and Tama 1 which form separate K_2O trends below the main envelope of data points. The lowest K_2O concentrations occur in the post-1.8 ka Red Crater lavas (minimum of 0.6 wt%), and the highest in Tongariro Trig and SW Oturere lavas (up to 2.2 wt% K_2O).

(i) **Phosphorous.** Considerable scatter marks the P_2O_5 versus SiO_2 variation diagram (Fig 6.5I), and it is not possible to make any general conclusions from this plot. There is no pronounced trend inflection to indicate a uniform onset of apatite crystallization. However, apatite phenocrysts have been noted in some Tongariro lavas (Section 4.5.6) and the variable P_2O_5 concentrations evident on Figure 6.5I are probably representative of variable apatite fractionation and possibly some apatite accumulation. P_2O_5 contents range from 0.08 wt% (Young Pukekaikiore) to 0.22 wt% (Ngauruhoe).

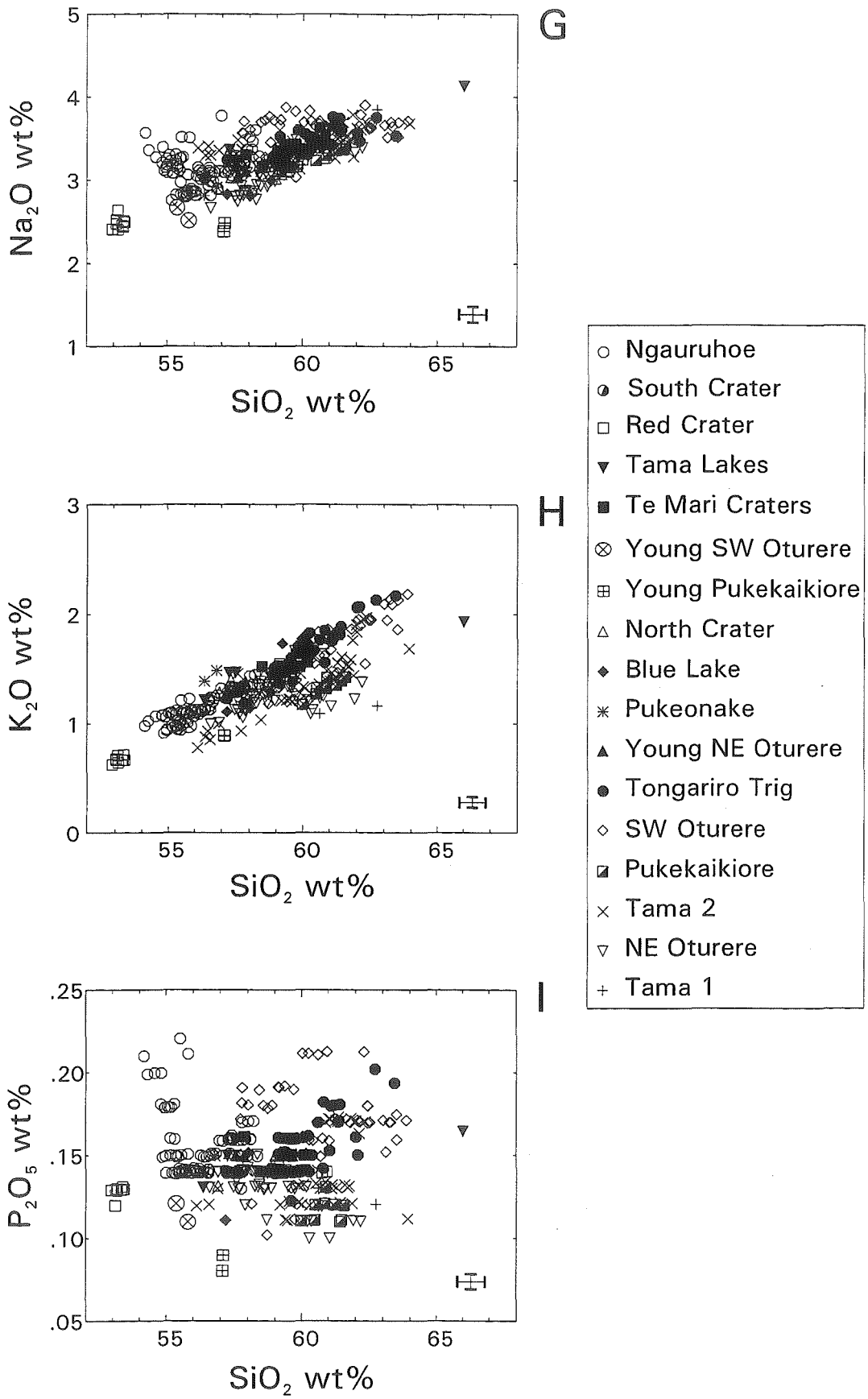

Figure 6.5 (continued) Major element concentrations in Tongariro eruptives (plotted according to volcano-stratigraphic unit) versus SiO_2. All data recalculated anhydrous. Error bars represent total error (2 sd from mean; Section A8.3.3).

6.5.2 Trace elements

All Tongariro rocks have been analysed for 16 trace elements (V, Cr, Ni, Zn, Ga, Rb, Sr, Ba, La, Ce, Nd, Y, Zr, Nb, Pb, Th) using the Canterbury University XRF facility. As reported in Appendix 8, precision varies for the different elements and some have been disregarded in Chapter 7 discussions in favour of more precise data obtained from another XRF facility (Royal Holloway, University of London) or from INAA (University of Massachusetts). The low precision elements La, Ce, Nd, Nb, Pb and Th are therefore not discussed directly in this chapter.

This section therefore serves to introduce the overall trace element composition of Tongariro eruptives and comment on broad trends, but limitations imposed by the varying data quality restrict interpretations to the general only. Compared to the major elements (Section 6.5.1), the trace elements show more scatter and more variable compositions when plotted against SiO_2. However, for the majority of trace elements the scatter in data points is beyond total analytical error as indicated by the error bars included on the plots. This supports the contention that the overall Tongariro data set represents many different magma batches (Section 6.5.1).

In summary, compatible behaviour is displayed by V, Cr and Ni which all decrease with increasing SiO_2 - although there are some aberrations from this overall trend. The large-ion-lithophile elements (LILE) of Rb and Ba display strong positive correlations with SiO_2, whereas Sr shows variable to constant trends with increasing SiO_2. Although considerable scatter (due to low precision) is present on variation diagrams of the light rare earth elements (REE) La, Ce and Nd, positive correlations with SiO_2 are evident. Likewise, when plotted against SiO_2 the heavy field strength elements (HFSE; Y, Zr and Nb) form variably defined positive trends. The incompatible elements exhibit varying enrichment factors; for example, Zr increases two-fold whereas Rb and Ba increase four-fold with increasing SiO_2.

(a) **Vanadium.** V contents range from 41 to 270 ppm, and correlate negatively with SiO_2 in a moderately well-defined sub-linear trend (Fig 6.6A). This compatible behaviour reflects substitution for Fe^{3+}, mainly in magnetite (Kd_V=30; compilation of Gill,

1981) but also in hornblende (Kd_V=32; compilation of Gill, 1981) for those magmas (from e.g. Tama 2, Pukekaikiore) which have experienced amphibole fractionation. The trends in V concentrations parallel those of Fe_2O_3* and TiO_2 abundances. The decrease in V from low to high SiO_2 compositions is quite regular, indicating the importance of early magnetite crystallization (Section 4.1). Scatter in the V-SiO_2 trend corresponds to some extent with different volcano-stratigraphic units.

(b) **Chromium.** The Cr-SiO_2 variation diagram (Fig 6.6B) shows a series of relatively steeply curved trends with Cr abundances decreasing rapidly from >200 ppm (up to 267 ppm for post-1.8 ka Red Crater and 460 ppm for Pukeonake) to values of <20 ppm (minimum of 3 ppm) in the flat part of the trend. This pattern demonstrates that the partition coefficient for Cr is >>1 for mafic minerals, with early removal of Cr via chrome spinel (Section 4.5.5b), pyroxene (Section 4.5.3), olivine (Section 4.5.1), Fe-Ti oxides (Section 4.5.5a), and hornblende. Most (but certainly not all) Tongariro rocks contain less than 100 ppm Cr, indicating that Tongariro magmas are fractionated relative to primary magmas.

As is the case for the MgO variation diagram (Fig 6.5F), there is a range in Cr abundances at any given SiO_2 content (except for the highest SiO_2 end) which correlates with the different volcano-stratigraphic units (Section 6.5.1f). The general trends and relationships between units are very similar on the two plots, and demonstrate the importance of mafic silicate phases in consistently differentiating the various magma batches involved in Tongariro petrogenesis. And as is the case for MgO, fractional crystallization cannot be invoked to simply relate the different groups evident on the Cr variation diagram, since some of the lowest SiO_2 samples also have the lowest Cr (and MgO) concentrations (e.g. one Ngauruhoe group).

(c) **Nickel.** Ni trends follow a similar pattern to Cr when plotted against SiO_2 (Fig 6.6C), although higher concentrations are not so prominent. There is a distinct break between the highest Ni contents of 220 ppm (Pukeonake) and the majority of Tongariro samples which contain less than 50 ppm Ni (the minimum of 3 ppm Ni occurs in a Tongariro Trig lava). Moderately curved decreasing Ni trends are still evident, however, and volcano-stratigraphic units and separate magma batches can be distinguished (although

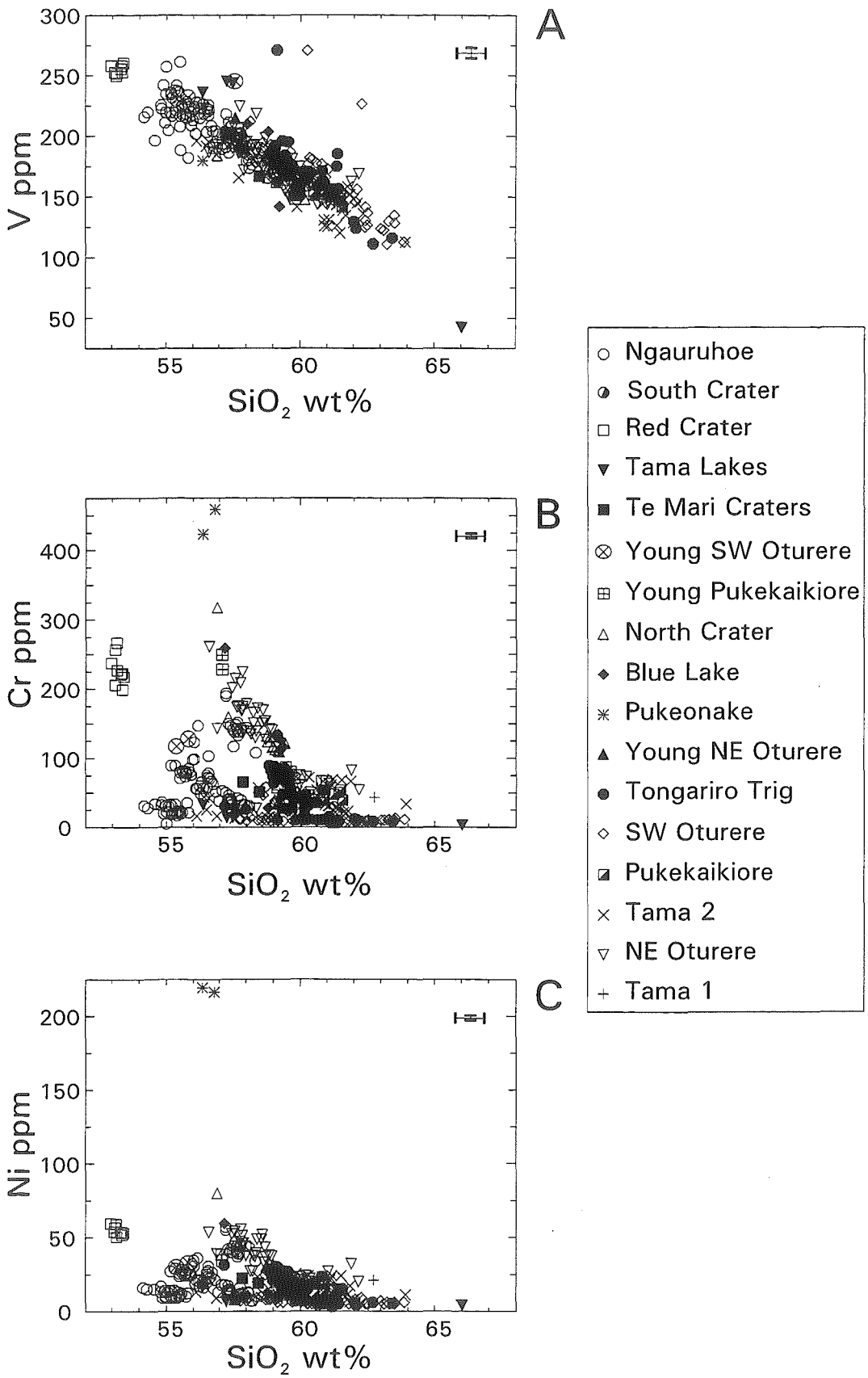

Figure 6.6 Trace element concentrations in Tongariro eruptives (plotted according to volcano-stratigraphic unit) versus SiO_2. All data recalculated anhydrous. Error bars represent total error (2 sd from mean; Section A8.3.3).

not to the extent as seen in MgO and Cr variation diagrams). Ni is extracted from magmas during early crystallization of particularly olivine (Kd_{Ni}=58, Luhr and Carmichael, 1980; Section 4.5.1), but also oxide and pyroxene phases, and the relatively low Ni values of most Tongariro rocks indicate that they have experienced considerable fractionation.

(d) Zinc. Zn contents in Tongariro andesites vary between 54 and 101 ppm, and show considerable scatter (partly attributable to analytical error) on a plot of Zn versus SiO_2 (Fig 6.6D). No particular trend is evident for the basaltic andesites, but the andesite-dacite compositions generally display a decrease in Zn with increasing SiO_2. Zn is not a useful discriminant of volcano-stratigraphic units. Higher precision analyses of Zn were obtained from the Royal Holloway XRF (Appendix 8, Section A8.5).

(e) Gallium. The scattered variation diagram for Ga (not shown) does not reveal any trend, and Ga concentrations vary between 12 and 25 ppm Ga over the entire Tongariro compositional range.

(f) Rubidium. Rb exhibits incompatible behaviour in Tongariro magmas, with a sharp increase in Rb contents corresponding to increasing SiO_2 (Fig 6.6E). Post-1.8 ka Red Crater eruptives contain the lowest Rb concentrations (minimum of 18 ppm), and Tongariro Trig and SW Oturere lavas are the most enriched in Rb (up to 80 ppm). For any given SiO_2 content, however, there exists a range of Rb abundances (as also occurs particularly for MgO and Cr). A number of sub-parallel trends can be distinguished on the Rb-SiO_2 plot (Fig 6.6E), and the distribution of volcano-stratigraphic units into these trends closely mirrors the pattern evident on the K_2O variation diagram (Fig 6.5H).

(g) Strontium. Sr contents do not show a systematic relationship with SiO_2 and many different clusters of data points and short linear trends are evident on the Sr-SiO_2 variation diagram (Fig 6.6F). The lower part of the diagram is rather crowded because of the need to accommodate the very high Sr (643 ppm) Young Pukekaikiore rocks. The lower Sr contents (194 to 408 ppm) of the rest of the Tongariro eruptives reflect substantial removal of plagioclase (Kd_{Sr}=1.6-2.8; compilation of Rollinson, 1993), consistent with petrographic observations. When the pattern is examined in detail for particular stratigraphic units, a decrease in Sr with increasing SiO_2 is exhibited by some, others define

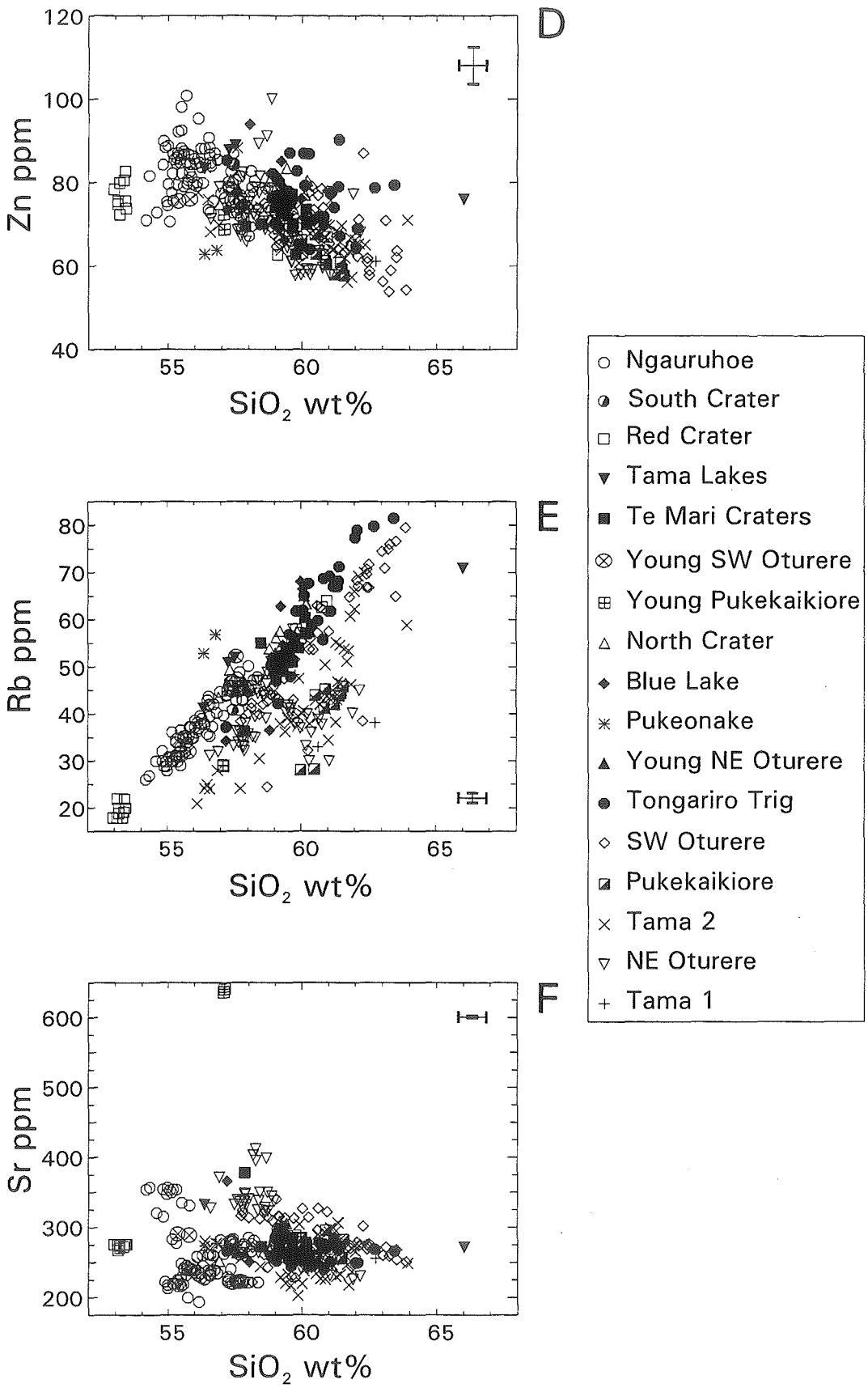

Figure 6.6 (continued) Trace element concentrations in Tongariro eruptives (plotted according to volcano-stratigraphic unit) versus SiO_2. All data recalculated anhydrous. Error bars represent total error (2 sd from mean; Section A8.3.3).

constant abundance trends, and yet others are highly scattered.

(h) **Barium.** Ba behaves incompatibly in Tongariro magmas, showing on a plot against SiO_2 (Fig 6.6G) the most coherent (although still scattered) positive linear trend of all the trace elements. Ba increases fairly regularly in concentration from a low of 117 ppm (post-1.8 ka Red Crater) up to 454 ppm (Tongariro Trig), apart from the Tama 2 ignimbrite (Tn144d) which is particularly enriched in Ba (561 ppm). Several samples also fall noticeably below the main broad trend on the Ba-SiO_2 variation diagram.

(i) **Yttrium.** Y concentrations vary from 14 to 57 ppm but remain relatively constant throughout the Tongariro SiO_2 range, with the majority of samples containing between 18 and 25 ppm Y (Fig 6.6H). A very subtle bias towards higher Y contents in the higher SiO_2 andesites and the dacites imparts a slightly positive overall correlation between Y and SiO_2. The amphibole-bearing lavas tend towards slightly lower Y abundances than other Tongariro eruptives. Royal Holloway XRF analyses of Y were found to be somewhat more precise than those obtained at Canterbury (Appendix 8; Chapter 7).

(j) **Zirconium.** Zr generally behaves incompatibly in Tongariro magmas, but the scatter about the overall positive trend greatly exceeds analytical error (Fig 6.6I) and instead is suggestive of different volcano-stratigraphic units and multiple magma batches. In particular, a group of Ngauruhoe analyses plots in a relatively high Zr position on the variation diagram relative to their low SiO_2 contents. In contrast, samples from Young Pukekaikiore, Pukekaikiore, Tama 2 and Tama 1 have comparatively lower concentrations of Zr than the main envelope of data points. It is possible, however, that Zr may be weakly compatible in some of these magmas, especially in those containing hornblende (Kd_{Zr}=1.4; Pearce and Norry, 1979). Overall, Zr abundances vary from 72 ppm (post-1.8 ka Red Crater basaltic andesite) to 156 ppm (SW Oturere dacite).

6.5.3 Elemental ratios

Rb/Sr ratios vary from 0.05 to 0.32 and show an overall increase with increasing SiO_2, although a scatter in this positive trend can be correlated with different subparallel

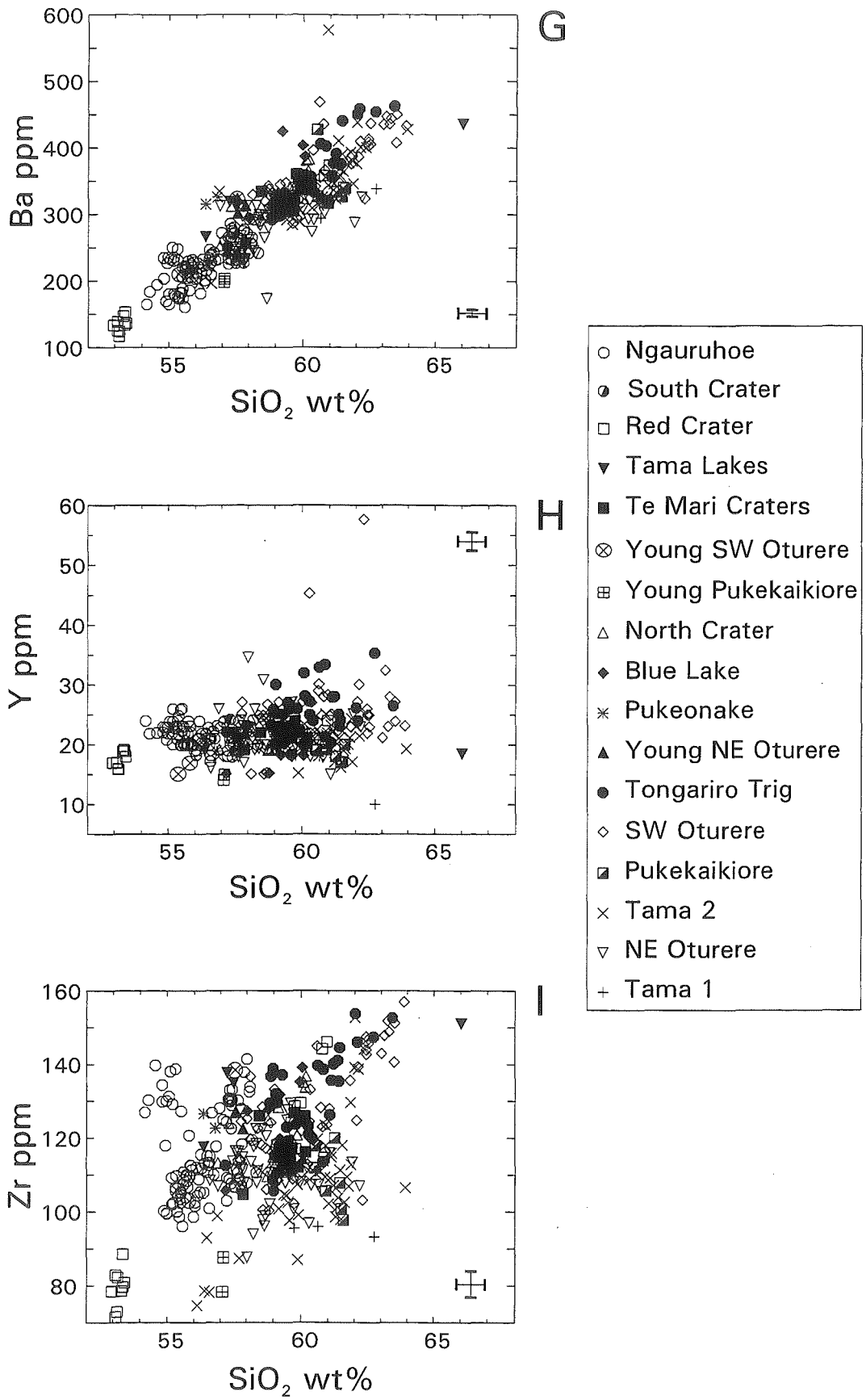

Figure 6.6 (continued) Trace element concentrations in Tongariro eruptives (plotted according to volcano-stratigraphic unit) versus SiO_2. All data recalculated anhydrous. Error bars represent total error (2 sd from mean; Section A8.3.3).

and partly overlapping trends of the different units (Fig 6.7A). For example, magmas from Ngauruhoe and other young eruptives have relatively high Rb/Sr ratios, whereas some of the older cones (e.g. Tama 1, NE Oturere, Tama 2 and Pukekaikiore) have comparatively low Rb/Sr ratios (Fig 6.7A). K/Rb ratios range from 401 to 210, showing a general decrease with increasing SiO_2 (Fig 6.7B). It is evident from the scattered groupings on Figure 6.7B that different units have different K/Rb ratios. Notably, the hornblende-bearing samples of Tama 1, Tama 2 and Pukekaikiore have distinctly higher K/Rb ratios than most other Tongariro units, indicating that relatively high K/Rb magmas are required before hornblende can crystallize. K/Ba ratios (not shown) vary from 57 to 21 and show a broadly decreasing trend with increasing SiO_2, but do not serve to distinguish volcano-stratigraphic units from each other particularly well.

A Rb versus Zr plot of Tongariro data (Fig 6.8A) shows considerable variation in Rb/Zr ratios (0.20-0.55), in part correlated with different volcano-stratigraphic units. Although many units exhibit a broad range in Rb/Zr ratios, within some units there are distinctive groupings of samples distinguished by contrasting Rb/Zr values (e.g. Red Crater, Section 6.6.8i; Ngauruhoe, Section 6.6.8k). Low Ba/Zr ratios (<2.5) distinguish Ngauruhoe and post-1.8 ka Red Crater lavas from other Tongariro eruptives (Ba/Zr mostly 2.5-5), but Ba is generally not as useful as Rb in discriminating between volcano-stratigraphic units. Ti/Zr ratios appear to distinguish Tongariro volcano-stratigraphic units to a certain extent (Fig 6.8B), and have an overall range of 15-58.

The patterns for individual units and the process or processes which may be responsible for these varying incompatible ratios are discussed in Section 6.6 and Chapter 7. Rb and Zr are assumed to be nearly equally incompatible (estimated bulk partition coefficients close to zero) particularly in the basaltic andesites (and most andesites) where plagioclase is the main fractionating phase and hornblende is absent. Therefore the range in Rb/Zr cannot be attributed to fractional crystallization processes and instead may be a result of variable degrees of partial melting or variable crustal contamination. Radiogenic isotope compositions provide a means by which these two processes may be distinguished (Section 7.4).

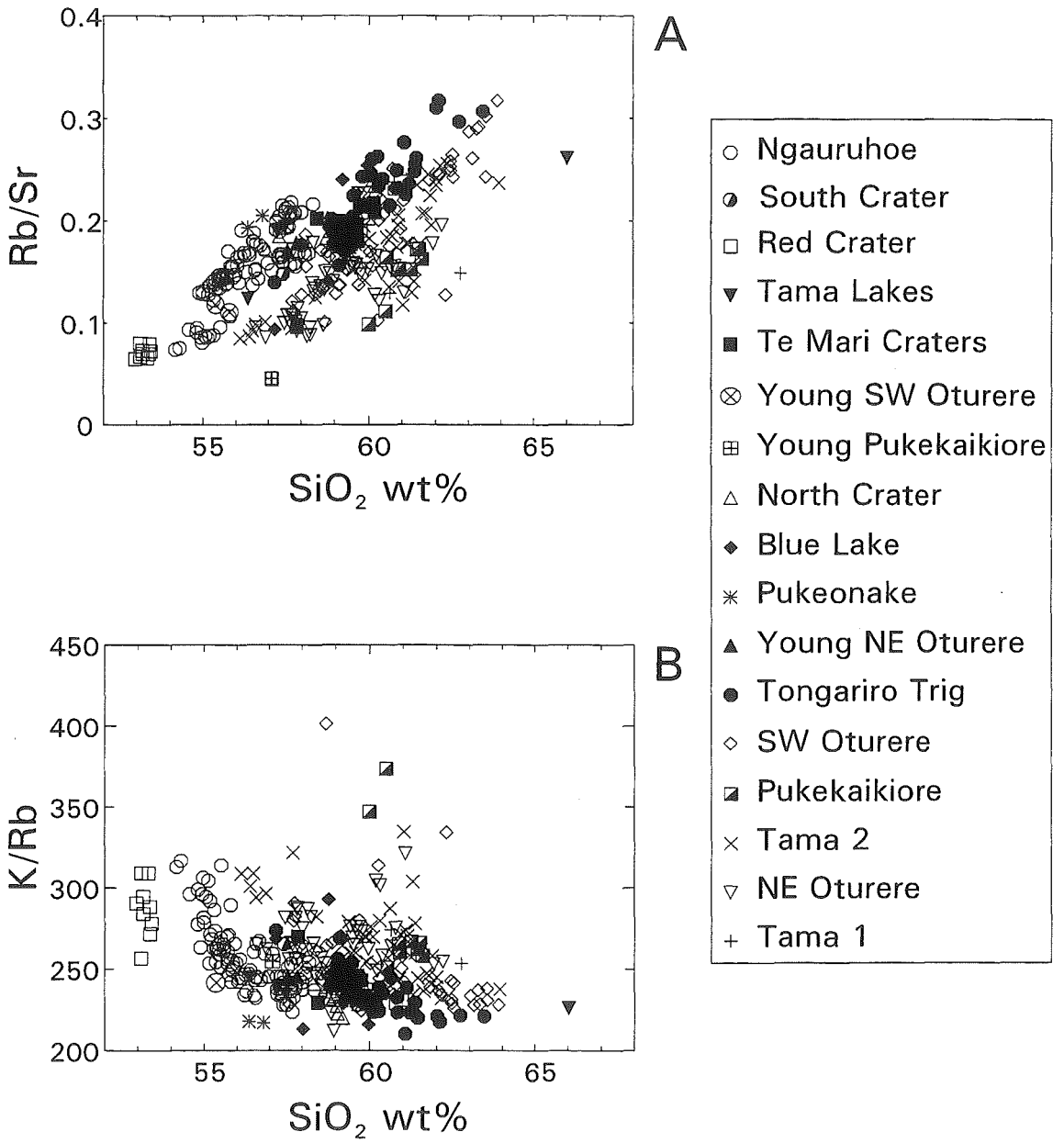

Figure 6.7 Rb/Sr (A) and K/Rb (B) ratios of Tongariro eruptives (plotted according to volcano-stratigraphic unit) versus SiO_2. All data recalculated anhydrous.

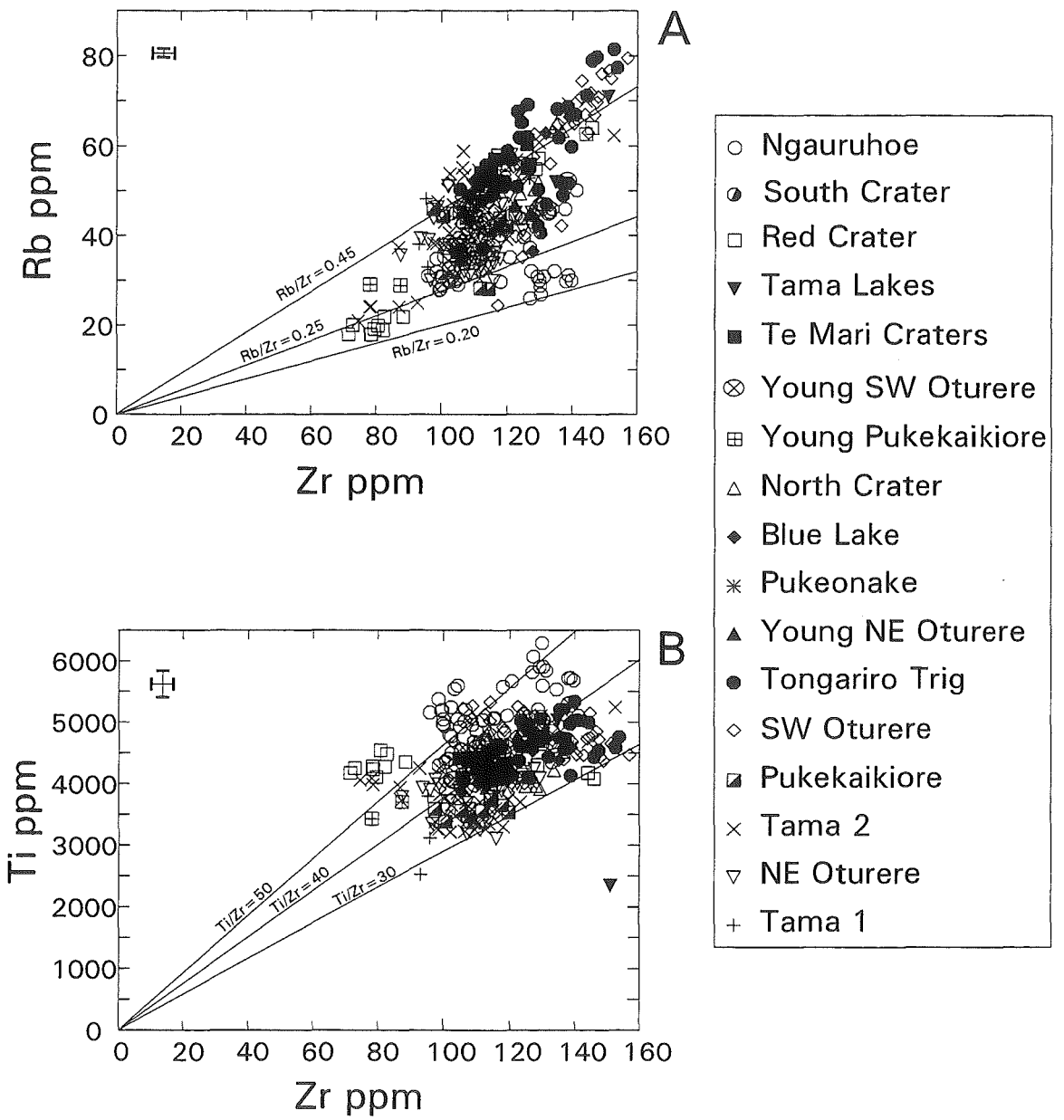

Figure 6.8 Rb versus Zr (**A**) and Ti versus Zr (**B**) for Tongariro eruptives (plotted according to volcano-stratigraphic unit). Selected constant ratio lines are shown. All data recalculated anhydrous. Error bars represent total error (2 sd from mean; Section A8.3.3).

6.6 CHEMICAL COMPOSITIONS AND RELATIONSHIPS OF VOLCANO-STRATIGRAPHIC UNITS

6.6.1 Introduction

In this section, the focus shifts from the broad overview taken in Section 6.5 of the chemical composition of all Tongariro eruptives, down to the level of each volcano-stratigraphic unit. Here it is possible to trace changes and similarities in the units' geochemical characteristics throughout the eruptive history of Tongariro Volcanic Complex. There is the opportunity to assess the degree of chemical 'order' on various temporal and spatial scales, i.e., compositional relationships between groups of units of similar age or area, between individual units, within one unit, and - for some of the young eruptives - between different historic eruptive units. Patterns on all these scales have been identified for Tongariro, and are described in the following sections.

The approach taken involves using the MgO-SiO_2 variation diagram as a basis for initial comparison between units, and with the overall Tongariro field of data (already presented in Section 6.5). As the units are described from the oldest to youngest, the fields of the previous units are overlain on the data points of the unit being described. This provides a relatively clear and accessible way of obtaining a feel for the gross geochemical relationships between units. For clarity, the fields of the older units are differentiated by colour at first, but then only outlined when the numerous coloured fields of the young eruptives are introduced. Besides the MgO-SiO_2 plot, selected diagrams illustrating key features are also presented (or the appropriate diagram from Section 6.5 is referred to), and the relative element abundances and chemical trends of the units are compared.

For each unit, any correlation between chemical composition and eruptive style, internal stratigraphy, cone volume, eruptive rate, mineralogy, and magmatic intensive parameters is assessed. Where sufficiently thick continuous sequences have been sampled, chemical stratigraphy diagrams are used to further highlight compositional trends with time. Where mineral compositional data are available, preliminary geochemical modelling, in the form of major element least-squares mixing calculations, is carried out to test the viability

of relating certain samples by closed system fractional crystallization. Procedures and results of this modelling are presented in Appendix 12.

Major elements are generally not significantly affected by open system processes and therefore in some cases the least-squares modelling may suggest a direct fractional crystallization relationship between magmas, whereas the trace element and isotope data (because they are more affected by open system processes) may negate the simple fractional crystallization model. Also, some least-squares models may not yield acceptable results, implying that other processes (such as crustal contamination, magma mixing) may be involved, or that the two magmas are not closely related. For these reasons, least-squares modelling referred to in this chapter provides only a first order approximation of the processes which may or may not be responsible for the chemical compositions and magmatic trends displayed by Tongariro lavas and pyroclastics. This theme is explored in more detail in Chapter 7, where trace element and isotopic compositions are used to refine the models.

6.6.2 Tama 1

(a) **Introduction and chemical characteristics.** The oldest (215-275 ka) exposed lavas on the Tongariro complex, from the small volume Tama 1 cone in the south (Section 3.5.2), have relatively high SiO_2 (59.5-62.6 wt%) and low MgO (2.8-3.8 wt%) contents compared to the overall Tongariro field (Fig 6.9A). The more evolved compositions of these holocrystalline, strongly porphyritic lavas are consistent with the dome-building eruptive style displayed by the cone, although note that the analysed samples are andesites rather than dacites. Other distinctive geochemical characteristics of these Tama 1 lavas (particularly Tn89) are their relatively low La, Ce, Y and Zr concentrations when compared to the overall Tongariro field (e.g. Figs 6.6H-I); features suggestive of relatively compatible behaviour during hornblende fractionation (e.g. Section 6.5.2j). Whole-rock analyses of pre-Tama Lakes lavas (D2, D11, D74) sampled by Wahyudin (1993) correspond to compositions determined for this study, and plot in a position intermediate between TG028 and TG136 on variation diagrams. This is consistent with the petrographic similarities noted in Section 4.4.2.

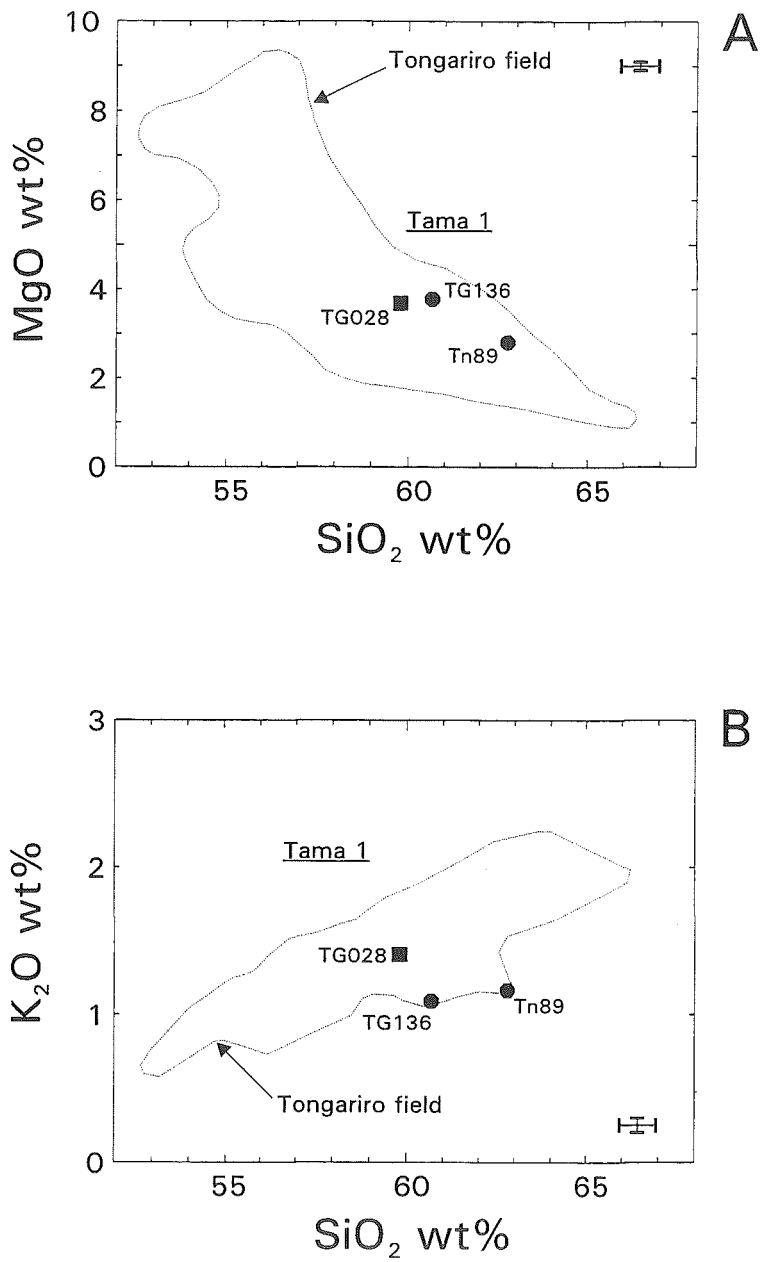

Figure 6.9 Variation diagrams for Tama 1 eruptives: (A) MgO versus SiO_2, (B) K_2O versus SiO_2. The compositional field for all Tongariro samples is shown for comparison. All data recalculated anhydrous. Error bars represent total error (2 sd from mean; Section A8.3.3).

(b) **Stratigraphic-compositional relationships.** With only three samples it is difficult to gain a sense of magmatic trends through time. The two oldest samples (TG136 and Tn89) are notable for their pale to dark green hornblende phenocrysts, and appear to be geochemically linked when MgO (Fig 6.9A), K_2O (Fig 6.9B), Cr, Rb (Fig 6.6E) and Ba are plotted against SiO_2. However, the youngest lava (TG028, which lacks hornblende) has lower MgO (Fig 6.9A) and Cr, and higher K_2O (Fig 6.9B), Rb and Ba than would be expected if it shared the same fractionation trend as the others. In addition, the two older lavas have significantly lower Rb/Sr (0.13-0.15) and higher K/Rb (253-274) ratios than the younger lava (Rb/Sr=0.19; K/Rb=242) (Fig 6.7).

(c) **Fractional crystallization models.** Modelling using least-squares mixing (Appendix 12) indicates that it is possible to obtain the Tn89 magma composition from fractional crystallization of the TG136 magma (removal of 13% [hbl+plag+opx] crystals; Model A12.1). The best-fit model produces a very low ΣR^2 of 0.03 and the calculated mineral proportions are similar to observed modal mineralogy. It is not geologically reasonable to model the more evolved TG136 and Tn89 as parental to the less evolved, younger TG028. Hence even with such limited sampling, at least two quite distinctive magma batches can be identified for the Tama 1 cone.

6.6.3 Northeastern Oturere

(a) **Introduction and chemical characteristics.** Approximately 8 km to the northeast of the Tama 1 vent (Fig 3.4), the NE Oturere sequence (Section 3.5.3) was built up between ?250 and 90 ka (although the main cone-building period was c.130-100 ka) from numerous basaltic andesite to andesite (55.4-62.2 wt% SiO_2) lava flows and pyroclastic deposits. Two distinctive curvilinear trends (A and B) are evident on the SiO_2-MgO variation diagram (Fig 6.10A):

A. a steeply-decreasing high-MgO trend (7.1-3.5 wt% MgO) spanning the entire NE Oturere SiO_2 range; and

B. a flatter, lower-MgO trend (4.2-3.5 wt% MgO) showing more limited SiO_2 variability (57.6-59.9 wt% SiO_2).

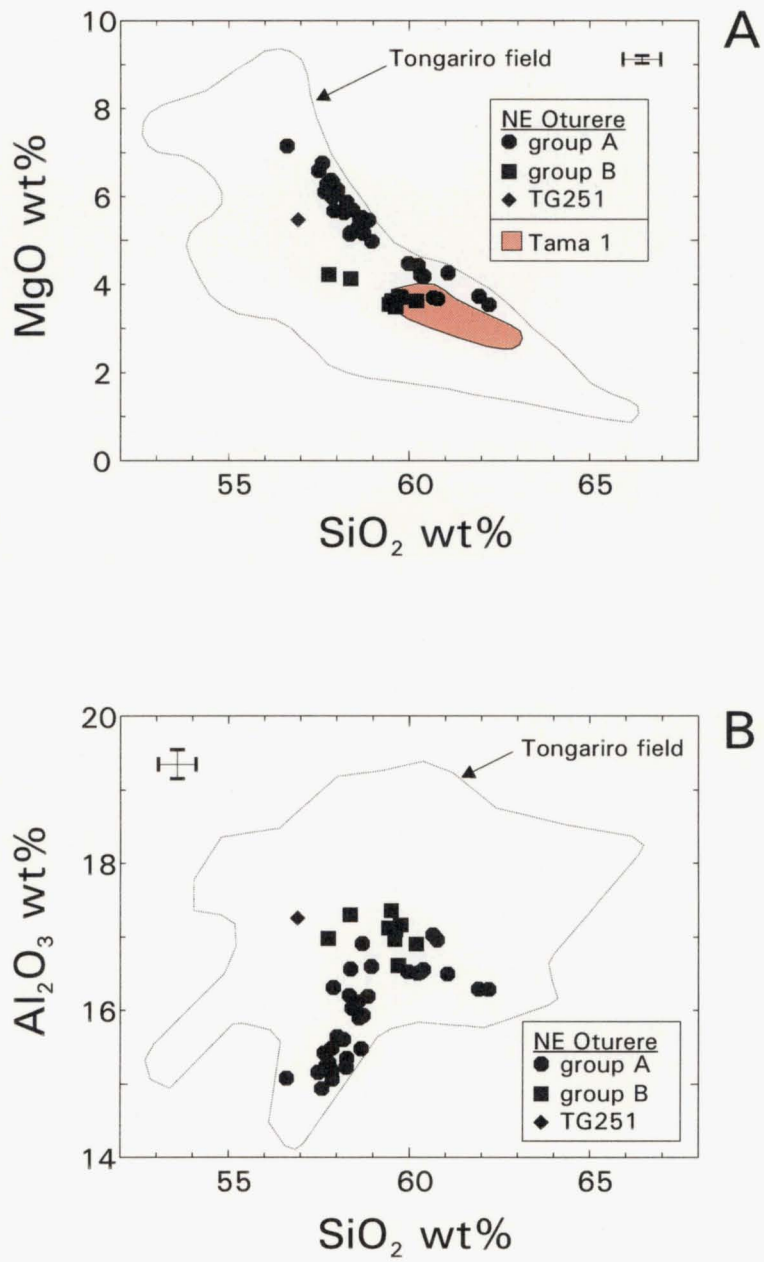

Figure 6.10 Variation diagrams for NE Oturere eruptives: (**A**) MgO versus SiO_2, (**B**) Al_2O_3 versus SiO_2. The compositional field for the older Tama 1 unit is shown in the MgO-SiO_2 diagram. The compositional field for all Tongariro samples is also shown for comparison. All data recalculated anhydrous. Error bars represent total error (2 sd from mean; Section A8.3.3).

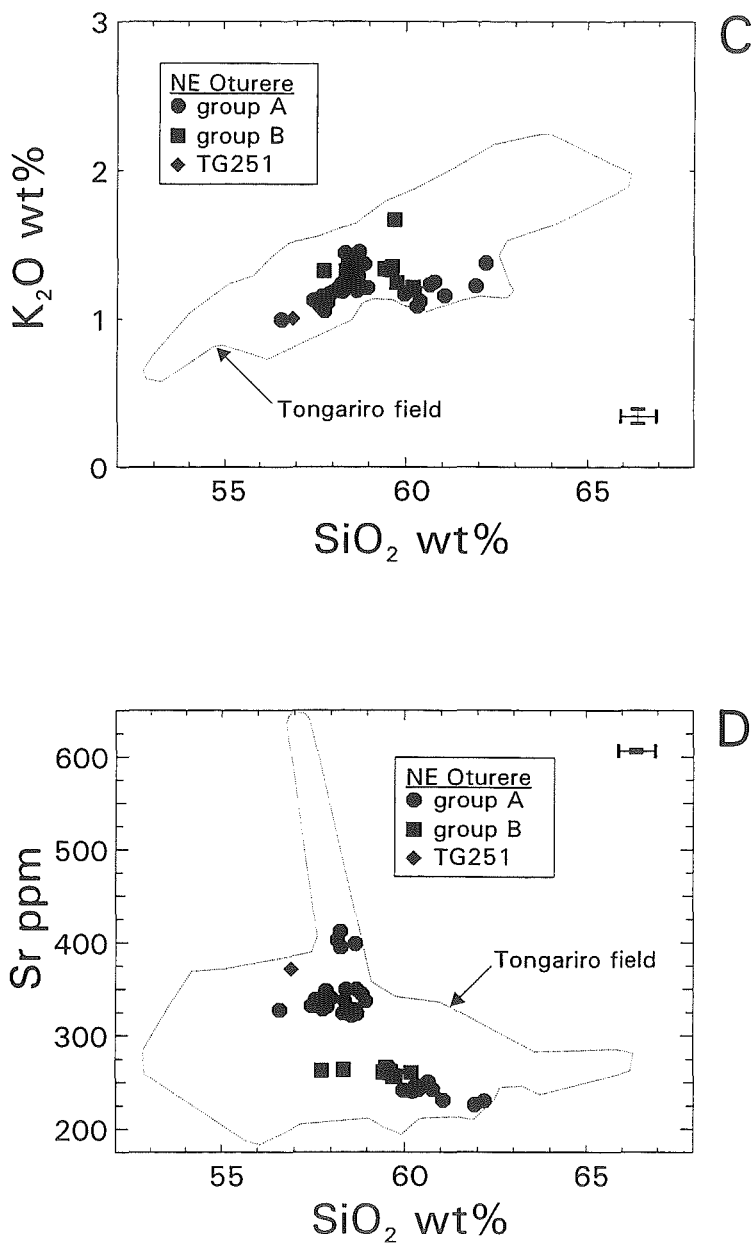

Figure 6.10 (continued) Variation diagrams for NE Oturere eruptives: (**C**) K_2O versus SiO_2, (**D**) Sr versus SiO_2. The compositional field for all Tongariro samples is also shown for comparison. All data recalculated anhydrous. Error bars represent total error (2 sd from mean; Section A8.3.3).

In addition to the samples plotting on the two main trends there is a basaltic andesite sample (TG251) which, because of inconsistent behaviour when other elements are plotted, is difficult to place in either group A or B. Apart from its relatively low MgO and high Al_2O_3, TG251 shares broadly similar chemical characteristics to samples from the lower SiO_2 part of group A (e.g. high Cr, Ni, Sr; see below).

Other chemical parameters serve to distinguish NE Oturere group A from group B, and these often also equate with petrographic differences. Samples plotting at the high-MgO end of trend A contain up to 5 modal% olivine phenocrysts whereas other NE Oturere eruptives are olivine-free. Compared to group B, group A samples also have higher concentrations of Cr (<260 ppm; Fig 6.6B) and Ni (<55 ppm; Fig 6.6C), among the highest of all the Tongariro eruptives. Dominance of clinopyroxene over orthopyroxene, especially in the group A basaltic andesites, reflects the higher CaO contents (<8.7 wt%) compared to other Tongariro eruptives of comparable SiO_2 (Fig 6.5B).

The Al_2O_3-SiO_2 variation diagram (Fig 6.10B) reveals a pattern of low and increasing Al_2O_3 contents for the group A basaltic andesites and low-SiO_2 andesites (which contain <10 modal% plag, cpx>plag), in contrast to the higher Al_2O_3, negative trend for the group A silicic andesites and group B andesites (which contain >15 modal% plag, plag>>cpx). K_2O (and Rb) contents show considerable variability; the group A silicic andesites define a lower K_2O (and Rb) trend than group B andesites and the less silicic samples of group A (Fig 6.10C). NE Oturere Sr contents are of interest because the lower SiO_2 part of group A are distinguishable by their very high Sr concentrations (326-408 ppm) from the rest of group A (225-253 ppm) and from group B (256-265 ppm) (Fig 6.10D). Most incompatible trace element ratios display considerable scatter when plotted against SiO_2 and do not show any marked differences between group A and B.

(b) **Stratigraphic-compositional relationships.** The detailed stratigraphy established for the NE Oturere cone (Appendix A2.16) does not correspond to neat divisions into chemical groupings. There are some correlations between stratigraphy and composition, however, such as the older eruptives from subunits 'f', 'g' and 'h' which plot as relatively coherent groups at the higher SiO_2 end of the range. In contrast, the large subunits 'd' and 'e' show considerable compositional diversity. There is also no simple

relationship between stratigraphy and the chemical groups A and B; group A comprises samples from nearly all subunits encompassing a wide age range, and group B represents a large geographic separation of samples from the upper valley subunit 'a' and parts of the lower valley subunits 'd', 'g' and 'h'.

(c) **Subunit 'd' chemical stratigraphy.** Stratigraphic trends in petrography for NE Oturere subunit 'd' eruptives were introduced in Section 4.8. Variation in major element and trace element composition throughout the section is now examined (Fig 6.10E). Numerous breaks and reversals in magma chemistry (beyond analytical error limits) up through the stratigraphy, or through time, are consistent with conclusions based on petrographic trends (Section 4.8) that this sequence of lava flows and pyroclastic deposits records frequent magma recharge and mixing events on a time scale of no more than thousands of years. The eruptives all plot along trend A on the SiO_2-MgO variation diagram (Fig 6.10A), except for TG114 (trend B) and TG251 (intermediate between A and B). That these geochemical groups (A, B and TG251) represent fundamental changes in magma dynamics can be demonstrated by the abrupt reversals apparent on the chemical stratigraphy plots (Fig 6.10E).

Lower sequence

Lavas of the lower sequence (TG114-119) are relatively uniform in composition with the exception of flow TG114 (from group B) at the base of the section which exhibits marked enrichment in SiO_2, Al_2O_3, K_2O, Rb, Ba, and Rb/Sr, and depletion in MgO, Cr, Ni, and Sr compared to the flows immediately above (Fig 6.10E). Petrographic evidence for magma mixing displayed by the overlying flow (TG115, Section 4.8) is also consistent with an influx of basic magma into the reservoir which produced TG114. The comparatively smooth compositional progression from TG115 to TG119 is interrupted at flow TG117 by pronounced spikes in the trend, particularly lower Ni and Zr, and higher Rb, Ba, Rb/Zr and Ti/Zr (Fig 6.10E), possibly signalling an additional small magma recharge event.

Middle sequence

The transition from the lower lava sequence to the middle scoria-dominated sequence does not coincide with major reversals in geochemical trends for many elements, except for a notable decrease in Ni and Zr, and increase in Sr concentrations between

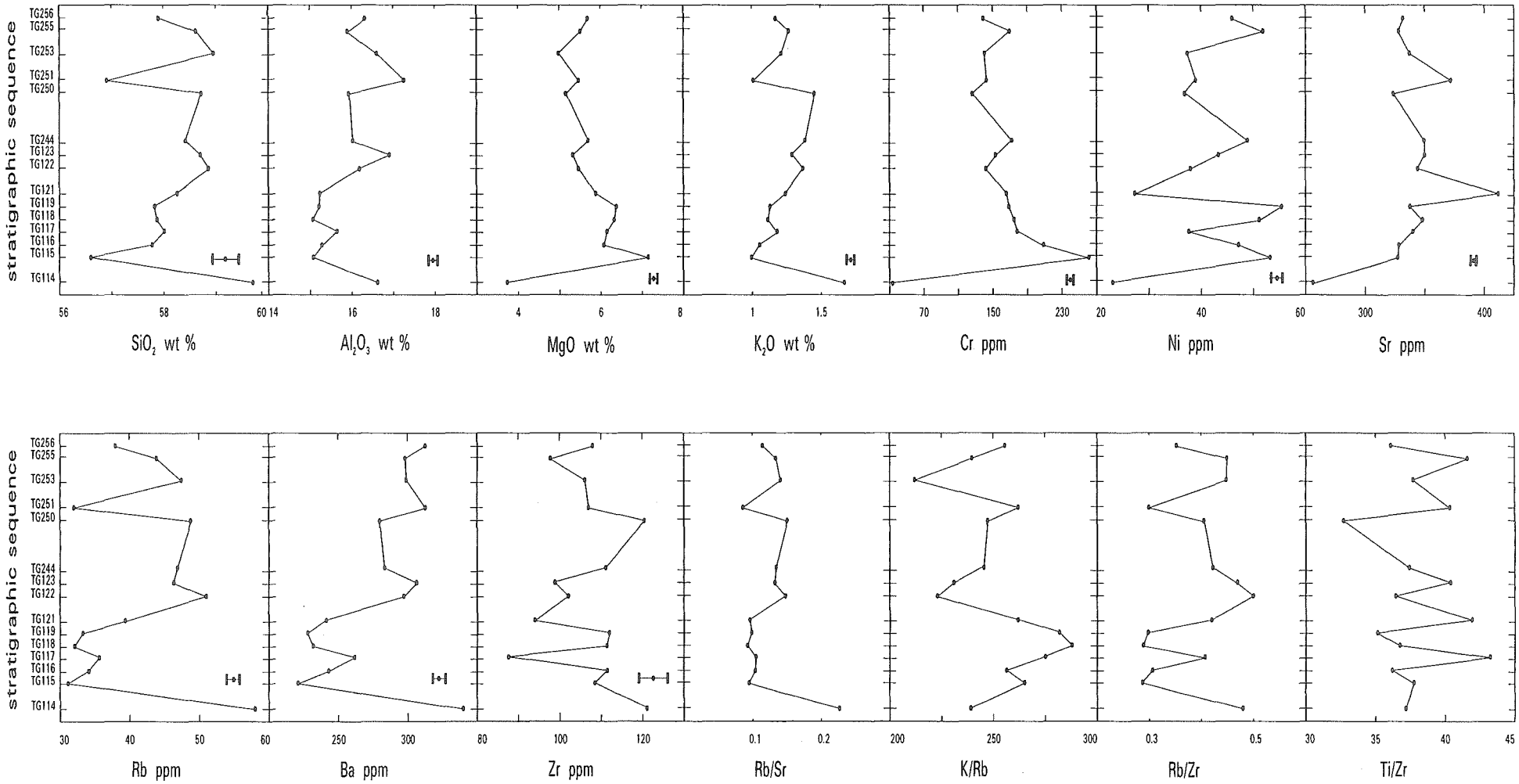

Figure 6.10 (continued) E. Selected whole-rock major and trace element compositions of NE Oturere subunit 'd' eruptives plotted in stratigraphic order. All data recalculated anhydrous. Error bars represent total error (2 sd from mean; Section A8.3.3). See Fig 4.45 for details of stratigraphic units and petrography.

TG119 and TG121 (Fig 6.10E), implying at least some compositional diversity between the lower and middle parts of the succession. The variability in Ni and Sr concentrations is reflected in the changing involvement of olivine and plagioclase, respectively, up through the section (Section 4.8). Within the middle scoria section, the intercalated lava flows (TG122-123) tend to have more evolved compositions than the scoria, creating breaks in the trends, especially for Al_2O_3, K_2O, Cr, Rb, and Ba (Fig 6.10E). Lack of chemical data for samples in the upper part of the middle sequence precludes a better understanding of these chemical trends.

Upper sequence

As for the lower-middle sequence boundary, the middle-upper sequence transition is not marked by many major compositional reversals, except for a decrease in Ni and Sr, and increase in Zr (the same elements noted for the lower boundary; Fig 6.10E). The upper sequence does not represent a simple fractional crystallization trend either, as indicated by decreasing SiO_2, K_2O, Rb, Zr, and increasing Ni up section (Fig 6.10E). In addition, striking inflections in the upper compositional trends are imparted by flow TG251, which is much lower in SiO_2, K_2O, Rb, and higher in Al_2O_3 and Sr compared to the flows between which it is sandwiched (Fig 6.10E). This case illustrates how fractional crystallization processes can render very compatible elements like MgO, Cr and Ni less capable of detecting new injections of basic magma (such as TG251), whereas Sr concentrations for example, retain strong evidence of the magma mixing event. TG251 is the other lava, along with TG114, which does not belong to the chemical group A which predominates in subunit 'd'. A complex magmatic plumbing system can thus be envisaged beneath NE Oturere cone over this time; eruptions mostly occurring from a constantly replenished group A type reservoir, but with occasional tapping of a group B type reservoir (or some chamber intermediate between the two).

Discussion

Thus the data suggest that rather than tapping one large, steadily evolving magma reservoir, multiple batches of magma have been erupted from a dynamic system over probably <10 ka. At least 5 cycles of basic magma influx and mixing are recorded over this time by subunit 'd'. Although the angular unconformities separating the three packages of eruptives do have certain petrographic significance (Section 4.8), they do not generally

correspond to petrological variability (which more often occurs within a package). Least-squares mixing calculations (see below) have shown that it is possible to relate the lower (TG115) to the middle (TG242) part of the subunit 'd' sequence by fractional crystallization, but this simplistic modelling obviously masks more complex chemical relationships which are suggested by the chemical stratigraphy plots in Fig 6.10E. Lack of mineral composition data for more of these subunit 'd' samples precludes in depth modelling of fractional crystallization links on a flow to flow basis. The influence of other processes on NE Oturere chemical stratigraphy, particularly magma mixing and crustal contamination, are discussed in Section 7.5.4.

(d) **Fractional crystallization models.** Step-wise least-squares calculations (Appendix 12) involving (from oldest to youngest) TG115-TG242-TG103 from trend A (models A12.2-A12.3) show satisfactory but not exceptionally good fits (ΣR^2=0.14-0.17) to fractional crystallization models, which require removal of 17% [plag+cpx+oliv+ilm] crystals from TG115 basaltic andesite and 30% [plag+opx+cpx+mag] crystals from TG242 andesite. Note, however, that calculated proportions of ferromagnesian silicate phases tend to differ from observed phenocryst proportions, and slight orthopyroxene accumulation is implied by model A12.2. Low K_2O (residual -0.33) in Model 12.3 suggests that crust needs to be added to the calculations; assimilation fractional crystallization (AFC) is probably a more realistic model than fractional crystallization for many Tongariro magmas. Lack of mineral composition data precludes similar fractional crystallization modelling of trend B. Modelling between A and B (e.g. TG115 initial magma to TG047 final magma) was not successful, producing poor fits of ΣR^2>0.2 and showing that group B magmas cannot be generated by fractional crystallization of group A magmas.

(e) **Relationship with older units and Tongariro complex in general.** The high-SiO_2 ends of both groups A and B overlap with the field for Tama 1 lavas (Fig 6.10A), which were erupted from a vent c.8 km to the SW prior to and during early NE Oturere activity. However, the NE Oturere eruptives show considerably more compositional variability than those from Tama 1, encompassing much lower SiO_2 and higher MgO compositions. Relative to the overall Tongariro field on the MgO-SiO_2 diagram, NE Oturere samples (especially those in group A) have MgO contents generally greater than those of other samples of comparable SiO_2 (Fig 6.10A).

(f) **Relationship between magma chemistry and eruptive style.** With respect to eruptive style, lava flow activity has been most commonly preserved in the NE Oturere stratigraphy and is represented by the entire compositional range of this unit. However the welded agglutinates and scoria deposits, reflecting hawaiian-strombolian explosive activity concurrent with lava extrusion in some localities, are confined to magma compositions of 57.3-58.8 wt% SiO_2 and 5.1-5.8 wt% MgO at the lower SiO_2 end of trend A (Fig 6.10A). Considering the much larger overall Tongariro field for these types of deposits (Fig 6.4), the narrow compositional range of the NE Oturere pyroclastics suggests that they may share a common magmatic history.

(g) **Summary.** Although the main theme to emerge from a study of NE Oturere chemical stratigraphy is one of multiple magma batches and magma mixing, the importance of fractional crystallization processes in generating NE Oturere magmas is also apparent from variation diagrams which show relationships between the main phenocryst phases (oliv, cpx, opx, plag) and chemical trends on variation diagrams (particularly of MgO, Cr, Ni, CaO, Al_2O_3, K_2O, Rb, Sr), and from least-squares modelling. Differences between groups A and B (and within group A) imply the presence of multiple magma batches with different fractionation histories. The strong petrographic evidence for magma mixing which is preserved in NE Oturere lavas (Section 4.4.3) indicates involvement of at least one other process (other than fractional crystallization), and this is supported by the complex series of compositional breaks and reversals seen on chemical stratigraphy plots. NE Oturere's magmatic stratigraphy and petrogenesis are examined in more detail in the light of precise trace element and isotope data in Section 7.5.4.

6.6.4 Tama 2

(a) **Introduction and chemical characteristics.** During early NE Oturere cone-building, at least 55 mostly hornblende-bearing lava flows were erupted at a relatively high rate (1 km^3/ka; Table 3.3) between 210 and 200 ka to form the Tama 2 cone in the south of the Tongariro complex, from a vent area c.4 km southwest of the NE Oturere vents (Fig 3.4; Section 3.5.4). These Tama 2 lavas exhibit noticeable major element variability

and do not always show tight trends on variation diagrams. However, it is possible to distinguish two groups on the MgO-SiO_2 diagram (Fig 6.11A):

A. andesites (most containing hornblende) which define a moderate- to high-SiO_2 (59.4-63.0 wt%) trend showing considerable scatter in MgO, decreasing from 4.5 wt% to 2.1 wt% with increasing SiO_2; and

B. a smaller group of hornblende-free basaltic andesites (and one andesite) of more restricted compositional range (56.4-57.5 wt% SiO_2 and 3.7-4.4 wt% MgO).

Intermediate between groups A and B is the hornblende-bearing lava TG291 (Fig 6.11A), although overall it has more affinity with group A.

Within group A, nine silicic andesite lavas from NE Waihohonu Valley differ in that they are higher in TiO_2 (Fig 6.5C), Fe_2O_3*, K_2O (Fig 6.5H) and Rb (Fig 6.6E) relative to the main trend of group A lavas, suggesting that multiple magma batches were involved in producing this group of lavas. Apart from these samples (which lack hornblende), note that Tama 2 lavas are typically lower in K_2O and Rb than most other Tongariro lavas of comparable SiO_2 (Figs 6.5H and 6.6E), a feature typical of all hornblende-bearing Tongariro lavas (Sections 6.5.1h and 6.5.2f). Hornblende crystallization thus leads to lesser enrichment of K, Rb, etc. compared to magmas crystallizing purely anhydrous mineral assemblages. Tama 2 magmas have higher K/Rb ratios than other Tongariro magmas of similar SiO_2 contents (Fig 6.7B; Section 6.5.3). Furthermore, La, Ce, Y and Zr concentrations of Tama 2 lavas are generally in the lower portion of the Tongariro field (e.g. Figs 6.6H-I), as observed for Tama 1 lavas (Section 6.6.2). The distinctive chemical signature of Tama 2 magmas may have some link with the exceptionally high rate of cone growth (compared with all other Tongariro units; Table 3.3), but the nature of this relationship is at present unclear.

Patterson and Graham (1988) presented a limited number of whole-rock analyses of Upper Tama Lake lavas. Sample localities provided by I.J. Graham indicate that most of these analyses were from the same units or adjacent lava flows as those sampled as part of this study. This is borne out in the similar trends displayed in variation diagrams: comparatively low TiO_2, K_2O, Rb, Ba, and Zr. However, Patterson and Graham (1988) state that all lavas contain anhydrous mineral assemblages. Considering the correspondence in

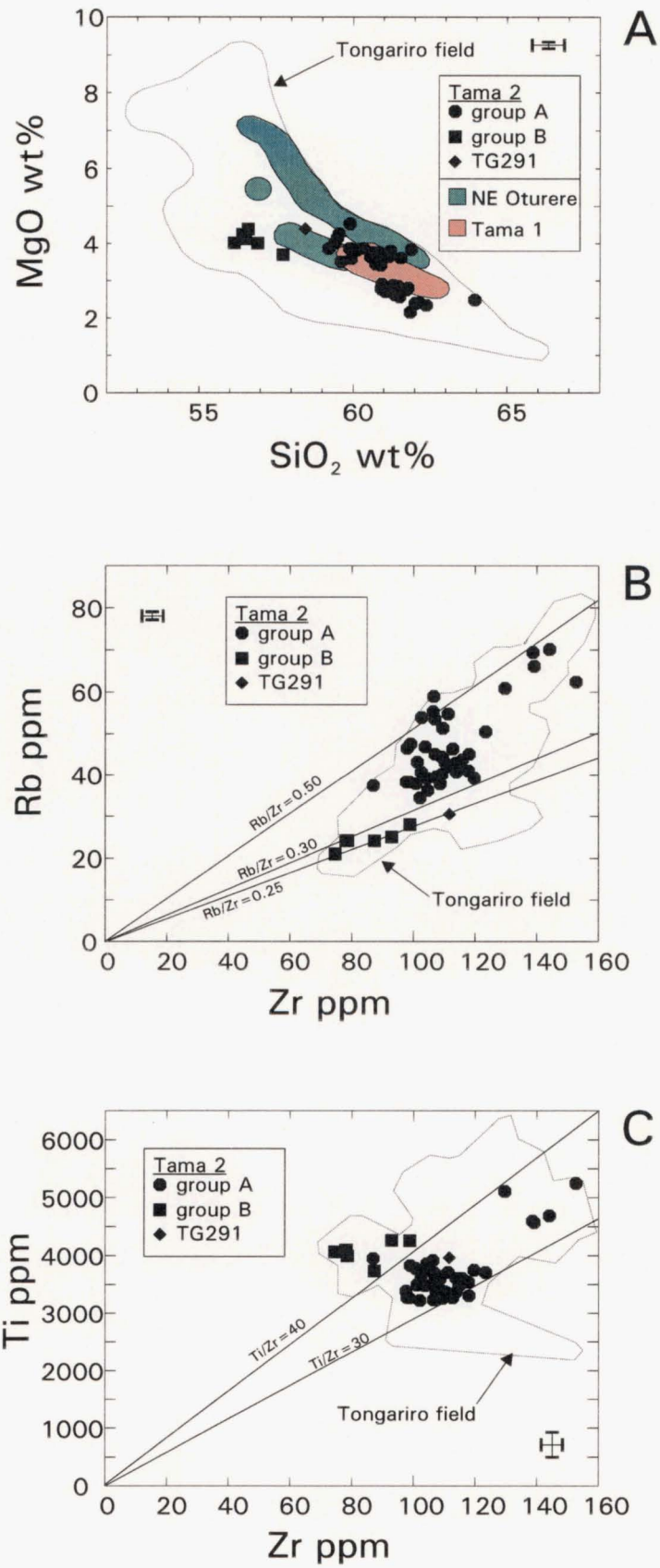

Figure 6.11 Variation diagrams for Tama 2 eruptives: (**A**) MgO versus SiO_2, (**B**) Rb versus Zr, (**C**) Ti versus Zr. The compositional fields for the older volcano-stratigraphic units are shown in the MgO-SiO_2 diagram. The compositional field for all Tongariro samples is also shown for comparison. All data recalculated anhydrous. Error bars represent total error (2 sd from mean; Section A8.3.3).

sample locality and geochemistry, it is probable that these workers overlooked the sparse (often pseudomorphed) hornblende phenocrysts present in these lavas. Patterson and Graham (1988) assigned the "Older Pukekaikiore-Upper Tama Lake andesites" to their Type 7 category, inferring an origin by POAM fractionation of a low-alumina basalt with very little or no crustal contamination (Section 4.2).

(b) Stratigraphic-compositional relationships. Most of the small volcano-stratigraphic subunits of Tama 2, each containing 2 to 10 lava flows (Appendix 2.15), have relatively wide-ranging compositions, and do not correspond to a neat division into either chemical group A or B. The smaller number of samples which comprise group B are from four subunits collected from spatially disparate lava flow outcrops on Ngauruhoe cone, Tama trig ridge, and NE Waihohonu Valley wall.

(c) Fractional crystallization models. It must be emphasised that because of the strong involvement of magma mixing processes, as indicated by petrographic evidence (Section 4.4.4), modelling of closed system crystal fractionation is not a very realistic approach. Using least-squares mixing (Appendix 12) to model major element fractional crystallization along trend A shows that it is possible to relate some of these samples by this process (e.g. Model A12.4), but often the calculated phase proportions differ somewhat from the observed modal mineralogy (e.g. a much less significant role for plagioclase and a much more significant role for hornblende than is suggested by phenocryst proportions).

Mineral compositional data were not acquired on samples of group B so it was not possible to test relationships within this group, nor between A and B. However, because the groups do not share the same trends on certain variation diagrams (e.g. MgO, Na_2O, Cr, Ni versus SiO_2) and because of contrasting K/Rb (A=232-334, B=294-322), Rb/Zr (A=0.33-0.55, B=0.27-0.31; Fig 6.11B), Ti/Zr (A=28-45, B=43-54;Fig 6.11C) ratios, they are interpreted to represent different magma batches. Consequently, at least three chemically distinctive magma types can be identified for Tama 2. For group A especially, the very scattered trends on incompatible element plots (e.g. Figs 6.11B and 6.11C) also suggest considerable heterogeneity which must be produced by processes other than fractional crystallization.

(d) **Relationship with older units and Tongariro complex in general.** The Tama 2 lavas overlap with the high-SiO_2 end of the NE Oturere suite (Fig 6.11A), but NE Oturere lavas contain lower Fe_2O_3*, TiO_2 and K_2O contents, and higher concentrations of REE and Zr than the Tama 2 lavas of comparable SiO_2. Tama 2 lavas exhibit some geochemical similarities to those of Tama 1, and partly overlap the field for Tama 1 lavas on Figure 6.11A. Attempts to model fractional crystallization of TG136 andesite (Tama 1) to derive a younger Tama 2 silicic andesite were not successful, however, yielding relatively high ΣR^2 and incongruous phase assemblages.

The only Tama 2 composition which could be successfully modelled (ΣR^2=0.12) from fractional crystallization of Tama 1 was the dacite Tn144e, which required extraction of 19% [plag+opx+hbl+mag] crystals (Model A12.5). Tn144d-e are samples of andesitic to dacitic pumice erupted as a pyroclastic flow, the only example of explosive activity preserved on the Tama 2 cone. The relatively wide compositional contrast (e.g. 59.2-63.0 wt% SiO_2) of these two samples is consistent with fractional crystallization; a zoned magma chamber may have existed prior to eruption of the ignimbrite.

The Tama 2 lavas span most of the SiO_2 range of the Tongariro eruptives (Fig 6.11A). The group A lavas encompass samples among the lowest and the highest MgO contents represented by the Tongariro field at those SiO_2 levels, whereas group B lavas plot in the moderate to low MgO portion of the Tongariro field at its lower-SiO_2 end (Fig 6.11A).

6.6.5 Pukekaikiore

(a) **Introduction and chemical characteristics.** Following Tama 2 activity, and during the ongoing eruptions which were building the NE Oturere cone, the Pukekaikiore cone formed from silicic andesite lava flows and coulées in the west of the Tongariro complex between 190 and 120 ka (Section 3.5.5). The inferred vent area for Pukekaikiore is c.2 km northwest of the Tama 2 vent, and c.5 km southwest of the NE Oturere vent (Fig 3.4). The samples plot as a restricted group on the MgO-SiO_2 diagram, ranging from 59.8 to 61.8 wt% SiO_2 and 3.6 to 4.3 wt% MgO (Fig 6.12A). Lack of mineral

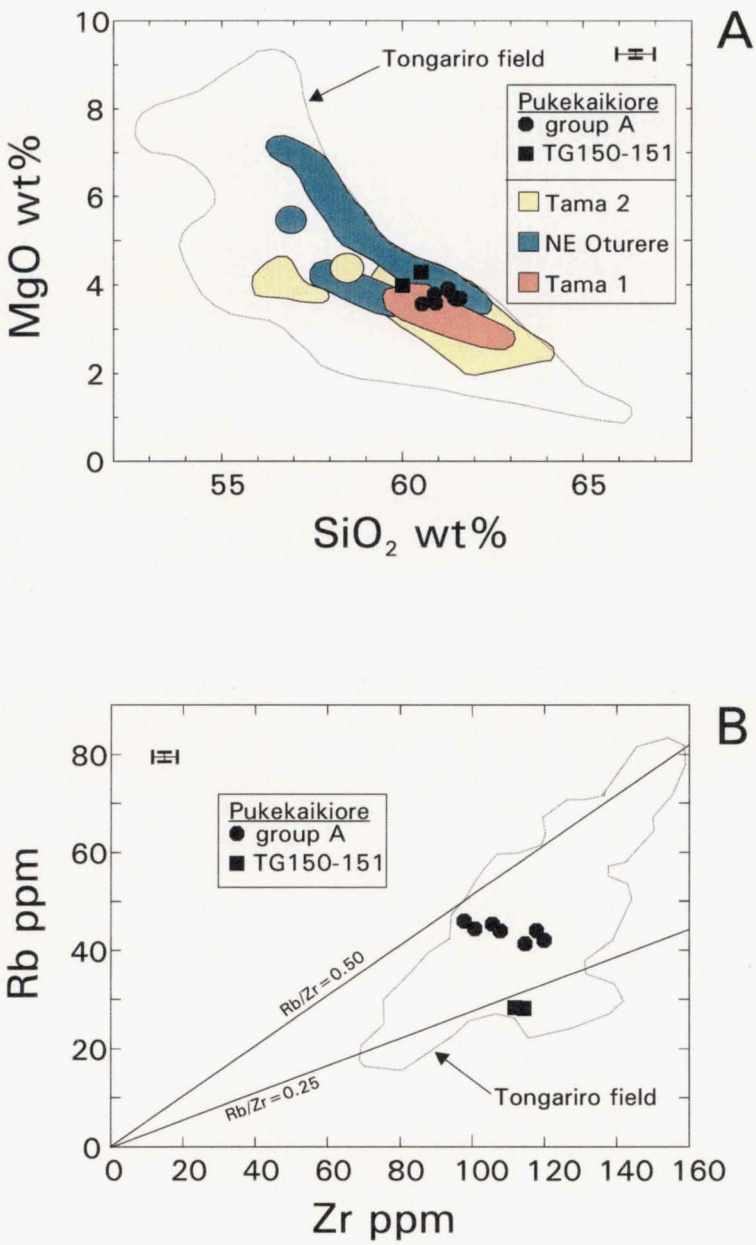

Figure 6.12 Variation diagrams for Pukekaikiore eruptives: (**A**) MgO versus SiO_2, (**B**) Rb versus Zr. The compositional fields for the older volcano-stratigraphic units are shown in the MgO-SiO_2 diagram. The compositional field for all Tongariro samples is also shown for comparison. All data recalculated anhydrous. Error bars represent total error (2 sd from mean; Section A8.3.3).

composition data precluded least-squares modelling of fractional crystallization processes linking Pukekaikiore lavas. However the petrographic evidence for magma mixing (e.g. disequilibrium phenocryst assemblages including embayed quartz, olivine and hornblende) indicate that open system processes were involved in Pukekaikiore petrogenesis.

(b) **Stratigraphic-compositional relationships.** Chemical relationships within the short stratigraphic section for Pukekaikiore (subunit 'a'; Appendix A2.14) represent a pattern of more evolved older lavas and more basic younger lavas. Although all the lavas generally behave as one chemically coherent group, the two youngest and hornblende-free lavas (TG150 and TG151) have significantly lower Rb contents (Fig 6.6E), Rb/Sr (Fig 6.7A) and Rb/Zr (Fig 6.12B) ratios. TG151 is also much lower in CaO than the other Pukekaikiore lavas. Thus at least two contrasting magma batches have contributed to the Pukekaikiore cone.

(c) **Relationship with older units and Tongariro complex in general.** Most Pukekaikiore lavas contain hornblende, and like other Tongariro hornblende-phyric lavas (Tama 1, Tama 2) they are characterised by relatively low K_2O (Fig 6.5H), Rb (Fig 6.6E), REE, and Zr (Fig 6.6I), and comparatively high K/Rb ratios (Fig 6.7B). Thus the similarities suggested by the overlap of the Pukekaikiore MgO-SiO_2 field with those of Tama 1 and Tama 2 (Fig 6.12A) are further supported by the distinctive elemental trends and abundances which all the units have in common. Least-squares modelling between Tama 1 and Pukekaikiore compositions was unsuccessful, but crystallization of 11% [plag+opx+hbl+mag] from a Tama 2 magma (TG381) could produce a Pukekaikiore magma (TG367) with $\Sigma R^2=0.18$ and calculated phase proportions similar to modal mineralogy - apart from a lack of fractionating clinopyroxene in the model (Model A12.6, Appendix 12). The fields for Pukekaikiore and NE Oturere also partly overlap (Fig 6.12A), but these two units do not share as many other common features as those mentioned above.

Compared to the Tongariro field overall, the Pukekaikiore lavas are confined to a moderately high SiO_2 and moderate MgO portion of the field (Fig 6.12A). Existing whole-rock analyses of Pukekaikiore lavas presented by Patterson (1986) plot in the same field defined by Pukekaikiore analyses from this study. Patterson and Graham (1988) also discuss these "Older Pukekaikiore" lavas, for which they did not attribute any hornblende

in the phenocryst assemblage - a discrepancy also noted for their Upper Tama Lake lavas (Section 6.6.4).

6.6.6 Southwestern Oturere

(a) Introduction and chemical characteristics. Soon after cessation of activity at Pukekaikiore, cone-building commenced from vents c.3 km to the east in the SW Oturere area (Fig 3.4), where numerous andesitic to dacitic lavas and pyroclastics were erupted between 115 and 70 ka (Section 3.5.6). When their compositions are plotted on an MgO-SiO_2 diagram, the eruptive products sampled from SW Oturere fall into three chemical groups (Fig 6.13A):

A. lavas on a gently-decreasing low-MgO trend (3.4-2.1 wt% MgO) extending over the complete SW Oturere SiO_2 range (57.2-65.5 wt% SiO_2); and

B. a smaller group of olivine-bearing lavas and agglutinates with slightly higher MgO (4.2-3.7 wt%) and moderately low SiO_2 (57.9-59.4 wt%) contents; and

C. a relatively high-MgO (5.5 wt%), low-SiO_2 (57.8 wt%) trend represented by the olivine-bearing scoria sample TG240 and lava flows TG274-275.

Other overall differences between the chemical groups are apparent. In addition to the lower MgO contents, the samples from group A are also lower in CaO, Cr and Ni, and higher in TiO_2 (Fig 6.13B), Al_2O_3, Na_2O, P_2O_5 and REE relative to trends for group B. The TiO_2 (<0.9 wt%), Na_2O (<3.9 wt%) and P_2O_5 (<0.2wt%) contents of the group A lavas are among the highest concentrations analysed for Tongariro eruptives (e.g. Figs 6.5G and 6.5I). In contrast, the relatively high-MgO group C includes the lowest TiO_2 (Fig 6.13B), Al_2O_3, Na_2O and P_2O_5 of the SW Oturere eruptives.

(b) Stratigraphic-compositional relationships. Within the SW Oturere unit itself, the internal volcano-stratigraphy (Appendix A2.13) does not relate simply to the chemical trends and groupings. The compositions of most subunits overlap to varying degrees along the length of trend A, although there is a broad correlation between age and composition; older subunits (e.g. 'g' and 'i') tend to be more evolved and younger subunits

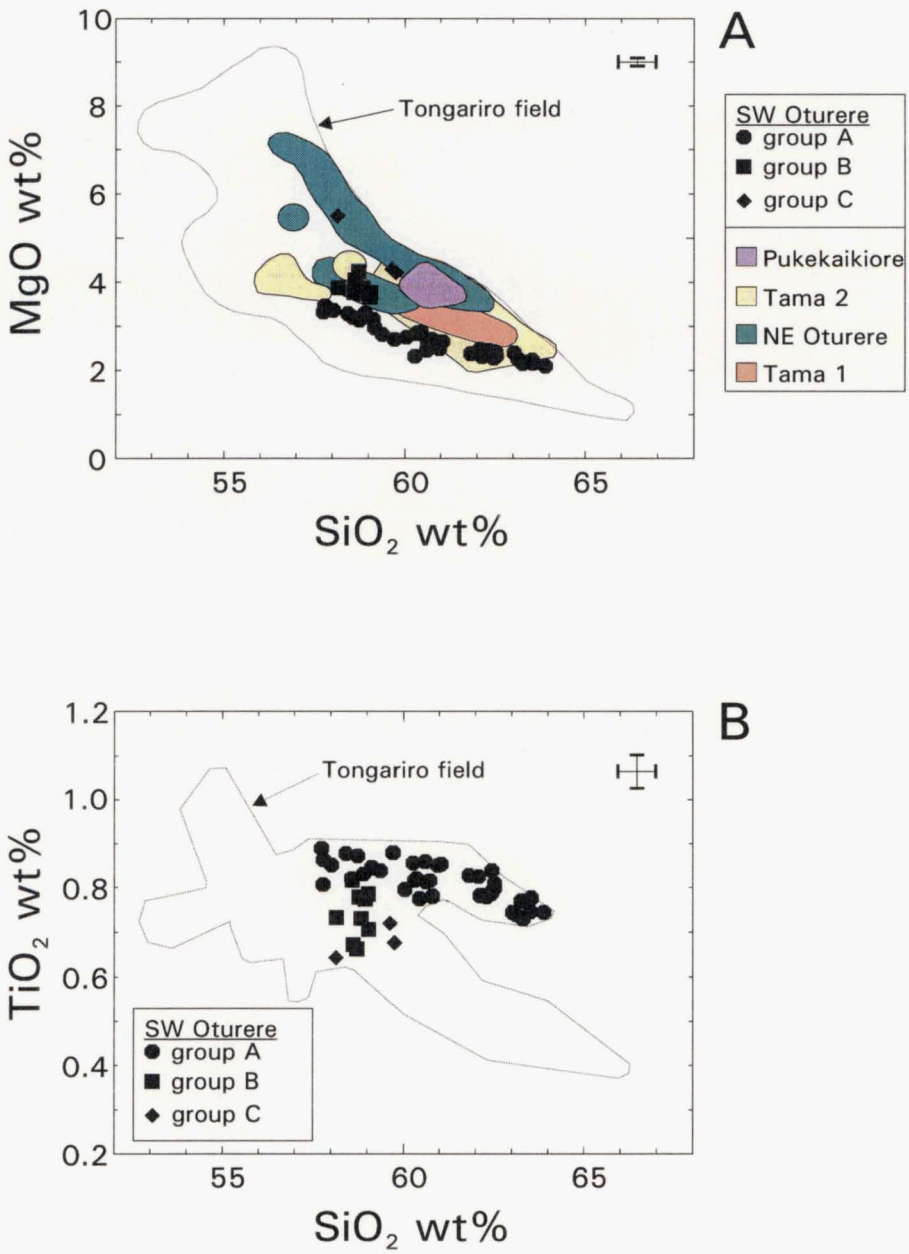

Figure 6.13 Variation diagrams for SW Oturere eruptives: (**A**) MgO versus SiO_2, (**B**) TiO_2 versus SiO_2. The compositional fields for the older volcano-stratigraphic units are shown in the MgO-SiO_2 diagram. The compositional field for all Tongariro samples is also shown for comparison. All data recalculated anhydrous. Error bars represent total error (2 sd from mean; Section A8.3.3).

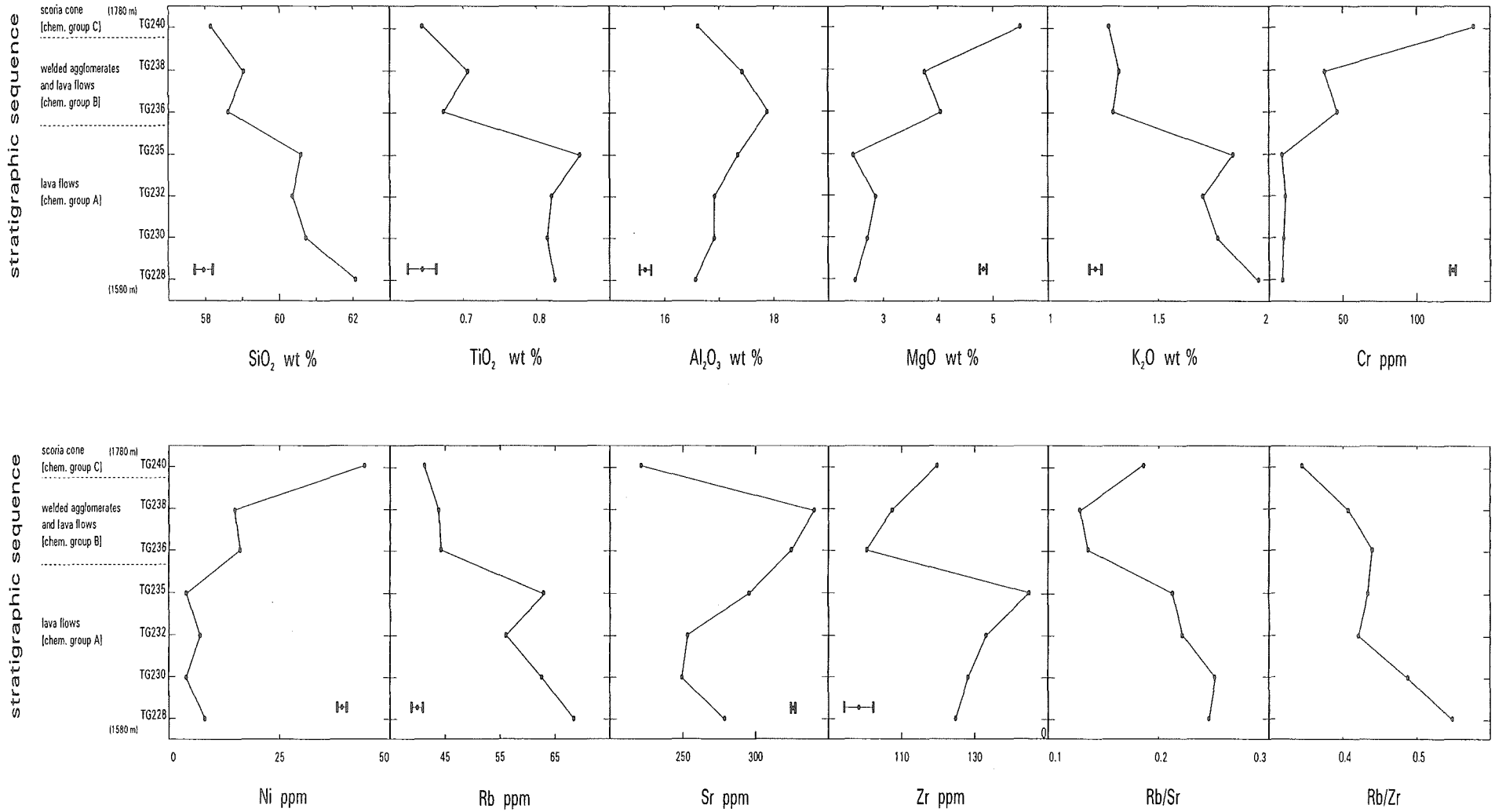

Figure 6.13 (continued) C. Selected whole-rock major and trace element compositions of SW Oturere subunit 'b' eruptives plotted in stratigraphic order. All data recalculated anhydrous. Error bars represent total error (2 sd from mean; Section A8.3.3).

(e.g. 'd') less evolved. *Within* any one subunit there are generally no systematic chemical trends. Chemical stratigraphy plots (e.g. Fig 6.13C, see below) demonstrate this compositional variability, and support the involvement of magma mixing processes, as determined from petrographic and mineral composition evidence (Section 4.7).

When plotted according to stratigraphic order (Fig 6.13C), the chemical compositions of subunit 'b' eruptives reveal a neat division into the chemical groups identified from variation diagrams. The lower lava flow sequence belong to group A and exhibit some chemical trends up section contrary to those expected for fractional crystallization (e.g. decreasing SiO_2, K_2O, Rb), whereas other elements such as Cr are remarkably consistent. Although the trends for these group A lavas are not entirely smooth and consistent, they may indicate eruption from a subtly zoned magma reservoir. A generally sharp chemical break towards more basic magma compositions marks the boundary between the lower group A flows, and the overlying group B welded agglutinates and flows. Subunit 'b' is capped by a scoria cone deposit which represents an influx of group C magma with dramatically higher MgO, Cr and Ni, and lower Sr concentrations than the previously erupted magmas. Geothermometry supports the occurrence of a significant magma mixing event; estimated crystallization temperatures for the TG240 scoria are c.865°C and 1175°C (Sections 4.6.2 and 4.7.5). The chemical differences between and also within chemical groups indicate input of multiple magma batches into the SW Oturere magmatic system during its lifetime.

(c) **Fractional crystallization models.** Least-squares calculations (Appendix 12) show that fractional crystallization is a valid process that could link certain lavas along the group A trend. The andesite sample TG235 can be derived from the more mafic andesite TG074 in this way by removal of 35% [plag+opx+ox] crystals, giving a very low ΣR^2 of 0.02 (Model A12.7). The andesite sample TG080 occurs midway along trend A, and can generate the younger dacite TG167 by extraction of 23% [plag+opx+cpx+ox] crystals, yielding an acceptable ΣR^2 of 0.20 (Model A12.8). However, applied rigorously and systematically, such models break down and it is not possible to simply model all successive lavas along trend A because the chemical trend does not follow a smooth path of decreasing age with increasing differentiation, which limits the number of geologically acceptable initial-final magma pairs available for modelling. This suggests that a number

of different magma batches, arising under similar melting conditions and then differentiating along similar paths, have contributed to form the chemical trend of group A lavas. It is possible to relate selected lavas from group B to group A by fractional crystallization (e.g. Model A12.9), but there is no consistent relationship linking these two groups by this process alone. It is not feasible to conduct similar modelling with the most primitive sample, TG240, because it cannot be reasonably derived from any other available SW Oturere composition.

(d) **Relationship with older units and Tongariro complex in general.** The main trend (group A) for SW Oturere magmas represents a significant departure from the earlier Tongariro units towards much lower MgO and more evolved compositions (Fig 6.13A). There is only limited overlap between the compositional fields of SW Oturere and those of NE Oturere and Tama 2 (Fig 6.13A). Least-squares modelling of the relationship between NE Oturere lava flow TG115 and SW Oturere group C scoria TG240 (eruptives which appear to lie on the same steep trend on the MgO-SiO_2 diagram) indicate that fractional crystallization may be a viable process (removal of 20% [cpx+plag+opx+oliv+ilm],ΣR^2 =0.08; Model A12.10). However, this model is unsatisfactory in that it requires little involvement of olivine and a much greater role for clinopyroxene than indicated by observed modal proportions. On the MgO-SiO_2 diagram, SW Oturere group B eruptives share a similar position to those of the NE Oturere group B, but lack of mineral compositional data prevents exploration of the magmatic relationship (if any) between these two groups. Similarly, mineral analyses are not available to test the association between Tama 2 group B eruptives and those of SW Oturere group A.

(e) **Relationship between magma chemistry and eruptive style.** The higher-MgO chemical groups B and C include some of the younger lavas, agglutinates and scoria deposits from subunit 'b', and illustrate that there is some degree of compositional control over eruptive style. In addition, the overthickened lava flows and coulées plot at the higher-SiO_2 end of trend A.

6.6.7 Tongariro Trig

(a) Introduction and chemical characteristics. At about the same time period that the SW Oturere cone was active, eruptions were also taking place from vents centred around the Tongariro Trig area, c.2 km northwest of the SW Oturere vents (Fig 3.4), between 110 and 65 ka (Section 3.5.7). Eruptives of these two volcano-stratigraphic units share a number of similar geochemical characteristics. On the SiO_2-MgO variation diagram (Fig 6.14A), the Tongariro Trig andesite-dacite lavas and welded agglutinates plot as two different trends or groups:

A. andesites and dacites lying on a low MgO (1.8-2.9 wt%) and relatively high SiO_2 (58.9-62.3 wt%) trend; and

B. andesites forming a relatively broad, moderate MgO-SiO_2 trend (3.3-4.6 wt% MgO, 58.2-60.5 wt% SiO_2).

The lowest- SiO_2 andesite sample, TG322 (57.0 wt% SiO_2), does not have correspondingly high MgO, Cr, etc., and therefore is not considered a logical member of either group A or group B. Further contrast between Tongariro Trig chemical groups A and B is illustrated on a Cr-SiO_2 diagram. Group A samples define a flat, very low Cr trend, whereas group B samples plot on a steep, moderately high Cr trend (Fig 6.14C). The analyses of Mangatepopo Valley lava flows presented by Patterson (1986) and Patterson and Graham (1988) generally coincide with those of this study from similar locations (mostly subunit 'f').

(b) Stratigraphic-compositional relationships and fractional crystallization models. It was not possible to apply rigorous least-squares fractional crystallization models to the eruptives of the two Tongariro Trig trends because of a lack of mineral composition data. However, there is no orderly chemical evolution of magma compositions with time within each of the Tongariro Trig subunits (Appendix A2.12), or for the unit as a whole. Open system processes are therefore more likely to have operated in the Tongariro Trig magmatic system, rather than fractional crystallization alone.

(c) Relationship with older units and Tongariro complex in general. The chemical trends displayed by Tongariro Trig are remarkably similar to those of SW Oturere, i.e. a main sublinear trend (group A) of low MgO magmas, and a shorter trend/grouping

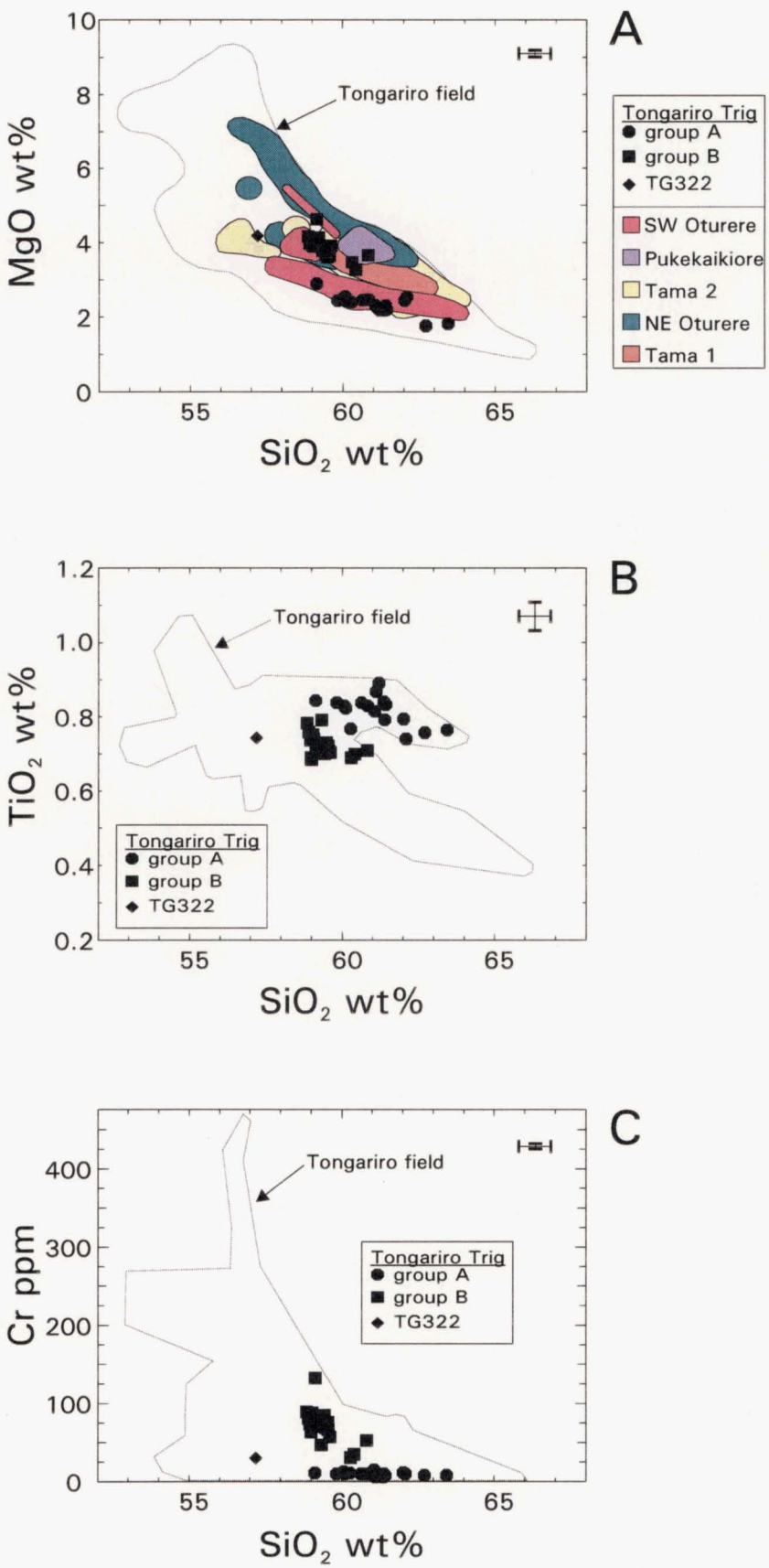

Figure 6.14 Variation diagrams for Tongariro Trig eruptives: (**A**) MgO versus SiO_2, (**B**) TiO_2 versus SiO_2, (**C**) Cr versus SiO_2. The compositional fields for the older volcano-stratigraphic units are shown in the MgO-SiO_2 diagram. The compositional field for all Tongariro samples is also shown for comparison. All data recalculated anhydrous. Error bars represent total error (2 sd from mean; Section A8.3.3).

(group B) of moderate MgO magmas (Fig 6.14A). Tongariro Trig eruptives also display the distinctive division into high TiO_2 (group A) and low TiO_2 (group B) trends (Fig 6.14B) also noted for SW Oturere. Thus these two units share close links in composition as well as in space and time. Least-squares calculations confirm this intimate relationship, showing that it is possible to derive Tongariro Trig magmas from SW Oturere magmas by fractional crystallization. Modelling along both the group A (TG080 to TG326) and group B (TG051 to TG355) trends indicates extraction of 26% and 19%, respectively, of [plag+opx+cpx+mag] (Models A12.11-12). These models achieve an excellent correspondence between calculated and observed phase proportions, and yield very low ΣR^2 values of between 0.04 and 0.06.

(d) Relationship between magma chemistry and eruptive style. The Tongariro Trig welded agglutinates plot at the lower SiO_2 end of both group A and B trends, reflecting the general relationship between more primitive magma chemistry and lower magma viscosities and this particular eruptive style noted in Section 6.4.

6.6.8 Young eruptives

For most of the young eruptive units there is not the same quantity of samples as for the older units, but this is offset by the greater degree of time control offered by (especially the historic) eruptions which have occurred from many of these post-25 ka vents. In many cases this allows a more detailed analysis of the scale of chemical ordering evident within one unit. Chemical groupings or trends can still be identified for many of the young eruptives. Note that to more clearly show the compositional fields on the MgO-SiO_2 variation diagram, the young eruptive units are colour-coded whereas the older units are outlined only. For convenience of presentation, samples from two or three young eruptive units are often plotted on the same variation diagrams.

Ngauruhoe is highlighted as a cameo study, for which the comprehensive data base provides an excellent opportunity to use stratigraphic constraints to refine and test petrogenetic models. It is important to recognise the more complete perspective on magmatic history given by Ngauruhoe; the detailed sampling of all sectors of this young

cone provides insights often different from those obtained for the older units where usually only one sector of the cone is exposed in a valley. Thus, the conclusions drawn from the Ngauruhoe study may be applicable to the older Tongariro cones, even though the different study approaches might make comparison more difficult.

(a) Young NE Oturere. The andesitic scoria fall deposit erupted around 20 ka from the NE Oturere area (Section 3.5.8) plot in a moderately low SiO_2 (57.6-58.1 wt%), moderate MgO (4.1-4.3 wt%) position relative to the overall Tongariro field (Fig 6.15). The three samples act as a coherent, tightly clustered chemical group on all variation diagrams. For its SiO_2 content, the Young NE Oturere scoria is relatively low in MgO, Cr (26-27 ppm) and Ni (8-10 ppm), and this is reflected in the lack of olivine phenocrysts (Section 4.4.8a). This young pyroclastic deposit has a very similar composition to the older welded agglutinates erupted in the vicinity possibly some tens of thousands of years earlier (subunit 'a', NE Oturere chemical group B). The fields for these two deposits overlap on variation diagrams for MgO (Fig 6.15), Al_2O_3, K_2O, Cr, Ni, and Ba. The close spatial and compositional relationship displayed by these two units could suggest a magmatic link to a pre-existing older batch of magma which, after a considerable period of time, was tapped via a reactivation of part of the magmatic plumbing system. This conclusion must undoubtedly be tempered, however, by the relative uncertainty surrounding the age of the Young NE Oturere scoria (Section 3.5.8a).

(b) Pukeonake. The olivine- and chrome spinel-bearing basaltic andesite scoria and lava flows erupted from the satellite vent Pukeonake (Section 3.5.8b) represent the most MgO-rich (8.9-9.2 wt%, Mg# =70.8), although not the most SiO_2-poor (56.5-57 wt%) of the Tongariro eruptives (Fig 6.15). They are also notably high in K_2O (Fig 6.5H), Cr (424-460 ppm; Fig 6.6B), Ni (217-220 ppm; Fig 6.6C), Rb (Fig 6.6C), and Ba (Fig 6.6G), and have the lowest Al_2O_3 contents (14.3-14.5 wt%; Fig 6.5A) of any eruptives from Tongariro. The ample evidence for disequilibrium indicated by the petrography (Sections 4.4.8b and 4.7), coupled with the distinctive chemical composition (high concentrations of both compatible and incompatible elements) is consistent with the influx and mixing of a very primitive magma batch into a pre-existing magma reservoir. Estimates of crystallization conditions indicate that Pukeonake magmas equilibrated at higher

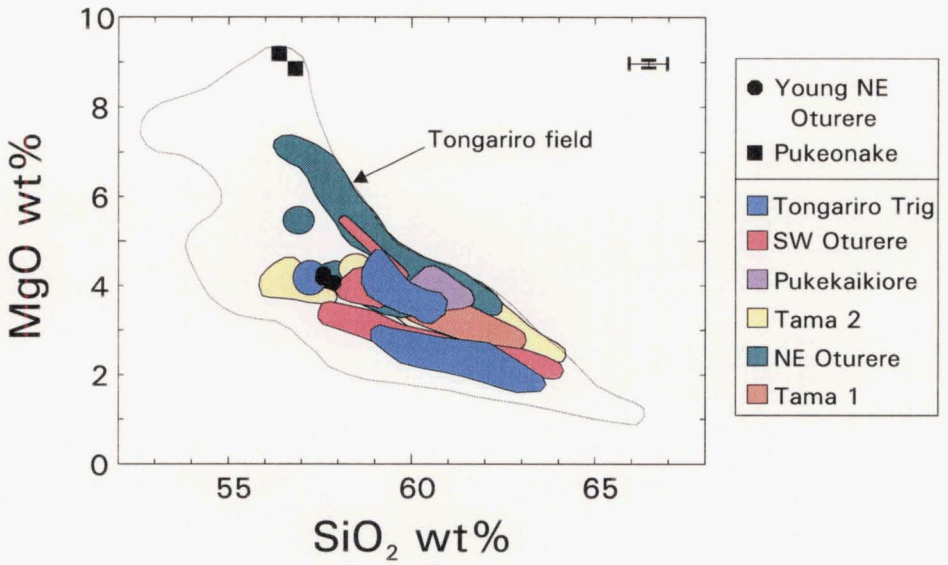

Figure 6.15 MgO versus SiO_2 diagram for Young NE Oturere and Pukeonake eruptives. The compositional fields for the older volcano-stratigraphic units are shown. The compositional field for all Tongariro samples is also shown for comparison. All data recalculated anhydrous. Error bars represent total error (2 sd from mean; Section A8.3.3).

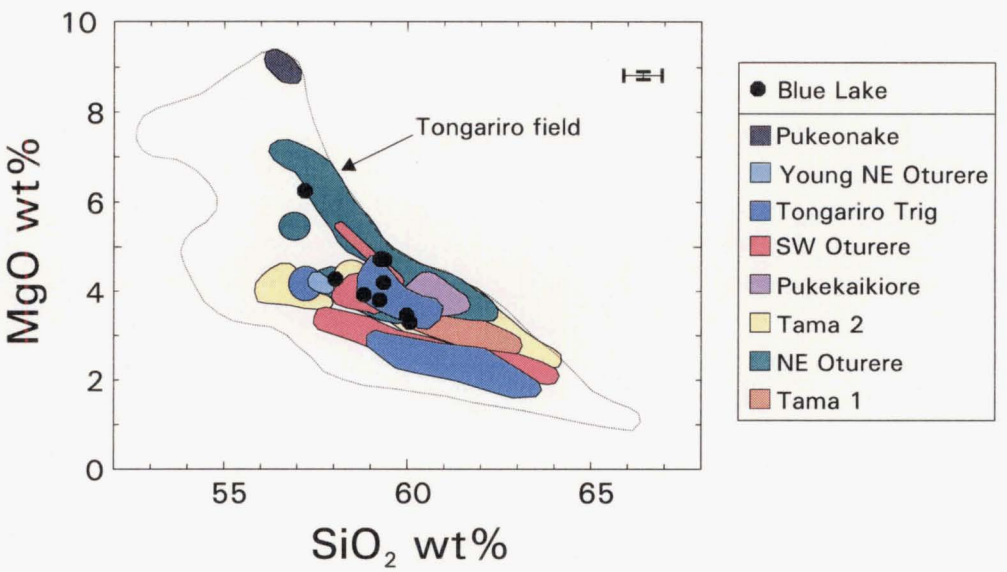

Figure 6.16 MgO versus SiO_2 diagram for Blue Lake eruptives. The compositional fields for the older volcano-stratigraphic units are shown. The compositional field for all Tongariro samples is also shown for comparison. All data recalculated anhydrous. Error bars represent total error (2 sd from mean; Section A8.3.3).

temperatures (c.1050-1200°C) and possibly higher pressures than most other Tongariro magmas (Section 4.6).

Nowhere else on the Tongariro complex has such a basic magma been tapped or such dramatic evidence for magma mixing been recorded. Thus Pukeonake represents a uniquely recognisable event in the magmatic history of Tongariro, when conditions in the magma source region and plumbing system led to the eruption of these exceptionally high-MgO-Cr-Ni magmas. Pukeonake compositions determined in this study are in agreement with Topping's (1974) and Cole's (1978) major element analyses of scoria and flows from Pukeonake cone and associated plugs. Hackett (1985) and Graham and Hackett (1987) have also presented petrological data on Pukeonake eruptives, and these data correspond well to analyses made for this study, although some higher Cr concentrations (<591 ppm) were measured by these previous workers. They found analogous magma compositions in lavas of the Mangawhero Formation of Ruapehu volcano, and grouped these together in their Type 6 hybrid lavas, modelled by mixing Waimarino basalt with Mangawhero Formation dacite (Section 4.2). The eruption of similar magmas from Ruapehu at about the same time that Pukeonake was active, and the lack of any eruptions from the Tongariro complex during this period suggests that these "Type 6" magmas were only available to the volcanic system during a relatively short interval when access to Tongariro conduits was not possible.

(c) **Blue Lake.** Eruptions from Blue Lake crater between c.20 and 10 ka produced andesitic scoria, agglutinate and lava flow deposits which span a moderately wide MgO range of 3.3 to 6.2 wt% and SiO_2 from 56.8 to 59.9 wt% (Fig 6.16). The samples do not form a single cohesive trend on the MgO-SiO_2 diagram, and stratigraphic/relative age relationships (Appendix A2.9) are inconsistent with a simple fractional crystallization process linking these eruptive products. The higher MgO ejecta are olivine-bearing and have correspondingly high Cr and Ni. The lower SiO_2 Blue Lake trend appears to be an extension of the Young NE Oturere magma composition (Fig 6.15); a shared magmatic history between these two units would be consistent with their relatively close temporal and spatial (c.1 km between vents) associations. Compared to the Tongariro field overall, Blue Lake eruptives plot in the centre of the field, overlapping with the 'B' chemical groups of Tongariro Trig, SW Oturere and NE Oturere (Fig 6.16). Thus these older Tongariro magma

compositions are echoed in the chemistry of younger eruptive units, suggesting some link in the type of magma available to the volcanic plumbing system over time and in the processes operating on these magmas.

(d) **North Crater.** The basaltic andesite to andesite scoria, agglutinate and solidified lava lake of the North Crater vent were produced around 10-15 ka. The moderate SiO_2 (56.3-60.1 wt%) and MgO (3.3-6.2 wt%) contents place this cone near the middle of the overall Tongariro field (Fig 6.17A). Analyses from Te Rato Lapilli and Pahoka Lapilli (Topping, 1974), which were erupted from North Crater around 10ka (Table 3.2), encompass more silicic compositions (<63.5 wt% SiO_2) than those sampled on the cone.

Samples from each stratigraphic unit (Appendix A2.8) tend to plot as clusters of points rather than as linear trends. North Crater eruptives lie in almost exactly the same compositional field as those from Blue Lake, both units sharing a similar pattern of a lower MgO trend, a slightly higher MgO cluster, and one or two high MgO outliers (Fig 6.17A). These groupings are also reflected in the Cr-SiO_2 variation diagram (not shown). Petrography and other chemical parameters are also closely matched between the two units. Eruptions from these 1 km-apart vents were occurring concurrently (especially around 10 ka) and there is strong petrological evidence that suggests North Crater and Blue Lake were derived from a common magma storage area.

(e) **Young Pukekaikiore.** A very distinctive magma type is represented by the clinopyroxene-rich, olivine-bearing andesitic scoria and lava flows erupted from a summit vent on Pukekaikiore about 15 ka (Section 3.5.8e). It plots among the highest MgO (6.9-7.0 wt%; Fig 6.18) and Cr (229-248 ppm; Fig 6.6B) compositions erupted from Tongariro complex, has moderately low SiO_2 (56.9-57.4 wt%; Fig 6.18), but is most remarkable for its extremely elevated Sr concentration (634-643 ppm; Fig 6.6F) and lack of plagioclase phenocrysts (Section 4.4.8e). The Young Pukekaikiore magma is also relatively high in CaO (Fig 6.5B) and Ni, and relatively low in Al_2O_3 (Fig 6.5A), TiO_2 (Fig 6.5C), Na_2O (Fig 6.5G), K_2O (Fig 6.5H), P_2O_5 (Fig 6.5I), and incompatible trace elements (Rb, Ba, Y, Zr) compared to the overall Tongariro trends. Patterson and Graham (1988) present chemical data for Young Pukekaikiore which show the same characteristics reported here, and they

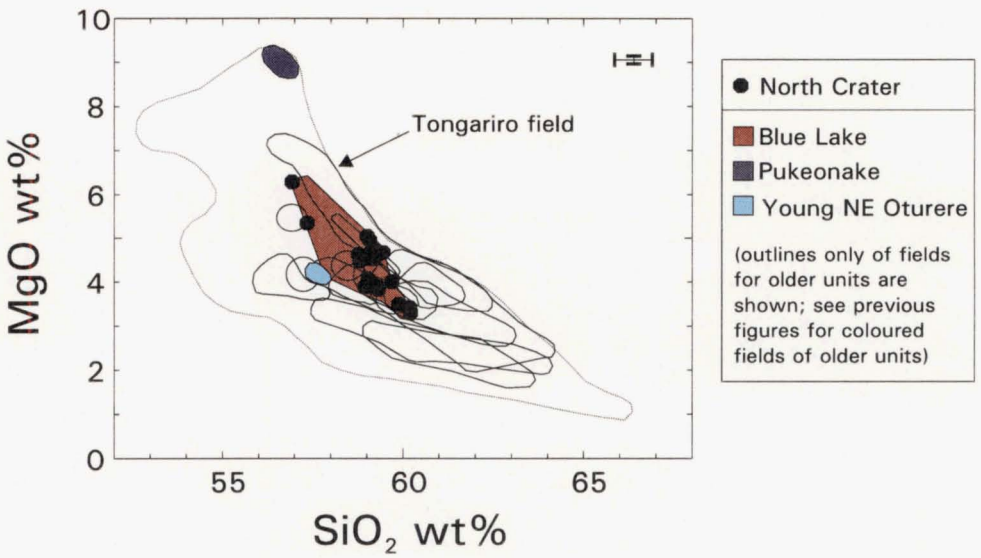

Figure 6.17 MgO versus SiO_2 diagram for North Crater eruptives. The compositional fields for the older volcano-stratigraphic units are shown. The compositional field for all Tongariro samples is also shown for comparison. All data recalculated anhydrous. Error bars represent total error (2 sd from mean; Section A8.3.3).

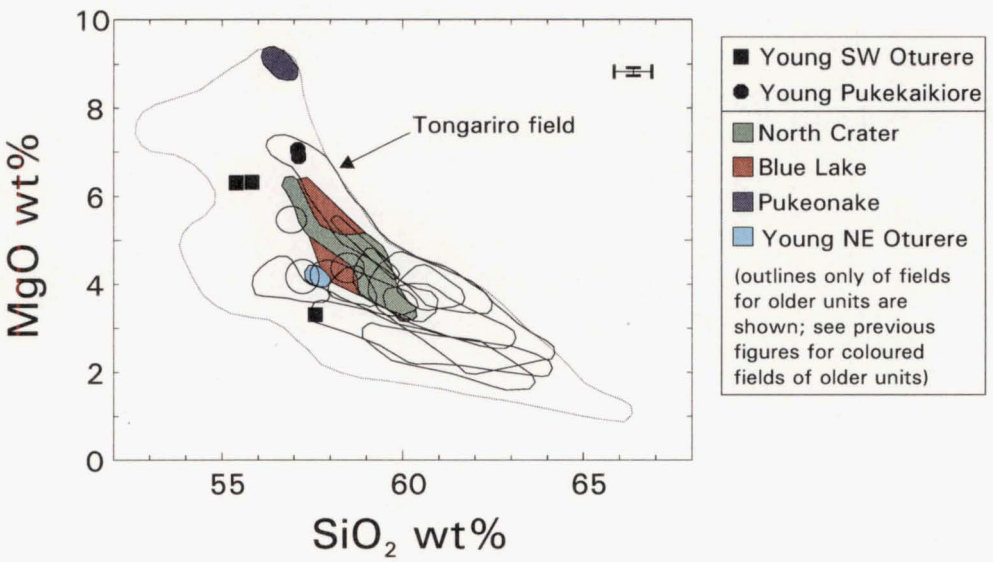

Figure 6.18 MgO versus SiO_2 diagram for Young Pukekaikiore and Young SW Oturere eruptives. The compositional fields for the older volcano-stratigraphic units are shown. The compositional field for all Tongariro samples is also shown for comparison. All data recalculated anhydrous. Error bars represent total error (2 sd from mean; Section A8.3.3).

model this variety of magma (their Type 5) by fractional crystallization of a quartz-tholeiite parent (Section 4.2).

No other Tongariro units can be reasonably or successfully modelled as parental to Young Pukekaikiore by means of fractional crystallization. There is no overlap of the younger and older Pukekaikiore compositional fields on the MgO-SiO_2 diagram, although the units do fall at either end of the steep trend defined by NE Oturere group A lavas (Fig 6.18). The combination of very low Al_2O_3 with very high Sr and absence of plagioclase phenocrysts precludes plagioclase accumulation as a significant petrological process, and suggests that the Young Pukekaikiore eruptives were derived from an unusually high-Sr parent magma feeding part of the Tongariro plumbing system around 15 ka, distinct from the magma being erupted at about the same time further north from the Blue Lake and North Crater vents.

(f) **Young SW Oturere.** Two (TG165-6) and one (TG176) scoria bombs were collected from two outcrops of young fall deposits less than 1 km apart in the upper SW wall of Oturere Valley. These samples of glassy, aphyric scoria bombs are thought to have erupted from a postulated vent in the upper SW Oturere Valley c.10-14 ka (Section 3.5.8f). They vary quite considerably in composition from relatively mafic (TG165-6; 55.0-55.9 wt% SiO_2, 6.3 wt% MgO, 116-128 ppm Cr, 30-33 ppm Ni) to more silicic (TG176; 57.4 wt% SiO_2, 3.3 wt% MgO, 13 ppm Cr, 8 ppm Ni) (Fig 6.18). TG165-6 contain relatively high CaO (Fig 6.5B), and relatively low Al_2O_3 (Fig 6.5A) and Na_2O (Fig 6.5G) when compared to overall Tongariro trends.

TG176 has geochemical characteristics suggesting that it could be derived by fractional crystallization from TG165-6, although lack of mineral data precludes quantitative modelling. This scenario would require a later eruptive pulse of greater dispersive power to produce the mapped distribution of more primitive proximal scoria (TG165-6) and more evolved medial-distal scoria (TG176). On the other hand, TG165-6 may correspond to the eruption of a younger batch of more mafic magma. Further field studies are required to clarify the relationship between the two outcrops of Young SW Oturere scoria.

On the MgO-SiO_2 diagram (Fig 6.18), TG165-6 are distinctive from other previously erupted Tongariro magma compositions. Extrapolation of the steeply decreasing trend from TG165-6 to TG176 follows the flattening out trend of the older SW Oturere group A lavas, perhaps signalling some degree of similarity in the parental magmas of these two units, which have such a close spatial association. Further differentiation of the Young SW Oturere magma would possibly have produced a magmatic trend similar to that displayed by the SW Oturere group A lavas.

(g) **Te Mari Craters.** The andesitic lava flows sampled from Upper and Lower Te Mari Craters range in age from c.14 ka to prehistoric (Section 3.5.8g), and form a slightly scattered trend on the MgO-SiO_2 diagram (Fig 6.19). Te Mari lavas contain moderate to low MgO (3.1-4.4 wt%) and SiO_2 (57.5-60.2 wt%) contents, and there is no consistent relationship between stratigraphy and composition. Te Mari compositional fields overlap with those of the neighbouring Blue Lake and North Crater eruptives (e.g. Fig 6.19) and they share similar incompatible element ratios (e.g. Rb/Zr typically 0.4-0.5, Ti/Zr typically 35-40), suggesting that all three of these young northern vents are in some way linked. Note that one of the lava flows east of the craters (TG347) has slightly lower Rb (Fig 6.6E) and higher Sr (Fig 6.6F) more akin to some of the Blue Lake lavas, with which it may be more closely associated.

Topping (1974) noted the similarity between major element analyses of Lower Te Mari Crater lavas and Rotoaira Lapilli. These correspond to the lower crater flows analysed in this study (TG345-6, TG350-1), although the lapilli are a slightly more evolved, lower MgO composition than the lava flows. Cole (1978) appears to have sampled a much more olivine-rich portion of the c.1500AD flow which is notably higher in MgO (6.66 wt%), Cr (445 ppm) and Ni (109 ppm) compared to the samples analysed in this study (TG281-2).

(h) **Tama Lakes.** Four samples from the c.10 ka pyroclastic material erupted in the Tama Lakes area in the south of the Tongariro complex (Section 3.5.8h) reveals a wide compositional range from basaltic andesite (56.1 wt% SiO_2, 4.5 wt% MgO) to dacite (64.2 wt% SiO_2, 1.1 wt% MgO). These samples could define a fractional crystallization trend in the lower-MgO portion of the overall Tongariro trend on the MgO-SiO_2 diagram (Fig 6.20); mineral data are not available to test this relationship, however. The two basaltic

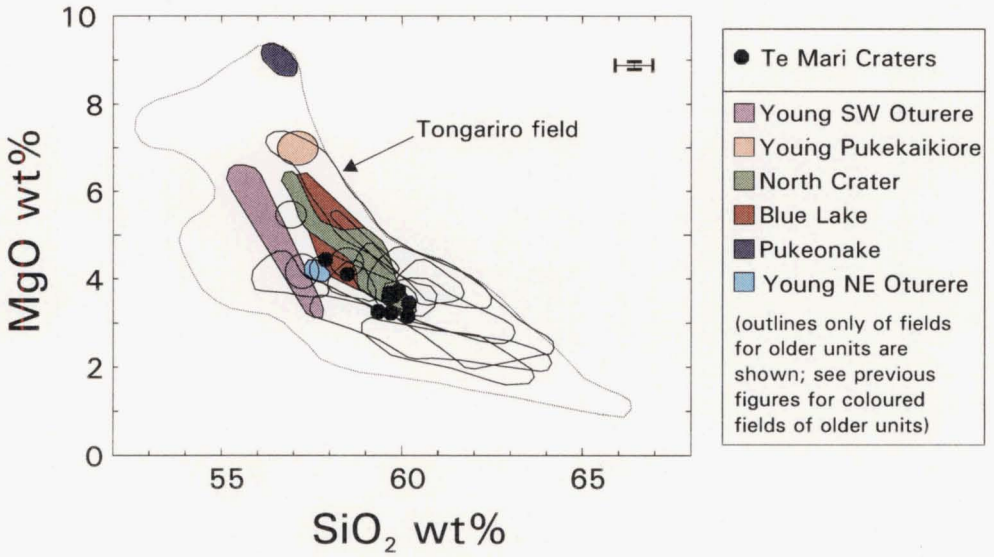

Figure 6.19 MgO versus SiO_2 diagram for Te Mari Craters eruptives. The compositional fields for the older volcano-stratigraphic units are shown. The compositional field for all Tongariro samples is also shown for comparison. All data recalculated anhydrous. Error bars represent total error (2 sd from mean; Section A8.3.3).

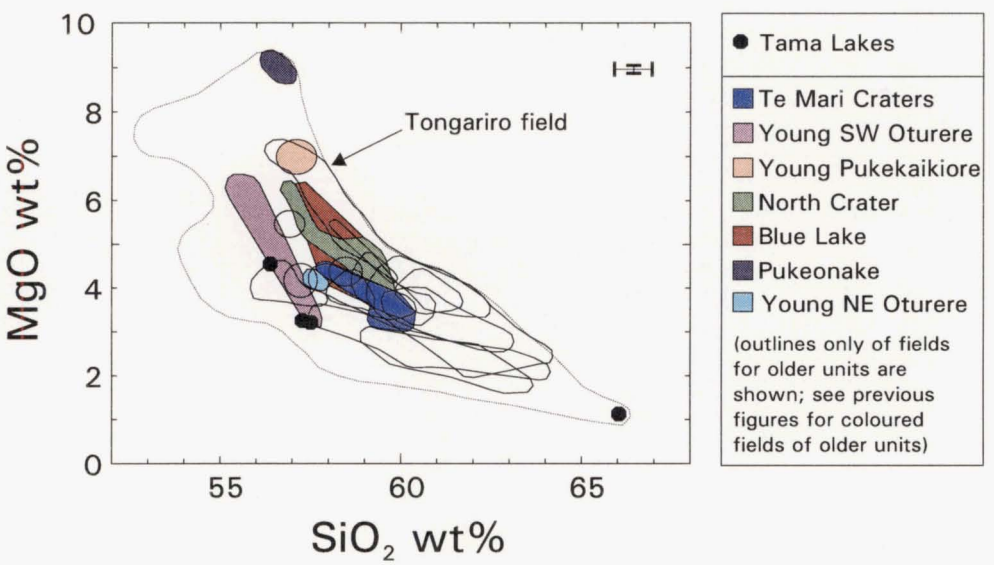

Figure 6.20 MgO versus SiO_2 diagram for Tama Lakes eruptives. The compositional fields for the older volcano-stratigraphic units are shown. The compositional field for all Tongariro samples is also shown for comparison. All data recalculated anhydrous. Error bars represent total error (2 sd from mean; Section A8.3.3).

andesite bombs sampled by Wahyudin (1993) are chemically very similar to (although slightly more silicic than) TG137, and plot on a trend between TG137 and TG033-034 (c.f. Section 4.4.8h). The relatively mafic Waihohonu Lapilli analysed by Topping (1974) and thought to be derived from Tama Lakes (Table 3.2) fall on a back projection of this trend. The Tama Lakes ejecta are characterised by relatively high Al_2O_3 contents compared to most Tongariro eruptives (Fig 6.5A). Despite the relatively low-SiO_2 nature of the basaltic andesite and andesite bombs, they contain very little Cr (14-32 ppm) and Ni (7-16 ppm).

The dacitic pumice (Tn141a) is the most silicic sample in the Tongariro data set, and also has the lowest compatible element contents (e.g. 3 ppm Cr) and the highest Na_2O (4.0 wt%). Tn141a does not contain the greatest abundances of other incompatible elements, however, and appears to fit the pattern of the older hornblende-bearing units which typically contained lower K_2O, Rb, Ba, La, Ce, Y, and Zr relative to other Tongariro eruptives of comparable SiO_2 contents (Section 6.6.4). Least-squares mixing calculations demonstrate that Tama 2 (TG381) and Tama Lakes (Tn141a) magmas can easily be related by fractional crystallization (removal of 30% [hbl+plag+cpx+mag+opx], ΣR^2=0.02; Model A12.13). Although a direct link over such a time span is unlikely, there may be distinctive conditions and processes at work under these southern vents which allow this magmatic signature to be repeated over time.

Of the other young eruptives produced around this 10 ka period, Tama Lakes is compositionally distinct from the northern vents (Te Mari Craters, North Crater, Blue Lake) but resembles to the Young SW Oturere trend (Fig 6.20). These relationships suggest that during this very active phase of Tongariro's eruptive history, there were probably two independently operating plumbing systems feeding magmas to the southern vents and to the northern vents. However, the magmas feeding into either the southern or northern vents respectively, probably did share a strong degree of inter-dependence with one another (reflected in their compositional similarities).

(i) **Red Crater.** The relatively young (0-c.3 ka) olivine-bearing lava flows and scoria erupted from the Red Crater vent near the centre of the Tongariro complex have a distinctive compositional-time relationship (Section 3.5.8i) already noted by previous workers (e.g. Topping, 1974). The older (pre-1.8 ka) lava flows are andesites which plot

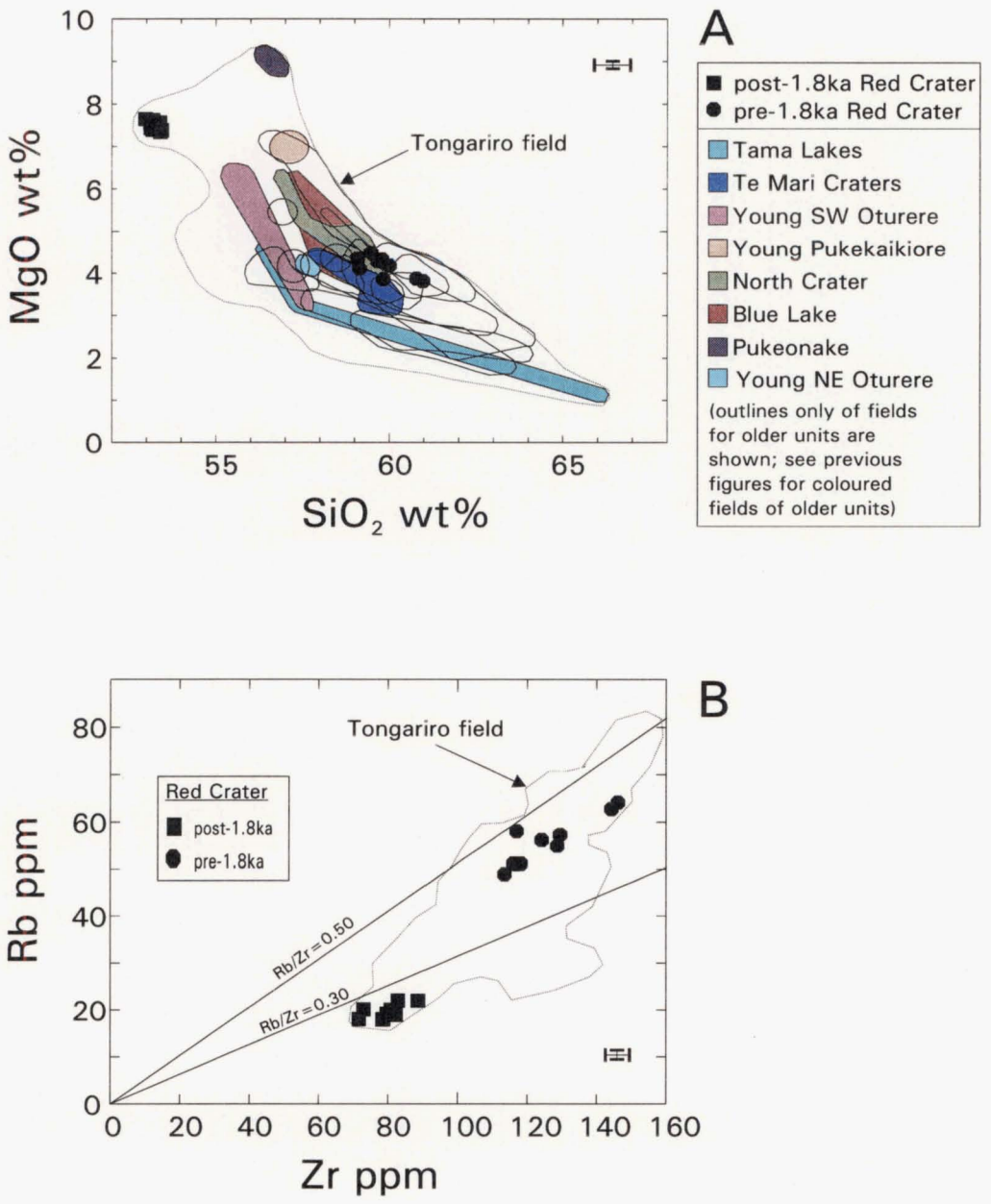

Figure 6.21 Variation diagrams for Red Crater eruptives: (**A**) MgO versus SiO_2, (**B**) Rb versus Zr. The compositional fields for the older volcano-stratigraphic units are shown in the MgO-SiO_2 diagram. The compositional field for all Tongariro samples is also shown for comparison. All data recalculated anhydrous. Error bars represent total error (2 sd from mean; Section A8.3.3).

in a relatively scattered trend between 59.1 and 61.1 wt% SiO_2 and 3.8-4.5 wt% MgO (Fig 6.21A). The younger (post-1.8 ka) flows are basaltic andesites which plot in a tight cluster at 53.0-53.7 wt% SiO_2 and 7.4-7.7 wt% MgO (Fig 6.21A). These post-1.8 ka lavas also contain correspondingly high concentrations of Cr (200-267 ppm; Fig 6.6B) and Ni (51-60 ppm; Fig 6.6C), CaO contents are displaced to higher values relative to the overall Tongariro trend (Fig 6.5B), and concentrations of Al_2O_3 (Fig 6.5A), alkalis (Figs 6.5G-H), and incompatible trace elements (e.g. Rb, Ba, Zr; Fig 6.6) are all very low. Analyses of Red Crater lava flows presented by Topping (1974) correspond closely with compositions determined for this study. Graham (1985a) and Graham and Hackett (1987) analysed the post-1.8 ka flow in Central Crater and included Red Crater "basalts" in their Type 1 lavas (Section 4.2). Red Crater "basalt" was tested as a parent composition in fractional crystallization models by Graham (1985a).

Stratigraphic-compositional relationships

Apart from the obvious stratigraphic break highlighted by the change in magma composition between pre-1.8 ka and post-1.8 ka lavas, the internal stratigraphy within these groups (and within one flow) may also be assessed for compositional trends. From the oldest and largest Red Crater flow, which probably represents a major withdrawal from the first Red Crater magma reservoir (Section 3.5.8i), a sampling sequence (TG087-090) up through a c.60m thick part of the flow margin reveals some degree of compositional variation within the flow (e.g. 3.9-4.4 wt% MgO, 56-75 ppm Cr, 317-344 ppm Ba, 114-129 ppm Zr) which can at least partly be attributed to fractional crystallization (although lack of appropriate mineral data precludes quantification by least-squares mixing calculations). Later lava flows (e.g. TG132-4) were slightly more mafic, suggesting that there may have been ongoing replenishment of the pre-1.8 ka magma reservoir.

The uniform composition of the post-1.8 ka eruptives precludes the establishment of any relationship between magma chemistry and stratigraphy (sequence of five lava flows; Appendix A2.3). However it does confirm that the dikes fed the lava flows and that all the flows and scoria were probably erupted over a relatively short time period, as short as years or decades, which did not allow for any significant magmatic differentiation between eruptions.

The distinct compositional break of over 5 wt% SiO_2 between the two Red Crater groups is inconsistent with fractional crystallization processes. Least-squares modelling between pre-1.8 ka and post-1.8 ka Red Crater lavas (e.g. Cole et al., 1983) is therefore not geologically reasonable. The strong petrographic and mineralogic evidence for magma mixing exhibited by the post-1.8 ka Red Crater eruptives (Sections 4.4.8i and 4.7) reflects the injection of a much more primitive batch of magma into the Red Crater plumbing system at this time. This is supported by other compositional differences such as the contrasting incompatible element ratios (e.g. Fig 6.21B) of the pre-1.8 ka lavas (Rb/Zr=0.43-0.50, Ti/Zr=28-39) compared to the post-1.8 ka lavas (Rb/Zr=0.23-0.27, Ti/Zr=49-58). Intermediate magma compositions transitional between the two extreme Red Crater groups have not been identified, suggesting that magma batches unrelated in time or chemistry can reoccupy the same shallow plumbing system..

Relationship with older units and Tongariro complex in general

With regards to their moderately high SiO_2 contents, the pre-1.8 ka Red Crater lava flows plot in the relatively high MgO part of the Tongariro field, overlapping with the NE Oturere field, and also parts of the Pukekaikiore and Tama 2 (group A) fields (Fig 6.21A). Of the other younger eruptives, these older Red Crater magma compositions correspond with those erupted earlier from Blue Lake and North Crater, but are displaced to higher MgO contents relative to the Te Mari Craters field (Fig 6.21A). Least-squares modelling shows that extraction of 12% crystals [plag+cpx+oliv+opx+mag] from a North Crater andesite produces a pre-1.8 ka Red Crater andesite with $\Sigma R^2=0.01$ and calculated phase proportions in reasonable agreement with those observed (Model A12.14).

In contrast to the earlier lava flows from Red Crater, the post-1.8 ka basaltic andesites bear no derivative relationship to any previously erupted magma compositions on the Tongariro complex. These lava flows, dikes and scoria represent the most SiO_2-poor of all the Tongariro eruptives (Fig 6.21A), although MgO, Cr, Ni, etc. are not as high as might be expected if the samples were following other Tongariro trends such as that defined by NE Oturere group A (Figs 6.6B-C, 6.21A).

Relationship between magma chemistry and eruptive style

A range of eruptive styles and eruptive products (lava flows, dikes, scoria fall) are represented by Red Crater, but do not relate specifically to certain compositions. The exposed dikes and scoria in the cone are post-1.8 ka basaltic andesites and the most accessible to sample. However further sampling, e.g. of scoriaceous lapilli associated with the older flows, would also show the existence of andesitic scoria. The broad eruptive style - compositional relationship of the pre-1.8 ka andesitic aa-block flows compared to the post-1.8 ka basaltic andesite pahoehoe-aa flows has already been noted in Section 3.5.8i.

(j) **South Crater**. Although a vent separate from Ngauruhoe has been recognised for the andesitic South Crater scoria (TG276; Section 3.5.8j), it is geochemically indistinguishable from the Ngauruhoe Group 3B lavas (Section 6.6.8k), plotting at the more silicic end of the trend (Fig 6.22A). It does not coincide with the Red Crater compositional fields, being less silicic (by c.2 wt% SiO_2) than pre-1.8 ka Red Crater andesites of comparable MgO contents (Fig 6.22A). The sampled scoria (TG276) contains 57.8 wt% SiO_2 and 4.1 wt% MgO. The eruption from the South Crater explosion pit took place prior to 1.8 ka (Section 3.5.8j), therefore this scoria represents one of only two pre-1.8 ka eruptive products with Group 3B affinities. The other is the long Ngauruhoe lava flow in Makahikatoa Valley (TG529), which is significantly less silicic than TG276. Further field investigation and sampling of the South Crater scoria deposit is needed to clarify its stratigraphic and compositional relationship to the Ngauruhoe eruptives.

(k) **Ngauruhoe.** The youngest cone of the Tongariro Volcanic Complex plays a central role in the quest for a fuller understanding of magma chamber dimensions, dynamics, and compositional relationships over time. The 2.5-0 ka Ngauruhoe cone represents a unique opportunity for well-constrained petrological investigation because of the large number (over 70) of historic and prehistoric lava flows preserved on its flanks. Furthermore, it is distinguished by its exceptionally diverse chemical composition, as outlined in Section 3.5.8k and Figures 3.30 and 3.31. This section serves to describe the compositional variability between and within Ngauruhoe lava groups in terms of the general whole-rock data set, and to discuss preliminary petrological modelling. A further assessment of Ngauruhoe time-space relationships, with the use of precise trace element and isotopic data, is reserved for Section 7.5. As noted at the beginning of Section 6.6.8,

the level of detail obtained for recognising the specific Ngauruhoe magma groupings may at least in part be a function of the excellent exposure of all sectors of the cone. In this way, Ngauruhoe geochemistry may not be unique amongst Tongariro units, but similar patterns in older cones may just be obscured by lack of full exposure or incomplete lava preservation.

Figures 3.30-31 depict the five distinct groups identified from Ngauruhoe in terms of composition (MgO-SiO_2), space (mapped distribution) and time (relative chronology of flows). These groups are also evident on Figure 6.22A, which places Ngauruhoe within the context of the other Tongariro volcano-stratigraphic units (see below). Ngauruhoe eruptives are predominantly basaltic andesites, with an overall geochemical range of 54.2-58.6 wt% SiO_2 and 2.2-5.6 wt% MgO. It is important to recognise this division of data into discrete groups and trends when confronted with such wide compositional diversity for a given SiO_2 content, e.g. the almost 3 wt% range in MgO contents for lavas of c.58 wt% SiO_2 (Figs 3.30B and 6.22A). Also important to note is the variation in slope, length and tightness of the trends formed by the different Ngauruhoe groups. These features have implications for such things as the magmatic intensive parameters, longevity of magma batches, extent of fractional crystallization, degree of crustal contamination, contrast between 'end member' mixing compositions, and degree of mixing (see also Section 7.5).

As noted in Section 4.4.8k, the occurrence of olivine phenocrysts is related to whole-rock MgO contents being >4 wt% (Groups 1A, 3A and most of 3B). Group 3A lavas, which are unexpectedly MgO-rich relative to their SiO_2 contents, contain chrome spinel-bearing olivines of composition Fo_{91} which are not in equilibrium with whole-rock Mg# (Fig 4.26), and which are surrounded by markedly more Fe-rich orthopyroxene rims (Fig 4.35). In contrast, Group 1A lavas, for which higher MgO would be anticipated based on the low SiO_2 contents, are characterised by disequilibrium Fo_{67} olivines (Fig 4.26) rimmed by more Mg-rich orthopyroxene. Other petrographic features (Table 4.1) such as particularly wide compositional ranges (e.g. An_{57-90}), strong reverse zoning, and sieved plagioclase, plus disparate crystallization temperature estimates (Fig 4.42B; Section 4.6) add to the evidence for magma mixing processes within the different Ngauruhoe lava groups. However, a simplistic model of mixing two Ngauruhoe magma types to get a third cannot be reconciled with the trends displayed on variation diagrams.

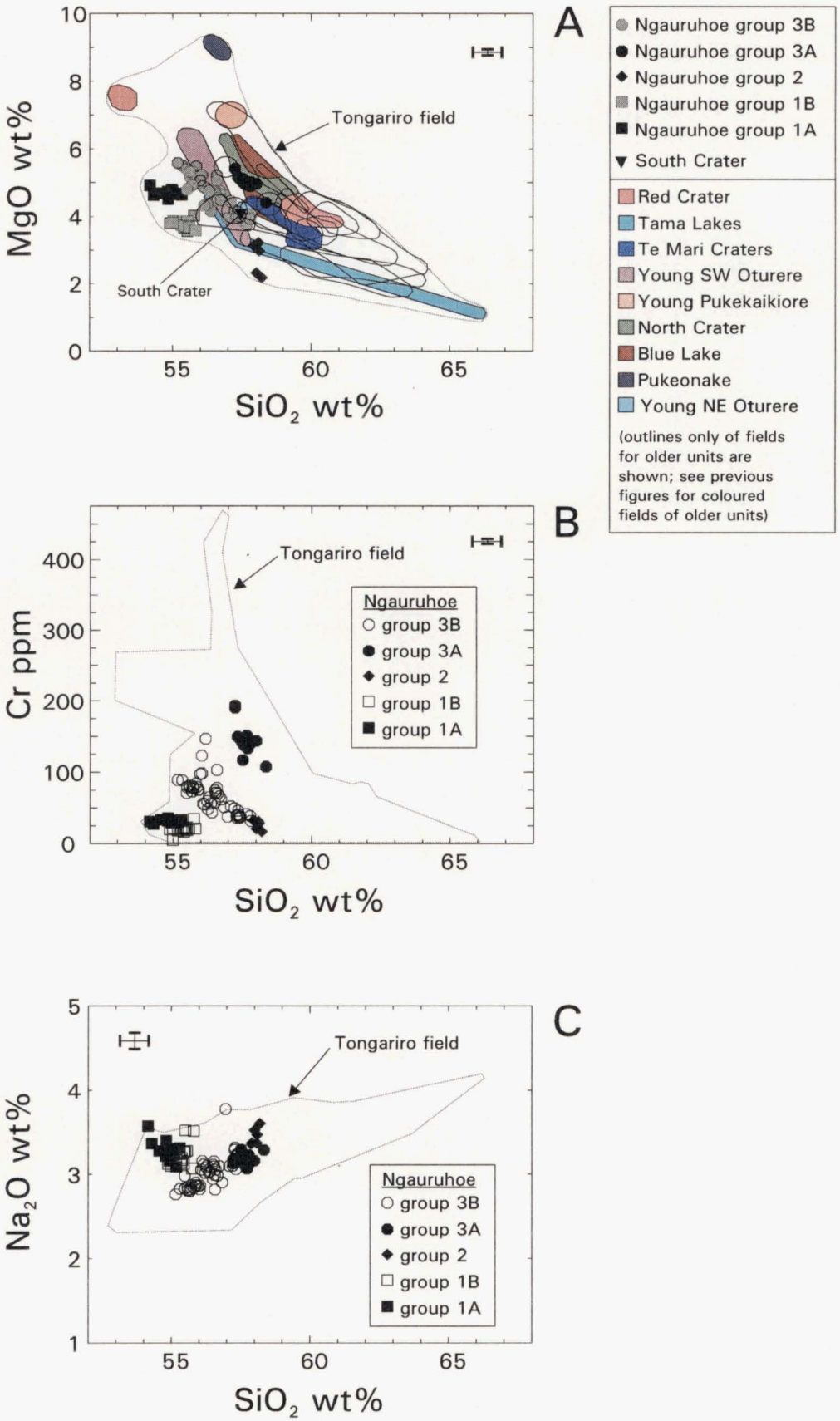

Figure 6.22 Variation diagrams for Ngauruhoe eruptives: (**A**) MgO versus SiO_2, (**B**) Cr versus SiO_2, (**C**) Na_2O versus SiO_2. The compositional fields for the older volcano-stratigraphic units are shown in the MgO-SiO_2 diagram. The compositional field for all Tongariro samples is also shown for comparison. All data recalculated anhydrous. Error bars represent total error (2 sd from mean; Section A8.3.3).

In addition, petrographic investigation of Ngauruhoe lavas and pyroclastics has revealed another important process which has helped shape patterns of magma chemistry. The occurrence of mm- to cm-sized quartzite xenoliths, especially prevalent in historic Ngauruhoe lavas, is attributed to incorporation of refractory quartz veins from the Torlesse metasedimentary basement (Chapter 5). Evidence of partial intergranular melting within xenoliths (Section 5.6.2) illustrates the involvement of crustal assimilation in Ngauruhoe magmas. Petrological modelling of this process is presented and discussed in Chapter 7.

Apart from the distinct geochemical groupings evident in MgO-SiO_2 compositional space, other chemical parameters serve to distinguish the Ngauruhoe groups from one another. In a pattern analogous to that revealed by the MgO-SiO_2 diagram, Cr (Fig 6.22B) and Ni abundances and trends also correspond with differences between groups. Note that for these trace elements, Group 3A is more elevated relative to the other groups than it is for MgO. Sometimes the distinctions between groups are not as sharply defined, such as for Na_2O versus SiO_2 (Fig 6.22C), but the contrasts in the slopes and lengths of trends still highlight the heterogeneous nature of Ngauruhoe magmas. For many compatible elements (e.g. CaO, Fe_2O_3*), the pattern of Ngauruhoe groups is masked by the overall fractional crystallization trend.

Some fundamental differences between (and within) groups are revealed in plots of Sr (Fig 6.22D) and Zr (Fig 6.22E) versus SiO_2. Group 1A lavas contain markedly higher concentrations of Sr, but so do two of the Group 1B samples which are split from the rest of their group. Contrasts in trends are also evident; Group 3A displays a very tight constant Sr trend, whereas the Group 3B 'trend' displays considerable scatter. Considerable scatter occurs on the Zr-SiO_2 plot, but once again Group 1A and the two Group 1B samples are significantly elevated in Zr relative to other lavas of comparable SiO_2 contents.

Incompatible element ratios also provide further clues to processes which operated to produce the distinct Ngauruhoe magma groups. Instead of remaining constant as would be expected during closed system fractional crystallization there is considerable scatter in Rb/Zr, for example, plus constant ratio lines can effectively separate the Ngauruhoe groups (Fig 6.22F). This separation is incomplete, however, because there is a small degree of overlap between Groups 2, 3B and 1B. Distinctions between groups are generally more

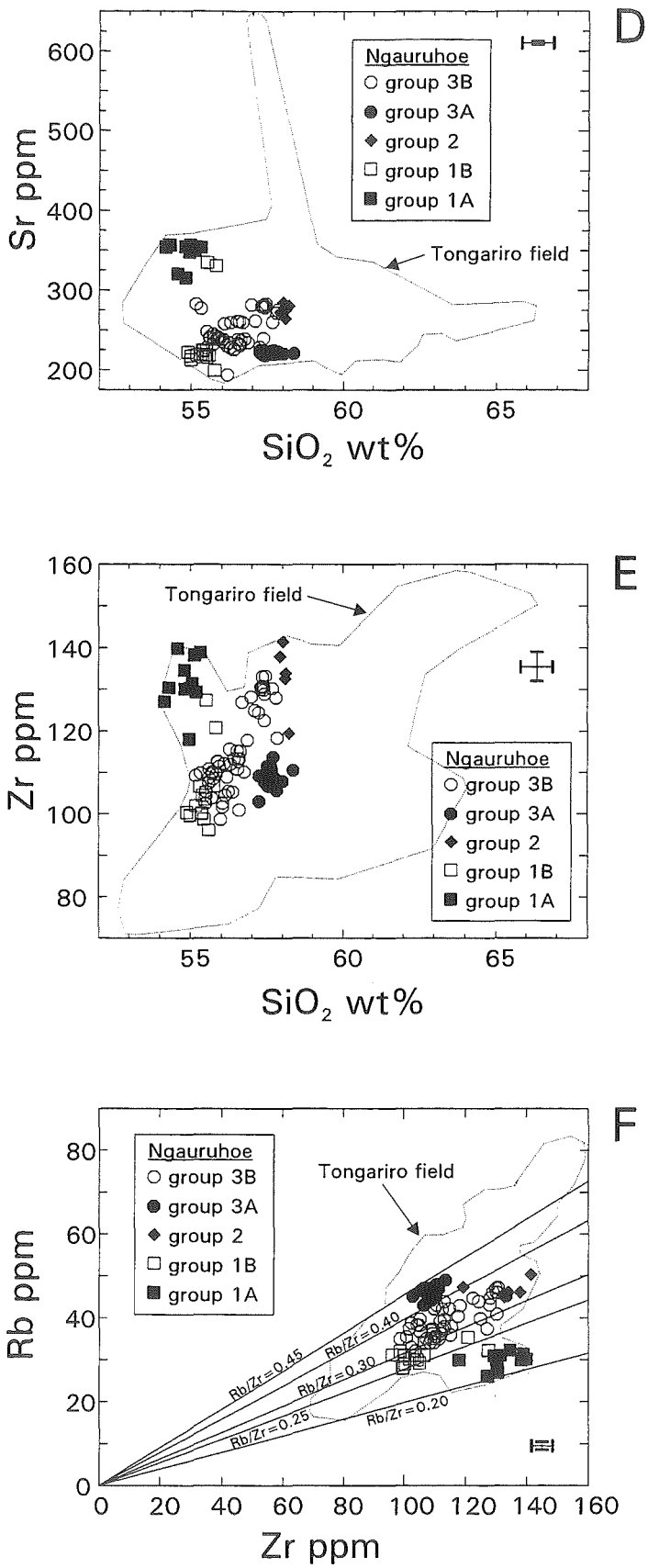

Figure 6.22 (continued) Variation diagrams for Ngauruhoe eruptives: (**D**) Sr versus SiO_2, (**E**) Zr versus SiO_2, (**F**) Rb versus Zr. The compositional field for all Tongariro samples is also shown for comparison. All data recalculated anhydrous. Error bars represent total error (2 sd from mean; Section A8.3.3).

blurred for other ratios, such as K/Zr, Ti/Zr, Ba/Zr, although some degree of separation is usually evident. To determine what process(es) are responsible for these different incompatible element ratios (e.g. variable source compositions, variable degrees of partial melting, variable crustal contamination) requires radiogenic isotope data (Chapter 7). The large range in incompatible element trace elements for Ngauruhoe lavas does not automatically require derivation from many different primary magmas. These differences may be reconciled by a process involving heterogeneous crustal contamination of a single parental magma in separate magma chambers (see Chapter 7). Thus even with the XRF data set, it is apparent that Ngauruhoe magma compositions are controlled by much more than just fractional crystallization, and that additional processes are operating at a variety of structural levels to produce the compositional variability observed in Ngauruhoe lavas and pyroclastics.

Table 6.1 provides a brief summary of the main geochemical differences between the five Ngauruhoe lava groups.

Table 6.1 Geochemical characteristics of the Ngauruhoe lava groups.

	Group 1A	Group 1B	Group 2	Group 3A	Group 3B
SiO_2 (wt%)	54.2 - 55.5	55.2 - 55.9	57.9 - 58.3	57.2 - 58.6	54.8 - 58.2
MgO (wt%)	4.5 - 4.9	3.6 - 4.0	2.2 - 3.2	4.4 - 5.4	3.8 - 5.6
Cr (ppm)	28 - 36	5 - 35	17 - 33	108 - 193	32 - 147
Ni (ppm)	13 - 17	9 - 13	7 - 13	34 - 57	9 - 36
Sr (ppm)	316 - 359	200 - 334	266 - 284	219 - 225	194-284
Zr (ppm)	119 - 142	96 - 127	119 - 141	103 - 114	99 - 133
Rb/Zr	0.20-0.25	0.25 - 0.32	0.33 - 0.39	0.40 - 0.44	0.29 - 0.39

Previous work

Prior to this study, whole-rock chemical analyses of Ngauruhoe lavas had focused on the historic eruptives. Steiner (1958) published one analysis each of prehistoric, 1928, 1949 and 1954 lavas/ejecta and these were subsequently quoted by other workers (e.g. Clark, 1960a). Because the original 1928 sample is no longer available, this analysis is used in Section 7.5.1 to further clarify the magmatic history of Ngauruhoe in historic times. Steiner's (1958) sample of the 1949 lava (P9997) was obtained courtesy of GNS, Lower Hutt, and re-analysed on the University of Canterbury XRF (Appendix 10). P9997 is almost identical to the 1949 sample collected for this study (TG019). More detailed analysis of the 1954 lava flow sequence (data for 10 flows) was provided much later by Cole (1979b), and these 12 samples were re-analysed by Graham (1985a), but were not widely published in either case. Graham's (1985a) analyses correspond well to those obtained for the same flows in this study. One of Graham's (1985a) analyses of Ngauruhoe 1954 lava was used in petrogenetic models in a study on Ruapehu (Graham and Hackett, 1987; Section 6.7). Patterson and Graham (1988) also present data on Ngauruhoe 1954 lava as part of their study of the Mangatepopo Valley - Upper Tama Lake area.

Nairn et al. (1976) presented major element analyses of Ngauruhoe 1974 ejecta; a lava spatter bomb (P39851) erupted in January and a solid lava block (P39864) erupted in March. Because the 1974 eruptions did not leave permanent deposits they were not sampled in this study. However, the two original samples used for the published analyses were obtained courtesy of GNS, Lower Hutt, and re-analysed to be included in the data set in Appendix 10. Major element data for lapilli ejected during the 19 February 1975 eruption were tabulated by Nairn and Wood (1987), and a sample (P40674) was also obtained from GNS, Lower Hutt, and re-analysed for the current study (Appendix 10).

This study has built on the existing geochemical data base for historic Ngauruhoe eruptives and extended it to include more 1975 analyses, 1954-75 scoria from the inner crater, and the two 1870 lava flows. Unfortunately, proximal ejecta from other eruptions this century were not collected or analysed, probably because of the relative isolation of Ngauruhoe in the earlier part of the century, in conjunction with limitations on resources available for formal volcanological research. Nevertheless, data for six eruptions over a 100 year interval (1870, 1928, 1949, 1954, 1974, 1975) provide ample opportunity for

composition-time relationships to be investigated (Section 7.5.1). The major contribution of this study is of course the comprehensive sampling and chemical analysis of virtually all exposed prehistoric lava flows from all sectors of the cone. Thus for the first time the distinctive Ngauruhoe lava groups have been identified.

Stratigraphic-compositional relationships

The stratigraphy, or chronology, of Ngauruhoe eruptives was introduced in Section 3.5.8k and is presented in Appendix 2.1. Each compositionally distinct lava group generally relates to a series of flows confined to a certain sector of the cone (Fig 3.31), representing a certain period in Ngauruhoe's eruptive history. However, this is not a simple composition-time relationship, as demonstrated by Figure 3.31. Group 3B lavas correspond with the youngest prehistoric and historic lavas directed down into Mangatepopo Valley, with the important exception of the long TG529 flow into Makahikatoa Valley which overlies Mangatawai Tephra (Topping, 1974) and therefore was erupted during the same period as the pre-Taupo Pumice Group 1A lavas (Fig 3.31). Most Group 1B lavas were erupted relatively early in Ngauruhoe's eruptive history, but several lavas (e.g. TG003, TG158) are much younger and overlie Group 3B lavas (Fig 3.30A).

These exceptions to the general pattern indicate that certain magmatic signatures can be repeated over time after an eruption interval which has produced contrasting magma types. This conflicts with the simplest scenario to explain Ngauruhoe geochemistry which would be to invoke a succession of different discrete magma batches feeding the eruptions, each batch existing just long enough to give rise to a different lava group, before the next (contrasting) batch arrived to take its place. But the situation represented by TG529, TG003, etc. seems to instead reflect the coexistence of more than one magma batch beneath Ngauruhoe at any one time. These 'exception to the rule' lavas may in effect represent 'leaky' magma batches from which an early aliquot (e.g. TG529) or the last remnants (e.g. TG003) are drawn, synchronous with eruptions from the main magma storage area at that time.

That the Ngauruhoe lava groups do not represent a continuum of steadily evolving magma compositions can be demonstrated by the failure of most major element fractional crystallization models (see below), along with geochemical and mineralogic evidence for

magma mixing and crustal contamination. A closer look at compositional-stratigraphic relationships within Group 3B reveals further complexity, which is dealt with on a number of time scales in Section 7.5. These include documentation of the variation from prehistoric to historic times, during historic eruptions over c.100 years (1870 to 1975), between recent eruption episodes separated by 20 years (1954-5 to 1974-5), and during one year (1954).

Fractional crystallization models

Least-squares mixing calculations give a first approximation to the viability of fractional crystallization as a process linking the different Ngauruhoe groups. The oldest lavas (Group 1A) occupy a position on variation diagrams (e.g. 6.22A) such that no other Ngauruhoe composition may be reasonably modelled as parental to them. Modelling fractional crystallization of a Group 1A initial magma to produce a Group 1B magma was unsuccessful, as expected from the lack of a fractional crystallization trend between the two groups (Fig 6.22A). The limited compositional variability of lavas in each of these groups prevents rigorous modelling within each group.

Group 2 magmas present a dilemma in terms of modelling because of the small data set which seems to plot as an almost vertical trend on the MgO-SiO_2 diagram (Fig 6.22A). Ngauruhoe may have erupted other lavas of a similar composition, which would possibly have augmented the Group 2 trend, but such lavas are not exposed for sampling. Group 1A cannot be modelled as parental to Group 2 via fractional crystallization; the least-squares mixing model required significant orthopyroxene accumulation. Conversely, removal of 22-26% [plag+cpx+opx+mag] crystals from TG020 of Group 1B can produce a Group 2 lava with low ΣR^2 (<0.03) and calculated phenocryst proportions comparable to those observed. Modelling was most successful with the higher MgO Group 2 lavas (e.g. Model A12.15). If it were possible to obtain more data from Group 2, trends may become apparent which would indicate that two magma groups (high and low MgO) are actually represented by Group 2. This uncertainty coupled with the compositional gap of 2 wt% SiO_2 between Group 1B and Group 2 compositions means the origin of Group 2 magmas remains equivocal. However, of the other Ngauruhoe lava groups they appear to be most closely related to Group 1B based on major element modelling.

Group 3A likewise cannot reasonably be derived from any other Ngauruhoe group due to its moderate-SiO_2, high-MgO position on the variation diagram (Fig 6.22A). Least-squares modelling along the Group 3A trend showed that the highest MgO lava (TG288) could not be successfully modelled to lower MgO lavas (e.g. TG289, TG283) by fractional crystallization. The calculations indicated that phenocrysts could not be extracted in modal proportions. Note that magma compositions do not simply get progressively more silicic with time. This coupled with the relatively straight trend on Fig 6.22A and petrographic evidence (see above) suggests that the Group 3A trend may represent a mixing line.

As is the case for most of the other Ngauruhoe lava groups, Group 3B eruptives plot as a discrete trend which does not share a fractional crystallization affinity with any of the preceding magma groups. On the MgO-SiO_2 diagram (Fig 6.22A), the Group 3B samples plot as a slightly scattered, relatively linear trend which along with irregular compositional-stratigraphic relationships and petrographic evidence suggests that magma mixing has played a role in developing this trend. To test the degree of involvement of fractional crystallization processes presents difficulties because the most mafic lavas (likely to be chosen as 'initial' magma compositions) are actually the young historic eruptives from 1870, 1954 and 1975, and should not be modelled as producing the older, more silicic prehistoric lavas. However, taking segments of the Group 3B trend for which logical age relationships can be established, step-wise least-squares mixing calculations reveal that parts of the trend may be related to fractional crystallization. Modelling the 1870 lava (TG001) by fractional crystallization to produce the 1949 (TG019) or 1954 (TG042-44) lavas failed to produce acceptable ΣR^2 values (0.2-0.7) and did not reconcile well with observed phenocryst proportions. But one of the relatively older prehistoric flows (TG156) can be successfully related via fractional crystallization to the younger flows on the upper cone. For example, Model A12.16 demonstrates the good fit (ΣR^2=0.02) when 16% [plag+opx+cpx+mag] crystals are removed from TG156 to produce TG501, with calculated phenocryst proportions very close to those observed.

The overall difficulty in modelling the major elements for Group 3B, and indeed for generally all the Ngauruhoe groups, highlights the importance of processes *other* than fractional crystallization in producing the observed compositions and trends. And these other processes, such as magma mixing, are also inherently variable. Compositions of

initial magma batches obviously vary between the Ngauruhoe groups, but because of the relatively short time span involved it is likely that segregation into different magma batches occurs at a higher level than a deep mantle source. Thus these Ngauruhoe groups do not represent separate mantle partial melts, but probably a shallower differentiation of one initial mantle-derived melt body. The degree of mixing and ongoing recharge of each magma batch also vary. Groups 1A and 1B may represent comparatively short-lived magma batches which were not undergoing constant replenishment and mixing, and therefore are of limited compositional variability. In contrast, the Group 3B trend may reflect a more prolonged, integrated magmatic system which experienced several episodes of magma recharge, between which a certain degree of fractional crystallization could occur.

Relationship with older units and Tongariro complex in general

Ngauruhoe eruptives occupy an almost unique position within the overall Tongariro compositional field. Although among the lowest-SiO_2 lavas erupted from the Tongariro complex, Ngauruhoe lavas contain only moderate MgO relative to their SiO_2 contents (Fig 6.22A). The MgO-SiO_2 space defined by Groups 1A, 1B, 2 and 3A is essentially unique to these Ngauruhoe groups, whereas the lower-MgO part of the Group 3B trend overlaps with parts of the South Crater, Tama Lakes, Young NE Oturere, Tongariro Trig, and Tama 2 fields (Fig 6.22A). Nevertheless, a significant change from the previous Tongariro magmatic conditions is reflected in the distinctive Ngauruhoe compositions.

Other chemical differences are evident on a broad scale. Compared to the trend towards low Al_2O_3 contents for some of the other mafic Tongariro eruptives (e.g. post-1.8 ka Red Crater), Ngauruhoe lavas tend to contain relatively high levels of Al_2O_3 (Fig 6.5A). In contrast to the hornblende-bearing lavas (e.g. Tama 1, Tama 2, Pukekaikiore) which tend to plot along a lower-K_2O (and Rb) trend relative to the main Tongariro trend (Sections 6.5.1h and 6.5.2f), note that Ngauruhoe eruptives generally plot along the high-K_2O (and Rb) side of the field, with Group 1A lavas forming a higher-K_2O (and Rb) trend subparallel to and above the Group 1B trend (Figs 6.5H and 6.6E). Ngauruhoe lavas are also notable for their comparatively high Rb/Sr trend in terms of their SiO_2 content, relative to the overall Tongariro field (Fig 6.7A).

The only other Tongariro unit which could reasonably be modelled as parental to Ngauruhoe is the post-1.8 ka Red Crater eruptives, which are distinctly more MgO-rich and slightly more SiO_2-poor than the Ngauruhoe lavas (Fig 6.22A). Extensive least-squares mixing calculations failed to produce a convincing model for fractional crystallization of post-1.8 ka Red Crater basaltic andesite to any Ngauruhoe lava. The best approximations were for Group 1A and 3B, but ΣR^2 values were still unacceptably high and/or calculated phenocryst proportions did not correspond well to modal proportions. Graham (1985a) concluded that a Ruapehu basalt (Mangawhero Formation) was better able to generate the Ngauruhoe 1954 basaltic andesite than the post-1.8 ka Red Crater "basalt". Thus the Ngauruhoe and Red Crater lavas do not share any direct link; their magmatic plumbing systems appear to have operated independently of one another.

Could the Ngauruhoe-type magma have the potential to fractionate to other Tongariro compositions? Although the age relationships do not hold, it is an interesting question to consider because it could represent a similar previous magma composition produced by the Tongariro complex (and perhaps now eroded or concealed) which could explain the occurrence of the low-MgO SW Oturere and Tongariro Trig group A trends which seem to be natural extensions of the Ngauruhoe Group 3B trend (Fig 6.22A). Least-squares mixing calculations (Models A12.17-18) demonstrate that Ngauruhoe lava TG156 could fractionate phenocrysts in roughly modal proportions to produce lavas of similar composition to those represented by SW Oturere (TG076) and Tongariro Trig (TG338). Calculated ΣR^2 values were low (0.03-0.04), although other samples tested were not all such good fits and the models did tend to underestimate plagioclase proportions and give varied clinopyroxene-orthopyroxene ratios. The success of at least some of these models, however, demonstrates that despite the comprehensive field sampling undertaken for this study, it cannot be assumed that the Tongariro complex has been as equally diligent in sampling (erupting) magmas representative of all compositions produced over the lifespan of the magmatic plumbing system. In other words, the availability of magma at a certain time is not necessarily reflected in what is actually being erupted.

Relationship between magma chemistry and eruptive style

Most of the eruptives sampled from Ngauruhoe are lava flows, which span the entire compositional range represented by this cone. The historic scoria and pyroclastic avalanche

deposits plot along the length of the Group 3B trend and do not show any strong compositional control (note that older pyroclastics are not so well exposed and were not sampled in this study). Thin aa transitional to pahoehoe flows are rarely preserved on the upper cone (Section 2.2.1a), but are not the most mafic of the Ngauruhoe flows (only moderate MgO contents of 4.7 wt%).

The majority of lava flows from Ngauruhoe are of the aa to block type (Section 2.2.1a), and they exhibit a certain degree of variability in terms of proportion of breccia versus sheet lava, levée development, surface relief, thickness, and length. Magma composition does not appear to exert any influence over flow length (Section 2.2.1a). A closer look at the morphologies and physical parameters of Ngauruhoe lava flows would be instrumental in establishing high level magma chamber/vent processes and flow emplacement mechanisms - which are important variables to consider in conjunction with composition-time relationships.

Summary

The Ngauruhoe eruptives, which occupy an almost unique low-SiO_2, moderate-MgO position within the overall Tongariro compositional field, are basaltic andesites and andesites of wide major and trace element variability, e.g. diverse MgO, Na_2O, Cr, Ni, Sr, Zr, Rb/Zr. They fall into five distinct lava groups (1A-3B) which represent flows which built different sectors of the cone at essentially different times, although some overlap between certain groups reflects coexistence of some magma reservoirs. Petrographic evidence for magma mixing is supported by compositional reversals along trends, and the general failure of major element fractional crystallization models in linking between and within the groups. The occurrence of crustal xenoliths indicates that assimilation processes are also involved in Ngauruhoe magma genesis.

On variation diagrams the Ngauruhoe lava groups differ in characteristics such as the length and slope of the trends, as well as the actual compositional space they occupy. These features highlight the contrasting magma chemistry of each group, and the varying degrees of fractional crystallization, assimilation, mixing, and replenishment experienced by each of the many magma batches over its lifetime. Groups 1A and 1B may represent comparatively short-lived magma batches which lacked continuous fresh magma influx and

associated mixing, and therefore are of limited compositional variability. In contrast, the Group 3B trend is consistent with a more prolonged, integrated magmatic system which experienced several episodes of magma recharge, between which a certain degree of fractional crystallization took place.

6.6.9 Summary of chemical relationships between cone-forming units

As has been shown by the preceding descriptions, there are varying degrees of similarity and diversity between and within the Tongariro volcano-stratigraphic units. Some of the key compositional parameters used to characterise the units from the general whole-rock data set are summarised in Table 6.2. However, as already demonstrated, the use of variation diagrams is usually a more effective way to give an immediate impression of the relationships between units. These diagrams highlight the differences which exist between and within units in terms of:

1. absolute major and trace element abundances for given SiO_2 contents,
2. degree of compositional variability (cluster of data points versus elongate trend; length of trends),
3. rate of compositional change with respect to SiO_2 (steepness of trends),
4. shape of trends (curvilinear versus linear),
5. conformity of data points to trends (scattered versus tight trends), and
6. distribution of chemical groups within observed SiO_2 ranges.

In considering the above factors, patterns emerge which link compositionally similar units. Thus a sense of chemical 'order' is obtained for which spatial and/or temporal connotations may also apply. Note that there are several scales or levels on which this chemical ordering becomes apparent. Within most units there are a number of different geochemical groups which between them usually represent multiple magma batches; certain units on their own represent a distinctive type of magma; and several units may share compositional-time-space characteristics which denote a similar origin. It is mainly the latter scale of magmatic ordering that this section is concerned with describing.

Table 6.2 Summary of some key compositional characteristics of Tongariro volcano-stratigraphic units. See Table 3.3 for summary of age, volume, eruptive rate, vent location and eruptive products of each unit. Rock type is based on the TAS classification (BA=basaltic andesite, A=andesite, D=dacite).

Volcano-stratigraphic unit	Rock type	SiO_2 (wt%)	MgO (wt%)	Cr (ppm)	Ni (ppm)	Sr (ppm)	K/Rb	Rb/Sr	Rb/Zr	Ti/Zr	No. of chemical groups
Ngauruhoe	BA - A	54.2 - 58.6	2.2 - 5.6	5 - 193	7 - 57	194 - 359	224 - 317	0.12 - 0.18	0.20 - 0.44	33 - 55	5
South Crater explosion pit	A	57.8	4.1	33	12	277	265	0.15	0.31	38	1
Red Crater	BA - A	53.0 - 61.1	3.8 - 7.7	56 - 267	18 - 60	269 - 295	229 - 309	0.06 - 0.24	0.23 - 0.50	28 - 58	2
Tama Lakes	BA -A - D	56.1 - 64.2	1.1 - 4.5	3 - 32	4 - 16	264 - 331	226 - 245	0.12 - 0.26	0.35 - 0.47	15 - 38	1?
Te Mari Craters	A	57.5 - 60.2	3.1 - 4.4	24 - 65	11 - 22	253 - 375	224 - 270	0.10 - 0.22	0.35 - 0.49	33 - 42	1?
Young SW Oturere	BA - A	55.0 - 57.4	3.3 - 6.3	13 - 128	8 - 33	268 - 289	231 - 254	0.11 - 0.19	0.31 - 0.38	38 - 43	1?
Young Pukekaikiore	A	56.9 - 57.4	6.9 - 7.0	229 - 248	35 - 38	634 - 643	255	0.05	0.33 - 0.37	42 - 44	1
North Crater	BA - A	56.3 - 60.1	3.3 - 6.2	33 - 314	10 - 79	249 - 309	220 - 246	0.17 - 0.24	0.38 - 0.50	30 - 42	3?
Blue Lake	A	56.8 - 59.9	3.3 - 6.2	26 - 257	10 - 59	248 - 363	213 - 293	0.09 - 0.25	0.29 - 0.50	32 - 39	3?
Pukeonake	BA	56.5 - 57.0	8.9 - 9.2	424 - 460	217 - 220	274 - 278	217 - 218	0.19 - 0.21	0.42 - 0.46	32 - 33	1
Young NE Oturere	A	57.6 - 58.1	4.1 - 4.3	26 - 27	8 - 10	264 - 265	243 - 245	0.17 - 0.18	0.35 - 0.38	38 - 39	1
Tongariro Trig	A - D	57.0 - 62.3	1.8 - 4.6	6 - 132	3 - 31	237 - 297	210 - 274	0.14 - 0.32	0.33 - 0.55	30 - 41	2
SW Oturere	A - D	57.2 - 65.5	2.1 - 5.5	8 - 138	4 - 44	220 - 342	228 - 334	0.10 - 0.32	0.21 - 0.55	28 - 49	3
Pukekaikiore	A	59.8 - 61.8	3.6 - 4.3	20 - 53	9 - 18	220 - 294	251 - 373	0.10 - 0.17	0.25 - 0.47	29 - 37	1
Tama 2	BA - A	56.4 - 63.0	2.1 - 4.5	7 - 79	4 - 25	200 - 306	234 - 334	0.08 - 0.26	0.27 - 0.55	28 - 54	2
NE Oturere	BA - A	55.4 - 62.2	3.5 - 7.1	21 - 260	7 - 55	225 - 408	212 - 321	0.09 - 0.23	0.26 - 0.50	27 - 43	2
Tama 1	A	59.5 - 62.6	2.8 - 3.8	25 - 57	11 - 21	248 - 255	242 - 274	0.13 - 0.19	0.34 - 0.51	27 - 40	2

Because conclusive evidence for many intensive parameters (e.g. total pressure) is lacking, it is difficult to envisage in detail the configuration of magma reservoirs feeding the Tongariro vents at different times. Relative magma reservoir volumes may be roughly approximated from relative cone volumes, although the precise ratio of intrusive to extrusive volumes cannot be readily determined from existing geophysical information. Crisp (1984) found that subduction-related settings represent typical intrusive:extrusive volume ratios of 10 to 1. However, magma storage areas inferred from geophysical data are often of a similar magnitude to the erupted material (Marsh, 1989). Most of the units do not represent particularly constant compositions over their lifetime, recording the effect of frequent new magma influx and mixing events, suggesting that their magma reservoirs were generally too small to even out and obscure the compositional variations produced by a dynamic magmatic system. The depths of the various magma storage areas are not known with any certainty, but the abundant plagioclase phenocrysts present in most eruptive products testify to considerable crystallization within the crust, although probably in reservoirs at more than one level.

Linking in the variables surrounding transport and storage of magma with geochemical studies is very challenging, but ultimately necessary to a fuller understanding of the dynamics of volcanoes (e.g. Iyer et al., 1990). It is not possible to create one unifying model for the entire Tongariro Volcanic Complex because of the diverse range of magma groups over a relatively long time period. Instead, a series of models for successive windows of time are more appropriate for illustrating the complex plumbing history and petrogenesis. Using the available information, a schematic representation of Tongariro magmatic relationships as interpreted (Fig 6.23) can at least establish the general context and the likely links between magma batches and reservoirs with respect to space, time, volume and composition. Note that although the diagrams in Figure 6.23 show a relatively stylised and simplified plumbing system of single conduits connected to one or two magma reservoirs, in reality the ascending magma may be more likely to follow much less straightforward pathways via more intricate networks of branching, discontinuous conduits. The broad relationships between units are also summarised in Table 6.3 and discussed below.

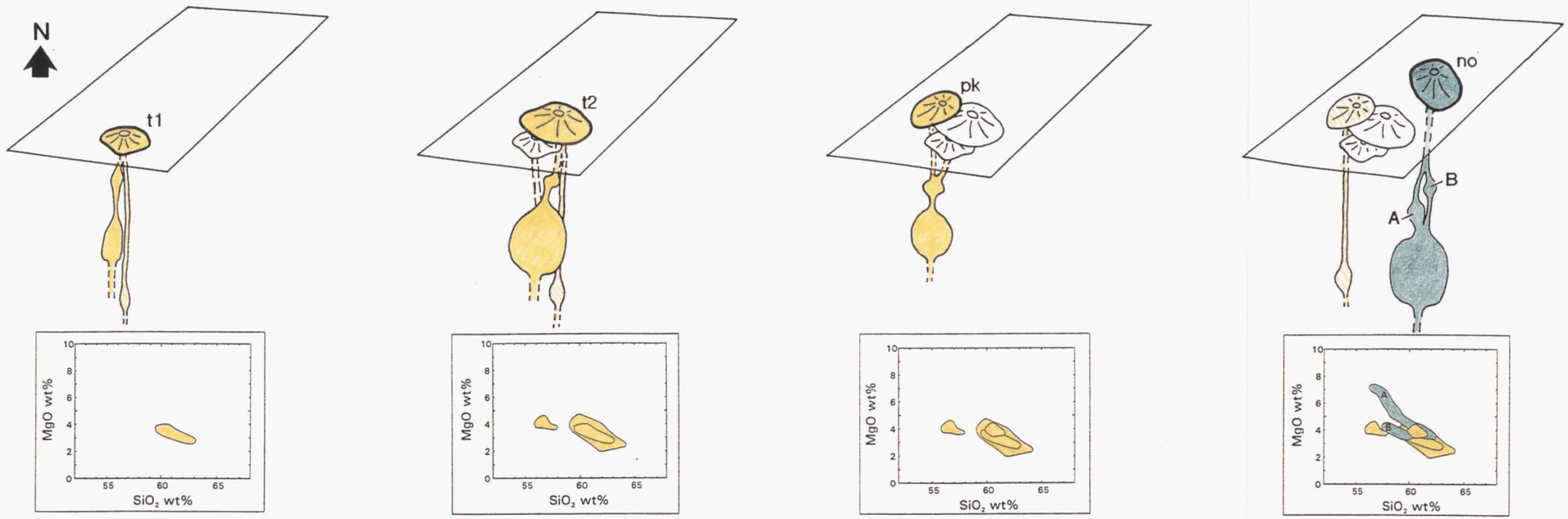

Figure 6.23 Schematic representation (not to scale) of Tongariro magmatic relationships in time and space in terms of crustal magma reservoirs, plumbing system dynamics and magma compositions (see text for discussion). Selected time windows are shown for main periods of cone growth and only the main volcano-stratigraphic units involved in each time period are depicted. Note that uncertainty surrounds the time of earliest initiation of NE Oturere activity. The interval 65-25 ka may represent a period of quiescence. See Figures 3.2 and 3.4 for maps of cone and vent distribution. Simplified MgO-SiO_2 diagrams for each time window relate to the more detailed plots of Figures 6.9 - 6.22 and are colour-coded to show compositional relationships between units (also summarised in Table 6.3).

Table 6.3 Relationships between Tongariro volcano-stratigraphic units with respect to composition (including type of trends on variation diagrams), age, spatial distribution within Tongariro complex, volume of cones and magma reservoirs, and eruptive rate (major cones only). See Tables 3.3 and 6.2 for abbreviations.

Units	Chemical composition	Age range (main period)	Spatial distribution	Original cone volume	Eruptive rate
Tama 1 Tama 2 Pukekaikiore	amphibole andesite high K/Rb short-moderate, broad shallow trends	275 - 160 ka	S - SW	small to large 2 - 10 km^3	very high t2 = 1 km^3/ka
NE Oturere	olivine BA - A high MgO long, steep trend A & shorter trend B	130 - 90 ka	central - NE	relatively large 11 km^3	moderate 0.4 km^3/ka
SW Oturere Tongariro Trig	andesite -dacite low MgO long, shallow trend A & shorter trend B	110 - 65 ka	central - NW - SE	moderate to large 5 - 12 km^3	moderately low 0.1 - 0.3 km^3/ka
Yg NE Oturere Blue Lake North Crater Te Mari Craters pre-1.8 ka Red Cr.	(olivine) andesite moderate MgO short, scattered, mod. steep trends	20 - 0 ka	N - central	small <0.5 km^3	
Yg SW Oturere Tama Lakes	BA - A - D relatively long, mod. steep trends	14 - 10 ka	central - S	small <0.1 km^3	
Ngauruhoe	(olivine) BA - A moderate MgO 5 distinct geological - chemical trends/groups	2.5 - 0 ka	central	moderately small 2.2 km^3	high 0.9 km^3/ka
Others: Pukeonake Yg Pukekaikiore post-1.8 ka Red Cr.	oliv BA-A scoria+flows high MgO, Cr, Ni (ypk = very high Sr) groups/short trends	23 - 0 ka	central - W	small <0.5 km^3	

(a) **Tama 1, Tama 2, Pukekaikiore.** Most eruptive products from these units are distinguished from others on Tongariro by the presence of amphibole in the phenocryst assemblage (Fig 4.8). These relatively silicic andesites also exhibit a distinctive chemical signature reflected in higher K/Rb for a given SiO_2 content, and comparatively low K_2O, Rb, La, Ce, Y and Zr abundances relative to other Tongariro units (Sections 6.6.2, 6.6.4, 6.6.5). When looking at variation diagrams, considerable data scatter along relatively short to medium-length (c.2-3 wt%SiO_2 range), shallow, broadly linear trends are features common to all three units (e.g. Figs 6.9A, 6.11A, 6.12A).

Trends on variation diagrams overlap for the units (e.g. Fig 6.12A), except for the Tama 2 group B lavas which lack amphibole or the other associated chemical characteristics. That there were a minority of amphibole-free lavas erupted from these southern vents over this early period (c.275-160 ka) in Tongariro's development indicates the involvement of at least two quite different, but coexisting, parental magma reservoirs (Fig 6.23). Magma chamber offshoots or discrete batches from these main storage areas would have allowed further diversification, e.g. the subtle mineralogical distinction between the green amphibole of Tama 1 and the brown amphibole of Tama 2 and Pukekaikiore (Section 4.5.4). Least-squares mixing calculations demonstrate that it is partly feasible to relate the three units via fractional crystallization, indicating some degree of shared history. However, there is also considerable evidence for magma mixing having played a major role in the genesis of these lavas and this process has no doubt complicated any obvious inter-relationships between units.

Tama 2 is also noteworthy for its particularly high volume (originally c.10 km^3) and very high eruptive rate (1 km^3/ka) compared to other Tongariro units (Table 3.3). Poorer exposure/sampling of Tama 1 and Pukekaikiore cones may possibly have influenced their much lower calculated rates of cone growth, but a strong relationship between the occurrence of amphibole-phyric magmas and a high eruptive rate cannot be proven. There does not appear to be a particularly long (if any) repose period between the close of Tama 1 activity and the initiation of the voluminous eruptions from Tama 2, suggesting sporadic magma recharge rather than a constant magma supply rate. Aside from the similarities of the three units, the Tama 2 cone appears to represent a rather special set of circumstances which allowed eruption of such a large volume of magma in probably less than ten

thousand years. In this case at least, it appears that the pattern of cone growth (eruptive rate, etc.) is not set at as deep a level as the parental magma reservoir, but is probably a higher level phenomenon.

Thus despite the variation displayed by these amphibole-phyric units, they all reflect involvement of a distinctive type of magma which was restricted to these southern vents and the earlier part of Tongariro's history. Magmatic diversity was probably established through differences in the dynamics of magma replenishment and withdrawal and perhaps also by variable crustal contamination of magmas. Since the great volume of hornblende-bearing magmas produced at this time, only one isolated instance of a similar magma has been recorded; a c.109 ka andesite lava flow (TG080) from SW Oturere which contains <0.5 modal % resorbed hornblende microphenocrysts. This flow appears to be anomalous relative to the rest of SW Oturere lava types. There is also the possibility that some of the much younger (c.10 ka) Tama Lakes eruptives (e.g. Tn141a) bear a similar chemical signature (Section 6.6.8 h), although thin sections are not available to confirm the presence of amphibole.

(b) Northeastern Oturere. A significant change in magmatic chemistry occurred after the amphibole-dominated petrogenesis of the older southern cones. The focus of eruptions moved towards the north where the NE Oturere cone was constructed, at a reasonably high eruptive rate of 0.37 km^3/ka, mainly between 130 and 90 ka. In contrast to most previous magma compositions, the olivine-bearing basaltic andesite and andesite magmas of NE Oturere are much more mafic, with higher MgO contents (up to 7.1 wt%), especially for the lower SiO_2 end of the spectrum (Fig 6.14A). The group A lavas in particular form a much steeper, longer, more tightly clustered trend of data points spanning a wider compositional range (c.7 wt% SiO_2) compared to prior trends. The occurrence of two chemical groups such that for a given SiO_2 content (e.g. 57.5 wt%) there is a relatively broad range in, for example, MgO content (e.g. 4.2 to 6.3 wt%) also distinguishes the NE Oturere type of behaviour from that demonstrated by the Tama-Pukekaikiore magmas.

The NE Oturere magmatic phase represents involvement of a magma reservoir beneath the Tongariro complex which was quite different from, and unrelated to, the magma reservoir feeding the amphibole-bearing magmas in terms of location, lifespan and

composition (Fig 6.23). The strong evidence for magma mixing events preserved in the NE Oturere eruptives (Section 6.6.3c) indicates a dynamic system of multiple magma batches derived from this main reservoir.

(c) **Southwestern Oturere and Tongariro Trig.** The two youngest of the pre-glacial cone-forming units represent another notable departure in compositional trends for the Tongariro complex. Erupted mainly between 110 and 60 ka from the central region of the complex, lavas and pyroclastics from these vents lie on a much lower MgO trend relative to the preceding units (Fig 6.14A). This appears to reflect a situation in which magma has been derived from an already quite differentiated parental magma and/or has resided longer than usual (compared to most other Tongariro units) in a high level reservoir enabling it to evolve more substantially. SW Oturere and Tongariro Trig eruptives also share other distinctive chemical characteristics such as a division into high and low TiO_2 groups (Section 6.6.7c) as well as common eruptive styles (Hawaiian-Strombolian spatter-scoria eruptions). Very good fits are achieved when SW Oturere is modelled as parental to Tongariro Trig, demonstrating that they probably share a common origin with the same parental magma reservoir. However, neither SW Oturere nor Tongariro Trig can readily be derived from any of the older lavas by modelling fractional crystallization relationships.

Although quite different in terms of the steepness of trends and the compositional space occupied on variation diagrams, these units share in common with NE Oturere a relatively tight, elongate trend (spanning up to 8 wt% SiO_2) representing considerable magmatic differentiation. There is also a certain degree of similarity between NE Oturere, SW Oturere and Tongariro Trig in their distribution of chemical groups into a main elongate trend (group A) and a more clustered, less chemically diverse group B. The group B compositional fields for these three units overlap in a moderate MgO-SiO_2 position relative to the entire Tongariro field, whereas the Tama 2 group B lavas contain comparable MgO contents but lower SiO_2 (Fig 6.14A). These overall similarities between units may be indicative of common controls operating within the Tongariro plumbing system which promote this kind of high level differentiation even though the original magma storage areas are often compositionally diverse. Magma mixing has taken place during production of all these compositional trends; the manner in which it occurs may be influenced by certain physical conditions repeatedly present during Tongariro's history.

(d) **Young NE Oturere, Blue Lake, North Crater, Te Mari Craters, pre-1.8 ka Red Crater.** These andesitic young eruptives occur in the northern and central part of the Tongariro complex and were produced over the last c.20ka. Their close spatial and temporal proximity is complemented by their similar geochemistry. The units contain moderate SiO_2 and MgO contents, plotting near the centre of the overall Tongariro compositional field on variation diagrams (Figs 6.15, 6.16, 6.17A, 6.19, 6.21A). The overlapping, moderately steep, short to medium length trends are generally quite scattered and do not represent consistent stratigraphic-compositional relationships. This composition and style of trend coincides with the 'B' chemical groups of Tongariro Trig, SW Oturere and NE Oturere, with which these younger northern units overlap. Their incompatible element ratios are all similar. In addition to lava flows, these units also comprise a significant proportion of welded spatter deposits. There is a strong case for a common magma reservoir shared by these vents (Fig 6.23), with only minor chemical variations produced by slight differences in the type and degree of higher level differentiation processes experienced by the various magma batches erupted over c.20 ka.

(e) **Young SW Oturere and Tama Lakes.** These central and southern vents - and probably some in between (I.A. Nairn, pers comm., 1995) - erupted over a similar time period (14 - 10 ka) to the young northern vents described above. However, they generally plot on a lower MgO trend relative to the northern vents, and also span a much wider compositional range, from 55.0 to 64.2 wt% SiO_2 (Figs 6.18 and 6.20). Further sampling and geochemical modelling is required to assess whether this long trend represents fractional crystallization, magma mixing, or both. Nevertheless, it is likely that the Young SW Oturere and Tama Lakes vents were fed by the same magma reservoir which was operating independently from the plumbing system beneath the young northern vents (Fig 6.23).

(f) **Ngauruhoe.** The cone of Ngauruhoe has been built up quite rapidly (0.88 km^3/ka) around the most recent (2.5 - 0 ka) vent in the centre of the Tongariro complex. Ngauruhoe eruptives are distinguished by their almost unique position at the left of the MgO-SiO_2 diagram and their division into five discrete geochemical groups which represent many more than that number of magma batches (Figs 3.30 and 6.22A; Section 6.6.8k). These diverse chemical groups also exhibit a wide range of characteristics in terms

of slope, length and tightness of trends. Magma mixing and crustal contamination processes have probably played just as important a role as fractional crystallization in Ngauruhoe petrogenesis. Ngauruhoe lavas and pyroclastics thus represent another distinctive magmatic signature in Tongariro petrogenesis, although to what extent this is owing to the comprehensive sampling enabled by the excellent exposure of the young cone is not certain. The main magma reservoir providing the characteristic Ngauruhoe type of magma has supplied a number of smaller magma chambers at higher levels in which the different geochemical groupings have developed (Fig 6.23).

(g) **Other: Pukeonake, Young Pukekaikiore, post-1.8 ka Red Crater.** These three units are not particularly closely related in time or space, but do represent several of the more extreme compositions erupted, as scoria cones and lava flows, from the Tongariro complex. They all occur as high MgO outliers on the MgO-SiO_2 diagram (Figs 6.15, 6.18, 6.21A) and cannot be derived by differentiation processes from any of the earlier Tongariro magma compositions. Pukeonake olivine basaltic andesite erupted c.23 ka to the west of the complex and represents a comparatively primitive magma which mingled with a more evolved magma prior to eruption (Section 6.6.8b). The Young Pukekaikiore (c.15 ka) olivine andesite erupted from a central-west location and is remarkable for its lack of plagioclase phenocrysts, very high Sr concentrations and low Al_2O_3 (Section 6.6.8e). The much younger post-1.8 ka Red Crater scoria and flows erupted from the centre of the complex (Section 6.6.8i), and are confined to a tightly clustered group of the lowest-SiO_2 compositions recorded from the Tongariro complex (Fig 6.21A). The Pukeonake, Young Pukekaikiore and post-1.8 ka Red Crater units represent three independent, very distinctive, and relatively primitive magma batches which probably followed atypical paths to the surface compared to the routes already established by the existing plumbing system beneath the Tongariro complex (Fig 6.23).

6.7 COMPARISON WITH RUAPEHU VOLCANO

It is appropriate at this stage to provide a general comparison of Tongariro whole-rock chemical compositions with those determined for Ruapehu volcano. Ruapehu represents the only other Taupo Volcanic Zone composite volcano studied in reasonable detail, and is also obviously of interest because of its close proximity to the Tongariro Volcanic Complex. Similarities between the two volcanoes in terms of eruptive styles and products have already been noted in Section 2.4. In tandem with these observations is a broad correspondence in chemical composition.

The classification of Ruapehu (and nearby) lavas into six main types by Graham and Hackett (1987) has already been described in Section 4.2. Compositional fields for these types (plus the type 7 of Patterson and Graham, 1988) are plotted on an MgO-SiO_2 diagram (Fig 6.24A) along with the overall compositional field for the Tongariro complex. There is considerable overlap between the fields for the two volcanoes, and they show a similar range in MgO and SiO_2 contents. Differences exist near the base of the diagram where Tongariro eruptives extend to lower MgO values for given SiO_2 contents, and for most of Ruapehu lava types 3 and 6 which occupy higher-MgO compositional space outside of the Tongariro field. Rb/Zr ratios are generally more restricted for Ruapehu eruptives than for those on Tongariro, which forms a much broader scattered field on a plot of Rb versus Zr (Fig 6.24C).

Further evidence of shared chemical patterns is provided by other variation diagrams (not shown) such as: Ruapehu TiO_2 contents decrease in two subparallel trends at high SiO_2 contents as is the case for Tongariro (Fig 6.5C); Ruapehu type 7 lavas form a lower-K_2O trend subparallel to the main trend as happens for Tongariro amphibole-bearing lavas (Fig 6.5H; Section 6.6.4a); and the irregular shape of the Tongariro Sr-SiO_2 field (imparted by the very high Sr Young Pukekaikiore eruptives; Fig 6.6F) is confirmed by the Ruapehu field, which also contains samples plotting intermediate between those from Young Pukekaikiore and the rest of the Tongariro eruptives.

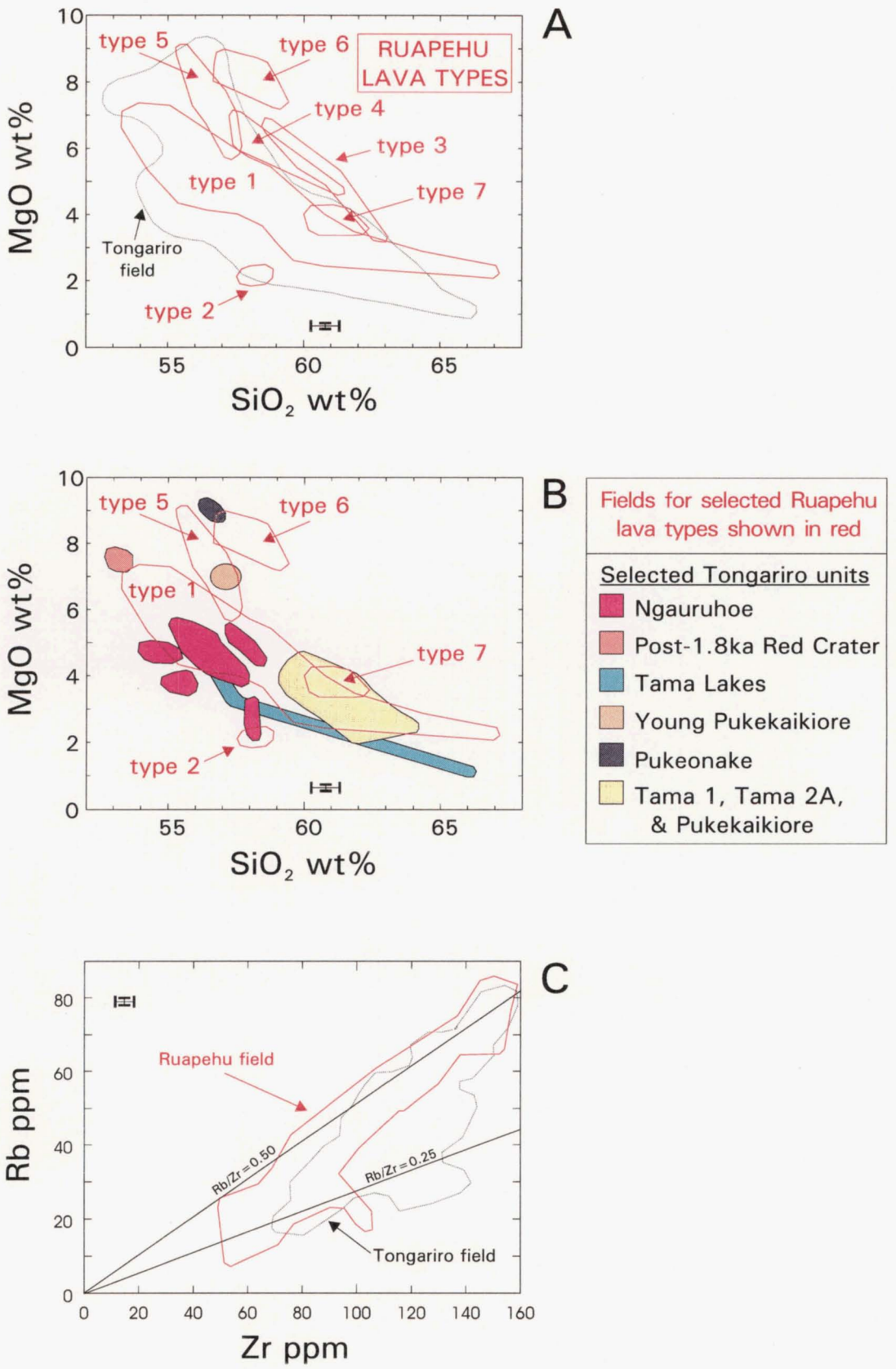

Figure 6.24 Comparison of Tongariro and Ruapehu geochemistry. Boundaries for Ruapehu compositional fields drawn from data kindly supplied by J.A. Gamble and I.J. Graham. (**A**) MgO-SiO_2 diagram of fields for Ruapehu lava types (Graham and Hackett, 1987) shown within context of overall Tongariro compositional field, (**B**) MgO-SiO_2 diagram of selected fields for Ruapehu lava type and Tongariro volcano-stratigraphic units (refer to text), (**C**) Rb versus Zr diagram showing overall compositional fields for Tongariro and Ruapehu. All data recalculated anhydrous. Error bars for Tongariro data represent total error (2 sd from mean; Section A8.3.3).

The reasons for not following Graham and Hackett's (1987) lava classification were outlined in Section 4.2, but it is interesting to compare these lava type fields with those of the Tongariro volcano-stratigraphic units. The Ruapehu lava types may also have a corresponding time-space dimension, but were not examined in detail for this purpose by Graham and Hackett (1987). Figure 6.24B shows the compositional fields for selected Ruapehu lava types and Tongariro units on the MgO-SiO_2 diagram. Most Tongariro units fall within the Ruapehu type 1 field and are not shown on the diagram. Certain Tongariro units fall into the "related vents" category of Graham and Hackett's (1987) study and thus not surprisingly overlap with their associated lava type. The fields for types 5 and 6, which contain Young Pukekaikiore and Pukeonake, respectively, are more extensive than the fields documented for the relevant Tongariro units (Fig 6.24B), indicating that other Ruapehu eruptives share these distinctive compositions. Patterson and Graham's (1988) additional type 7 from Upper Tama Lake - Pukekaikiore lavas coincides with the compositional fields for Tama 1, Tama 2 and Pukekaikiore (Fig 6.24B; as discussed in Sections 6.6.4a and 6.6.5c). Units such as Ngauruhoe (groups 1A, 1B, 2), post-1.8ka Red Crater, and Tama Lakes are unique compositions to Tongariro and plot mostly outside of any Ruapehu field (Fig 6.24B). SW Oturere and Tongariro Trig eruptives plot on or just below the Ruapehu type 1 field at lower-MgO values. The low-SiO_2 end of the NE Oturere A trend overlaps with the high-MgO field of Ruapehu type 5 (not shown).

It is apparent from this brief overview of Ruapehu geochemistry in relation to Tongariro that there are underlying controls on magmatic evolution shared by both volcanoes. It is probably a rather artificial boundary between them in some respects, and with further volcano-stratigraphic-magmatic study of Ruapehu, a sense of a more transitional relationship between Tongariro and Ruapehu activity may emerge. However in light of the new geochemical data presented from this study and the various departures of Tongariro compositions from those of Ruapehu, it is clear that the Ruapehu lava classification scheme does not adequately describe all TVZ andesites, as suggested by Graham et. al. (1995).

6.8 DISCUSSION AND SUMMARY

6.8.1 Implications of research strategy

By design, this study has been built around a comprehensive data base made possible by extensive field sampling within a known chronostratigraphic framework. It is believed, therefore, that conclusions drawn from this study are based upon a solid foundation. For example, this thorough surface sampling should reliably reflect the relative volumes of the different types of magma tapped by the plumbing system of Tongariro Volcanic Complex. A question not to be overlooked, however, is how faithfully do the collected samples reflect those magma compositions actually involved in Tongariro petrogenetic processes?

It may well be the case that either end of the spectrum of magmatic compositions (e.g. basalt or dacite) are being produced beneath Tongariro in much larger quantities than are represented by the material being erupted. However, true basalts rarely survive as such because of the significant degree of fractional crystallization occurring at various levels within the plumbing system as evidenced by the majority of Tongariro eruptives. The strong involvement of magma mixing processes also probably prevents Tongariro magmas evolving much beyond silicic andesites, or occasionally dacites, before the next influx of basic magma replenishes the reservoir. This last deduction must be viewed with a certain degree of caution, however, when one recalls the tendency for minimal preservation of silicic pyroclastic material on the cone (Section 2.1). Ultimately, it is very difficult to judge whether or not the availability of magma at a certain time is always reflected in what is being erupted, but this assumption is often necessary if some kind of model is to be developed.

This study has been successful in highlighting a number of distinctive, broad groupings of magma compositions which have contributed to the growth of the Tongariro cone complex (Section 6.6.9). Some of these have not previously been identified or described. The detailed sampling approach taken here has thus proved valuable in characterising much more fully the range of magmatic compositions involved, and has

allowed recognition of recurring geochemical patterns. The combination of magmatic processes involved, coupled with the complexity of the time-space-volume-composition relationships determined for the Tongariro complex demonstrate the need for representative sampling over the entire exposed area and lifespan of a composite volcano if a full picture of its eruptive and magmatic history is to be attained.

A random and insufficient sampling of Tongariro lavas would not have revealed the characteristic geochemical groups and trends, and would have rendered it difficult to make sense of seemingly unrelated, isolated data points on variation diagrams. Some studies of other composite volcanoes may suffer from this approach, in which individual magma batches have not been identified and instead modelling is conducted as if all samples belonged to the same fractionated suite. During detailed geochemical monitoring of the 1989-1993 eruptive activity from Mount Etna, Tonarini et al. (1995) noted that a single lava sample should not serve as representative of a given eruption, since so many processes are involved in producing chemical variability even over the relatively short time span of a few months. On Tongariro it has also been possible to demonstrate this for Ngauruhoe, where detailed sampling of historic and prehistoric eruptions has revealed considerable compositional diversity.

Just as inadequate sampling of a cone can be limiting to a full understanding of petrogenesis, it is also possible to overlook chemical variation within single lava samples. The scope of the Tongariro study does not extend to multiple sampling of each lava flow or pyroclastic unit and therefore the degree of heterogeneity on this scale is generally not known. Only for Ngauruhoe and a few other young eruptives were multiple samples occasionally collected, e.g. for the Ngauruhoe 1975 pyroclastic avalanche deposit which revealed significant variability.

6.8.2 Summary of time-space-volume-composition relationships

Tongariro's magmatic history represents a complex interplay between a number of contrasting magma reservoirs and magma batches which experienced varying degrees of differentiation by a variety of processes, namely magma mixing, fractional crystallization

and crustal assimilation. The major compositional differences reflected in the broad groupings of volcano-stratigraphic units (summarised in Section 6.6.9) represent periods in Tongariro's development when a break in magmatic evolution occurred, resulting from a structural change in the complex subvolcanic plumbing system via the influx of a new batch of 'parental' magma, establishment of new configurations of magma reservoirs, and the ensuing modification of the magmatic intensive parameters controlling differentiation. The time period represented by one group of similar magmas, however, often reflected a relatively long-term dominance of a particular magmatic signature (e.g. amphibole magmas between 275 and 160 ka, low MgO magmas between 110 and 60 ka). Some magma groupings share a common eruptive style (e.g. the lava flows, coulees and domes of the southern amphibole-bearing units, the welded agglutinates of the young northern cones), whereas others exhibit a range of eruptive styles which do not appear to be uniquely related to any one magmatic grouping.

These magma storage areas existed at a variety of levels beneath the volcano, and some operated independently whereas others shared some degree of connection. Initially, primitive magmas derived from the mantle would probably collect as relatively deep crustal reservoirs in which some AFC would occur. Certain units which share an underlying geochemical signature and overlap in compositional space on variation diagrams, e.g. the distinctive amphibole lavas of the three southern cones, were probably fed from the same parental crustal reservoir which existed over that particular time period and in that particular location. The ascending magmas may have branched out onto slightly differing paths via shallow crustal conduits/chambers within which further differentiation imparted the subtle variations observed between these commonly-sourced units. Other more compositionally distinct units which were not derived from a common reservoir, but instead often mirror each other in the characteristics of their chemical trends or groupings (e.g. the long trend A and clustered trend B of NE Oturere, SW Oturere and Tongariro Trig) suggest that similar shallow differentiation processes have been in operation in higher level magma chambers (which share similar dimensions and crystallization conditions?) that were fed from the different parental magma reservoirs below.

Note that there is no overall pattern during Tongariro's history to tend towards a particular type of chemical trend; compositional patterns vary throughout its lifespan.

However it is possible to speculate that the more basic compositions of the most recent eruptives (Ngauruhoe, Red Crater, etc.) may in part owe their existence to exploitation of established paths to the surface which were unavailable to some of the earlier magmas which tended to be stalled within the crust and thus fractionated to a greater extent. This scenario does not explain the very MgO-rich magmas erupted much earlier from NE Oturere though.

Examination of the spatial occurrence of the various cone-forming units through time reveals a general pattern with respect to vent location, which also ties in with compositional relationships. Between about 275 and 130 ka magma was finding its way to the surface principally in the south and west of the complex to form Tama 1, Tama 2 and Pukekaikiore cones. From around 130 to 60 ka the plumbing system was focused towards delivering magma to the centre and north of the complex, building up the NE Oturere, SW Oturere and Tongariro Trig cones. The young eruptives produced within the last c.25 ka have occurred more extensively across the complex, exploiting a NE-trending vent lineation which extends from Tama Lakes in the southwest to Te Mari Craters in the northeast. Apart from the spatial dimension, there is also obvious evidence for several coexisting magma reservoirs at certain periods during Tongariro's history and there was usually some overlap in time between different cone-building eruptions, rather than a sequential and discrete progression from one to another.

This detailed geochemical study of the Tongariro complex has also provided the opportunity to consider any links between the young eruptive units and the older cones. Keeping in mind the differing levels of detail concerning time-space relationships obtained for these different periods in Tongariro's history, it appears that there are certain magmatic signatures repeated over time. For example, the young northern vents of Young NE Oturere, Blue Lake, North Crater and Te Mari Craters have erupted compositions which closely resemble those which comprise the 'B' chemical trends of Tongariro Trig, SW Oturere and NE Oturere. In the case of Ngauruhoe, however, its five distinctive geochemical groups occupy an almost unique position in compositional space with respect to the rest of the Tongariro field. The pattern of lava groups is also characteristic only of Ngauruhoe, but this could be a consequence of the very detailed sampling possible on most sectors of the cone. Most Tongariro units exhibit evidence of a dynamic system of periodic magma

replenishment and withdrawal, but this interplay between different magma batches is most clearly evident for Ngauruhoe.

6.8.3 Differentiation processes

Petrographic, mineralogical and geochemical evidence preserved in most units points to significant involvement of magma mixing and crustal contamination processes in Tongariro petrogenesis. The entire Tongariro compositional field when plotted on one variation diagram reflects a series of mixing and AFC trends which have originated from a multitude of separate magma batches sourced from a number of main parental magma reservoirs that have existed at varying times during Tongariro's lifespan. These differentiation mechanisms complicate attempts to model major element variations by least-squares mixing because they will generally shift compositions away from a closed system liquid line of descent. Consequently, calculated fits to actual compositions during modelling are often poorer than would be expected if closed system fractional crystallization was solely responsible for the trends. Where detailed chemical stratigraphy plots are available (e.g. for NE Oturere), their characteristic zig-zag pattern shows that repeated basic magma influx and only short periods of uninterrupted fractional crystallization have occurred, rather than the eruption of a steadily fractionating or zoned magma chamber.

Simple bulk mixing was not considered a realistic process to model for a number of reasons. It is difficult to identify end members or estimate mixing proportions because Tongariro magmas are generally well-blended hybrid magmas (lacking mafic inclusions or banding), and any one trend is not a pure mixing line but represents a complex interplay of fractional crystallization, magma influx and mixing. Using mixing calculations of a fixed rhyolite composition and variable mafic end members, Sparks and Marshall (1986) suggest that relatively large proportions of mafic magma must be involved to produce hybrid magmas. Because mixing of Tongariro magmas is typically between much more closely related compositions than rhyolite and basalt (Section 4.7), the proportion of mafic magma involved may actually be less than that predicted by Sparks and Marshall (1986). Many variables, such as the temperature, crystallinity and water content of the silicic end member,

and the P_{H2O} and cooling rate of the mafic end member, combine to influence the mixing process (Sparks and Marshall, 1986). For the likely Tongariro scenario of a basalt or basaltic andesite magma recharging an andesite magma reservoir, there would be insufficient viscosity contrast to allow preservation of any obvious evidence for mingling (e.g. banded texture), and relatively thorough mixing would instead take place.

As is often the case with composite volcanoes, Tongariro represents a complex, dynamic system of constant magma replenishment, mixing, fractional crystallization, and variable crustal contamination. This combination of differentiation mechanisms has been actively involved throughout virtually all of Tongariro's history and there is no one time period which stands out as particularly representing more exclusively one or the other process. Variations in the relative importance of these mechanisms will correspond with differences in such things as the magma batch size, available magma residence time, frequency of new magma influx, and degree of communication with surrounding crustal wallrock. It is also not really possible to easily categorise magmatic behaviour with time (e.g. progressively more basic, more silicic, etc.) because compositional trends switch back and forth so rapidly.

6.8.4 The big(ger) picture

Tongariro's close neighbour Ruapehu is compositionally very similar, as described above (Section 6.7), but has not been studied in quite the same way so that it is not possible to compare magma batches and plumbing systems in any detail. In the broader context of the Taupo Volcanic Zone, Sutton et al. (1995), in a comprehensive and ongoing study of Taupo volcanic centre, identified a number of distinct rhyolitic magma types on the basis of petrology and time/space relationships which they used to determine the development of the magmatic system beneath the volcano. There are very few examples in the literature of attempts to integrate time-space-volume-composition data in studies of composite volcanoes. The extensive investigation carried out on Mount St. Helens is an obvious exception. Having the considerable advantage of real time geophysical data on the magma reservoir dimensions, ascent rate, and eruption chronology, magmatic models could

incorporate the known chemical cycles within a wider volcanological context (e.g. Pallister et al., 1992).

Magmatic evolution should ultimately be explained by the ascent process, vent dynamics and eruption characteristics, in addition to inferences regarding the deep source and higher level magma reservoir (e.g. Marsh, 1989). Much is yet to be learned about the total workings of a volcanic system, and this will be greatly assisted as more research is conducted which integrates all the variables involved. Geophysical studies suggest that magma storage areas are much more complex than usually depicted in petrogenetic models. Physical models are necessary to constrain the actual mechanisms involved and to assess the plausibility of chemical models, in which the large number of adjustable parameters invoked for complex magma chamber dynamics almost guarantees an acceptable fit to the data (Jaupart and Tait, 1995). The present study on the Tongariro complex has at least demonstrated that it is possible to conduct more realistic and meaningful geochemical characterisation and modelling within a framework where the timing, spatial distribution and volume of cone-forming units and their inferred magma reservoirs is specified.

Chapter 7

Petrogenetic Processes and Time-Space Relationships: Magma Batches at Tongariro

CHAPTER 7
PETROGENETIC PROCESSES AND TIME-SPACE RELATIONSHIPS: MAGMA BATCHES AT TONGARIRO

7.1 INTRODUCTION

This chapter marks a progression from the general geochemical parameters provided by whole-rock XRF data described in the Chapter 6, to more discriminating parameters afforded by precise trace element and isotopic data. Using selected samples from a variety of Tongariro volcano-stratigraphic units, this chapter explores in more detail the petrological processes involved in Tongariro magmatism over a range of time scales. The previous chapter dealt mainly with the compatible elements and their ability to test the viability of fractional crystallization as a process creating diversity in Tongariro magmas. This was approached by examining trends on variation diagrams and by least-squares mixing calculations. It was shown that fractional crystallization models often fail to predict the actual compositions of Tongariro lavas. In this chapter, incompatible trace elements, including the rare earth elements, and various isotopic ratio data are used to identify the effects of other magmatic processes, such as crustal contamination, and test their involvement in Tongariro petrogenesis.

General major and trace element data for the Tongariro complex reveal patterns of shared deep parental magma reservoirs and/or higher level differentiation processes between certain cone-forming units (see Chapter 6). The more precise data set used in this chapter allows a more discriminating examination of particular time-space relationships (chosen from units with maximum exposure and age-control) and a refinement of the various scales or levels on which chemical order and diversity exist.

Data used in the following sections (Appendix 13) include precise trace element, rare earth element (REE), radiogenic and stable isotopic analyses for 66 samples chosen from the total Tongariro data base of c.370 samples. Analytical procedures and data precision are described in Appendix 8 (Sections A8.3.4, A8.4, A8.6-8.8). Optimum sample selection was not always possible due to the analytical schedules of the various laboratories used (see Appendix 13). Consequently, the selected samples are not fully representative of all Tongariro units, nor (in the case of certain trace elements) are they all analysed at the same laboratory. Interlaboratory variation was investigated and in some cases corrections were applied to ensure the data sets were comparable (Appendix 8, Section A8.5). Appendix 14 contains tables of partition coefficient (Kd) values (Table A14.1) and crustal assimilant compositions used in trace element and isotopic modelling (Tables A14.2-14.3).

This chapter is divided into essentially two parts. The first deals with the total 'precise' geochemical data base and examines trends and processes revealed by incompatible trace elements, rare earth elements, and isotopic ratios (Sections 7.3 and 7.4). These data are also assessed in light of published TVZ data. These sections are not intended as an exhaustive investigation of Tongariro andesite petrogenesis and source compositions. Instead, the main focus is on different time-space windows of the Tongariro complex and their associated petrological relationships. To this end, the second part (Section 7.5) is concerned with the sizes, lifespans and degree of independence of magma batches involved in individual eruptions and clusters of eruptions. The best exposed volcano-stratigraphic units are reviewed in Section 7.5 and include Ngauruhoe, Red Crater, Tama 2 and NE Oturere.

Some important findings highlighted in this chapter are:

1. A considerable variation in incompatible trace element ratios (e.g. Ba/Zr, Nb/Ta, La/Yb, Zr/Hf) and radiogenic isotopic compositions for closely-related samples is best explained by processes of assimilation fractional crystallization (AFC) involving contamination of Tongariro magmas by varying amounts of compositionally heterogeneous Torlesse crust, giving rise to a family of different AFC trends.

2. Complex dynamics in the magma-plumbing system are evident on time scales as short as 100 years. For the case of Ngauruhoe historic eruptions, relatively high-level processes of magma mixing, fractional crystallization, and complex crustal contamination have combined to produce an isotopically diverse suite of lavas.

3. Although relatively closely associated in time and space, the intensively-sampled products of the last 1000 years of activity at three vents of the Tongariro complex (Ngauruhoe, post-1.8 ka Red Crater, c.1500AD Upper Te Mari Crater) cannot be directly linked to one another via fractional crystallization alone. The non-systematic age relationships along geochemical trends, compositional reversals and compositional loops formed by these samples represent instead many small, short-lived magma batches which have been produced at relatively shallow crustal levels in several independent plumbing systems, and which have been affected by varying degrees of crustal contamination.

4. Comparable compositional variability and rates of magmatic change over three 10 ka time intervals spanning different parts of Tongariro's history (0-10 ka young eruptives, c.120-130 ka NE Oturere, c.200-210 ka Tama 2) suggest that similar magmatic processes have been operating throughout Tongariro's lifetime, although each time interval displays a subtly different trend pattern. Thus the regularity/rate of magma batch production may vary somewhat, but all batches appear to be small (probably $<<0.1$ km^3) and short-lived (probably c.1 ka).

7.2 PREVIOUS WORK

This study and other recent ones have greatly expanded the availability of high precision geochemical data for Tongariro and the TVZ. As the first isotopic and trace element analyses became available, workers concentrated on using the data to establish petrogenetic models for a wide range of volcanic rocks in the TVZ. Ewart and Stipp (1968) presented $^{87}Sr/^{86}Sr$ ratios for mainly rhyolites, but included andesites from Tongariro

($^{87}Sr/^{86}Sr$=0.7057), Pukekaikiore (0.7053), Tama Lakes (0.7055-0.7058) and 1954 Ngauruhoe (0.7060), for which they proposed an origin by crustal contamination of a basalt or primary andesite magma (in line with the work of Steiner, 1958, and Clark, 1960a). The first Pb isotope analyses on TVZ rocks, revealing little variability, included analyses from Mangatepopo ($^{206}Pb/^{204}Pb$=18.828, $^{207}Pb/^{204}Pb$=15.683, $^{208}Pb/^{204}Pb$=38.739), Pukekaikiore (18.784, 15.611, 38.649) and Tama Lakes (18.682, 15.518, 38.382) (Armstrong and Cooper, 1971). Ewart et. al. (1977) reviewed and compared TVZ andesites with those of the Tonga-Kermadec arc. Concentrating mostly on the origin of the rhyolites, Blattner and Reid (1982) presented the first oxygen isotope data for TVZ, including samples from Tongariro ($\delta^{18}O$=+8.5), Pukekaikiore ($\delta^{18}O$=+8.1), 1954 Ngauruhoe ($\delta^{18}O$=+7.6), and 1954 Ngauruhoe xenoliths ($\delta^{18}O$=+11.0-12.6). In an early investigation of the rare earth element (REE) geochemistry of TVZ andesites and basalts, Cole et. al. (1983) identified a light REE-enriched pattern and negative Eu anomalies for samples which included Tongariro, Pukekaikiore and Te Mari Craters, and Red Crater (the latter containing among the lowest abundances of REE and highest La/Yb of the high-Al_2O_3 basalts).

Because of the greater levels of analytical precision now attainable, data from only studies of the last decade or so are considered suitable for comparison with the new Tongariro data of this study. The doctoral thesis of Graham (1985a) focused on the Sr isotopic ratios of Ruapehu lavas and xenoliths, but also contained several analyses of Pukeonake ($^{87}Sr/^{86}Sr$=0.70479±33 - 0.70483±32), Young Pukekaikiore (0.70440±46), Red Crater (0.70462±25), and 1954 Ngauruhoe (0.70551±72) eruptives (note errors are 1 sd). Graham (1985a) found that each of the Ruapehu lava types (Sections 4.2 and 6.7) exhibited characteristic Sr isotope compositions, which he attributed to variable degrees of crustal contamination although this was not quantitatively modelled.

To this initial work were added some $^{143}Nd/^{144}Nd$ data for Ruapehu samples and also for eruptives from Pukeonake ($^{143}Nd/^{144}Nd$=0.51275), Red Crater (0.51280), and 1954 Ngauruhoe (0.51273), published by Graham and Hackett (1987). For the Type 1 lavas they noted a general trend of increasing SiO_2 content and $^{87}Sr/^{86}Sr$ from the oldest to the youngest lavas (from basic andesites, $^{87}Sr/^{86}Sr$=0.70520, to silicic andesites to dacites, $^{87}Sr/^{86}Sr$=0.70520-0.70620) (Graham and Hackett, 1987). A plot of $^{143}Nd/^{144}Nd$ versus $^{87}Sr/^{86}Sr$ identified crustal contamination as a major process, which caused the data to trend

towards the compositional field of Torlesse greywacke (Graham and Hackett, 1987). AFC calculations suggested that addition of 1-30% crustal assimilant was required to produce the Type 1 lavas (Graham and Hackett, 1987). Both the exposed sedimentary basement (Mesozoic Torlesse and Waipapa terranes and Tertiary sediments) and the crustal xenoliths found in Tongariro Volcanic Centre lavas (see Chapter 5) have been the subject of intensive study and analysis by Graham (1985a, 1985b, 1987), Graham et. al. (1988, 1990), Graham and Adams (1990), Roser and Grapes (1990), George and Graham (1991), and Adams and Graham (1993).

New $^{87}Sr/^{86}Sr$ data were obtained by Patterson and Graham (1988) for Ngauruhoe ($^{87}Sr/^{86}Sr$=0.70526-0.70536), Young Pukekaikiore (0.70435), Tongariro (0.70542), Mangatepopo (0.70603), Pukekaikiore (0.70471), and Upper Tama Lake (0.70472). The Ngauruhoe, Tongariro and Mangatepopo lavas were modelled as requiring 3-8% crustal contamination, along with fractional crystallization, of a low-Al_2O_3 basalt, whereas the older Pukekaikiore and Upper Tama Lakes lavas required only fractional crystallization of a similar parent magma. Fractionation of a quartz-tholeiite basalt was believed to be the origin of the young Pukekaikiore olivine andesite.

A major boost to the TVZ isotope data base came in the form of new Pb isotope analyses for basalts, andesites, rhyolites, and basement metasediments which further refined the AFC models (Graham et. al., 1992). Samples from the Tongariro complex comprised lavas from 1954 Ngauruhoe ($^{206}Pb/^{204}Pb$=18.795, $^{207}Pb/^{204}Pb$=15.606-15.609, $^{208}Pb/^{204}Pb$=38.642-38.653), Red Crater (18.799-18.805, 15.598-15.607), and Pukeonake (18.781-18.784, 15.594-15.600, 38.588-38.624). Graham et. al. (1992) also presented an average Torlesse assimilant composition which has the following characteristics: $^{87}Sr/^{86}Sr$=0.71459, $^{143}Nd/^{144}Nd$=0.512407, $^{206}Pb/^{204}Pb$=18.859, $^{207}Pb/^{204}Pb$=15.646, $\delta^{18}O$=+12.0. A Torlesse terrane assimilant was favoured over Waipapa terrane, but AFC trends were equivocal and a limited contribution from the Waipapa basement was not ruled out (Graham et. al., 1992).

Within the context of investigations of TVZ basalt petrogenesis, Gamble et. al. (1993a, 1996) presented data on Red Crater including REE analyses and isotopic ratios ($^{87}Sr/^{86}Sr$ = 0.704456±12 - 0.704569±12, $^{143}Nd/^{144}Nd$ = 0.512830±9 - 0.512862±10). On a

$^{143}Nd/^{144}Nd$ - $^{87}Sr/^{86}Sr$ diagram the TVZ basalts plot on an AFC curve which trends towards the fields for TVZ andesites, rhyolites and Torlesse and Waipapa metasediments (Gamble et. al., 1993a). Other recent studies dealing with North Island andesite petrology include those on White Island (Graham and Cole, 1991), Whale Island (Burt et. al., 1996) and Egmont Volcano (Price et. al., 1992), for which AFC processes were also invoked. The overall geochemistry and petrogenesis of TVZ eruptives were recently reviewed by Graham et. al. (1995) under the three major subdivisions of high-Al_2O_3 basalt, andesite, and rhyolite.

Note that most of these previous studies have been focused on using trace element and isotopic data to examine *overall* TVZ petrogenesis in terms of this broad division into basalts, andesites and rhyolites. Chronostratigraphic relationships of the samples analysed have largely been ignored in favour of the generalised approach. Much effort has been concentrated towards developing a petrogenetic model which explains the broad relationships between the three compositional groups of high-Al_2O_3 basalts, andesites and rhyolites. A solution which satisfies all the available geochemical data has yet to be agreed upon. A somewhat different approach is employed in this study. Although the new Tongariro data presented in the following sections are treated firstly in terms of the total data set, the volcano-stratigraphic divisions are kept to the forefront, and then attention is directed towards selected time-space windows which allow a closer examination of inter-relationships of the magma batches and plumbing systems involved.

7.3 INCOMPATIBLE TRACE ELEMENTS (INCLUDING RARE EARTH ELEMENTS)

The previous chapter primarily investigated the compatible behaviour of elements during fractional crystallization. This section provides the opportunity to examine incompatible element concentrations and trends which have the potential to tell us about source compositions, partial melting, and contamination. Of the expanded trace element data set used in this chapter, new elements not previously referred to include Cs, REE, Nb, Hf, Ta, Pb, Th and U. Higher precision analyses were also attained for Zn and Y. The

addition of the REE and the high field strength elements (HFSE) in particular greatly enhance the ability to conduct rigorous geochemical modelling. As an aside, note that the samples in this select data set have also been analysed for the compatible elements Sc and Co. These two elements correlate positively with each other and produce slightly curved negative trends when plotted versus SiO_2 on variation diagrams involving MgO, Fe_2O_3, CaO, Cr, and Ni - indicating their involvement in the fractionation of clinopyroxene and olivine.

7.3.1 Primitive mantle-normalized spiderdiagrams

Multi-element (spider) diagrams showing a range of incompatible elements normalised to primitive mantle are presented in Fig 7.1 for a representative range of Tongariro samples. The selected samples are arranged in plots according to the broad groupings of volcano-stratigraphic units identified in Section 6.69 (and summarised in Table 6.3). Note that Pb and Nb analyses of sufficient precision are not available for some samples (Section A8.5), although Ta provides an indication of the likely extent of the negative Nb anomaly. Only the comparatively high precision data (Appendix 13) are plotted so as to avoid the occurrence of spurious inflections in the spiderdiagram patterns due to low analytical precision. The range of normalised incompatible element abundances for all fully analysed Tongariro samples is shown for comparison as a shaded background on all the plots. All volcano-stratigraphic units are represented apart from the young southern units of Tama Lakes or Young SW Oturere, for which a full set of precise trace element analyses were not acquired.

All the Tongariro spiderdiagrams share the same strongly spiked pattern typical of subduction-related magmas. The relatively high concentrations of the large ion lithophile elements (LILE) such as Rb, Ba, and K are thought to be a consequence of enrichment of the mantle wedge by fluids released from the subducted slab (e.g. Tatsumi et al., 1986). Debate is ongoing concerning the relative role of fluids (or melt) from the subducted slab and the contribution from the mantle wedge itself (e.g. Pearce, 1983; Hawkesworth and Ellam, 1989; Hawkesworth et al., 1991; Arculus, 1994). It appears that points of view very much depend on which trace elements are investigated, as the apparent relative slab/wedge

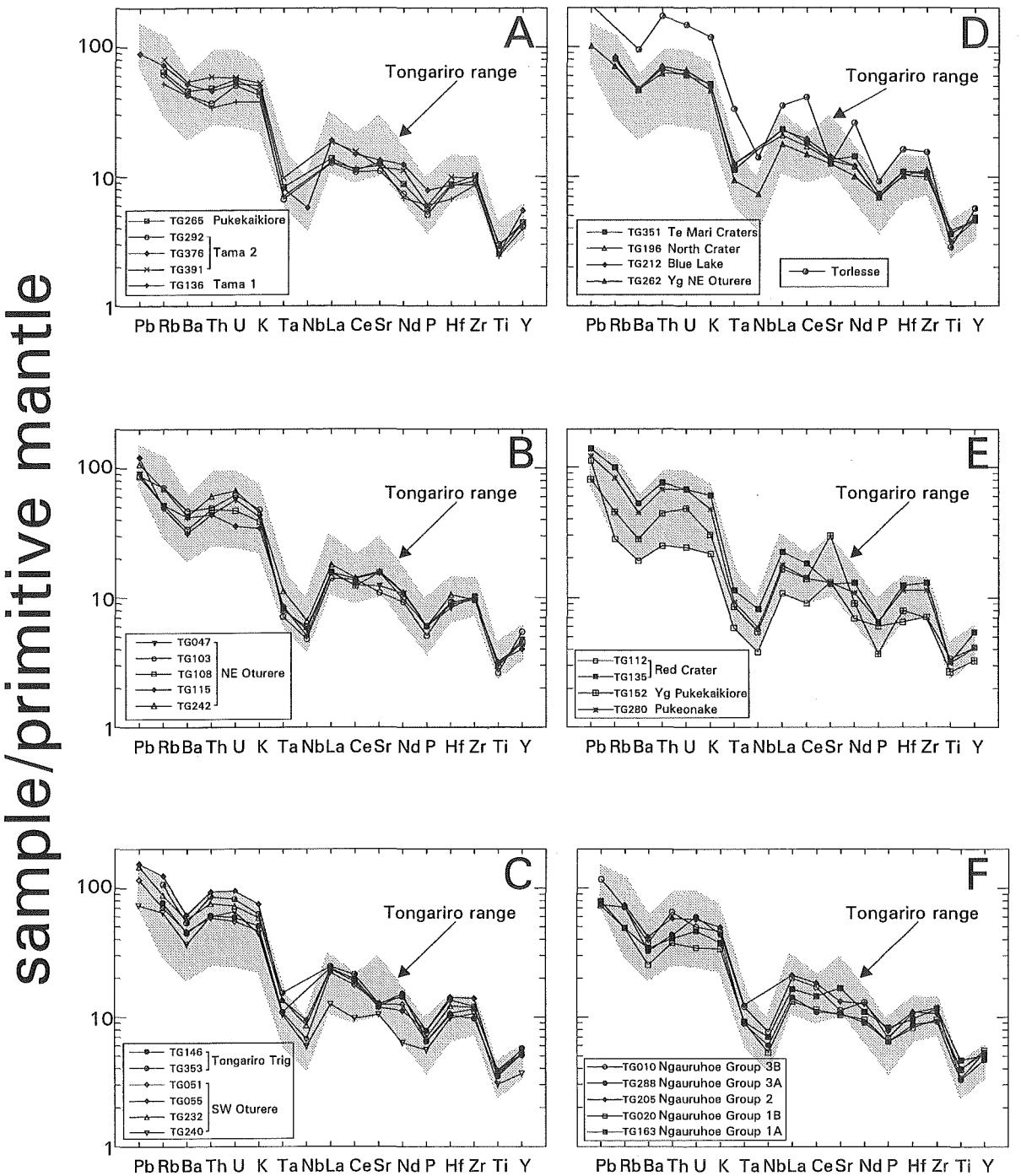

Figure 7.1 Primitive mantle-normalised abundances of incompatible trace elements in selected Tongariro samples, arranged in groupings of similar volcano-stratigraphic units. Absence of symbol for Nb or Pb indicates lack of data. Shaded pattern shows range of all analysed Tongariro samples. Incompatible element pattern for average Torlesse crust is shown for comparison in D. Normalisation factors from McDonough et al. (1992).

contribution varies for different elements (Hawkesworth et al., 1994). Low high field strength element (HFSE) concentrations, including the pronounced negative Ta and Nb anomalies present on all the Tongariro spiderdiagrams, are also a characteristic feature of arc rocks and have alternatively been explained by minor refractory phases in the source which retain these elements during partial melting, higher degrees of partial melting, or by derivation from an already depleted mantle wedge (e.g. Pearce, 1982; Arculus and Powell, 1986, McCulloch and Gamble, 1991; Thirlwall et al., 1994; Stolz et al., 1996). Some of the spikes on the spiderdiagrams may be the result of certain of the elements behaving compatibly; the troughs at P (apatite fractionation) and Ti (magnetite and ilmenite fractionation), for example (Fig 7.1).

Whereas a role for contamination of Tongariro magmas by Torlesse metasedimentary basement rocks is indicated by the presence of crustal xenoliths (Chapter 5), it is more difficult to confidently identify this process using multivariate trace element plots alone. Incompatible element ratios (Section 7.3.5) and radiogenic isotopic ratios (Sections 7.4.1-7.4.2), however, allow more successful geochemical modelling of crustal contamination. Note however that although modelling of contamination by a Torlesse partial melt has not been attempted here, it is significant that when the average Torlesse crust composition is plotted on a primitive mantle-normalised spiderdiagram it exhibits a remarkably similar pattern of troughs and peaks (but at higher relative abundances) as shown by the Tongariro lavas (Fig 7.1D). This is because Torlesse sediments have a broadly calc-alkaline active margin provenance. Thus features such as the high Rb, Th, U, and K, and the negative anomalies for Ba, P and Ti exhibited by most Tongariro magmas are also shared by Torlesse crust, thus Torlesse contamination would not be detectable on spiderdiagrams.

A comparison of the spiderdiagrams for Tongariro volcano-stratigraphic units reveals some interesting differences. The amphibole-bearing magmas of the older southern cones are distinguished from other Tongariro units by a relatively subdued or absent Ba trough and almost flat pattern from Ba through to K (Fig 7.1A), demonstrating the comparatively high concentrations of K relative to Rb which give rise to the relatively high K/Rb typical of these lavas (Fig 6.7; Section 6.5.3). NE Oturere eruptives show reasonably similar patterns to each other on a spiderdiagram (Fig 7.1B), but differences exist in the

magnitude of the peaks at U and Sr. Tongariro Trig and SW Oturere lavas exhibit some of the highest normalised incompatible element concentrations (Fig 7.1C); an expected consequence of their relatively evolved nature compared to other Tongariro eruptives. The exception to this pattern is TG240 which contains overall lower concentrations (particularly of the REE) and displays a slight positive Sr anomaly in contrast to the Sr trough of the other samples from these two units (Fig 7.1C). TG240 has already been described as a chemically distinctive magma composition (Section 6.6.6a).

The young northern eruptives show markedly similar patterns when plotted on a spiderdiagram, with only minor variation in the light REE (Fig 7.1D). Pukeonake and pre-1.8 ka Red Crater samples have very similar patterns, whereas the post-1.8 ka Red Crater sample displays much lower incompatible element concentrations and a moderate peak at Sr (Fig 7.1E). Note that the exceptionally Sr-rich Young Pukekaikiore sample (Section 6.6.8e) has a correspondingly large positive Sr anomaly (Fig 7.1E), reflecting its Sr-rich source. Ngauruhoe eruptives from the different lava groups show a certain degree of variability in their spiderdiagram patterns, including flat trends, troughs or a peak at Sr, for example (Fig 7.1F).

7.3.2 Rare earth element patterns

Representative REE patterns for each broad grouping of volcano-stratigraphic units (identified in Section 6.69 and summarised in Table 6.3) are shown (Fig 7.2) superimposed on the overall REE range of all the Tongariro samples analysed. Note, however, that REE data were not acquired on the young southern units of Tama Lakes or Young SW Oturere.

All the samples exhibit a moderately light REE-enriched pattern, with La abundances ranging from 23 to 65 times chondritic values, and Lu at 7-14, fairly typical of subduction-related rocks. $(Ce/Yb)_N$ ranges from 1.8 to 3.9 and the degree of REE fractionation increases with increasing REE content (Fig 7.3). The actual degree of light REE enrichment (steepness of trend as indicated by $(La/Sm)_N$) also increases with differentiation (Fig 7.4), corresponding especially with the fractionation of orthopyroxene and clinopyroxene which all have higher partition coefficients for the heavy REE than the

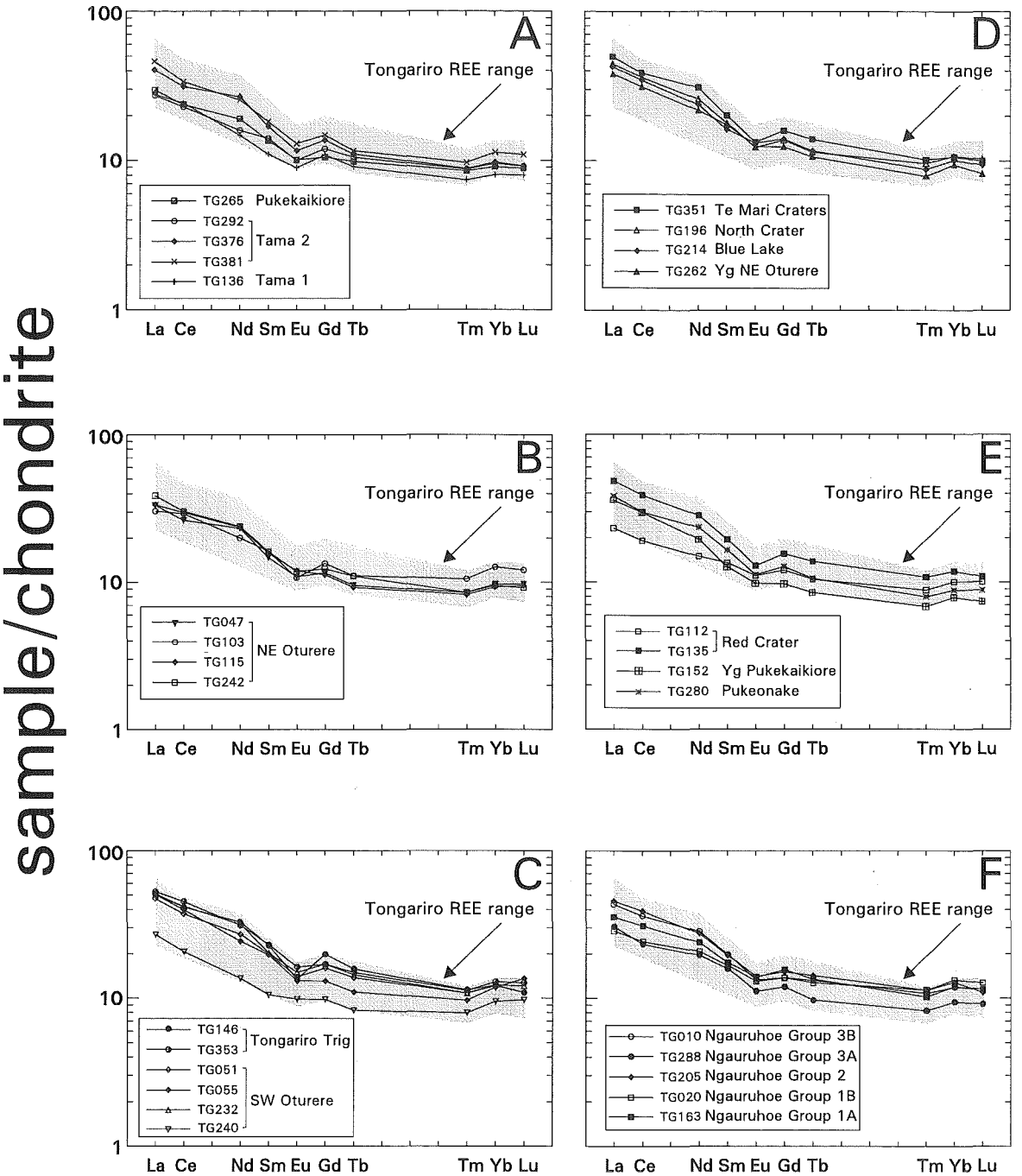

Figure 7.2 Chondrite-normalised abundances of rare earth elements in selected Tongariro samples, arranged in groupings of similar volcano-stratigraphic units. Shaded pattern shows range of all analysed Tongariro samples. Normalisation factors from Nakamura (1974).

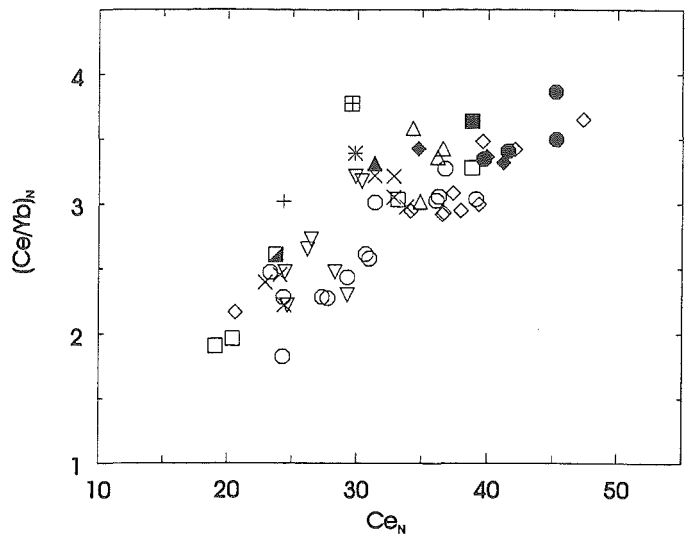

Figure 7.3 $(Ce/Yb)_N$ versus Ce_N contents in selected Tongariro samples, plotted according to volcano-stratigraphic unit (see key).

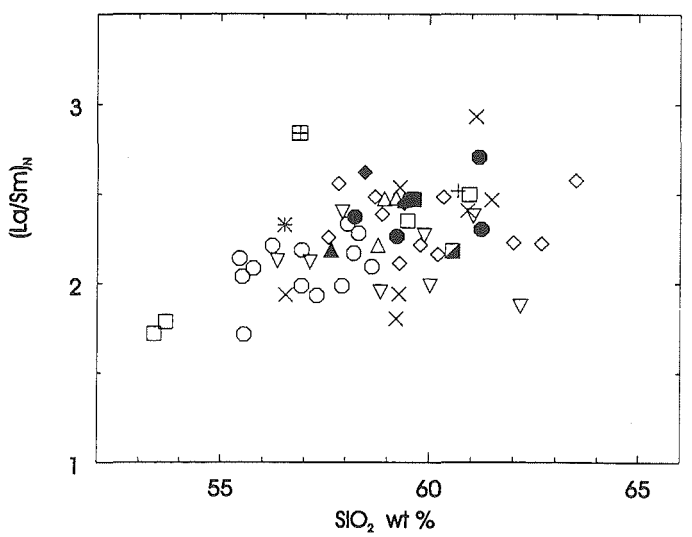

Figure 7.4 $(La/Sm)_N$ versus SiO_2 contents in selected Tongariro samples, plotted according to volcano-stratigraphic unit (see key).

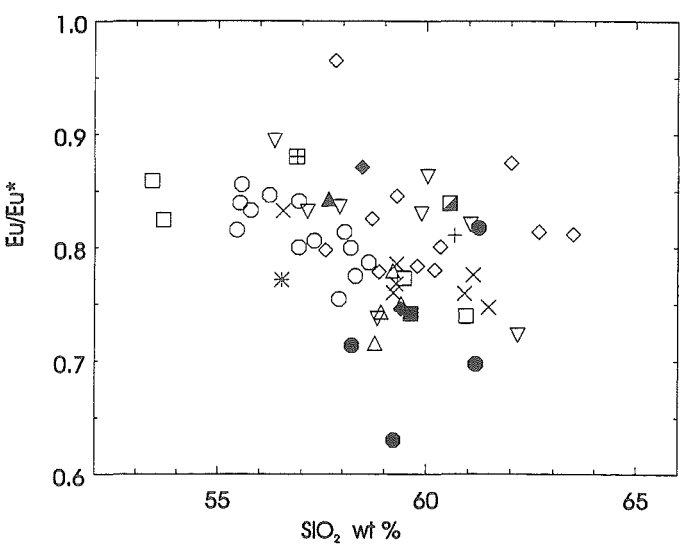

Figure 7.5 Eu/Eu* versus SiO_2 contents in selected Tongariro samples, plotted according to volcano-stratigraphic unit (see key).

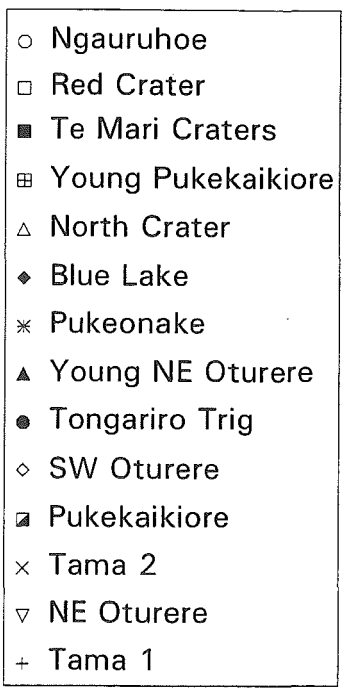

light REE (although since the Kd's are still less than 1, the effect is not extreme). The middle REE patterns are invariably characterised by a negative europium anomaly (Eu/Eu*=0.63-0.97), the magnitude of which shows a weak increase with differentiation (Fig 7.5). Negative Eu anomalies indicate relatively low oxygen activities which allow Eu^{2+} (high Kd for plagioclase) to predominate over Eu^{3+}, consistent with the major role played by plagioclase in the fractionating assemblage (Section 4.5.2). Note that the slight Gd peak evident in some REE plots is probably due to analytical error. Rather than being completely flat, the heavy REE patterns typically display a slight kink in the trend, of which the low Tm may be due to analytical error (Fig 7.2).

As expected from fractional crystallization, REE abundances generally increase with increasing SiO_2. The lowest abundances are represented by basaltic andesites and andesites such as those from post-1.8ka Red Crater, Young Pukekaikiore, and SW Oturere scoria TG240, whereas the silicic andesites and dacites of Tongariro Trig and SW Oturere tend to contain higher REE contents (Fig 7.2). However, there are considerable deviations from this pattern (Fig 7.2) such that two of the highest SiO_2 samples analysed (TG055 and TG103) plot mainly in the middle of the Tongariro REE range, and some of the hornblende-bearing lavas from Tama 1 & 2 and Pukekaikiore contain some of the lowest REE abundances (plotting at much lower values than samples of similar SiO_2 content from other units).

The REE patterns for the southern units of Tama 1, Tama 2 and Pukekaikiore (Fig 7.2A) do not show a marked depletion of middle REE's as might be expected given the presence of amphibole phenocrysts in these lavas, although the generally lower REE contents (of the middle and heavy REE in particular) may reflect fractionation of amphibole in these magmas. Samples from NE Oturere display similar REE patterns and concentrations, although the much more silicic TG103 (62.2 wt% SiO_2) has more elevated heavy REE abundances (Fig 7.2B). SW Oturere and Tongariro Trig lavas have relatively high concentrations of both light and heavy REE, with the noticeable exception of TG240 which contains much lower REE concentrations (particularly light REE; Fig 7.2C), this difference being consistent with other chemical differences which mark TG240 as representing a chemically distinctive type of magma (Section 6.6.6).

The REE patterns of the young northern units mirror each other, with slight differences in abundances reflecting small contrasts in degree of differentiation (Fig 7.2D). The Young Pukekaikiore sample is notable for its relatively high $(Ce/Yb)_N$ (Fig 7.3) and $(La/Sm)_N$ (Fig 7.4), with light REE abundances in the middle of the Tongariro range but among the lowest middle and heavy REE abundances (Fig 7.2E). A distinctive REE signature is in keeping with the other unusual chemical characteristics of the Young Pukekaikiore magma (Section 6.6.8e). A major contrast is obvious between the shape of the REE patterns for pre-1.8 ka and post-1.8 ka Red Crater lavas. The pre-1.8 ka sample shows comparatively strong light REE enrichment (Fig 7.2E) with $(Ce/Yb)_N$=3.3, whereas the post-1.8 ka sample displays much less REE fractionation (Fig 7.2E) with $(Ce/Yb)_N$=1.9 and the lowest $(La/Sm)_N$ of all analysed Tongariro samples (Fig 7.4). Gamble et al. (1993a, 1996) obtained very similar REE contents and patterns for a post-1.8 ka Red Crater lava (TVZ-10). REE patterns of Ngauruhoe samples are similar (Fig 7.2F), but the relative REE abundances of the different Ngauruhoe groups bear little relationship to SiO_2 content. For example, the Group 3A lava has lower REE abundances than less differentiated samples, which together with petrographic (Section 4.7) and geochemical evidence (Section 6.6.8k) for mixing suggest that some of these REE relationships may result primarily from magma mixing rather than fractional crystallization (c.f. Pallister et. al., 1992).

7.3.3 Incompatible trace element plots

As is the case for most subduction-related rocks (e.g. Hawkesworth et al., 1994), Tongariro lavas contain low HFSE abundances compared to those of the REE and LILE. Tongariro eruptives exhibit trace element ratios typical of orogenic andesites (e.g. Gill, 1981; Thorpe, 1982) such as relatively high Ba/La (17-33), Ba/Ta (440-1120), and La/Nb (2-4). Bivariate trace element plots using the full data set are now examined in order to provide a more expanded view than allowed by the multivariate diagrams. In this way, geochemical trends and patterns may be examined more closely. As expected, the incompatible elements show positive linear correlations when plotted against differentiation indices such as SiO_2 or Rb, although the strength of these correlations does vary. The varying degrees of enrichment reflect the relative incompatibilities of the elements. Cs, Rb, Ba, Th and U (Fig 7.6) experience increases in concentration by factors of 3 to 5 times over

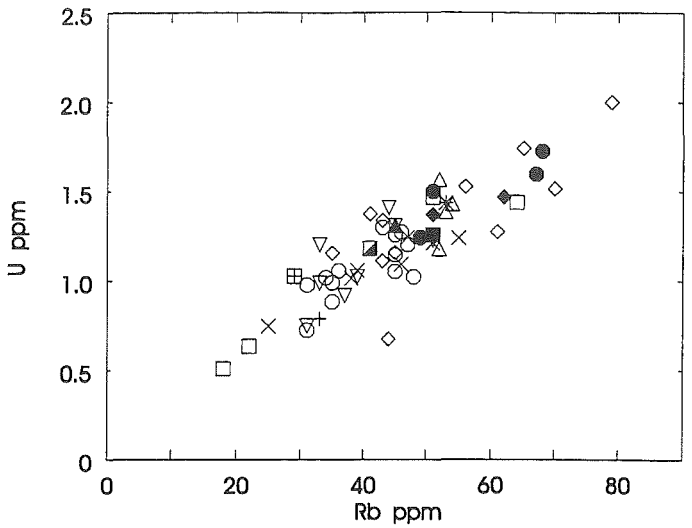

Figure 7.6 U versus Rb concentrations in selected Tongariro samples, plotted according to volcano-stratigraphic unit (see key).

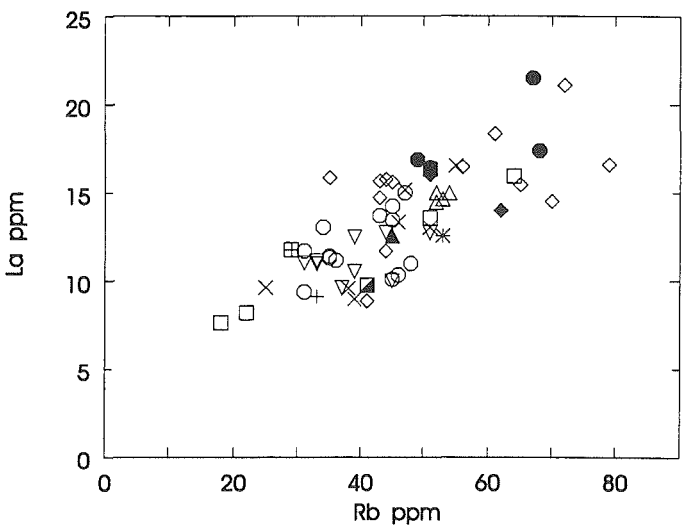

Figure 7.7 La versus Rb concentrations in selected Tongariro samples, plotted according to volcano-stratigraphic unit (see key).

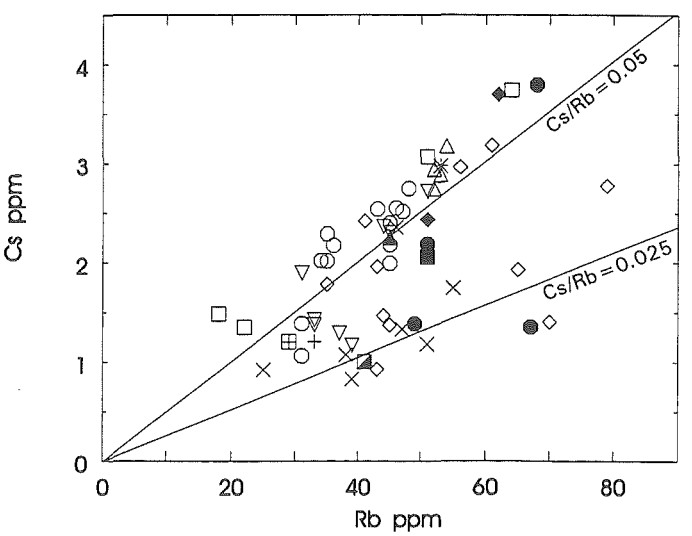

Figure 7.8 Cs versus Rb concentrations in selected Tongariro samples, plotted according to volcano-stratigraphic unit (see key). Selected constant ratio lines are shown.

the analysed SiO_2 range of just over 10 wt% (and Rb range of 62 ppm), whereas the other incompatible trace elements exhibit two- to three-fold increases over the same range (e.g. La, Fig 7.7).

Some noticeable sub-trends and compositional-stratigraphic relationships are evident in some of these variation diagrams. For example, the feature of relatively low Cs (Fig 7.8), Th (Fig 7.9), U (Fig 7.6), Nb, Ta, and Hf concentrations for the amphibole-bearing magmas of the old southern cones is consistent with the general pattern of low incompatible element abundances already observed for these units (i.e. low K, Rb, La, Ce, Zr, Y; Section 6.6.9a). Samples mainly from Tama 1, Tama 2, and Pukekaikiore fall on a Cs/Rb constant ratio line of around 0.025, whereas most other Tongariro eruptives contain higher Cs/Rb of c.0.5 (Fig 7.8). The Th-SiO_2 plot (Fig 7.9) also reveals this pattern, and in addition highlights the geochemical similarity of four younger (and amphibole-free) NE Oturere lavas (TG047, TG098, TG100, TG103) which consistently plot with the amphibole magmas in most incompatible element plots. These relationships suggest that some of the magmatic conditions leading to the formation of the distinctive southern magmas have subsequently been repeated, but not to the extent of preserving amphibole phenocrysts in the erupted lavas. A ratio-ratio plot of Ba/Zr versus Ta/Zr (Fig 7.10) shows a distinct division between the Ngauruhoe lavas at the base of the diagram, the amphibole-bearing units at the top, and the other Tongariro units in between.

A further example of compositional-stratigraphic inconsistency is illustrated by a plot of Pb versus SiO_2 (Fig 7.11). As well as the wide range in Pb contents exhibited by Tongariro eruptives, it is evident that lavas from SW Oturere plot on two quite distinct trends of different Pb concentrations and slopes. These trends do not equate with a straightforward time/stratigraphic relationship. Although with the full data set there is often no particular trend with time displayed by incompatible trace element ratios (which tend to fluctuate throughout the history of the volcanic complex), a more detailed examination of smaller time windows into Tongariro's history allows more meaningful examination of these fluctuations (Section 7.5).

Highly incompatible elements are especially sensitive to varying degrees of partial melting, and relatively small degrees of partial melting can cause significant changes in the

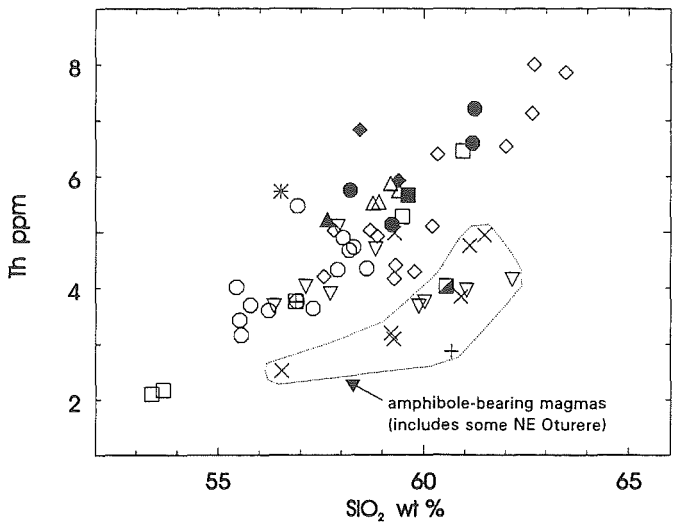

Figure 7.9 Th versus SiO_2 contents in selected Tongariro samples, plotted according to volcano-stratigraphic unit (see key).

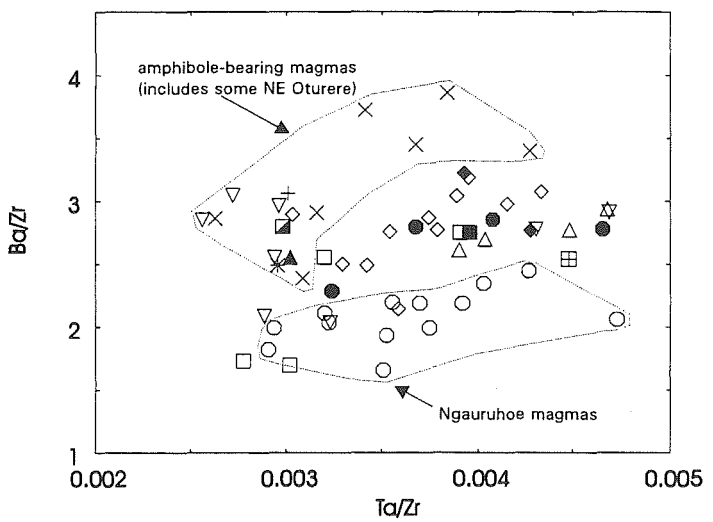

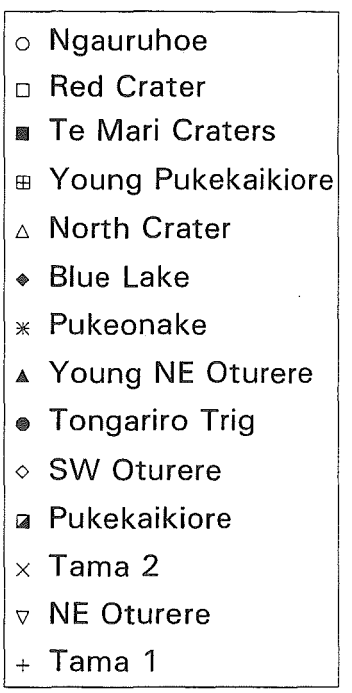

Figure 7.10 Ba/Zr versus Ta/Zr contents in selected Tongariro samples, plotted according to volcano-stratigraphic unit (see key).

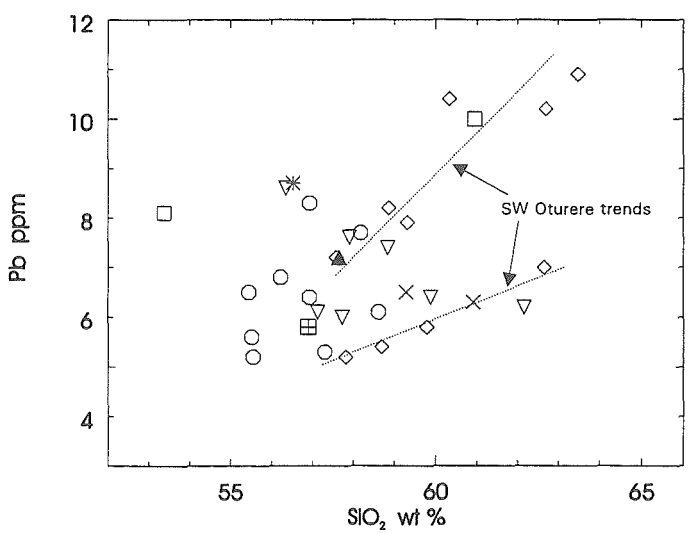

Figure 7.11 Pb versus SiO_2 contents in selected Tongariro samples, plotted according to volcano-stratigraphic unit (see key).

ratio of two incompatible elements with slightly different bulk partition coefficients (D). For the case of Tongariro, such a pair of elements are Rb and Zr, because Rb behaves somewhat more incompatibly than does Zr. The wide range in Rb/Zr values (0.20-0.55) for Tongariro eruptives has already been described in Section 6.5.3 and illustrated in Fig 6.8A. This variability could be attributed to changes in conditions at source whereby small degrees of partial melting (which concentrate Rb in the melt relative to Zr, producing higher Rb/Zr) or larger degrees of partial melting (lowering Rb/Zr) have predominated at different times. However, there is no consistent relationship between Rb/Zr and sample age, and there is often in fact a wide range in Rb/Zr for very closely associated samples - which might suggest that an insufficient time interval is likely to have elapsed to allow differences created at source to be translated into variable composition of the magmas erupted. On the other hand, it is not known how the eruption age of the magma relates to its residence time in shallow magma storage areas or deeper magma reservoirs. Also, the degree of partial melting is unknown.

Although variable degrees of partial melting may be a viable process responsible for generating the diverse Rb/Zr of Tongariro magmas, different source compositions or crustal contamination could also conceivably produce these compositional disparities. To test this idea further, it is appropriate to look at the ratios of pairs of incompatible elements with almost identical D's - upon which degree of partial melting (and of course extent of fractional crystallization) will have essentially no effect. Plots of Nb vs Ta (Fig 7.12), Zr vs Hf (Fig 7.13), and Th vs Ta (Fig 7.14) reveal considerable scatter in the data points and thus variation in the slopes of constant ratio lines, which on these plots cannot be explained by partial melting differences. Nb/Ta values range from 9.0 to 13.6 (Fig 7.12), which also coincide with the model continental crustal composition of Nb/Ta~11 (Taylor and McLennan, 1988; Green, 1995). Zr/Hf varies from 30 to 46 (Fig 7.13), similar to the range reported by Hildreth and Drake (1992) for the 1932 Volcán Quizapu eruptives. They concluded that such ranges of trace element ratios for magma erupted from the same reservoir over a period of only a few hours must represent the influence of crustal processes and therefore such ratios should not be relied upon to signify mantle sources (Hildreth and Drake, 1992).

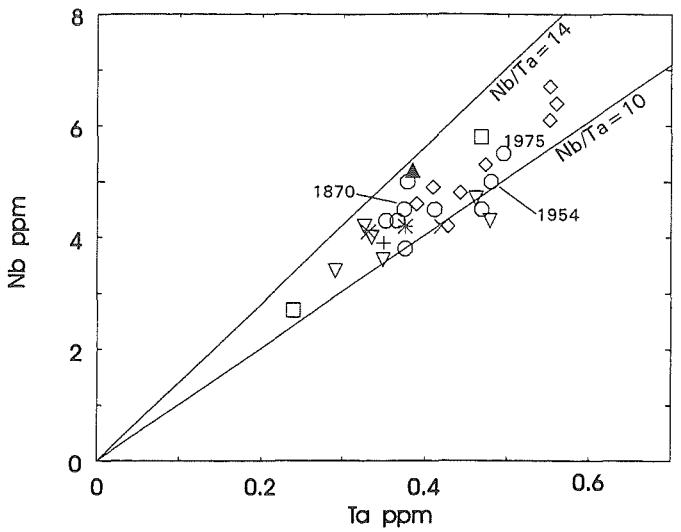

Figure 7.12 Nb versus Ta contents in selected Tongariro samples, plotted according to volcano-stratigraphic unit (see key). Selected constant ratio lines are shown. Historic Ngauruhoe samples are labelled.

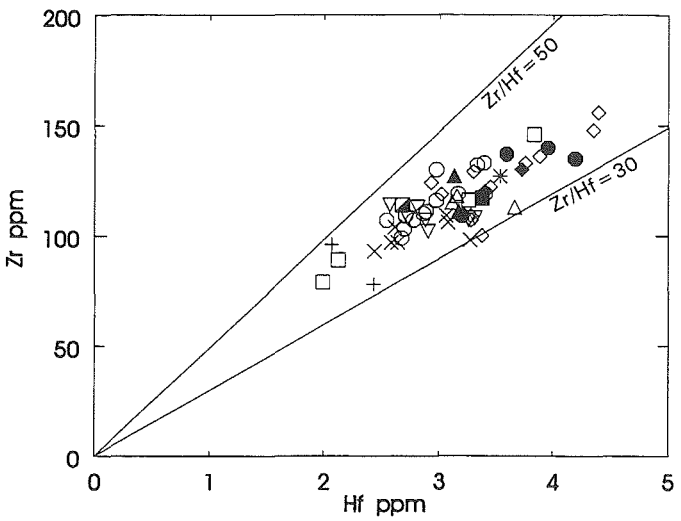

Figure 7.13 Zr versus Hf contents in selected Tongariro samples, plotted according to volcano-stratigraphic unit (see key). Selected constant ratio lines are shown.

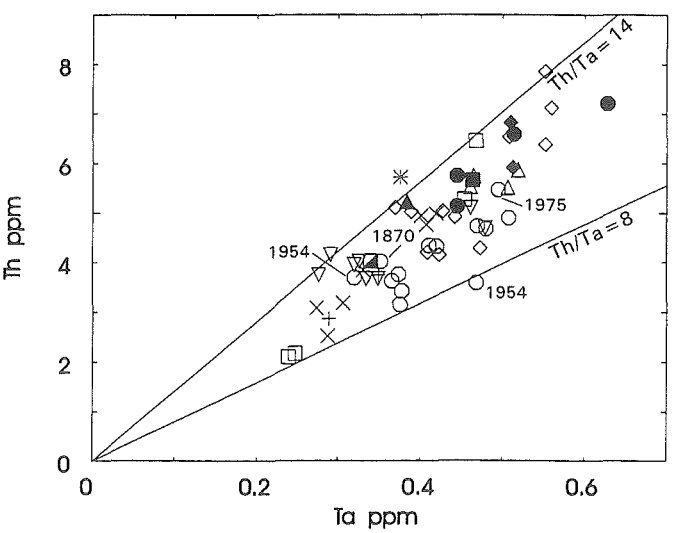

Figure 7.14 Th versus Ta contents in selected Tongariro samples, plotted according to volcano-stratigraphic unit (see key). Selected constant ratio lines are shown. Historic Ngauruhoe samples are labelled.

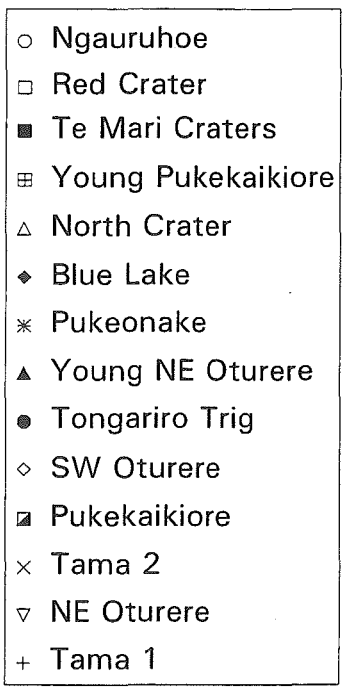

The observed variation in these particular Tongariro incompatible trace element ratios therefore seems more likely to reflect the influence of crustal contamination rather than different mantle sources or partial melting. Open system differentiation processes have already been implied from the inability of least-squares mixing models to satisfactorily predict major element compositions for many of the chemical groups and volcano-stratigraphic units (Section 6.6). Furthermore, modelling partial melting trends from a given mantle source is not practicable for Tongariro magmas because the Tongariro source is most likely an already somewhat evolved parent magma (probably at mid or lower crustal regions) rather than a primary mantle melt. Even the most 'primitive' basalts erupted from the Taupo Volcanic Zone (e.g. the Kakuki basalt and Ruapehu basalt end members of Graham et. al., 1992) are not primary mantle melts, having themselves experienced some fractionation. Thus the original mantle source composition for Tongariro eruptives remains uncertain.

7.3.4 Role of amphibole

The significant difference in mineralogy between the amphibole-phyric lavas of the Tama 1, Tama 2 and Pukekaikiore cone-building units and the other Tongariro eruptives is reflected in contrasting minor and trace element abundances at similar SiO_2 contents (Sections 6.6.9a, 7.3.3). Thus it appears that of the factors which control amphibole stability in andesites (bulk composition, temperature, total pressure, P_{H2O}, f_{O2}; Gill, 1981), bulk composition can be invoked as at least one of the influences promoting the occurrence of amphibole in these lavas. It is therefore perhaps somewhat surprising that more striking evidence for amphibole fractionation is not revealed by elements such as the middle REE (Section 7.3.2) or Y (Section 6.5.2i) for which hornblende Kd's are greater than 1. However, it is probable that the relatively low modal abundance of amphibole phenocrysts in Tongariro lavas (typically less than 5%) is a factor in the lack of geochemical evidence for a strong control by hornblende fractionation. The other more dominant phases effectively mask any major influence that amphibole might have on, for example, the REE patterns.

7.3.5 Modelling AFC processes using trace elements

The role of crustal contamination may be further examined by calculating model fractional crystallization and assimilation fractional crystallization (AFC) trends and comparing them with the patterns of Tongariro data on selected variation diagrams. For Tongariro magmas AFC is probably a more realistic process to model than bulk assimilation. A qualitative appraisal of many of these trace element variation diagrams is enough to reveal the Tongariro data being pulled away from a constant ratio trend (expected for fractional crystallization) towards crustal compositions along an AFC curve. Some plots show AFC trends diffused by fractional crystallization effects, e.g. Ba/Nb ratios generally increase with increasing Ba (e.g. NE Oturere), but part way along this AFC trend, SW Oturere magmas deviate from an increasing to a constant Ba/Nb trend - probably indicative of fractional crystallization unaccompanied by any crustal assimilation (Fig 7.15).

For the generalised models described below, unless stated otherwise, the initial magma composition upon which AFC modelling is based is taken to be the overall most primitive Tongariro magma erupted, i.e. that represented by the post-1.8ka Red Crater sample TG112. Thus in order to first examine general petrological processes, these models do not take strict account of age relationships (an approach reserved for Sections 7.4.1 and 7.5) and hence the relatively young Red Crater composition is used as a representative of the type of primitive magma that could also perhaps have been erupted earlier in Tongariro's history. Fractional crystallization trends are calculated according to the Rayleigh Law, $C_L/C_O=F^{(D-1)}$. Partition coefficients (Kd's) for trace elements used in the models are tabulated in Appendix 14; these were used in conjunction with known phase proportions to calculate the bulk partition coefficients (D's). AFC modelling is carried out according to the equations of DePaolo (1981), using an Excel spreadsheet modified from a programme kindly provided by J.P. Davidson. These arrangements also apply to the radiogenic isotope modelling of Section 7.4.

The Mesozoic Torlesse and Waipapa metasediments are both used to represent the potential crustal assimilants in the AFC models, of which the Torlesse terrane is the basement lithology thought most likely to underlie the Tongariro complex (supported by evidence from crustal xenoliths incorporated into Tongariro magmas; Chapter 5). Crustal

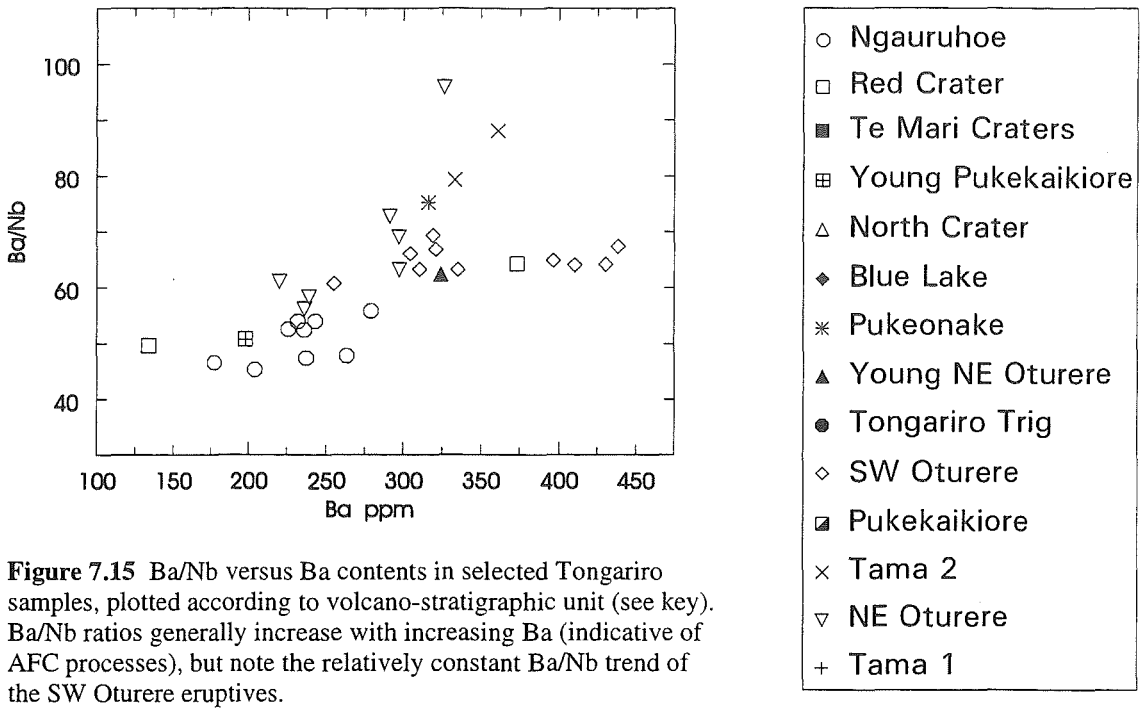

Figure 7.15 Ba/Nb versus Ba contents in selected Tongariro samples, plotted according to volcano-stratigraphic unit (see key). Ba/Nb ratios generally increase with increasing Ba (indicative of AFC processes), but note the relatively constant Ba/Nb trend of the SW Oturere eruptives.

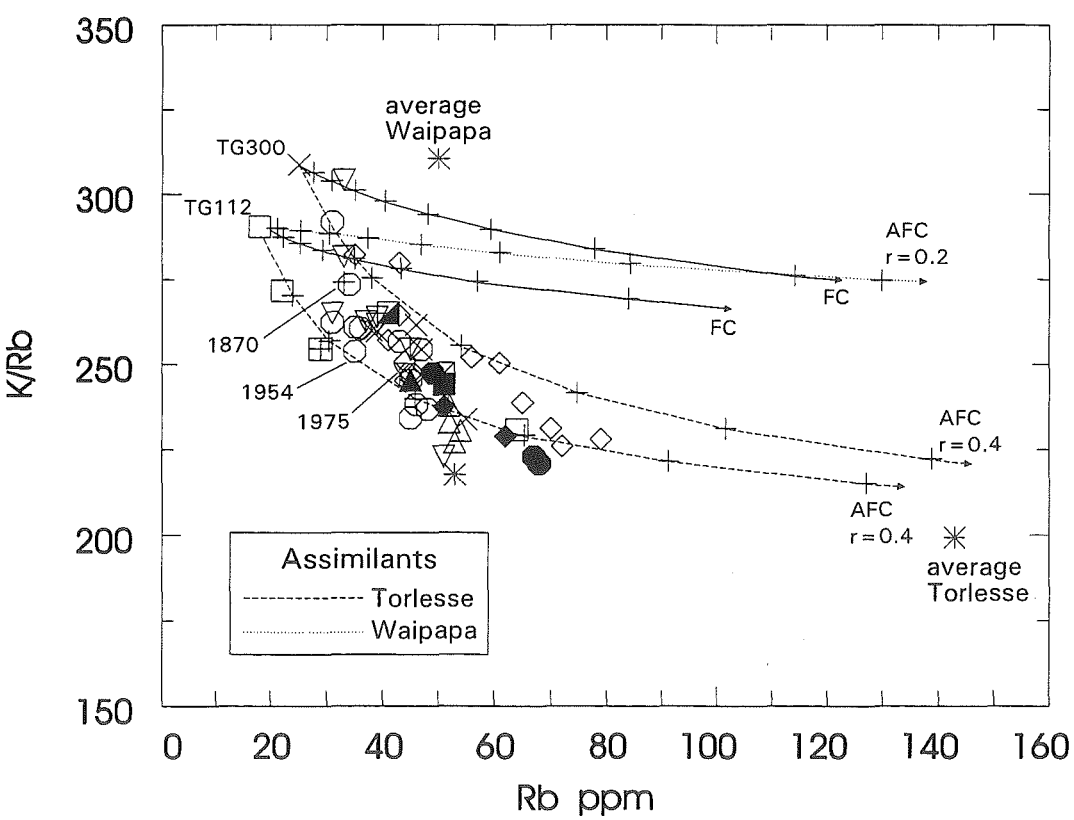

Figure 7.16 K/Rb versus Rb contents in selected Tongariro samples, plotted according to volcano-stratigraphic unit (see key). Fractional Crystallization (FC) and AFC curves calculated for both Torlesse and Waipapa assimilants are shown modelled from TG112 and TG300 starting compositions. Average Torlesse and Waipapa compositions are also plotted. Tick marks are denoted as crosses at 0.1 increments. Historic Ngauruhoe samples are labelled.

compositions were selected to be as representative as possible, although this objective was often constrained by limited availability of appropriate data. Isotopic compositions used in Section 7.4 were the averages of Graham et. al. (1992) (Table A14.2). XRF trace element crust compositions were obtained from Graham (1985a) along with unpublished INAA data of I.J. Graham (Table A14.3), and these correspond well with other part analyses of Torlesse published by Reid (1983) and Frost and Coombs (1989).

The overall contrast in trace element and isotope compositions between Torlesse basement and Tongariro magmas fulfills a basic requirement for recognition of AFC processes (Powell, 1984). The ratio of the concentration of the trace element in the assimilated country rock to the concentration in the initial magma (e.g. post-1.8ka Red Crater) is particularly high (C_A/C_O=2-7) for Rb, Ba, light REE, Zr, Nb, Hf, Ta, Pb, Th, and U. Note however that the Torlesse terrane is compositionally variable and the averaged compositions used in AFC modelling (Appendix 14) are thus by necessity a compromise for a complex reality which would be very difficult to model successfully otherwise.

The scale of crustal contamination is important with regards to the greywacke-argillite alternations; Graham (1985a) described how chemical trends correspond to greywacke-argillite differences. If some contamination occurs in relatively thin dikes rather than larger magma chambers then the compositional banding may have a significant effect on the compositional diversity of the magmas. However, there is probably not much validity in conducting highly complex AFC models for variable contaminant compositions. In addition, although the actual contaminant is likely to be a partial melt of the wallrock (rather than bulk assimilation), the slightly different composition of this melt and the variable degrees of partial melting possible are not incorporated into the AFC models.

Besides the compositions of the initial magma and the crustal assimilant, another important variable of the AFC model is designation of the ratio of the rate of assimilation to fractional crystallization (r). This has important consequences for the degree of enrichment of incompatible elements in the model. It is likely that in the case of Tongariro r is reasonably small, since the magma reservoirs are likely to be at relatively high levels in the crust. Contamination in the higher temperature environment existing at much deeper levels would increase the assimilation rate (and thus increase r) and cannot be completely

ruled out for Tongariro. Tongariro AFC trends were calculated using r values ranging between 0.2 and 0.4.

The trend of decreasing K/Rb with increasing SiO_2 has been described in Section 6.5.3 and plotted in Fig 6.7B. A convincing case may be made for this trend being the result of contamination of Tongariro magmas with the high Rb, low K/Rb Torlesse crust. K/Rb remains relatively constant with simple fractional crystallization (decreasing only very slightly due to Rb being marginally more incompatible than K), whereas assimilation of Torlesse crust will drag K/Rb values down an AFC curve which describes a path through much of the Tongariro data (Fig 7.16). The amphibole-bearing units (and some others) lie on a comparatively higher K/Rb trend (c.f. Fig 6.7B) which is better explained by Torlesse contamination of Tama 2 sample TG300, rather than Red Crater TG112 (Fig 7.16). The range in K/Rb of potential initial magmas suggests that variable parental magma compositions have been subjected to open system differentiation giving rise to a family of AFC curves (c.f. Davidson et. al., 1988). Note that the Waipapa crust cannot be responsible for the trend of the Tongariro data on this diagram; it contains lower Rb and higher K/Rb than Torlesse such that the calculated AFC curve predicts almost constant K/Rb with increasing Rb - a path clearly not followed by the plotted Tongariro compositions.

Fractional crystallization is not expected to have any significant effect on La/Yb ratios, whereas contamination with the comparatively La-rich Torlesse crust will increase La/Yb. Calculations confirm these predictions and show that assimilation of either Torlesse or Waipapa average crust could be responsible for the trend of the Tongariro data (Fig 7.17). Similarly, Ba/Zr versus Ba trends may also be explained by AFC processes (Fig 7.18). The average crustal compositions plotted on this diagram do not appear to explain the occurrence of the highest Ba/Zr Tongariro samples, but note that Torlesse greywacke and argillite Ba/Zr values do actually range up to around 7 (Graham, 1985a). Thus the compositional variability of the Torlesse may be responsible for much of the scatter on these diagrams, and when magmas encounter a compositionally similar (e.g. low Ba/Zr) portion of the crust, AFC processes may effectively be masked. It is also interesting to note that on the Ba/Zr-Ba diagram sediments from the Kermadec-Hikurangi Margin (Gamble et. al., 1996) plot in a similar compositional field to the Torlesse crust - which creates problems when trying to distinguish between sediment subduction and crustal assimilation.

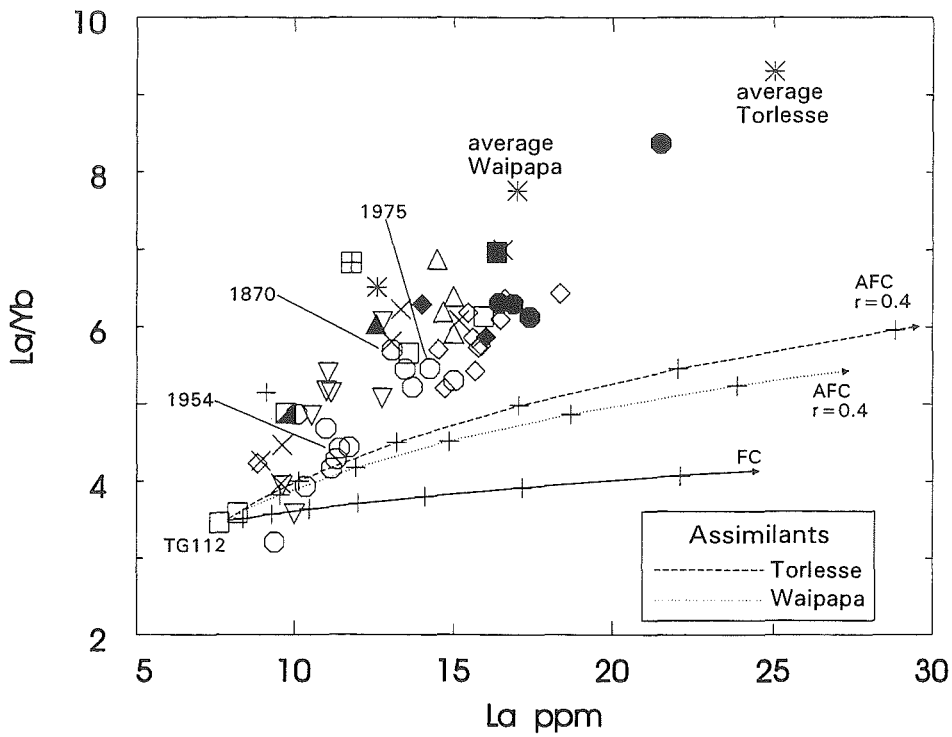

Figure 7.17 La/Yb versus La contents in selected Tongariro samples, plotted according to volcano-stratigraphic unit (see Fig 7.15 for key). Fractional Crystallization (FC) and AFC curves calculated for both Torlesse and Waipapa assimilants are shown modelled from TG112 starting composition. Average Torlesse and Waipapa compositions are also plotted. Tick marks are denoted as crosses at 0.1 increments. Historic Ngauruhoe samples are labelled.

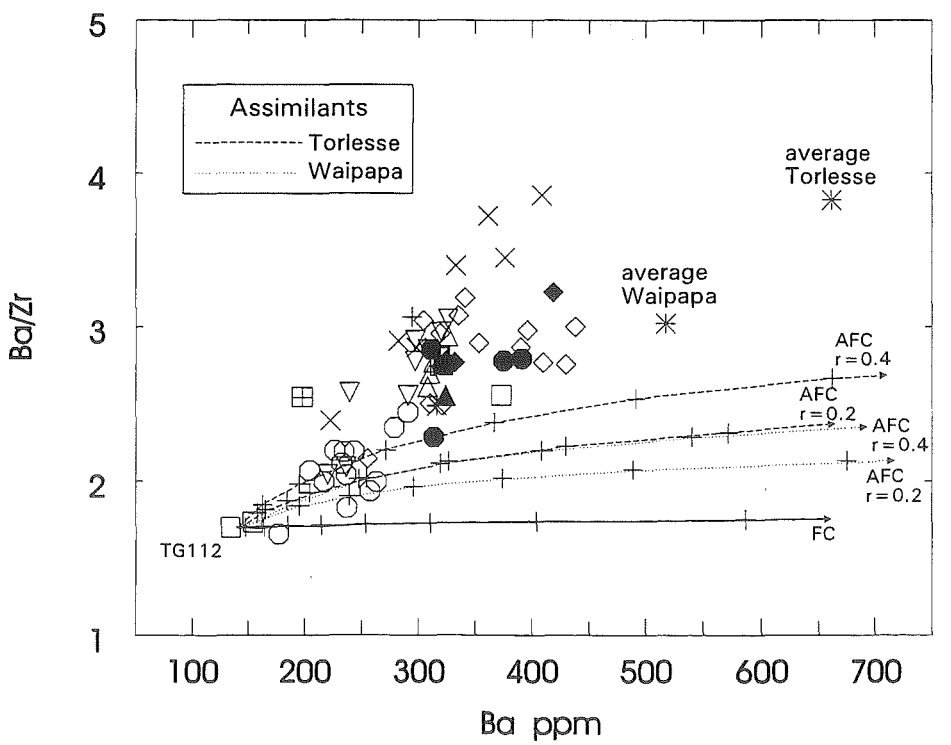

Figure 7.18 Ba/Zr versus Ba contents in selected Tongariro samples, plotted according to volcano-stratigraphic unit (see Fig 7.15 for key). Fractional Crystallization (FC) and AFC curves calculated for both Torlesse and Waipapa assimilants are shown modelled from TG112 starting composition. Average Torlesse and Waipapa compositions are also plotted. Tick marks are denoted as crosses at 0.1 increments.

In conclusion, as supported by petrographic evidence (crustal xenoliths; Chapter 5) and radiogenic isotope data discussed in the next section, crustal contamination (plus or minus a contribution from subducted sediments) is favoured as the process principally responsible for creating these diverse incompatible element ratios in Tongariro magmas.

7.4 ISOTOPE COMPOSITIONS

Radiogenic and stable isotope data are now brought in to further test AFC relationships in Tongariro petrogenesis. It is found that the isotopic data provide additional support for the involvement of AFC as a driving force in producing the observed compositional differences in Tongariro magmas. Variation both in the composition of the crustal assimilant and the amount of contamination appears likely to be responsible for the considerable isotopic diversity observed within some units and chemical groups.

The approach taken to obtaining isotopic data was to analyse a few selected volcano-stratigraphic units in as much detail as possible, thereby concentrating on explaining particular trends or groupings already identified from XRF data. To this end, a disproportionate number of samples from Ngauruhoe, SW Oturere and NE Oturere were analysed for their isotopic compositions, with isolated samples chosen from the compositionally distinctive units of Red Crater, Young Pukekaikiore, Young NE Oturere, Pukeonake, and Tama2 making up the data set. Thus although a significant number of Tongariro units are not represented in the following discussion, the approach taken is in keeping with the aims of this project, i.e. rather than documenting total compositional variation from a random scatter of samples, concentration on particular units allows a more detailed characterisation of magmatic trends in time and space. Note that published isotopic analyses (Section 7.2) of Ngauruhoe 1954, Red Crater, Young Pukekaikiore, Pukeonake, Tongariro Trig, Pukekaikiore, and Tama 2 have also been plotted alongside the new Tongariro data in some of the diagrams.

7.4.1 Strontium and neodymium isotope compositions

The analysed range in measured $^{87}Sr/^{86}Sr$ for Tongariro magmas is 0.704442 (TG152, Young Pukekaikiore) to 0.706193 (TG232, SW Oturere). When plotted versus sample age (Fig 7.19), no obvious patterns or cycles of isotopic variation with time are apparent, although some broad trends can be identified. Data are sparse for the pre-125 ka period, but indicate relatively constant $^{87}Sr/^{86}Sr$ at around 0.70495. Lower $^{87}Sr/^{86}Sr$ (down to 0.70460) magmas are recorded for NE Oturere between c.125 ka and 90 ka. Partly synchronous with the activity at NE Oturere, much more radiogenic compositions (0.70512-0.70619) were erupted from SW Oturere from 114 to 77 ka, whereas the youngest lava and scoria (c.40-50 ka) mark a return to lower $^{87}Sr/^{86}Sr$ (0.70488-0.70494).

The last 25 ka of Tongariro's history has considerable isotopic variability, including within cone-forming sequences, e.g. Red Crater 0.70456-0.70513 and Ngauruhoe 0.70453-0.70617. The Sr-rich Young Pukekaikiore lava (TG152) has the least radiogenic $^{87}Sr/^{86}Sr$ (0.704442), Pukeonake (TG280) is also relatively low (0.704758), whereas the Young NE Oturere scoria (TG262) contains one of the highest $^{87}Sr/^{86}Sr$ ratios analysed (0.705700). Note that a similar total range of $^{87}Sr/^{86}Sr$ ratios was erupted over the post-glacial period as was erupted c.80 ka earlier (Fig 7.19). Thus rather than each unit representing a distinctive isotopic 'fingerprint' of a different source, most of them seem to have suffered variable enrichment by way of crustal contamination (as shown in the following discussion), smearing out their isotopic signatures to cover a broad range of values.

When plotted against a measure of fractionation such as MgO (Fig 7.20), Tongariro $^{87}Sr/^{86}Sr$ ratios increase towards the more radiogenic values of three quartzose xenoliths analysed from the 1975 Ngauruhoe pyroclastic avalanche deposit. Similarly, $^{87}Sr/^{86}Sr$ correlates positively with SiO_2, a relationship suggestive of AFC and also exhibited by other TVZ andesites (Fig 7.21). The new Tongariro data obtained from this study overlap with the compositional fields for Ruapehu (supporting other evidence for their geochemical similarity; Section 6.7) and White Island andesites, and the Red Crater basaltic andesites overlap with the TVZ basalt field (Fig 7.21). Young Pukekaikiore eruptives plot in the satellite vents Type 5 compositional field (Fig 7.21), the magma type within which they have already been classified (Graham and Hackett, 1987), and also overlap with the Rolles

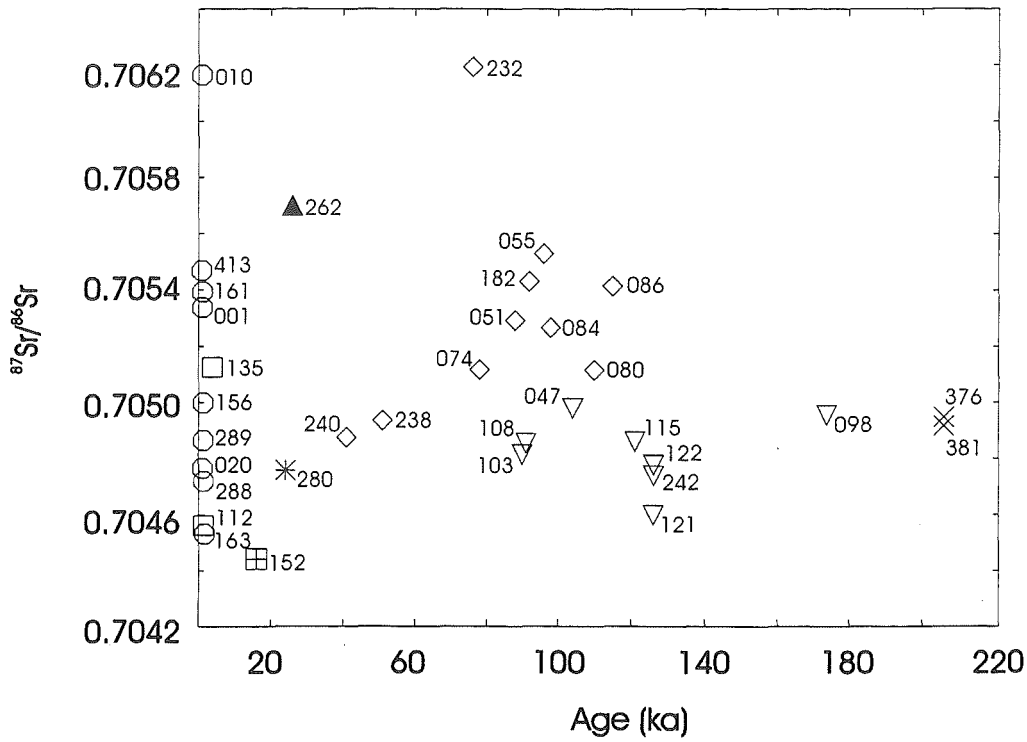

Figure 7.19 Plot of $^{87}Sr/^{86}Sr$ versus time for all those Tongariro samples analysed for isotopic composition. Samples are plotted according to volcano-stratigraphic unit (see Fig 7.15 for key) and are labelled with sample number (all have TG prefix). Prehistoric sample ages are derived from tephra chronology, K-Ar age determinations or by extrapolation (see Appendix 13). Errors on the $^{87}Sr/^{86}Sr$ measurements are usually much less than the size of the symbols used.

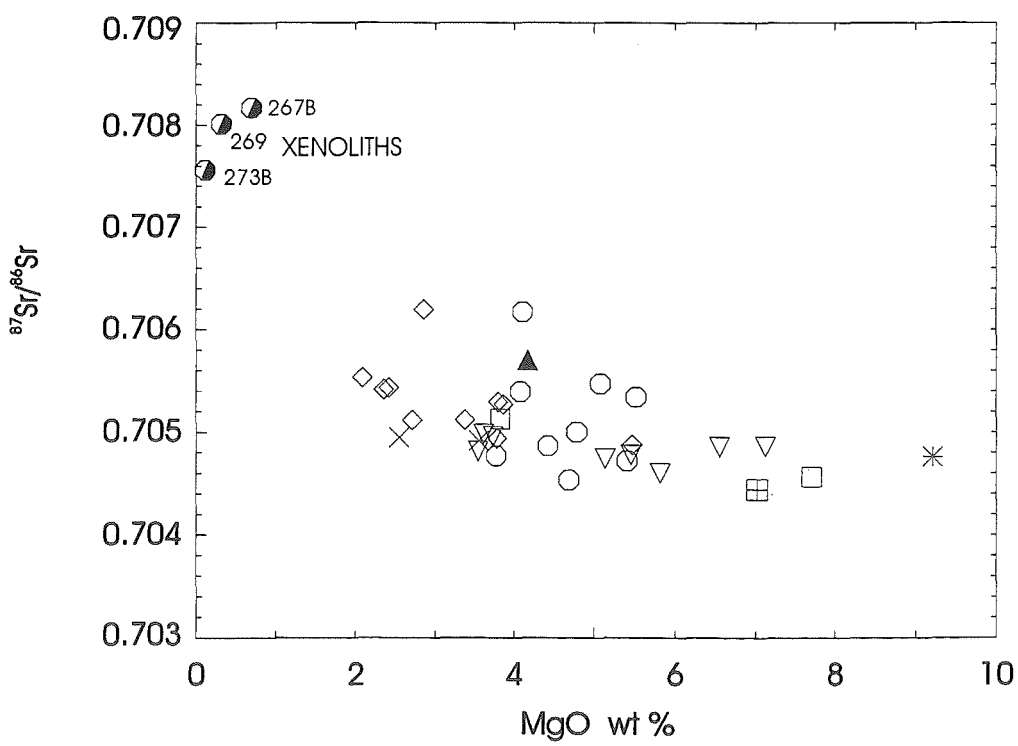

Figure 7.20 $^{87}Sr/^{86}Sr$ versus MgO contents in selected Tongariro samples, plotted according to volcano-stratigraphic unit (see Fig 7.15 for key). $^{87}Sr/^{86}Sr$ ratios increase in a broad trend towards the compositions of the crustal xenoliths (hosted by the 1975 Ngauruhoe pyroclastic avalanche deposit). Errors on the $^{87}Sr/^{86}Sr$ measurements are usually much less than the size of the symbols used.

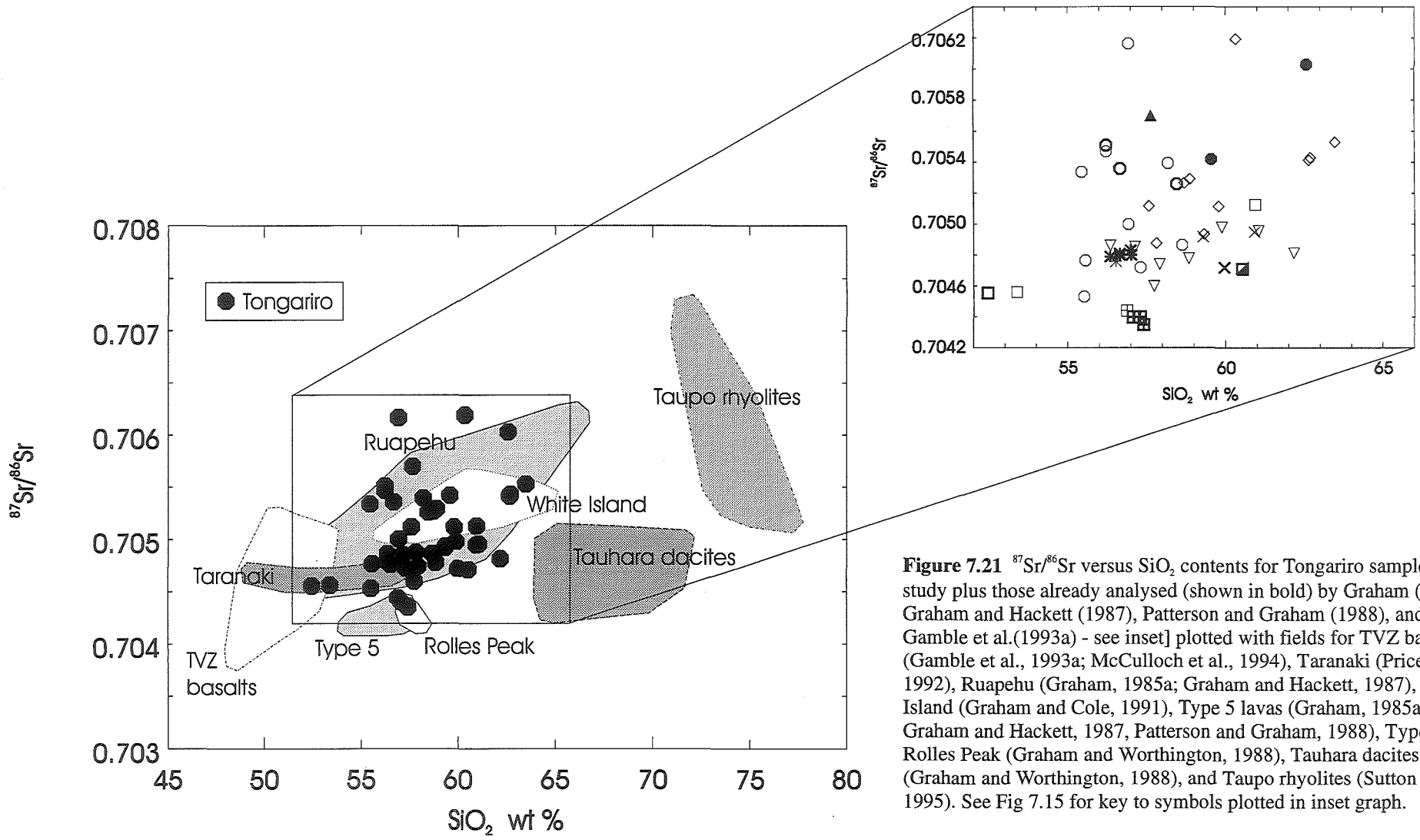

Figure 7.21 $^{87}Sr/^{86}Sr$ versus SiO_2 contents for Tongariro samples [this study plus those already analysed (shown in bold) by Graham (1985), Graham and Hackett (1987), Patterson and Graham (1988), and Gamble et al.(1993a) - see inset] plotted with fields for TVZ basalts (Gamble et al., 1993a; McCulloch et al., 1994), Taranaki (Price et al., 1992), Ruapehu (Graham, 1985a; Graham and Hackett, 1987), White Island (Graham and Cole, 1991), Type 5 lavas (Graham, 1985a; Graham and Hackett, 1987, Patterson and Graham, 1988), Type 8 Rolles Peak (Graham and Worthington, 1988), Tauhara dacites (Graham and Worthington, 1988), and Taupo rhyolites (Sutton et al., 1995). See Fig 7.15 for key to symbols plotted in inset graph.

Peak samples (Graham and Worthington, 1988; Type 8 andesite) - but these andesites differ in several respects such as their petrography and substantially higher Sr contents (919-1035 ppm) than those from Young Pukekaikiore (634-643 ppm).

When the new Tongariro data are examined in more detail (Fig 7.21 inset), the considerable scatter evident in the generally positive trend make it clear that these samples have not evolved along a unique AFC trend. NE Oturere eruptives scatter about a relatively gently sloping trend, whereas SW Oturere samples plot on a steeper (but also scattered) trajectory, and Ngauruhoe displays a family of trends of varying steepness (Fig 7.21 inset). There are no major discrepancies between the published analyses of Ngauruhoe, Red Crater, Young Pukekaikiore, Pukeonake, Pukekaikiore, and Tama 2 and the equivalent samples from this study (Fig 7.21 inset). Two published analyses of Tongariro Trig lavas show relatively radiogenic $^{87}Sr/^{86}Sr$ compositions which plot close to SW Oturere eruptives (Fig 7.21 inset) - with which they have already been shown to have a close association (Section 6.6.9c).

Just under half the samples analysed for $^{87}Sr/^{86}Sr$ were also analysed for $^{143}Nd/^{144}Nd$, and the systematic covariation of these two radiogenic isotope ratios is shown in Fig 7.22. The new Tongariro data fit into the published fields and trends of TVZ andesites, and as observed for the $^{87}Sr/^{86}Sr$-SiO_2 diagram (Fig 7.21) there is reasonably good correspondence between existing and new analyses of Ngauruhoe and Young Pukekaikiore (Fig 7.22 inset). Tongariro $^{143}Nd/^{144}Nd$ values range from 0.512629 to 0.512862. Note that the Young Pukekaikiore eruptives (along with published analyses of 'Type 5' lavas) fall off the main trend towards lower $^{87}Sr/^{86}Sr$ values (Fig 7.22). Published data for Red Crater and Pukeonake are plotted in place of data from this study as new $^{143}Nd/^{144}Nd$ analyses were not made on these samples.

Graham et al. (1992, 1995) have shown how compared with MORB, the Tonga-Kermadec and TVZ basalts plot along the higher $^{87}Sr/^{86}Sr$ side of the mantle array, and that calculated AFC trends between TVZ basalts and Torlesse crust explain the trends for Ruapehu andesites. AFC models using post-1.8 ka Red Crater lava as the initial magma show that the main trend for Tongariro data on the $^{87}Sr/^{86}Sr$ - $^{143}Nd/^{144}Nd$ diagram can be satisfactorily explained by contamination with Torlesse crust, which provides a better fit

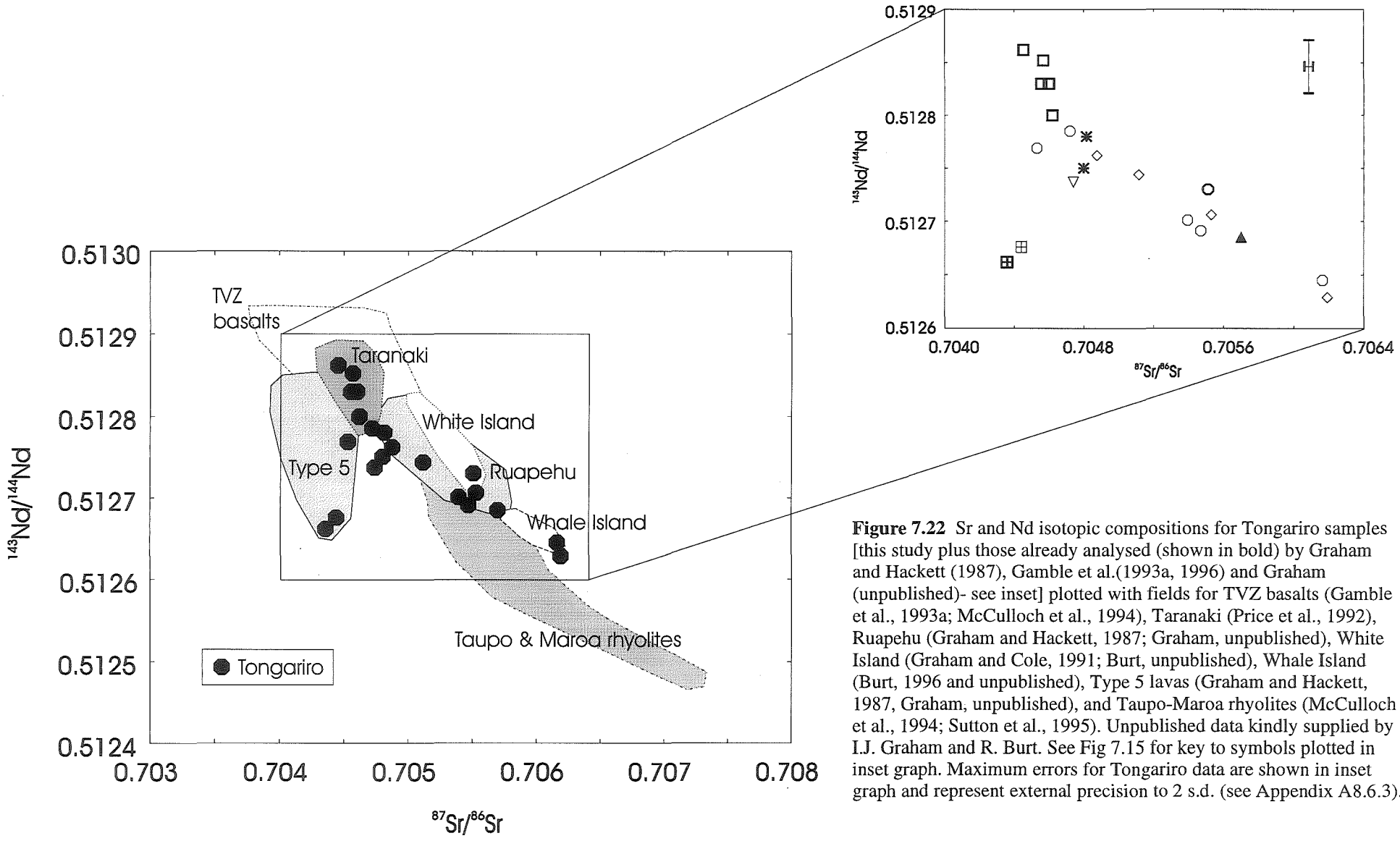

Figure 7.22 Sr and Nd isotopic compositions for Tongariro samples [this study plus those already analysed (shown in bold) by Graham and Hackett (1987), Gamble et al.(1993a, 1996) and Graham (unpublished)- see inset] plotted with fields for TVZ basalts (Gamble et al., 1993a; McCulloch et al., 1994), Taranaki (Price et al., 1992), Ruapehu (Graham and Hackett, 1987; Graham, unpublished), White Island (Graham and Cole, 1991; Burt, unpublished), Whale Island (Burt, 1996 and unpublished), Type 5 lavas (Graham and Hackett, 1987, Graham, unpublished), and Taupo-Maroa rhyolites (McCulloch et al., 1994; Sutton et al., 1995). Unpublished data kindly supplied by I.J. Graham and R. Burt. See Fig 7.15 for key to symbols plotted in inset graph. Maximum errors for Tongariro data are shown in inset graph and represent external precision to 2 s.d. (see Appendix A8.6.3).

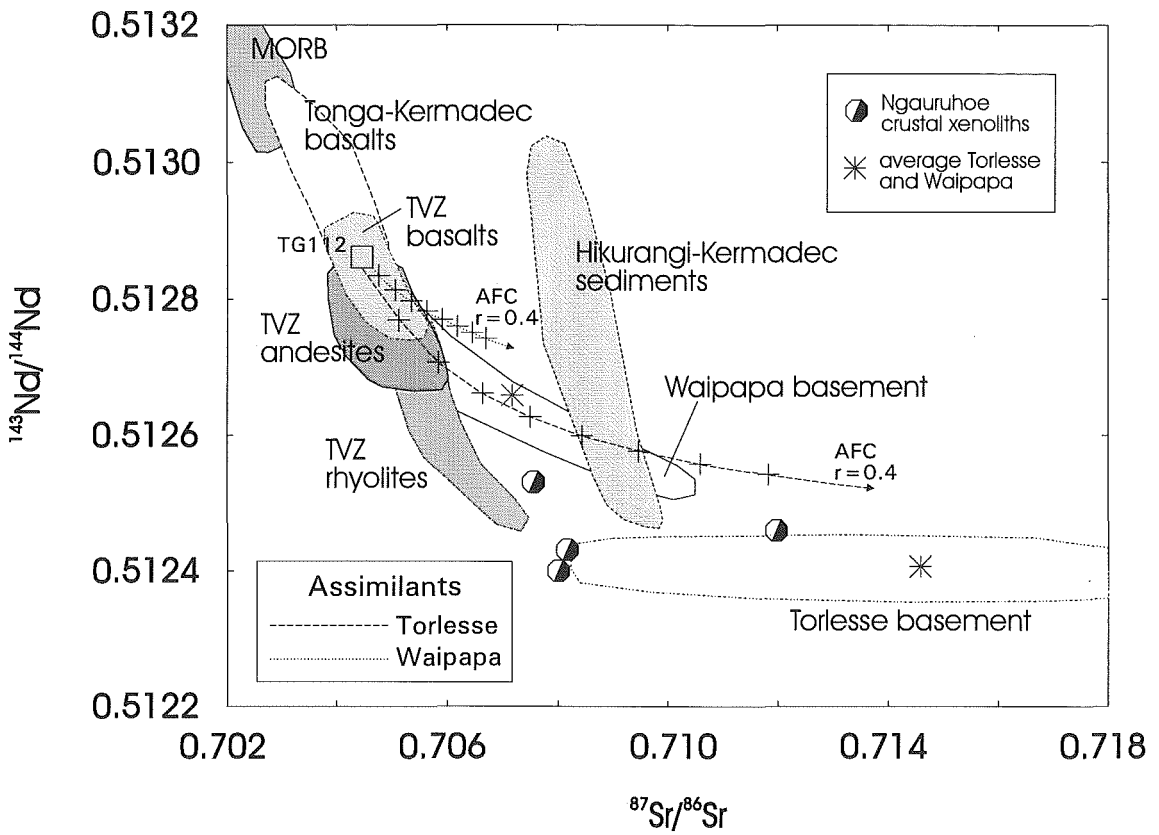

Figure 7.23 Sr and Nd isotopic compositional fields for TVZ basalts (Gamble et al., 1993a; McCulloch et al., 1994), TVZ andesites (this study; Graham and Hackett, 1987; Graham and Cole, 1991; Gamble et al., 1993a, 1996; Burt et al., 1996 and unpublished; Graham, unpublished), TVZ rhyolites (McCulloch et al., 1994; Sutton et al., 1995), Tonga-Kermadec basalts (Ewart and Hawkesworth, 1987; Gamble et al., 1993a, 1995, 1996), MORB (Ito et al., 1987), Torlesse and Waipapa crust (McCulloch et al., 1994; Graham, unpublished), and Hikurangi-Kermadec sediments (Gamble et al., 1996). Unpublished data kindly supplied by I.J. Graham and R. Burt. AFC curves calculated for both Torlesse and Waipapa assimilants are shown modelled from TG112 starting composition. Tick marks are denoted as crosses at 0.1 increments.

to the data than Waipapa crust (Fig 7.23). Note also that xenoliths found in Ngauruhoe lavas also plot in or close to the Torlesse compositional field (Fig 7.23).

Considerable scatter is revealed when the incompatible trace element ratios used in AFC calculations in Section 7.3.5 (K/Rb, La/Yb, Ba/Zr) are plotted against $^{87}Sr/^{86}Sr$. When examined in the light of age relationships, in addition to not defining a single AFC curve, the data do not even seem to relate to a family of AFC trends. For example, on these diagrams SW Oturere and NE Oturere samples plot from oldest to youngest in a seemingly random and almost opposite direction to that of increasing AFC (e.g. Fig 7.24).

On the other hand, eruptives from Ngauruhoe do progress from the oldest and least contaminated to the youngest and most contaminated, although the data are widely scattered (e.g. Fig 7.24). The historic Ngauruhoe lavas follow a steep trend which can be modelled as an AFC curve between the older TG163 lava and average Torlesse crust, with r=0.4 (Fig 7.24). Unrealistically high rates of assimilation relative to fractional crystallization are required to pull even slightly the AFC curve towards the other older Ngauruhoe lavas which appear to track along a much less steep trend than the historic lavas. However, when a less radiogenic Torlesse composition from Graham's (1985a) data set is modelled as the contaminant for these lavas, the AFC curve becomes more plausible (Fig 7.24). This is a relatively crude but useful demonstration of the influence of variable crustal composition on Tongariro isotopic and incompatible element compositions.

Although Tongariro magmas have ascended through a relatively limited horizontal distance of crust, their vertical traverse provides opportunity to interact with a compositionally diverse basement. Strontium isotopic compositions of samples taken from different depths of the same drill core (Graham, 1985a) demonstrate this heterogeneity. When examined in this way, data for Torlesse greywacke samples from borehole "r" (east of Tama Saddle at the foot of the Kaimanawa Ranges) for example, reveal the following $^{87}Sr/^{86}Sr$ isotopic range: 35.7m=0.70924, 39.6m=0.71289, 46.3m=0.70921, 64m=0.70930, 89.9m=0.70908, 93.3m=0.70867, 180.7m=0.70922, 198.4m=0.71334. Note that the variation over 4m (difference of 0.00365 between 35.7m and 39.6m) can be almost as large as that encountered over 160m (difference of 0.0041 between 35.7m and 198.4m). A similar situation exists for the Waipapa basement (borehole "b2" west of Tongariro sampled

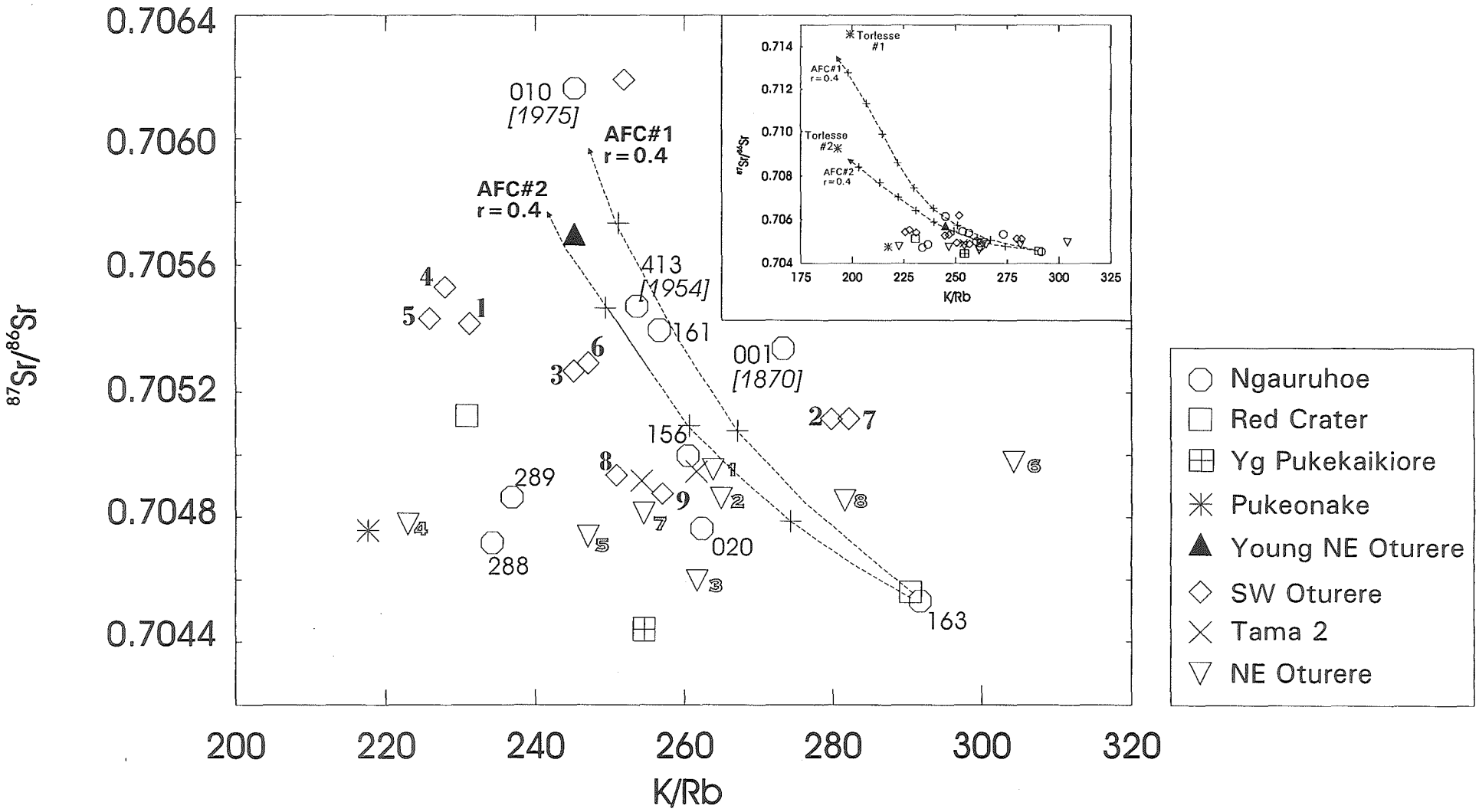

Figure 7.24 $^{87}Sr/^{86}Sr$ versus K/Rb ratios in selected Tongariro samples, plotted according to volcano-stratigraphic unit (see key). AFC curves calculated for different Torlesse assimilant compositions (see text) are shown modelled from a Ngauruhoe TG163 starting composition. Tick marks are denoted by crosses at 0.1 increments. Ngauruhoe samples are labelled with sample number (all have TG prefix) and historic samples are labelled with date. Time progression of SW Oturere and NE Oturere samples are indicated by numbered sequences. Inset graph shows AFC models in their entirety.

Waipapa crust ranging from $^{87}Sr/^{86}Sr$=0.70499 to 0.70845 for depths spanning 96.6m to 53m). Based on evidence from drillcores in such close proximity to Tongariro, it is thus more than likely that a similarly compositionally diverse crust exists beneath the Tongariro complex. If the Torlesse basement is also structurally complex (e.g. isoclinally folded), then considerable horizontal compositional variability may also exist. Thus vertical, as well as lateral, heterogeneity in the crust (rather than the mantle) may be the primary cause of the diverse $^{87}Sr/^{86}Sr$ ratios measured for Tongariro lavas closely related in time and space. However, for reasons already touched upon in Section 7.3.5, it is generally not feasible to rigorously quantify contamination with such a wide range of crustal compositions.

The lack of a strong correlation between incompatible element ratios and $^{87}Sr/^{86}Sr$ ratios may indicate a certain degree of decoupling between trace element and isotopic systematics. Certainly, variations (between and within units) in parental magma compositions, degree of fractional crystallization and crustal contamination of the different magma batches, and heterogeneity of the crustal assimilant will all contribute much complexity to any perceived overall AFC trends. Thus in contrast to the general approach of calculating an AFC trend to fit a large data set (e.g. Fig 7.23), which is still a useful exercise, when Tongariro data are examined in detail it is much more difficult to obtain geologically-realistic AFC models which satisfy both compositional and age relationships (e.g. the young, relatively non-radiogenic Red Crater lava strictly should not be modelled as parental to much older - and more radiogenic - units). It is important to be aware of the more detailed information concerning the complexity of AFC processes which may be gained from this latter approach.

7.4.2 Lead isotope compositions

The subset of Tongariro samples analysed for radiogenic Pb isotopes are plotted in Fig 7.25 along with published Tongariro and other TVZ volcanics. The Ngauruhoe 1954 analyses of Graham et al. (1992) are much less radiogenic than not only the new 1954 sample (TG413), but also all the new Ngauruhoe analyses (Fig 7.25 inset). This may indicate strong isotopic heterogeneity of the 1954 eruption products, although analytical variation between laboratories cannot be discounted. Even when the published Ngauruhoe

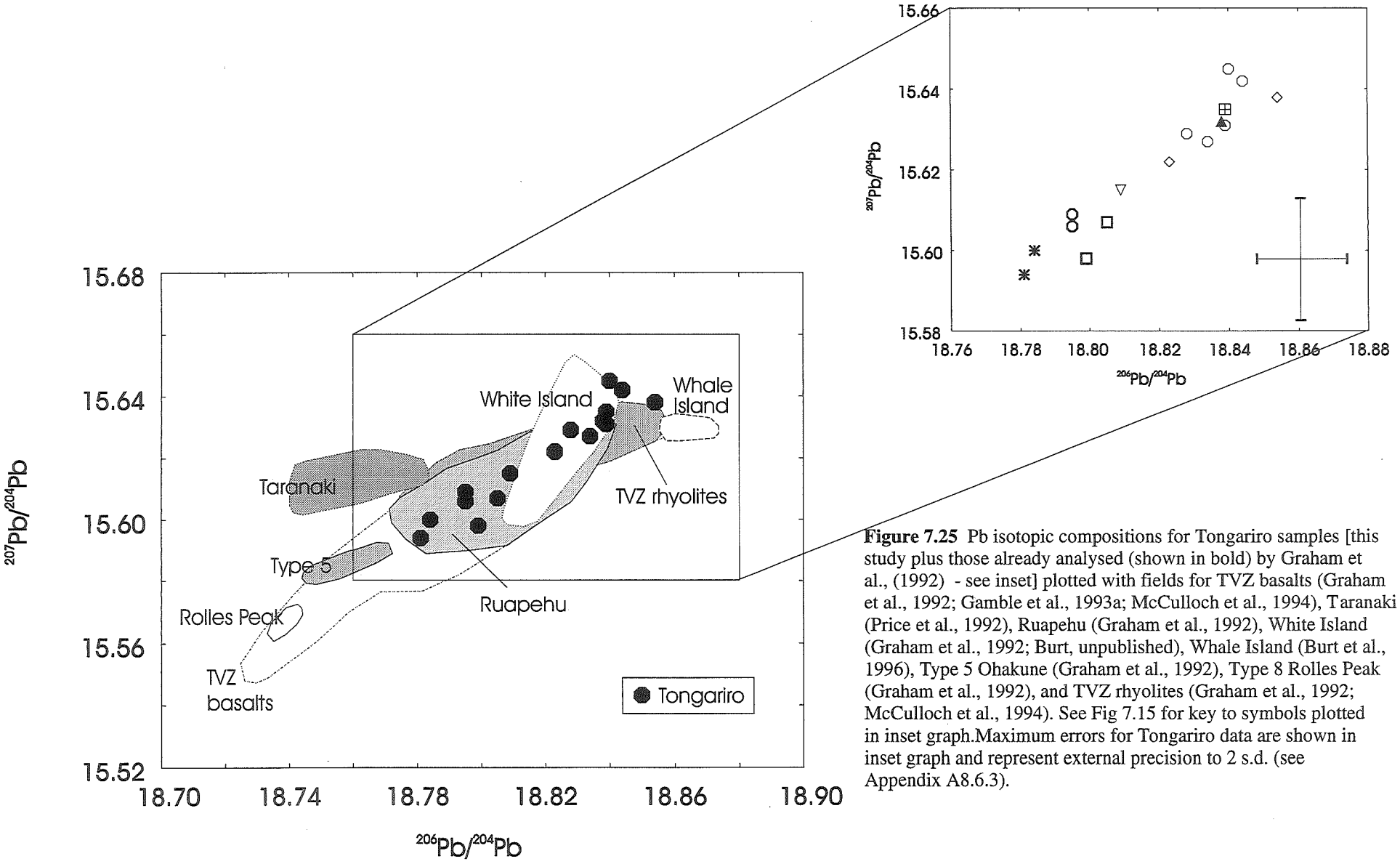

Figure 7.25 Pb isotopic compositions for Tongariro samples [this study plus those already analysed (shown in bold) by Graham et al., (1992) - see inset] plotted with fields for TVZ basalts (Graham et al., 1992; Gamble et al., 1993a; McCulloch et al., 1994), Taranaki (Price et al., 1992), Ruapehu (Graham et al., 1992), White Island (Graham et al., 1992; Burt, unpublished), Whale Island (Burt et al., 1996), Type 5 Ohakune (Graham et al., 1992), Type 8 Rolles Peak (Graham et al., 1992), and TVZ rhyolites (Graham et al., 1992; McCulloch et al., 1994). See Fig 7.15 for key to symbols plotted in inset graph.Maximum errors for Tongariro data are shown in inset graph and represent external precision to 2 s.d. (see Appendix A8.6.3).

analyses are ignored, the Ngauruhoe data do not plot sequentially along a time line because the youngest sample (1975, TG010) is less radiogenic than two older ones (TG288, TG413). The young eruptives from Red Crater and Pukeonake contain the lowest Pb isotope ratios, thus representing separate magma batches from, rather than AFC end-products of, the older units (c.f. Fig 7.22 inset). The new Tongariro analyses overlap with the Ruapehu compositional field (Fig 7.25). Note that the new Young Pukekaikiore analysis plots in a much more radiogenic position than the published examples of Graham and Hackett's (1987) Type 5 (taken from the Ohakune scoria cone), to which it is supposed to belong (Fig 7.25).

The new Tongariro data form a relatively linear trend of increasing $^{207}Pb/^{204}Pb$ with increasing $^{206}Pb/^{204}Pb$. Generally the same Tongariro samples that are highest in $^{87}Sr/^{86}Sr$ and lowest in $^{143}Nd/^{144}Nd$ (Fig 7.22) also contain the most radiogenic Pb isotope compositions (Fig 7.25 inset), thus isotope patterns of these three systems are consistent with a crustal contamination signature. However, the order of samples on these diagrams is not always strictly maintained, for example although TG163 and TG288 are relatively low in $^{87}Sr/^{86}Sr$ and high in $^{143}Nd/^{144}Nd$ (Fig 7.22 inset), their Pb isotope ratios are among the most radiogenic measured for Tongariro (Fig 7.25 inset).

As was shown by Graham et al. (1992), Ruapehu andesites plot along a mixing line between Ruapehu basalt (itself already contaminated) and Torlesse metasediment (although a small role for Waipapa crust was not ruled out). Figure 7.26 shows the Tongariro data plotting along an AFC trend between the relatively primitive Red Crater lava and Torlesse crust. Some of the Tongariro analyses actually plot very near to or within the Torlesse field (Fig 7.26), providing further evidence that Torlesse is probably the main contaminant. Note that all the TVZ samples, including the basalts, plot well above the Northern Hemisphere Reference Line (NHRL) indicating more than one stage of contamination which has firstly elevated the basalts above the NHRL (combination of source and lower crustal contamination?, Graham et al., 1992) and then these in turn have become even more radiogenic through further contamination within the upper crust.

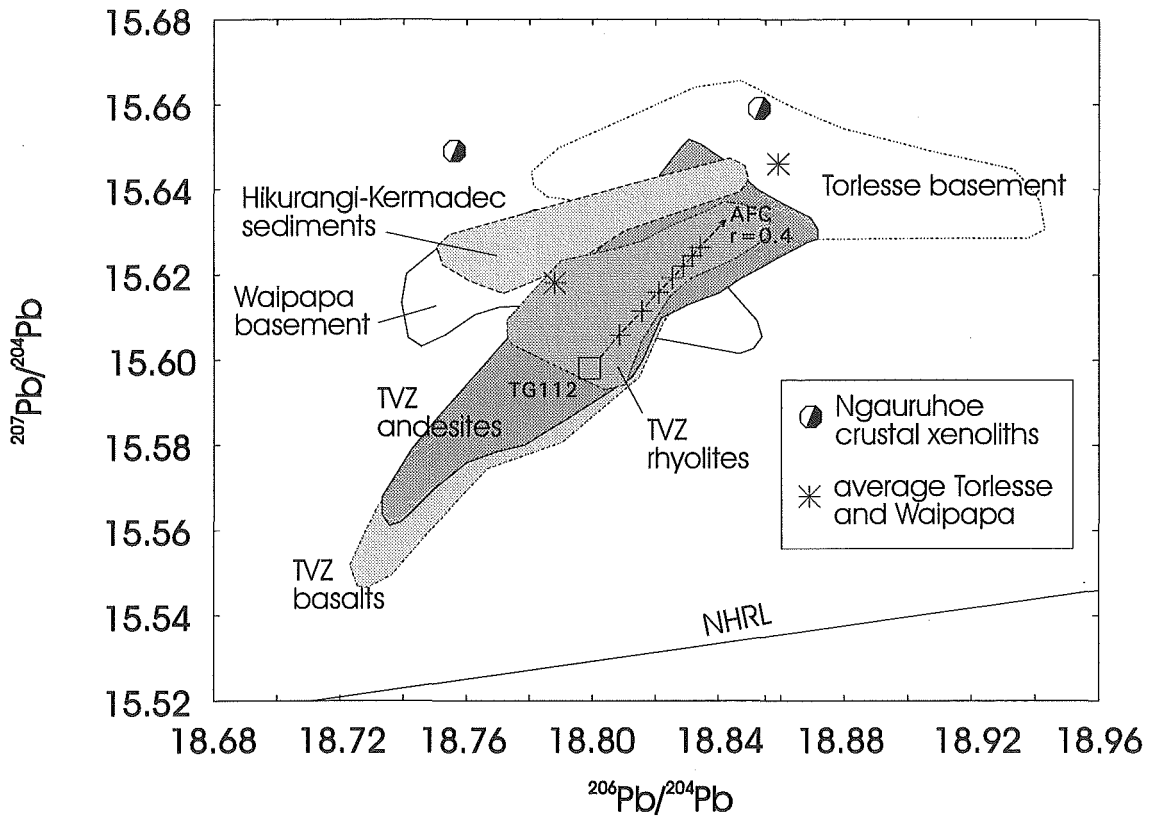

Figure 7.26 Pb isotopic compositional fields for TVZ basalts (Graham et al., 1992; Gamble et al., 1993a; McCulloch et al., 1994), TVZ andesites (this study; Graham et al., 1992; Burt et al., 1996 and unpublished), TVZ rhyolites (Graham et al., 1992; McCulloch et al., 1994), Torlesse and Waipapa crust (Graham et al., 1992; McCulloch et al., 1994), and Hikurangi-Kermadec sediments (Gamble et al., 1996). AFC curves calculated for Torlesse assimilant is shown modelled from TG112 starting composition. Tick marks are denoted as crosses at 0.1 increments. DPb=0.1. Northern Hemisphere Reference Line (NHRL) from Hart (1984).

7.4.3 Oxygen isotope compositions

Stable isotope data are not widely available for Tongariro volcanics, although some have been presented by Blattner and Reid (1982) and Graham et al. (1992). Compared to the andesites compositional field on the $^{87}Sr/^{86}Sr$ versus $\delta^{18}O$ diagram of Graham et al. (1992), the new Tongariro data from this study (obtained in a preliminary investigation of $\delta^{18}O$) display a comparatively low and limited range in $\delta^{18}O$ values (+6.16-6.59), showing a less steep trend of increasing $\delta^{18}O$ with increasing $^{87}Sr/^{86}Sr$ (Fig 7.27). If these data are comparable, it appears that contamination of Tongariro magmas may not be as straightforward as the crustal contamination invoked for the other TVZ andesites (Graham et al., 1992).

The published data fields define a steep trend of rapidly increasing $\delta^{18}O$ relative to $^{87}Sr/^{86}Sr$, which is taken to represent the significant increase in $\delta^{18}O$ resulting from the relatively large amounts of crustal contamination required to produce a small $^{87}Sr/^{86}Sr$ increase in an already Sr-rich melt (Taylor, 1980; James, 1981) . Although the Tongariro data do not seem to follow this trend, they equally do not fit the convex-downward mixing curve predicted for source contamination. The unusually flat Tongariro trend may perhaps correspond to part of a sigmoidal-shaped trend (e.g. Taylor, 1980) which represents a crustal contamination curve affected by extreme plagioclase fractionation such that it renders the magma more sensitive to contamination by a $^{87}Sr/^{86}Sr$-rich crust. Crustal contamination is unlikely to be a simple mixing process, and operating in conjunction with fractionation, variations of the curve trajectories on $^{\text{the}}\ ^{87}Sr/^{86}Sr$ versus $\delta^{18}O$ diagram would be expected.

One other possibility to consider is whether or not analyses of pyroxene crystal separates (as used for the Tongariro samples) are comparable with analyses of whole-rock. The range in $\delta^{18}O$ compositions for Tongariro lavas is much more limited than would be expected considering their measured $^{87}Sr/^{86}Sr$ range. Data from Blattner and Reid (1982) showed a $\delta^{18}O$ range of +7.6-8.5 for Ngauruhoe, Pukekaikiore and Tongariro. Some recent studies (e.g. Cortini and van Calsteren, 1985; Mazzone and Grant, 1988; Tilling and Arth, 1994) have indicated that isotopic heterogeneity may exist between crystals and whole-

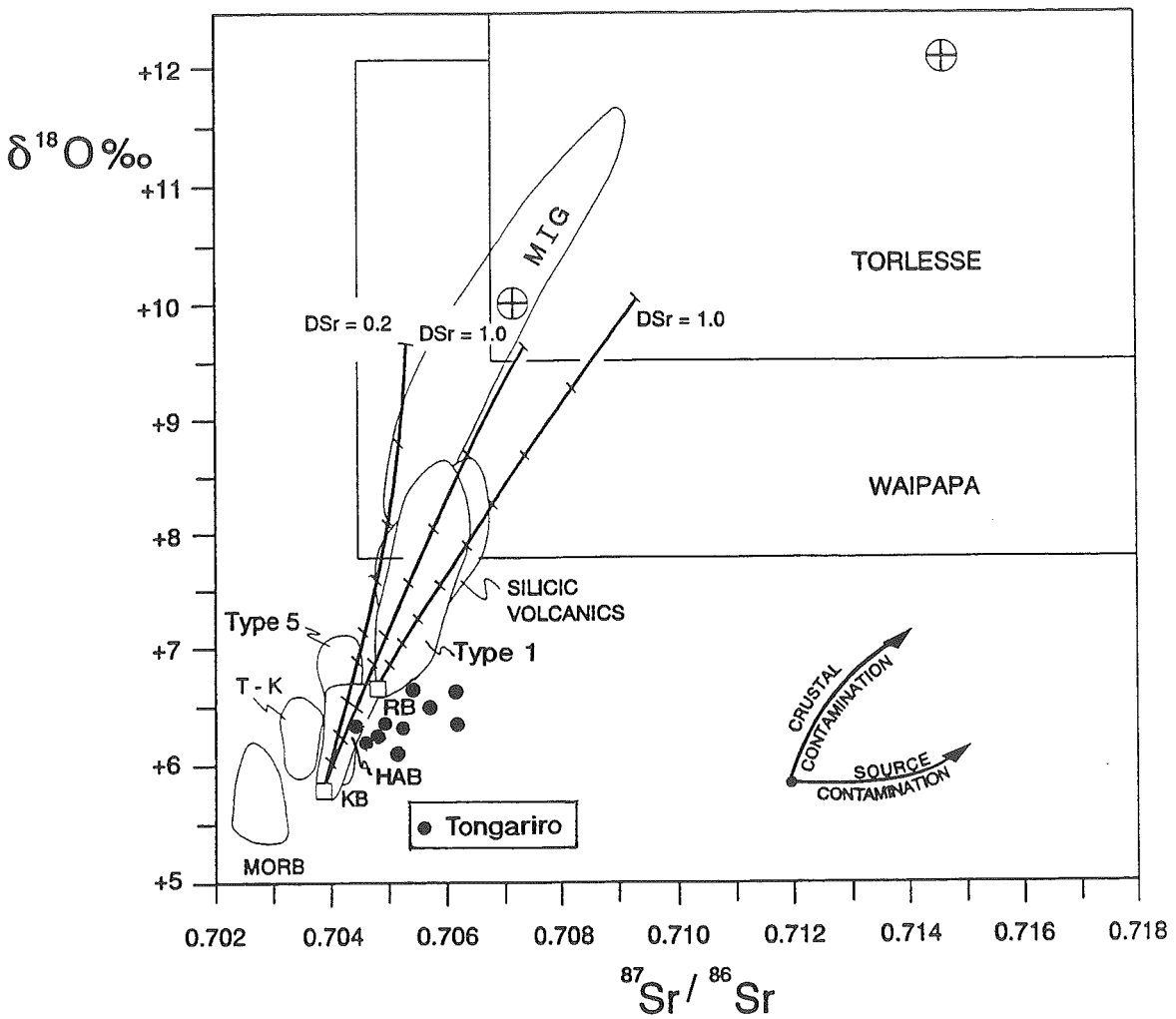

Figure 7.27 $^{87}Sr/^{86}Sr$ versus $\delta^{18}O$ for Tongariro samples (analysed for this study) plotted on the TVZ diagram of Graham et al. (1992) which shows AFC curves (r=0.2) using average Torlesse (denoted by circled cross symbol) as the assimilant and Kakuki Basalt (KB) and Ruapehu Basalt (RB) as the starting compositions. Tick marks are given in intervals of 0.1 to a maximum of 0.9. Compositional fields are shown for MORB, Tonga-Kermadecs (T-K), TVZ high alumina basalts (HAB), Type 1and 5 andesites, TVZ silicic volcanics, meta-igneous granulites (MIG), Torlesse and Waipapa basement. See Graham et al. (1992) for data sources.

rock, thus caution must be exercised when using diagrams such as $^{87}Sr/^{86}Sr$ versus $\delta^{18}O$ to constrain petrogenetic models. Could the $\delta^{18}O$ signature of the Tongariro pyroxene phenocrysts represent a more primitive, pre-crustal contamination composition which is overprinted by open system processes in the whole-rock $\delta^{18}O$ analyses? Another factor which cannot be ignored is the degree of fluid exchange and $\delta^{18}O$ heterogeneity in the crust which may complicate simple AFC calculations. Further detailed $\delta^{18}O$ analysis of more Tongariro samples is required before these ambiguities can be addressed properly.

7.4.4 Beryllium isotope compositions

Be-B isotopic studies of volcanic arcs have increasingly been used to provide evidence for sediment subduction (Morris, 1991; Morris and Tera, 1989; Morris et al., 1990; Ishikawa and Nakamura, 1993 &1994). ^{10}Be is mainly produced in the atmosphere, from which it is removed (principally by precipitation) and incorporated into deep sea sediments. ^{10}Be-rich pelagic sediments are subducted at convergent margins and the high ^{10}Be signature is believed to be transferred from the subducted slab to the source of arc magmas in the mantle (Morris and Tera, 1989). A pilot project to investigate the ^{10}Be content of TVZ lavas was undertaken in 1993 by I.J. Graham and co-workers (see Section A8.8) with the two-fold aim of using the samples to improve chemical preparation and isotopic analysis techniques, and to determine the presence (or otherwise) of ^{10}Be in TVZ (including Tongariro) lavas which might imply the presence of subducted sediment in their source magmas.

Samples selected were those which spanned a wide range of Ba/La, La/Th, K/La, and Ba/Rb in order to maximise probable variation in $^{10}Be/^{9}Be$. The results of the ^{10}Be analysis for the 8 samples are summarised in Table 7.1. For most samples, the normalised ^{10}Be spectra were indistinguishable from zero (c.f. published $^{10}Be/^{9}Be \times 10^{-11}$ values of up to 28; Morris et al., 1990, Gill et al., 1993), indicating the absence of ^{10}Be, at least at the determined detection limit. The only substantially positive result was for TG240 which yielded $26.6\pm4.7 \times 10^{9}$ $^{10}Be/g$. Lower, but statistically significant, positive results were also obtained for TG074 ($4.3\pm2.1 \times 10^{9}$ $^{10}Be/g$) and TG280 ($4.6\pm1.9 \times 10^{9}$ $^{10}Be/g$). Graham (pers. comm., 1993) suggested that the two older SW Oturere samples (TG240, TG074) may have

Table 7.1 Results of preliminary study of ^{10}Be contents of Tongariro lavas. Full analytical details may be obtained from the investigators (Graham and others, see Section A8.8).

Sample	Volcano-stratigraphic unit	Age (ka)	$^{10}Be/^{9}Be \times 10^{-11}$	$^{10}Be/gram \times 10^{9}$
TG001	Ngauruhoe historic lava flow	0.125 (1870)	-0.082 ± 0.098	-5.471 ± 6.572
TG135	Red Crater lava flow	c.3	-0.046 ± 0.023	-3.086 ± 1.552
TG196	North Crater lava lake	c.10	-0.021 ± 0.044	-1.393 ± 2.926
TG280	Pukeonake lava flow	c.23	0.069 ± 0.028	4.597 ± 1.855
TG035	Ruapehu flow near Tama Lakes	37±5	0.038 ± 0.023	2.525 ± 1.546
TG240	SW Oturere lava bomb	c.40	0.398 ± 0.071	26.608 ± 4.732
TG074	SW Oturere lava flow	77±14	0.065 ± 0.031	4.349 ± 2.100
TG098	NE Oturere lava flow	173±10	-0.010 ± 0.017	-0.701 ± 1.123

incorporated ^{10}Be from either the atmosphere or from groundwater, although these lavas are only weakly to moderately vesicular. The result for the younger Pukeonake sample (TG280) may provide a real indication of a subducted sediment component in the parental magma, but alternatively could be an artifact of the measuring system (Graham, pers. comm., 1993).

In Tongariro rocks, the general lack of strong ^{10}Be isotope evidence for sediment subduction cannot be taken as confirmation of the absence of this process because of various factors such as the relatively short half-life of ^{10}Be. The convergence rate at the Hikurangi Trough (c.5 cm/yr) may be too slow to allow preservation of the ^{10}Be signal. In addition, it is not known if enough ^{10}Be has been supplied to the trench and survived subduction in order to be incorporated as a chemical signature of the magmas. Possibly some geochemical process may be operating to allow the ^{10}Be to escape from the system. In the case of the positive results, analytical uncertainties cannot be discounted; for example, although the samples were first leached to remove any effects of surface contamination it is not clear whether or not this procedure was totally effective, especially for the older samples (e.g. TG240?) which may have built up significant inventories of ^{10}Be through surface alteration or cosmic ray bombardment (c.f. Morris and Tera, 1989).

A very recent study by Gamble et al. (1996) presented geochemical data for sediments collected along a transect across the Kermadec-Hikurangi Margin, integrated with the arc basalt data. Noting the common origin of the subducted sediments and the continental crust in New Zealand, Gamble et al. (1996) addressed the problem of distinguishing between the very different processes of source contamination versus crustal contamination. An important role for sediment subduction was invoked to explain the overlap between data from the oceanic and continental portions of the plate boundary, a transition not marked by any significant change in chemical parameters usually indicative of crustal contamination (Gamble et al., 1996). Future detailed work on Be-B isotopic compositions of the Kermadec Arc and TVZ could provide an interesting and useful addition to the debate surrounding sediment subduction versus crustal contamination.

7.5 A CLOSER LOOK AT TIME-SPACE RELATIONSHIPS

Inspection of the chemical trends and patterns displayed by those units which have been sampled comprehensively and for which age relationships are reliably known provides a way of clarifying magma batch relationships in time and space. In the following sections, magmatic trends of selected units are examined in more detail to characterise the sizes, frequency and chemical variability of magma batches on a variety of time scales. This approach has not previously been applied to Tongariro, or indeed to many other composite volcanoes, but is crucial to understanding magmatic history. In addition, by looking at a variety of time windows, for example it is possible to assess how representative the 1954 eruptive period (spanning c.1 year) is of historic activity at Ngauruhoe, historic Ngauruhoe (c.100 years) of all Ngauruhoe, and Ngauruhoe itself (c.2500 years) of the Tongariro complex as a whole. Caution must be exercised, however, when comparing Ngauruhoe's development with the older cone-building episodes which generally have a much lower level of exposure (c.f. introduction to Section 6.6.8).

7.5.1 One year period: 1954 Ngauruhoe

Samples have been collected and analysed from eight different lava flows which were erupted from Ngauruhoe over a four month period between June and September 1954 (Figs 3.30A & 3.32). This represents the most sustained lava-producing eruption episode witnessed in historic times, and can be investigated within the context of compositional variation over the smallest examined time window of (less than) a year.

The 10 whole-rock XRF analyses available for these 1954 flows (Appendix 10) indicate a certain degree of chemical diversity, but of a limited extent as the concentration range for most elements is very near to or within analytical error. The 1954 lavas span 54.80-56.25 wt% SiO_2 and 5.14-5.38 wt% MgO. The flows of 4 June and 14 July appear to be slightly more mafic than the others (Fig 7.28). These slight compositional differences correlate in part with subtle variations in the abundances and ratios of ferromagnesian phenocrysts and plagioclase. The 1954 samples plot in a cluster at the low-SiO_2 end of the

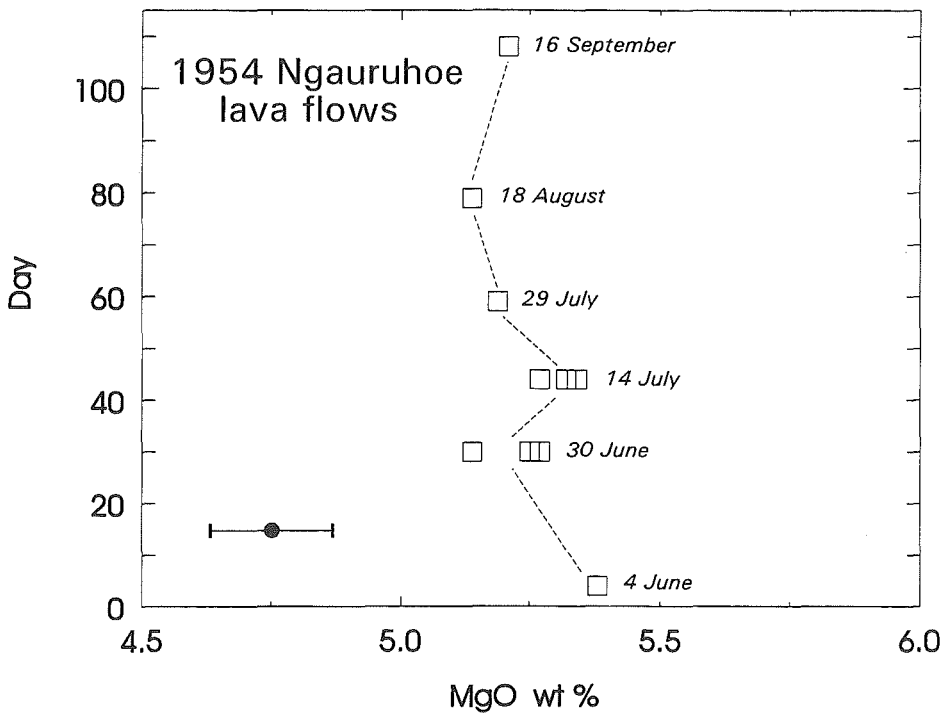

Figure 7.28 MgO contents of 1954 Ngauruhoe lava flows plotted against day of eruption. The actual date of each eruption is labelled beside the data points. MgO error bar is for 2 s.d. (see Appendix A8.3.3).

Ngauruhoe Group 3B trend (Fig 7.29), and as discussed in the following section, the slight variation in 1954 lava compositions may suggest active mixing of a new basic magma influx with the residual (pre-1954) magma, which effectively smeared out the magma compositions towards the slightly more evolved host magma (Fig 7.30). Mixing must have been either nearly complete, or between very compositionally similar magmas however, because XRF major and trace element concentration and ratio (e.g. K/Rb, Ba/Zr) variations are insignificant when compared to the total variation observed for Ngauruhoe as a whole.

Unfortunately, a full data set for precise trace elements and isotopes is only available for one 1954 sample (TG413, crater wall scoria), so variation of these parameters during the 1954 eruptive episode cannot be examined. This may be an interesting line of inquiry to pursue further, as indicated by a noticeable discrepancy (Fig 7.25; Section 7.4.2) between measured radiogenic Pb isotopic compositions of TG413 ($^{206}Pb/^{204}Pb$=18.844, $^{207}Pb/^{204}Pb$=15.642) and the published values of $^{206}Pb/^{204}Pb$=18.795, $^{207}Pb/^{204}Pb$=15.606 in Graham et al. (1992).

Further investigation is required to evaluate analytical uncertainties and establish whether or not there is significant compositional variability between different 1954 flows. If, as seems most likely, there is no profound difference in magma erupted over the four month period, it could be postulated that higher level physical controls on magma ascent were primarily responsible for triggering each discrete eruptive event, rather than the influx of new mafic magma batches. Note that the volume of magma erupted at any one event does not seem to correlate with compositional parameters, e.g. the two days which produced the largest volumes of magma (30 June and 14 July, Fig 3.32) represent the two 'extremes' of the 1954 compositional range (Fig 7.28).

7.5.2 100 year period: 1870-1975 Ngauruhoe

The last 127 years have seen frequent eruptions from Ngauruhoe (Section 3.4.3) and of these, five have been sampled and analysed for major and trace elements (1870, 1949, 1954, 1974, 1975), one for major elements only (1928), and three also for isotopes (1870, 1954, 1975). The 1928 data are taken from Steiner (1958), whereas all other analyses were

conducted during this study. Details of other published analyses are contained in Section 6.6.8k. The Ngauruhoe historic data set thus provides the opportunity to assess just over 100 years of magmatic variability at a single vent, and allows a comparison with the compositional patterns exhibited by just one eruptive episode (1954, described above).

Having demonstrated in Section 7.5.1 that, on the whole, the compositions of the 1954 eruptive products are essentially indistinguishable from one another, it is evident that a more complex magmatic history is represented by the1870-1975 lava suite. An enlarged version of the MgO-SiO_2 variation diagram (Fig 7.29) reveals compositional-age relationships inconsistent with a systematic evolution from one magma reservoir. The 1870-1928-1949 samples do plot logically as a possible fractional crystallization trend, but the 1954 eruptives return to more basic compositions, and the 1974 and 1975 ejecta are highly variable and may in part define other trend(s). A cautious approach to the 1975 data is warranted as all samples may not be strictly classed as juvenile, and the relatively high xenolith content in some samples may be affecting whole-rock compositions.

MgO plotted versus time (Fig 7.30) shows the distinct change in composition at 1954, and the relatively broad MgO ranges of 1954 and 1975 ejecta which are suggestive of mixing following recharge event(s). A possible scenario could involve fractional crystallization of magma between 1870 and 1949 which was interrupted by injection of a new magma pulse from which the 1954 magma erupted, some of which then fractionated to 1975 compositions - although some of the 1974-75 eruptives may represent the products of another separate magma recharge event. This scenario on its own cannot be invoked for the historic Ngauruhoe eruptives, however, because least-squares mixing calculations in Section 6.6.8k demonstrated that these samples (1870 to 1949, for example) could not be satisfactorily related by fractional crystallization.

The other process most likely to be contributing to the compositional diversity is crustal contamination. Incompatible trace element ratios not expected to vary during fractional crystallization show significant variation, e.g. Nb/Ta=9.6-12.2, Th/Ta=7.6-11.5, La/Yb=4.4-5.7 (cf. Figs 7.12, 7.14, 7.17) which can more easily be explained by assimilation fractional crystallization (AFC). Even this is not a straightforward process, however, because the samples either do not plot along just one AFC curve (e.g. Fig 7.16)

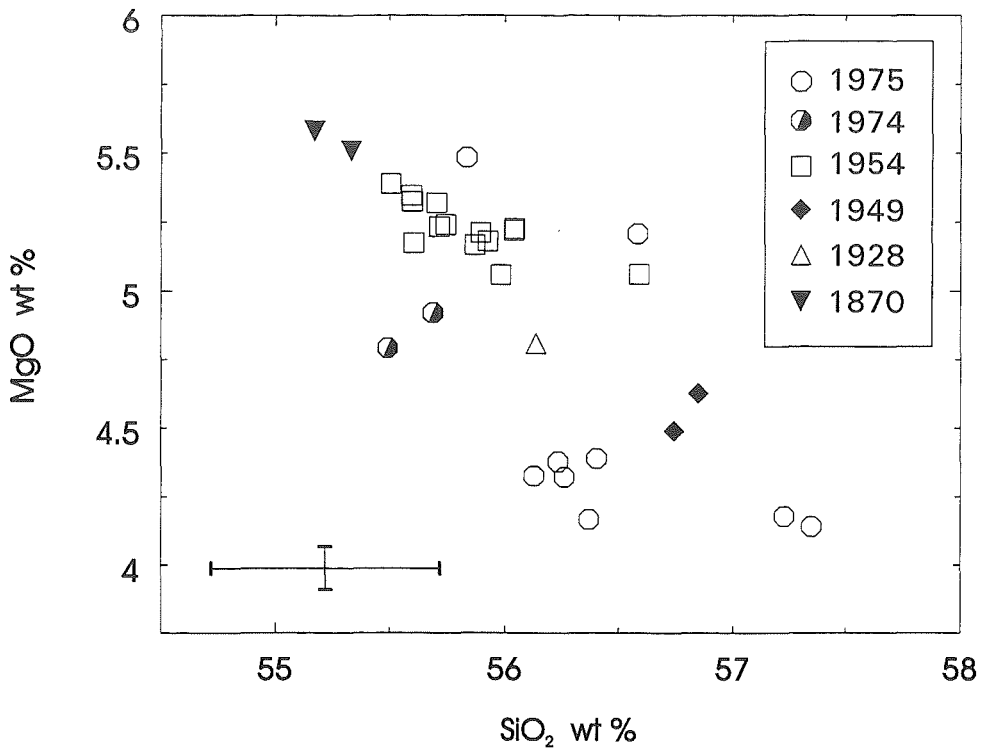

Figure 7.29 MgO versus SiO_2 contents for historic Ngauruhoe lava flows and pyroclastics, plotted according to year of eruption (see key). Error bars are for 2 s.d. (see Appendix A8.3.3).

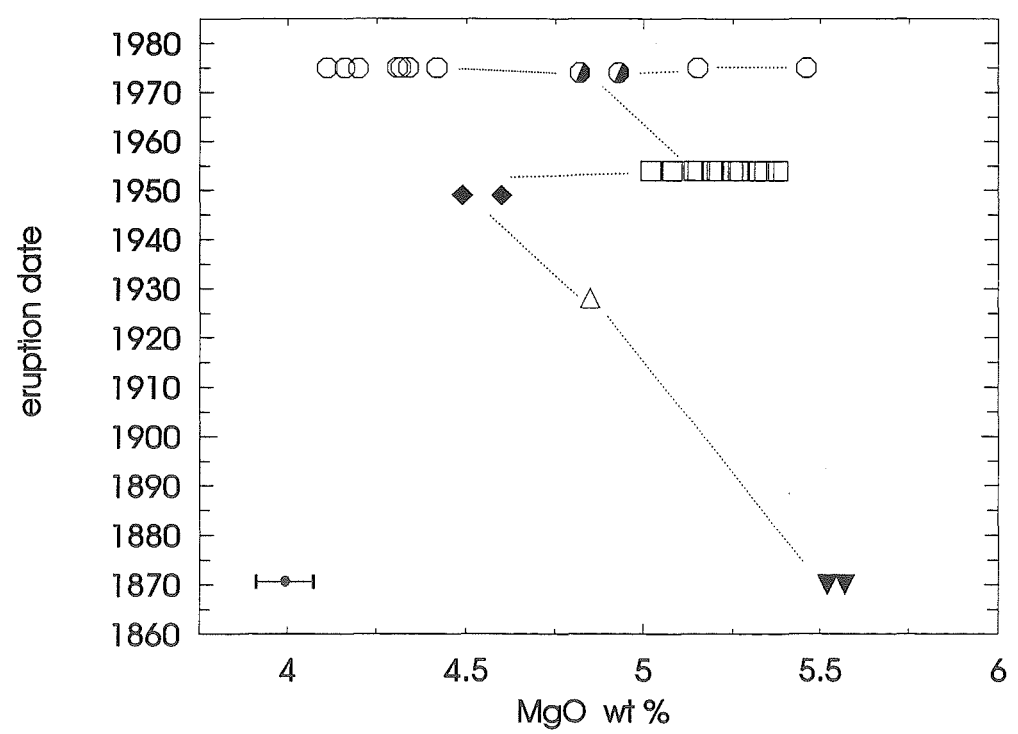

Figure 7.30 MgO contents of historic Ngauruhoe eruptives plotted against eruption date. Error bars are for 2 s.d. (see Appendix A8.3.3).

or they show age relationships inconsistent with one AFC history (Fig 7.17). These findings are consistent with those of Section 7.3.5, and show that it is possible for variable crustal contamination to exert a considerable influence over magma compositions over the comparatively short time span of 100 years.

From the limited isotopic data available for historic Ngauruhoe lavas, an interesting story emerges. For example, $^{87}Sr/^{86}Sr$ ratios increase with time from 1870 (0.705339) to 1975 (0.706165), with a remarkable increase of 0.0007 over just 20 years between 1954 (0.705470) and 1975. An added advantage of knowing the precise dates of these eruptions is that the time *intervals* between eruptions are also known. These place some constraints on what processes are feasible in physical and chemical terms over various time periods. Twenty years is almost certainly insufficient time for a new partial melt from an isotopically distinct mantle source to make its way to the surface as an andesite (migration velocity of andesitic magma is estimated at less than 5 m/year, Basaltic Volcanism Study Project, 1981) - even if the new melt started rising only slightly later then the previous one. Therefore it is much more likely that the marked variation in historic $^{87}Sr/^{86}Sr$ ratios is due to assimilation of varying amounts of a compositionally diverse crustal contaminant (Torlesse metasediment, Sections 7.3.5 and 7.4). Note that the normalised incompatible element and REE patterns are very similar for the 1870, 1954 and 1975 samples (Fig 7.31), although the slight decrease in light REE abundances with increasing SiO_2 between 1870 and 1954 could be taken as an indication of magma mixing (instead of fractional crystallization for which REE contents would be expected to increase).

7.5.3 1000 year period: historic and prehistoric Ngauruhoe, post-1.8 ka Red Crater, and c.1500AD Upper Te Mari Crater

By increasing the time window by an order of magnitude, magma dynamics over roughly 1000 years can now be examined. Comparison between magma batches erupted from different vents, e.g. Ngauruhoe and Red Crater, can also be made. Although absolute ages for the prehistoric Ngauruhoe flows are not available, it is likely that these represent the latter part of the cone's c.2.5 ka period of activity, and thus all Ngauruhoe samples are incorporated into the <1 ka data set. The post-1.8 ka Red Crater eruptives, thought to be

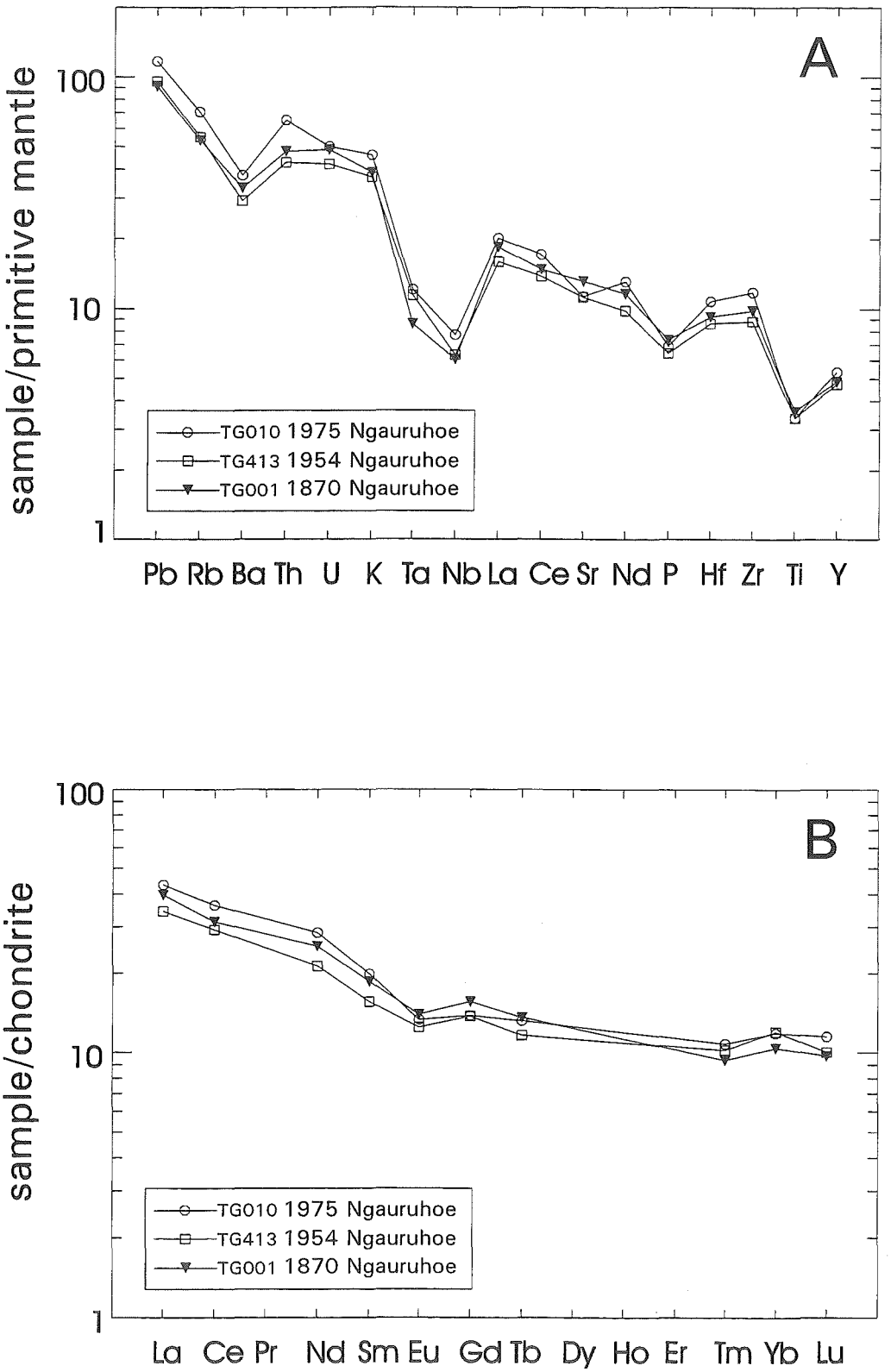

Figure 7.31 Normalised abundances of trace elements in historic Ngauruhoe eruptives: (A) Primitive mantle-normalised incompatible element plot, normalisation factors from McDonough et al. (1992); (B) Chondrite-normalised REE plot, normalisation factors from Nakamura (1974).

around 0.5 ka (Appendix A2.3), and the c.1500 AD Te Mari Crater flows (Section 3.3.2e) are also included in the <1 ka data set. The relative age of these Red Crater and Te Mari Crater samples is not known for certain, but the Te Mari Crater flows are most likely to be the oldest.

The compositional variability and complex age relationships evident on variation diagrams for the historic eruptives of Ngauruhoe Group 3B are also reflected in the patterns for the 1 ka period eruptives. These may be assessed in terms of the relationships between the Ngauruhoe chemical groups identified in Section 3.5.8k (and discussed in Section 6.6.8k), along with the Red Crater and Te Mari Crater groups. The compositional-time-space associations within the groups as well as between them are examined particularly with reference to the precise geochemical data set of incompatible elements and radiogenic isotopes (thus corresponding to a subset of selected samples).

Least-squares mixing calculations have demonstrated the difficulty of relating Ngauruhoe chemical groups by simple fractional crystallization trends (Section 6.6.8k). Expanding on these models, with reference to Fig 7.32, show that only a very limited portion of the 1 ka history could be satisfactorily explained solely by fractional crystallization. The results of least-squares modelling are summarised below, from the oldest to youngest groups.

The Te Mari Crater flows occupy the highest SiO_2 part of the MgO-SiO_2 diagram (Fig 7.32) and therefore it is not geologically reasonable to model them as parental to any other of the 1 ka eruptives. However, bearing in mind the uncertainty over some of the age relationships, it is interesting to note that an excellent fit to the data is obtained when Ngauruhoe Group 3A (TG288) is modelled by fractional crystallization to Te Mari Craters (TG282) (Appendix 12, Model 12.19). This is considered noteworthy because on the whole these types of models failed to predict the various Ngauruhoe compositions (Section 6.6.8k). Ngauruhoe Group 3A and prehistoric Te Mari Craters eruptives also share other similar chemical characteristics such as the same Rb/Zr ratios, but more detailed precise trace element and isotopic data (and absolute age data) are necessary to properly evaluate the petrological and geological relationships between these two groups. Note that even if the post-1.8 ka Red Crater eruptives were found to be older than those from Te Mari, they

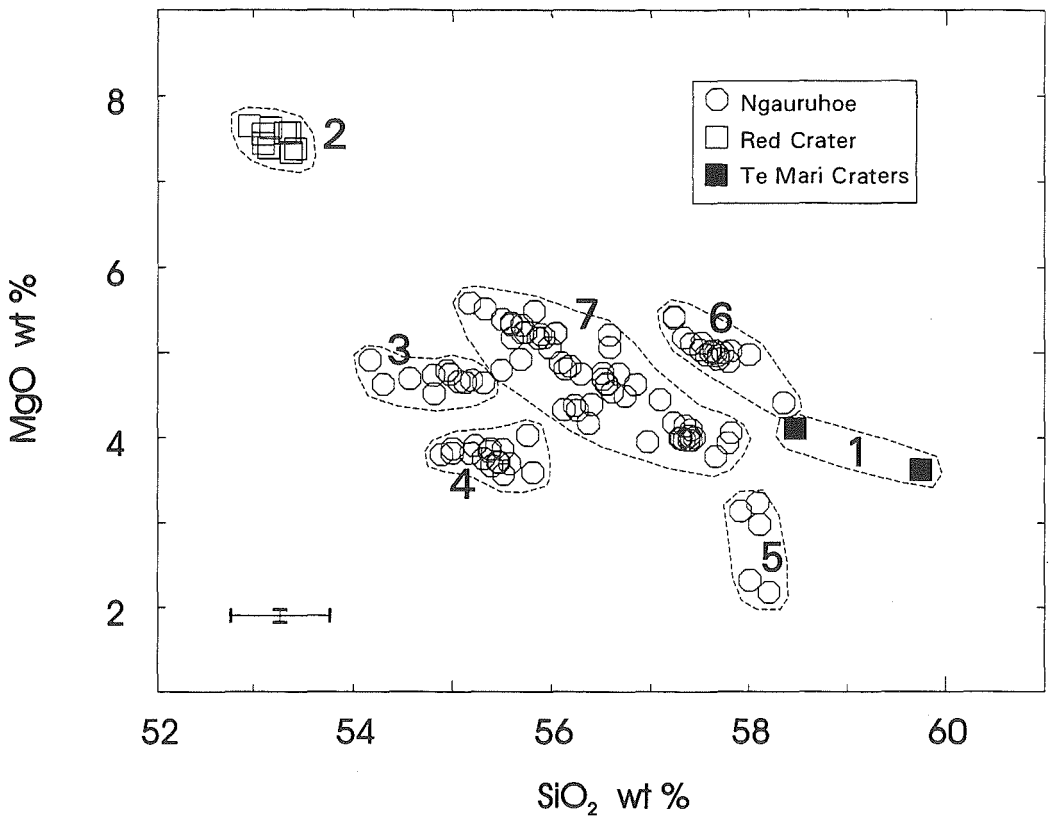

Figure 7.32 MgO versus SiO_2 contents for lava flows and pyroclastics erupted from Ngauruhoe, Red Crater and Upper Te Mari Crater over the last 1000 years. Best interpretation of time progression of lava groups is indicated by numbered sequence (see text). Error bars are for 2 s.d. (see Appendix A8.3.3).

would not represent logical parent magmas for the Te Mari flows because least-squares models yielded unacceptably poor fits to the data.

The post-1.8 ka Red Crater lavas cannot be modelled as fractionating to any of the Ngauruhoe chemical group compositions (Section 6.6.8k). Modelling between the five Ngauruhoe groups also failed to indicate any obvious links via fractional crystallization, with the exception of some of the Group 2 lavas which could be produced by fractional crystallization of a Group 1B lava (Section 6.6.8k). Least-squares modelling along the trends of Group 3A and 3B showed that fractional crystallization could only rarely be demonstrated, and a combination of magma mixing and AFC processes appeared to be involved. This contention is supported by the non-systematic age relationships along these trends.

To further clarify the processes responsible for the magmatic patterns of the last 1000 years it is necessary to turn attention to more precise incompatible elements and isotope ratios. Variability in the shapes and normalised abundances of these elements on spiderdiagrams and REE diagrams (Figs 7.1E-F and 7.2E-F) provide an indication of their diverse histories. Incompatible element ratios, considered unaffected by fractional crystallization and partial melting processes, show small yet significant variations over time (Fig 7.33). Only rarely do these ratios show smooth and regular changes with time; for example Ba/Nb increases from c.0.8 to 0.1 ka suggestive of a single AFC trend (cf. Fig 7.15) - but then drops significantly in the last 100 years (Fig 7.33). Most incompatible element ratios display much more random patterns with time (Fig 7.33) which once again serve as reminders of the complexity of Tongariro magmatic inter-relationships. Over the interval of 1000 years it is generally not possible to trace any persistent differentiation trends with logical age progressions. This supports the concept (already promoted in Sections 7.3.3, 7.3.5 and 7.4) of diversity being created at a relatively high level by variable crustal contamination affecting many discrete magma batches. To further test this idea, age relationships on AFC process diagrams are now examined.

Convincing evidence for crustal contamination operating in tandem with fractional crystallization on Tongariro magmas was revealed in Section 7.3.5. A closer inspection of the post-1 ka data on the Ba/Zr versus Ba diagram (Fig 7.34A) shows a variety of trends

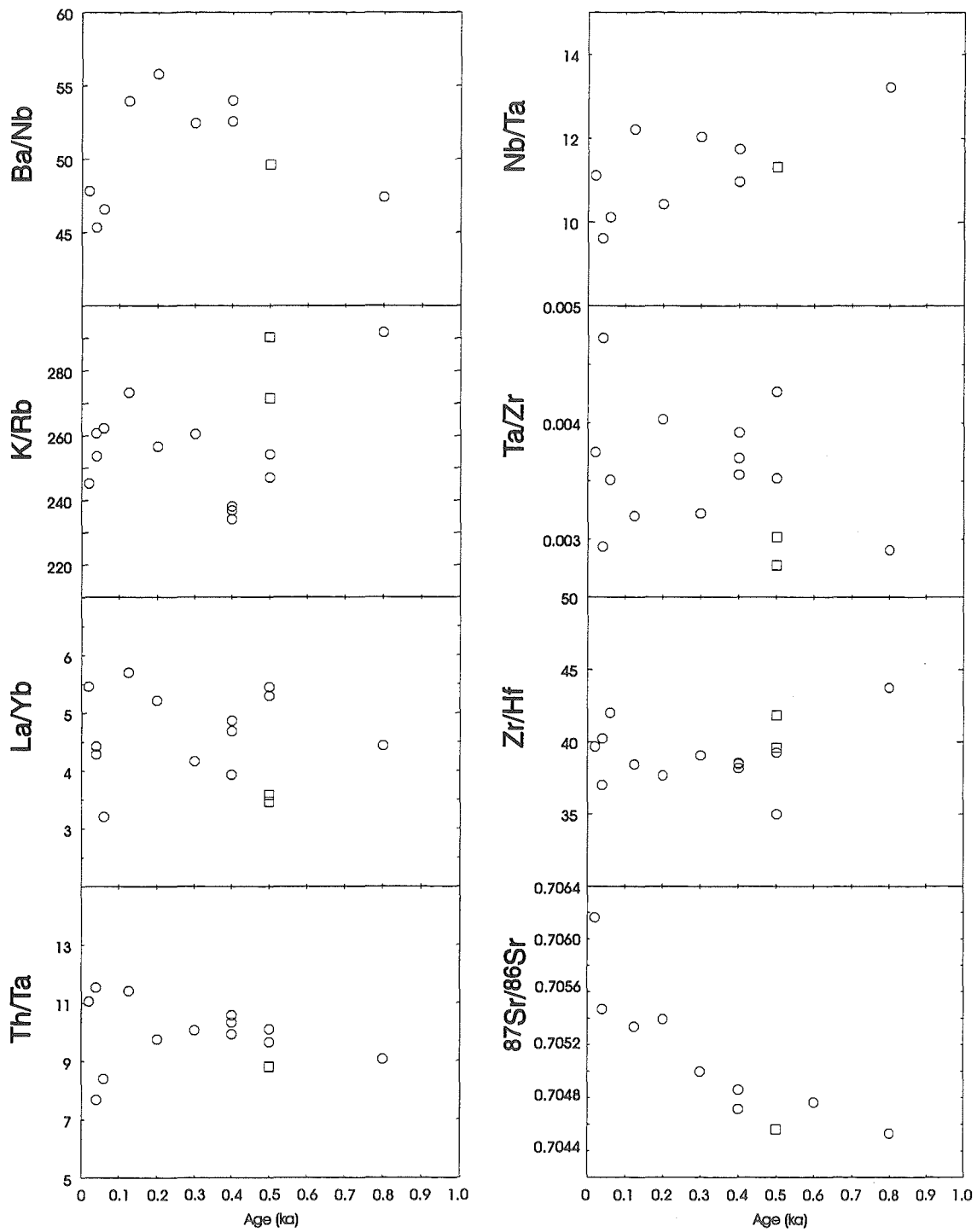

Figure 7.33 Incompatible element and isotopic ratios plotted versus time for lava flows and pyroclastics erupted from Ngauruhoe (circles) and Red Crater (squares) within the last 1 ka.

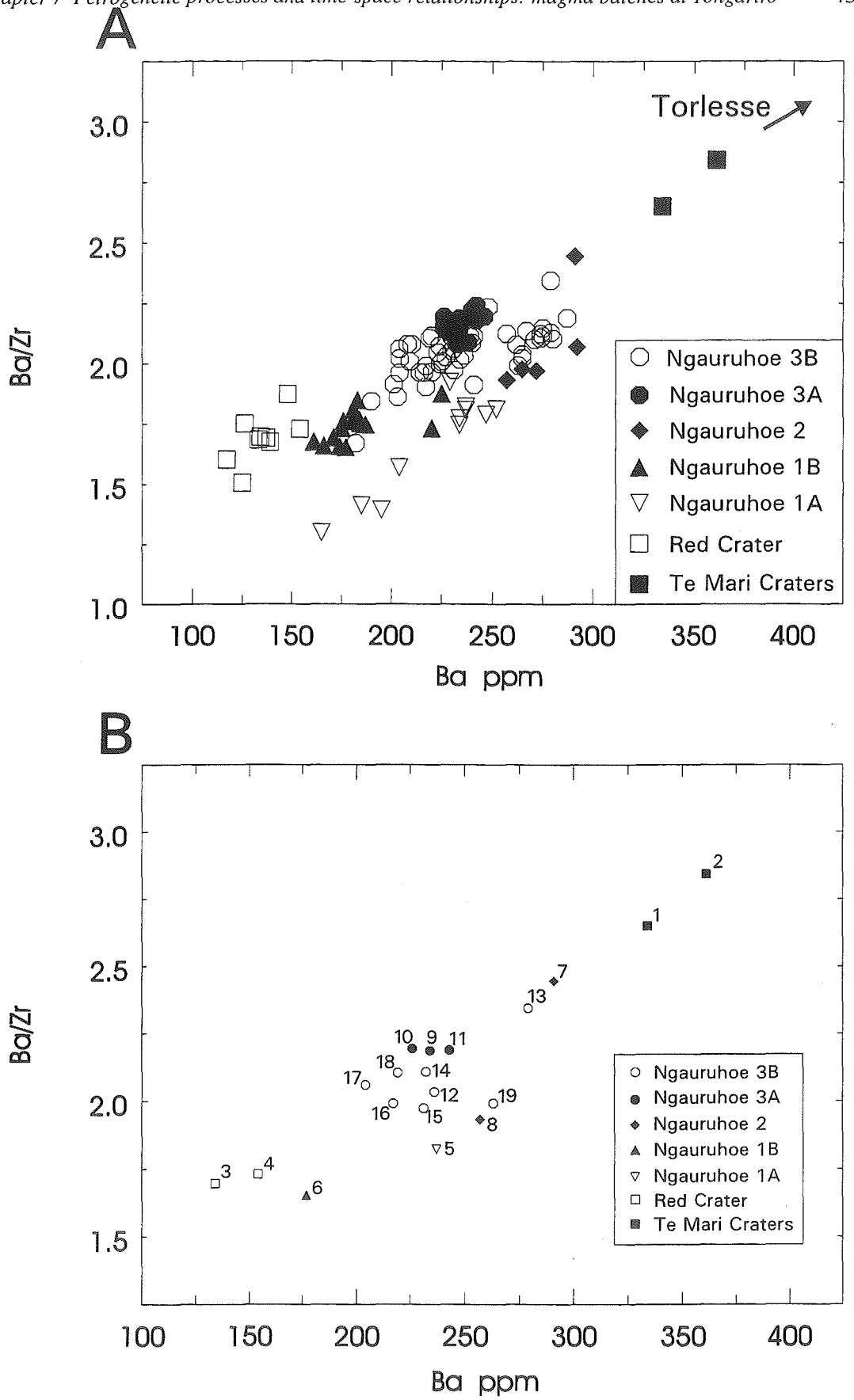

Figure 7.34 Ba/Zr versus Ba contents for lava flows and pyroclastics erupted from Ngauruhoe, Red Crater and Upper Te Mari Crater over the last 1000 years. (A) shows all data for this time period, and (B) shows selected samples, numbered in best interpretation for time progression (see text). Direction of Torlesse contaminant indicated by arrow. Refer to Fig 7.18 for AFC models

and data groupings. There is no one overall AFC trend shared by all the data, although all samples plot on trajectories heading towards the average Torlesse crust composition. Modelling AFC from the Red Crater lava does produce a trend which passes through some of the Ngauruhoe data (Figs 7.16-7.18), although for example Group 1A magmas (which may in fact be older than post-1.8ka Red Crater) cannot be logically derived from Red Crater magmas by AFC (Fig 7.34A). After the failure of closed system fractional crystallization models to relate Red Crater to Ngauruhoe (Section 6.6.8k), it appears that the two units may be more plausibly linked by AFC processes, although the highly variable nature of the crustal contamination process precludes a straightforward relationship.

The relatively elongate trend of Ngauruhoe Group 1A magmas suggests that they may have experienced more extensive interaction with the crust than others such as Groups 1B and 3A which plot as more tightly clustered short trends (Fig 7.34A). Group 3B magmas plot as a diverse group, obviously comprising more than one AFC trend. The variability in the AFC trends and the non-systematic age relationships between groups (e.g. the comparatively old Te Mari Craters lavas appearing to have suffered the most AFC) provide further evidence for variable amounts of AFC involving compositionally diverse crustal contaminants. When selected samples only are plotted on the Ba/Zr versus Ba diagram, and numbered according to their relative age in the sequence of lavas, it is clear that there is no orderly progression of erupted lavas advancing up an AFC trend (Fig 7.34B). This rather haphazard arrangement of reversing trends and loops is also observed for other incompatible element ratio diagrams indicative of AFC, such as K/Rb versus Rb (Fig 7.16) and La/Yb versus La (Fig 7.17), reinforcing the impression of complex interactions between numerous short-lived magma batches and variable amounts of a compositionally variable crust.

Preliminary findings from an ion microprobe study of prehistoric and historic Ngauruhoe lavas indicate that phenocrysts within a given rock have had different chemical histories (Rogan and Blake, 1994). Contrasting trend slopes for different mineral phases on trace element log-log plots (e.g. Ce versus Y) show that the phenocrysts did not grow during closed system fractionation. Trace element zonation profiles (e.g. K/Ce, K/La) across single crystals reveal complex patterns produced by combinations of magma mixing, crustal contamination, and crystallization (Rogan and Blake, 1994).

Radiogenic isotope compositions provide further evidence for the importance of variable crustal contamination in producing the compositional diversity observed in lavas over the last 1000 years. There has been a significant increase in $^{87}Sr/^{86}Sr$ over this period (Fig 7.33), as well as in historic times (Section 7.5.2). The broad scatter of data points on the $^{87}Sr/^{86}Sr$-SiO_2 diagram (Fig 7.35) can more easily be explained by a family of AFC trends, rather than just one. Since it is unlikely that the magmas are unrelated and represent different source compositions over such a short time span, their isotopic diversity is more consistent with higher level differences in crustal contamination, as maintained in the previous section and supported by trace element modelling (Section 7.3.5). Ngauruhoe isotopic and trace element ratio trends are best explained by contamination with variable crustal compositions (Fig 7.24; Section 7.4.1). Although there are no obvious simple fractional crystallization relationships within the different chemical magma groups erupted over the last 1000 years, the reasonably coherent trends on most variation diagrams for e.g. Ngauruhoe Group 3B also reflect the higher level differentiation processes of magma mixing and AFC rather than different sources.

The degree of magmatic diversity and complexity for the 1000 year period appears magnified in comparison to the 100 year time window. We have already seen how several small, distinctive magma batches (each identified by only a few lava flows) were involved over 100 years (Section 7.5.2), and this pattern seems to be repeated many times over for the 1 ka period as indicated by the frequent compositional reversals. The volume or number of lava flows per chemical group provide a guide to the volume of each magma batch (which will be around one order of magnitude larger than the material actually erupted). Thus it appears that quite small aliquots of magma periodically escape from the main reservoir, experiencing varying degrees and types of differentiation processes at different crustal levels beneath the vent, thereby obtaining their distinctive magmatic character. Since there is little evidence for protracted periods of differentiation having taken place in any of these magma batches, the lifespan of any one batch is probably not great and magma does not tend to reside for very long in the high level reservoir. Other factors which may have contributed to magmatic diversity include the possibility of an irregular magma rise rate over a variety of time scales, and the effect of changes in the proportion of stored versus erupted magma. The findings from this part of the study serve as a reminder of the dynamic

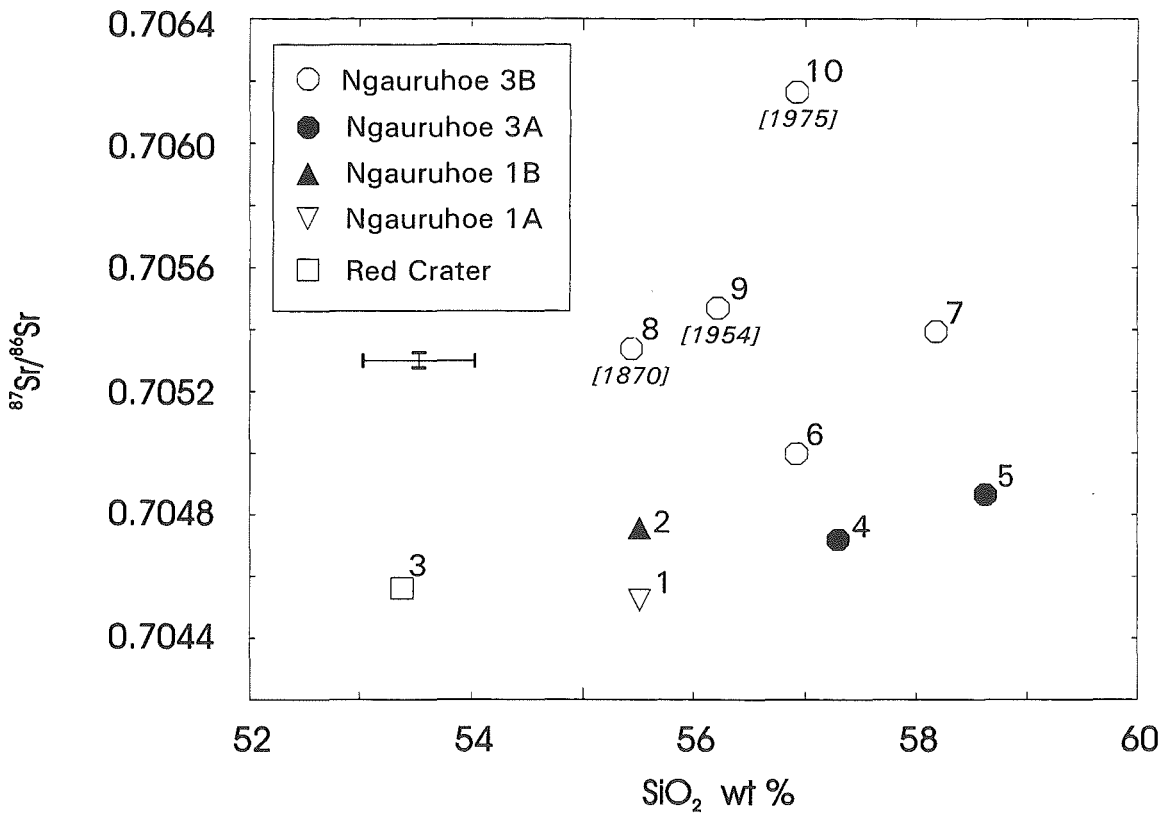

Figure 7.35 $^{87}Sr/^{86}Sr$ versus SiO_2 contents for lava flows and pyroclastics erupted from Ngauruhoe and Red Crater within the last 1000 years. Samples are numbered to indicate time progression (see text). Historic Ngauruhoe samples are also labelled with eruption year. Error bars represent external precision to 2 s.d. (see Appendix 8).

plumbing system involved in Tongariro magmatism which complicates any attempts to produce a simple petrogenetic model.

Based on their distinctive geochemical characters and lack of age-consistent tight AFC trends, it does not appear likely that the plumbing systems for Ngauruhoe, Red Crater and Te Mari Craters have been closely inter-connected over the last thousand years or so. Thus at certain periods it is probable that several spatially separate magma reservoirs coexisted at different levels beneath the Tongariro complex, feeding vents separated by a few kilometres, as depicted in Fig 6.23H. The lack of both central and flank eruptions from these young cones on the Tongariro complex precludes a closer look at spatial control on magmatic variability. More detailed geochemical data are required to ascertain whether or not some degree of interaction may have occurred at some stage between e.g. Te Mari Craters and Ngauruhoe Group 3A. The inter-relationships between the Ngauruhoe groups have been discussed in Section 6.6.8k. These distinctive magma types were probably generated in a number of sub-reservoirs (each experiencing variable degrees of AFC and magma mixing) from which many discrete magma batches have risen, probably having undergone varying ascent histories prior to eruption.

7.5.4 10 000 year period: 0-10 ka young eruptives, c.120-130 ka NE Oturere, and c.200-210 ka Tama 2

The largest time window examined in detail in this chapter is that of 10 000 years. In this section, three 10 k yr eruptive intervals, which together span most of Tongariro's lifetime, are compared in terms of trace element and isotopic patterns to assess how similar the degree of magmatic variability is over this time period. Thus rather than concentrating on relationships between lavas within each 10 k yr period, the focus is more on using the three case studies to provide an indication of any parallel trends which might reveal common underlying controls on Tongariro magmatism and differentiation which have operated throughout its history. The time intervals of 0-10 ka (Young Eruptives), 120-130 ka (NE Oturere, lower and middle sequences of subunit 'd') and 200-210 ka (Tama 2) were chosen for their detailed sampling, precise trace element and isotopic analysis, and good age control. However, bearing in mind that these data sets could nonetheless be improved

upon by conducting more detailed analyses on a wider selection of samples, the interpretation of trends must remain tentative.

Geochemical modelling reported in previous sections has demonstrated the very open system nature of the Tongariro plumbing system. Most samples could not be linked solely by a simple fractional crystallization pattern in a logical age sequence, and instead variable crustal contamination in conjunction with fractional crystallization and mixing of different batches of magma was invoked to explain the pervasive chemical variability (Sections 6.6, 7.3.5, 7.4). The 0-10 ka young eruptives represent many different magma batches (even within just the last 1k yr; Section 7.5.3), although certain units appear to have shared a common magma reservoir from which similar magma batches have arisen (Section 6.6.9d-g). At least five cycles of magma influx and mixing are represented by the NE Oturere sequence, for which fractional crystallization alone could not satisfy the observed chemical trends (Section 6.6.3c). Tama 2 magmas also could not easily be related by fractional crystallization, with several magma batches identified (Section 6.6.4).

Some of the incompatible element ratios shown in Section 7.3.5 to reflect AFC processes have been used in plots of the 10 ka period data (Figs 7.36-7.39). Significant fluctuations are apparent in K/Rb, La/Yb, Ba/Zr and Th/Ta over each of the three 10 ka periods. The variations in these ratios most likely correspond to variable degrees of contamination (with a compositionally-diverse crust) of multiple magma batches, creating several different AFC trends.

The full range in K/Rb for the 0-10 ka eruptives is concentrated in just 1 k yr (as it is for Tama 2) but a similarly wide K/Rb range occurs across almost the entire 10 k yr period for NE Oturere (Fig 7.36). NE Oturere La/Yb values appear relatively constant compared to those of the young eruptives and Tama 2 (Fig 7.37), but this is more probably a function of the small data set. The sinusoidal Ba/Zr trend for NE Oturere (Fig 7.38) is almost a mirror image of that for K/Rb (Fig 7.36), reflecting the opposing effects of AFC on these two ratios (cf. Figs 7.16 and 7.18). The patterns for Th/Ta variation for the respective time periods (Fig 7.39) are similar to those for Ba/Zr and La/Yb. Thus each 10 ka interval seems to be characterised by a particular type of trend (e.g. sinusoidal for NE

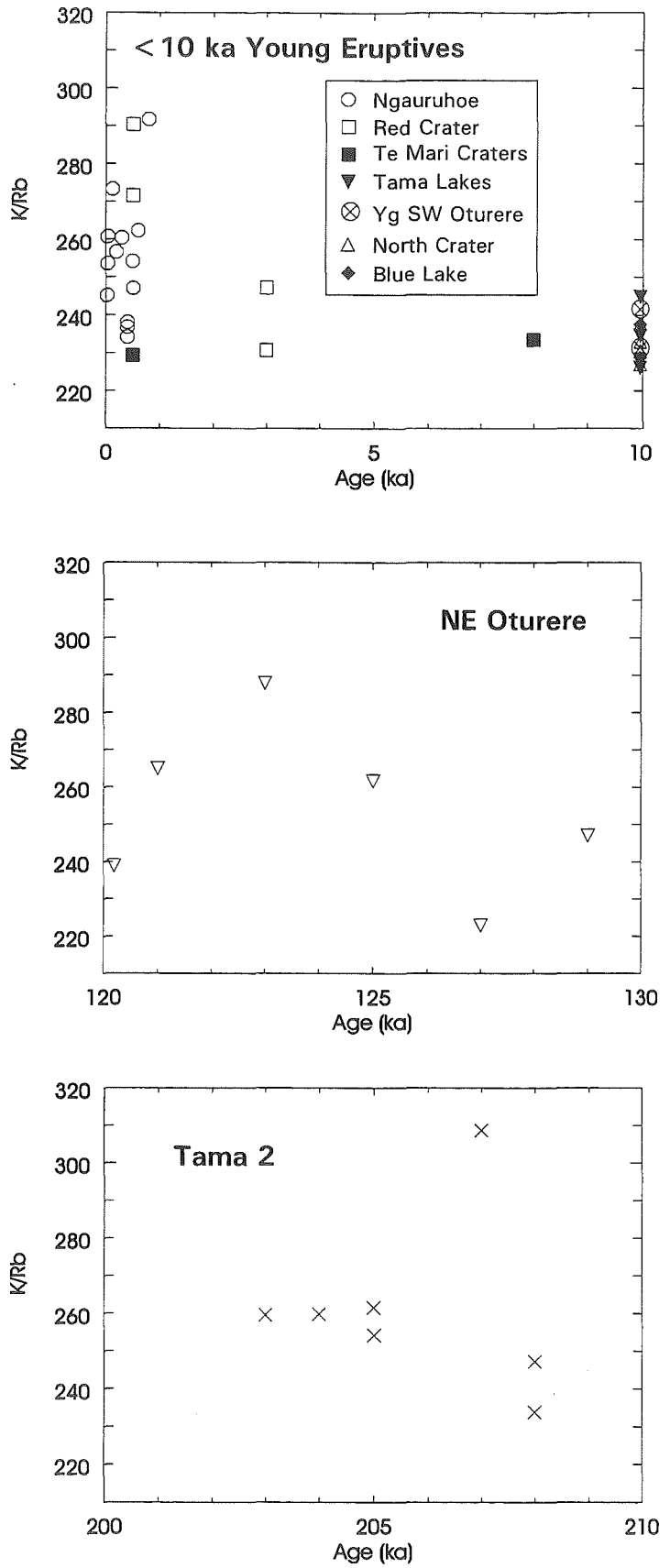

Figure 7.36 K/Rb ratios plotted versus time for three eruptive periods of 10 ka duration: 0-10 ka young eruptives, c.120-130 ka NE Oturere, and c.200-210 ka Tama 2. Prehistoric sample ages are derived from tephra chronology, K-Ar age determinations, or by extrapolation (see Appendix 13).

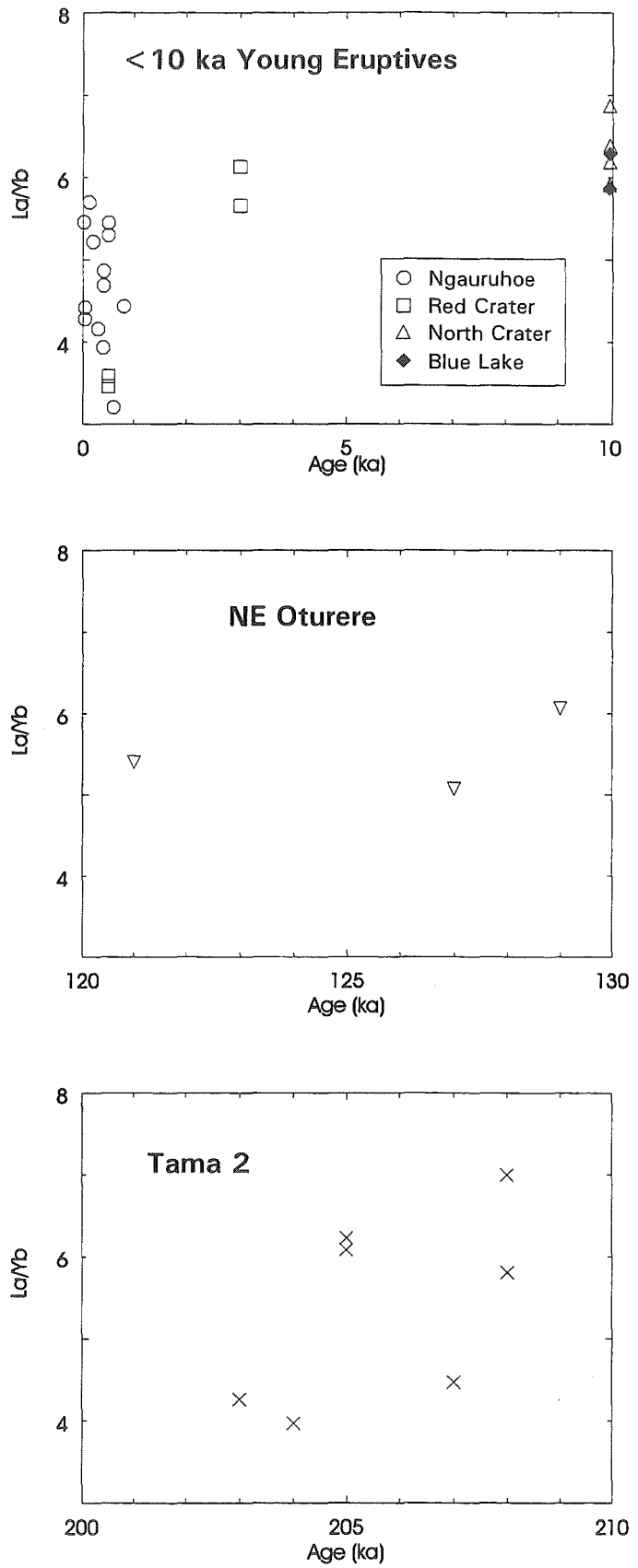

Figure 7.37 La/Yb ratios plotted versus time for three eruptive periods of 10 ka duration: 0-10 ka young eruptives, c.120-130 ka NE Oturere, and c.200-210 ka Tama 2. Prehistoric sample ages are derived from tephra chronology, K-Ar age determinations, or by extrapolation (see Appendix 13).

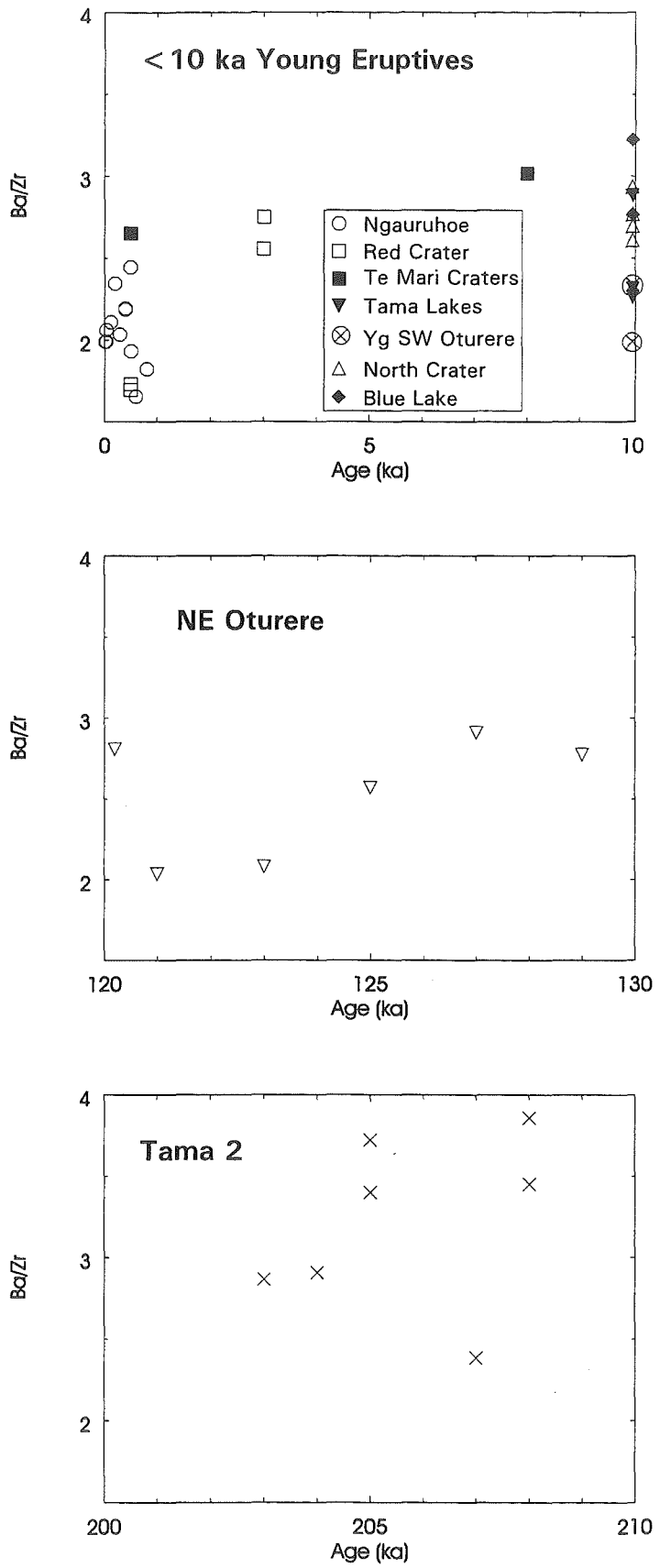

Figure 7.38 Ba/Zr ratios plotted versus time for three eruptive periods of 10 ka duration: 0-10 ka young eruptives, c.120-130 ka NE Oturere, and c.200-210 ka Tama 2. Prehistoric sample ages are derived from tephra chronology, K-Ar age determinations, or by extrapolation (see Appendix 13).

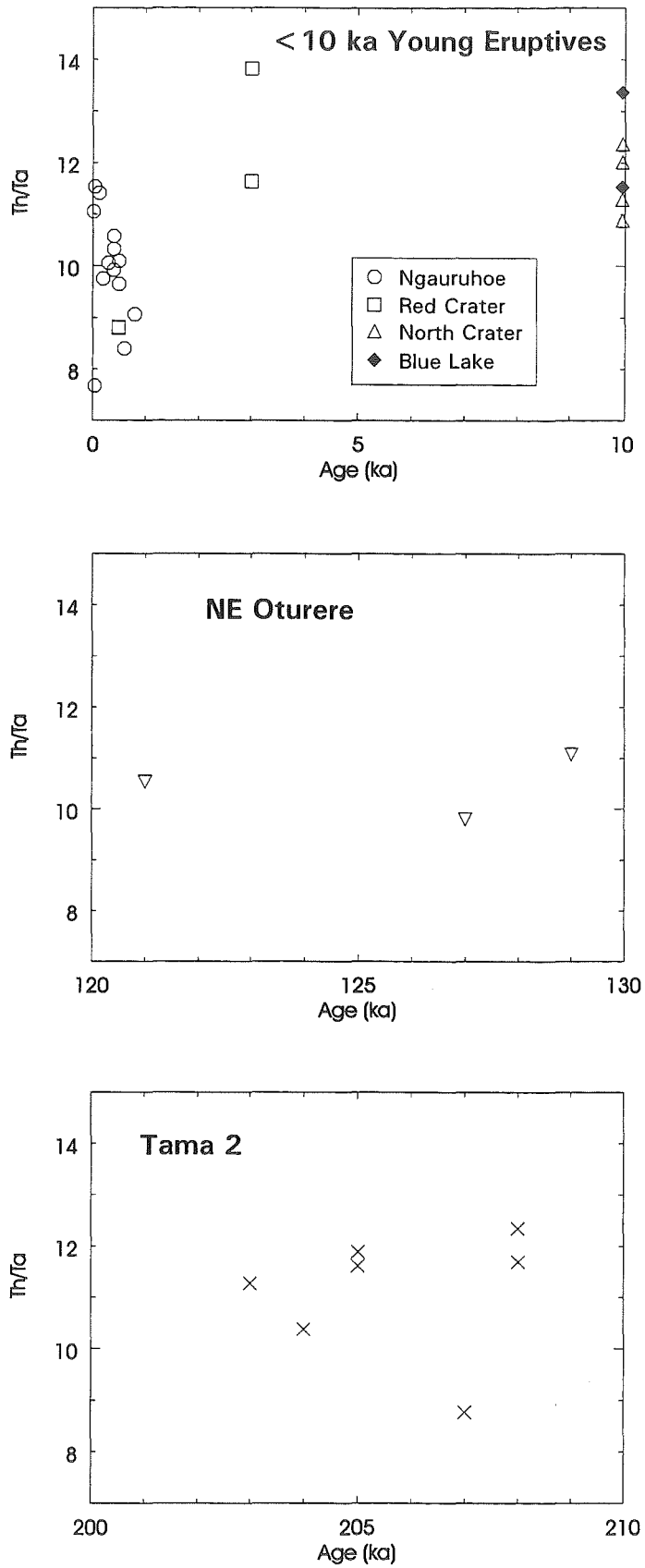

Figure 7.39 Th/Ta ratios plotted versus time for three eruptive periods of 10 ka duration: 0-10 ka young eruptives, c.120-130 ka NE Oturere, and c.200-210 ka Tama 2. Prehistoric sample ages are derived from tephra chronology, K-Ar age determinations, or by extrapolation (see Appendix 13).

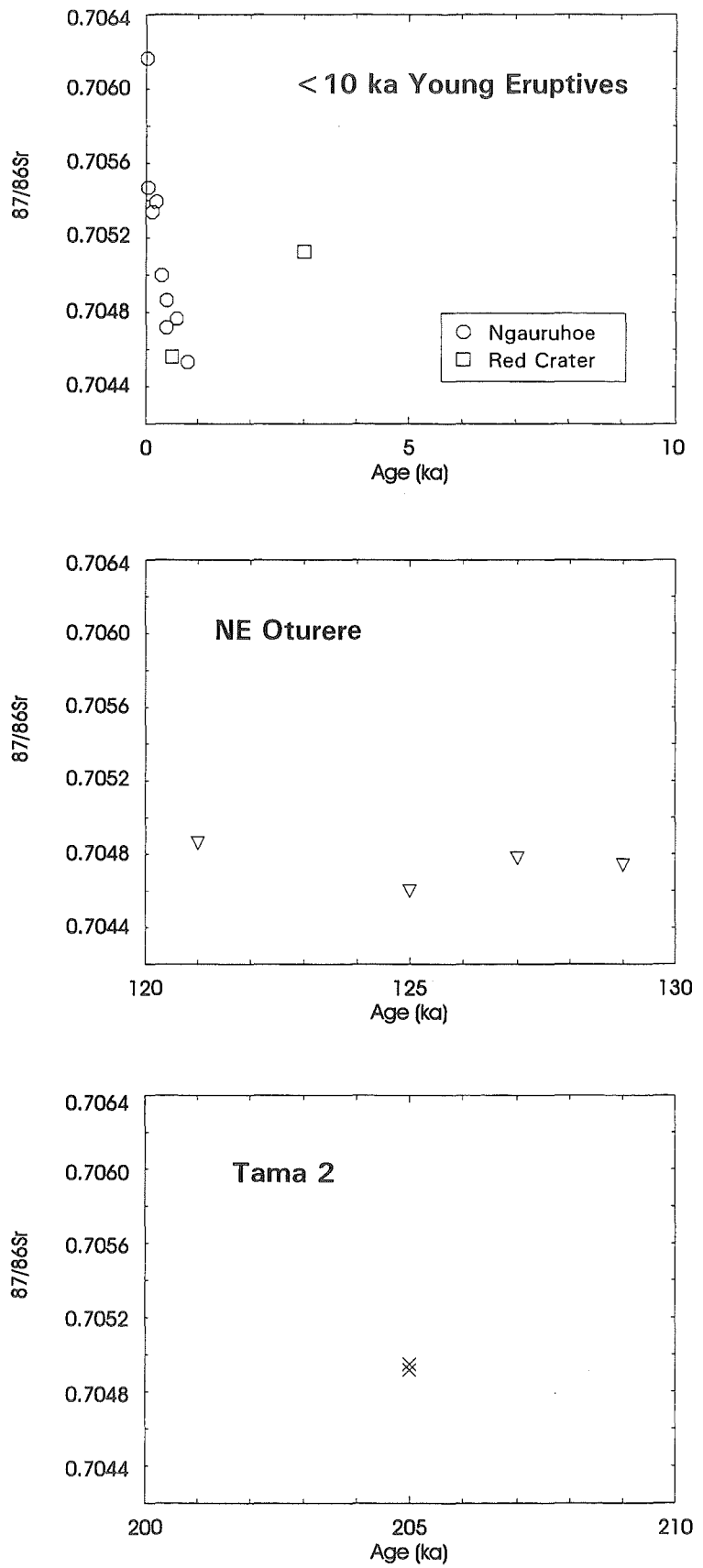

Figure 7.40 $^{87}Sr/^{86}Sr$ ratios plotted versus time for three eruptive periods of 10 ka duration: 0-10 ka young eruptives, c.120-130 ka NE Oturere, and c.200-210 ka Tama 2. Prehistoric sample ages are derived from tephra chronology, K-Ar age determinations, or by extrapolation (see Appendix 13).

Oturere, more broadly scattered for Tama 2), although the amount of variation in each incompatible element ratio appears comparable for the three intervals.

The $^{87}Sr/^{86}Sr$ versus time diagrams (Fig 7.40) are less revealing probably because of the more restricted data set available. The wide isotopic variability in the eruptives of the last 1 k yr has been attributed to differences in crustal contamination (in both the degree of interaction with the crust and the composition of the contaminant; Section 7.5.3). The NE Oturere and Tama 2 sequences appear more isotopically constant in comparison, but any conclusions are seriously limited by the inadequate number of analyses. Note that NE Oturere patterns on isotope-incompatible element ratio diagrams are highly irregular with respect to sample age, thought to indicate the involvement of complex interactions with the crust (Fig 7.24; Section 7.4.1).

Comparison of the three time periods is slightly hindered by the irregular spread of data across the 10 k yr intervals for the young eruptives and the Tama 2 lavas. Addition of samples of intermediate ages to existing ones would benefit interpretation of chemical trends of all three time periods. The enhanced level of detailed sampling and time control available for Ngauruhoe compared to the other units must also be kept in perspective. It is likely that the Ngauruhoe plots in Figs 7.36-7.40 are somewhat distorted by the amount of data for eruptives from the last 1000 years. In all likelihood, if similar exposure and preservation of lavas had permitted a similar degree of sampling for the other units, they may have demonstrated a similarly wide compositional range at various 'points' in the 10 ka history. Thus the data plotted on the NE Oturere and Tama 2 plots probably represent a blurred pattern and an averaging of a series of magma batches which is more clearly defined for the last 1 ka interval of the young eruptives.

The rates of change in magma chemistry over the 3 time intervals appear broadly similar in that there are no instances of a very constant ratio for one interval contrasting with a rapidly varying ratio for another. However as noted above, the nature of the chemical trends does vary between time periods, which may belie variations in the frequency or regularity of arrival of new magma batches into the different plumbing systems. For all these windows into 10 k yr periods of Tongariro's history, the relatively frequent chemical

fluctuations suggest that the typical size of magma batches is small (probably much less than 0.1 km^3) and their lifespans correspondingly short (less than a few ka).

7.6 DISCUSSION AND SUMMARY

The lack of coherent relationships on major and trace element variation diagrams (Chapter 6), coupled with the highly variable and non-systematic age relationships of incompatible element ratios and isotope ratios (Chapter 7) provide strong indications that the Tongariro lavas and pyroclastics sampled on the surface are products of complex differentiation processes operating within a number of dynamic open plumbing systems.

The various Tongariro volcano-stratigraphic units display subtle differences in the shapes of their patterns on normalized incompatible element and REE spiderdiagrams. All samples exhibit the spiked trace element pattern typical of subduction-related magmas, including troughs at Ta and Nb. Sr anomalies range from positive to flat to negative, and are not generally very conspicuous. Light REE-enriched patterns [$(Ce/Yb)_N$=1.8-3.9] prevail, and small to moderate negative Eu anomalies occur on all plots. Incompatible trace element ratios such as Ba/La, Ba/Ta and La/Nb are typically high. Bivariate incompatible trace element plots (involving Rb, Cs, Ba, La, Zr, Nb, Hf, Ta, Pb, Th, U) reveal differences between (and within) some volcano-stratigraphic units which point to their differing parental magmas and/or crustal contamination histories. The chemistry of individual Tongariro lavas (on diagrams such as K/Rb versus Rb, La/Yb versus La, and Ba/Zr versus Ba) can be modelled by assimilation of Torlesse crustal components into relatively uniform parental magmas. However this process does not appear to have produced consistent AFC trend lines on time scales of 1000 to 10 000 years which are compatible with the known ages of the lavas. Instead the assimilation process probably has involved very small magma batches on the time scale of years to decades (or centuries) each mixing with a chemically distinct Torlesse component.

Tongariro $^{87}Sr/^{86}Sr$ isotopic ratios range from 0.704442 to 0.706193, encompassing considerable variability, even for samples closely related in time. $^{87}Sr/^{86}Sr$ ratios increase towards more radiogenic values when plotted against indices of fractionation. Tongariro $^{143}Nd/^{144}Nd$ values range from 0.512629 to 0.512862. Successful AFC models on $^{87}Sr/^{86}Sr$-$^{143}Nd/^{144}Nd$ and Pb isotope diagrams confirm the involvement of Torlesse crust in contaminating Tongariro magmas to varying degrees. Preliminary $\delta^{18}O$ and ^{10}Be data provide ambiguous evidence for crustal contamination and require further investigation.

Magma batch relationships in time and space were examined on a variety of time scales. The 1954 Ngauruhoe eruption produced lava flows which showed only subtle compositional differences, whereas all the historic Ngauruhoe eruptions over the last 100 years or so represent a more complex interaction of several magma batches which have experienced ongoing fractional crystallization and variable crustal contamination. The sharp increase in $^{87}Sr/^{86}Sr$ (0.705339-0.706165) over the relatively short time intervals between historic eruptions cannot represent separate mantle sources and instead relates to differences in the degree of contamination of magmas with the compositionally variable Torlesse crust.

A similar story is represented by the time window an order of magnitude larger; the last thousand years have seen eruptions of many different magma batches from three main vents on Tongariro (Ngauruhoe, Red Crater, Upper Te Mari Crater). Variable AFC and also magma mixing are the principal processes responsible for creating the diverse compositional trends which lack any systematic age relationships. Magmatic variations over three 10 ka time intervals (young eruptives, 120-130 ka NE Oturere, 200-210 ka Tama 2) all indicate multiple magma batches contaminated and fractionated to varying degrees implying that similar magma dynamics have been prevalent over the lifespan of the Tongariro complex. Thus it appears that historic Ngauruhoe behaviour is representative of longer periods of the cone's growth in as much as all the time windows reveal frequent episodes of complex interactions between small (<0.1 km^3) short-lived (< a few ka) magma batches which have experienced varying degrees of AFC.

Tongariro magmatic trends generally do not appear to reflect the distinct signatures of significant batches of fractionating magma, as seen at some other composite volcanoes

where coherent trends are occasionally broken by sharp changes consistently observed across all chemical parameters. The rapid chemical fluctuations every few Tongariro lava flows represent the eruption of numerous small magma batches. Non-systematic variability rather than constant change appears to be the norm with Tongariro magmas, with each reversal in composition signalling a new incoming batch of magma. The variety of physical controls (such as total pressure, water pressure, rise rate) on magma ascent histories of magma batches probably contribute to the chemical variability observed. For example, magma may reside for different periods in short 'pauses' on its way to the surface - these irregularities in magma ascent provide opportunities for different degrees of crustal interactions and magma mixing, and varying time for fractional crystallization, and will ultimately influence when a given body of magma will erupt.

Chapter 8

Discussion and Conclusions

CHAPTER 8
DISCUSSION AND CONCLUSIONS

8.1 IMPORTANCE OF DETAILED MAPPING AND DATING FOR UNDERSTANDING THE ERUPTIVE AND MAGMATIC HISTORY OF A COMPOSITE VOLCANO

Ngauruhoe and the other young cones and craters of the Tongariro Volcanic Complex have long been an obvious source of interest and general study (e.g. Gregg, 1960; Clark, 1960a; Cole, 1978; Graham, 1985a), but little was known about how the older volcanic stratigraphy related to the more recent cone-building style in terms of eruptive pattern, frequency and volume, and rates and processes of magmatic differentiation. This study has attempted to fill this gap in knowledge by undertaking a rigorous mapping, sampling and dating programme covering all sectors of the Tongariro complex, with particular emphasis on the thick successions of lava flows and pyroclastic deposits preserved in steep glaciated valley walls. In this way the older portions of the complex have now been characterised as a complex system of cone-forming units with which comparisons of the younger, post-glacial cones may now be made. To gain a thorough appreciation of the magmatic history of a composite volcano requires that the eruptive history is reconstructed as far back in time as possible to ensure that conclusions are weighted according to events over the entire lifespan of the volcano and not to what is most conveniently exposed or dated (i.e. historic or recent pre-historic activity).

A key focus of this study has been to utilise the newly-acquired knowledge of stratigraphic, time and volume relationships of the samples collected in formulating volcanologically plausible models for magma batches and time-space relationships of the

subvolcanic plumbing system. Conducting petrological modelling within this chronostratigraphic framework has led towards a valuable integration of time-space-volume-composition data which has not been attempted for the majority of composite volcanoes (exceptions include Hopson and Melson, 1990 - for Mount St Helens; Feeley et al., 1993 - for Volcan Ollague; Hildreth and Lanphere, 1994 - for Mount Adams). This approach is vital in linking petrological models to realistic geological relationships (such as truly viable 'parent-daughter' affiliations), rather than focusing on the geochemical data at the expense of meaningful interpretations in a volcano-stratigraphic sense.

The integrated approach adopted for this study enables some fundamental questions about how composite volcanoes work to be considered more satisfactorily than possible by a more conventional approach. Compositional relationships have been investigated on a number of different temporal and spatial scales: between individual volcano-stratigraphic (cone-forming) units, within one of these units, and between different historic eruptions of one unit. In addition to establishing the eruptive and magmatic history for the known lifespan of the Tongariro complex, two cones (Ngauruhoe, NE Oturere) were chosen as cameo studies for which magma batches could be investigated in more depth. The conclusions reached then provided a framework for looking at the other cone-forming units and the Tongariro complex as a whole.

This study of the Tongariro complex differs markedly to previous investigations of composite volcanoes in the Taupo Volcanic Zone. Andesite volcanoes in the TVZ have typically been viewed within the context of an essentially three-way division into basalt-andesite-rhyolite magma types which in effect ignore the geological and chronological relationships of the samples analysed. From the petrological investigations of Ruapehu volcano (Hackett, 1985, Graham, 1985a, Graham and Hackett, 1987) a lava classification into nine 'types' was developed, based on petrographic and geochemical characteristics rather than chronostratigraphy, and therefore not adopted for this study. The results of the Tongariro study bring into question the validity of conventional sampling programmes at composite volcanoes such as Tongariro. If say, only 50-100 samples are taken to determine a petrogenetic overview with little or no regard to chronostratigraphy, then any models which attempt to explain relationships between magma compositions will be seriously

flawed, or fail outright. Not until the spatial and temporal distribution of magmatic activity is understood will the dynamics of the petrogenetic processes responsible be clarified.

Schematic diagrams representing the conceptual framework of the preferred model for Tongariro magmatic plumbing systems are presented in Figures 8.1 and 8.2 and referred to throughout the following discussion.

8.2 VOLCANOLOGICAL FRAMEWORK

8.2.1 Chronology and volcano-stratigraphy

A comprehensive field mapping programme on the Tongariro complex yielded over 400 samples for petrological study, many collected from thick vertical lava-scoria stratigraphic sequences which have been used to construct detailed internal stratigraphies for each cone-forming unit. K-Ar age determinations on 41 selected samples were used in conjunction with field data to identify six pre-glacial (275-65 ka) cone-forming sequences: Tama 1, NE Oturere, Tama 2, Pukekaikiore, SW Oturere, and Tongariro Trig (see Section 8.5). This work represents the first detailed division of Tongariro geology (particularly this earlier history) in terms of units constrained by absolute age limits. The projected convergence of radiating dip patterns of lava flows, together with the presence of hydrothermally-altered lapilli-tuff vent breccias, steeply dipping lavas and rare dikes were used to identify the vent areas of the older cones. Over the last c. 25 k yr, a relatively complex system of more than 20 young vents has developed, dominated by the rapid growth of Ngauruhoe cone since c.2.5 ka. Eleven young intra- and post-glacial eruptive units are recognised: Young NE Oturere, Pukeonake, Blue Lake, North Crater, Young Pukekaikiore, Young SW Oturere, Te Mari Craters, Tama Lakes, Red Crater, South Crater explosion pit, and Ngauruhoe. A map of the cone-forming or volcano-stratigraphic units is presented in Figure 3.2 in a simplified form, and in more detail in the map contained in the back pocket of Volume 2. The characteristics of the volcano-stratigraphic units are summarised in Table 3.3, and eruptive chronology depicted in Figure 3.33.

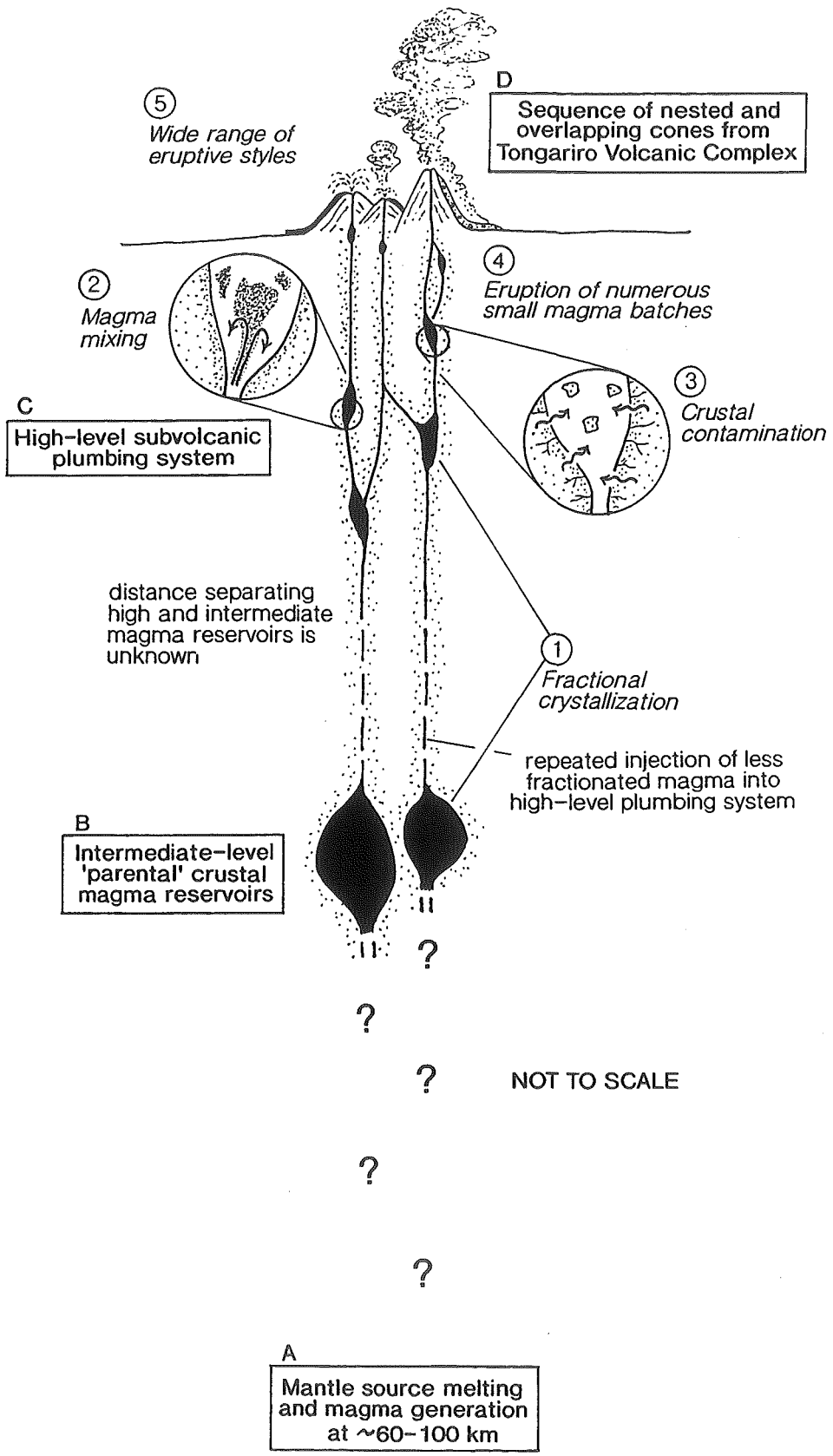

Figure 8.1 Schematic diagram (not to scale) depicting generalised inferred crustal-level magmatic plumbing system beneath Tongariro Volcanic Complex. Main parts of the system (lettered boxes) and main petrological processes (numbered) are shown. See Fig 8.2 for expanded information. Two 'parental' magma reservoirs are shown, but more or less than that number existed at different periods during Tongariro's lifetime (Fig 6.23).

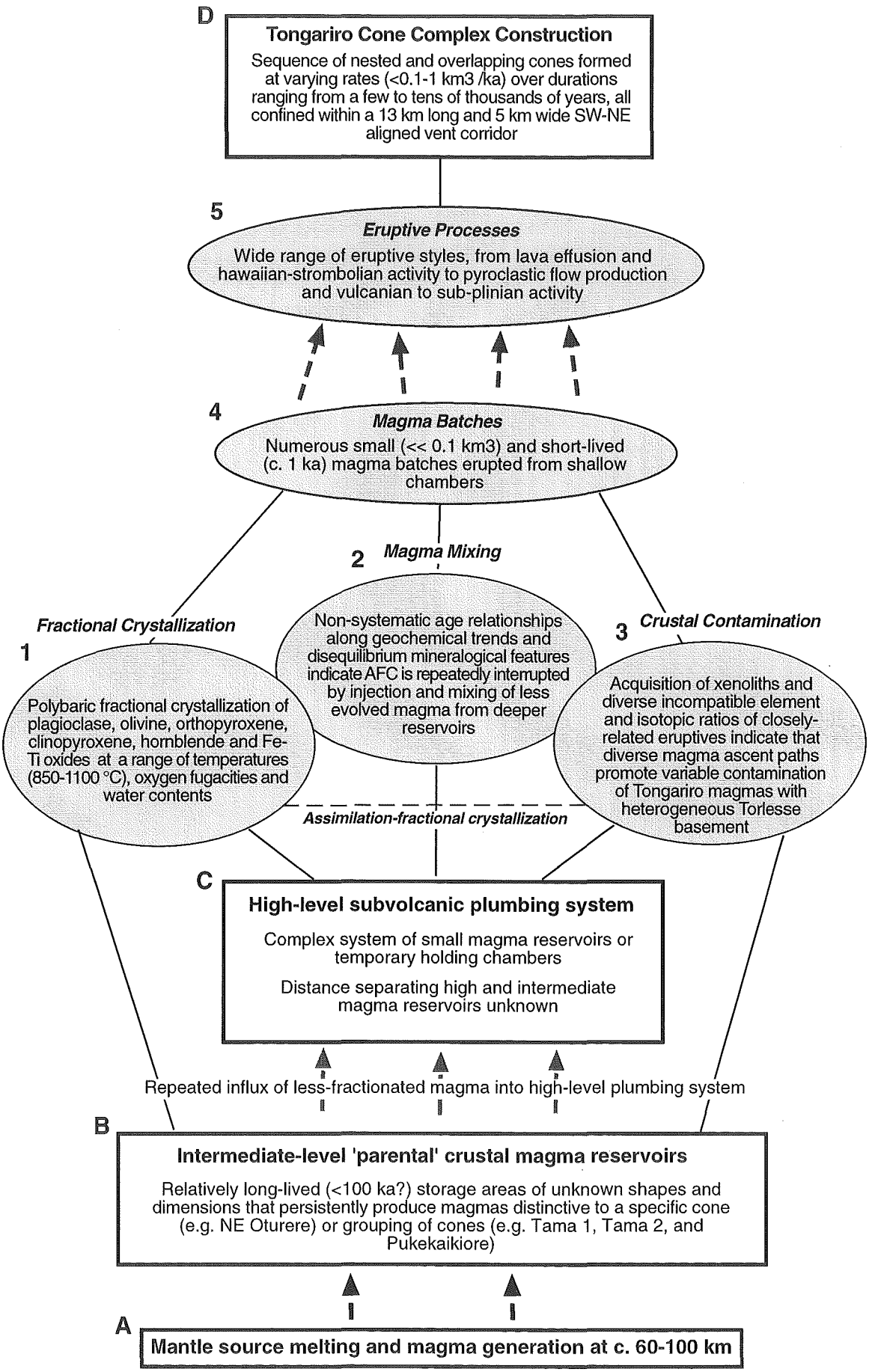

Figure 8.2 Schematic model of Tongariro crustal-level magmatic plumbing system showing a generalised scenario, consistent with geological and petrological evidence, of the main reservoirs or parts of the system (lettered) and petrological and eruptive processes (numbered).

The Tongariro magmatic system has remained almost continuously active throughout its history, with episodes of rapid cone growth at 210-200 ka and 130-80 ka, and possibly one period of quiescence at 65-25 ka. The rate and duration of cone growth has varied throughout the eruptive history of Tongariro (Fig 8.2). At one extreme, Tama 2 represents a short-lived (<10 k yr) and rapidly formed (1km^3/ka) cone that forms a marked contrast to many of the other cones which were active for periods often five times longer than Tama 2 and at substantially lower (often by an order of magnitude) eruptive rates. There are no orderly time-space relationships between cone-building events; the locus of activity has shifted non-systematically over the lifetime of the complex within a 13 km-long and 5 km-wide SW-NE aligned vent corridor (Fig 3.4). Cone-building events also tended to overlap in time rather than be sequential, thus more than one cone was often being constructed over the same time period (e.g. SW Oturere and Tongariro Trig).

8.2.2 Cone-building behaviour over Tongariro's lifetime

The detailed investigation of the older portions of the complex has enabled a comparison between the recent cone-building styles represented by the young eruptives with the earlier episodes of cone growth represented by the six pre-glacial cones. Eruptive rates calculated from both extremes of the volcano's lifetime are comparable; the high magma output of the 2.5-0 ka Ngauruhoe cone (0.9 km^3/ka) almost matches that of the 210-200 ka Tama 2 cone (1.0 km^3/ka). The location of older vents shifts non-systematically with time as is the case for the young vents, and together with the fact that vents of all ages share the same alignment or vent corridor it appears that similar magmatic plumbing system dynamics have endured for most of Tongariro's development. Despite the lower levels of preservation for the pre-glacial cones, the same variety of eruptive products and hence eruption styles can be found represented by the earlier history of the complex as are demonstrated by the most recent cones.

8.2.3 Eruptive styles

The wide variety of eruptive product types at Tongariro reflect an equally wide range of eruption styles (Figs 8.1-8.2). Cone growth at Tongariro has been dominated by repeated effusion of numerous aa and block lava flows from virtually all the summit and flank vents on the complex. Frequent hawaiian to strombolian fire fountaining eruptions have formed significant but localised welded spatter deposits and scoria cones (e.g. Red Crater, North Crater, Blue Lake, Pukeonake, Tongariro Trig, SW Oturere, NE Oturere). Small phreatic to phreatomagmatic eruptions creating explosion craters or tuff cones and pyroclastic surge deposits have often been associated with scoria cone growth (e.g. Emerald Lakes, Tongariro Trig, NE Oturere). More infrequently preserved on the cone complex is evidence for formation of lava lakes ponded in craters (e.g. North Crater), vulcanian style eruptions which have generated pyroclastic flows or avalanches (e.g. Ngauruhoe 1975), and subplinian to plinian eruptions - the latter have, however, deposited extensive tephra on the ring plain.

The in depth facies model presented for Ruapehu volcano by Hackett and Houghton (1989) can also be applied to the Tongariro complex, although the vent association on Tongariro is comparatively less well exposed than on Ruapehu. Note that an abrupt lateral change in eruptive products (related to preservation) is a feature shared by the neighbouring volcanoes; lava flows and localised pyroclastic deposits dominate the proximal cone whereas widespread pyroclastic fall deposits and reworked volcaniclastic material dominate the distal part of the complex.

8.3 OVERVIEW OF MAGMA COMPOSITIONS AND PETROLOGICAL PROCESSES

8.3.1 General rock types and their mineralogy

Within the volcano-stratigraphic framework established for the Tongariro complex during this study, mineralogical and geochemical characteristics and patterns were assessed

(see Section 8.5). In some instances it was also pertinent to examine the 'whole history' of Tongariro as one study unit - effectively as a c.300 k yr time window - in order to establish, for example, what affinity of conditions persisted with time in the source region of Tongariro melts and what degree of 'common history' is shared by all Tongariro magmas. In broad terms, the petrography and mineral and whole-rock chemical compositions of Tongariro eruptives do not encompass too wide a range (Tables 4.6 and 6.2). This is all the more reason to pay careful attention to time-space relationships of compositional patterns so as to avoid a 'broad brush' interpretation of the petrogenesis which is blind to the complex interplay of magma batches on a variety of scales.

This study first conducts general surveys and characterisations of the overall range in mineralogical and petrological compositions by way of a prelude to the main time-space focus of the investigation. The eruptive products from the Tongariro complex range almost continuously in composition from 53.0 to 64.2 wt% SiO_2, forming a calc-alkaline, medium-K suite. Mg# ranges from 37 up to 71, but no Tongariro eruptives have the primitive characteristics representative of direct mantle melts and no true basalts have been documented. Throughout the growth of the volcanic complex, eruptive products have been dominated by strongly porphyritic two-pyroxene andesites, although hornblende-pyroxene andesites were also erupted from the older southern cones (Tama 1, Tama 2, Pukekaikiore), and the young (<25 ka) cones (particularly Ngauruhoe, Red Crater and Pukeonake) have produced the most basic compositions in the form of olivine-bearing basaltic andesites and andesites. Dacite is a volumetrically minor product erupted principally as lava flows from SW Oturere and as pumice ejecta from Tama Lakes.

Mineralogical compositions may be summarised as follows. Olivine (Fo_{67-92}; <2 modal %) typically occurs as resorbed microphenocrysts in almost a third of Tongariro lavas. Plagioclase phenocrysts (An_{45-90}; average 19 modal %) display complex zoning patterns, sieve textures, and resorption features, and single samples often contain wide core compositional ranges of 20-35 mol% An. Orthopyroxene ($Ca_{1-5}Mg_{55-86}Fe_{11-42}$; 1-10 modal %) is usually dominant over augite ($Ca_{35-46}Mg_{35-52}Fe_{7-24}$; 1-15 modal %), and both may be moderately to strongly zoned. Green or red-brown hornblende (mostly magnesio-hornblende to tschermakite; generally <5 modal %) is typically resorbed and rimmed or

pseudomorphed by oxides ± plag ± pyx. Minor phases are dominated by magnetite, and also include ilmenite, chrome spinel, apatite, and quartz.

8.3.2 Fractional crystallization: not the sole process

The recurrence of identical or very similar plagioclase-two pyroxene mineral assemblages and andesitic compositions for many cone-forming units indicates a strong control by low pressure phase equilibria, and emphasises the importance of delayed ascent or stalling of magmas in relatively high-level reservoirs or chambers, as well as earlier crystallization in intermediate-level 'parental' reservoirs (Figs 8.1-8.2). The phenocryst-rich nature of Tongariro magmas and the moderate success of selected least-squares mixing models indicates that (polybaric) fractional crystallization has obviously played a role in Tongariro magma petrogenesis. Where detailed chemical stratigraphy plots are available (e.g. for NE Oturere), however, their characteristic zig-zag pattern shows that repeated basic magma influx and only short periods of uninterrupted fractional crystallization have occurred, rather than the eruption of a steadily fractionating or zoned magma chamber.

Thus strong evidence suggests that often fractional crystallization has been over-shadowed by other processes, principally crustal assimilation and magma mixing (Figs 8.1-8.2). Apart from any obvious differences in the presence or absence of hornblende or olivine, the mineralogical variability between volcano-stratigraphic units is generally more subtle (given the constraints of the available data) with the main distinction being the degree of disequilibrium displayed.

8.3.3 Role of magma mixing

Evidence for disequilibrium between phenocryst phases and groundmass and the involvement of magma mixing processes is especially prevalent in lavas from Tama 2, NE Oturere, SW Oturere, Pukeonake, Red Crater, and Ngauruhoe, and includes: plagioclase containing zones of intense concentrations of glass inclusions (sieve texture) coinciding with major compositional breaks/reversals and inner resorption surfaces; strongly reverse

and/or patchy zoned crystals; co-existing high-temperature and low-temperature phases showing evidence of disequilibrium such as resorption (corroded/embayed crystal edges) and reaction rims; olivine phenocrysts with much higher Fo contents than expected from whole-rock Mg#; bimodal or very widely ranging crystallization temperature estimates for some samples; and rare compositional banding. Magma mixing at Tongariro generally appears to have occurred between closely related compositions. Chemical stratigraphy plots (for e.g. NE Oturere), and variation diagrams assessed in terms of the time sequence of the plotted data (for e.g. Ngauruhoe), reveal numerous chemical breaks and reversals which mark the incoming of multiple magma batches over time periods as short as decades or centuries (Figs 8.1- 8.2).

8.3.4 Role of crustal contamination

Abundant metasedimentary crustal xenoliths (see Section 8.4) and AFC patterns on incompatible trace element and isotope plots provide strong evidence for crustal contamination of Tongariro magmas by the Torlesse metasedimentary basement. A considerable variation in incompatible trace element ratios (e.g. Ba/Zr, Nb/Ta, La/Yb, Zr/Hf) and radiogenic isotopic compositions (e.g. Ngauruhoe $^{87}Sr/^{86}Sr$ ratios increase from 0.705470 in 1954 to 0.706165 in 1975) for closely-related samples is best explained by processes of assimilation fractional crystallization (AFC) involving contamination of Tongariro magmas by varying amounts of compositionally heterogeneous Torlesse crust, giving rise to a family of different AFC trends or AFC events. Thus the assimilation process probably has involved very small magma batches on the time scale of years to decades (or centuries) each mixing to varying degrees with a chemically distinct Torlesse component (Figs 8.1-8.2).

8.3.5 Crystallization conditions

Mineral chemistry was also utilised to provide estimates of crystallization conditions for the majority of Tongariro lavas. Subtle differences between and within some units were revealed. For example, Ngauruhoe lava groups appear to have crystallized at

slightly different temperatures. Further mineral analyses would provide valuable additional information on crystallization conditions of different magma batches. In summary, magmatic parameters determined for Tongariro are: equilibration temperatures of 850-1100°C; oxygen fugacities on or up to 1 log unit above the NNO buffer curve; relatively low total pressures of <7 kb (possibly only 1-3 kb); and water contents of up to 2-5 wt% H_2O.

8.4 A XENOLITHIC PERSPECTIVE ON THE SUBVOLCANIC BASEMENT

Sampling of quartzose xenoliths, particularly in Ngauruhoe lavas, has provided an additional line of inquiry for considering the influence of crustal contamination of Tongariro magmas. A new finding arising from a petrographic study of the quartzite xenoliths is that they provide evidence for an origin as quartz *veins* in Torlesse basement rather than as quartzose segregations of gneissic Torlesse sandstone as proposed by Graham (1985a, 1987). The medium to coarse grained white xenoliths range from small (2-5 mm) subangular to subrounded inclusions within andesite, to larger (2-8 cm) intact inclusions. Many of the xenoliths also contain 5-40 modal % calc-silicates (wollastonite, anorthite, diopside) which are concentrated in irregular patches between quartz mosaics and thin, irregular, closely-spaced bands (often overgrown by larger quartz grains) which cross-cut a dominant banding. These features are interpreted to represent the original structure of calcite/dolomite-quartz veining within the Torlesse, and cannot be reconciled with a bedded sandstone or chert origin.

A granular texture to the xenoliths in hand specimen, and the observation of colourless glass along quartz grain boundaries, both provide evidence for partial melting within the xenoliths. These partial melts have most probably contaminated their host magmas and thus xenolith disaggregation and total assimilation of these crustal fragments is likely to be an important process affecting Tongariro magma compositions (Figs 8.1-8.2). The scarcity of recognisable greywacke xenoliths in Tongariro lavas is probably a result of their high susceptibility to rapid melting or reaction once incorporated into the magma, and

consequently only the much more refractory quartz-rich veins survive as the main type of crustally-derived xenolith.

8.5 COMPOSITIONAL VARIATIONS IN TIME AND SPACE

The volcano-stratigraphic units defined for this study are used here as the framework for describing the composition of Tongariro magmas throughout the eruptive history of the complex. Groupings of cone-forming units which appear to be closely associated in terms of a wide range of factors (age, spatial distribution, cone volume, eruptive rate, mineralogy, and chemical composition) may be viewed together. Seven major unit groupings have been identified (Fig 6.23 and Table 6.3; Section 6.6.9): (1) the older (c.275-160 ka) southern amphibole-andesite cones of Tama 1, Tama 2 and Pukekaikiore; (2) the c.130-90 ka NE Oturere olivine basaltic andesite to andesite cone; (3) the c.110-65 ka low-MgO andesite-dacite cones of SW Oturere and Tongariro Trig; (4) the young (c.20-0 ka) northern andesite cones and eruptives of Young NE Oturere, Blue Lake, North Crater, Te Mari Craters, and pre-1.8 ka Red Crater; (5) the young (c.14-10 ka) southern basaltic andesite to dacite eruptives from Young SW Oturere and Tama Lakes; (6) the young (c.2.5-0 ka) olivine-bearing basaltic andesite to andesite Ngauruhoe cone; and (7) the young (c.23-0 ka) MgO-rich olivine basaltic andesite to andesite eruptives from Pukeonake, young Pukekaikiore, and post-1.8 ka Red Crater. The distinctive similarities shared by each 'grouping' of units suggest that spatial-temporal domains with unique magma geochemistry may be associated with plumbing/conduit systems which operate more or less independently from any adjacent domains.

8.5.1 Southern amphibole-andesite cones (275-160 ka)

The earliest known history of the complex is recorded in the hornblende-bearing silicic andesite (59.5-62.6 wt% SiO_2) lava flow and dome remnants exposed in the Tama Lakes area (Tama 1 cone; c.275-215 ka). The distinctive green hornblende phenocrysts of

Tama 1 lavas contrast with the red-brown amphiboles found in Tama 2 and Pukekaikiore lavas. These later cones represent the persistent focus of activity in the south of the complex. The rapid growth (1.00 km^3/ka) of the large (c.10 km^3) Tama 2 cone between c.210 and 200 ka produced at least 55 hornblende-phyric andesite (56.4-63.0 wt% SiO_2) lava flows which have been mapped dipping southwards away from hydrothermally-altered vent breccias now exposed on the flanks of Ngauruhoe. The final phase of this concentration of hornblende-andesite production in the southern portion of the complex is represented by the Pukekaikiore cone situated just west of the Tama centres, which between c.190 and 160 ka produced thick, columnar-jointed amphibole-bearing silicic andesite flows (59.8-61.8 wt% SiO_2) from a vent now concealed beneath Ngauruhoe.

In addition to their characteristic amphibole-bearing phenocryst assemblages, these southern cones also exhibit a distinctive chemical signature reflected in higher K/Rb for a given SiO_2 content, and comparatively low K_2O, Rb, La, Ce, Y and Zr abundances relative to other Tongariro units. When looking at variation diagrams, considerable data scatter along relatively short to medium-length (c.2-3 wt%SiO_2 range), shallow, broadly linear trends are features common to all three units. Little variation in isotopic composition is evident ($^{87}Sr/^{86}Sr$ = 0.704917-0.704948), although these units have not been extensively analysed for isotopic ratios. The eruptive products of these cones reflect involvement of a distinctive type of 'parental' magma which was restricted to these southern vents and the earlier part of Tongariro's history (Fig 6.23). Higher level magma chamber offshoots from this main storage area probably allowed further diversification (Fig 8.1). Multiple magma batches have been erupted from these cones, as demonstrated by the considerable petrographic evidence for magma mixing (e.g. coexisting resorbed quartz and olivine phenocrysts in obvious disequilibrium, compositionally banded lava) and non-systematic age relationships along geochemical 'trends' on variation diagrams.

8.5.2 NE Oturere olivine basaltic andesite-andesite cone (130-90 ka)

The first obvious indication of the SW-NE vent corridor which dominates the overall Tongariro vent configuration is provided by the NE Oturere cone, which represents a shift in vent location from the south to the northeast by at least 130 ka when an intense

period of activity commenced. Between 130 and 90 ka the bulk of the c.11 km^3 cone was formed (0.37 km^3/ka) by eruption of more than 70 often olivine-bearing basaltic andesite and andesite (55.4-62.2 wt% SiO_2) block lava flows and intercalated scoria-tuff deposits, now exposed as thick stratigraphic sequences (bounded by angular unconformities) in the glacial valley wall.

The NE Oturere eruptives represent a significant change to more mafic (up to 7.1 wt% MgO) compositions and a much steeper, longer, more tightly clustered trend of data points spanning a wider compositional range (c.7 wt% SiO_2) on variation diagrams compared to the preceding silicic hornblende lavas of the southern cones. $^{87}Sr/^{86}Sr$ ranges from 0.704600 to 0.704980. The occurrence of two main chemical groups such that for a given SiO_2 content (e.g. 57.5 wt%) there is a relatively broad range in, for example, MgO content (e.g. 4.2 to 6.3 wt%) also distinguishes the NE Oturere type of behaviour from that demonstrated by the Tama-Pukekaikiore magma. This suggests the involvement of a 'parental' magma reservoir compositionally distinct from and unconnected with the magma reservoir feeding the amphibole-bearing cones. The wide compositional range, reverse zoning, resorption and sieve textures common to many phenocrysts (particularly plagioclase and orthopyroxene), the rare corroded quartz, and the numerous breaks and reversals in magma chemistry up through the subunit 'd' stratigraphy, all indicate disequilibrium and the involvement of mixing between multiple magma batches on a time scale of not more than thousands of years (Fig 8.2).

8.5.3 SW Oturere and Tongariro Trig andesite-dacite cones (110-65 ka)

As activity waned in the northeast, the central portion of the complex between the southern hornblende-bearing cones and NE Oturere was filled with material erupted synchronously from two cones, SW Oturere and Tongariro Trig, mainly between 110 and 65 ka. Thick stacks of andesitic-dacitic (57.0-65.5 wt% SiO_2) autobrecciated lavas, pyroclastic and epiclastic deposits are exposed along the walls of the SW Oturere and north Mangatepopo valleys and South-Central Crater. The Tongariro Trig cone appears to have originally been larger (12 km^3) and more productive (0.27 km^3/ka) than the SW Oturere cone (5 km^3, 0.11 km^3/ka), although the SW Oturere cone preserves evidence of a greater

number of flows and pyroclastic units (c.65) compared to the Tongariro Trig cone (c.45). Old vent areas can be recognised for both cones, in the form of extensively hydrothermally-altered lavas and lapilli-tuff breccias, dike-like intrusive bodies, proximal scoria and spatter deposits, and lava flows with steep and opposing dips.

These two youngest of the pre-glacial cone-forming units represent another notable departure in compositional trends for the Tongariro complex; data lie on a much lower MgO trend at a given SiO_2 content relative to the preceding units. This appears to reflect a situation in which magma has been derived from an already quite differentiated 'parental' magma and/or has resided longer than usual (compared to most other Tongariro units) in a high level reservoir enabling it to evolve more substantially (Fig 8.1). SW Oturere and Tongariro Trig eruptives also share other distinctive chemical characteristics such as a division into high (0.77-0.89 wt%) and low TiO_2 (0.64-0.76 wt%) groups, and widely ranging $^{87}Sr/^{86}Sr$ (0.704876-0.706193). Chemical stratigraphy plots show considerable compositional variability tied in to the divisions between chemical lava groups, but also indicate chemical breaks and reversals within these groups which demonstrate the involvement of multiple magma batch influxes. Bimodal crystallization temperature estimates (e.g. 865 and 1175°C) support the occurrence of significant magma mixing.

8.5.4 Establishment of young summit vents

Following a possible lull in eruptive activity between c.65 and 25 ka, the complex system of vents comprising the "young eruptives", small-volume cones and pyroclastic deposits, was established on the eroded remnants of the six older cone-forming units. Recognisable cone and original flow morphology has been preserved for most of these units, and they dominate the summit landscape and skyline. These young eruptives were typically more mafic than those erupted previously, with generally higher proportions of olivine-bearing basaltic andesites. Many of the eruptions occurred around 10 ka, signifying that this was a period of intensive volcanic activity and peak productivity of magma for the Tongariro complex.

8.5.5 Young northern andesitic vents: Young NE Oturere, Blue Lake, North Crater, Te Mari Craters, pre-1.8 ka Red Crater (20-0 ka)

A cluster of small two-pyroxene andesitic (56.3-60.2 wt% SiO_2) cones started to form on the north flanks of the Tongariro complex around 20 ka with the eruption of the Young NE Oturere scoria fall deposit, Blue Lake spatter cone, North Crater spatter cone and lava lake, Te Mari Crater cone, and pre-1.8 ka Red Crater scoria cone and lava flows. Of these units, the Upper Te Mari Crater has also erupted historically, but has not produced a lava flow since c.1500AD. The close spatial and temporal proximity of these cones is complemented by their similar geochemistry, including similar incompatible element ratios such as K/Rb and Rb/Zr, and $^{87}Sr/^{86}Sr$ ranging 0.705126-0.705700. The overlapping, moderately steep, short to medium length trends are generally quite scattered and do not represent consistent stratigraphic-compositional relationships. There is a strong case for a common deep magma reservoir shared by these vents, with only minor chemical variations produced by slight differences in the type and degree of higher level differentiation processes experienced by the various magma batches erupted over c.20 ka (Figs 8.1-8.2).

8.5.6 Young southern basaltic andesite to dacite vents: Young SW Oturere and Tama Lakes (14-10 ka)

During the establishment of the young northern vents, discrete eruptions also occurred further to the south from multiple vents between SW Oturere and Tama Lakes, forming explosion craters and scoria and pumice deposits. They generally plot on a lower MgO trend at a given SiO_2 content relative to the northern vents, and also span a much wider compositional range, from 55.0 to 64.2 wt% SiO_2. Isotopic compositions have not been measured on these samples. It is likely that the Young SW Oturere and Tama Lakes vents were fed by the same magma reservoir which was operating independently from the coeval plumbing system beneath the young northern vents (Fig 8.1).

8.5.7 Ngauruhoe olivine basaltic andesite to andesite cone (2.5-0 ka)

By far the most productive of all the post-glacial vents has been that of Ngauruhoe, which has issued numerous basaltic andesite to andesite (54.2-58.6 wt% SiO_2) lava flows (c.80 exposed) and built a 2.2 km^3 cone within its 2.5 ka lifetime at an average rate of 0.88 km^3/ka. Ngauruhoe has been frequently active in historic times with its last major eruption in 1975. Ngauruhoe eruptives are distinguished from the rest of the Tongariro eruptives by their almost unique position at the left of the MgO-SiO_2 diagram and their division into five discrete geochemical groups which represent an even larger number of magma batches. These diverse chemical groups also exhibit a wide range of characteristics in terms of slope, length and tightness of trends. Ngauruhoe lavas are also characterised by considerable isotopic heterogeneity ($^{87}Sr/^{86}Sr$ = 0.704532-0.706165). Magma mixing and crustal contamination processes have played just as important a role as fractional crystallization in Ngauruhoe petrogenesis. Ngauruhoe lavas and pyroclastics thus represent another distinctive magmatic signature in Tongariro petrogenesis, although to what extent this is owing to the comprehensive sampling enabled by the excellent exposure of the young cone is not certain. The main magma reservoir providing the characteristic Ngauruhoe type of magma has supplied a number of smaller magma chambers at higher levels in which the different geochemical groupings have developed, and from which numerous magma batches have been erupted (Fig 8.1). A fuller summary of Ngauruhoe eruptive and magmatic history is presented in Section 8.7.

8.5.8 Young olivine basaltic andesite eruptives: Pukeonake, Young Pukekaikiore, post-1.8 ka Red Crater (23-0 ka)

These three units are only moderately related in time or space, but do represent several of the more extreme compositions erupted from the Tongariro complex as olivine-bearing scoria cones and lava flows. They all occur as high MgO outliers on the MgO-SiO_2 diagram (53.0-57.4 wt% SiO_2, 6.9-9.2 wt% MgO) and cannot be derived by differentiation processes from any of the earlier Tongariro magma compositions. These units are also characterised by containing among the least radiogenic $^{87}Sr/^{86}Sr$ (0.704442-0.704758) values of all Tongariro eruptives.

The basaltic andesite Pukeonake scoria cone, lava flows, and associated vents formed c.23 ka and represent the only known eruptions *peripheral* to the main Tongariro complex, and are also distinguished by their relatively primitive compositions (<9.2 wt% MgO, <460 ppm Cr, <220 ppm Ni) and strong evidence for disequilibrium resulting from magma mixing (e.g. strong reverse zoning, sieve textures, reaction rims, bimodal crystal populations). The Young Pukekaikiore (c.15 ka) olivine andesite erupted from a central-west location and is remarkable for its lack of plagioclase phenocrysts, very high Sr concentrations (up to 643 ppm) and low Al_2O_3 (less than 14.8 wt%). Post-1.8 ka eruptions from the low-SiO_2 (53.0-53.7 wt%) basaltic andesite Red Crater vent have continued to build up the small scoria cone and have sent small to large lava flows in many directions, with ash and steam eruptions occurring last century. The Pukeonake, Young Pukekaikiore and post-1.8 ka Red Crater units represent three independent, very distinctive, and relatively primitive magma batches which probably followed atypical, more direct paths to the surface compared to the routes already established by the existing plumbing system beneath the Tongariro complex (Fig 8.1).

8.5.9 Summary

Variation diagrams for the Tongariro cone-forming units reveal differences in the absolute elemental abundances for given SiO_2 contents, in the length, steepness and shape of chemical trends, and in the distribution of chemical groups within compositional space. Certain volcano-stratigraphic units do share, however, similar patterns of chemical ordering which suggest derivation from a common deep magma reservoir, e.g. the amphibole-bearing andesites of southern cones (Tama 1, Tama 2, Pukekaikiore). Other compositionally distinct units nevertheless often exhibit analogous trend patterns which may signify a common high level differentiation history involving (to varying degrees) magma mixing, fractional crystallization and crustal contamination. A relatively complex history is envisaged for the plumbing system of the Tongariro Volcanic Complex, in which different configurations and combinations of both deep and shallow magma reservoirs, some operating independently and others interconnected, have existed at different time periods throughout Tongariro's development (Figs 8.1-8.2).

8.6 WINDOWS INTO TIME-SPACE RELATIONSHIPS OF MAGMA BATCHES

Modelling using incompatible trace element and isotopic data over time scales of 1 year, 100 years, 1000 years and 10 000 years provided useful 'windows' into the behaviour of magma batches in time and space. Considerable diversity in magma chemistry over the latter three time intervals is revealed by tracking time-compositional sequences on variation diagrams and examining chemical stratigraphies. The fundamental process which is the key to explaining this chemical diversity is variable amounts of crustal assimilation of a heterogeneous Torlesse contaminant affecting many discrete magma batches at a relatively high level (Figs 8.1-8.2).

Although broad magmatic signatures may be developed at moderate depths in 'parental' magma reservoirs (i.e. represented by the groupings of volcano-stratigraphic units discussed in Section 8.5), the many discrete magma batches that have risen from them have typically diversified through higher level variable interaction with the crust and mixing with other magmas in the higher level plumbing system beneath the volcano - on time scales as short as 100 years. Any one magma batch may equate with one eruption or may be vented over a series of eruptive episodes. Comparable compositional variability and rates of magmatic change over three 10 k yr time intervals spanning different parts of Tongariro's history (0-10 ka young eruptives, c.120-130 ka NE Oturere, c.200-210 ka Tama 2) suggest that similar magmatic processes have been operating throughout Tongariro's lifetime, although each time interval displays a subtly different pattern. Thus the regularity/rate of magma batch production may vary somewhat, but all batches appear to be small (probably $<<0.1$ km^3) and short-lived (probably c.1 ka).

Crucial parts of the Tongariro petrogenetic model which require further clarification include a more thorough assessment and quantification of the uniformity of source conditions for magmas related on a variety of temporal and spatial scales, and determination of the depth range over which some magmas may have shared a common history before compositionally diversifying at a higher level (and at what depth is this

'chemical signature' finally determined?). In other words, more rigorous testing must be carried out as to where exists the highest degree of connectivity between various eruptives; is it in the source melting region, in shallow 'parental' magma reservoirs, or in the high-level plumbing system? It is also not clear at present whether magmas could be linked to one source composition but still be unrelated in the sense of representing different melting events, or whether they also represent the same melting event.

Considering the AFC process in more detail also throws up some intriguing questions. For example, does the scatter of data represent a *family* of AFC *trends*, or not trends at all but a series of 'one-off' AFC *events*? Each magma batch may in fact be fairly homogeneous, representing mixing of one deep and one crustal component, but the 'batches' may be small and frequent giving the illusion of 'trends'. It is often difficult on Tongariro AFC 'trends' to see where one batch ends and another begins. If magma from a 'parental' reservoir, released as numerous magma batches, is subject to a whole series of crustal contamination events, then smooth, long-lived AFC trends would not be expected, and this is what is found for Tongariro eruptives. Because the Torlesse crustal contaminant is so compositionally variable and the amount of magma:crust interaction also varies, chemical modelling of Tongariro AFC 'trends' is actually of questionable value since these unknown parameters so significantly affect the outcome of any model.

8.7 NGAURUHOE: A SPECIAL CASE

Although essentially the entire Tongariro complex has been mapped and sampled in detail, and a comprehensive volcano-stratigraphic framework established for assessing the magmatic history, Ngauruhoe has been singled out as a cameo study. The well-constrained stratigraphy enabled by the preservation of numerous young lava flows erupted from Ngauruhoe over the last thousand years provides a unique opportunity for detailed petrological modelling paying careful attention to age relationships. It is important to recognise the more complete perspective on magmatic history given by Ngauruhoe; the detailed sampling of all sectors of this young cone provides insights often different from

those obtained for the older units where usually only one sector of the cone is exposed in a valley wall. Thus, the conclusions drawn from the Ngauruhoe study may be applicable to the older Tongariro cones, even though the different study approaches might make comparison more difficult.

Activity at Ngauruhoe has been characterised by effusive, strombolian (e.g. 1954-55 eruption), vulcanian (e.g. 1974-75 eruption) and possibly subplinian styles of activity, which have produced a correspondingly wide range of eruptive products, although preservation of aa to block lava flows has dominated. Ngauruhoe has an estimated volume of 2.2 km^3, the largest volume of the young eruptive units. The frequency of eruption from Ngauruhoe is demonstrated in both the large number of recognisable lava flows and pyroclastic units (c.80) and in the relatively high eruptive rate of c.0.88 km^3/ka - second only to that of the Tama 2 cone. Approximate instantaneous eruptive rates calculated for the historic lava flow-producing eruptions vary from 1-4 m^3/s, whilst the 1975 pyroclastic avalanche eruption occurred at a rate of c.70 m^3/s.

Comprehensive sampling of lava flows (and some pyroclastic avalanches and scoria) from all sectors of the volcano has enabled the construction of a detailed volcano-stratigraphy. On the basis of field relationships and inferred flow chronology, the lava flows have been divided into 5 groups which also have a chemical distinction. There are not straightforward compositional-time relationships between these groups, however, as demonstrated by several instances when two compositional types were erupted during the same time period. This situation seems to reflect the coexistence of more than one high level magma reservoir feeding into Ngauruhoe at any one time, the contrasting (anomalous) magma group represents a 'leaky' magma batch from which an early aliquot or the last remnants are drawn, synchronous with eruptions from the main magma storage area at that time. Ngauruhoe eruptives are predominantly basaltic andesites, with an overall geochemical range of 54.2-58.6 wt% SiO_2 and 2.2-5.6 wt% MgO. It is important to recognise the division of data into the 5 discrete groups and trends when confronted with the characteristically wide compositional diversity for a given SiO_2 content, e.g. the almost 3 wt% range in MgO contents for lavas of c.58 wt% SiO_2 (see Tables 4.1 and 6.1).

The oldest (>1.8 ka) exposed Ngauruhoe lavas belong to Groups 1A and 1B and helped build up the eastern and N-NW sectors of the cone. The olivine-bearing (Fo_{67} rimmed by more Mg-rich orthopyroxene) Group 1A basaltic andesites are of restricted composition (54.2-55.5 wt% SiO_2, 4.5-4.9 wt% MgO) and contain the lowest Rb/Zr (0.20-0.25) and $^{87}Sr/^{86}Sr$ (0.704532) of all the Ngauruhoe groups, plus the highest Sr (316-359 ppm) and, of other lavas of comparable SiO_2 contents, the highest Zr concentrations (119-142 ppm). The disequilibrium olivine compositions, wide plagioclase compositional range (An_{57-90}), reverse zoning, and sieve textures suggest a strong involvement of magma mixing processes in the petrogenesis of Group 1A magmas. Group 1B basaltic andesites record a shift to slightly more silicic (55.2-55.9 wt%SiO_2) and lower MgO compositions (3.6-4.0 wt%) compared to Group 1A, and also contain higher Rb/Zr (0.25-0.32) and $^{87}Sr/^{86}Sr$ (0.704766). A distinctive split into high (329-334 ppm) and low (200-225 ppm) Sr samples is another feature of Group 1B lavas. Group 2 andesites (57.9-58.3 wt% SiO_2) comprise several relatively long flows on the south flanks of the cone, and represent the most MgO-poor (2.2-3.2 wt%) of all Ngauruhoe eruptives, with Rb/Zr between 0.33 and 0.39 (isotopic compositions were not measured).

A series of andesitic (57.2-58.6 wt%) lava flows represented by Group 3A added to the SW sector of the cone, and mark a significant change back to higher (and more widely ranging compared to Groups 1A-B) MgO compositions (4.4-5.4 wt%). These Group 3A lavas also contain the highest Rb/Zr (0.40-0.44) of all the Ngauruhoe groups, and $^{87}Sr/^{86}Sr$ (0.704720-0.704865) similar to Groups 1A-B. Group 3A lavas, which are unexpectedly MgO-rich relative to their SiO_2 contents, contain chrome spinel-bearing olivines of composition Fo_{91} which are not in equilibrium with whole-rock Mg#, and which are surrounded by markedly more Fe-rich orthopyroxene rims, all indicative of the involvement of magma mixing processes.

The youngest pre-historic plus all historic (1870, 1949, 1954-55, 1974-75) flows and pyroclastics belong to Group 3B which are concentrated in the N-NW sector of the cone. These olivine-bearing (Fo_{80}) basaltic andesite to andesite samples plot as a broad linear trend spanning the widest SiO_2 (54.8-58.2 wt%) and MgO (3.8-5.6 wt%) range of all Ngauruhoe groups, with Rb/Zr ranging between 0.29-0.39. Group 3B rocks (particularly the historic eruptives) often contain crustal quartzite xenoliths (Section 8.4) which exhibit

evidence of partial melting and are considered to indicate involvement of crustal contamination of these magmas. Group 3B eruptives are more radiogenic than the other Ngauruhoe groups and also much more isotopically variable ($^{87}Sr/^{86}Sr$=0.705000-0.706165) with non-systematic age relationships along AFC 'trends', factors taken to suggest variable amounts of crustal assimilation (of a heterogeneous Torlesse crust) by magmas from a number of batches. Complex dynamics in the Ngauruhoe Group 3B magma-plumbing system are evident on time scales as short as decades or centuries. The non-systematic age relationships along geochemical trends, compositional reversals and compositional loops formed by these isotopically diverse samples represent many small, short-lived magma batches which have been produced at relatively shallow crustal levels in several independent plumbing systems, and which have been affected by varying degrees of crustal contamination (Figs 8.1-8.2).

That the Ngauruhoe lava groups do not represent a continuum of steadily evolving magma compositions can also be demonstrated by the failure of most major element fractional crystallization models. The variability in incompatible element ratios (e.g. Rb/Zr) and radiogenic isotope compositions between and within the Ngauruhoe groups are believed to result principally from variable degrees of crustal contamination with a compositionally diverse Torlesse assimilant. Many magma batches, mixing with each other and the crust, have been involved in Ngauruhoe petrogenesis and can be identified in association with the lava groups but also for any one group.

Ngauruhoe provides a unique opportunity in New Zealand to investigate the size and lifespans of magma batches to aid in the prediction of future activity. Knowledge of the pre-historic patterns of magma interactions and eruption from Ngauruhoe can provide models for predicting the most likely sequences of events that could occur in the future, based on the assumption that future activity will probably resemble past behavioural patterns. This study has shown that much can be learned from such a well-exposed, frequently active cone as Ngauruhoe, and further detailed investigation of magma batch relationships would greatly enhance the ability to identify and prepare for the volcanic hazards likely to be encountered.

8.8 IMPLICATIONS FOR ANDESITIC MAGMA PLUMBING SYSTEMS

This study has been successful in highlighting a number of distinctive, broad groupings of magma compositions related to volcano-stratigraphy which have contributed to the growth of the Tongariro cone complex. Some of these have not previously been identified or described. The detailed sampling approach taken here has thus proved valuable in characterising much more fully the range of magmatic compositions involved, and has allowed recognition of recurring geochemical patterns related to the complex interplay of magma batches with each other and with the crust through which they pass. The combination of magmatic processes involved (fractional crystallization, magma mixing, AFC), coupled with the complexity of the time-space-volume-composition relationships determined for the Tongariro complex demonstrate the need for representative sampling over the entire exposed area and lifespan of a composite volcano if a full picture of its eruptive and magmatic history is to be attained. Thus it is not possible to be confident of "representative" samples from composite volcanoes because of the chemical variability of multiple magma batches involved over very short time spans (decades to centuries).

A petrogenetic model of Tongariro (or any other composite volcano) must attempt to account for a number of fundamental questions which arise from the complex time-space-compositional relationships. Some of these major issues are listed below. The duration, configuration and size of magma reservoirs, and their degree of connectedness to other reservoirs is a pertinent problem when looking at the magmatic history of composite volcanoes. How does magma rise at Tongariro and from what depths? Age relationships must be carefully examined on geochemical diagrams before geologically feasible modelling can be attempted (e.g. relating 'parent-daughter' compositions by least-squares mixing fractional crystallization models). If certain volcano-stratigraphic units share a common 'parental' magma reservoir - what depths are we talking about and did the units share a reservoir in the sense of all being present together at any one time or did they pass through the reservoir sequentially with no overlap in time and hence no common history? How much magma was present at shallow crustal levels at any one time? The widespread sub-plinian fall deposits on the Tongariro ring plain suggest that relatively large shallow magma chambers have existed at various times during Tongariro's history. There is a strong

need to more clearly distinguish 'parental magma batches' from 'erupted' or 'final' magma batches from Tongariro, and to clarify the likely size and life span of a magma batch at Tongariro. Further work is required to characterise these important aspects of the magmatic system.

The distribution of magma chambers and conduits is fundamental to the understanding of volcanic eruptions, and contributes to a basis for reliable forecasting techniques that may reduce volcanic hazards. Ngauruhoe provides an especially good opportunity to assess these factors (see Section 8.7). The next step for this study would be to consider whether the pre-historic and historic pattern of Ngauruhoe's behaviour will continue, or will there be some more fundamental change in the dynamics of its magmatic system. Future work on the Tongariro complex could involve an even more detailed study (with a more comprehensive chemical analytical base) expanding the chemical stratigraphy of Ngauruhoe and NE Oturere, plus also applying these techniques to other suitable units such as SW Oturere. Somewhat of a drawback of the wide scope of this study has been that in order to conduct detailed time-space-composition modelling, the overall volcano-stratigraphic framework and magmatic history had first to be established in order to identify the general patterns and relationships of the cone-forming units. This first aim required considerable field and laboratory investigation which by necessity reduced the time available to concentrate on the specific time windows.

Because relatively few time-space-volume-composition studies have been conducted, it is rather difficult to assess with any degree of certainty how typical Tongariro's eruptive behaviour and magmatic history are compared to other composite volcanoes. In general, the lifespan, size, eruptive products, and overall magma compositions of the Tongariro complex all have aspects in common with other andesite volcanoes (e.g. Hackett and Houghton, 1989; Ferguson et al., 1992; Feeley et al., 1993). A particularly useful comparison is with the detailed investigation of Mount Adams by Hildreth and Lanphere (1994). The findings for this study of the Tongariro complex in many ways parallel their implications for understanding the workings of composite volcanoes.

The Mount Adams study highlighted how the construction of an arc volcano often encompasses several growth spurts when magma production rates are particularly high, interspersed with much longer periods of sporadic, low-level background activity (Hildreth and Lanphere, 1994). A pattern of long-term behaviour whereby certain periods of peak productivity were responsible for adding significant volumes to the Tongariro cone complex was also revealed by this study. Thus volumetric eruption rates are generally more meaningful when calculated within the context of the time scales of a detailed volcano-stratigraphy, as attempted here. Otherwise, if only an average rate for the lifetime of the volcano had been estimated, the unique rhythms in varying peak and background magma production rates now evident for Tongariro's history would not have been revealed.

8.9 SUMMARY OF MAIN CONCLUSIONS

(1) A detailed mapping, sampling and dating programme has enabled a comprehensive volcano-stratigraphy to be developed. The eruptive history of the Tongariro Volcanic Complex is divided into 17 units: six relatively large (<12 km^3 original volume), nested and overlapping pre-glacial cone-forming units - Tama 1 (275-215 ka), NE Oturere (250-90 ka), Tama 2 (210-200 ka), Pukekaikiore (190-120 ka), SW Oturere (115-70 ka), and Tongariro Trig (110-65 ka), upon which eleven mostly post-glacial eruptive units or small cones (<2 km^3) are superimposed - Young NE Oturere (20+ ka), Pukeonake (23 ka), Blue Lake (20-10 ka), North Crater (15-10 ka), Young Pukekaikiore (15 ka), Young SW Oturere (14-10 ka), Te Mari Craters (14+-0 ka), Tama Lakes (10 ka), Red Crater (3-0 ka), South Crater explosion pit (2-1.8 ka), Ngauruhoe (2.5-0 ka).

(2) The Tongariro complex has been almost continuously active throughout its history, with episodes of rapid cone growth at 210-200 ka (Tama 2 eruptive rate = 1km^3/ka) and 130-80 ka (NE Oturere, SW Oturere and Tongariro Trig cones all under construction), and possibly one period of quiescence at 65-25 ka. There is no orderly time-space relationship between cone-building events; the locus of activity shifted non-systematically over the

lifetime of the complex within a 13 km-long and 5 km-wide SW-NE aligned vent corridor. Recent cone-building styles share much in common with the older eruptive behaviour.

(3) Detailed internal stratigraphies developed for each cone-forming unit reveal a dominance of thick aa and block (often autobrecciated) lava flow sequences which often contain intercalated scoria, tuff, welded agglutinate and laharic breccias. The wide variety of eruptive products at Tongariro reflect an equally wide range of eruptive styles, from hawaiian-strombolian style fire-fountaining, to phreatic-phreatomagmatic eruptions, to vulcanian-style explosions, to subplinian eruptions (evidence for the latter is restricted to tephra of the ring plain).

(4) Although a typical mineral assemblage dominated by plagioclase along with orthopyroxene and clinopyroxene prevails on the Tongariro complex, hornblende is a significant phase confined to the older southern cones of Tama 1 and 2, and Pukekaikiore, and olivine is particularly prominent in the young eruptives, suggesting an overall time-space relationship with petrography and mineralogy.

(5) Mineral compositions used to infer crystallization conditions revealed some subtle differences between and within some units, for example, Ngauruhoe lava groups appear to have crystallized at slightly different temperatures. Overall crystallization conditions encompass equilibration temperatures of 850-1100°C, oxygen fugacities on or up to 1 log unit above the NNO buffer curve, relatively low total pressures of <7 kb (possibly only 1-3 kb), and water contents of up to 2-5 wt% H_2O.

(6) Petrographic evidence for disequilibrium between phenocryst phases and groundmass and the involvement of magma mixing processes is especially prevalent in lavas from Tama 2, NE Oturere, SW Oturere, Pukeonake, Red Crater, and Ngauruhoe, and includes: plagioclase sieve texture coinciding with major compositional breaks/reversals and inner resorption surfaces; strongly reverse and/or patchy zoned crystals; co-existing high-temperature and low-temperature phases showing evidence of disequilibrium such as corrosion/embayments and reaction rims; olivine phenocrysts with much higher Fo contents than expected from whole-rock Mg#; and bimodal or very widely ranging crystallization temperature estimates for some samples.

(7) On the basis of variations in phenocryst mineralogy and abundances, grainsize, vesicularity, and numerous breaks and reversals in magma chemistry up section, at least five episodes of magma recharge and mixing have been identified in the NE Oturere subunit 'd' stratigraphic sequence. These subtle cyclical changes in magma petrography and chemistry suggest that multiple batches of magma and differing ascent histories have played an important role on a time scale of no more than thousands of years.

(8) Cognate feldspathic xenoliths, common in all volcano-stratigraphic units, are interpreted as coarse-grained equivalents of the host groundmass which crystallized hypabyssally at conduit margins. Quartzite xenoliths (particularly common in Ngauruhoe lavas) contain a thin, irregular, closely-spaced layering of calc-silicates between the quartz grains which is interpreted to represent the original structure of calcite/dolomite-quartz veins within the Torlesse crustal basement. Evidence for partial melting of these quartzite xenoliths is suggestive of their involvement in crustal contamination of Tongariro magmas.

(9) Tongariro eruptive products range from basaltic andesites to andesites to rare dacites, and vary almost continuously in composition from 53.0 to 64.2 wt% SiO_2 forming a calc-alkaline, medium-K suite. MgO contents vary from 1.1 to 9.2 wt%, Mg# range from 37 to 71, Cr ranges from 3 to 460 ppm and Ni from 3 to 220 ppm, but no truly primitive magmas representing direct mantle melts have been recorded from Tongariro. Tongariro rocks exhibit light-REE enriched patterns ($[Ce/Yb]_N$=1.8-3.9), contain relatively low high field strength abundances (e.g. Nb=2.7-6.7, Ta=0.24-0.63), and display the strongly spiked patterns on incompatible element spiderdiagrams that are typical of subduction-related magmas. Tongariro rocks encompass a wide range in $^{87}Sr/^{86}Sr$ (0.704442-0.706193), with slightly less variability in $^{143}Nd/^{144}Nd$ (0.512629-0.512862), Pb isotopic ratios ($^{206}Pb/^{204}Pb$=18.781-18.854, $^{207}Pb/^{204}Pb$=15.594-15.645, $^{208}Pb/^{204}Pb$=38.588-38.802), and $\delta^{18}O$ (+6.16-6.59).

(10) Variation diagrams for the Tongariro cone-forming units reveal differences in the absolute elemental abundances for given SiO_2 contents, in the length, steepness and shape of chemical trends, and in the distribution of chemical groups within compositional space. However, certain volcano-stratigraphic units do share similar patterns of chemical ordering which suggest derivation from a common deep magma reservoir, e.g. the amphibole-

bearing andesites of the older southern cones. Some compositionally distinct units nevertheless often exhibit analogous trend patterns which may signify a similar high level differentiation history involving (to varying degrees) processes of magma mixing, fractional crystallization and crustal contamination.

(11) A considerable variation in incompatible trace element ratios (e.g. Ba/Zr, Nb/Ta, La/Yb, Zr/Hf) and radiogenic isotopic compositions (e.g. Ngauruhoe $^{87}Sr/^{86}Sr$ ratios increase from 0.705470 in 1954 to 0.706165 in 1975) for closely-related samples is best explained by processes of assimilation fractional crystallization (AFC) involving contamination of Tongariro magmas by varying amounts of compositionally heterogeneous Torlesse crust, giving rise to a family of different AFC trends or AFC 'events'.

(12) Complex dynamics in the magma-plumbing system are evident on time scales as short as 100 years. For the case of Ngauruhoe historic eruptions, relatively high-level processes of magma mixing, fractional crystallization, and complex crustal contamination have combined to produce an isotopically diverse suite of lavas.

(13) Although relatively closely associated in time and space, the intensively-sampled products of the last 1000 years of activity at three vents of the Tongariro complex (Ngauruhoe, post-1.8 ka Red Crater, c.1500AD Upper Te Mari Crater) cannot be directly linked to one another via fractional crystallization alone. The non-systematic age relationships along geochemical trends, compositional reversals and compositional loops formed by these samples represent instead many small, short-lived magma batches which have been produced at relatively shallow crustal levels in several independent plumbing systems, and which have been affected by varying degrees of crustal contamination.

(14) Comparable compositional variability and rates of magmatic change over three 10 k yr time intervals spanning different parts of Tongariro's history (0-10 ka young eruptives, c.120-130 ka NE Oturere, c.200-210 ka Tama 2) suggest that similar magmatic processes have been operating throughout Tongariro's lifetime, although each time interval displays a subtly different trend pattern. Thus the regularity/rate of magma batch production may vary somewhat, but all batches appear to be small (probably $<<0.1$ km^3) and short-lived (probably c.1 ka).

(15) A relatively complex history is envisaged for the plumbing system of the Tongariro Volcanic Complex, in which different configurations and combinations of both deep and shallow magma reservoirs, some operating independently and others interconnected, have existed at different time periods throughout Tongariro's development.

ACKNOWLEDGEMENTS

Bearing in mind the rather voluminous proportions of this thesis, I should endeavour to keep the acknowledgements as brief as possible. However, this is somewhat difficult because this study was conducted and written up within such a broad time-space context (somewhat ironically paralleling the main themes of the investigation) that numerous people must be thanked for their contributions.

Many people at the Department of Geological Sciences of the University of Canterbury have greatly assisted me throughout this study. My supervisor Steve Weaver provided constant academic and logistic support and good-humoured encouragement, fruitful discussions and thorough reviews and feedback of my work in progress, sound analytical advice, and is also to be specially thanked for obtaining the necessary funding to make possible a trip to London to obtain isotopic analyses. I would like to thank David Shelley, who was also involved in supervising my thesis, for contributing many stimulating discussions on the petrography of the lavas and xenoliths, and for taking such an interest in my project. Jim Cole is also thanked for his ongoing support (and thanks to Jim and Christine for giving us a taste of professorial living with the interlude as house-sitters). The technical staff of the department are also thanked for their many and varied services, particularly: Rob Spiers for all the thin sections, jokes, and boxes; Stephen Brown for running the XRF analyses; Lee Leonard for expertly draughting many figures; Michael Finnemore for always fixing my (frequent) computer problems with a smile; and Albert Downing and Kerry Swanson for photographing hand specimens and advising on the photomicroscopy.

Funding for this study was provided by the award of a NZ Universities' Postgraduate Scholarship and a Ministry of Research, Science and Technology Postgraduate Scholarship. A number of grants from the Mason Trust Fund of the Department of Geological Sciences, University of Canterbury, contributed greatly towards field expenses.

I am extremely grateful to scientists and staff of the Wairakei Research Centre of the Institute of Geological and Nuclear Sciences. Principally, my supervisor Bruce Houghton is thanked for initiating the project and coordinating the K-Ar dating programme, providing excellent field instruction and support throughout the first field season (and ensuring a constant chocolate supply), collecting some additional Ngauruhoe samples, and providing continual inspiration and motivation through stimulating discussions and critical reviews of my written work. Ian Nairn gave generously of his time for discussion of field aspects of the volcanology, and provided several additional samples collected as part of the GNS Tongariro mapping project. Peter Wood helped obtain some historic Ngauruhoe samples from the GNS collection. Brad Scott kindly provided information and references on volcanic surveillance at Tongariro. Ashley Cody gave cheerful assistance during the first field season. I would also like to thank the Wairakei staff (and Steve Weaver for the airfares!) for the opportunity to take part in the scientific monitoring of the Ruapehu eruptions of 1995-96, which provided my first close encounter with an erupting volcano

and further renewed and inspired my fascination for volcanology (just a pity it wasn't Tongariro!).

A number of other people made field work possible. The Department of Conservation are thanked for permission to take samples from Tongariro National Park, Harry Keys for initial discussion of the project, and Neil Small for arranging use of the hut warden's quarters, providing field radios, and enthusiastically driving us to and from track road ends. Sacha Baldwin and Kay Cooper were invaluable assistants during the second field season - thanks also for your companionship, fine conversation and needing no encouragement to end a long day in the field with a soak in the hot pools! Thanks also go to Lois and Ian Smith for their generous hospitality and support, and for having a bach so conveniently located in Taupo just when it was needed most!

Analytical work was undertaken at or by a number of other organisations. Marvin Lanphere of US Geological Survey, Menlo Park, carried out K-Ar age determinations on over 40 samples, and gave useful feedback on interpretation of the geochronology. I obtained mineral analyses on the electron probe analyser at the University of Otago, under the direction of Yosuke Kawachi who provided much useful advice. Nelson Eby of University of Massachusetts, Lowell, provided INAA data on 60 samples along with stimulating and helpful discussions. I carried out radiogenic isotope analysis at Royal Holloway & Bedford New College (RHBNC), University of London, under the direction of Matthew Thirlwall, with assistance from Gerry Ingram, Joel Baker, and Pieter Vroon. Matthew and Joel are also thanked for enthusiastic and useful discussions which greatly benefited my interpretation of the data. Thanks also go to Emily Forde and Orlando Vaselli for helping to enliven the long hours spent in the lab. Whilst at RHBNC, selected samples were also re-analysed for trace elements using XRF by Gis Marriner and Matthew Thirlwall. Oxygen isotope analyses were also obtained at RHBNC, under the direction of David Mattey and with considerable assistance from Joel Baker and Colin Macpherson. Finally, Tongariro samples were involved in a pilot project to investigate the ^{10}Be content of TVZ lavas, undertaken by Ian Graham and co-workers at GNS, Lower Hutt.

Other people who I have been fortunate to have contact with and who have provided comment and discussion, and/or given feedback on problems or dilemmas, include: Ian Graham, who also kindly supplied some unpublished data; John Gamble for his continued interest and helpfulness; John Tarney for some early inspiration on the use of geochemical data; Steve Blake for information on his ion microprobe investigation of Ngauruhoe; Vince Neall, Alan Palmer and Bob Stewart for the ring plain perspective; Jon Davidson for discussions and advice on computer modelling; Thor Thordarson for his interest and discussions; and Wes Hildreth for advice on volume calculations.

The latter part of my thesis has been completed in Hamilton whilst based at the University of Waikato. Many thanks go to the staff of the Earth Sciences Department for their support, particularly Roger Briggs and Cam Nelson for their encouragement and making available the necessary facilities, Megan Balks for cheerfully and generously sharing her room and IBM computer with me, Frank Bailey for draughting additional figures, Bruce Parkinson for expert computer advice, and all the postgraduates (particularly the Monday lunch group!). Lideweij, Geerten and Dave are especially thanked for the much-needed but regrettably infrequent days at Raglan beach (and other adventures) which have made living in Hamilton just that much better!

I was lucky enough to be part of a lively group of postgraduates during my time at Canterbury University who must be thanked for their friendship and support over the years, particularly Stu (special thanks for the pep talks, witty repartee and setting such a fine example!), Rose (special thanks for the enthusiastic discussions and support, and playing host in Dublin), Ali, Tod, Simon, Roddie, Jens, Rod, Ritva, Viv, Hugh, Andy, and my various room-mates (always so quiet!) Tim, Alan and Toti. Other (mostly non-geological) friends, who have also made significant contributions to maintaining my sanity and enhancing my enjoyment of doctoral life, include: Sacha (for her enduring friendship); Stephen and Rachael (they were the best of times); Megan (especially for the retail therapy and being my London tour guide); Lisa, Sarah, Jennie, Katherine, Janine, Helen, Kathryn and Leisa (for support and friendship extending way back); Jens and Kathrin; and Zinzuni and Cosa.

I am also extremely grateful to my parents and brother James for their love, ongoing interest (and concern!), and moral and emotional support (along with all those garden-fresh veges!). Also glad you finally made it over the Tongariro Crossing walk this summer and saw what all the fuss was about. A special thanks (for financial as well as moral support) also go to my grandparents, Barbara and Len, who in the year of their 60th wedding anniversary finally get to see me leave school! And finally, to my partner Richard, an incredibly big thank you for all your love, understanding and support. Thanks for your constant encouragement, thoughtful advice, acting as a sounding board for my ideas, fixing my computer hassles, cheering me up whenever I needed it, helping so much during the final stages, making great creamy chicken pasta, and for being a most wonderful companion in life and all things volcanological.

REFERENCES

Adams, C. J. and Graham, I. J. (1993) K-Ar and Rb-Sr age studies of the metamorphism and quartz vein Au mineralisation on Terawhiti Hill, near Wellington, New Zealand. *Chem. Geol.* **103**, 235-249.

Allen, L. R. (1948) Activity at Ngauruhoe, April - May 1948. *NZ J. Sci. Tech.* **B30**, 187-193.

Allen, L. R. (1949) The eruption of Ngauruhoe, February-March 1949. *NZ Sci. Rev.* **7**, 180-183.

Allen, J. C. and Boettcher, A. L. (1978) Amphiboles in andesite and basalt. II Stability as a function of P-T-f_{H2O}-f_{O2}. *Am. Min.* **63**, 1047-1087.

Allen, J. C. and Boettcher, A. L. (1983) The stability of amphibole in andesite and basalt at high pressures. *Am. Min.* **68**, 307-314.

Allen, J. C., Boettcher, A. L. and Marland, G. (1975) Amphiboles in andesite and basalt. I. Stability as a function of P-T-f_{H2O}-f_{O2}. *Am. Min.* **60**, 1069-1085.

Anderson, D. J. and Lindsley, D. H. (1988) Internally consistent solution models for Fe-Mg-Mn-Ti oxides: Fe-Ti oxides. *Am. Min.* **73**, 714-726.

Arculus, R. J. (1994) Aspects of magma genesis in arcs. *Lithos* **33**, 189-208.

Arculus, R. J. and Powell, R. (1986) Source component mixing in the regions of arc magma generation. *J. Geophys. Res.* **91**, 5913-5926.

Armstrong, R. L. and Cooper, J. A. (1971) Lead isotopes in island arcs. *Bull. Volcanol.* **35**, 27-63.

Atkinson, I. A. E. (1981) *Vegetation map of Tongariro National Park, North Island, New Zealand, scale 1:50 000.* Wellington: NZ DSIR.

Bacon, C. R. and Hirschmann, M. M. (1988) Mg/Mn partitioning as a test for equilibrium between coexisting Fe-Ti oxides. *Am. Min.* **73**, 57-61.

Barley, M. E. (1987) Origin and evolution of mid-Cretaceous, garnet-bearing, intermediate and silicic volcanics from Canterbury, New Zealand. *J. Volcanol. Geotherm. Res.* **32**, 247-267.

Barton, M. and Wyers, G. P. (1991) Estimates of P, T, P_{H2O} and f_{O2} for lavas from Patmos (Greece) and implications for magmatic evolution. *J. Volcanol. Geotherm. Res.* **47**, 265-297.

Basaltic Volcanism Study Project (1981) *Basaltic volcanism on the terrestrial planets.* New York, Pergamon. 1286 pp.

Battey, M. H. (1949) The recent eruption of Ngauruhoe. *Rec Auck Inst Mus.* **3**, 387-395.

Beddoe-Stephens, B., Petterson, M. G., Millward, D. and Marriner, G. F. (1995) Geochemical variation and magmatic cyclicity within an Ordovician continental-arc volcanic field: the lower Borrowdale Volcanic Group, English Lake District. *J. Volcanol. Geotherm. Res.* **65**, 81-110.

Beetham, R. D. and Watters, W. A. (1985) Geology of Torlesse and Waipapa terrane basement rocks encountered during the Tongariro Power Development project, North Island, New Zealand. *NZ. J. Geol. Geophys.* **28**, 575-594.

Bibby, H. M., Caldwell, T. G., Davey, F. J. and Webb, T. H. (1995) Geophysical evidence on the structure of the Taupo Volcanic Zone and its hydrothermal circulation. *J. Volcanol. Geotherm. Res.* **68**, 29-58.

Blattner, P. and Reid, F. (1982) The origin of lavas and ignimbrites of the Taupo Volcanic Zone, New Zealand, in the light of oxygen isotope data. *Geochim. Cosmochim. Acta* **46**, 1417-1429.

Broughton, A. K. (1988) *The geology of the Manawahe Volcano*, Bay of Plenty. Unpublished B.Sc(Hons) project. Victoria University of Wellington.

Brown, W. L. and Parsons, I. (1993). Feldspars in igneous rocks. In *Feldspars and their reactions.* (Edited by I. Parsons). Netherlands, Kluwer Acad. Pub., 449-499.

Buddington, A. F. and Lindsley, D. H. (1964) Iron-titanium oxide minerals and synthetic equivalents. *J. Petrology* **5**, 310-357.

Burt, R. M., Cole, J. W. and Vroon, P. Z. (1996) Volcanic geology and geochemistry of Motuhora (Whale Island), Bay of Plenty, New Zealand. *NZ J. Geol. Geophys.* **39**, 565-580.

Carey, S. N. (1991). Transport and deposition of tephra by pyroclastic flows and surges,. In: R. V. Fisher and G. A. Smith (eds) *Sedimentation in volcanic settings.* SEPM Spec. Publ., 39-57.

Carmichael, I. S. E. (1967) The iron-titanium oxides of salic volcanic rocks and their associated ferromagnesian silicates. *Contrib. Mineral Petrol.* **14**, 36-64.

Carmichael, I. S. E., Turner, F. J. and Verhoogen, J. (1974) *Igneous Petrology.* San Francisco, McGraw-Hill. 739 pp.

Cas, R. A. F. and Wright, J. V. (1987) *Volcanic successions: Modern and ancient.*

London, Allen & Unwin. 528 pp.

Christenson, B. W. and Crump, M. E. (1994) Chemistry of springs and lakes in Tongariro National Park, 1989-1992. *NZ Volcanol. Rec.* **21**, 98-99.

Clark, R. H. (1960a). Appendix 2: Petrology of the volcanic rocks of Tongariro Subdivision. In: D. R. Gregg (ed) The geology of Tongariro Subdivision. *N.Z. Geol. Survey. Bull.* **40**, 107-123.

Clark, R. H. (1960b) Andesite lavas of the North Island, New Zealand. *Proc. 21st Int. Geol. Cong. Norden.* **13**, 123-131.

Clocchiatti, R., Del Moro, A., Gioncada, A., Joron, J. L., Mosbah, M., Pinarelli, L. and Sbrana, A. (1994) Assessment of a shallow magmatic system: the 1888-90 eruption, Vulcano Island, Italy. *Bull. Volcanol.* **56**, 466-486.

Cloud, P. E. (1951) The 1949 eruption of Ngauruhoe. *Scientific Monthly* **72**, 241-251.

Cockayne, L. (1908) Report on a botanical survey of the Tongariro National Park. *App. J. House Rep. NZ.* **C11, Vol II**, 1-42.

Cole, J. W. (1978) Andesites of the Tongariro Volcanic Centre. *J. Volcanol. Geotherm. Res.* **3**, 121-153.

Cole, J. W. (1979a) Structure, petrology and genesis of Cenozoic volcanism, Taupo Volcanic Zone, New Zealand - a review. *NZ J. Geol. Geophys.* **22**, 631-657.

Cole, J. W. (1979b) Chemical analyses of lavas and ignimbrites of the Taupo Volcanic Zone. *Victoria University of Wellington Geology Dept Publ* **13**, 31pp.

Cole, J. W. (1981) Genesis of lavas of the Taupo Volcanic Zone, North Island, New Zealand. *J. Volcanol. Geotherm. Res.* **10**, 317-337.

Cole, J. W. (1982). Tonga - Kermadec - New Zealand. In: R. S. Thorpe (ed) *Andesites: orogenic andesites and related rocks.* Chichester, Wiley. 245-258.

Cole, J. W. (1984). Taupo-Rotorua Depression: an ensialic marginal basin of North Island, New Zealand. In: B. P. Kokelaar and M. F. Howells (eds) Marginal Basin Geology. *Geol Soc Lond Spec Pub* **16**, 109-120.

Cole, J. W. (1990) Structural control and origin of volcanism in the Taupo Volcanic Zone, New Zealand. *Bull. Volcanol.* **52**, 445-459.

Cole, J. W., Cashman, K. V. and Rankin, P. C. (1983) Rare-earth element geochemistry and the origin of andesites and basalts of the Taupo Volcanic Zone, New Zealand. *Chem. Geol.* **38**, 255-274.

Cole, J. W. and Graham, I. J. (1989) Petrology of strombolian and phreatomagmatic ejecta from the 1976-82 White Island eruption sequence. *NZ Geol. Survey Bull.* **103**, 61-68.

Cole, J. W., Graham, I. J., Hackett, W. R. and Houghton, B. F. (1986). Volcanology and petrology of the Quaternary composite volcanoes of Tongariro Volcanic Centre, Taupo Volcanic Zone. In: I. E. M. Smith (ed) Late Cenozoic volcanism in New Zealand, *Roy. Soc. N.Z. Bull.* **23**, 224-250.

Cole, J. W. and Nairn, I. A. (1975) *Catalogue of the active volcanoes of the world including solfatora fields. Part 22 New Zealand.* International Association of Volcanology and Chemistry of the Earth's Interior. Rome. 156 pp.

Cortini, M. and van Calsteren, P. W. C. (1985) Lead isotope differences between whole-rock and phenocrysts in recent lavas from south Italy. *Nature* **314**, 343-345.

Cowan, J. (1927) *The Tongariro National Park, New Zealand.* Wellington, Tong. Nat. Park Board. 157 pp.

Crisp, J. A. (1984) Rates of magma emplacement and volcanic output. *J. Volcanol. Geotherm. Res.* **20**, 177-211.

Cronin, S. J., Neall, V. E. and Palmer, A. S. (1994) Contribution to the geological history of Ruapehu volcano prior to 22.5 ka BP. (Abst). *Geol. Soc. NZ Misc. Publ.* **80A**, 52.

Cronin, S. J., Neall, V. E., Stewart, R. B. and Palmer, A. S. (1996) A multiple-parameter approach to andesitic tephra correlation, Ruapehu volcano, New Zealand. *J. Volcanol. Geotherm. Res.* **72**, 199-215.

Cullen, J. (1926) Eruption of Ngauruhoe. *App. J. House Rep. NZ.* **C13**, 5-6.

Cussen, L. (1891) Report on the topographical survey of the Tongariro mountains. *App. J. House Rep. NZ.* **C1A**, 36-38.

Dalrymple, G. B. and Lanphere, M. A. (1969) *Potassium-argon dating*. San Francisco, Freeman, 53-83.

Davidson, J. P., Ferguson, K. M., Colucci, M. T. and Dungan, M. A. (1988) The origin and evolution of magmas from the San Pedro-pellado Volcanic Complex, Southern Chile: multicomponent sources and open system evolution. *Contrib. Mineral Petrol.* **100**, 429-445.

Davidson, P. M. and Lindsley, D. H. (1989) Thermodynamic analysis of pyroxene-olivine-quartz equilibria in the system CaO - MgO- FeO- SiO_2. *Am. Min.* **74**, 18-30.

DePaolo, P. J. (1979) Estimation of the depth of origin of basic magmas: A modified thermodynamic approach and a comparison with experimental studies. *Contrib. Mineral. Petrol.* **69**, 265-278.

DePaolo, D. J. (1981) Trace element and isotopic effects of combined wallrock assimilation and fractional crystallization. *Earth Planet Sci. Lett.* **53**, 189-202.

Dick, H. J. B. and Bullen, T. (1984) Chromian spinel as a petrogenetic indicator in abyssal and alpine-type peridotites and spatially associated lavas. *Contrib. Mineral Petrol.*

86, 54-76.

Donaldson, C. H. (1985) The rates of dissolution of olivine, plagioclase, and quartz in a basalt melt. *Mineral. Mag.* **49**, 683-693.

Donoghue, S. L. (1991) *Late Quaternary volcanic stratigraphy of the southeastern sector of the Mount Ruapehu ring plain, New Zealand.* Unpublished PhD thesis. Massey University.

Donoghue, S. L., Neall, V. E. and Palmer, A. S. (1995) Stratigraphy and chronology of late Quaternary andesitic tephra deposits, Tongariro Volcanic Centre, New Zealand. *J. Roy. Soc. NZ.* **25**, 115-206.

Donoghue, S. L., Stewart, R. B. and Palmer, A. S. (1991) Morphology and chemistry of olivine phenocrysts of Mangamate Tephra, Tongariro Volcanic Centre, New Zealand. *J. Roy. Soc. NZ.* **21**, 225-236.

Downey, W. S., Kellet, R. J., Smith, I. E. M., Price, R. C. and Stewart, R. B. (1994) New palaeomagnetic evidence for the recent eruptive history of Mt Taranaki, New Zealand. *J. Volcanol. Geotherm. Res.* **60**, 15-28.

Droop, G. T. R. (1987) A general equation for estimating Fe^{3+} concentrations in ferromagnesian silicates and oxides from microprobe analyses, using stoichiometric criteria. *Mineral. Mag.* **51**, 431-435.

Duncan, A. R. (1970) *The petrology and petrochemistry of andesite-dacite volcanoes in eastern Bay of Plenty, New Zealand.* Unpublished Ph.D thesis. Victoria University of Wellington.

Dungan, M. A. and Rhodes, J. M. (1978) Residual glasses and melt inclusions in basalts from DSDP Legs 45 and 46: evidence for magma mixing. *Contrib. Mineral. Petrol.* **64**, 417-431.

Eggler, D. H. (1972) Water-saturated and undersaturated melting relations in a Paricutin andesite and an estimate of water content in the natural magma. *Contrib. Mineral. Petrol.* **34**, 261-271.

Eggler, D. H. and Burnham, C. W. (1973) Crystallization and fractionation in the system andesite - H_2O - CO_2 - O_2 at pressures up to 10kb. *Geol. Soc. Am. Bull.* **84**, 2517-2532.

Ewart, A. (1965). *Petrology of the andesites.* In: B. N. Thompson, L. O. Kermode and A. Ewart (eds) New Zealand volcanology, Central Volcanic Region. *NZ DSIR Info Ser* **50**, 86-93.

Ewart, A. (1971) Notes on the chemistry of ferromagnesian phenocrysts from selected volcanic rocks, Central Volcanic Region. *NZ J. Geol. Geophys.* **14**, 323-340.

Ewart, A. (1982). The mineralogy and petrology of Tertiary-Recent orogenic rocks with special reference to the andesite-basaltic compositional range. In: R. S. Thorpe (ed)

Andesites: Orogenic andesites and related rocks. Chichester, Wiley. pp 25-95.

Ewart, A., Brothers, R. N. and Mateen, A. (1977) An outline of the geology and geochemistry, and the possible petrogenetic evolution of the volcanic rocks of the Tonga-Kermadec-New Zealand island arc. *J. Volcanol. Geotherm. Res.* **2**, 205-250.

Ewart, A. and Hawkesworth, C. J. (1987) The Pleistocene-Recent Tonga-Kermadec arc lavas: interpretation of new isotopic and rare earth data in terms of a depleted mantle source model. *J. Petrology* **28**, 495-530.

Ewart, A. and Stipp, J. J. (1968) Petrogenesis of the volcanic rocks of the central North Island, New Zealand, as indicated by a study of $^{87}Sr/^{86}Sr$ ratios, and Sr, Rb, K, U and Th abundances. *Geochim. Cosmochim. Acta.* **32**, 699-736.

Ewart, A., Taylor, S. R. and Capp, A. C. (1968) Trace and minor element geochemistry of the rhyolitic volcanic rocks, central North Island, New Zealand. *Contrib. Mineral. Petrol.* **18**, 76-104.

Feeley, T. C. and Davidson, J. P. (1994) Petrology of calc-alkaline lavas at Volcan Ollague and the origin of compositional diversity at Central Andean stratovolcanoes. *J. Petrology* **35**, 1295-1340.

Feeley, T. C., Davidson, J. P. and Armendia, A. (1993) The volcanic and magmatic evolution of Volcan Ollague, a high-K, late Quaternary stratovolcano in the Andean Central Volcanic Zone. *J. Volcanol. Geotherm. Res.* **54**, 221-245.

Ferguson, K. M., Dungan, M. A., Davidson, J. P. and Colucci, M. T. (1992) The Tatara-San Pedro Volcano, 36°S, Chile: A chemically variable, dominantly mafic magmatic system. *J. Petrology* **33**, 1-43.

Fisher, R. V. and Schmincke, H.-U. (1984) *Pyroclastic rocks.* Berlin, Springer-Verlag. 472 pp.

Fleming, C. A. (1953) The geology of Wanganui subdivision. *N.Z. Geol. Survey Bull.* **52**, 362.

Fleming, C. A. and Steiner, A. (1951) Sediments beneath Ruapehu volcano. *N.Z. J. Sci. Tech.* **B32**, 31-32.

Friedlaender, B. (1898) Some notes on the volcanoes of the Taupo district. *Trans. N.Z. Inst.* **31**, 498-510.

Frost, C. D. and Coombs, D. S. (1989) Nd isotope character of New Zealand sediments: implications for terrane concepts and crustal evolution. *Am. J. Science.* **289**, 744-771.

Frost, B. R. and Lindsley, D. H. (1991). Occurrence of iron-titanium oxides in igneous rocks. In: D. H. Lindsley (ed) *Oxide minerals: Petrologic and magnetic significance.* Michigan, Min. Soc. Am. pp 433-468.

Frost, B. R. and Lindsley, D. H. (1992) Equilibria among Fe-Ti oxides, pyroxene, olivine, and quartz: Part II. Application. *Am. Min.* **77**, 1004-1020.

Gabites, I. (1986) *Roots of Fire: A guide to the plant ecology of Tongariro National Park.* Wellington, Tongariro Natural History Society. 112 pp.

Gamble, J. A., Smith, I. E. M., McCulloch, M. T., Graham, I. J. and Kokelaar, B. P. (1993a) The geochemistry and petrogenesis of basalts from the Taupo Volcanic Zone and Kermadec Island Arc, S.W. Pacific. *J. Volcanol. Geotherm. Res.* **54**, 265-290.

Gamble, J. A., Woodhead, J. D., Wright, I. C. and Smith, I. E. M. (1996) Basalt and sediment geochemistry and magma petrogenesis in a transect from oceanic island arc to rifted continental margin arc: the Kermadec-Hikurangi Margin, SW Pacific. *J. Petrology* **37**, 1523-1546.

Gamble, J. A., Wright, I. C. and Baker, J. A. (1993b) Seafloor geology and petrology in the oceanic to continental transition zone of the Kermadec-Havre-Taupo Volcanic Zone arc system, New Zealand. *N.Z. J. Geol. Geophys.* **36**, 417-435.

Gamble, J. A., Wright, I. C., Woodhead, J. D. and McCulloch, M. T. (1995). Arc and back-arc geochemistry in the southern Kermadec Arc - Ngatoro Basin and offshore Taupo Volcanic Zone, S.W. Pacific. In: J. L. Smellie (ed) Volcanism associated with extension at consuming plate margins. *Geol. Soc. Spec. Pub.* **81**, 193-212.

Garcia, M. O. and Jacobson, S. S. (1979) Crystal clots, amphibole fractionation and the evolution of calc-alkaline magmas. *Contrib. Mineral. Petrol.* **69**, 319-327.

Gardner, J. E., Carey, S., Sigurdsson, H. and Rutherford, M. J. (1995) Influence of magma composition on the eruptive activity of Mount St Helens, Washington. *Geology* **23**, 523-526.

George, A. D. and Graham, I. J. (1991) Whole-rock Rb-Sr isochrons and pseudo-isochrons from turbidite suites from the Torlesse accretionary prism, New Zealand. *Chem. Geol.* **87**, 11-20.

Gerbe, M.-C., Gouraud, A., Sigmarsson, O., Harmon, R. S., Joron, J.-L. and Provost, A. (1992) Mineralogical and geochemical evolution of the 1982-1983 Galunggung eruption (Indonesia). *Bull. Volcanol.* **54**, 284-298.

Giannetti, B. and Luhr, J. F. (1983) The white trachytic tuff of Roccamonfina Volcano (Roman Region, Italy). *Contrib. Mineral. Petrol.* **84**, 235-252.

Gill, J. B. (1981) *Orogenic andesites and plate tectonics.* Berlin, Springer-Verlag. 390 pp.

Gill, J. B., Morris, J. D. and Johnson, R. W. (1993) Timescale for producing the geochemical signature of island arc magmas: U-Th-Pb and B-Be systematics in recent Papua New Guinea lavas. *Geochim. Cosmochim. Acta* **57**, 4269-4283.

Graham, I. J. (1985a) *Petrochemical and Sr isotopic studies of lavas and xenoliths from Tongariro Volcanic Centre - implications for crustal contamination in calcalkaline*

magmas. Unpublished PhD thesis, Victoria University of Wellington.

Graham, I. J. (1985b) Rb-Sr geochronology and geochemistry of Torlesse metasediments from the central North Island, New Zealand. *Chem. Geol.* **52**, 317-331.

Graham, I. J. (1987) Petrography and origin of metasedimentary xenoliths in lavas from Tongariro Volcanic Centre. *N.Z. J. Geol. Geophys.* **30**, 139-157.

Graham, I. J. and Adams, C. J. (1990) Rb-Sr and K-Ar geochronology of turbidites and metavolcanics at Red Rocks, Wellington, New Zealand. *N.Z. J. Geol. Geophys.* **33**, 193-200.

Graham, I. J., Blattner, P. and McCulloch, M. T. (1990) Meta-igneous granulite xenoliths from Mount Ruapehu, New Zealand: fragments of oceanic crust? *Contrib. Mineral. Petrol.* **105**, 650-661.

Graham, I. J. and Cole, J. W. (1991) Petrogenesis of andesites and dacites of White Island volcano, Bay of Plenty, New Zealand, in the light of new geochemical and isotopic data. *N.Z. J. Geol. Geophys.* **34**, 303-315.

Graham, I. J., Cole, J. W., Briggs, R. M., Gamble, J. A. and Smith, I. E. M. (1995) Petrology and petrogenesis of volcanic rocks from Taupo Volcanic Zone: a review. *J. Volcanol. Geotherm. Res.* **68**, 59-87.

Graham, I. J., Grapes, R. H. and Kifle, K. (1988) Buchitic metagreywacke xenoliths from Mount Ngauruhoe, Taupo Volcanic Zone, New Zealand. *J. Volcanol. Geotherm. Res.* **35**, 205-216.

Graham, I. J., Gulson, B. L., Hedenquist, J. W. and Mizon, K. (1992) Petrogenesis of Late Cenozoic volcanic rocks from the Taupo Volcanic Zone, New Zealand, in the light of new lead isotope data. *Geochim. Cosmochim. Acta* **56**, 2797-2819.

Graham, I. J. and Hackett, W. R. (1987) Petrology of calc-alkaline lavas from Ruapehu Volcano and related vents, Taupo Volcanic Zone, New Zealand. *J. Petrology* **28**, 531-567.

Graham, I. J. and Worthington, T. J. (1988) Petrogenesis of Tauhara dacite (Taupo Volcanic Zone, New Zealand) - evidence for magma mixing between high-alumina andesite and rhyolite. *J. Volcanol. Geotherm. Res.* **35**, 279-294.

Grange, L. I. (1928) Eruption of Ngauruhoe, March 1928. *N.Z. J. Sci. Tech.* **10**, 143-147.

Grange, L. I. and Hurst, J. A. (1929) Tongariro Subdivision. *NZG. 23rd Ann. Rep.*, 5-8.

Grange, L. I. and Williamson, J. H. (1930) Tongariro Subdivision. *NZGS 24th Ann. Rep.*, 10-13.

Grange, L. I. and Williamson, J. H. (1933) Tongariro District. *NZ.S 27th Ann. Rep.*, 18-21.

Grapes, R. H. (1986) Melting and thermal reconstitution of pelitic xenoliths, Wehr

Volcano, East Eifel, West Germany. *J. Petrology* **27**, 343-396.

Green, T. H. (1972) Crystallization of calc-alkaline andesite under controlled high-pressure hydrous conditions. *Contrib. Mineral. Petrol.* **34**, 150-166.

Green, T. H. (1995) Significance of Nb/Ta as an indicator of geochemical processes in the crust-mantle system. *Chem. Geol.* **120**, 347-359.

Gregg, D. R. (1956) Eruption of Ngauruhoe 1954-1955. *N.Z. J. Sci. Tech.* **B37**, 675-688.

Gregg, D. R. (1957a) Eruption of Ngauruhoe, January 1956. *N.Z. J. Sci. Tech.* **B38**, 683-685.

Gregg, D. R. (1957b) The tectonic setting of the Tongariro Volcanoes, New Zealand. *Proc 9th Pac. Sci. Cong.*, 218-224.

Gregg, D. R. (1960) The geology of Tongariro Subdivision. *N.Z. Geol. Survey Bull.* **40**, 152pp.

Grindley, G. W. (1960) *Sheet 8, Taupo. Geological map of New Zealand 1:250 000.* Wellington, DSIR.

Hackett, W. R. (1985) *Geology and petrology of Ruapehu Volcano and related vents.* Unpublished PhD thesis. Victoria University of Wellington, Wellington.

Hackett, W. R. and Houghton, B. F. (1985) Pinnacle Ridge Member, Whakapapa Formation: a welded airfall deposit from Ruapehu Volcano, Taupo Volcanic Zone. *N.Z. Geol. Surv. Rec.* **8**, 24-29.

Hackett, W. R. and Houghton, B. F. (1989) A facies model for a Quaternary andesitic composite volcano: Ruapehu, New Zealand. *Bull. Volcanol.* **51**, 51-68.

Hart, S. R. (1984) A large-scale isotope anomaly in the southern hemisphere mantle. *Nature* **309**, 753-757.

Harvey, P. K., Taylor, D. M., Hendry, R. D. and Bancroft, F. (1973) An accurate fusion method for the analysis of rocks and chemically related materials by X-ray fluorescence spectrometry. *X-ray Spectrum* **2**, 33-44.

Hawkesworth, C. J. and Ellam, R. M. (1989) Chemical fluxes and wedge replenishment rates along Recent destructive plate margins. *Geology* **17**, 46-49.

Hawkesworth, C. J., Gallagher, K., Hergt, J. M. and McDermott, F. (1994) Destructive plate margin magmatism: geochemistry and melt generation. *Lithos* **33**, 169-188.

Hawkesworth, C. J., Hergt, J. M., Ellam, R. M. and McDermott, F. (1991) Element fluxes associated with subduction related magmatism. *Spec. Publ. Roy. Soc. Lond.* **A335**, 393-405.

Healy, J. (1962). Structure and volcanism in the Taupo Volcanic Zone, New Zealand. In: G.

A. Macdonald and H. Kuno (eds) *The crust of the Pacific basin.* Geophys. Monogr. Ser., 151-157.

Healy, J. (1963) Welded pyroclastic rock at Tongariro. *N.Z. J. Geol. Geophys.* **6**, 712-713.

Hector, J. D. (1870) Eruption of the volcano Tongariro, New Zealand. *Nature* **2**, 477-479.

Helz, R. (1973) Phase relations of basalts in their melting ranges at PH20=5kb as a function of oxygen fugacity. I. Mafic phases. *J. Petrology* **14**, 249-302.

Higgins, M. D. (1996) Crystal size distributions and other quantitative textural measurements in lavas and tuffs from Egmont Volcano (Mt Taranaki), New Zealand. *Bull. Volcanol.* **58**, 194-204.

Hildreth, W. and Drake, R. E. (1992) Volcan Quizapu, Chilean Andes. *Bull. Volcanol.* **54**, 93-125.

Hildreth, W. and Lanphere, M. A. (1994) Potassium-argon geochronology of a basalt-andesite-dacite arc system: The Mount Adams volcanic field, Cascade Range of southern Washington. *Geol. Soc. Am. Bull.* **106**, 1413-1429.

Hill, H. (1891) Ruapehu and Ngauruhoe. *Trans. N.Z. Inst.* **24**, 603-625.

Hill, H. (1894) The volcanic outburst at Te Mari, Tongariro, in November 1892. *Trans. N.Z. Inst.* **26**, 388-392.

Hobden, B. J., Houghton, B. F., Lanphere, M. A. and Nairn, I. A. (1996) Growth of the Tongariro volcanic complex: new evidence from K-Ar age determinations. *N.Z. J. Geol. Geophys.* **39**, 151-154.

Hochstein, M. P. (1985) Steaming ground at Red Crater and in the Te Mari Craters, Mount Tongariro geothermal system (New Zealand). *Proc. 7th N.Z. Geotherm. Workshop.*, 177-180.

Hochstetter, F. (1867) *Geology of New Zealand; contributions to the geology of the provinces of Auckland and Nelson.* Wellington, Govt Printer. 320 pp.

Hodgson, K. A. (1993) *Late Quaternary lahars from Mount Ruapehu in the Whangaehu River valley, North Island, New Zealand.* Unpublished PhD thesis. Massey University.

Holcomb, R., Champion, D. and McWilliams, M. (1986) Dating recent Hawaiian lava flows using paleomagnetic secular variation. *Geol. Soc. Am. Bull.* **97**, 829-839.

Hopson, C. A. and Melson, W. G. (1990) Compositional trends and eruptive cycles at Mount St Helens. *Geoscience Canada* **17**, 131-141.

Houghton, B. F. and Hackett, W. R. (1984) Strombolian and phreatomagmatic deposits of Ohakune Craters, Ruapehu, New Zealand: a complex interaction between external water and rising basaltic magma. *J. Volcanol. Geotherm. Res.* **21**, 207-231.

Houghton, B. F., Latter, J. H. and Hackett, W. R. (1987) Volcanic hazard assesment for Ruapehu composite volcano, Taupo Volcanic Zone, New Zealand. *Bull. Volcanol.* **49**, 737-751.

Houghton, B. F. and Nairn, I. A. (1991) The 1976-82 strombolian and phreatomagmatic eruptions of White Island, New Zealand: eruptive and depositional mechanisms at a 'wet' volcano. *Bull. Volcanol.* **54**, 25-49.

Houghton, B. F., Wilson, C. J. N., McWilliams, M. O., Lanphere, M. A., Weaver, S. D., Briggs, R. M. and Pringle, M. S. (1995) Chronology and dynamics of a large silicic magmatic system: central Taupo Volcanic Zone, New Zealand. *Geology* **23**, 13-16.

Huebner, J. S. and Sato, M. (1970) The oxygen fugacity relationships of manganese oxide and nickel oxide buffers. *Am. Min.* **55**, 934-952.

Hurst, A. W. (1986) Monitoring of volcanoes of Tongariro National Park. *N.Z. Geol. Survey Rec.* **10**, 23-34.

Ingamells, C. O. (1970) Lithium metaborate flux in silicate analysis. *Analitica Chimica Acta.* **52**, 323-334.

Irvine, T. N. and Baragar, W. R. A. (1971) A guide to the chemical classification of the common volcanic rocks. *Can. J. Earth. Sci.* **8**, 523-548.

Ishikawa, T. and Nakamura, E. (1993) Boron isotope systematics of marine sediments. *Earth Planet. Sci. Lett.* **117**, 567-580.

Ishikawa, T. and Nakamura, E. (1994) Origin of the slab component in arc lavas from across-arc variation of B and Pb isotopes. *Nature* **370**, 205-208.

Ito, E., White, W. M. and Gopel, C. (1987) The O, Sr, Nd and Pb isotope geochemistry of MORB. *Chem. Geol.* **62**, 157-176.

Iyer, H. M., Evens, J. R., Dawson, P. B., Stauber, D. A. and Achauer, U. (1990). Differences in magma storage in different volcanic environments as revealed by seismic tomography: silicic volcanic centers and subduction-related volcanoes. In: M. P. Ryan (ed) *Magma transport and storage.* Chichester, Wiley. pp 293-316.

Jakes, P. and White, A. J. R. (1972) Hornblendes from calc-alkaline volcanic rocks of island arcs and continental margins. *Am. Min.* **57**, 887-902.

James, D. E. (1981) The combined use of oxygen and radiogenic isotopes as indicators of crustal contamination. *Ann. Rev. Earth Planet. Sci.* **9**, 311-344.

Jaupart, C. and Tait, S. (1995) Dynamics of differentiation in magma reservoirs. *J. Geophys. Res.* **100B**, 17615-17636.

Johnson, M. C., Anderson, A. T. and Rutherford, M. J. (1994). Pre-eruptive volatile contents of magmas. In: M. R. Carroll and J. R. Holloway (eds) *Volatiles in magmas.* Washington, Min. Soc. Am., pp 281-330.

Johnston, T. A. (1909) Eruption of Ngauruhoe, 11th March 1909, as seen from the Waimarino Plain. *App. J. House Rep. N.Z.* **C1**, 45-46.

Kontak, D. J., Clark, A. H. and Pearce, T. H. (1984) Recognition of simple and complex zoning in olivine and orthopyroxene phenocrysts using laser interference microscopy. *Mineral. Mag.* **48**, 547-550.

Kouchi, A. and Sunagawa, I. (1985) A model for mixing basaltic and dacitic magmas as deduced from experimental data. *Contrib. Mineral. Petrol.* **89**, 17-23.

Latter, J. H. (1981) Location of zones of anomalously high s-wave attenuation in the upper crust near Ruapehu and Ngauruhoe volcanoes, New Zealand. *J. Volcanol. Geotherm. Res.* **10**, 125-156.

Latter, J. H. (1986). Surveillance, research and mitigation of risk at individual volcanoes. In: J. G. Gregory and W. A. Watters (eds) Volcanic hazards assessment in New Zealand. *N.Z. Geol. Survey Rec.* **10**, 81-92.

Latter, J. H. (1989) *Volcanic hazard map of Tongariro National Park region, scale 1:100 000.* DSIR, Wellington.

Latter, J. H. and Ahmed, A. O. (1992) Tectonic and volcano-tectonic earthquakes in and near Tongariro National Park during 1990. *N.Z. Volcanol. Rec.* **19**, 72-84.

Latter, J. H., Alloway, B. V., Sherburn, S. and Hurst, A. W. (1990) Volcano-seismic activity at Ngauruhoe and Tongariro during 1989. *N.Z. Volcanol. Rec.* **18**, 48-55.

Latter, J. H., Harris, J. S., Waters, D. W. and Rogers, M. (1987) Volcano-seismic activity at Ngauruhoe and Tongariro during 1985. *N.Z. Volcanol. Rec.* **15**, 27-32.

Le Bas, M. J., Le Maitre, R. W., Streckeisen, A. and Zarettin, B. (1986) A classification of igneous rocks based upon the alkali-silica diagram. *J. Petrology* **27**, 745-750.

Le Maitre, R. W. (1989) *A classification of igneous rocks and glossary of terms: Recommendations of the I.U.G.S.* Subcomission on the systematics of igneous rocks. 193pp.

Leake, B. E. (1978) Nomenclature of amphiboles. *Mineral. Mag.* **42**, 533-563.

Lindsley, D. H. (1983) Pyroxene thermometry. *Am. Min.* **68**, 477-493.

Lindsley, D. H. and Anderson, D. J. (1983) A two-pyroxene thermometer. Proceedings of the 13th Lunar and Planetary Sciences Conference. *J. Geophys. Res. Supplt.* **88B**, A887-A906.

Lindsley, D. H. and Frost, B. R. (1992) Equilibria among Fe-Ti oxides, pyroxene, olivine, and quartz. Part I. Theory. *Am. Min.* **77**, 987-1003.

Lipman, P. W. and Banks, N. G. (1987) Aa flow dynamics, Mauna Loa 1984. *USGS Prof. Pap.* **1350**, 1527-1567.

Lockwood, J. P. and Lipman, P. W. (1980) Recovery of datable charcoal beneath young lavas: lessons from Hawaii. *Bull. Volcanol.* **43**, 609-615.

Lockwood, J. P. and Lipman, P. W. (1987) Holocene eruptive history of Mauna Loa Volcano. *USGS Prof. Pap.* **1350**, 509-527.

Lofgren, G. E. and Norris, P. N. (1981) Experimental duplication of plagioclase sieve and overgrowth textures. *Geol. Soc. Am. Abstr. Programs.* **13**, 498.

Luhr, J. F. and Carmichael, I. S. E. (1980) The Colima Volcanic Complex, Mexico I. Post-caldera andesites from Volcan Colima. *Contrib. Mineral. Petrol.* **71**, 343-372.

Marsh, B. D. (1989) Magma chambers. *Ann. Rev. Earth Planet. Sci.* **17**, 439-474.

Marshall, P. (1909) Crater of Ngauruhoe. *Trans. N.Z. Inst.* **41**, 102-105.

Mason, D. R. (1978) Compositional variations in ferromagnesian minerals from porphyry copper-generating and barren intrusions of the Western Highlands, Papua New Guinea. *Econ. Geol.* **73**, 878-890.

Mathews, W. H. (1967) A contribution to the geology of the Mount Tongariro massif, North Island, New Zealand. *N.Z. J. Geol. Geophys.* **10**, 1027-1038.

Mattey, D. and Macpherson, C. (1993) High-precision oxygen isotope microanalysis of ferromagnesian minerals by laser fluorination. *Chem. Geol.* **105**, 305-318.

Matthews, S. J., Jones, A. P. and Gardeweg, M. C. (1994) Lascar Volcano, Northern Chile: Evidence for steady-state disequilibrium. *J. Petrology* **35**, 401-432.

Maury, R. C. and Didier, J. (1991). Xenoliths and the role of assimilation. In: J. Didier and B. Barbarin (eds) *Enclaves and granite petrology.* Amsterdam, Elsevier. pp 529-542.

Maury, R. C., Didier, J. and Lameyre, J. (1978) Comparative magma/xenolith relationships in some volcanic and plutonic rocks from the French Massif Central. *Contrib. Mineral. Petrol.* **66**, 401-408.

Mazzone, P. and Grant, N. K. (1988) Mineralogical and isotopic evidence for phenocryst-matrix disequilibrium in the Garner Mountain andesite. *Contrib. Minera.l Petrol.* **99**, 267-272.

McArthur, J. L. and Shepherd, M. J. (1990) Late Quaternary glaciation of Mount Ruapehu, North Island, New Zealand. *J. Roy. Soc. N.Z.* **20**, 287-296.

McBirney, A. R. (1979). Effects of assimilation. In: H. S. Yoder (ed) *The evolution of igneous rocks:fiftieth anniversary perspectives.* New Jersey, Princeton University Press. pp 307-338.

McBirney, A. R. (1989). Xenolith. In: D. R. Bowes (ed) *The encyclopedia of igneous and metamorphic petrology.* New York, Van Nostrand Reinhold, pp 626-627.

McCulloch, M. T. and Gamble, J. A. (1991) Geochemical and geodynamical constraints on subduction zone magmatism. *Earth Planet. Sci. Lett.* **102**, 358-374.

McCulloch, M. T., Kyser, T. K., Woodhead, J. and Kinsley, L. (1994) Pb-Sr-Nd-O isotopic constraints on the origin of rhyolites from the Taupo Volcanic Zone of New Zealand: evidence for assimilation followed by fractionation from basalt. *Contrib. Mineral. Petrol.* **115**, 303-312.

McDonough, W. F., Sun, S.-S., Ringwood, A. E., Jagoutz, E. and Hofmann, A. W. (1992) Potassium, rubidium and cesium in the Earth and Moon and the evolution of the mantle of the earth. *Geochim. Cosmochim. Acta.* **56**, 1001-1012.

McGlone, M. S. and Topping, W. W. (1973) Late Otiran/early Aranuian vegetation in the Tongariro area, central North Island, New Zealand. *N.Z J. Botany.* **11**, 283-290.

McGlone, M. S. and Topping, W. W. (1977) Aranuian (post-glacial) pollen diagrams from the Tongariro region, North Island, New Zealand. *N.Z. J. Botany.* **15**, 749-760.

McGlone, M. S. and Topping, W. (1983) Late Quaternary vegetation, Tongariro region, central North Island, New Zealand. *N.Z. J. Botany.* **21**, 53-76.

Merzbacher, C. and Eggler, D. H. (1984) A magmatic geohygrometer: application to Mt St Helens and other dacitic magmas. *Geology.* **12**, 587-590.

Michaelis, F. B. (1981) *The lakes of Tongariro National Park.* Report to the National Parks and Reserves Authority. 35 pp.

Montgomery, R. L. and Keys, (H). R. (1993) Volcanic hazard management in Tongariro National Park. *DOC Sci. Res. Ser.* 11 pp.

Moore, P. R. and Brock, J. L. (1981) A physical and chemical survey of Ketatahi Hot Springs, Mt Tongariro, New Zealand. *N.Z. J. Sci.* **24**, 161-177.

Morimoto, N. (1988) Nomenclature of pyroxenes. *Mineral. Mag.* **52**, 535-550.

Morris, J. D. (1991) Applications of cosmogenic ^{10}Be to problems in the earth sciences. *Am. Rev. Earth Planet. Sci.* **19**, 313-350.

Morris, J. D., Leeman, W. P. and Tera, F. (1990) The subducted component in island arc lavas: constraints from Be isotopes and B-Be systematics. *Nature* **344**, 31-36.

Morris, J. D. and Tera, F. (1989) ^{10}Be and ^{9}Be in mineral separates and whole rocks from volcanic arcs: implications for sediment subduction. *Geochim. Cosmochim. Acta* **53**, 3197-3206.

Nairn, I. A. (1976) Atmospheric shock waves and condensation clouds from Ngauruhoe explosive eruptions. *Nature* **259**, 190-192.

Nairn, I. A., Hewson, C. A. Y., Latter, J. H. and Wood, C. P. (1976). Pyroclastic eruptions of Ngauruhoe Volcano, central North Island, New Zealand, 1974 January and March.

In: R. W. Johnson (ed) *Volcanism in Australasia.* Amsterdam, Elsevier. pp 385-405.

Nairn, I. A. and Self, S. (1978) Explosive eruptions and pyroclastic avalanches from Ngauruhoe in February 1975. *J. Volcanol. Geotherm. Res.* **3**, 39-60.

Nairn, I. A. and Wood, C. P. (1987) Active volcanoes of Taupo Volcanic Zone. *N.Z. Geol. Survey Rec.* **22**, 5-84.

Nakamura, N. (1974) Determination of rare earth elements, Ba, Fe, Mg, Na, and K in carbonaceous and ordinary chondrites. *Geochim. Cosmochim. Acta* **38**, 757-775.

Napp, J. B. (1983) *Physical volcanology of Pukeonake scoria cone, Tongariro Volcanic Centre, New Zealand.* Unpublished Bsc(Hons) thesis, Victoria University of Wellington.

Natland, J. H. (1989). Partial melting of a lithologically heterogeneous mantle: inferences from crystallization histories of magnesian abyssal tholeiites from the Siqueiros Fracture Zone. In: A. D. Saunders and M. J. Norry (eds) Magmatism in the oceanic basins. *Geol. Soc. Lond. Spec. Pub.* **42**, 41-70.

Neall, V. E., Stewart, R. B. and Smith, I. E. M. (1986). History and petrology of the Taranaki volcanoes. In: I. E. M. Smith (ed) Late Cenozoic volcanism in New Zealand. *Roy. Soc. N.Z. Bull.* **23**, 251-263.

Negendank, J. F. W. (1972) Volcanics of the Valley of Mexico. Part II: The opaque mineralogy. *Neues Jahrb. Mineral. Abh.* **117**, 183-195.

Nelson, S. T. and Montana, A. (1992) Sieve-textured plagioclase in volcanic rocks produced by rapid decompression. *Am. Min.* **77**, 1242-1249.

Nixon, G. T. (1988a) Petrology of the younger andesites and dacites of Iztaccihuatl Volcano, Mexico: I, Disequilibrium phenocryst assemblages as indicators of magma chamber processes. *J. Petrology* **29**, 213-264.

Nixon, G. T. (1988b) Petrology of the younger andesites and dacites of Iztaccihuatl Volcano, Mexico: II: Chemical stratigraphy, magma mixing, and the composition of basaltic magma influx. *J. Petrology* **29**, 265-303.

Nixon, G. T. and Pearce, T. H. (1987) Laser-inferometry study of oscillatory zoning in plagioclase: The record of magma mixing and phenocryst recycling in calc-alkaline magma chambers, Iztaccihuatl volcano, Mexico. *Am. Min.* **72**, 1144-1162.

Norrish, K. and Chappel, B. W. (1977). X-ray fluorescence spectrometry. In: J. Zussman (ed) *Physical methods in determinative mineralogy.* London, Academic Press. pp 201-272

Norrish, K. and Hutton, J. T. (1969) An accurate X-ray spectrograph method for the analysis of a wide range of geological samples. *Geochim. Cosmochim. Acta* **33**, 431-453.

Otway, P. M. (1986) Volcanic deformation surveys in Tongariro Volcanic Centre. *N.Z. Geol. Survey Rec.* **10**, 35-40.

Otway, P. M. (1987) Ngauruhoe and Tongariro deformation surveys. *N.Z. Volcanol. Rec.* **15**, 33.

Otway, P. M. (1994a) Ngauruhoe and Tongariro geodetic observations, 1992. *N.Z. Volcanol. Rec.* **21**, 96-97.

Otway, P. M. (1994b) Ngauruhoe crater inspection on 29 April and deformation survey on 30 March and 29 April 1994. *Unpublished Immediate Report*, Institute of Geological and Nuclear Sciences.

Otway, P. M. (1995) Ngauruhoe and Tongariro geodetic observations, 1993. *N.Z. Volcanol. Rec.* **22**, 83.

Otway, P. M., Hodgson, K. A. and Nairn, I. A. (1995) Whakapapa skifields lahar study. *IGNS Science Report* **95/39**, 90.

Pallister, J. S., Hoblitt, R. P., Crandell, D. R. and Mullineaux, D. R. (1992) Mount St Helens a decade after the 1980 eruptions: magmatic models, chemical cycles, and a revised hazards assessment. *Bull. Volcanol.* **54**, 126-146.

Palmer, B. A., Alloway, B. V. and Neall, V. E. (1991). Volcanic-debris-avalanche deposits in New Zealand - lithofacies organisation in unconfined, wet-avalanche flows. In: R. V. Fisher and G. A. Smith (eds) *Sedimentation in volcanic settings.* SEPM Spec Publ. pp 89-98.

Palmer, B. A., Purves, A. M. and Donoghue, S. L. (1993) Controls on accumulation of a volcaniclastic fan, Ruapehu composite volcano, New Zealand. *Bull. Volcanol.* **55**, 176-189.

Patterson, D. B. (1986) Petrochemistry and structure of the lavas of the Mangatepopo Valley, Tongariro Volcanic Centre, New Zealand. Unpublished B.Sc(Hons) Thesis. Victoria University of Wellington.

Patterson, D. B. and Graham, I. J. (1988) Petrogenesis of andesitic lavas from Mangatepopo Valley and Upper Tama Lake, Tongariro Volcanic Centre, New Zealand. *J. Volcanol. Geotherm. Res.* **35**, 17-29.

Pearce, J. A. (1982). Trace element characteristics of lavas from destructive plate boundaries. In: R. S. Thorpe (ed) *Andesites: orogenic andesite and related rocks.* Chichester, Wiley. pp 525-548.

Pearce, J. A. (1983). Role of the sub-continental lithosphere in magma genesis at active continental margins. In: C. J. Hawkesworth and M. J. Norry (eds) *Continental basalts and mantle xenoliths.* Nautwich, Shiva. pp 230-249.

Pearce, J. A. and Norry, M.J. (1979) Petrogenetic implications of Ti, Zr, Y and Nb variations in volcanic rocks. *Contrib. Mineral. Petrol.* **69**, 33-47.

Pearce, T. H. (1993). Recent work on oscillatory zoning in plagioclase. In: I. Parsons (ed) *Feldspars and their reactions*. Netherlands, Kluwer Acad Pub. pp 313-349.

Pearce, T. H., Russell, J. K. and Wolfson, I. (1987) Laser-interference and Nomarski interference imaging of zoning profiles in plagioclase phenocrysts from the May 18 1980 eruption of Mt St Helens, Washington. *Am. Min.* **72**, 1131-1143.

Pillans, B. (1994) Direct marine-terrestrial correlations, Wanganui Basin, New Zealand: the last one million years. *Quat. Sci. Rev.* **13**, 189-200.

Pillans, B., McGlone, M., Palmer, A., Mildenhall, D., Alloway, B. and Berger, G. (1993) The last glacial maximum in central and southern North Island, New Zealand: a paleoenvironmental reconstruction using the Kawakawa Tephra Formation as a chronostratigraphic marker. *Paleogeog. Paleoclim. Paleoecol.* **101**, 283-304.

Pinkerton, H. and Wilson, L. (1994) Factors controlling the lengths of channel-fed lava flows. *Bull. Volcanol.* **56**, 108-120.

Potton, C. (1987) *Tongariro: a sacred gift.* Nelson & Auckland, Craig Potton & Landsdowne Press, 192 pp.

Powell, R. (1984) Inversion of the assimilation and fractional crystallization (AFC) equations; characterization of contaminants from isotope and trace element relationships in volcanic suites. *J. Geol. Soc. Lond.* **141**, 447-452.

Price, R. C., McCulloch, M. T., Smith, I. E. M. and Stewart, R. B. (1992) Pd-Nd-Sr isotopic compositions and trace element characteristics of young volcanic rocks from Egmont Volcano and comparisons with basalts and andesites from the Taupo Volcanic Zone, New Zealand. *Geochim. Cosmochim. Acta* **56**, 941-953.

Ramsey, J. G. (1980) The crack-seal mechanism of rock deformation. *Nature* **284**, 135-139.

Reid, F. (1983) Origin of the rhyolitic rocks of the Taupo Volcanic Zone, New Zealand. *J. Volcanol. Geotherm. Res.* **15**, 315-338.

Robinson, P., Spear, F. S., Schumacher, J. C., Laird, J., Klein, C., Evans, B. V. and Doolan, B. L. (1981). Phase relations of metamorphic amphiboles: natural occurrence and theory. In: D. R. Veblen and P. H. Ribbe (eds) *Amphiboles: Petrology and experimental phase relations.* Michigan, Min Soc Am. pp 1-227.

Roeder, P. L. and Emslie, R. F. (1970) Olivine-liquid eqilibrium. *Contrib. Mineral. Petrol.* **29**, 275-289.

Rogan, W. and Blake, S. (1994) Trace element zonation of phenocrysts from Ngauruhoe Volcano, New Zealand: constraints on magmatic processes. *Mineral. Mag.* **58A**, 783-784.

Rollinson, H. R. (1993) *Using geochemical data: evaluation, presentation, interpretation.* Harlow, Longman. 352 pp.

Romick, J. D., Kay, S. M. and Kay, R. W. (1992) The influence of amphibole fractionation on the evolution of calc-alkaline andesite and dacite tephra from the central Aleutians, Alaska. *Contrib. Mineral. Petrol.* **112**, 101-118.

Roser, B. and Grapes, R. (1990) Geochemistry of a metabasite - chert - coloured-argillite - turbidite association at Red Rocks, Wellington, New Zealand. *N.Z. J. Geol. Geophys.* **33**, 181-191.

Rubin, M., Gargulinski, L. K. and McGeehin, J. P. (1987) Hawaiian radiocarbon dates. *US Geol. Survey Prof. Pap.* **1350**, 213-242.

Rutherford, M. J. and Devine, J. D. (1988) The May 18 1980 eruption of Mt St Helens 3. Stability and chemistry of amphibole in the magma chamber. *J. Geophys. Res.* **93B**, 11948-11959.

Rutherford, M. J. and Hill, P. M. (1993) Magma ascent rates from amphibole breakdown: an experimental study applied to the 1980-1986 Mt St Helens eruptions. *J. Geophys. Res.* **98B**, 19667-19685.

Rutherford, M. J., Sigurdsson, H., Carey, S. and Davis, A. (1985) May 18 1980 eruption of Mount St Helens 1. Melt composition and experimental phase equilibria. *J. Geophys. Res.* **90B**, 2929-2947.

Sachs, P. M. and Stange, S. (1993) Fast assimilation of xenoliths in magmas. *J. Geophys. Res.* **98B**, 19741-19754.

Sakuyama, M. (1978) Petrographic evidence of magma mixing in Shirouma-Oike volcano, Japan. *Bull. Volcanol.* **41**, 501-512.

Sakuyama, M. (1979) Evidence of magma mixing: petrological study of Shirouma-Oike calc-alkaline andesite volcano, Japan. *J. Volcanol. Geotherm. Res.* **5**, 179-208.

Sakuyama, M. (1981) Petrological study of the Myoko and Kurohime volcanoes, Japan, Crystallization sequence abd evidence for magma mixing. *J. Petrology* **22**, 553-583.

Sato, H. (1975) Diffusion coronas around quartz xenocrysts in andesite and basalt from Tertiary Volcanic Region in northeastern Shikoku, Japan. *Contrib. Mineral. Petrol.* **50**, 49-64.

Searle, E. J. (1962) Quartzose xenoliths and pyroxene aggregates in the Auckland basalts. *N.Z. J. Geol. Geophys.* **5**, 130-140.

Self, S. (1975) Explosive activity of Ngauruhoe, 27-30 March 1974 (Note). *N.Z. J. Geol. Geophys.* **18**, 189-195.

Self, S., Wilson, L. and Nairn, I. A. (1979) Vulcanian eruption mechanisms. *Nature* **277**, 440-443.

Shelley, D. (1975) Temperature and metamorphism during cleavage and fold formation of the Greenland Group north of Greymouth. *J. Roy. Soc. N.Z.* **5**, 66-75.

Sherburn, S. (1994) Volcano-seismic activity at Ngauruhoe and Tongariro, 1992. *N.Z. Volcanol. Rec.* **21**, 95.

Sherburn, S. (1995) Tongariro area seismicity. *N.Z. Volcanol. Rec.* **22**, 77.

Sigurdsson, H. (1968) Petrology of acid xenoliths from Surtsey. *Geol. Mag.* **105**, 440-453.

Smith, A. L. and Roobol, M. J. (1982). Andesitic pyroclastic flows. In: R. S. Thorpe (ed) *Andesites: orogenic andesites and related rocks.* Chichester, Wiley. pp 415-433.

Smith, A. L. and Roobol, M. J. (1990) Mt Pelee, Martinique; A study of an active island-arc volcano. *Geol. Soc. Am. Mem.* **175**, 105.

Smith, E. G. C., Stern, T. and Reyners, M. (1989) Subduction and back-arc activity at the Hikurangi convergent margin, New Zealand. *Pure Appl. Geophys.* **129**, 203-231.

Smith, G. A. (1991). Facies sequences and geometries in continental volcaniclastic sediments. In: R. V. Fisher and G. A. Smith (eds) *Sedimentation in volcanic settings.* SEPM Spec. Publ. pp 109-121.

Smith, G. A. and Lowe, D. R. (1991). Lahars: volcanic-hydrologic events and deposition in the debris flow - hyperconcentrated flow continuum. In: R. V. Fisher and G. A. Smith (eds) *Sedimentation in volcanic settings.* SEPM Spec. Publ. pp 60-70.

Sparks, R. S. J. (1976) Grain size variations in ignimbrites and implications for the transport of pyroclastic flows. *Sedimentology* **3**, 147-188.

Sparks, R. S. J. and Marshall, L. A. (1986) Thermal and mechanical constraints on mixing between mafic and silicic magmas. *J. Volcanol. Geotherm. Res.* **29**, 99-124.

Speight, R. (1908). Geology of Tongariro National Park. In Report on a botanical survey of the Tongariro National Park. (Edited by L. Cockayne), *App. J. House Rep. N.Z.* **C11**, 7-13.

Spry, A. (1969) *Metamorphic textures.* Oxford, Pergamon. 350 pp.

Stamatelopoulou-Seymour, K., Vlassopoulos, D., Pearce, T. H. and Rice, C. (1990) The record of magma chamber processes in plagioclase phenocrysts at Thera Volcano, Aegean Volcanic Arc, Greece. *Contrib. Mineral. Petrol.* **104**, 73-84.

Stasiuk, M. V., Jaupart, C. and Sparks, R. S. J. (1993) Influence of cooling on lava flow dynamics. *Geology* **21**, 335-338.

Steiger, R. H. and Jager, E. (1977) Submission on geochronology: convention on the use of decay constants on geo- and cosmochronology. *Earth Planet. Sci. Lett.* **36**, 359-362.

Steiner, A. (1958) Petrogenetic implications of the 1954 Ngauruhoe lava and its xenoliths. *N.Z. J. Geol. Geophys.* **1**, 325-363.

Stern, T. A. (1986). Geophysical studies of the upper crust within the Central Volcanic

Region, New Zealand. In: I. E. M. Smith (ed) Late Cenozoic volcanism in New Zealand. *Roy. Soc. N.Z. Bull.* **23**, 92-111.

Stern, T. A. (1987) Asymmetric back-arc spreading, heat flux and structure associated with the Central Volcanic Region of New Zealand. *Earth Planet. Sci. Lett.* **85**, 265-276.

Stimac, J. A. and Pearce, T. H. (1992) Textural evidence of mafic-felsic magma interaction in dacite lavas, Clear Lake, California. *Am. Min.* **77**, 795-809.

Stipp, J. J. (1968) *The geochronology and petrogenesis of the Cenozoic volcanics of the North Island, New Zealand.* Unpublished PhD thesis, Australian National University.

Stolz, A. J., Jochum, K. P., Spettel, B. and Hofmann, A. W. (1996) Fluid- and melt-related enrichment in the subarc mantle: evidence from Nb/Ta variations in island-arc basalts. *Geology* **24**, 587-590.

Stormer, J. C. (1973) Calcium zoning in olivine and its relationship to silica activity and pressure. *Geochim. Cosmochim. Acta* **37**, 1815-1821.

Stormer, J. C. and Nicholls, J. (1978) XLFRAC: A program for the interactive testing of magmatic differentiation models. *Computers and Geosciences* **4**, 143-159.

Sutton, A. N., Blake, S. and Wilson, C. J. N. (1995) An outline geochemistry of rhyolite eruptives from Taupo volcanic centre, New Zealand. *J. Volcanol. Geotherm. Res.* **68**, 153-175.

Tatsumi, Y., Hamilton, D. L. and Nesbitt, R. W. (1986) Chemical characteristics of fluid phase released from a subducted lithosphere and origin of arc magmas: evidence from high-pressure experiments and natural rocks. *J. Volcanol. Geotherm. Res.* **29**, 293-309.

Taylor, H. P. and 1980 (1980) The effect of assimilation of country rocks by magmas on $^{18}O/16O$ and $^{87}Sr/^{86}Sr$ systematics in igneous rocks. *Earth Planet. Sci. Lett.* **47**, 243-254.

Taylor, S. R. and McLennan, S. M. (1988). Ch. 79 The significance of the rare earths in geochemistry and cosmochemistry. In: K. A. Gschneidner and L. Eyring (eds) *Handbook on the physics and chemistry of rare earths.* Netherlands, Elsevier. pp 485-578.

Tatara-San Pedro Project Team (1992) The life history of an Andean volcano. *Eos* **73**, 406-407.

Thirlwall, M. F. (1991) Long-term reproducibility of multicollector Sr and Nd isotope ratio analysis. *Chem. Geol.* **94**, 85-104.

Thirlwall, M. F., Smith, T. E., Graham, A. M., Theodorou, N., Hollings, P., Davidson, J. P. and Arculus, R. J. (1994) HFSE anomalies in arc lavas: source or process? *J. Petrology* **35**, 819-838.

Thomas, A. P. W. (1888) Notes on the volcanic rocks of the Taupo district and King Country. *Trans. N.Z. Inst.* **20**, 306-311.

Thomas, A. P. W. (1889) Notes on the geology of Tongariro and the Taupo district. *Trans. N.Z. Inst.* **21**, 338-353.

Thomson, J. A. (1926) Volcanoes of the New Zealand - Tonga volcanic zone. *N.Z. J. Sci. Tech.* **8**, 354-371.

Thorpe, R. S. (1982) *Andesites:Orogenic andesite and related rocks.* Chichester, Wiley. 697 pp.

Tilling, R. I. and Arth, J. G. (1994) Sr and Nd isotopic composition of sulfur-rich magmas of El Chichon Volcano, Mexico. (Abst) *IAVCEI General Assembly*, Ankara, Turkey,

Tonarini, S., Armienti, P., D'Orazio, M., Innocenti, F., Pompilio, M. and Petrini, R. (1995) Geochemical and isotopic monitoring of Mt Etna 1989-1993 eruptive activity: bearing on the shallow feeding system. *J. Volcanol. Geotherm. Res.* **64**, 95-115.

Tongariro National Park Board (1981) *The restless land: the story of Tongariro National Park.* Wellington. 112 pp.

Topping, W. W. (1973) Tephrostratigraphy and chronology of late Quaternary eruptives from the Tongariro Volcanic Centre, New Zealand. *N.Z. J. Geol. Geophys.* **16**, 397-423.

Topping, W. W. (1974) *Some aspects of Quaternary history of Tongariro Volcanic Centre.* Unpublished PhD thesis, Victoria University of Wellington.

Topping, W. W. and Kohn, B. P. (1973) Rhyolitic tephra marker beds in the Tongariro area, North Island, New Zealand. *N.Z. J. Geol. Geophys.* **16**, 375-395.

Tsuchiyama, A. (1985) Dissolution kinetics of plagioclase in the melt of the system diopside - albite - anorthite, and origin of dusty plagioclase in andesites. *Contrib. Mineral. Petrol.* **89**, 1-16.

Tsuchiyama, A. (1986) Melting and dissolution kinetics: application to partial melting and dissolution of xenoliths. *J. Geophys. Res.* **91B**, 9395-9406.

Turner, E. P. (1911) Appendix VI - A short account of a visit to Ngauruhoe and Tongariro volcanoes. *App. J. House Rep. N.Z.* **C1**, 34-35.

Tuttle, O. F. and Bowen, N. L. (1958) Origin of granite in the light of experimental studies in the system $NaAlSi_3O_8$ - $KAlSi_3O_8$ - SiO_2 - H_2O. *Geol. Soc. Am. Mem.* **74**, 153 pp.

Ussler, W. and Glazner, A. F. (1989) Phase equilibria along a basalt-rhyolite mixing line: implications for the origin of calc-alkaline intermediate magmas. *Contrib. Mineral. Petrol.* **101**, 232-244.

Vance, J. A. (1965) Zoning in igneous plagioclase: Patchy zoning. *J. Geol.* **73**, 636-651.

Wahyudin, D. (1993) *Volcanology and petrology of Tama Lakes area, Tongariro Volcanic Centre, New Zealand.* Unpublished M.Sc. thesis, Victoria University of Wellington.

Walcott, R. I. (1978) Present tectonics and Late Cenozoic evolution of New Zealand. *Geophys. J. Roy. Astr. Soc.* **52**, 137-164.

Walker, G. P. L. (1973) Lengths of lava flows. *Phil. Trans. R. Soc Lond.* **A274**, 107-118.

Walker, G. P. L. (1982). Eruptions of andesite volcanoes. In: R. S. Thorpe (ed) *Andesites: orogenic andesites and related rocks*. Chichester, Wiley. pp 403-413.

White, F. W. G. (1929) The crater of Ngauruhoe. *N.Z. J. Sci. Tech.* **11**, 48-52.

Wilson, S. H. (1960). Physical and chemical investigation of Ketatahi Hot Springs. In: D. R. Gregg (ed) The geology of Tongariro Subdivision. *N.Z. Geol. Survey Bull.* **40**, 124-144

Wilson, L., Sparks, R. S. J. and Walker, G. P. L. (1980) Explosive volcanic eruptions - IV. The control of magma properties and conduit geometry on eruption column behaviour. *Geophys. J. Roy. Astr. Soc.* **63**, 117-148.

Wilson, C. J. N., Houghton, B. F., McWilliams, M. O., Lanphere, M. A., Weaver, S. D. and Briggs, R. M. (1995) Volcanic and structural evolution of Taupo Volcanic Zone, New Zealand: a review and synthesis. *J. Volcanol. Geotherm. Res.* **68**, 1-28.

Wilson, C. J. N., Rogan, A. M., Smith, I. E. M., Northey, D. J., Nairn, I. A. and Houghton, B. F. (1984) Caldera volcanoes of the Taupo Volcanic Zone, New Zealand. *J. Geophys. Res.* **89**, 8463-8484.

Wolff, J. A. and Wright, J. V. (1981) Rheomorphism of welded tuffs. *J. Volcanol. Geotherm. Res.* **10**, 13-34.

Wright, J. V., Smith, A. L. and Self, S. (1980) A working terminology of pyroclastic deposits. *J. Volcanol. Geotherm. Res.* **8**, 315-336.

Warrior mountains do battle:
According to Maori legend, Tongariro defeats Taranaki as they vie for the love of Pihanga.
(Illustration by John Bevan Ford, in "The Warrior Mountains" by Katerina Mataira, Te Ataarangi Publications, Raglan.)